ACTA PHYSICA

ACADEMIAE SCIENTIARUM HUNGARICAE

ADIUVANTIBUS
L. JÁNOSSY, I. KOVÁCS, K. NAGY, A. SZALAY

REDIGIT
P. GOMBÁS

TOMUS XXIX FASCICULUS 1

AKADÉMIAI KIADÓ, BUDAPEST
1970

ACTA PHYS. HUNG.

ACTA PHYSICA

A MAGYAR TUDOMÁNYOS AKADÉMIA FIZIKAI KÖZLEMÉNYEI

SZERKESZTŐSÉG ÉS KIADÓHIVATAL: BUDAPEST V., ALKOTMÁNY UTCA 21.

Az *Acta Physica* német, angol, francia és orosz nyelven közöl értekezéseket a fizika tárgyköréből.

Az *Acta Physica* változó terjedelmű füzetekben jelenik meg: több füzet alkot egy kötetet.

A közlésre szánt kéziratok a következő címre küldendők:

Acta Physica, Budapest 502, P. O. B. 24.

Ugyanerre a címre küldendő minden szerkesztőségi és kiadóhivatali levelezés.

Megrendelhető a belföld számára az Akadémiai Kiadónál (Budapest V., Alkotmány utca 21. Bankszámla 05-915-111-46), a külföld számára pedig a „Kultúra" Könyv- és Hírlap Külkereskedelmi Vállalatnál (Budapest I., Fő u. 32. Bankszámla 43-790-057-181 sz.), vagy annak külföldi képviseleteinél és bizományosainál.

Die *Acta Physica* veröffentlichen Abhandlungen aus dem Bereich der Physik in deutscher, englischer, französischer und russischer Sprache.

Die *Acta Physica* erscheinen in Heften wechselnden Umfanges. Mehrere Hefte bilden einen Band.

Die zur Veröffentlichung bestimmten Manuskripte sind an folgende Adresse zu richten:

Acta Physica, Budapest 502, P. O. B. 24.

An die gleiche Anschrift ist auch jede für die Redaktion und den Verlag bestimmte Korrespondenz zu senden. Abonnementspreis pro Band: $ 16.00.

Bestellbar bei dem Buch- und Zeitungs-Aussenhandels-Unternehmen »Kultura« (Budapest I., Fő u. 32. Bankkonto Nr. 43-790-057-181) oder bei seinen Auslandsvertretungen und Kommissionären.

ACTA PHYSICA

ACADEMIAE SCIENTIARUM HUNGARICAE

ADIUVANTIBUS
L. JÁNOSSY, I. KOVÁCS, K. NAGY, A. SZALAY

REDIGIT
P. GOMBÁS

TOMUS XXIX

AKADÉMIAI KIADÓ, BUDAPEST
1970

ACTA PHYSICA

Tomus 29

D. Berényi and *D. Varga:* The Details of the Critical Study of the Internal Bremsstrahlung Spectrum from ^{32}P. — *Д. Берени* и *Д. Варга:* Подробности критического изучения спектра внутреннего тормозного излучения 32p 1

G. Fáy: A Phenomenological Foundation of Quantum Logic. — *Г. Фаи:* Феноменологическое обоснование квантовой логики 27

J. Balázs and *B. Pődör:* On the Theory of Galvanomagnetic Effects in Semiconductors with Anisotropic Scattering. — *Й. Балаж* и *Б. Педер:* К теории гальваномагнитных явлений с анизотропным рассеянием 35

B. Rősner, Z. Bodó, T. Sebestyén and *B. Wohn:* Transmitted Phonon Drag Measurements in Ge. — *Б. Рэзнер, З. Бодо, Т. Шебештен* и *Б. Вон:* Измерение фононной тяти в Ge 45

I. Tamássy-Lentei: Potential Curves for One-Electron Heteronuclear Diatomic Systems in One-Centre Treatment. — *И. Тамаши-Лентеи:* Потенциальные кривые для одноэлектронных гетероядерных двухатомных систем в одноцентровом рассмотрении 67

J. Gyulai: Energy Distribution of Traps in GaP Crystals. — *Й. Дьюлаи:* Распределение энергии ловушек в кристаллах GaP 75

I. Hevesi, A. Süli and *J. Gyulai:* Contact Potential Difference Measurements on (010) Surfaces of Vanadium Pentoxide. — *И. Хевеши, А. Шюли* и *Й. Дьюлаи:* Измерения контактной разности потенциалов на поверхности (010) пятиокиси ванадия 79

I. Kovács and *V. M. Korwar:* On the Anomalous Multiplet Splitting of the Triplet Terms of the ND Molecule. — *И. Ковач* и *В. М. Корвар:* Об аномальном мультиплетном расщеплении триплетных термов молекулы ND 85

T. Gémesy and *G. Surányi:* A Note on the Observation of S° Meson 91

RECENSIONES 93

I. Szép and *I. Bársony:* Oxygen Content Determination in Thin Silicon Slices. — *И. Сейп* и *И. Баршонь:* Определение содержания кислорода в тонких пластинках кремния 97

S. K. Sangal and *P. K. Sharma:* Vibration Spectra and Debye Temperatures of Transition Metals. — *С. К. Сангал* и *П. К. Шарма:* Колебательные спектры и температура Дэбая переходных металлов 107

M. S. El-Manharawy: The Influence of Cobalt on the Photo-Luminescence of Silver-Activated ZnS: CdS Phosphors Containing Nickel. — *М. С. Эл-Манхаравы:* Влияние кобальта на фотолюминесценцию фосфоров активизированных серебром и содержащих никель 117

M. El-Nadi, A. Osman and *T. H. Rihan:* Finite Range Coulomb Stripping in (t, p) and (He^3, n) Reactions. — *М. Эл-Нади, А. Осман* и *Т. Х. Рихан:* Кулоновская реакция срыва (t, p) и (He^3, n) с конечным радиусом взаимодействия 127

M. El-Nadi, A. Osman and *T. H. Rihan:* Cluster Transfer Reactions at Low Energies — *М. Эл-Нади, А. Осман* и *Т. Х. Рихан:* Реакции при низких энергиях с передачей «кластеров» 143

R. G. Nousratoullin and *I. Ts. Lyast:* Application of Variation-Perturbation Theory to the Study of the Inductive Effect in Saturated Molecules by the Method of Geminals II. Halogen-Substituted Hydrocarbons. — *Р. Г. Нусратуллин* и *И. Ц. Лят:* Применение вариационной теории возмущения к изучению индуктивного эффекта в насыщенных молекулах методом геминалей II. Галогенозамещенные углеводороды 159

G. Fáy: On the Correspondence Principle. — *Г. Фаи:* О принципе соответствия 167

I. Hevesi and *B. Karvaly:* Optical Reflection of V_2O_5 Single Crystals. — *И. Хевеши* и *Б. Карваль:* Оптическое отражение монокристаллов V_2O_5 183

E. Balázs: Collective Vibrations of the Statistical Nuclear Model. — *Э. Балаж:* Коллективные колебания в статистической ядерной модели 193

B. Karvaly and *F. Pintér:* Investigations on the Connections between the Bulk Absorption and Diffuse Reflectance Spectra of Powdered Solids II. — *Б. Карваль* и *Ф. Пинтэр:* Исследования о взаимосвязи между спектрами истинного (массивного) поглощения и диффузного отражения порошкообразных веществ II 203

L. Szalay and *Z. Várkonyi:* Investigations on Connections between Fluorescence Polarization and Foreign Quenching in Viscous Solutions. — *Л. Салаи* и *З. Варкони:* Исследования соотношений между флуоресцентной поляризацией и посторонним погласителем в вискозных растворах 221

R. M. Gupta and *N. L. Varma:* Penetration of Electromagnetic Waves into Plasma. — *Р. М. Гупта* и *Н. Л. Варма:* Проникновение электромагнитных волн в плазму 229

I. Kovács, L. Nagy and *I. Vinnay:* Angular Anisotropy of Fission Fragments in Ternary Fission of ^{235}U and ^{238}U Induced by 14 MeV Neutrons. — *И. Ковач, Л. Надь* и *И. Виннаи:* Угловая анизотропия осколков деления в тройном делении ^{235}U и ^{238}U вызванная нейтронами 14 МэВ 239

I. Kirschner, A. Stark and *I. I. Falko:* The Collective Effect of Paramagnetic and Diamagnetic Impurities on the Temperature of Superconducting Transition. — *И. Киршнер, А. Штарк* и *И. И. Фалко:* Совместное влияние пара и диамагнитных примесей на температуру сверхпроводящего перехода 243

K. L. Nagy: Complex Poles, Cuts, Indefinite Metric and Unitarity. — *К. Л. Надь:* Комплексные полюсы, разрезы, неопределенная метрика и унитарность 251

P. Gombás und *D. Kisdi:* Über die Grundlagen der statistischen Theorie des Atomkerns. — *П. Гомбаш* и *Д. Кишди:* Об основах статистической теории атомных ядер 267

J. Balázs and *Z. Bodó:* Theoretical Study of Space-Charge-Limited (SCL) Currents and its Application to ZnS Single Crystals. — *Й. Балаж* и *З. Бодо:* Теоретическое изучение тока ограниченного пространственным зарядом (топз) и его применение к изучению монокристаллов ZnS 279

J. Dombi: Some Remarks on Corrections Concerning Energy Transfer Processes in Luminescent Mixed Solutions 297

RECENSIONES 301

N. D. Sen Gupta: On the Symmetry Properties of the Equations of Motion. — *Н. Д. Сен Гупта:* О свойствах симметрии уравнения движения 305

A. M. Molla: Punch Problem of Transversely Isotropic Material for a Half-Space with Mixed Thermal Conditions. — *А. М. Молла:* Проблема ударной волны в поперечно изотропном материале, заполняющем полупространство со смешанными термическими условиями 309

И. Киршнер: Аналогические черты матрицы энтропии и матрицы проводимости — *I. Kirschner:* Analogous Features of the Entropy and Conductivity Matrices ... 319

I. Ketskeméty and *L. Kozma:* A Method for the Spectrophotometric Investigation of Absorption and Fluorescence Emission in Media of Extremely Weak Absorption. — *И. Кечкемети* и *Л. Козма:* Метод для спектрофотометрического изучения поглощения и флуоресцентного излучения слабо поглощающих сред 331

Х. Д. Андросенко, С. Б. Ермагамбетов, Г. Н. Смиренкин, Д. Л. Шпак и *И. Ковач:* Угловая анизотропия деления ядер нейтронами и структура барьера. — *H. D. Androsenko, S. B. Ermagambetov, G. N. Smirenkin, D. L. Shpak* and *I. Kovács:* Angular Anisotropy of Nuclear Fission by Neutrons and the Barrier Structure.... 341

A. Dobay-Szegleth: Calculation of Electron Scattering on the Basis of the Statistical Atom Model in which the Electrons are Grouped according to the Principal Quantum Number. — *А. Добаи-Сеглет:* Расчет рассеяния электронов по статистической модели атома, в которой электроны сгруппированы по главному квантовому числу 359

L. Meskó, V. Schlenk and *A. Valek:* Experimental Study of the $^{24}Mg(d,p)^{25}Mg$ Reaction in the Energy Range 650—500 keV. — *Л. Мешко, Б. Шленк* и *А. Валек:* Исследование ядерной реакции $^{24}Mg(d, p)^{25}Mg$ в области энергии 650—500 кэв 365

J. Cunningham: A Ghostless Lee Model. — *Дж. Канингэм:* Модель Ли без призрачных состояний 373

J. Cunningham: A Differential Approach to High Energy Behaviour of Feynman Amplitudes. — *Дж. Канингэм:* Дифференциальное приближение поведения амплитуд Фейнмана в области высоких энергий 379

K. Somogyi: On the Apparent Deviation from Ohm's Law in GaP. — *К. Шомоди:* О появлении кажущегося отклонения от закона Ома в GaP 383

T. Tietz: Potential Energy Curves for Diatomic Molecules. — *Т. Титц:* Кривые потенциальной энергии для двухатомных молекул 391

I. Kovács and *V. M. Korwar:* Re-investigation of the Coupling Constants of the Revised Molecular States of TiO. — *И. Ковач* и *В. М. Корвар:* Повторное исследование констант связи исправленных молекулярных состояний 399

A. Szalay and *E. Csongor:* Fission Products in the Atmospheric Precipitation in Debrecen, Hungary, during 1968 and 1969. — *А. Салаи* и *Е. Чонгор:* Продукты деления в атмосферных осадках в г. Дебрецен (Венгрия) в 1968 и 1969 гг. 407

Gy. Farkas: Higher Order Coherence Effects of Laser Light on the Photoelectron Distribution Detected by Third Order Photoeffect. — *Д. Фаркаш:* Когерентные эффекты высшего порядка распределения фотоэлектронов от лазерного излучения, измеренные фотоэффектом третьего порядка 415

L. Jánossy: On the Physical Significance of the Vector Potential. — *Л. Яноши:* Роль векторного потенциала 419

RECENSIONES 427

Acta Physica Academiae Scientiarum Hungaricae, Tomus 29 (1), pp. 1–26 (1970)

THE DETAILS OF THE CRITICAL STUDY OF THE INTERNAL BREMSSTRAHLUNG SPECTRUM FROM ^{32}P

By

D. BERÉNYI and D. VARGA

INSTITUTE OF NUCLEAR RESEARCH OF THE HUNGARIAN ACADEMY OF SCIENCES, DEBRECEN

(Received 26. VI. 1969)

On the basis of a critical analysis of the measuring conditions and the evaluation process in the measurement of the internal bremsstrahlung (IB), an experimental study of the integral IB spectrum from ^{32}P was carried out. To eliminate the sources of possible systematic errors both in the measurement and in the evaluation, special care was devoted to the following items. 1) To check the effect of external bremsstrahlung (EB), the magnetic deflection and the "classical" absorption method for the elimination of direct electrons of the source were applied in the same experiment. 2) The detector efficiency (photopeak efficiency) for the correction of the spectrum was determined experimentally using the IAEA, Vienna, standards with known activities (errors from 1 to 3%). 3) The correction for the detector resolution was carried out by the method of OWEN and PRIMAKOFF instead of the mostly used LIDÉN—STARFELT procedure. 4) With the geometrical arrangement of the experiment a low Compton distribution (relative to the photopeak) in the spectra of the monoenergetic gamma rays was provided with practically no backscatter peak. 5) The theoretical spectrum was converted into pulse-height distribution. 6) The experimental and theoretical spectrum shape was compared by normalization of the distributions to avoid errors. arising from the absolute determination of beta activity of the source.

As a result of the investigation, the observed maximum deviation of the experimental distribution from the NILSSON-corrected KUB theory of IB was about 6% in the energy region from 60 to 1060 keV. Even if the possible maximum errors are taken into consideration, the deviation from the KUB-NILSSON theory cannot be more than 15% in the above region in contrast with e.g. recent contradictory results [21, 22] in one of which a deviation amounting to 30—40% from the KUB-NILSSON theory was observed in the region from about 100 keV to 800 keV, while an agreement was found for higher energies up to about 1200 keV, and in the other an increasing disagreement with the above mentioned theory was indicated from 500 keV towards the higher energies up to about 1300—1400 keV (the deviation is about 80% at 1000 keV). At the same time, the present measurements definitely disprove the considerable disagreements (the greatest disagreement ever observed from the theory in an IB study) which were found in the only earlier experiment of this kind [17] where the direct electrons from the source were prevented to reach the gamma-ray detector by applying a magnetic field.

1. Introduction

Although many experimental and theoretical works have been devoted to the clarification of the details of the internal bremsstrahlung (IB) process, there are various disagreements not only between theory and experiment but eve n among the individual experiments on the IB spectrum (see e.g. the recent surv ey of PERSSON [1]).

It was, therefore, decided to carry out a critical analysis of the relevant literature and the measuring conditions as well as the evaluation procedure of

the experimental data and on the basis of this to perform a new experiment for the study of the IB spectrum from ^{32}P. Namely, it is the IB from ^{32}P that has been mostly studied, compared with IB from other isotopes. The number of published articles on the IB from ^{32}P is more than ten.

In the early works carried out by scintillation techniques only the low energy region (to several hundred keV at most) of the IB spectrum was studied [2—5]. A good agreement with the theory of KNIPPP and UHLENBECK [6] and BLOCH [7] was found only by BOLGIANO et al.[4] in the region from about 30 to 120 keV. In the other three works the experimental values are generally higher than the theoretical ones up to about 50 per cent. RENARD [8] investigated the lowest energy section of the spectrum from 3 to 30 keV using a combination of magnetic field and proportional counter, and obtained a good agreement with the theoretical curve but this was lower than that used by others [16].

In the following years the study of the spectrum was extended up to 1 MeV and higher energies and it was investigated not only integrally but also differentially (IB quanta in coincidence with electrons emitted in a definite solid angle to the direction of the emission of the quanta or with electrons of definite energy). In these works partly agreements [9—13] with the Coulomb corrected KUB theory [14—15] were found in the whole region studied, but partly different deviations were observed [16—22]. E.g. LIDÉN and STARFELT [16], as well as LANGEVIN-JOLIOT [17] found a deviation in practically the whole spectrum. Their experimental values lie above the theoretical ones. With LIDÉN and STARFELT, however, the deviation increases with energy and is about 60% at 1 MeV, while according to LANGEVIN-JOLIOT the number of photons observed at about 150 keV is 150% in excess of the theory, and at 1 MeV the surplus is 85%. In the first work [18] of KOROTKOV and his collaborators the overall pattern of the deviations is similar to that in LIDÉN and STARFELT's measurement. Nevertheless, in one of their later papers [20] the discrepancy is observable only from 900 keV and up to this energy value there is a good agreement between experiment and theory. In their other later measurement [19] the discrepancy appears in the whole region of the spectrum studied from 300 to 1400 keV, increasing with energy.

In the last two published measurements [21, 22, 30] of the IB spectrum of ^{32}P discrepancy was also observed between the experimental and theoretical spectra but the character of the deviation is definitely different in the two cases. According to [21] the experimental points lie above the theoretical curve from 100 to 800 keV (the maximum deviation is about 40—50% at 650 keV) but from that energy value to 1200 keV there is an agreement between experiment and theory. On the contrary, in [22, 30] an increasing positive deviation of the experimental values from the theoretical ones was found, starting from about 600—700 keV. In this work, however, the deviation is

about 100% at 1200 keV and there is also a smaller increase in the experimental data from 200—250 keV toward the lowest energy (20—25%) within the limits of the errors, but systematically.

2. The analysis of the measuring conditions and the evaluation procedure

On the basis of the short survey given in the earlier Section, it seems that the discrepancies have their origin in the measuring conditions and the evaluation procedure because the deviations are so different and contradictory to one another in the various measurements.

In this way we are trying to carry out a critical analysis of the chief problems of the experimental techniques and procedures in the study of the IB spectrum to find the probable reasons for the different deviations and, on the basis of such an analysis, to construct a suitable arrangement and procedure for the measurement of the IB spectrum and to perform a new measurement of the IB spectrum of ^{32}P.

The experimental difficulties are undoubtedly great in the study of the IB beta-decay. The chief difficulties are as follows:

1) The probability of the IB process is relatively low and even the intensity distribution in the spectrum shows a very steep decrease toward the higher energies (the intensity changes about two orders of magnitude from 100 to 1000 keV).

2) A central problem in the various measurements is the elimination of the external bremsstrahlung originating from the electrons which are emitted from the source with an intensity several orders of magnitude higher than that of the studied IB.

3) The numerous corrections (for detection efficiency, for gamma-absorption, for pile-up, for energy resolution, etc.) and the whole unscrambling process of the continuous pulse-height distribution from the scintillation detector in the evaluation of the experimental data might be a real source of the different systematic errors.

A further experimental difficulty in absolute measurements is the precise measurement of the absolute activity of the source.

The three problems enumerated will be discussed separately in following sub-sections.

2.1. Low background and high statistical accuracy

Of the three problems considered as the chief difficulties, the first seems to be relatively the easiest to overcome. To reduce the background proper shielding has to be used, and to increase the statistical accuracy (especially

at the high energy end of the spectrum) a strong enough source and a long enough measuring time have to be employed.

In different works, various shieldings were made which surrounded the NaI(Tl) crystal with a lead layer of thicknesses from 2 [12] to 8 [16, 21] and 10 [18] cms. For coincidence measurements (where e.g. the coincidences between beta-particles and the relevant IB quanta are measured) generally no shielding against the background has been used.

Published data on the actual value of the background are very scarce (10% [16] or 30% [21] of the IB intensity at 1000 keV and 15% [18] of it at 1200 keV) but the high background can be compensated by a sufficiently long measuring time.

The strength of the sources varied from ≈ 100 μC [4] to 10 mC [9] and the measuring times from several hours to several weeks (chiefly in the coincidence measurements).

Contrary to the broad variety in background, source strength, and measuring time in the individual measurements, it does not seem likely that these conditions can contribute considerably to the discrepancy between theory and experiment and among different experiments. The statistical accuracy attained eventually is better than 3% even at 1000 keV and higher energies in practically every singles measurement (in the case of coincidence arrangements it is not worse than 10—15% in the considered region of energy) and at the same time the calibration changes (instability) of the measuring systems can be maintained within low and strong limits relatively easily (e.g. 0.5% in [13], 1.0% in [19] and [20], 1.5% in [21]). But the observed deviations could not be explained even by a much higher instability. It is also a reassuring fact that in several cases [12, 17, 18, 21] among them in measurements where high deviations from the theory were found [17, 18] measurements were carried out with sources of different strength (the difference is higher than an order of magnitude, e.g. in [17] and [18]) and the same result was obtained. Thus, the possibility of explaining some part of the deviations by a pile-up effect is excluded.

2.2. The elimination of the beta-electrons and the external bremsstrahlung

In the study of IB a difficult problem is the presence of beta-particles, having an intensity orders of magnitude higher then that of the IB. If we want to eliminate the electrons by absorption, the external bremsstrahlung (EB) will appear as a disturbance in the measurement of IB.

To eliminate the direct beta-particles and to get rid of the EB, three main types of methods have generally been used: reducing the solid angle of EB relative to IB (method of transformation of the solid angle), the coincidence method, and the magnetic deflection.

Magnetic deflection of the beta-electrons coming from the source was applied in the study of the IB spectrum only by RENARD [8] when investigating the lowest energy region of the IB spectrum (from 3 to 30 keV), and by LANGEVIN-JOLIOT [17] who obtained the greatest discrepancy from the theory of all in IB measurements ($\approx$ 150% at about 150 keV).

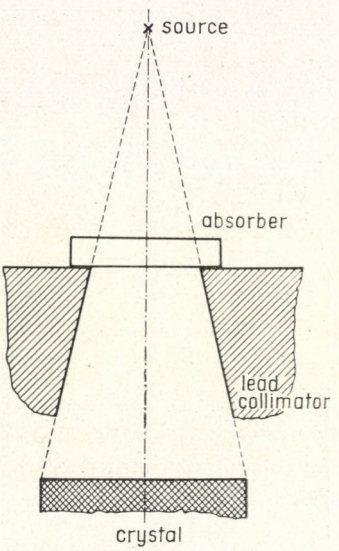


Fig. 1. The sketch of the arrangement in IB measurements where the electrons from the source are stopped by an absorber between the source and the detector crystal

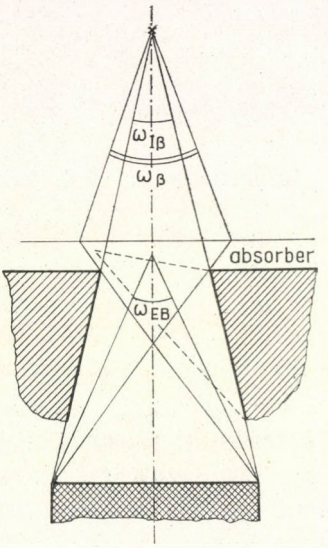


Fig. 2. The approximate plane equivalents of the solid angles in the geometrical arrangement of IB measurements in which the electrons from the source are stopped by an absorber. The dashed lines indicate the EB gamma rays which go directly to the wall of the collimator and indirectly can scatter into the crystal

In the coincidence arrangement a gamma and a beta detector work in coincidence with a proper lead shield between them. Electrons producing external bremsstrahlung in the absorber before the gamma crystal are not able to reach the beta spectrometer [10, 13]. (The triple coincidence arrangement in [20] belongs to this type in principle while the double gamma coincidence system of [19] results practically in a singles spectrum measurement but with an elimination of the Compton distribution in the scintillation spectrum.)

The most frequently used method for eliminating the electrons coming from the source is to place an absorber of low atomic number between the source and the detector using a proper lead collimator (see the sketch of the arrangement in Fig. 1). In this case, the distribution of the EB produced in the thick absorber is supposed to be nearly isotropic. Below we should like to

deal with this arrangement in more detail because most of the measurements were carried out with this method and a good statistics can be attained by this in a wide energy region over a reasonable measuring time.

In the arrangement under consideration the task is to choose the conditions in such a way that the ratio of the external bremsstrahlung to the internal one should be a minimum. If

$$N_{IB}(E_\gamma) = N_0 f_{IB}(E_\gamma)\,\omega_{IB}\,,$$
$$N_{EB}(E_\gamma) = N_0 f_{EB}(E_\gamma, Z_{abs})\,\omega_\beta\,\omega_{EB}\,,$$

then

$$\frac{N_{EB}(E_\gamma)}{N_{IB}(E_\gamma)} = \frac{f_{EB}(E_\gamma, Z_{abs})}{f_{IB}(E_\gamma)}\,\frac{\omega_\beta}{\omega_{IB}}\,\omega_{EB}\,,$$

where N_{IB} and N_{EB} are the counting rate from the IB and EB, respectively, N_0 is the number of the beta particles emitted per time unit, f_{IB} and f_{EB} are the probability of the emission of IB and EB per one beta particle (here, the complete stoppage of beta particle for f_{EB} is assumed) and ω are the corresponding solid angles (see Fig. 2).

As far as the geometrical arrangement is concerned the f_{EB}/f_{IB} ratio does not depend on the geometry in a first approximation (disregarding for the time being e.g. the effect of a possible small non-isotropic EB component from the absorber especially at higher energies). Now let us see how the N_{EB}/N_{IB} ratio will depend on the three ω. Their approximate plane equivalents are shown in Fig. 2. The ω_β/ω_{IB} is always higher than the unit (see the Figure) and it is the higher the nearer the absorbent is located to the source at a fixed source—detector distance. At the same time ω_{EB} decreases monotonically if the distance of the absorber from the crystal increases (i.e. if the absorber—source distance decreases at a fixed source detector distance). Thus, for the $(\omega_\beta/\omega_{IB})\ \omega_{EB}$ there will be a minimum in the function of the location of the absorber between the source and the detector. In Fig. 3 the change of the solid angles (and their combinations) can be seen for a 22.5 cm crystal—source distance and at a crystal size of 6.3 cm $\varnothing \times 5.1$ cm and an absorbent thickness of 1 cm.

It can be seen from these approximate geometrical considerations that the ω_β/ω_{IB} changes very slowly with the crystal—absorber distance (at a fixed crystal—source distance) except when the absorber is in the immediate neighbourhood of the source and the ω_{EB} changes steeply except when close to the source. Thus, for a given crystal size a sufficiently long crystal—source distance must be chosen, and for a fixed crystal—source distance the location of the absorber must be as far as possible from the crystal (16—17 cm crystal—absorbant distance in the case of Fig. 3) is more advantageous (to have a small enough product $(\omega_\beta/\omega_{IB})\ \omega_{EB}$).

Actually, the ω_β can be even higher than estimated above because of the penetration of the gamma rays through the edge of the lead collimator. In Fig. 4 it can be seen that EB reaches directly and indirectly to the crystal from a much bigger volume of the absorber than was considered above. For example, a 2 cm thickness of lead let through 1/4 of the original beam without any change at 1 MeV energy and a further part with an energy decrease. The ratio of the solid angle corresponding to ω'_β and ω_β is about five, e.g. with

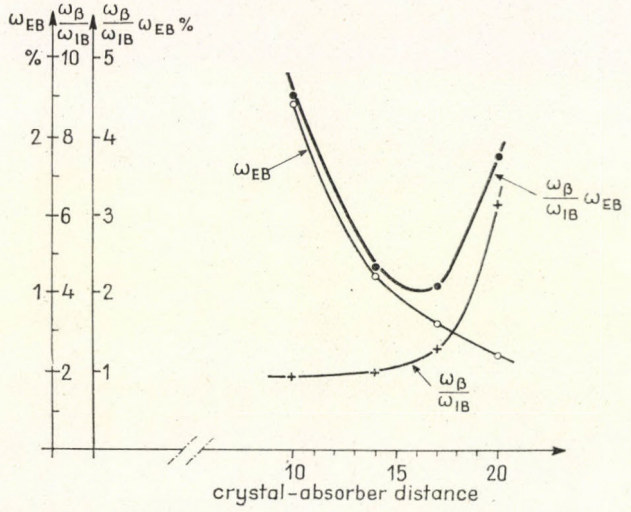


Fig. 3. The variation of the solid angles (and their combinations) as a function of the crystal—absorber distance (crystal—source distance 22,5 cm, crystal size 6,3 ∅ × 5,1 cm and absorber thickness 1 cm)

the actual geometry of Fig. 3. At the same time the scattering of EB from the walls of the collimator can be rather high especially with a "bad geometry" where the absorber and the crystal are relatively near (ω_{EB} not being large enough).

This penetration effect through the collimator modifies the optimum place of the absorber but the displacement is not considerable because of the significance of ω_{EB}.

Let us mention here the effect of the f_{EB}/f_{IB} factor (see the formula above), which is a function of the energy and in some energy regions it is greater than unity (see below Fig. 15).

It has to be noted here that some probable anisotropy in the EB even in the case of a thick target [16] also contributes to the EB part of the measured spectrum which is even greater if the distance between the absorber and the crystal is shorter.

As a conclusion, the total contribution from the EB can vary from several per cent to several times ten per cent depending on the actual geometry (c.f. the corresponding experimental indication in Section 4).

This increase of the IB spectrum from EB contributions will not completely vanish (especially with a bad geometry) after the extrapolation of the observed distribution to $Z = 0$ to eliminate the EB contribution, this is

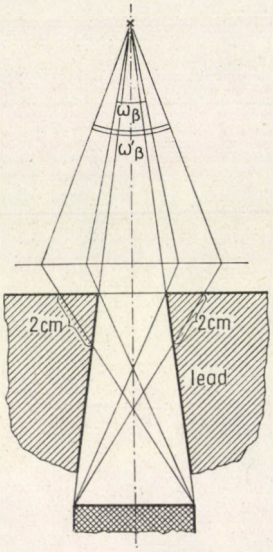


Fig. 4. The effect of the penetration of gamma rays through the lead collimator on the magnitude of ω_β

understandable from the above considerations and has been confirmed experimentally (see below in Section 4) but even such a correction has not been made in every case.

On the basis of all this it is also clear why the use of a cylindrical collimator is so disadvantageous [16]. Here not only is the scattering higher but there is a large difference between ω_{IB} (determined here by the lower end of the collimator) and ω_β. Thus, rather intense EB will appear in practically the whole energy region.

2.3. Correction of the measured pulse height distribution

Reviewing all the corrections made by different authors for the experimental data obtained in the study of IB, i.e. the correction for Compton distribution, iodine K X-ray escape, backscatter distribution, photopeak efficiency, instrumental energy resolution, pile-up, thickness of the source,

gamma absorption (in addition to these in coincidence measurements the chance coincidences, beta absorption, efficiency of the coincidence circuit, etc.), the correction of the photopeak efficiency seems to be one of the largest and most problematic. That is why we wish to deal with this correction first.

In nearly all cases this correction has been calculated using either a tabulation of X-ray attenuation coefficients (e.g. [23]) for calculations of total detection efficiency (ε_t) or a tabulation with calculated total detection efficiency (e.g. [24]). The difficulties of such calculations are evident. Not only is taking into consideration the actual conditions (source size, collimation, scattering, etc.) problematic but so also is the consideration of double, triple, etc. Compton processes. Such problems are the most definite at higher energies.

Having the ε_t values from calculations the ε_p are obtained by the formula

$$\varepsilon_p(E_\gamma) = R(E_\gamma)\,\varepsilon_i(E_\gamma)\,,$$

where the $R(E_\gamma)$, the peak-to-total ratio, is generally determined by experiment. In the experimental value of R the actual arrangements are reflected, i.e. because of scatterings, etc. the Compton distribution will be higher and so R is smaller than the "ideal" value. In this way the R values might decrease the ε_p values obtained further which might possibly already be lower because of the smaller than real values of ε_t. If the geometry is bad from the viewpoint of the scattering (a relatively high Compton-distribution) the error because of R will be higher in ε_p.

An additional energy dependent error might originate from the calculation of the solid angle factor. The error of whole efficiency correction was recently estimated to be of the order of 10% [21] and it seems evident, on the basis of the above mentioned facts, that the question is most problematic at higher energies.

In connection with the corrections is should be still noticed here that if the geometrical arrangement of the measurement is bad from the view-point of scattering (i.e. if the Compton distribution is high relative to the photo-peak), the error in the correction for the Compton distribution may be more significant.

The problems in connection with the correction for the finite energy resolution of the detector should also be mentioned. The situation is very contradictory in this respect. In any case this correction must be more considerable at higher energies (not regarding now the lowest energy region below 40—50 keV) because of the increasing experimental half-width of the monoenergetic lines and of the quicker change in the shape of the spectrum from about 1000—1100 keV towards the higher energies. This fact shows the significance of this correction particularly from the view-point of the deviations from the theory observed in the higher energy region of the spectrum by some of the authors. At the same time in most of the papers e. g. [16, 18—21] on IB

from ^{32}P (where this correction has been made at all) the LIDÉN and STARFELT procedure [16, 25] was used for the resolution correction which appears to be incorrect [26] (it is less than the OWEN—PRIMAKOFF method [27] by a factor of two which is one of the possible partial solutions of the integral equation of the problem). If an insufficiently large correction is made for this effect, it can result in an excess in the experimental values above the theory increasing with the energy. The OWEN—PRIMAKOFF correction, e.g. amounts to 16—17% (cf. Fig. 14) at about 1450 keV in an actual case (according to LIDÉN—STARFELT only $\approx$ 8%). The PALMER—LASLETT procedure [28] which is based on another correct partial solution of the integral equation generally gives a smaller correction value than that of OWEN and PRIMAKOFF, for higher energies (from about 1100—1200 keV). However, both methods give practically the same result.

The fact that HAKEEM and GOODRICH [12] found this correction negligible experimentally having measured the spectrum both with 8.5 and a 13% resolution, makes the question even more problematic. It seems to us that a more detailed experimental and mathematical investigation particularly of these problems is very necessary. In our measurements the OWEN—PRIMAKOFF correction was used for the correction of the finite energy resolution (see the details in 3.3).

The contribution to the error from the measurement of the absolute activity of the source is also considerable. According to a recent estimates [22] it amounts to 20—25%. Such an error, however, does not cause any change in the spectrum shape.

2.4. Conclusions on the measuring conditions

On the basis of the above considerations it seems probable that the most important distortions in the IB spectrum shape come from the EB and the photo-efficiency correction of the crystal and may be from the effect of the finite energy resolution of the detector at the lowest (below $\approx$ 50 keV) and at the higher energies (mainly from about 1100 keV towards the higher energies). A bad geometrical arrangement (resulting in EB contribution to the spectrum) of the IB measurement (section 2.2) might cause an increase in a wide energy region starting from the lowest energies depending on the actual geometry while the errors in photo efficiency might enhance the spectrum mainly in the higher energy region.

3. Experimental study of the IB from ^{32}P

3.1. The experimental arrangement and the plan for the evaluation of the measurements

To avoid the possible and probable sources of errors already discussed in the study of the IB spectrum the investigation was carried out in the following way.

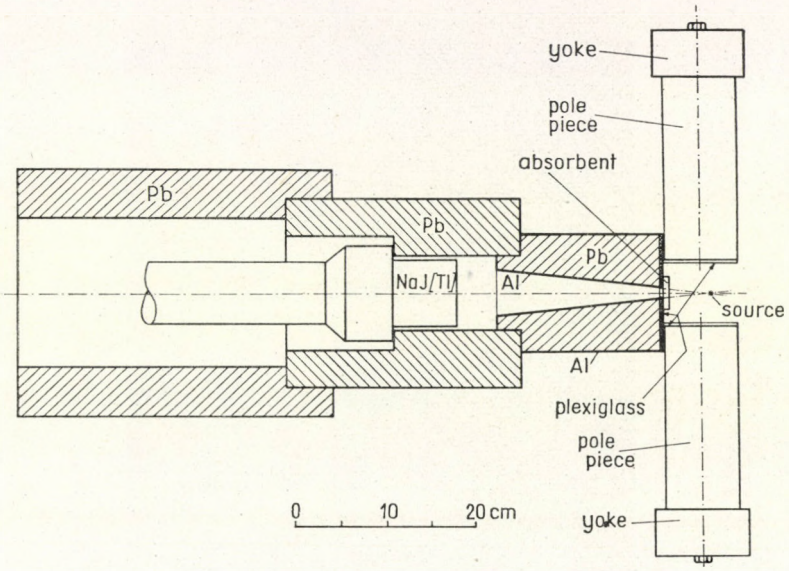


Fig. 5. Cross-section of the experimental arrangement for the investigation of IB in the present study

According to the considerations in 2.2. a rather good geometrical arrangement was chosen and, at the same time, the elimination of the electrons from the source by a magnetic field was made possible. In this way in the same experiment a comparison was possible between the frequently used solid angle transformation arrangement and the use of the magnetic field to eliminate the direct electrons, i.e. the EB from the IB spectrum. The measurement in such an arrangement will also be a control for the only measurement where the magnetic elimination has been used and where a maximum discrepancy from the theory has been found [17]. The cross-section of our equipment and the general view of it can be seen in Figs. 5 and 6.

The photopeak efficiency for the correction procedure, which is the other highly problematic point in IB spectrum studies, was determined experimentally by using a gamma standard series of IAEA, Vienna. In this, the error in the absolute activity of the sources is partly 1%, partly 2% and 3%. Thus, the efficiency curve was determined to an accuracy of about 9 per cent below 600 keV and of 3% above that energy value.

The pulse height spectrum of the gamma-rays from the ^{137}Cs standard source as taken by our arrangement is given in Fig. 7 and the photopeak efficiency curves in Fig. 8. Two efficiency curves have been determined; one with a 7 mm plexiglass absorber before the collimator gap and the other without this absorber. In the measurement some secondary standards were used besides the IAEA standards (see Fig. 8).

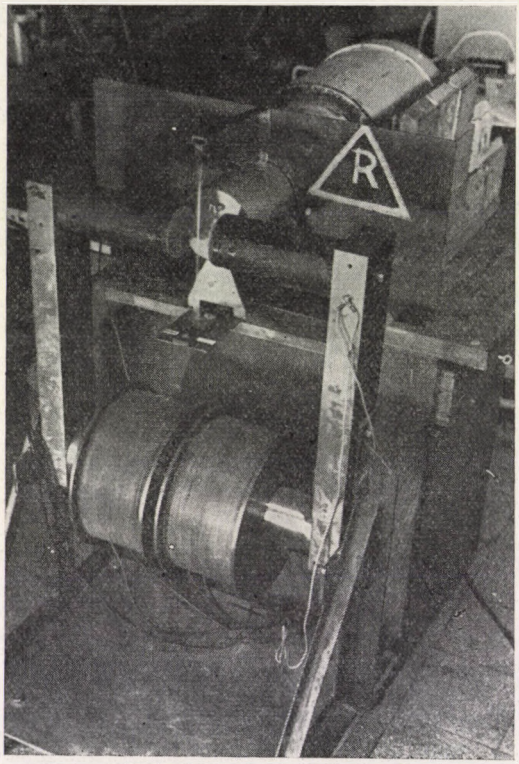


Fig. 6. General view of the equipment

Otherwise, the evaluation process made with an ODRA 1013 computer was the following. From the experimental pulse-height spectrum only the background was subtracted, all other corrections were applied for the theoretical spectrum (according to the KUB theory [6, 7]) corrected for the Coulomb field of the nucleus [14] i.e. the theoretical photon distribution was converted into pulse-height distribution. This seems to be advantageous for several reasons. For example, the use of the theoretical spectrum is advantageous from the view-point of resolution correction and the Compton correction because if we have the theoretical spectrum throughout the whole energy range an extrapolation of the experimental distribution is not necessary for the Compton correction.

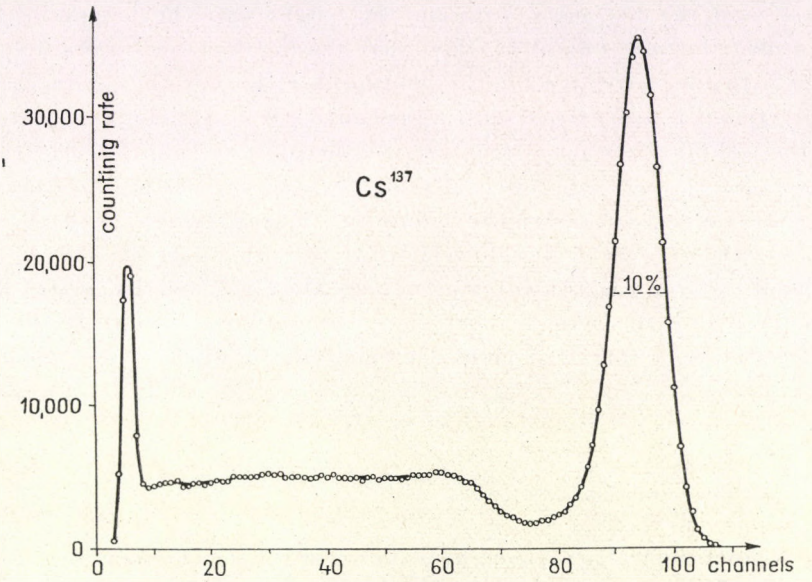


Fig. 7. Pulse-height spectrum of the gamma rays (662 keV) from the ^{137}Cs IAEA standard source

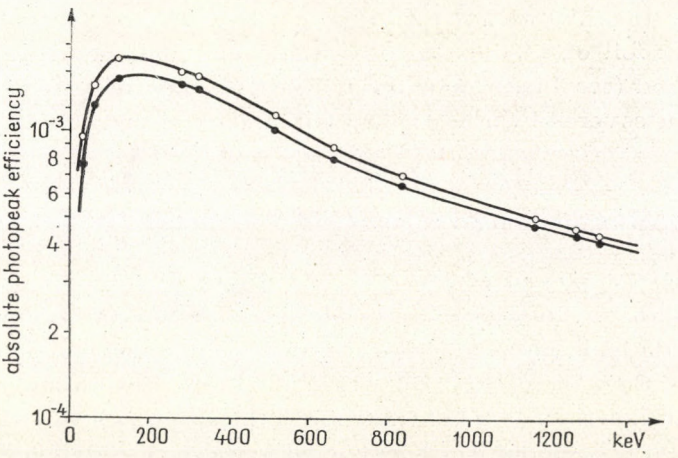


Fig. 8. Photopeak efficiency curves with a 7 mm plexiglass absorber before the gap of the collimator (●) and without such an absorber (○)

In the actual procedure the theoretical values corresponding to every channel were first multiplied by the photopeak efficiency, then the correction for the Compton distribution was made, and finally the resolution correction was made according to OWEN and PRIMAKOFF [27]. The Compton correction was made by summing the contributions from the higher channels using the

computer, and the necessary data for the height and the beginning of the Compton distribution (Compton edge) were taken from the standard spectra. Together with the correction for the photopeak efficiency the gamma absorption correction was also carried out (in the can of the crystal and in the absorber before the collimator, when it was present) because the photopeak efficiency curve was determined experimentally in the presence of the absorbers. The pile-up, the source thickness, the iodine X—K ray escape* and the backscatter corrections were negligible relative to the other corrections.

Finally, our measurement was not an absolute one. By matching the experimental and theoretical spectra we eliminated the considerable error from the absolute source strength measurement in the study of the IB spectrum shape.

3.2. Further experimental details

Our experimental arrangement is shown in Fig. 5. The size of the NaI(Tl) crystal was $65 \varnothing \times 65$ mm mounted on a DuMont 6363 multiplier. The pulse-height distribution was analysed by a 200 channel TMC pulse-height analyser.

The strength of the source was about 0.5 mC during the measurements, and its thickness was about 1 mg/cm^2. The carrier-free ^{32}P preparation was supplied by the ISOCOMMERZ GmbH, GDR. The backing of the source was a cellux foil of several mg/cm^2 without any solid source holder in the neighbourhood (see Fig. 6) and the radioactive material with a diameter of $\approx$ 3 mm was covered by a hostaphan foil of about 1 mg/cm^2.

3.3. Measurements and results

During the measurements the pulse-height distribution from ^{32}P was measured with an absorber (7 mm plexiglass) before the collimator in the absence of the pole pieces ("classical arrangement") and in the presence of these (but without magnetic field). Then the same distribution was detected at a proper magnetic field (1150 Gauss) with the absorber before the collimator and without it in each run. The background was also measured and the calibration checked several times in the individual runs and the changes were less than 0.5—1.0 per cent in every case. The runs were doubled. After finishing the measurements listed above they were repeated in the reverse order to compensate for the decay of the source. The statistical error was less than 2.5% even at 1000 keV.

* This correction was also included in part in our correction for the photopeak efficiency.

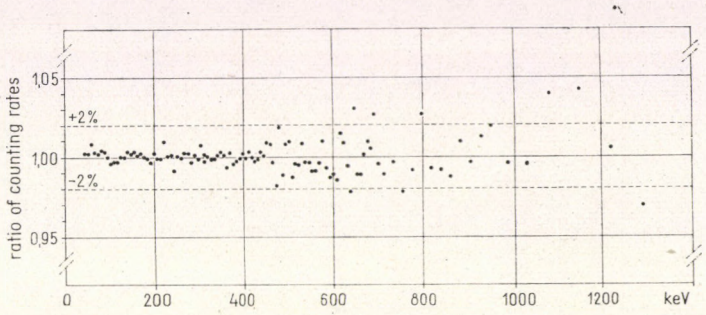


Fig. 9. The ratio of the counting rates measured in the "classical arrangement" (absorber before the collimator gap) in the presence of the pole pieces and in their absence, respectively

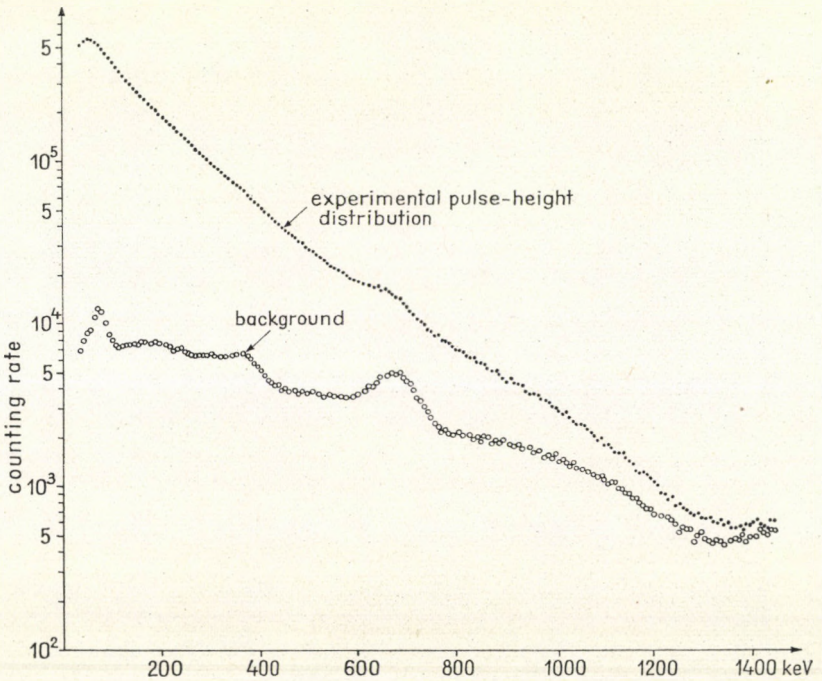


Fig. 10. The experimental pulse-height distributions without any corrections, and the background

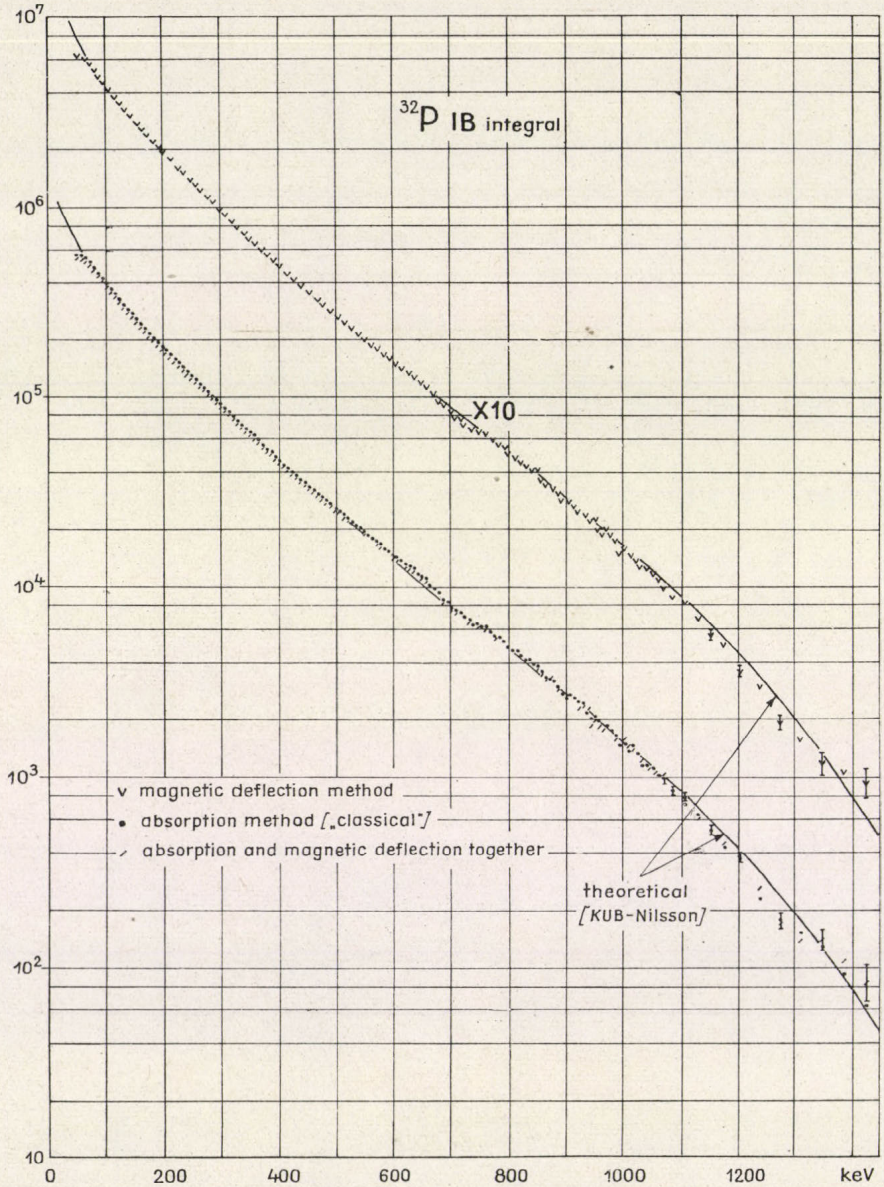


Fig. 11. Pulse height distributions corresponding to the different experimental conditions and the NILSSON [14] corrected KUB [6,7] theoretical IB spectra converted into pulse height distribution with all the necessary experimental corrections. The error from the counting statistics is smaller than the signs except in the region where indicated by vertical bars

The distance of the pole pieces and their actual geometry were chosen on the basis of calculations, designs and preliminary measurements.

In Fig. 9 the pulse-height distributions are compared in the "classical arrangement" (absorber before the collimator gap) both with and without pole pieces (but without a magnetic field). As can be seen the presence of the pole pieces does not cause any systematic distortion in the pulse distribution.

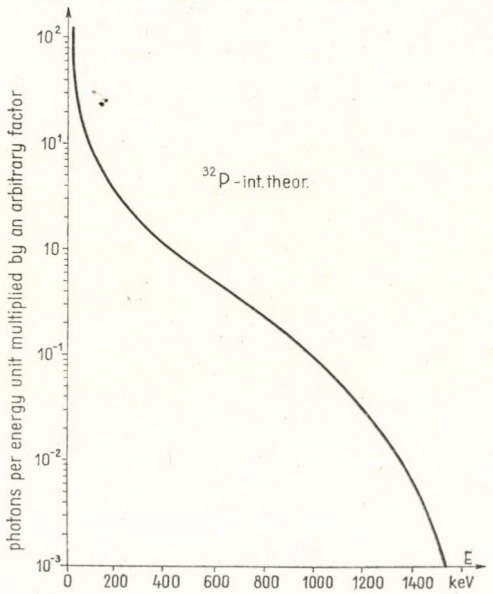


Fig. 12. The theoretical IB spectrum from ^{32}P according to the KUB theory [6,7] and corrected for the Coulomb effect of the nucleus by NILSSON's method [14]

Our experimental pulse-height distributions (background subtracted) and the NILSSON [14] corrected KUB [6, 7] theoretical IB spectra are given in Fig. 11 (Fig. 10 shows the experimental pulse-height distributions without any correction and the background). As has been mentioned (Section 3.1) all the necessary corrections have been applied for the theoretical spectrum converted into pulse-height distribution. The "clear" theoretical IB spectrum is shown in Fig. 12. In this way there are two theoretical curves in Fig. 11 because of the two experimental photopeak efficiency curves (taken with and without the absorber before the collimator gap). At the same time there are three different experimental distributions according to the measurements under different experimental conditions. i.e. 1) only with an absorber for preventing the electrons from reacting the detector crystal from the source, 2) only with a magnetic field for that purpose and 3) the absorber and the magnetic field applied together. For 1) and 3) the theoretical curve is the same.

The experimental and theoretical curves were normalized in the following way. The corresponding theoretical distribution (theory corrected by the photopeak efficiency curve taken with an absorber) was matched to the

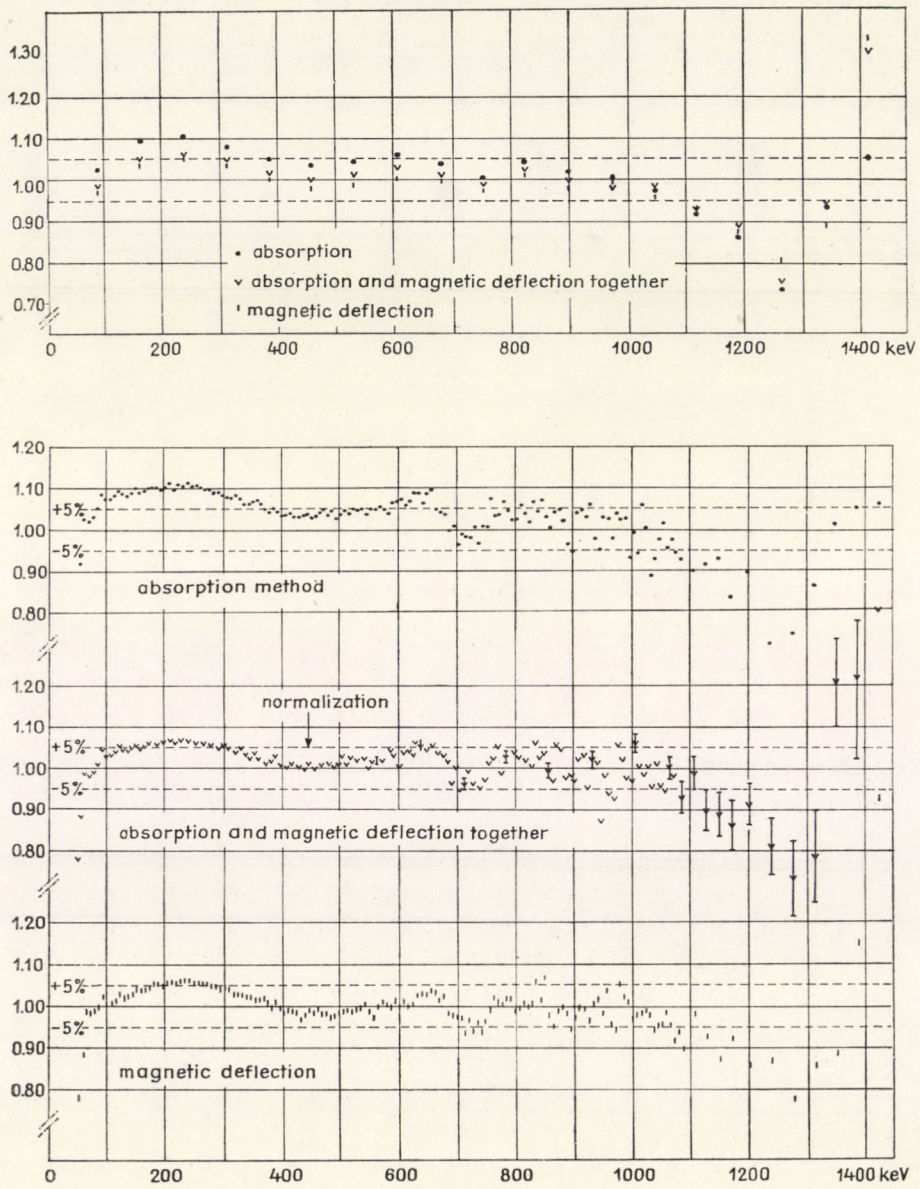


Fig. 13. The ratio of the experimental and the converted theoretical IB spectrum for different experimental conditions as a function of the energy. The upper plot was made by summing the counting rate in every ten channels. In the middle of the lower triple plot the statistical error for orientation is indicated in several cases

experimental pulse-height distribution, obtained by applying the absorber and the magnetic field together, in the region of 430 keV. For the other two experimental distributions the same normalization factor was used which was obtained as previously outlined. The reason for this method of normalization being chosen is that, in principle, the probability of having EB in the IB spectrum is the lowest when both methods of elimination of the electrons from the source i.e. both methods for the elimination of EB have been applied together. As to the normalization for the 430 keV region, it seems to be suit-

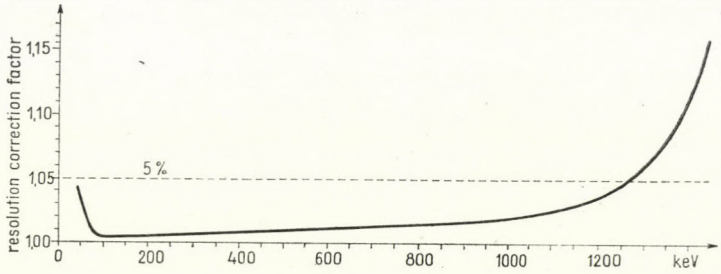


Fig. 14. The values of correction for finite energy resolution of the detector by the method of OWEN and PRIMAKOFF [27]. If it is not the theoretical curve that is corrected (as in this case) but the experimental data, the correction factor will be less than a unit and it will decrease the experimental spectrum by the same percentage as the increase is here

able for normalization because our aim has been to study the shape of the IB spectrum and using the chosen factor a good agreement between experiment and theory was obtained in the widest region. The statistics about 430 keV is good enough ($\approx 0.5\%$ error). It should also be noted here that the place of the normalization (in energy) means only about a 5% deviation from the agreement with the theory in the energy region from 60 to 1060 keV (see Fig. 13).

For a more detailed comparison between experiment and theory the ratio of the experimental and the theoretical distributions is plotted in Fig. 13 for the different experimental conditions.

At the beginning of this Section the extent of the statistical error was mentioned. Let us now see how big the errors of the corrections are, which have been made for the theoretical IB spectrum. The largest correction factor comes from the photopeak efficiency and its error is not higher than 6% in the low energy region (to about 600 keV) and less than 3% from 600 keV towards the higher energies.

The extent of the Compton correction also changes as a function of the energy. For energies higher than 1000 keV it is less than 10% of the value to be corrected. It has a maximum relative value at about 550 keV (16%) and from here it decreases to $\approx 6\%$ at 60 keV.

As was mentioned in 3.1 the correction in our measurements for the finite energy resolution has been made by the method of OWEN and PRIMAKOFF [27]. Although this method gives a somewhat higher correction value in a wide region (from the lowest energies to about 1200 keV) than the PALMER—LASLETT [28] procedure even this higher value is very small (not more than about 1 or 2%) from 60 to 1000—1100 keV. From 1100—1200 keV toward the higher energies where the correction will be more considerable (see Fig. 14) the two methods ([27] and [28]) give the same result in a good approximation.

4. Supplementary measurements

To investigate why we obtained a surplus in the lower energy part of the spectrum using the absorption method (cf. Fig. 13) and to check more directly our considerations in Section 2 (especially in 2.2) some supplementary investigations have been carried out.

4.1. The determination of the f_{EB}/f_{IB} ratio and the effective Z of the plexiglass

As we have seen in Section 2.2. the determination of f_{EB}/f_{IB} might be important for the estimation of the contribution of EB to the measured IB spectrum.

The ratio concerned was determined with a $65\varnothing \times 65$ mm size NaI(Tl) crystal and a lead collimator as well as a proper lead shield. In these measurements the pulse height distributions were taken by completely surrounding the ^{32}P source by materials of different atomic number, i.e. Be, plexiglass, C, Al, Cu, Sn, Pb. Then the counting rates have been plotted as a function of the atomic number of the absorbers using the gamma energy (determined channel numbers or pulse heights) as a parameter (cf. Fig. 15). By an extrapolation of these curves to $Z = 0$, the IB contribution is determined at the selected energy and thus the f_{EB}/f_{IB} can be determined for the absorbers of different atomic numbers and given energies.

By means of the above curves the effective atomic number of the plexiglass or another absorber of mixed material can be determined. For plexiglass a value of 5.2 was obtained. This figure is important at the extrapolation to $Z = 0$ absorber of the IB spectrum for the elimination of EB from it.

Fig. 16 shows the change of the f_{EB}/f_{IB} ratio as a function of energy for the plexiglass absorber. Otherwise, the ratio is characteristic for the relative shape of the EB and IB spectra. If the EB and IB spectra have the same shape, the ratio would be constant as a function of energy.

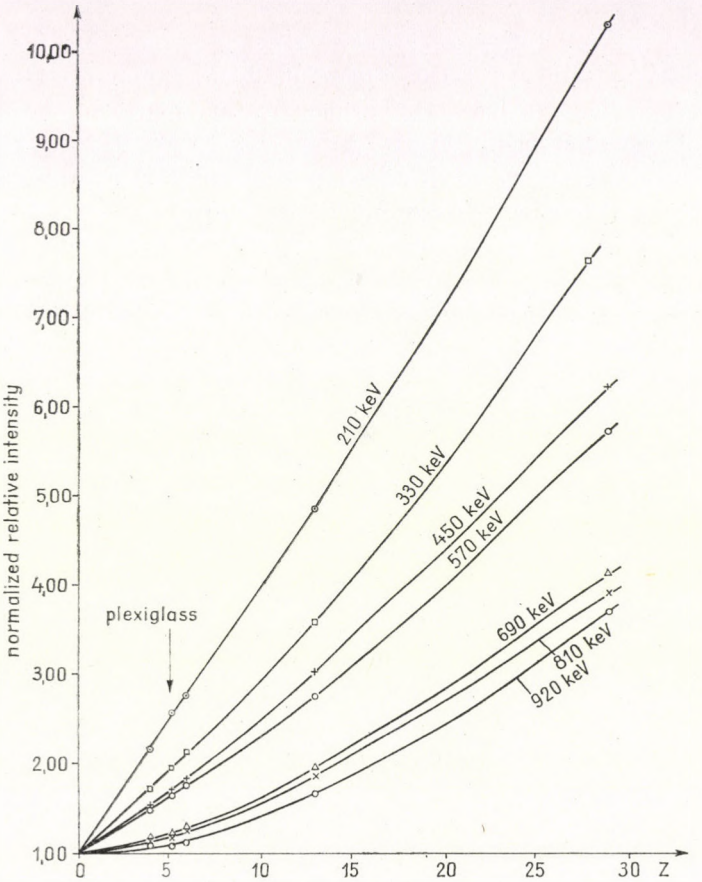


Fig. 15. The bremsstrahlung from ^{32}P source (internal and external together) as a function of the atomic number of the absorbers and in a normalized plotting. During the measurement the source was completely surrounded here with various absorbers. The energy of the gamma-rays was used as a parameter

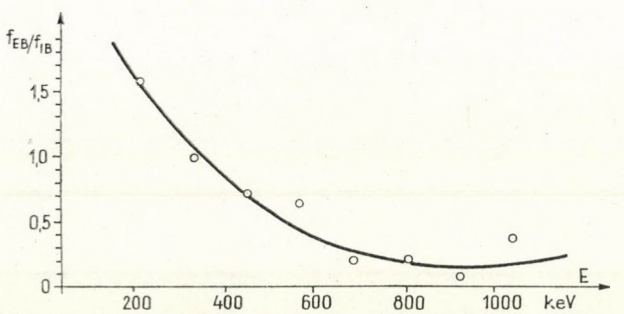


Fig. 16. The f_{EB}/f_{IB} ratio for a plexiglass absorber as a function of the energy (f_{EB} and f_{IB} are the probabilities of the emission of EB and IB per beta particle, respectively, provided that the beta particles in the production of EB are completely stopped)

4.2. The effect of "bad" geometry

A pilot experiment for the effects of "bad" geometry (cf. Section 2.2) has also been carried out. The actual geometrical arrangements in these measurements have been sketched in Fig. 17.

Several complete runs with background, calibration control, etc. were made in the two geometrical arrangements indicated in Fig. 17. After the correction (by using the experimental photopeak efficiences) of the pulse-height distribution obtained in the greater distance of the crystal from the source for its smaller detection efficiency (because of the larger distance), the ratio of the pulse-height spectra in the two arrangements have been formed. As can be seen in Fig. 18 a definite surplus appears in the case of "bad" geometry (detector and source near each other).

Considering that no correction has been made here for the effect of the Compton distribution, the points in Fig. 18 can be a little lower (less than 5% at every point) but this does not affect the general conclusions. It should be noted here that our "bad" geometry was not the worst that has actually been used according to the published literature.

Fig. 19 shows the ratio of the relative deviation of the IB spectra taken by the "classical" absorption method and with magnetic deflection and absorbent together in use (in Fig. 13). The deviation as a percentage is very small because the geometry was fairly good in our IB spectrum study but, as has been shown, such a type of surplus can be explained by the presence of some EB.

4.3. Extrapolation to the absorber with $Z = 0$

An extrapolation to $Z = 0$ has been performed in the case of our pilot experiment for both distributions ("bad" and "good" geometry). In the runs of the pilot experiment, the pulse-heigt distributions were taken using different absorbers (plexiglass, Al, Cu). Plotting the counting rates as a function of the atomic number for different energies, the extrapolation to $Z = 0$ has to be carried out.

The extrapolated values for "bad" geometry are considerably higher than those for "good" geometry. This fact and the actual forms of the extrapolation curves are related to the effects considered in Section 2.2 (cf. Figs. 2—4) and they are explicable by them.

In Fig. 18 the corresponding ratio is also indicated for the extrapolated pulse-height distributions (i.e. for the distributions corrected for EB by the method of extrapolation to $Z = 0$). The spectrum obtained in a "bad" arrangement is 10—15 per cent higher in a rather wide range than that in the better arrangement. Therefore, an extrapolation to $Z = 0$ will not result in the correct IB spectrum if the measurement is carried out in a "bad" geometry.

It should be noticed here that similar deviations shown in Fig. 18 (sometimes probably together with other types of deviations) have been observed

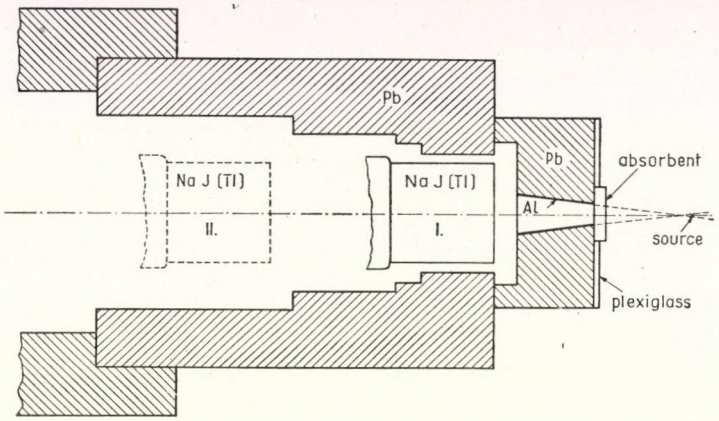


Fig. 17. The sketch of the geometrical arrangements in pilot experiments to study the effect of "bad" geometry

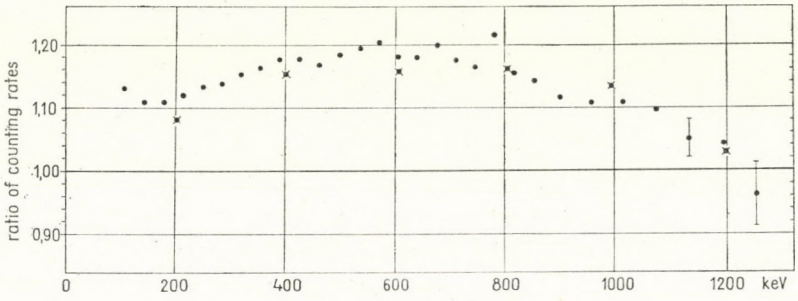


Fig. 18. The ratio of pulse-height distributions taken in "bad" and "good" geometries, respectively. The crosses indicate the ratio of the values when both have been corrected for EB by the method of extrapolation to $Z = 0$

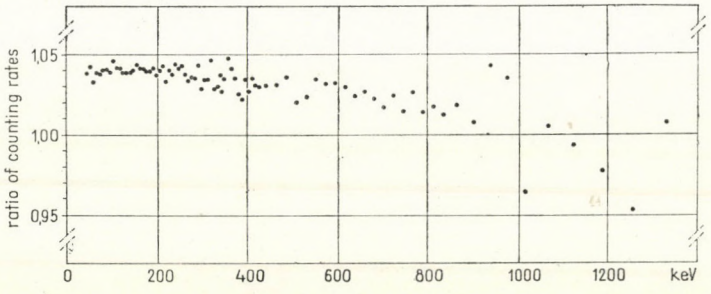


Fig. 19. The ratio of counting rates taken by the "classical" absorption method and using magnetic deflection (the relative deviations are shown in Fig. 13)

in several older and recent works [3, 5, 16—19, 21]. In [22] such a hump is also guessable but because of the high error (25%) of the experimental data the phenomenon is not explicitly expressed.

5. Conclusions

It can be seen in Fig. 13 that the agreement between the experimental and theoretical IB spectrum shape is better than 6% in the range from 60 to 1060 keV in the case of ^{32}P decay. Taking the possible maximum systematic errors in the same direction for the different corrections, our measurements might allow a deviation not higher than 15 per cent from the NILSSON corrected KUB theory in the above energy range. The reproducibility of our photopeak efficiency curve e.g., has been shown by the good agreement between the relative difference curves for the magnetic deflection method and for the magnetic deflection and absorption method applied together (the deviation is only 1 or 2%) because in both methods separate measurements were performed to determine the photopeak efficiency.

The present results on IB from ^{32}P were obtained in a study in which the measuring conditions and the evaluation process had been thoroughly analysed to avoid the possible systematic errors.

1) To eliminate the disturbing effect of the EB the "classical" absorption method using a "good" geometry and the magnetic deflection were used in the same measurements.

2) The detector efficiency correction was made by the experimental determination of the photopeak efficiency using the standards of IAEA, Vienna, the absolute activities of which are given with an accuracy from 1 to 3 per cent. The gamma absorption and partly the iodine K—X-ray corrections were also included in the correction according to the photopeak efficiency so avoiding an additional error due to such separate corrections.

3) The correction for the detector resolution has been critically analysed and the OWEN—PRIMAKOFF procedure has been used.

4) The theoretical photon spectrum was corrected, and not vice-versa. To do so is advantageous from the view-point of the evaluation process because the handling of the continuous theoretical curve is easier than that of the experimental values with statistical errors which can be relatively high, mainly in the high energy section of the spectrum. In addition, by the conversion of the theoretical spectrum, an extrapolation of the pulse-height distribution to the end-point was not necessary for the Compton correction.

Correcting the theoretical spectrum is also very important for the correction for finite energy resolution of the detector.

5) The form of the standard spectra was good, i.e. the photopeak Compton ratio is high, and there was no backscatter peak in the spectra (cf.

Fig. 7). It is important to avoid possible errors from the Compton correction and to avoid the necessity for additional correction for the backscatter peak.

6) The comparison of the theoretical and experimental distributions was normalized so as to eliminate the error from the absolute beta activity determination.

The present study definitely disproves the large discrepancy between experiment and theory obtained in [17] using a magnetic field to deflect the direct electrons from the source. It should be emphasized, however, that agreement with the NILSSON-corrected KUB theory was found previously, too, when the measuring conditions were chosen carefully and some possible mistakes were avoided in the evaluation. For example in 1962, HAKEEM and GOODRICH [12] measured the ^{32}P IB spectrum in a "good" geometry. In addition to that, they also used empirical data for the correction for the detector efficiency. They found a good agreement between the theory concerned and the experimental spectrum shape in the energy range from about 60 to 1100 keV. PERSSON [13] also found an agreement in about the same region in his differential measurements even at 90° between the direction of the beta particle and the IB quantum using a coincidence arrangement, though the statistics here were much worse than in the integral measurement, but if there is any disagreement between the theory and experiment it is most definite at 90°.

Finally, the situation for the energies higher than 1100 keV should be dealt with. According to our measurements (cf. Fig. 13) the agreement with the theory under consideration in this section of the spectrum (to about 1400 keV) exists only within a 20—25 per cent limit and the deviation of the experiment from the theory is negative. A probable reason for this phenomenon is the very high background in our measurement here and the neighbourhood of the ^{40}K gamma line in it. The statistical error, however, is rather high here and undoubtedly a more detailed study is necessary in this region with an even higher efficiency and/or a better resolution at an even lower background. Nevertheless, it is remarkable that HAKEEM and GOODRICH in their above-mentioned study found a deviation similar in magnitude and direction like that in the present investigations. So also did NARASIMHAMURTY and JANANANDA [21] in an absolute measurement who otherwise obtained a positive deviation at smaller energies.

On the basis of the present study it seems to be very probable that the disagreements in the earlier measurements have an instrumental origin. To prove the validity of the NILSSON-corrected KUB theory of IB more precisely, further investigations are very much needed, expecially in the high energy region above 1000 keV using the new information and experiences of this study.

A preliminary report on our results was given at the Debrecen Conference in July, 1968 [29] and the essence of the work without the details was published in Nuclear Physics [31].

Acknowledgments

The authors are indebted to Professor A. SZALAY for the excellent working condition in this Institute, and to Dr. E. VATAI for help in the calculations, as well as to Dr. Cs. UJHELYI for the preparation of the sources.

REFERENCES

1. B. PERSSON, Proc. Conf. on the Electron Capture and Higher Order Processes in Nuclear Decays, Debrecen, July 15—18, 1968. Eötvös Loránd Physical Society, Budapest, 1968. p. 142.
2. L. MADANSKY and F. RASETTI, Phys. Rev., **83,** 187, 1951.
3. T. B. NOVEY, Phys. Rev., **89,** 672, 1953.
4. P. BOLGIANO, L. MADANSKY and F. RASETTI, Phys. Rev., **89,** 679, 1953.
5. A. MICHALOWICH, Journ. Phys. Radium, **15,** 156, 1954.
6. J. K. KNIPP and G. E. UHLENBECK, Physca, **3,** 425
7. F. BLOCH, Phys. Rev., **50,** 272, 1936.
8. G.-A. RENARD, Journ. Phys. Radium, **14,** 261, 1953.
9. M. GOODRICH and W. B. PAYNE, Phys. Rev., **94,** 405, 1954.
10. B. PERSSON and S. A. E. JOHANSSON, Nucl. Phys., **12,** 432, 1959.
11. J. E. THUN, W. D. HAMILTON, K. SIEGBAHN and K. E. ERIKSSON, Ark. f. Fys., **22,** 565, 1962.
12. M. A. HAKEEM and M. GOODRICH, Nucl. Phys., **31,** 322, 1962.
13. B. PERSSON, Nucl. Phys., **55,** 49, 1964.
14. S. B. NILSSON, Ark. f. Fys., **10,** 467, 1956.
15. R. R. LEWIS Jr. and G. W. FORD, Phys. Rev., **107,** 756, 1957.
16. K. LIDÉN and N. STARFELT, Phys. Rev., **97,** 419, 1955.
17. H. LANGEVIN-JOLIOT, Ann. de physique, **2,** 16, 1957.
18. K. A. KOROTKOV and A. M. CHERNIKOV, Izv. AN SSSR, Ser. fiz., **24,** 899, 1960.
19. K. A. KOROTKOV and A. P. SHUMEYKO, Izv. AN SSSR, Ser. fiz., **29,** 2243, 1965.
20. K. A. KOROTKOV and V. I. KRYSHKIN, Izv. AN SSSR, Ser. fiz., **29,** 2247, 1965.
21. K. NARASIMHA MURTY and S. JANANANDA, Nuovo Cim., **46,** 217, 1966.
22. W. KREISCHE, W. LAMPERT und G. LOOS, Nucl. Phys., **A107,** 601, 1968.
23. G. R. WHITE, Nat. Bur. Stand. Report, No. 1003, 1952.
24. E. A. WOLICKI, R. JASTROW and F. BROOKS, Naval Res. Lab. Report, NRL-4833, 1956.
25. K. LIDÉN and N. STARFELT, Ark. för Fys., **7,** 427, 1954.
26. W. R. DIXON and J. H. ATTKEN, Can. J. Phys., **36,** 1624, 1958.
27. G. E. OWEN and H. PRIMAKOFF, Phys. Rev., **74,** 1406, 1948.
28. J. P. PALMER and L. J. LASLETT, AEC Report, ISC-174, Ames Laboratory, 1950. p. 35.
29. D. BERÉNYI and D. VARGA, Proc. Conf. on the Electron Capture and Higher Order Processes in Nuclear Decays, Debrecen, July 15—18, 1968. Eötvös Loránd Phys. Soc. Budapest, 1968. p. 176.
30. G. LOOS, W. KREISCHE, W. LAMPERT and H.—J. TREBST, Proc. Conf. on the Electron Capture and Higher Order Processes in Nuclear Decays, Debrecen, July 15—18, 1968. Eötvös Loránd Phys. Soc. Budapest, 1968. p. 182.
31. D. BERÉNYI and D. VARGA, Nuclear Physics, **A138,** 685, 1969.

ПОДРОБНОСТИ КРИТИЧЕСКОГО ИЗУЧЕНИЯ СПЕКТРА ВНУТРЕННЕГО ТОРМОЗНОГО ИЗЛУЧЕНИЯ ^{32}P

Д. БЕРЕНИ и Д. ВАРГА

Резюме

Проводя критический анализ условий измерений и обработки данных внутреннего тормозного излучения описывается эксперименальное изучение интегрального спектра внутреннего тормозного излучения ^{32}P.

Acta Physica Academiae Scientiarum Hungaricae, Tomus 29 (1), pp. 27—33 (1970)

A PHENOMENOLOGICAL FOUNDATION OF QUANTUM LOGIC

By

G. FÁY

DEPARTMENT OF HISTORY AND PHILOSOPHY OF SCIENCE, CHELSEA COLLEGE OF SCIENCE AND TECHNOLOGY, UNIVERSITY OF LONDON, LONDON, ENGLAND*

(Received in revised form 8. VII. 1969)

On general physical grounds and from symmetry considerations we derive some important lattice theoretical properties of quantum logic.

Introduction

Quantum logic (QL) is defined as a set of quantum mechanical propositions (about a physical system) together with the logical operations defined between them. As a set with algebraic operations QL is a lattice of all the subspaces of a denumerably infinite dimensional Hilbert space.

Research into QL was initiated by GARRET BIRKHOFF and JOHN VON NEUMANN [1] in a paper published in 1936. As the axioms upon which the deductive development of quantum mechanics is based are somewhat heuristic [17], attempts have been made from an early stage to derive them from more plausible physical axioms. Fundamental physical research is nowadays turning increasingly to quantum logic.

Among the investigations into the foundations of QL four main lines can be discerned. I will give the categories and then list some of the more important researches in the fields. Of course this list can not be complete.

1. *Logical* foundations of quantum logic: P. DESTOUCHES-FÉVRIER [2], K. KOTAS [13], H. KUNSEMÜLLER [14], P. MITTELSTAEDT [16], H. REICHENBACH [19] and C. F. VON WEIZSÄCKER [23].

2. *Probabilistic* foundations: A. I. FINE [5], G. GRAWERT [6], S. P. GUDDER [7], J. M. JAUCH and C. PIRON [8], F. KAMBER [12], K. URBANIK [21] and A. VARADARAJAN [22].

3. *Lattice* theoretical foundations: G. EMCH and C. PIRON [3], P. JORDAN [10], C. PIRON [18] and N. ZIERLER [24].

4. *Physical* foundations: F. KAMBER [11] and G. LUDWIG [15].

Accepting the programme set by LUDWIG [15] I would like to join the latter group. The present article is part of the author's doctoral thesis [4]. Further details and proofs can be found there.

* Present address: KGM ISZSZI, Budapest, Hungary

Preliminaries

According to the deductive development of quantum mechanics physical propositions can be treated as special physical quantities and as such, Hermitian hypermaximal operators of Hilbert space can be ascribed to them. The eigenvalues of operators belonging to physical quantities being the possible values of the relevant quantities, the operators belonging to physical propositions are projectors with eigenvalues 0 and 1 corresponding to the truth values 'true' and 'false' of the proposition.

The set of all the projectors of Hilbert space is isomorphic with the set of all the subspaces of Hilbert space. Therefore quantum logic (as the set of all the propositions about a physical system) is isomorphic with the latter subspace-lattice.

This isomorphism is to be understood as follows. Let A, B, C, ... denote physical propositions of the form: 'A physical quantity a has one of its values in the interval (λ', λ'') in the state ψ'.

Then there exists a one-to-one correspondence $S(X)$ between quantum logic (i.e. the set of A, B, C, ...) and the subspace lattice $L(\mathcal{H})$ of $\mathcal{H}$ (Hilbert space) such that for all propositions A, B, C, ...

$$S(A \wedge B) = S(A) \cap S(B),$$
$$S(A \vee B) = S(A) \cup S(B),$$
$$S(A') = S^{\perp}(A).$$

Here $\wedge$, $\vee$, and $'$ denote the logical connective conjunction, disjunction and negation ('and', 'or', 'no') respectively, whereas $\cap$, $\cup$, and $\perp$ denote the lattice theoretical operations meet, joint, and orthocomplementation, respectively.

From now on by a quantum logic Q(L) is meant a lattice L isomorphic with the lattice $L(\mathcal{H})$.

Now, quantum logic as a lattice has the following lattice theoretical properties. (For the terminology see e.g. [8].)

Theorem 1. Quantum logic is a

(1) complete
(2) absolutely atomic
(3) orthomodular

lattice.

Here, by an 'absolutely atomic' lattice is meant an atomic lattice L such that for every $a \in L$ there exists an atom $p \in L$ with

$$a \prec p \cup a \qquad (a \text{ is covered by } p \cup a).$$

Although theorem 1 does not characterise quantum logic completely, PIRON [18] has shown that properties contained in theorem 1 are the most

important ones contained in a complete lattice theoretical characterisation of quantum logic.

In this article we report some theorems by which properties (1), (2) and (3) can be derived from deeper and intuitively more plausible principles than usual.

For property (3) we have

Theorem 2. For any orthocomplemented lattice L the following nine conditions are mutually equivalent:

(A) L is uniquely orthocomplemented.
(B) L is orthomodular.
(C) $a \leqslant b$, $a^{\perp} \cap b = 0$ implies $a = b$.
(D) $a \leqslant c$, $b \leqslant c^{\perp}$ implies $a = (a \cup b) \cap c$.
(E) $a \geqslant c$, $b \geqslant c^{\perp}$ implies $a = (a \cap b) \cup c$.
(F) $a = a \cap (b \cup (a \cap b^{\perp}))$ iff $b = b \cap (a \cup (b \cup a^{\perp}))$.
(G) $a = (a \cap b) \cup (a \cap b^{\perp})$ iff $b = (b \cap a) \cup (b \cap a^{\perp})$.
(H) $a \leqslant x \leqslant b$ implies that $(a \cup x^{\perp}) \cap b$ is a relative orthocomplement of x with respect to the interval a, b. (C.f. [18].)
(I) If $a \cup b = a \cup c$, $a \leqslant b^{\perp}$, $c^{\perp}$, $b \leqslant c$ then $b = c$.

A detailed proof of this theorem can be found in the author's doctoral thesis [4].

Now one can define a 'commensurability relation' between the elements of an orthomodular lattice as follows [18].

a is commensurable with b iff $a = (a \cap b) \cup (a \cup b^{\perp})$. The relation 'commensurable' is detoned by $\leftrightarrow$ or $C(a, b)$. As is well known (see e.g. [18]), an orthomodular lattice L is a Boolean algebra if for every $a, b \varepsilon L$

$$a \leftrightarrow b, \text{ (or } C(a, b)).$$

According to (3) in theorem 1, Q(L) (Quantum Logic) has all the properties (A) . . . (I) of theorem 2.

Besides commensurability one can define two more relations between elements of a uniquely orthocomplemented (and atomic) lattice.

Definition 1. An element a is called a *modular pair* of an element b of a lattice L, if

$$a \leqslant c \text{ implies } a \cup (b \cap c) = (a \cup b) \cap c.$$

This relation is denoted by $M(a, b)$. If the relation M is symmetric in a lattice L, then L is called a *modular-symmetric* lattice.

The other relation which can be defined in an atomic lattice is as follows:

Definition 3. Let L be an atomic lattice and p, q be atoms of L such that for an element a

$$a \cap p = a \cap q \text{ implies } q \leqslant a \cup p.$$

In this case P is called an *atomic pair* of q, in symbols: $A(p, q)$. If in an (atomic) lattice L the relation A is symmetric then L is called *symmetrically atomic.*

It can be shown that quantum logic has the following three symmetry properties:

Theorem 3 [4]. In quantum logic
the 'atomic pair' relation A,
the 'commensurability' relation C and
the 'modular pair' relation M are symmetric.

Moreover we have

Theorem 4 [4]. For any orthocomplemented atomic lattice the symmetry of A implies the symmetry of M

and

Theorem 5 [4]. Every complete, symmetrically atomic lattice is absolutely atomic.

Having disposed of these preliminaries I shall attempt to derive the lattice theoretical properties (1)—(3) (in theorem 1) of quantum logic.

A proposed new foundation for quantum logic

We become acquainted with physical objects and systems via their effects. Effetcs alone, however, do not make it possible to recognize the essence beyond the phenomena. For this purpose, it is necessary to know some sets of effects and some relations between them.

Both KAMBER's and LUDWIG's development [11, 15] were essentially based on a certain grouping of effects (or observations). Beside this, a binary relation viz. 'co-existence' played an important role.

Let us postulate axiomatically only the following:

Axiom 1. On set Σ of all the possible effects of a given physical system there is defined a symmetric, irreflexive relation $\mathcal{R}$.

For instance the relation 'being different' satisfies axiom 1.

Let us consider a physical system and all its possible effects $a, b, c, \ldots \varepsilon\Sigma$. In our discussion 'effect' and 'physical system' are considered as basic concepts. They are implicitly defined by axioms 1 and 2 (given above and below). Let us be given the set Σ and the relation R satisfying axiom 1. It is intuitively evident, that some subsets of Σ are 'essential' and that some are not from some physical point of view. We do not define what is an 'essential' set of physical effects but suppose that there exist such sets and will characterise their properties.

Firstly we suppose that they can be selected from other sets by using only the given relation R. In other words one can speak of an 'essential' set (of physical effects) *with respect to* a relation R.

The selection of essential sets can be carried out by the following procedure.

Consider an arbitrary 'initial' element of a of Σ. If the singleton $\{a\}$ is essential then keep it, if not, consider a further element b. If the subset $\{a, b\} \varepsilon \Sigma$ is essential, keep it, if not, find another element c and examine whether the set $\{a, b, c\}$ is essential or not and so on. The procedure is to be repeated with each initial element a of Σ. This procedure is called 'essentialisation' by which every subset X of $\Sigma (X \varepsilon \Sigma)$ an essential subset Y can be ascribed:

$$Y = \varepsilon(X),$$

where function ε is the 'essence-operation' or 'essentialisation' of X.

Secondly, we assume that every subset $X \subseteq \Sigma$ can be made essential by adding suitable elements to it. This means that operation ε has the following property:

$$\varepsilon(X) \supseteq X. \tag{1}$$

Thirdly, we suppose that essentialisation can be finished in the sense that repeated application of the essentialisation yields no new result.

Mathematically this means the following:

$$\varepsilon(\varepsilon(X)) = \varepsilon(X). \tag{2}$$

As the last assumption we suppose that essentialisation does not spoil the original ordering relation between sets of effects. This means

$$X_1 \subseteq X_2 \text{ implies } \varepsilon(X_1) \subseteq \varepsilon(X_2). \tag{3}$$

The mapping satisfying (1), (2) and (3) is known as a *closure operation* so we postulate as a second axiom the following.

Axiom 2. On the power set 2^{Σ} of Σ (which is partially ordered by the set theoretical inclusion relation) there is defined a closure operation ε which depends only on the relation $\mathcal{R}$ in axiom 1. $\varepsilon = \varepsilon_{\mathcal{R}}$.

Now we will identify quantum logical or physical propositions with the essential subsets of Σ. In other words every subset of Σ of the form $\varepsilon(X)$ with $X \subseteq \Sigma$ is called a 'proposition'.

For these propositions we have

Theorem 6. The set L of all the physical propositions (about a physical system) is a complete lattice with respect to the set theoretical inclusion relation.

Proof: Can be found in [4].

In addition, it can be proved that

Theorem 7. The set L of all the physical propositions is an orthocomplemented lattice.

Proofs of theorems 6 and 7 are based on the well known properties of closure operations. C.f. e.g. SZASZ [20].

If the relation $\mathcal{R}$ of axiom 1 is given then one can find a closure operation $\varepsilon_{\mathcal{R}}$ as follows:

Let

$$\mathcal{R}(x) \overset{\text{def}}{=} \{y : x \mathcal{R} y, \quad x, y \in \Sigma\}$$

$$\mathcal{R}(X) \overset{\text{def}}{=} \bigcap_{x \in X} \mathcal{R}(x) \qquad \mathcal{R} \subseteq \Sigma,$$

then

$$\varepsilon_{\mathcal{R}}(X) \overset{\text{def}}{=} \mathcal{R}\big(\mathcal{R}(X)\big).$$

For this $\varepsilon_{\mathcal{R}}$ it is provable that it is in fact a closure operation.

For the sake of brevity let the set L be called *quantum logic.*

If we assume that the commensurability relation defined in L is symmetric, then we have

Theorem 8. Quantum logic is an orthomodular lattice.

If we assume that every singleton is essential (which can hardly be rejected on physical grounds) then we get

Theorem 9. Quantum logic is a complete, orthomodular atomic lattice.

On general physical grounds it seems reasonable to make two more assumptions:

(H) (L is symmetrically atomic
    (L is modular symmetric.

These latter assumptions ensure that L satisfies the statements (1), (2) and (3) of theorem 1. As these properties are considered by many authors (c.f. [18]) the most important ones of QL, axioms 1 and 2 together with hypotheses (*H*) may be regarded as one kind of phenomenological foundation for quantum logic.

Acknowledgements

Part of the work for this paper was done during the tenure of a post doctoral fellowship at the Department of History and Philosophy of Science, University of London, Chelsea College of Science and Technology. I would like to acknowledge my indebtedness to Dr. H. R. POST, Head of the Department and to Professor A. I. FINE, Visiting Professor at Chelsea College.

REFERENCES

1. G. Birkhoff and J. von Neumann, Ann. Math., **37,** 823, 1936.
2. P. Destouches-Février, Logical Structure of Physical Theories. The axiomatic Method. Ed. L. Henkin, P. Suppes, A. Tarski, Amsterdam, 1959, 376—389.
3. G. Emch and C. Piron, J. Math. Phys., **4,** 469, 1963.
4. G. Fáy, Dissertation (unpublished) University of Miskolc (Hungary), 1969. Investigations into Quantum Logic.
5. A. I. Fine, Logic, Phil. Sci., **35,** 101, 1968.
6. G. Grawert, Z. Phys., **136,** 206, 1953.
7. S. Gudder, J. Math. Mech. **18,** 325, 1968.
8. J. M. Jauch, Foundations of Quantum Mechanics. Addison Wesley, London, 1968.
9. J. M. Jauch and C. Piron, Helv. Phys. Acta, **36,** 827, 1963.
10. P. Jordan, Quantenlogik und das kommutative Gesetz. In: The Axiomatic Method. Ed. L. Henkin, P. Suppes, A. Tarski, Amsterdam, 1959, 365—375.
11. F. Kamber, Nachr. Ak. Wiss. Göttingen, Math. Phys. Kl., 103, 1964.
12. F. Kamber, Math. Ann., **158,** 158, 1965.
13. J. Kotas, Bull. Ac. Polon., **9,** 629, 1963.
14. H. Kunsemüller, Philos. Natur., **8,** 363, 1964.
15. G. Ludwig, An Axiomatic Foundation of Quantum Mechanics on a Nonsubjective Basis. In: Quantum Theory and Reality. Ed. M. Bunge, Berlin, 1967, 98—104.
16. P. Mittelstaedt, Fortschr. Phys., **9,** 106, 1961.
17. J. von Neumann, Mathematical Foundations of Quantum Mechanics. Princeton, N. J. 1955.
18. C. Piron, Quantum Axiomatics. Dissertation translated by M. Cole, G. P. O. Engineering Department, Research Station, Dollis Hill, London, N. W. 2.
19. H. Reichenbach, Philosophical Foundations of Quantum Mechanics. Berkeley, Calif. 1944.
20. G. Szasz, Introduction into Lattice Theory. Academic Press, New York and London, 1963.
21. K. Urbanik, Studia Mathematica, **21,** 117, 1961.
22. V. S. Varadarajan, Commun. Pure Appl. Math., **15,** 189, 1962.
23. C. F. von Weizsäcker, Naturw., 42, 521, 545, 1955.
24. N. Zierler, Axioms for Nonrelativistic Quantum Mechanics, Pacific J. Math., **11,** 115, 1961.

ФЕНОМЕНОЛОГИЧЕСКОЕ ОБОСНОВАНИЕ КВАНТОВОЙ ЛОГИКИ

Г. ФАИ

Резюме

Исходя из общих физических принципов и соображений симметрии выводится несколько теоретических свойств квантовой логики.

Acta Physica Academiae Scientiarum Hungaricae, Tomus 29 (1), pp. 35—44 (1970)

ON THE THEORY OF GALVANOMAGNETIC EFFECTS IN SEMICONDUCTORS WITH ANISOTROPIC SCATTERING

By

J. BALÁZS and B. PŐDÖR

RESEARCH INSTITUTE FOR TECHNICAL PHYSICS OF THE HUNGARIAN ACADEMY OF SCIENCES, BUDAPEST

(Received 8. VII. 1969)

In this work the galvanomagnetic coefficients are determined for the case of anisotropic scattering. The scattering anisotropy is described by introducing a relaxation time tensor into the scattering term of the Boltzmann equation. A power series solution of the Boltzmann equation is given according to the powers of the magnetic field for the case when the surfaces of constant energy are ellipsoids. The transport (galvanomagnetic) coefficients are determined for the multiple ellipsoidal energy valley model of semiconductors. This model describes the transport effects in *n*-type Ge and Si.

1. Introduction

The theory of transport phenomena in semiconductors is usually applied to the simplest case, i.e. to a semiconductor having a single spherical energy minimum or maximum in the centre of the Brillouin zone and with an isotropic scattering mechanism of the charge carriers. This latter assumption means that in the relaxation time approximation the relaxation time of the charge carriers is scalar. However, the band structure of the most common semiconductors i.e. Ge and Si, is rather complicated. In the conduction band of Ge and Si there are four and six equivalent energy valleys, respectively. In each valley the surfaces of constant energy are ellipsoids of rotation. On the other hand, even in the case of crystals of high symmetry like semiconductors with diamond-type lattice the acoustical phonon, the optical phonon and the ionized impurity scattering are anisotropic [1], [2]. The anisotropy of the scattering of charge carriers can be increased as a result of scattering by lattice defects, e.g. by dislocations. Scattering anisotropy can be described in the framework of relaxation time approximation by introducing a relaxation time tensor instead of the scalar relaxation time.

In crystals with high symmetry the principal axes of the relaxation time tensor, neglecting the scattering by lattice defects, coincide with those of the effective mass tensor. The theory of transport phenomena of *n*-type Ge and Si taking into account their multi-valley band structure and the above mentioned symmetry property of the relaxation time tensor was developed by HERRING and VOGT [1]. In this case the principal axes of the relaxation time tensor coincide with those of the effective mass tensor and the scattering anisotropy is merged in that of the effective masses. Thus, the Boltzmann equation can be solved in the usual way. KORENBLIT [3] has solved the Boltzmann equation for a somewhat more general case, when not all the nondiagonal elements of

the relaxation time tensor are zero. He has applied a successive approximation which resulted in a solution which is linear in the electric field and contains terms up to the second order in the magnetic field. A general solution of the Boltzmann transport equation with a relaxation time tensor for arbitrary magnetic fields has been given by ZUKOTYNSKI and GRYNBERG [4], and HÜBNER [5].

In this paper a general power series solution of the Boltzmann equation with a relaxation time tensor is given for the case when the surfaces of constant energy are ellipsoids. On the basis of this solution the transport (galvanomagnetic) coefficients for n-type Ge and Si can be determined.

2. The Boltzmann equation and its solution

2.1. Basic assumptions

In the following we calculate the transport coefficients on the basis of the solution of the Boltzmann equation for the case when the surfaces of constant energy are composed of equivalent ellipsoidal valleys (e.g. n-type Ge and Si) and the relaxation time of charge carriers is anisotropic. During the calculations the following assumptions were made.

a. The energy of electrons in the separate valleys is a quadratic function of the wave number vector i.e.

$$\varepsilon = \frac{\hbar^2}{2}\left(\frac{k_1^2}{m_1} + \frac{k_2^2}{m_2} + \frac{k_3^2}{m_3}\right), \tag{1}$$

where m_i is the i-th component of the effective mass tensor referred to the principal axis system of the energy ellipsoid, k_i is the i-th component of the wave number vector.

b. The surfaces of constant energy of electrons in Ge and Si are composed of four and six equivalent ellipsoids of revolution with their axis of symmetry coinciding with the directions $\langle 111 \rangle$ and $\langle 100 \rangle$, respectively.

c. The effects of electron transitions between the separate valleys are neglected.

d. The relaxation time of the electrons is anisotropic, and can be described by introducing a relaxation time tensor. In the most general case the relaxation time tensor referred to the principal axis system of the separate energy ellipsoids has the general form:

$$\bar{\bar{\tau}} = \begin{pmatrix} \tau_{11} & \tau_{12} & \tau_{13} \\ \tau_{21} & \tau_{22} & \tau_{23} \\ \tau_{31} & \tau_{32} & \tau_{33} \end{pmatrix}. \tag{2}$$

Introducing the collision time tensor $\overline{\nu}$, as the inverse of the relaxation time tensor we have

$$\nu_{ij}\tau_{jk} = \delta_{ik}. \tag{3}$$

Here and throughout this paper the summation convention over repeated indices is applied.

In the separate energy valleys the relaxation time tensors may be different, e.g. when the symmetry of the scattering mechanism is not the same as the symmetry of the crystal. This is the case when the scattering is caused by dislocations. The elements of the relaxation time tensor depend on the energy i.e. $\tau_{ij} = \tau_{ij}(\varepsilon)$ and this energy dependence is not necessarily the same for each element.

2.2. *The Boltzmann equation*

The Boltzmann equation is given in the following form

$$\frac{e}{\hbar}(\vec{E} + \vec{v}\times\vec{B})\nabla_{\vec{k}} f = \left(\frac{\partial f}{\partial t}\right)_c, \tag{4}$$

where f is the distribution function of charge carriers and e is the elementary charge, for electrons $e < 0$. According to KORENBLIT [3], the scattering anisotropy in the collision term can be taken into account in the following manner. The velocity change of electrons due to collisions is written as

$$\left(\frac{\partial v_i}{\partial t}\right)_c = -\nu_{ij} v_j. \tag{5}$$

Making use of this, the following expression is derived for the collision term

$$\left(\frac{\partial f}{\partial t}\right)_c = \frac{\partial f}{\partial v_i}\left(\frac{\partial v_i}{\partial t}\right)_c = -\frac{\partial f}{\partial v_i}\nu_{ij} v_j. \tag{6}$$

Substituting (6) into (4) we get the Boltzmann equation for anisotropic scattering

$$\frac{e}{\hbar}(\vec{E} + \vec{v}\times\vec{B})\nabla_{\vec{k}} f = -\frac{\partial f}{\partial v_i}\nu_{ij} v_j. \tag{7}$$

The collision term used by ZUKOTYNSKI and GRYNBERG [4], and by H ÜBNER [5] is essentially the same as ours in (6) or (7).

It is advantageous to introduce elliptic coordinates in the wave vector space and rewrite the Boltzmann equation in this new coordinate system. Let us put

$$\xi_i = \frac{k_i}{\sqrt{m_i}} . \tag{8}$$

In these new coordinates the Boltzmann equation has the following form

$$e\left(\vec{E}' + \frac{\vec{\xi} \times \vec{B}'}{\sqrt{m_2 m_3}}\right) \nabla_{\vec{\xi}} f = - \sum_{i,j} \sqrt{\frac{m_j}{m_i}}\, \nu_{ij}\, \xi_i F_j, \tag{9}$$

where

$$E_i' = \frac{E_i}{\hbar \sqrt{m_i}}; \quad B_i' = B_i \sqrt{\frac{m_i}{m_1}}; \quad F_i = \frac{\hbar}{\sqrt{m_i}} \frac{\partial f}{\partial v_i} . \tag{10}$$

2.3. Solution of the Boltzmann equation

We are looking for the solution of Eq. (9) which has the form of a power expansion according to the small perturbation $\vec{E}$ and $\vec{B}$, containing terms linear in the electric field $\vec{E}$ and terms up to the second order in the magnetic field $\vec{B}$.

Taking (10) into account, the solution of (9) is looked for in the form

$$f = f^{(0)} + \vec{F}\vec{\xi} = f^{(0)} + F_i^{(1)}\xi_i + F_i^{(2)}\xi_i + F_i^{(3)}\xi_i + \ldots, \tag{11}$$

where $f^{(0)}$ is the equilibrium distribution function and $F_i^{(k)}$ depends linearly on the electric field and in $(k-1)$-th order on the magnetic field.

To get the solution of (9) in the form of (11) we apply the Zener—Jones series expansion to our case (see e.g. [6]). This procedure yields all the terms in expansion (11).

Let us introduce the following notation

$$T_{ij} = \sqrt{\frac{m_j}{m_i}}\, \nu_{ij}. \tag{12}$$

Considering (11) and (12), Eq. (9) can be written as

$$\begin{aligned} &e\vec{E}' \nabla_{\vec{\xi}} f^{(0)} + e\vec{E}' \nabla_{\vec{\xi}} \vec{F}\vec{\xi} + \frac{e}{\sqrt{m_2 m_3}} \vec{\xi} \times \vec{B}' \nabla_{\vec{\xi}} f^{(0)} + \\ &+ \frac{e}{\sqrt{m_2 m_3}} \vec{\xi} \times \vec{B}' \nabla_{\vec{\xi}} \vec{F}\vec{\xi} = - \vec{\xi}\vec{\bar{T}}\vec{F}. \end{aligned} \tag{13}$$

Here the second term on the left-hand side of Eq. (13) is a small quantity of the second order, so it is negligible. Further considering that

$$\nabla_{\vec{\xi}} = \frac{\partial \varepsilon}{\partial \vec{\xi}} \cdot \frac{\partial}{\partial \varepsilon} = \hbar^2 \vec{\xi} \frac{\partial}{\partial \varepsilon} \tag{14}$$

the third term of Eq. (13) is zero. Applying (14) to the remaining two terms on the left hand side of Eq. (13) we finally obtain the following equation for $\vec{F}$

$$\vec{\xi}\left[e\hbar^2 \frac{\partial f^{(0)}}{\partial \varepsilon} \vec{E}' + \overline{\overline{T}}\vec{F} + \frac{e}{\sqrt{m_2 m_3}} \vec{B}' \times \vec{F}\right] = 0. \tag{15}$$

Since only the $\vec{F}\vec{\xi}$ scalar product has any physical meaning we can exclude the case when the two vectors appearing in (15) are perpendicular to each other and so Eq. (15) can be written in the simpler form

$$-e\hbar^2 \frac{\partial f^{(0)}}{\partial \varepsilon} \overline{\overline{T}}^{-1} E' = \left[1 + \frac{e}{\sqrt{m_2 m_3}} \overline{\overline{T}}^{-1} \vec{B}' \times\right] \vec{F}. \tag{16}$$

Let us denote the operator containing the vector product on the right hand side of Eq. (16) by $\hat{\Omega}$

$$\hat{\Omega} = \frac{e}{\sqrt{m_2 m_3}} \overline{\overline{T}}^{-1} \vec{B}' \times. \tag{17}$$

Taking into account (17) Eq. (16) can be written as

$$-e\hbar^2 \frac{\partial f^{(0)}}{\partial \varepsilon} \overline{\overline{T}}^{-1} \vec{E}' = [1 + \hat{\Omega}] \vec{F}. \tag{18}$$

The solution of Eq. (18) can be obtained formally in the following manner (see e.g. DAVIS [7] and ZIMAN [6])

$$\begin{aligned} \vec{F} &= \frac{1}{1+\hat{\Omega}^2}\left(-e\hbar^2 \frac{\partial f^{(0)}}{\partial \varepsilon} \overline{\overline{T}}^{-1} \vec{E}'\right) = \\ &= (1 - \hat{\Omega}^2 + \hat{\Omega}^2 - \hat{\Omega}^3 + \ldots)\left(-e\hbar^2 \frac{\partial f^{(0)}}{\partial \varepsilon} \overline{\overline{T}}^{-1} \vec{E}'\right). \end{aligned} \tag{19}$$

Let us write down $F_i^{(1)}$, $F_i^{(2)}$ and $F_i^{(3)}$ i.e. the contributions to the distribution function containing the zeroth, first and second power of the magnetic field, respectively. Writing $\vec{E}$ and $\vec{B}$ instead of $\vec{E}'$ and $\vec{B}'$

$$\begin{aligned} F_i^{(1)} &= -\frac{e\hbar}{\sqrt{m_i}} \frac{\partial f^{(0)}}{\partial \varepsilon} \tau_{ij} E_j, \\ F_i^{(2)} &= \frac{e^2\hbar}{\sqrt{m_i}} \frac{\partial f^{(0)}}{\partial \varepsilon} \varepsilon_{hkl} \tau_{ih} B_k \frac{\tau_{lj}}{m_l} E_j, \\ F_i^{(3)} &= -\frac{e^3\hbar}{\sqrt{m_i}} \frac{\partial f^{(0)}}{\partial \varepsilon} \varepsilon_{hkm} \frac{\tau_{hj}}{m_h} B_k \frac{\tau_{gm}}{m_g} E_j \varepsilon_{gln} B_l \tau_{in}, \end{aligned} \tag{20}$$

where ε_{ijk} is the antisymmetric tensor of Levy-Civita. Its value is $+1$ or -1 for even or odd permutations of the indices, respectively, and 0 for the other cases. The summation convention is applied to the indices which are repeated in the numerator only.

It should also be noted that if the relaxation time tensor is diagonal the solution given in (19) and (20) turns into the solutions valid for the corresponding special cases known from the literature [1], [6], [8]. Eq. (9) was solved by KORENBLIT [3], for the special case when the nondiagonal elements of the relaxation time tensor are zero except for τ_{13} and τ_{31}. ZUKOTYNSKI and GRYNBERG [4] have solved Eq. (7) for arbitrary magnetic fields, without using the Zener—Jones expansion. In the case of small magnetic fields the solution found by them is equivalent to that reported by us in Eq. (19), but our solution is more practical for low magnetic fields while the solution given in [4] can yield more tractable formulae for high magnetic fields.

3. Calculation of the current density

3.1. Calculation of the current density for one energy valley

Knowing the distribution function the current density can be calculated simply as

$$\vec{I} = \frac{e}{4\pi^3} \int f \vec{v}\, d^3\vec{k}. \tag{21}$$

Since the equilibrium distribution function does not contribute to the current we get from (21) and (11)

$$\vec{I} = \frac{e}{4\pi^3} \int (f - f^{(0)})\, \vec{v}\, d^3\vec{k} = \frac{e}{4\pi^3} \int (\vec{F}\,\vec{\xi})\, \vec{v}\, d^3\vec{k}. \tag{22}$$

Changing the integration in $\vec{k}$ space to that in $\vec{\xi}$ space the i-th component of the current will be

$$I_i = \frac{e\hbar\sqrt{m_1 m_2 m_3}}{4\pi^3} \int \frac{\xi_i}{\sqrt{m_i}} F_l\, \xi_l\, d^3\vec{\xi}. \tag{23}$$

Since $\vec{F}$ is independent of $\vec{\xi}$ the integral in (23) is not zero only if $i = l$ because of the $\xi_i\, \xi_l$ product in the integrand. Switching over to integration according to the energy instead of (23) we get the following expression for the current

$$I_i = \frac{2e\sqrt{2\, m_1 m_2 m_3}}{3\pi^2\hbar^4} \int \frac{F_i}{\sqrt{m_i}}\, \varepsilon^{3/2}\, d\varepsilon. \tag{24}$$

Substituting (11) and (20) into Eq. (24) the current density can be calculated as a function of the electric and magnetic fields. Comparing this with the phenomenological expression for the current density

$$I_i = \sigma_{ij} E_j + \sigma_{ijk} E_j B_k + \sigma_{ijkl} E_j B_k B_l , \tag{25}$$

the conductivity coefficients σ_{ij}, σ_{ijk} and σ_{ijkl} are obtained. Here σ_{ij} is the conductivity tensor for zero magnetic field, σ_{ijk} accounts for the Hall effect and σ_{ijkl} describes the change of conductivity in magnetic fields.

Substituting (20) into Eq. (24) and comparing this with (25) we get the following expressions for the conductivity coefficients

$$\begin{aligned}
\sigma_{ij} &= \frac{e^2 n}{m_i} \langle \tau_{ij} \rangle , \\
\sigma_{ijk} &= -\frac{e^3 n}{m_i} \varepsilon_{hkl} \frac{\langle \tau_{ih} \tau_{lj} \rangle}{m_l} , \\
\sigma_{ijkl} &= \frac{e^4 n}{m_i} \langle \tau_{hj} \tau_{gm} \tau_{in} \rangle \frac{\varepsilon_{hkm} \varepsilon_{gln} + \varepsilon_{hlm} \varepsilon_{gkn}}{2 m_h m_g} .
\end{aligned} \tag{26}$$

Here n is the electron density in a separate valley

$$n = \frac{1}{4\pi^3} \int f^{(0)} d^3 \vec{k} = -\frac{2\sqrt{2 m_1 m_2 m_3}}{3\pi^2 \hbar^3} \int \frac{\partial f^{(0)}}{\partial \varepsilon} \varepsilon^{3/2} d\varepsilon \tag{27}$$

and the symbol $\langle\ \rangle$ denotes the following integral average

$$\langle A \rangle = \frac{\int_0^\infty \frac{\partial f^{(0)}}{\partial \varepsilon} \varepsilon^{3/2} A d\varepsilon}{\int_0^\infty \frac{\partial f^{(0)}}{\partial \varepsilon} \varepsilon^{3/2} d\varepsilon} . \tag{28}$$

We should like to note that the factor of 2 in the numerator of the last equation in (26) arises from the usual symmetrization of σ_{ijkl}. The formulae of the conductivity coefficients given in (26) contain the special cases known from the literature, too, when the relaxation time is a scalar quantity [8], or the relaxation time tensor is diagonal [1], [6].

3.2. Calculation of the transport coefficients for multiple energy valley models

As was mentioned above in the conduction band of Ge and Si there are four and six equivalent ellipsoidal energy valleys, respectively. For such multiple energy valley models knowing the relaxation time tensor for each

energy ellipsoid, the conductivity coefficients are easily determined on the basis of equation (26). After transforming the conductivity coefficients of the separate energy valleys into a common coordinate system which have axes parallel to the cubic axes of the crystal, they are summed up and the final expressions for the conductivity coefficients are obtained. Denoting by $S_{ij}^{(\alpha)}$ the matrix of transformation from the coordinate system defined in the α-th valley to the cubic coordinate system we get

$$\begin{aligned} \sigma_{ij} &= \sum_{\alpha=1}^{N} S_{ip}^{(\alpha)} S_{jr}^{(\alpha)} \sigma_{pr}^{(\alpha)}, \\ \sigma_{ijk} &= \sum_{\alpha=1}^{N} S_{ip}^{(\alpha)} S_{jr}^{(\alpha)} S_{ks}^{(\alpha)} \sigma_{prs}^{(\alpha)}, \\ \sigma_{ijkl} &= \sum_{\alpha=1}^{N} S_{ip}^{(\alpha)} S_{jr}^{(\alpha)} S_{ks}^{(\alpha)} S_{lt}^{(\alpha)} S_{prst}^{(\alpha)}, \end{aligned} \tag{29}$$

where N is the number of equivalent valleys.

In the case of Ge the major axes of the energy ellipsoids coincide with the $\langle 111 \rangle$ directions. Table I shows a possible choice of the axes of coordinate systems in the separate valleys referred to the cubic axes of the crystal.

Table I

Major axis of ellipsoid	x	y	z
[111]	[111]	[$\bar{1}$10]	[$\bar{1}\bar{1}$2]
[$\bar{1}$11]	[$\bar{1}$11]	[$\bar{1}\bar{1}$0]	[1$\bar{1}$2]
[$\bar{1}\bar{1}$1]	[$\bar{1}\bar{1}$1]	[1$\bar{1}$0]	[112]
[1$\bar{1}$1]	[1$\bar{1}$1]	[110]	[$\bar{1}$12]

In this case the $\overline{\overline{S}}^{(\alpha)}$ transformation matrices can be written as

$$\overline{\overline{S}}^{(\alpha)} = \begin{bmatrix} \dfrac{S_2^{(\alpha)}}{\sqrt{3}} & -\dfrac{S_1^{(\alpha)}}{\sqrt{2}} & -\dfrac{S_2^{(\alpha)}}{\sqrt{6}} \\ \dfrac{S_1^{(\alpha)}}{\sqrt{3}} & \dfrac{S_2^{(\alpha)}}{\sqrt{2}} & -\dfrac{S_1^{(\alpha)}}{\sqrt{6}} \\ \dfrac{1}{\sqrt{3}} & 0 & \dfrac{2}{\sqrt{6}} \end{bmatrix}, \tag{30}$$

where the values of $S_1^{(\alpha)}$ and $S_2^{(\alpha)}$ are found in Table II.

Table II

Major axis of ellipsoid	$S_1^{(\alpha)}$	$S_2^{(\alpha)}$
[111]	1	1
$[\bar{1}11]$	1	—1
$[1\bar{1}1]$	—1	—1
$[\bar{1}11]$	—1	1

For the case of Si the transformation matrices can be constructed similarily.

At the comparison of the experimental and theoretical results it is more convenient to use the resistivity coefficients instead of the conductivity coefficients. They are defined phenomenologically with the aid of the following equation

$$E_u = \varrho_{uv} I_v + \varrho_{uvw} I_v B_w + \varrho_{uvwz} I_v B_w B_z . \tag{31}$$

Inverting equation (31) the resistivity coefficients can be expressed with the aid of the conductivity coefficients of the whole crystal as

$$\begin{aligned} \varrho_{uv} &= (\overline{\overline{\sigma}}^{-1})_{uv} , \\ \varrho_{uvw} &= \varrho_{ui}\, \sigma_{ijw}\, \varrho_{jv} , \\ \varrho_{uvwz} &= -\frac{\varrho_{ui}}{2} (\sigma_{ijz}\, \varrho_{jvw} + \sigma_{ijw}\, \varrho_{jvz}) - \varrho_{ui}\, \sigma_{ijzw}\, \varrho_{jv} . \end{aligned} \tag{32}$$

4. Conclusions

Using a relaxation time tensor instead of a scalar relaxation time we have solved the Boltzmann transport equation for semiconductors in the form of a power series according to the powers of the magnetic field. The galvanomagnetic coefficients were calculated for the multiple energy valley model of semiconductors which is the case of *n*-type Ge and *n*-type Si. Our results can be used for the description of transport processes in semiconductors with anisotropic scattering of current carriers. These results can be applied, e.g. to describe the galvanomagnetic effects in *n*-type Ge, containing high densities of dislocations as anisotropic scattering centres [9], [10].

Acknowledgements

We thank Dr. G. Szigeti, Director of the Institute for his interest and encouragement as well as Dr. Z. Bodó, Mr. T. Geszti and Mr. F. Beleznay for valuable discussions.

REFERENCES

1. C. HERRING and E. VOGT, Phys. Rev., **101,** 943, 1956.
2. А. Г. Самойлович, И. Я. Коренблит, И. В. Даховский, В. Д. Искра, ФТТ, **3**, 2939, 1961.
3. I. YA., KORENBLIT, Sov. Phys. Sol. State, **2,** 2738, 1961.
4. S. ZUKOTYNSKI and M. GRYNBERG, phys. stat. sol., **9,** 549, 1965.
5. U. HÜBNER, Zs. f. Naturforschung, **22a,** 2086, 1967.
6. J. M. ZIMAN, Electrons and Phonons, Clarendon Press, Oxford, 1960.
7. L. DAVIS, Phys. Rev., **56,** 93, 1939.
8. B. ABELES and S. MEIBOOM, Phys. Rev., **95,** 31, 1954.
9. Б. Пёдёр, ФТП, **2**, 384, 1968.
10. J. BALÁZS and B. PŐDÖR, phys. stat. sol., **37,** 119, 1970.

К ТЕОРИИ ГАЛЬВАНОМАГНИТНЫХ ЯВЛЕНИЙ С АНИЗОТРОПНЫМ РАССЕЯНИЕМ

Й. БАЛАЖ и Б. ПЁДЁР

Резюме

В данной работе определяются гальваномагнитные коэффициенты для анизотропного рассеяния носителей тока. Анизотропия рассеяния описывается введением тензора времени релаксации в член столкновения кинетического уравнения. Решение кинетического уравнения дается в виде разложения по степеням магнитного поля в случае изоэнергетических поверхностей описываемых эллипсоидами. Гальваномагнитные коэффициенты определяются для полупроводников, зона проводимости которых описывается несколькими эквивалентными эллипсоидами. Эту модель можно применять для германия и кремния *n*-типа.

Acta Physica Academiae Scientiarum Hungaricae. Tomus 29 (1), pp. 45–65 (1970)

TRANSMITTED PHONON DRAG MEASUREMENTS IN Ge

By

B. RŐSNER, Z. BODÓ, T. SEBESTYÉN and B. WOHN

RESEARCH INSTITUTE FOR TECHNICAL PHYSICS OF THE HUNGARIAN ACADEMY OF SCIENCES
BUDAPEST

(Received 10. VII. 1969)

The transmitted phonon drag effect in germanium (which is based on the pronounced phonon—electron interaction at low temperatures) is described. Its applications include:
(a) evaluation of phonon-phonon scattering parameters;
(b) investigation of phonon reflection at a free surface;
(c) experimental results on the influence of a twin boundary on phonon propagation will be also presented.

1. Introduction

A large contribution to the thermoelectric power due to nonequilibrium phonon distribution was first revealed experimentally in n — Ge by FREDERIKSE [1]. An extensive review of phonon drag effect has been given by HERRING [2]. In semiconductors at low temperatures the long wavelength

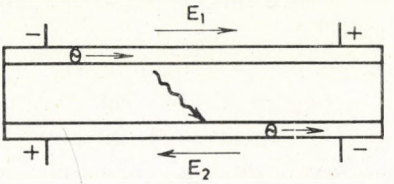


Fig. 1

acoustic phonons' relaxation is partly controlled by the charge-carrier-phonon interaction. Those phonons which interact with carriers are called relevant phonons. In the presence of a temperature gradient, phonons travel together with free carrier diffusion from the hot to the cold end of the sample. Phonons drag along the carriers and this appears as an increase in the Seebeck and Peltier coefficient, i.e. these coefficients can be expressed as the sum of an electronic and a phonon term. The phonon-drag contribution to low temperature thermoelectric power has been observed in most semiconductors: Ge [3], Si [4], InSb [5], [6], Te [7], GASs [8], CdS [9], ZnO [10]. In high transverse magnetic fields ($\hbar\omega \gg kT$, where ω is the cyclotron frequency) the phonon drag part in thermogalvanomagnetic effects becomes more pronounced [6]. The low temperature anomaly of thermopower in semiconductors led to the discovery of transmitted phonon drag effect [11]. Fig. 1 shows the sample arrangement suitable for investigating this effect. If an electric field $\vec{E}_1$ is

applied to the top n-layer the electron current disturbs the phonon distribution. Part of this nonequilibrium phonon momentum penetrates into the p-type layer. After decaying caused by various possible phonon interactions the rest phonon momentum reaches the bottom n-layer, where phonons drag along the electrons, thereby setting up an electric field $\vec{E}_2$ of opposite polarity to the input field. The E_2/E_1 ratio is proportional to the phonon momentum reaching the receiver layer. Considering the role of the layers they are called in turn emitter (or transmitter, phonon source), propagating medium, and receiver layer. As SHOCKLEY pointed out in his pioneer work [11] the center p-layer may serve as a medium, where various phonon interactions take place. As far as we know the following types of experiments have been carried out until now:

i) Varying the center layers' thicknesses phonon—phonon interaction controlled phonon mean free path measurements in Si [21] and in Ge [13].

ii) Interaction of relevant phonons with grain boundary in silicon [14], interaction of phonons with the stacking fault in Ge [15].

iii) Phonon reflection experiments in samples having a special structure in silicon [16] and in Ge [17].

iv) Low temperature estimate of Peltier heat in Ge [18].

This paper is concerned with giving a detailed review of our investigations with Ge. Some of these results have already been published in short notes [13, 15, 17]. We also deal with the main results of similar studies on Si. Section 2 deals with the sample preparation. Our equipment and measuring method is described in Section 3. The relevant phonon mean free path measurements are presented in Section 4. Section 5 contains our theory for interpreting the experimental data given in the fourth part. Our analysis makes it possible to compare the results of transmitted phonon drag measurements with thermal conductivity [19] and thermoelectric measurements [3, 4, 20]. Section 6 deals with the phonon plane type defect interaction employing the transmitted phonon drag effect as an experimental tool.

2. Sample preparation

The p-type Ge single crystals were produced by the CZOCHRALSKI method. The growth direction was [111]. They were doped with Ga to obtain an impurity concentration of 3.3×10^{15} cm^{-3}. Slices were cut perpendicular to the growth axis and were polished both mechanically and chemically. On both sides of the slices the 15 mμ deep n-type layers were made by antimony diffusion in oxygen and aqueous vapour-free H_2 atmosphere. We maintained the Ge slices at a temperature of 780 °C and the antimony source at 560 °C with an accuracy of 1 °C for the sake of reproducibility. The diffusion process lasted 3 hours. By bevelling and staining the diffused wafers we could control the diffusion

depth with an interference microscope, and found it to be 15 mμ at room temperature. Measuring the sheet resistivity by the four point method [21] the average carrier concentration could be estimated, and amounted to $3 \times$ $\times 10^{18}$ cm^{-3}. The final geometry and dimensions of our samples are illustrated in Fig. 2. Dimensions are given in millimeters. In many cases "mesa etching" was used to reveal a small area of p-type material.

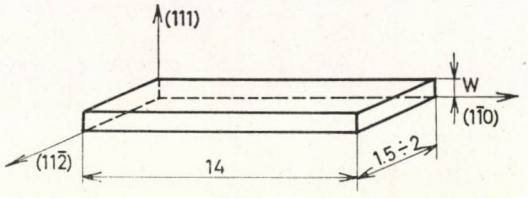


Fig. 2

In purified H_2 atmosphere dots of 95% Pb, 4% Sn and 1% Sb composition were alloyed to the sample to obtain ohmic contacts. The advantage of this alloy was that owing to the large amount of neutral dopant Pb, it did not penetrate into the p-layer. The alloying processes were performed in alloying jigs thus ensuring reproducible location of contacts. The shortest possible 100 μm dia annealed Ni wires lead to the shielded cables. The H_2O_2 surface treatment produced a protective oxide layer and this assured the stability and minimized the leakage current through the $p - n$ junctions.

3. Measurements and results

It is clear from the first section that the measurements should be carried out under isothermal conditions. With the use of direct current as input no reproducible output signals were obtained. The disturbances were attributed to thermoelectric effects caused by power dissipation at the current-carrying input contacts. Detailed analysis of this problem is described in [22]. The usual method to eliminate such disturbances is to apply alternating current as an input signal. Fig. 3 illustrates the electrical arrangement used for our purposes. A tunable R. C. oscillator and a power amplifier generated the 1000 c/s input field. The signals caused by the phonons were measured by a high input resistance selective amplifier. The phase relation between the input and the phonon drag signals was detected by a double beam oscilloscope. Obviously, the linearity of E_2/E_1 function and the 180° phase shift between the input and output signals prove that we are dealing with the transmitted phonon drag effect. The depletion layer thickness of $p - n$ junctions was estimated and the corresponding capacity found to be negligible at the applied

frequency. According to [22] the capacitive coupling between the input and output circuits plays a predominant role in the megacycle range. At room temperature the leakage current through the diodes surmounts the transmitted phonon drag signals. Thus, the input and output signals are in phase. When cooling the sample gradually down to liquid N temperature the "phase-in" output is continuously decreasing and at a certain temperature it comple-

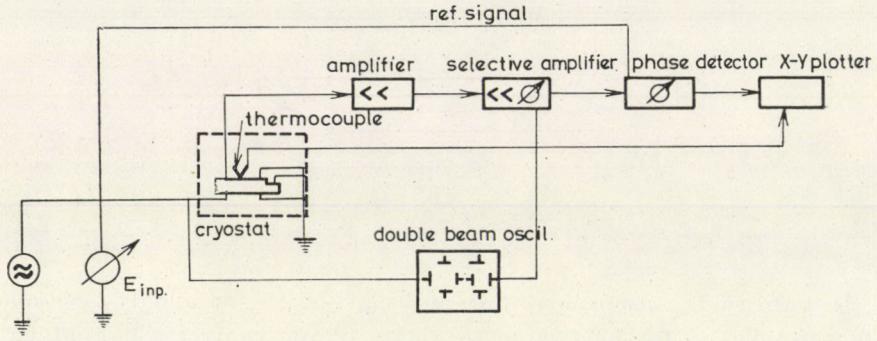


Fig. 3

tely disappears, i.e. it becomes lower than 10^{-7} V. This critical temperature depends on the properties of the samples, but it always lies between 150—200 °K. As cooling continues the opposite phase appears and increases very quickly. The above process is visualized by the traces of the double beam cathode ray oscilloscope. The phase detector served two purposes: its d.c. output (f.s.d. 10V) led directly to the input of Y axis of an XY plotter, while in the case of very low phonon signals (e.g. phonon reflection experiments) its noise filtering effect was exploited. An iron—constantan thermocouple measured the temperature of the sample. Its cold end was in a liquid N_2 bath and its output voltage was connected to the input of the X axis. We could work only in the temperature interval from 77 °K to 110 °K (at these temperatures the leakage current through the diodes could be neglected). A simple cryostat construction was used to establish the temperature of samples (Fig. 4). Liquid N_2 was flowing between the walls of a double walled dewar. The inner part of this dewar contained the sample which was immersed in oil — such a kind of thermal contact suited our purposes. After cooling with liquid N_2 had stopped about 30 minutes were necessary to reach temperatures near 110 °K. The cooling and heating of the sample were repeated successively. In the preliminary experiments the Y — Y plots exhibited hysteresis loops indicating that the sample and the thermocouple were not at the same temperature. Such disturbing effects could be eliminated by mounting a copper block on the sample holder, and by soldering the thermocouple to it. Increas-

ing the input voltage up to 0.5—2 Volts a deviation from the linearity (see in the next paragraph) of $E_2(E_1)$ function was observed. In this case the phonon signal was surmounted by the current passing through the diodes. The sudden increase and the 180° phase shift of the output signal indicated this "breakdown phenomenon". In many instances reverse bias was applied to the $n-p$ layers thus enlarging the differential resistivity between the layers. Applying

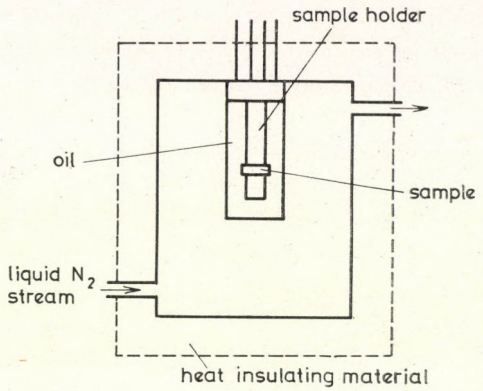


Fig. 4

the bias the input voltage could be extended by one order of magnitude. In the above mentioned temperature range, however, no appreciable change in the transmission ratio with or without reverse bias could be observed except for the phonon reflection experiments [17].

4. Relevant thermal phonon mean free path measurements and comparison with earlier theories

On the basis of HERRING's simplified model [2] SHOCKLEY [11] performed a calculation in order to obtain a relation for the E_2/E_1 transmission ratio. According to this model the frequency of both phonon — electron, and phonon—phonon interactions are supposed to be proportional to some effective charge carrier concentrations. He obtained for E_2/E_1:

$$\frac{E_2}{E_1} \sim \frac{e^{-w/L}}{\left(1+\frac{n}{n_i}\right)\left(1+\frac{n_\Phi}{n}\right)\left(1+\frac{n}{n_\Phi}\right)}, \tag{1}$$

where w is the width of the center p-layer;

L is the phonon mean free path caused only by the phonon—phonon scattering;

n is the actual electron concentration in the n-type layers;

n_i and n_Φ are the reference effective carrier concentrations at the given temperature if lattice and impurity scattering relaxation times are equal and if the phonon—phonon and the phonon—charge carrier relaxation times are equal, respectively.

From (1) it is obvious that by varying the thickness of the middle p-layers the relevant phonon mean free path can be determined. Such an experiment was carried out by R. GERETH and K. HÜBNER in Si [12]. For our investigations we chose germanium. The transmitted phonon drag signals were measured over a temperature range of 77 °K—110 °K in samples as illustrated in Fig. 2. They differed only in the thicknesses of their center layers. From SHOCKLEY's formula a linear dependence for the ln $E_2/E_1(w)$ function was to be expected. But in the case of thin samples this function deviates from linearity. The deviation is due to the change in the relevant thermal phonon distribution, i.e. phonon distribution generated in the emitter is varying continuously when propagating through the p-layer. In accordance with the general rule of wave physics the longer the wavelength the less is its scattering probability. With the phonons traversing the p-layer, the maximum of generated phonon distribution shifts gradually towards the longer wavelengths. Though our theory in the next section is devoted to an analysis of such measurement results we present the evaluation of our data on the basis of the model given in [12]. Calculating the phonon momentum F reaching the bottom n-layer the authors used the following simplifying assumptions:

1. The relevant phonon distribution is assumed to be of the form q^{-1}; q is the phonon wave number with a cut-off q_0.

2. Both longitudinal and transverse modes are present.

3. According to HERRING's calculation [23] the phonon mean free path depends on q as q^{-2} for longitudinal and q^{-1} for transverse modes, respectively.

4. The electron distribution is spherical.

5. Phonon—phonon scattering determines the mean free path in the center layer only.

The coordinate system is shown in Fig. 5. Then after suitable substitutions and considering the geometrical situation (see [12]) the authors obtained an integral in the following form:

$$\frac{E_2}{E_1} \sim P_x \sim \int_0^1 \int_0^{\pi/2} \exp\left(-\frac{ax}{\cos\vartheta}\right) x^s \sin^3\vartheta \, dx \, d\vartheta \,, \tag{2}$$

where $s = 1/2$ for longitudinal and $s = 2$ for transverse branches, respectively. The quantity $a = w/L_0$ and L_0 is the mean free path of phonons with cut-off (maximum) wave number. This integral has been solved by us for the case of

longitudinal phonons. The normalized (at $w = 0$, $F_{(a)} = 1$) formula is given in the Appendix (A1). Possessing no thin samples we could not judge whether longitudinal or transverse phonons are present in our case. Thus by applying formula (A1) and the curve fitting analysis detailed in [12] we just show the temperature dependence of L_0 in Fig. 6 assuming that we are dealing with longitudinal acoustic phonons. The curve has a similar character to that published in [12] for silicon.

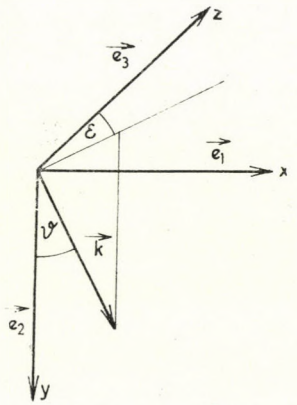


Fig. 5

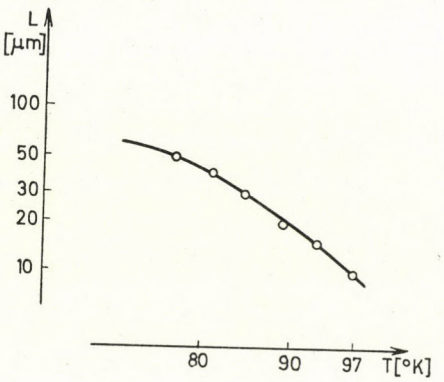


Fig. 6

5. General theory for evaluating phonon—phonon scattering coefficient from transmitted phonon drag measurements

The difficulty in establishing the phonon mean free path from these and from thermal conductivity measurements arises from the fact that the phonon distribution investigated depends upon the temperature and the length of the path travelled by the given phonon packet. The model proposed by us is an attempt to overcome the above complications. The simplifying assumptions used in our calculation are the following:

1. The Boltzman equation for electrons is solved using the relaxation time approximation in the case of a parabolic band.

2. The collisions of electrons with lattice vibrations are considered to be elastic and isotropic, i.e. the scattering probability equals to $\delta(k - k')/4\pi k'^2\tau_p$, where τ_p is the relaxation time for electrons determined by the lattice scattering only.

3. The generated non-equilibrium distribution of phonons does not undergo any change in the emitter.

4. All the phonon momenta arriving at the receiver layer are absorbed there and set up the E_2 electric field.

5. The excess phonon momentum decay caused by phonon—phonon interaction takes place only in the center p-layer. According to HERRING's [20, 23] calculations the relevant phonons are predominantly longitudinal acoustic ones and their mean free path caused by the phonon—phonon relaxation only is of the form

$$L(q) = \frac{c_l}{A_l q^2 T^3}, \tag{3}$$

where c_l is the averaged sound velocity and A_l is called the phonon—phonon scattering constant.

6. Neglecting the slowly varying function in the denominator in the Brooks—Herring formula the relaxation time τ_i of electrons for impurity scattering in the emitter is proportional to k^3. Furthermore, we utilize the assumptions

$$\tau_p \sim k^{-1} \text{ and } \tau_p \gg \tau_i.$$

The transmission ratio can be written in the form:

$$\frac{E_2}{E_1} = \eta_{1(T)} H_{(w,T)}, \tag{4}$$

where $\eta_{1(T)}$ is a temperature dependent function and $H_{(w,T)}$ is that part of the phonon momentum dependent on the p-layer's thickness reaching the receiver layer. The spectral and directional distribution of relevant phonons must also be considered. The changed phonon distribution is calculated from the electron distribution perturbed by E_1. The coordinate system used is illustrated in Fig. 5. The equilibrium distribution function of electrons is

$$f_0 = n \left(\frac{\hbar^2}{2\pi m^* k_B T} \right)^{3/2} \exp \left(- \frac{\hbar^2 k^2}{2 m^* k_B T} \right) = G e^{-Fk^2} \tag{5}$$

and an approximate solution of Boltzmann equation, if only lattice scattering is taken into account, is:

$$\frac{f - f_0}{\tau_p} = - \frac{e E_1 \hbar}{k_B T m^*} k_x f_0 = C k_x f_0. \tag{6}$$

Thus, in the $\vec{k}$ wave number space the net number of electrons scattering out of a cell around a given $\vec{k}$ is expressed by the following integral in $\vec{k}$, space:

$$\int \frac{\delta(k-k')}{4\pi k'^2 \tau_p} (f - f_0)\, d^3 k' = C \int \frac{\delta(k-k')}{4\pi k'^2} k_x f_0\, d^3 k' . \tag{7}$$

At first sight the elimination of τ_p seems to be surprising. According to the solution of the Boltzmann equation, however, the number of excess electrons accumulating in a certain cell in the $\vec{k}$ space is inversely proportional to the probability of scattering from it. Since the number of net scatterings in unit time is proportional to the product of the quantity of excess electrons and the scattering probability, the above number does not depend on the scattering probability.

Supposing that a phonon with wave vector $\vec{q}$ is generated at the scattering of an electron from $\vec{k}$ into $\vec{k}'$, the crystal momentum conservation rule reads:

$$\vec{k} = \vec{k}' + \vec{q} . \tag{8}$$

Using (7) the total x component of phonon momentum imparted by the electrons in unit time is given by the integral:

$$P_x \sim \int\int \frac{\delta(k-k')}{4\pi k'^2} k_x q_x f_0\, d^3 k d^3 k' . \tag{9}$$

For our further purposes we transform the above (9) integral into an integral determined in the $\vec{k}$ and $\vec{q}$ space. Introducing polar coordinates into our previous system shown in Fig. 5 the components of phonon wave vectors are:

$$q_x = q \sin\vartheta \sin\varepsilon , \qquad q_y = q\cos\vartheta , \qquad q_z = q \sin\vartheta \cos\varepsilon . \tag{10}$$

In order to integrate over $\vec{k}$ at a fixed $\vec{q}$ value we introduce new polar coordinates as is shown in Fig. 7. The unit vector $\vec{e}_4$ coincides with $\vec{q}$, $\vec{e}_5$ is perpendicular to $\vec{e}_1$ and $\vec{e}_4$, and $\vec{e}_6$ is perpendicular to $\vec{e}_5$ and $\vec{e}_4$. The corresponding transformation formulae are:

$$\begin{aligned}
\vec{e}_4 &= \frac{1}{q}(q_x \vec{e}_1 + q_y \vec{e}_2 + q_z \vec{e}_5) , \\
\vec{e}_5 &= \frac{1}{\sqrt{q_y^2+q_z^2}} (-q_z \vec{e}_2 + q_y \vec{e}_1) , \\
\vec{e}_6 &= \frac{1}{q\sqrt{q_y^2+q_z^2}} [(q_y^2+q_z^2)\vec{e}_1 - q_x q_y \vec{e}_2 - q_x q_z \vec{e}_3] .
\end{aligned} \tag{11}$$

Fig. 8 illustrates the momentum conservation rule. Thus k' can be expressed by q and k.

$$k' = \sqrt{k^2+q^2-2qk\cos\Theta} \tag{12}$$

and taking into account the well-known property of δ function we obtain:

$$\delta(k-k') = \delta(k - \sqrt{k^2+q^2-2qk\cos\Theta}) = \frac{\delta\left(k-\frac{q}{2\cos\Theta}\right)}{2\cos^2\Theta}. \tag{13}$$

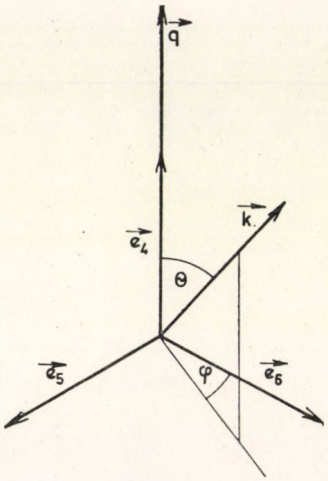


Fig. 7

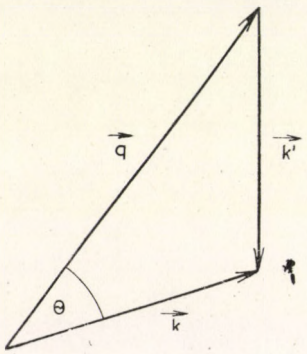


Fig. 8

Applying (10, 11, 12, 13) the integral (9) is of the form:

$$P_x = \int_{q=0}^{\infty}\int_{\vartheta=0}^{\pi}\int_{\varepsilon=0}^{2\pi}\int_{\Theta=0}^{\pi/2}\int_{\varphi=0}^{2\pi}\int_{k=0}^{\infty} \frac{\delta\left(k-\frac{q}{2\cos\Theta}\right) q\sin\vartheta\sin\varepsilon}{8\pi\cos^2\Theta\,(k^2+q^2-2kq\cos\Theta)} \times$$

$$\times(k\cos\Theta\sin\vartheta\sin\varepsilon + k\sin\Theta\cos\varphi)\sqrt{\cos^2\vartheta+\sin^2\vartheta\cos^2\varepsilon}\times \tag{14}$$

$$\times G[\exp - Fk^2]\,k^2\sin\Theta\,q^2\sin\vartheta\,dk\,d\varphi\,d\Theta\,d\varepsilon\,d\vartheta\,dq.$$

This (14) defined integral's value equals the x component of the force acting upon the electrons in unit volume i.e. — eE_xn as it should be in the stationary case. The transformed integral (14) is suitable for considering the filtering

and momentum-reducing effect of a layer with thickness w. If the phonon with wave number q has a mean free path of $L(q)$ the decay factor of

$$\exp\left[-\frac{w}{L\cos\vartheta}\right]$$

is to be put into the integrand (14) when calculating the x component of reduced momentum of the phonon beam reaching the receiver. Here, $w/(\cos\vartheta)$ is the effective length of the phonon path in the p-layer. The integration over ϑ is to be performed between the values of 0 and $\pi/2$ because of the sample geometry. Thus, we obtain for the phonon momentum arriving at the receiver in unit time

$$P_x = \frac{\pi}{8}\hbar CG\int_0^{\infty}\int_0^{\pi/2}\int_0^{\pi/2} q^4 \exp\left[-\frac{F q^2}{4\cos^2\Theta}\right]\times \\ \times\frac{\sin\Theta}{\cos^2\Theta}\exp-\frac{w}{L\cos\vartheta}\sin\vartheta\, d\vartheta\, d\Theta\, dq. \tag{15}$$

The integrations over $\vec{k}$, φ and ε have been executed and after elementary calculation we get:

$$P_x = \frac{\pi^{3/2}\hbar CG}{8F^{1/2}}\int_0^{\infty}\left[q^3\left(1-\Phi\left(\sqrt{\frac{Fq^2}{4}}\right)\right)\right]\left[\left(\frac{2}{3}+\frac{w}{6L}-\frac{w^2}{6L^2}\right)\times\right. \\ \left.\times\exp\left(-\frac{w}{L}\right)+\left(\frac{w}{L}-\frac{w^3}{6L^3}\right)E_i\left(-\frac{w}{L}\right)\right]dq. \tag{16}$$

Substituting (3) into the integral (16) and performing the integration we obtain:

$$P_x = -\frac{1}{2}eE_x nH(\xi), \quad \text{where} \quad \xi = \frac{8A_l m^* k_B T^4 w}{\hbar^2 C_l} \tag{17}$$

and the analytical form for $H(\xi)$ is given in the Appendix (A2). The main result of our calculation is that H depends only on the quantity of wT^4. The theoretical $H(\xi)$ shows surprisingly good agreement with our experimental results. Without going into further details it should be pointed out that in the low temperature interval investigated the ionized impurity scattering with τ_i relaxation time plays a more predominant role than the lattice scattering in the heavily doped n-type emitter layer — assumption (6) has to be considered.

In the integrand of (7) τ_p cannot be eliminated because the electron distribution is mainly influenced by τ_i, while the phonon generation is again proportional to τ_p^{-1}. We have a new factor in (7):

$$\frac{\tau_i}{\tau_i+\tau_p} \approx \frac{\tau_i}{\tau_p} . \tag{18}$$

Employing the assumption (6) and formula (18) we obtain instead of (9) an integral:

$$\iint \frac{\delta(k-k')}{4\pi k'^2} k_x q_x f_0 k^4 d^3 k' d^3 k . \tag{19}$$

Applying the transformation formulae (10, 11, 12, 13) and making similar steps as made in calculation of $H(\xi)$ we obtain defined integrals (A3, A4) and the transmission ratio is of the form:

$$\frac{E_2}{E_1} = \eta_2(T) S(\xi) . \tag{20}$$

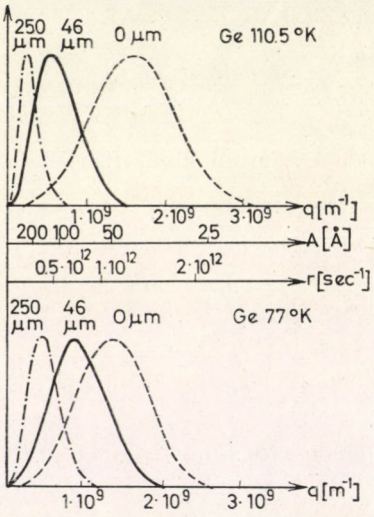


Fig. 9

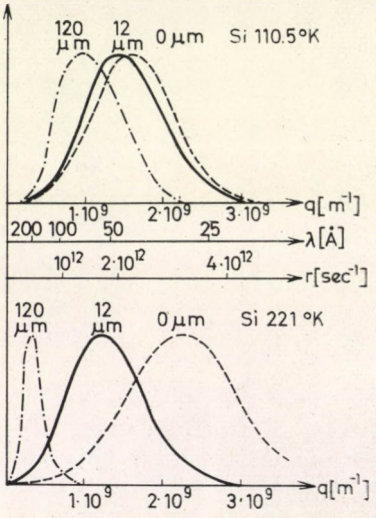


Fig. 10

The analytical form of $S(\xi)$ function is of (A5). When evaluating integral (19) for P_x an integral similar to (16) is obtained. This integrand appears to be the spectral function of the non-equilibrium relevant phonons with respect to the wave number. They are plotted in Fig. 9 for Ge and Fig. 10 for Si at various temperatures and sample thicknesses. The maxima of distributions are at 0.2—0.3 k_BT. Though the assumptions (2, 5) do not hold for such energies, (HERRING's [23] calculation is valid up to about 0.15 k_BT only), it does not cause any great deviation from this theory comparing it with our measurement results as will be seen further on. Plotting the E_2/E_1 data versus wT^4, both in logarithmic scale, we obtain four curves for the four sample

thicknesses. When fitting the theoretical $S(\xi)$ with this experimental curve the horizontal translation gives the quantity of $A_i\, m_n/m$. The different phonon—phonon scattering coefficient values A_l obtained from

i) transmitted phonon drag [12 and present paper]
ii) low temperature anomaly of thermopower [3, 4, 20]
iii) thermal conductivity measurements [19]

are presented in Table I.

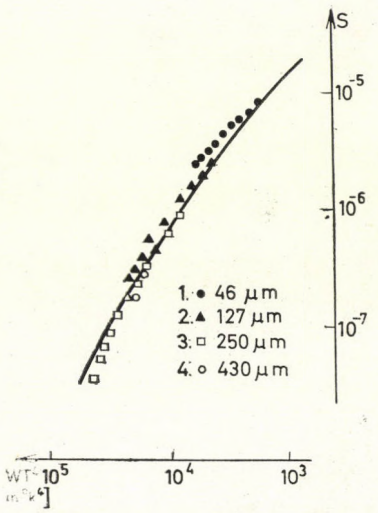


Fig. 11

Table I

	Ge	Si
transmitted phonon drag $A_l \frac{m_n}{m}$	$1.8 \cdot 10^{-12}$	$3.1 \cdot 10^{-13}$
thermopower $A_l \frac{m_n}{m} \frac{1}{f_l^*}$	$3.6 \cdot 10^{-12}$	$6.2 \cdot 10^{-13}$
thermal conductivity A_l	$1.67 \cdot 10^{-12}$	$1.44 \cdot 10^{-12}$

* f_l is a value near to unity

The data fitting for Ge are illustrated in Fig. 11 while the similar correspondence for silicon (employing [12] measured data) is shown in Fig. 12. They show good agreement with our theory. We can conclude that phonons taking part in transmitted phonon drag effect are predominantly longitudinal acoustic ones over the whole temperature interval in measurements of the authors of [12]. The same conclusion can be drawn on our measurement in the mentioned

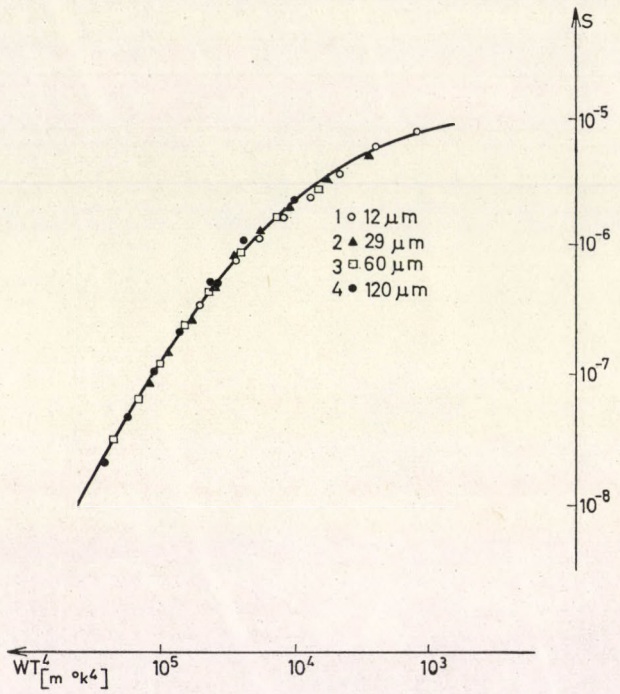


Fig. 12

temperature interval. Our approximation does not make it possible to choose m_r/m values with proper accuracy. As the case may be knowing that $(m_n/m)_{Ge} < (m_r/m)_{Si}$ our evaluation shows that the mean free path of long wavelength longitudinal phonons in silicon is longer than that in germanium.

6. Relevant phonon-plane type defect interaction

A family of transmitted phonon drag experiments has been used to investigate anharmonic damping of relevant phonons owing to their interactions with vibrations localized to certain crystalline plane defects.

In [14] the role of a low angle grain boundary sited in the middle layer of silicon samples was discussed. Marked reducing effect on the transmission ratio was observed in samples with dislocation row. The mobility of dislocations was so high that relevant phonons made them oscillate. On increasing the phonon path up to the grain boundary the phonon distribution maximum shifted towards the longer wavelength and greater attenuation was observed. The authors came to the conclusion that phonon scattering by dislocations increases with the phonon wavelength. However, on copper diffusion along the dislocations, the E_2/E_1 ratio increased corresponding to the immobilizing effect of copper precipitations on the dislocations.

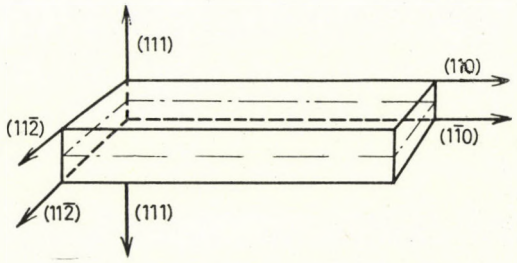


Fig. 13

We performed transmitted phonon drag measurements in Ge crystals with a twin boundary in the middle p-layer at liquid N_2 temperature. The geometry of samples used in our examinations is shown in Fig. 13. The cross-section of the [211] plane which is of importance in phonon propagation is shown in Fig. 14, symbolizing three atomic layers behind each other: the first by full, the second by lined, the third by empty circles. Control samples containing no twin boundaries but having the same dimensions and orientation were also measured. For samples with twin boundaries we obtain $E_2/E_1 = 0.5 \times 10^{-4}$ and for control samples $E_2/E_1 = 10^{-4}$. The accuracy of our measurements is better than 10%.

There are two possible explanations for this observed reduction of transmission ratio in specimens with twin boundaries. There is a large density of local phonon modes near a plane defect [25] and an interaction between relevant phonons and localized phonons takes place near the boundary and this decreases the relevant phonon momentum propagating towards the receiver layer. The second interpretation is that the relevant phonons are scattered by the boundary owing to the abrupt local change of interatomic potential but there is no phonon—phonon interaction, i.e. this phenomenon can be described within the framework of harmonic approximation. By comparing the relevant phonon wavelength to the dimensions of a twin boundary which

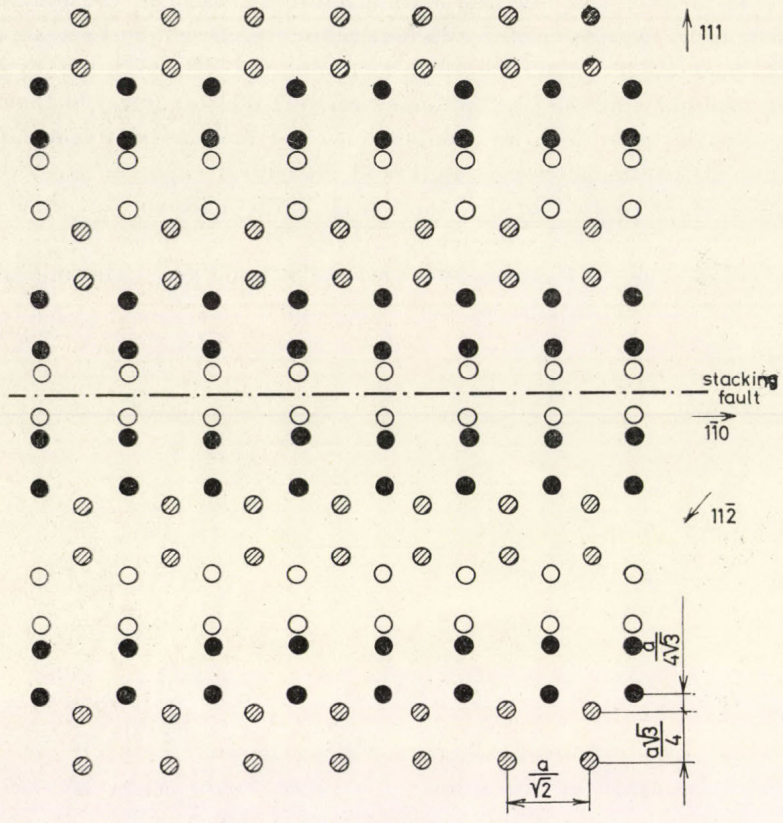


Fig. 14

extends up to a few lattice spacings it can be seen that the second interpretation is not very probable as was established by ZIMAN [26]. Thorough investigation showed, however, that it was not just one but a whole set of stacking faults that were located in the center layer. A set of stacking faults may cause various "optical" effects and not knowing the details of its structure we chose relevant phonon-free surface interaction as a subject for our investigation. This kind of experiment can yield information on bulk-phonon—surface-phonon interaction. Two possible processes can take place at a free surface:

i) Simple spectacular reflection;

ii) Bulk phonons reaching the free surface may interact with thermal surface modes.

If the reflection is spectacular and if we could select the phonons with different polarizations, performing calculations for a diamond lattice, as has

already been done for the simple cubic case by LUDWIG and PICK [27] we should have obtained numerical relations between the matrix elements of the atomic force constants near the disturbed surface region. It is very important to possess information on the surface modes not only because in certain cases the influence on semiconductor properties like surface recombination [28] plays a considerable role but they determine the physical properties of powders as well. In our opinion such experiments can generally be regarded as the first step to the investigation of heat transfer between two different materials.

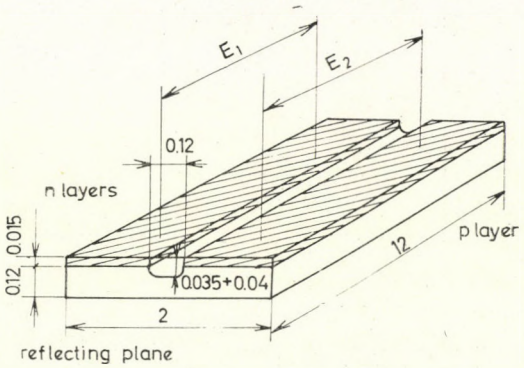


Fig. 15

The geometry of our samples is shown in Fig. 15. The dimensions are given in millimeters. The technology of their preparation is similar to that described in Section 2 except for the groove. They were made by masked etching. The reflector surface was polished both mechanically and chemically. In the reflection measurements the samples were at liquid N_2 temperature.

Phonons generated in one of the n-layers traverse into the p-layer. Some phonons reach the free surface of the p-layer where the phonon—free-surface interaction takes place. If reflection occurs the phonon "beam" is directed towards the detection n-layer. Fig. 16 shows the reflected phonon signal E_2 vs the input field. The full line represents the output E_2 in the presence of reverse bias, and the dotted line in its absence. We have already referred to this fact in Section 3.

In the course of our work R. GERETH and K. HÜBNER published similar investigations for silicon [16]. They outlined the development of "phonon optics" by such experiments. Their detailed experimental analysis showed that the quality of the surfaces of n-layers of samples used in transmitted phonon drag experiments strongly affected the magnitude of the E_2/E_1 transmission ratio as had been predicted by SHOCKLEY [11]. Direct evidence of phonon reflection was established by them on sample arrangements similar

to our specimens. Our work originally aimed at clarifying the problem whether anharmonic effects play pa redominant role in relevant phonon — free surface interactions. Samples with geometry illustrated in Fig. 17 were prepared in order to obtain the reflection coefficient of a free surface. The transmitted

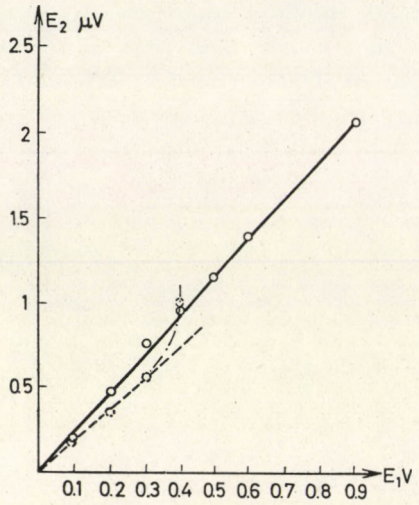


Fig. 16

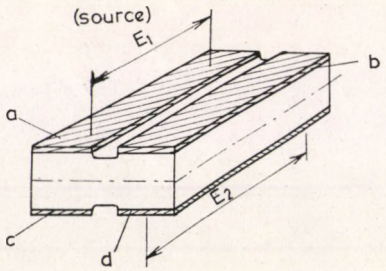


Fig. 17

phonon drag signals in these samples were measured in a diagonal direction. The reflection coefficient is a measure of the anharmonic damping taking place at the free surface. The dimensions and geometry of samples were chosen so that in these samples the length of the phonon path in a diagonal direction is equal to the reflected phonons in samples with a reflector plane. The only difference between E_2/E_1 ratios, if any, might be caused by the phonon surface interaction. Thus, the ratio of the transmission ratios of these two sample

groups gives the reflection coefficient. Five samples were measured from each of the two series and the average results are:

$$E_2/E_{1\,\text{reflection}} = 1.6\times10^{-6} \pm 0.4\times10^{-6},$$
$$E_2/E_{1\,\text{transmission}} = 2.1\times10^{-6} \pm 0.7\times10^{-6},$$

i.e. there is no significant difference between the two series of samples. Owing to the large error limits, the anharmonic effect could not be detected by this experiment. It is probable that anharmonic effects do not play any important role, i.e. the phonon reflection is mainly spectacular.

One would have expected the relevant thermal phonons to interact with thermally excited surface waves. There is a wider variety of interactions at the surface than in the mass because the vertical momentum component does not need to be conserved in such interactions.

A. A. MARADUDIN [29] has made calculation on bulk transverse phonons controlled surface wave mean free path. Similar calculations for longitudinal bulk phonons have not been performed so far.

Acknowledgements

Acknowledgements are due to Dr. G. SZIGETI, Director of the Institute and to Dr. G. GERGELY, Head of the Semiconductor Department for their valuable interest.

The authors are highly indebted to F. BELEZNAY, T. GESZTI and L. GUTAI for helpful discussions. Acknowledgements are due to B. PŐDÖR for the sample qualification measurements and to Miss MÉSZÁROS and Mrs. MIKLÓSSY for the careful sample preparation, to K. CSEPI and A. TÓTH for performing one part of the phonon mean free path measurements. Thanks are due to Miss FOGARASI for drawing the figures.

Appendix

All the determined integrals contained in our article were deduced to tabulated integrals [30, 31]. Here we present the explicit formulae related to in the text:

$$F(a) = \int_0^1 \int_0^{\pi/2} e^{-\frac{ax}{\cos\vartheta}} \sin^3\vartheta x^{1/2}\, d\vartheta\, dx =$$

$$= \frac{44}{135} e^{-a} - \frac{8}{45}\frac{e^{-a}}{a} + \frac{1}{27} a\, e^{-a} - \frac{1}{27} a^2 e^{-a} +$$

$$+ \left(\frac{2a}{5} - \frac{a^3}{27}\right) E_i(-a) - \frac{4}{45}\frac{\sqrt{\pi}}{a^{3/2}} \Phi(\sqrt{a}).$$

$$E_i(-x) \quad \text{and} \quad \Phi(x) \text{ are defined in [30].} \tag{A1}$$

From integral (16) and using formula (3) the following integral can be derived:

$$\begin{aligned} H(\xi) = \frac{4}{3}\xi^{-3/2}\int_0^\infty [1-\Phi(\xi^{-1/2}u)]\left\{(4u^3+u^5-u^7)e^{-u^2}+(6u^5-u^9)E_i(-u^2)\right\}du = \\ = \frac{1}{120\xi^2(1+\xi)^{9/2}}(-64-288\xi-384\xi^2+790\xi^3+3165\xi^4+ \\ +2631\xi^5-2638\xi^6-6204\xi^7-4095\xi^8-945\xi^9)- \\ -\left[\ln\frac{1+\sqrt{\xi+1}}{\sqrt{\xi}}\right]\frac{600\xi-945\xi^3}{120}+\frac{8}{15}\xi^{-2}. \end{aligned} \tag{A2}$$

When taking into account the impurity scattering we obtain from integral (19) similarly to the derivation of (45):

$$\begin{aligned} P_x = -\frac{\pi}{8}\hbar CGAT\cdot\int_{q=0}^{\infty}\int_0^{\pi/2}\int_0^{\pi/2} q^4\exp\left[-\frac{Fq^2}{4\cos^2\Theta}\right]\sin^3\vartheta\exp\times \\ \times\left[\frac{-w}{L\cos\vartheta}\right]\frac{q^4}{16\cos^4\Theta}\,d\vartheta\,d\Theta\,dq. \end{aligned} \tag{A3}$$

After differentiating (15) with respect to F we can easily see that $S(\xi)$ satisfies the following equation:

$$S(\xi) = H(\xi) + \frac{4}{7}\xi\frac{dH(\xi)}{d\xi} + \frac{4}{35}\frac{\xi^2 dH^2(\xi)}{d\xi^2}. \tag{A4}$$

Further we obtain from (A2):

$$\begin{aligned} S(\xi) = \frac{1}{4200\xi^2(1+\xi)^{13/2}}(-1216-7904\xi-17\,536\xi^2+ \\ +38\,746\xi^3+275\,759\xi^4+433\,969\xi^5-235\,909\xi^6- \\ -1\,700\,711\xi^7-2\,520\,979\xi^8-1\,863\,741\xi^9-712\,215\xi^{10}- \\ -112\,455^{11})+\left[\ln\frac{1+\sqrt{1+\xi}}{\sqrt{\xi}}\right]\frac{7497\xi^3-2200\xi}{280}+\frac{152}{525}\xi^{-2}. \end{aligned} \tag{A5}$$

REFERENCES

1. H. P. R. FREDERIKSE, Phys. Rev., **91,** 491, 1953.
2. C. HERRING, Semiconductors and Phosphors (Interscience Publishers, Inc. New York, 1958) p. 184.
3. T. H. GEBALLE and G. W. HULL, Phys. Rev., **98,** 940, 1955.
4. T. H. GEBALLE and G. W. HULL, Phys. Rev., **94,** 1134, 1954.

5. H. P. R. Frederikse and E. Mielczarek, Phys. Rev., **99,** 1889, 1955.
6. S. M. Puri and T. H. Geballe, Phys. Rev., **136,** 1767, 1964.
7. И. Н. Тимченко и С. С. Шалыт, ФТТ, **4,** 934, 1962.
8. O. V. Emelyanenko et al., phys. stat. sol., **12,** K89, 1965.
9. K. Morikawa, J. Phys. Soc. Japan, **20,** 786, 1965.
10. A. R. Hutson, J. Appl. Phys., **32,** 2287, 1961.
11. W. Shockley, Structure and Properties of Thin Films, Ed. by C. A. Neugebauer et al. (John Wiley and Sons, Inc. New York 1959), p. 326.
12. R. Gereth and K. Hübner, Phys. Rev., **134,** A235, 1964.
13. Z. Bodó, B. Rősner and T. Sebestyén, Phys. Letters, **29A,** 191, 1969.
14. K. Hübner and W. Shockley, Proceedings of the International Conference on Physics of Semiconductors, Exeter (The Institute of Physics and Physical Society, London, 1962), p. 157.
15. B. Rősner et al., phys. stat. sol., **15,** K127, 1966.
16. R. Gereth and K. Hübner, Solid State Electronics, **10,** 935, 1967.
17. Z. Bodó, B. Rősner and T. Sebestyén, Proceedings of the International Conference on the Physics of Semiconductors, Moscow (Publishing House "Nauka", Leningrád, 1968), p. 686.
18. E. J. Walker and R. W. Keyes, Phys. Rev. Letters, **12,** 217, 1964.
19. M. G. Holland, Phys. Rev., **132,** 2461, 1963.
20. C. Herring, Phys. Rev., **96,** 1163, 1954.
21. G. Nyerges et al., Acta Phys. Hung., **18,** 299, 1965.
22. R. Gereth et al., Solid State Electronics, **8,** 789, 1965.
23. C. Herring, Phys. Rev., **95,** 954, 1954.
24. H. J. McSkimi, J. Appl. Phys., **24,** 988, 1956.
25. А. М. Косевич и В. И. Хохлов, ФТТ, **10,** 56, 1968.
26. J. M. Ziman, Electrons and Phonons (Oxford: Clarendon Press) p. 239, 1960.
27. W. Ludwig and H. Pick, phys. stat. sol., **19,** 313, 1967.
28. J. D. Vagner, et al., phys. stat. sol., **31,** 481, 1969.
29. D. L. Mills and A. A. Maradudin, Bull. Am. Phys. Soc. Ser. II. **13,** 450, 1968.
30. I. M. Ryshik and I. S. Gradstein, Tables of series products and integrals (VEB Deutscher Verlag der Wissenschaften, Berlin, 1957).
31. Jahnke—Emde—Lösch: Tables of higher functions (B. G. Teubner Verlag, Stuttgart, 1960).

ИЗМЕРЕНИЕ ФОНОННОЙ ТЯГИ В Ge

Б. РЭЗНЕР, З. БОДО, Т. ШЕБЕШТЕН и Б. ВОН

Резюме

Описывается эффект фононной тяги в германии, (который основывается на определенном фононно-электронном взаимодействии при низких температурах). В работе содержится: а) вывод параметров фонон-фононного рассеяния; б) исследование отражения фононов на свободной поверхности; в) сообщаются также экспериментальные результаты влияния двойной границы на распространение фононов.

Acta Physica Academiae Scientiarum Hungaricae, Tomus 29 (1), pp. 67–74 (1970)

POTENTIAL CURVES FOR ONE-ELECTRON HETERONUCLEAR DIATOMIC SYSTEMS IN ONE-CENTER TREATMENT

By

I. TAMÁSSY-LENTEI

INSTITUTE OF THEORETICAL PHYSICS, KOSSUTH LAJOS UNIVERSITY, DEBRECEN

(Received 31. VII. 1969)

Calculations were carried out for the heteronuclear diatomic systems HeH^{++}, LiH^{3+}, HBe^{4+}, $HeLi^{4+}$, $HeBe^{5+}$, $LiBe^{6+}$, LiB^{7+} in the $1s\sigma$ and $2p\pi$ unstable states with one-center one-electron analytic trial wave functions. The total energy values, as a function of the internuclear distance R, are improved by the variation of the center of the wave function.

In quantum chemistry extensive investigations have been carried out with one of the simplest possible methods, the one-center method or united atom model. Detailed calculations have so far been found primarily for high-symmetry molecules of type X_2, XH_n ($n = 2, 3, 4$), as well as for the XH hydrides of the first two rows of the periodic system [1]. In these cases the choice of the centre for symmetry reasons is fairly natural; the expansion centre of the wave function has been, as a rule, coincident with the symmetry center or the heavier nucleus, respectively.

Two-center one-electron problems can be easily solved in both homonuclear and heteronuclear cases, although they require considerable numerical work. With this method for the ground- and 4 lower excited states of HeH^{++} accurate data have been given by BATES and CARSON [2], and so other values, obtained by approximate methods can be compared with these.

Although, when using the one-center method for diatomic hydrides XH with a not too low atomic number for X, the choice of the heavier nucleus X as center has proved to be correct. Results can be improved, however, according to [3], for the HeH^{++} one-electron system by shifting the center from the He nucleus, since treating the coordinate of the center as a variation parameter indicates the origin to be a point different from He. In the above case the $1s\sigma$ ground state was described by a single hydrogen-like $1s$ function as molecular orbital, the $2p\pi$ excited state by a hydrogen-like $2p$ function, in the exponents with variation parameters α and β, respectively.

The position of the center may be significant in the united atom model. This can be seen, e.g. in a special form of the one-center treatment, in the method of the partial waves theory. With a series of partial waves RABINOVICH [4] made calculations for HeH^{++}, choosing the charge center as the expansion point of the wave-function.

Table I contains the total energy values obtained after the numerical solution of the radial Schrödinger equation, in the ground state, in the zeroth, first and second order approximation obtained as a function of the internuclear distance R, together with the energies calculated with the one-term one-center functions centered on He ($x = 0$) and centered on an arbitrary point ($x \neq 0$), respectively, and together with the exact values (all data are given henceforth in atomic units). According to Table I, the convergence of expansion would surely be faster if instead of choosing the charge center, as expansion center, quite obviously from the physical point of view, in the homonuclear diatomic molecule cases, the expansion center were to be determined by way of variation. The location of the center, especially for great internuclear distances is seen to be far from the charge center. So the position of the expansion center has an influence on the accuracy of the energy value of the ground state, unless a large number of terms is kept in the series expansion. This is even more valid for the excited state.

With the united atom model the location of the center can be significant for other small diatomic problems, too. Thus, further investigations have been made on several one-electron diatomic heteronuclear systems, which, owing to the lack of nuclear symmetry, seem less suitable for one-center calculations. The systems under study were: LiH^{3+}, HBe^{4+}, $HeLi^{4+}$, $HeBe^{5+}$, $LiBe^{6+}$, LiB^{7+}. Energy calculations were made for these systems for the $1s\sigma$, the lowest σ state which is the ground state, and the $2p\pi$, the lowest π state. For the systems given above these states are unstable, and the energy curves have no minima.

Table I

Values (in atomic units) for HeH^{++} in the ground state

R	$E^{a}_{(0)}$	$E^{b}_{(1)}$	$E^{c}_{(2)}$	E^{d}	E^{e}	E^{f}_{exact}
0.5	0.4244	0.39075	0.3434	0.47574	0.42668	0.33445
1.0	—0.79155	—0.89475	—0.9976	—0.94872	—0.96332	—1.03335
2.0	—0.94475	—1.16285	—1.34755	—1.49919	—1.50063	—1.51219
3.0	—0.83585	—1.1022	—1.3293	—1.66665	—1.66694	—1.66882
4.0	—0.7792	—1.0047	—1.24655	—1.74999	—1.75009	—1.7506

[a] zeroth order energy from [4]
[b] first order energy from [4]
[c] second order energy from [4]
[d] on He centered ($x = 0$) one-center value from [3]
[e] on arbitrary point centered ($x \neq 0$) one-center value from [3]
[f] exact value from [2]

The trial wave function was, this time too, chosen as $1s$ and $2p$ hydrogen-like type, with parameters α and β, respectively, in the exponents. The energy values obtained with these simple one-term functions are given as a function of the internuclear distance R in Tables II and III, for the cases when they are centered on the heavier nucleus ($x = 0$) and when centered on an arbitrary point ($x \neq 0$). In addition to the above mentioned heteronuclear molecules, for the sake of completeness, the data obtained for HeH^{++} in [3] are also included.

For the simplest heteronuclear two-center systems, HeH^{++}, for the states $1s\sigma$ and $2p\pi$, too, besides the work of BATES and CARSON, there are other possibilities for comparison in papers [5] and [6]. Calculations concerning further systems, however, can only be found in the works of WILSON [7] and WILSON and GALLUP [8]. In addition to HeH^{++}, they have considered the lower lying σ states of heteronuclear systems LiH^{3+}, and $HeLi^{4+}$, by numerically solving the Schrödinger equation for several internuclear distance values. Their calculations can be regarded as exact. Thus, for the cases mentioned above comparisons are possible. Calculated or experimental data for the HBe^{4+}, $HeBe^{5+}$, $LiBe^{6+}$, LiB^{7+} systems, further for the $2p\pi$ excited states are not available. With the very easily manageable one-term analytic wave function corresponding to the united atom, reasonable results can be obtained for heteronuclear diatomic systems even in the case of low atomic number nuclei, and the variation of the center is very important to achieve this. This holds particularly for small internuclear distances and for excited states. (In $2p\pi$ state the center is always further from the heavier nucleus than in the ground state.) For the cases $R = 0$ and $R = \infty$ the one-term one-center function is the exact solution of the problem and so shows full agreement with the exact values. The free variation of the center is obviously increasingly significant as the atomic number is lowered and there is no great difference in the charges of the two nuclei. So, of all the cases under study, it is most effective, for HeH^{++}.

Quite naturally, the variation of the center is significant only with simple trial functions. When taking too many configurations into account, the position of the center is of no interest. However, in a great number of cases of practical interest, convergence can be accelerated by the choice of an appropriate center.

Table II

Values (in atomic units) for HeH^{++}, LiH^{3+}, HBe^{4+}, $HeLi^{4+}$, $HeBe^{5+}$, $LiBe^{6+}$, LiB^{7+} in the $1s\sigma$ state

R	HeH^{++}	LiH^{3+}	HBe^{4+}	$HeLi^{4+}$	$HeBe^{5+}$	$LiBe^{6+}$	LiB^{7+}
0.5	$x = 0$	$= 0$	$= 0$	$= 0$	$= 0$	$= 0$	$= 0$
	$\alpha = 2.33$	$= 3.17$	$= 4.09$	$= 3.29$	$= 4.16$	$= 4.23$	$= 5.11$
	$E_0 = 0.47574$	$= -0.26839$	$= -1.894$	$= 3.93619$	$= 4.20508$	$= 10.2984$	$= 11.6347$
	$x = 0.065$	$= 0.022$	$= 0.009$	$= 0.051$	$= 0.02$	$= 0.032$	$= 0.014$
	$\alpha = 2.33$	$= 3.17$	$= 4.08$	$= 3.28$	$= 4.14$	$= 4.18$	$= 5.08$
	$E_x = 0.42668$	$= -0.29472$	$= -1.90801$	$= 3.8197$	$= 4.14673$	$= 10.1595$	$= 11.5637$
	$E_{ex} = 0.33445$						
	$E_w = 0.33446$	$= -0.37801$		$= 3.42728$			
1.0	$x = 0$	$= 0$	$= 0$	$= 0$	$= 0$	$= 0$	$= 0$
	$\alpha = 2.08$	$= 3.02$	$= 4$	$= 3.04$	$= 4.01$	$= 4.01$	$= 5$
	$E_0 = -0.94872$	$= -2.49022$	$= -4.99832$	$= -0.48076$	$= -1.99665$	$= 1.00499$	$= -0.49918$
	$x = 0.039$	$= 0.0091$	$= 0.003$	$= 0.019$	$= 0.0061$	$= 0.0093$	$= 0.0037$
	$\alpha = -2.07$	$= 3.01$	$= 4$	$= 3.02$	$= 4$	$= 4$	$= 5$
	$E_x = -0.96332$	$= -2.49442$	$= -4.99977$	$= -0.49817$	$= -2.00255$	$= 0.99149$	$= -0.50469$
	$E_{ex} = -1.03335$						
	$E_w = -1.03336$	$= -2.52098$		$= -0.65096$			
2.0	$x = 0$	$= 0$	$= 0$	$= 0$	$= 0$	$= 0$	$= 0$
	$\alpha = 2.01$	$= 3$	$= 4$	$= 3$	$= 4$	$= 4$	$= 5$
	$E_0 = -1.49919$	$= -3.49997$	$= -6.49999$	$= -2.49995$	$= -4.99999$	$= -3.49999$	$= -6.49999$
	$x = 0.012$	$= 0.0023$	$= 0.00073$	$= 0.0051$	$= 0.0015$	$= 0.0022$	$= 0.0009$
	$\alpha = 2$	$= 3$	$= 4$	$= 3$	$= 4$	$= 4$	$= 5$
	$E_x = -1.50063$	$= -3.50027$	$= -6.50009$	$= -2.50113$	$= -5.00036$	$= -3.50083$	$= -6.50033$
	$E_{ex} = -1.51219$						
	$E_w = -1.51217$	$= -3.50204$		$= -2.50938$			

3.0	$x = 0$	$= 0$	$= 0$	$= 0$	$= 0$	$= 0$	$= 0$
	$\alpha = 2$	$= 3$	$= 4$	$= 3$	$= 4$	$= 4$	$= 5$
	$E_0 = -1.66665$	$= -3.83333$	$= -6.99999$	$= -3.16666$	$= -5.99999$	$= -4.99999$	$= -8.49999$
	$x = 0.005$	$= 0.001$	$= 0.00033$	$= 0.0021$	$= 0.00065$	$= 0.001$	
	$\alpha = 2$	$= 3$	$= 4$	$= 3$	$= 4$	$= 4$	
	$E_x = -1.66694$	$= -3.83339$	$= -7.00001$	$= -3.16689$	$= -6.00007$	$= -5.00016$	
	$E_{ex} = -1.66882$						
	$E_w = -1.66851$	$= -3.8337$		$= -3.16815$			
4.0	$x = 0$	$= 0$	$= 0$	$= 0$	$= 0$	$= 0$	$= 0$
	$\alpha = 2$	$= 3$	$= 4$	$= 3$	$= 4$	$= 4$	$= 5$
	$E_0 = -1.74999$	$= -3.99999$	$= -7.24999$	$= -3.49999$	$= -6.49999$	$= -5.74999$	$= -9.49999$
	$x = 0.003$	$= 0.0006$		$= 0.0012$	$=$	$= 0.0006$	
	$\alpha = 2$	$= 3$		$= 3$		$= 4$	
	$E_x = -1.75009$	$= -4.00001$		$= -3.50007$		$= -5.75005$	
	$E_{ex} = -1.7506$						
	$E_w = -1.7506$	$= -4.0001$		$= -3.50045$			
5.0	$x = 0$	$= 0$	$= 0$	$= 0$	$= 0$	$= 0$	$= 0$
	$\alpha = 2$	$= 3$	$= 4$	$= 3$	$= 4$	$= 4$	$= 5$
	$E_0 = -1.8$	$= -4.09999$	$= -7.39999$	$= -3.69999$	$= -6.79999$	$= -6.19999$	$= -10.0999$
	$x = 0.0019$						
	$\alpha = 2$						
	$E_x = -1.80003$						
	$E_{ex} = -1.80023$						
	$E_w = -1.80023$	$= -4.10004$		$= -3.70017$			
6.0	$x = 0$	$= 0$	$= 0$	$= 0$	$= 0$	$= 0$	$= 0$
	$\alpha = 2$	$= 3$	$= 4$	$= 3$	$= 4$	$= 4$	$= 5$
	$E_0 = -1.83333$	$= -4.16666$	$= -7.5$	$= -3.83333$	$= -7$	$= -6.49999$	$= -10.49999$
	$E_w = -1.83344$	$= -4.16669$		$= -3.8334$			
∞	$x = 0$	$= 0$	$= 0$	$= 0$	$= 0$	$= 0$	$= 0$
	$\alpha = 2$	$= 3$	$= 4$	$= 3$	$= 4$	$= 4$	$= 5$
	$E = -2$	$= -4.5$	$= -8$	$= -4.5$	$= -8$	$= -8$	$= -12.5$

E_{ex}: values from [2]
E_w: values from [7], [8]

Table III

Values (in atomic units) for HeH^{++}, LiH^{3+}, HBe^{4+}, $HeLi^{4+}$, $HeBe^{5+}$, $LiBe^{6+}$, LiB^{7+} in the $2p\pi$ state

R	HeH^{++}	LiH^{3+}	HBe^{4+}	$HeLi^{4+}$	$HeBe^{5+}$	$LiBe^{6+}$	LiB^{7+}
0.5	x = 0	= 0	= 0	= 0	= 0	= 0	= 0
	β = 2.84	= 3.75	= 4.66	= 4.37	= 5.19	= 5.67	= 6.46
	E_0 = 2.91978	= 4.09653	= 5.04615	= 9.19014	= 11.9935	= 18.8648	= 23.3483
	x = 0.155	= 0.103	= 0.0707	= 0.182	= 0.131	= 0.19	= 0.141
	β = 2.87	= 3.78	= 4.68	= 4.49	= 5.28	= 5.85	= 6.56
	E_x = 2.9081	= 4.0812	= 5.0288	= 9.1113	= 11.9119	= 18.6527	= 23.1507
	E_{ex}= 2.90683						
1.0	x = 0	= 0	= 0	= 0	= 0	= 0	= 0
	β = 2.6	= 3.45	= 4.33	= 3.8	= 4.59	= 4.82	= 5.61
	E_0 = 0.99842	= 1.24232	= 1.27058	= 3.5648	= 4.51685	= 7.74489	= 9.44223
	x = 0.262	= 0.138	= 0.0761	= 0.285	= 0.154	= 0.259	= 0.138
	β = 2.64	= 3.46	= 4.33	= 3.84	= 4.59	= 4.79	= 5.61
	E_x = 0.97798	= 1.2239	= 1.25595	= 3.47957	= 4.4543	= 7.58957	= 9.33701
	E_{ex}= 0.97168						
2.0	x = 0	= 0	= 0	= 0	= 0	= 0	= 0
	β = 2.3	= 3.16	= 4.08	= 3.29	= 4.16	= 4.22	= 5.13
	E_0 = 0.12921	=—0.05092	=—0.45484	= 1.01757	= 1.08868	= 2.63075	= 2.96233
	x = 0.309	= 0.106	= 0.0424	= 0.225	= 0.087	= 0.136	= 0.06
	β = 2.29	= 3.14	= 4.07	= 3.22	= 4.13	= 4.16	= 5.1
	E_x = 0.11357	=—0.058799	=—0.45876	= 0.98415	= 1.0728	= 2.59419	= 2.94395
	E_{ex}= 0.10035						

3.0	$x = 0$	$= 0$	$= 0$	$= 0$	$= 0$	$= 0$	$= 0$
	$\beta = 2.15$	$= 3.06$	$= 4.03$	$= 3.1$	$= 4.05$	$= 4.08$	$= 5.04$
	$E_0 = -0.11824$	$= -0.43432$	$= -0.98621$	$= 0.25552$	$= 0.027388$	$= 1.04082$	$= 0.90144$
	$x = 0.243$	$= 0.064$	$= 0.0234$	$= 0.131$	$= 0.046$	$= 0.07$	$= 0.03$
	$\beta = 2.13$	$= 3.05$	$= 4.03$	$= 3.08$	$= 4.04$	$= 4.05$	$= 5.03$
	$E_x = -0.1263$	$= -0.43712$	$= -0.98732$	$= 0.24409$	$= 0.02299$	$= 1.03077$	$= 0.89692$
	$E_{ex} = -0.13767$						
4.0	$x = 0$	$= 0$	$= 0$	$= 0$	$= 0$	$= 0$	$= 0$
	$\beta = 2.08$	$= 3.03$	$= 4.01$	$= 3.07$	$= 4.02$	$= 4.03$	$= 5.02$
	$E_0 = -0.22782$	$= -0.61468$	$= -1.24415$	$= -0.10454$	$= -0.48834$	$= 0.26742$	$= -0.11378$
	$x = 0.172$	$= 0.041$	$= 0.0136$	$= 0.078$	$= 0.028$	$= 0.041$	$= 0.018$
	$\beta = 2.07$	$= 3.02$	$= 4.01$	$= 3.05$	$= 4.02$	$= 4.02$	$= 5.01$
	$E_x = -0.23179$	$= -0.61579$	$= -1.24455$	$= -0.109$	$= -0.48992$	$= 0.26386$	$= -0.11533$
	$E_{ex} = -0.23887$						
5.0	$x = 0$	$= 0$	$= 0$	$= 0$	$= 0$	$= 0$	$= 0$
	$\beta = 2.04$	$= 3.01$	$= 4.01$	$= 3.03$	$= 4.01$	$= 4.02$	$= 5.01$
	$E_0 = -0.2883$	$= -0.71968$	$= -1.397$	$= -0.31443$	$= -0.79401$	$= -0.19103$	$= -0.71925$
	$x = 0.123$	$= 0.026$	$= 0.0085$	$= 0.055$	$= 0.019$	$= 0.027$	$= 0.011$
	$\beta = 2.04$	$= 3.01$	$= 4.01$	$= 3.02$	$= 4.01$	$= 4.01$	$= 5.01$
	$E_x = -0.29033$	$= -0.72018$	$= -1.39716$	$= -0.31648$	$= -0.7947$	$= -0.19257$	$= -0.71994$
	$E_{ex} = -0.29422$						
6.0	$x = 0$	$= 0$	$= 0$	$= 0$	$= 0$	$= 0$	$= 0$
	$\beta = 2.03$	$= 3.01$	$= 4$	$= 3.02$	$= 4$	$= 4.01$	$= 5$
	$E_0 = -0.32648$	$= -0.78858$	$= -1.49826$	$= -0.45219$	$= -0.99692$	$= -0.4948$	$= -1.12166$
	$x = 0.089$	$= 0.0109$	$= 0.006$	$= 0.039$	$= 0.01$	$= 0.02$	$= 0.01$
	$\beta = 2.02$	$= 3.01$	$= 4$	$= 3.01$	$= 4$	$= 4.01$	$= 5$
	$E_x = -0.32759$	$= -0.78886$	$= -1.49834$	$= -0.45321$	$= -0.99692$	$= -0.49557$	$= -1.12196$
∞	$x = 0$	$= 0$	$= 0$	$= 0$	$= 0$	$= 0$	$= 0$
	$\beta = 2$	$= 3$	$= 4$	$= 3$	$= 4$	$= 4$	$= 5$
	$E = -0.5$	$= -1.125$	$= -2$	$= -1.125$	$= -2$	$= -2$	$= -3.125$

E_{ex} values from [2]

REFERENCES

1. For references see e.g. B. D. Joshi, J. Chem. Phys., **46**, 875, 1967; D. M. Bishop, Adv. Quant. Chem., **3**, 25, 1967.
2. D. R. Bates and T. R. Carson, Proc. Roy. Soc., **A234**, 207, 1956.
3. I. Tamássy-Lentei, Acta Phys. Chim. Debr., XI/IV, 5, 1965.
4. H. Rabinovich, J. Chem. Phys., **43**, 3144, 1965.
5. M. Cohen, R. P. Eachran and S. D. McPhee, Canad. J. Phys., **45**, 2231, 1967.
6. R. L. Matcha, W. D. Lyon and J. O. Hirschfelder, Canad. J. Phys., **46**, 1647, 1968.
7. L. Y. Wilson, Ph. D. thesis, University of Nebraska, 1964.
8. L. Y. Wilson and G. A. Gallup, J. Chem. Phys., **45**, 586, 1966.

ПОТЕНЦИАЛЬНЫЕ КРИВЫЕ ДЛЯ ОДНОЭЛЕКТРОННЫХ ГЕТЕРОЯДЕРНЫХ ДВУХАТОМНЫХ СИСТЕМ В ОДНОЦЕНТРОВОМ РАССМОТРЕНИИ

И. ТАМАШИ-ЛЕНТЕИ

Резюме

Проводятся вычисления для гетероядерных двухатомных систем HeH^{++}, LiH^{3+}, HBe^{4+}, $HeLi^{4+}$, $HeBe^{5+}$, $LiBe^{6+}$, LiB^{7+} в неустойчивых состояниях $1s\sigma$ и $2p\pi$ с помощью одноцентровых одноэлектронных аналитических пробных волновых функций. Значения полной энергии — как функция междуядерного расстояния R-улучшались варьировнием сосредоточивания волновой функции.

Acta Physica Academiae Scientiarum Hungaricae, Tomus 29 (1), pp. 75—78 (1970)

ENERGY DISTRIBUTION OF TRAPS IN GaP CRYSTALS

By

J. GYULAI

RESEARCH GROUP ON LUMINESCENCE AND SEMICONDUCTORS OF THE HUNGARIAN ACADEMY OF SCIENCES, SZEGED

(Received 31. VII. 1969)

Current-voltage characteristics in the [111] direction of slightly p-type GaP : Cu crystals were investigated. Temperature variations of the power dependence of current on voltage indicate the presence of two sets of traps having exponential distribution in energy. Because of the slight p-type conduction and Cu centres present, the interpretation of the characteristics was based on an ASHLEY—MILNES type [4] two-carrier model extended for the case of trapping.

Dark current density — voltage characteristics were investigated on thin (0.02—0.05 cm) slices of highly compensated and slightly p-type GaP : Cu crystals under d.c. conditions (Fig. 1) and with pulse measurements (5 cps, pulse length 2 msec, Fig. 2) at different temperatures. Slices had ohmic Sn : Zn contact on one side and slightly blocking Au contact on the other [1]. In both figures, two distinct regions are to be observed in the non-ohmic part of the curves.

After ROSE [2], taking an exponential distribution of traps, i.e. $N_t(E) = A\exp[-(E_c - E)/kT_c]$, into account, two characteristic temperatures can be calculated from lines of the lower-voltage region and from those of the high-voltage region (T_{c1} and T_{c2}). The intersection points of the lines [(V_{m1}, i_{m1}) and (V_{m2}, i_{m2})], on the analogy with the case treated by SUSSMAN [3], give the following results:

Sample	T_{c1} (°K)	T_{c2} (°K)	V_{m1} (volt)	V_{m2} (volt)	$kT_{c1}A_1$ (cm^{-3})	$kT_{c2}A_2$ (cm^{-3})
2/3—11	304	1150	9.0×10^5	8.0×10^5	1.1×10^{16}	1.0×10^{13}
2/3—12	296	770	6.3×10^6	8.1×10^3	3.5×10^{16}	4.5×10^{13}

The concentration of trap-system 1 is consistent with the Te concentration in our samples.

We recall that on the basis of our experiments an exponential distribution of shallow (Te) traps is to be concluded: the slopes belonging to this system ($T_{c1} \approx$ room temperature) increase with lower ambient temperatures.

Because of the slightly p-type conduction and the Cu centres present, it seems that the $i - V$ curves are to be explained on the basis of an ASHLEY and MILNES type injection [4]. Photoconductivity lifetimes ($\tau_n \approx 10^{-9}$—10^{-8}

sec) from [5] and ohmic relaxation times ($\tau_{p\Omega} \approx 10^{-4}$ sec at room temperature, $\approx 10^{-1}$ sec, at 175°K) calculated from reverse currents (Fig. 1, broken lines) give a reasonable explanation for the downward shift of the $i - V$ curves [6]. Thus, it seems that our experiments point to a double carrier mechanism with two sets of traps. With the Poisson equation and particle conservation equation

$$\frac{\varepsilon}{4\pi e}\frac{dE}{dx} \approx \delta p_r - n_t \tag{1}$$

and

$$\frac{1}{e}\frac{di_n}{dx} = \frac{n}{\tau_n} + r_{ct1} + r_{ct2} = -\frac{1}{e}\frac{di_p}{dx}$$

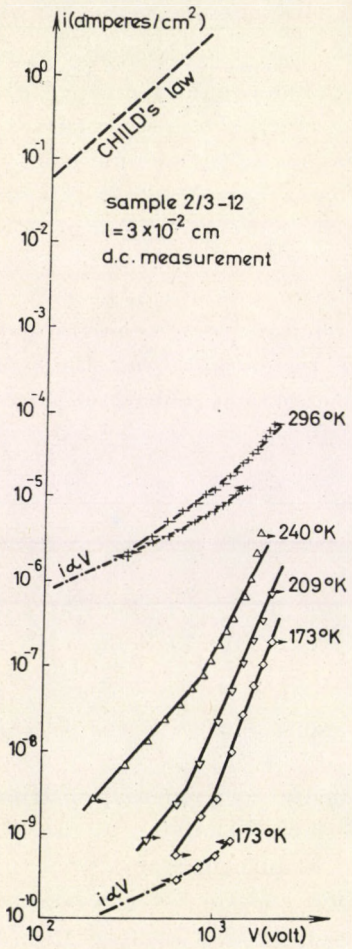


Fig. 1

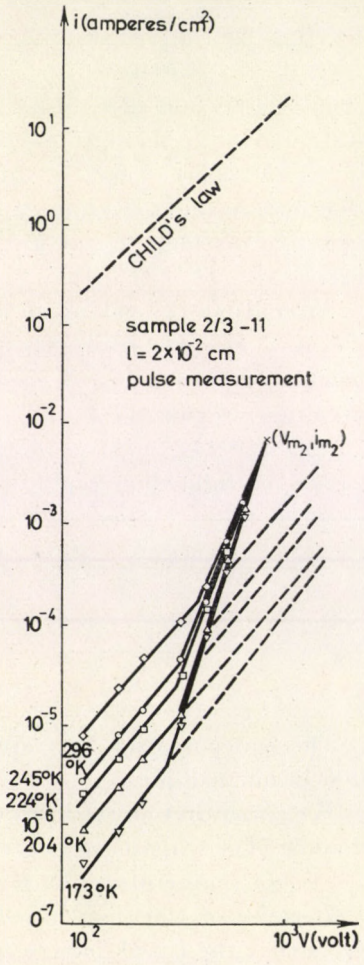


Fig. 2

(where δp_r is the recombination charge and n_t the trapped charge, both per unit volume, ε the static dielectric constant, $i_n + i_p = i$), and with r_{ctj} $(j = 1, 2)$

$$r_{ctj} = nS_{ntj}\, vkT_{cj}\, A_j [1 - \exp\left(-(E_c - E_{fn})/kT_{cj}\right)] \equiv nr'_{ctj}, \tag{2}$$

(where S_{ntj} is the capture cross-section, v the thermal velocity, E_{fn} the quasi-Fermi level) neglecting thermal re-emission, we have

$$\delta p_r - n_t \approx -n\,(1/\tau_n + r'_{ct1} + r'_{ct2})\,\tau_{p\Omega}\,, \tag{3}$$

which is a generalization of the results of ASHLEY and MILNES [4] for the case including trapping by traps having an exponential distribution in energy. The current-voltage curves cannot be exactly calculated in this case, but the role of the above formula supports the supposition that the downward shift of the experimental $i - V$ curves is connected with the recombination charge plus trapped charge densities.

As further evidence, an approximate treatment is proposed. Let us write the charge in the l long sample of unit cross-section (C the capacity of the plate condenser) in the following form

$$CV = -el\,\delta p_r + el \sum_{j=1,2} kT_{cj}\, A_j \exp\left[-(E_c - E_{fn})/kT_{cj}\right],$$

or with the results in (2) and (4)

$$CV = el\left[(\tau_{p\Omega}/\tau_n)\,n + \sum_{j=1,2} kT_{cj}\, A_j (n/N_c)^{T/T_{cj}}\right], \tag{4}$$

where N_c denotes the effective density of states. This form, like Eq. (3), cannot be solved exactly (the elimination of n is not possible), but, using our experimental results (e.g. curve belonging to 240 °K in Fig. 1), the following can be stated. For rather low voltages (200 volts), the terms in Eq. (4) have the values $CV \approx el\,(5 \times 10^{12} + 1 \times 10^{12})$, i.e. the term connected with recombination charge density dominates, while for high voltages (1000 volts), the relations are reversed: $CV \approx el\,(1 \times 10^{13} + 1.5 \times 10^{14})$, i.e. trapped charge density grows more quickly. This fact is consistent with our model: the charge lying in the deep recombination centres seems to be responsible for the lower voltage behaviour of the currents in our samples (ASHLEY and MILNES type injection), while for higher voltages, i.e. for higher Fermi levels, the role of the trapped charge predominates.

Acknowledgement

The author's gratitude is due to the late Prof. A. BUDÓ, Director of the Research Group, for his sustained interest, to Dr. Z. BODÓ (Institute for Technical Physics, Budapest) for helpful discussions and to Mrs. M. SALLAI-NÉMETH for preparing the samples.

REFERENCES

1. J. Gyulai, phys. stat. sol., **29,** K85, 1968.
2. A. Rose, Concepts in Photoconductivity and Allied Problems, Interscience Publ., New York—London, 1963, p. 72.
3. A. Sussman, J. Appl. Phys., **38,** 2738, 1967.
4. K. L. Ashley and A. G. Milnes, J. Appl. Phys., **35,** 369, 1964.
5. J. Gyulai, V. K. Subashiev and G. A. Chalikyan, Acta Phys. et Chem. Szeged, **13,** 25, 1967; J. Gyulai, Acta Phys. et Chem. Szeged, **15,** to be published.
6. R. Williams, J. Appl. Phys., **39,** 57, 1968.

РАСПРЕДЕЛЕНИЕ ЭНЕРГИИ ЛОВУШЕК В КРИСТАЛЛАХ GaP

Й. ДЬЮЛАИ

Резюме

Исследовались вольт-амперные характеристики кристаллов GaP: Cu с небольшой дырочной проводимостью в направлении [111]. Температурные изменения показательной зависимости тока от напряжения говорит о наличии двух типов ловушек, имеющих экспоненциальное распределение энергии. Из-за небольшой дырочной проводимости и наличия центров Cu интерпретация характеристик основывается на модели двух носителей Эшли—Милнса, распространенная на случай ловушек.

Acta Physica Academiae Scientiarum Hungaricae, Tomus 29 (1), pp. 79—83 (1970)

CONTACT POTENTIAL DIFFERENCE MEASUREMENTS ON (010) SURFACES OF VANADIUM PENTOXIDE

By

I. HEVESI, A. SÜLI and J. GYULAI

INSTITUTE OF EXPERIMENTAL PHYSICS, JÓZSEF ATTILA UNIVERSITY, SZEGED

(Received 31. VII. 1969)

Changes in contact potential difference (C. P. D.) between freshly cleaved (010) vanadium pentoxide surfaces and a platinum electrode were investigated using different ambients. Experiments show the logarithmic time dependence of C. P. D. during stabilization and also the important role of the presence of humidity.

The investigation of surface properties of vanadium pentoxide seems to be of importance from both theoretical and practical points of view. Previous publications deal mainly with measurements of electric conductivity, thermoelectric power on single crystals, thin layers and pressed powders for different atmospheres and temperatures [1]. Despite the numerous investigations which are mainly connected with catalytic activity and with physico-chemical problems of the surface, many unclarified details remained. It seems to be proved that the lower oxide structures on the surfaces of vanadium pentoxide are in some way responsible for the catalytic and semiconducting behaviour.

Later, FIERMANS and VENNIK [2] studied the structure of monocrystal surfaces by LEED techniques. From changes of the diffraction patterns it could have been concluded that the V_2O_5 structure, corresponding to bulk composition, of the freshly cleaved (010) surfaces turned to a structure of $V_{12}O_{26}$, — a process accompanied by oxygen loss. These conclusions supported those obtained by GILLIS [3] with EPR measurements.

The present paper deals with our investigations of contact potential difference between (010) surfaces of vanadium pentoxide and a polished platinum reference electrode, the latter being stabilized at room atmosphere.

The results obtained with this different method can be fitted to those quoted above and support a new aspect of the problem.

Results

The C.P.D. measurements were performed using a Zisman-type arrangement having an accuracy of ± 2 mV. The cleavage of the monocrystals took place in room atmosphere and the measurements were begun within 100—150 seconds after cleavage. The figures show some results of typical measurements. The circles in Fig. 1 show the changes in C.P.D. of a freshly cleaved surface

as a function of elapsed time in room atmosphere. It can be seen on the curve that there are three linear portions with different slopes (linearity in logarithmic scale). The end of the curve shows the nearly stabilized value of the C.P.D. Similar measurements on numerous samples indicated that the time needed for stabilization is approximately 24 hours and the C.P.D. value

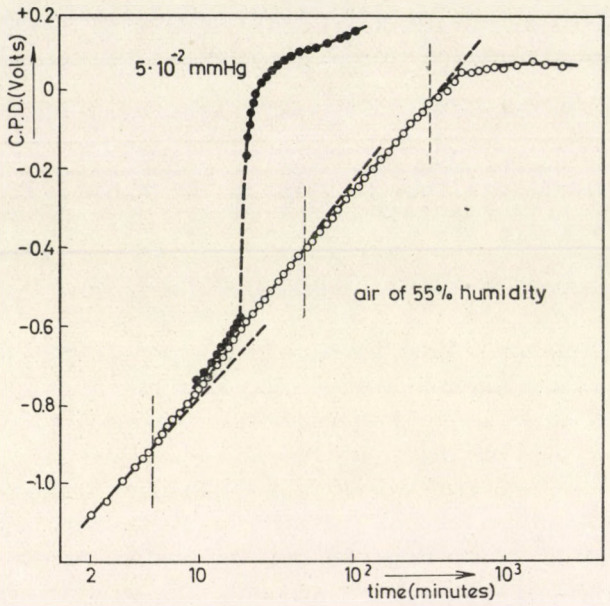


Fig. 1. C.P.D. changes of a freshly cleaved (010) surface with elapsed time

reached is about (+60)—(+80) mV in room atmosphere. This value is in accordance with late results of A. V. IOFFE [4]. The typical values of C.P.D. at the beginning of our measurements were (−1.1)—(−1.2) volts. The curve represented by dots shows the effect of vacuum on the stabilization process. It can be seen that at the beginning the rate of changes is much higher in vacuum than in room atmosphere.

The influence of humidity on C.P.D. changes is represented in Fig. 2. In order to get comparable results, the cycling of the ambient took place in a time interval corresponding to the intermediate linear portion in Fig. 1. The slopes belonging to humid air (portions I and III) are equal, while that corresponding to dry air (portion II) is somewhat less, which points to the slowing down of the reactions in dry atmospheres.

Fig. 3 shows the effect of ambient cycling on a surface stabilized in room atmosphere, showing the diminution of C.P.D. in wet atmospheres.

The effect of various dry gas ambients (e.g. O_2, N_2 and air) of long duration has also been studied. One of our results is represented in Fig. 4. The

lower rate of stabilization due to the dry ambient can clearly be observed (see the curve denoted by circles in Fig. 1). Employing various, otherwise dry gases, no detectable deviations were found compared with the curve shown in Fig. 4.

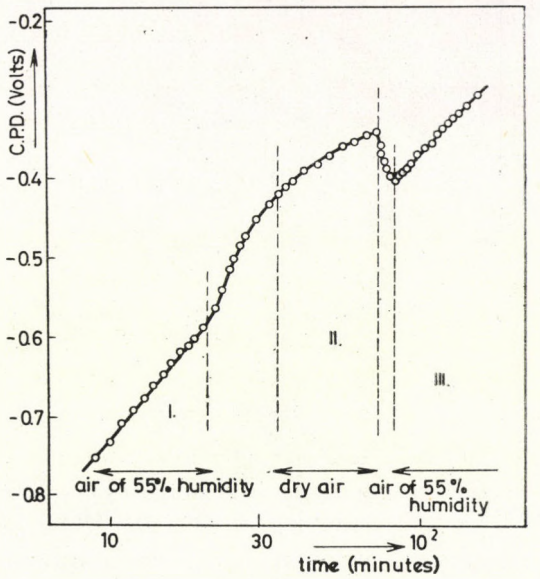


Fig. 2. C.P.D. changes of a freshly cleaved (010) surface vs time in humid and dry air

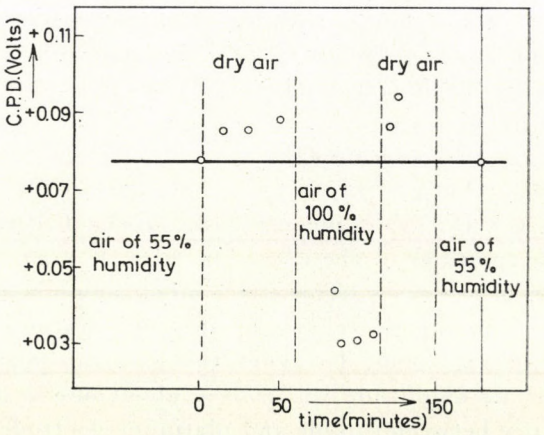


Fig. 3. C.P.D. changes of a stabilized (in room atmosphere) surface subjected to ambient cycling

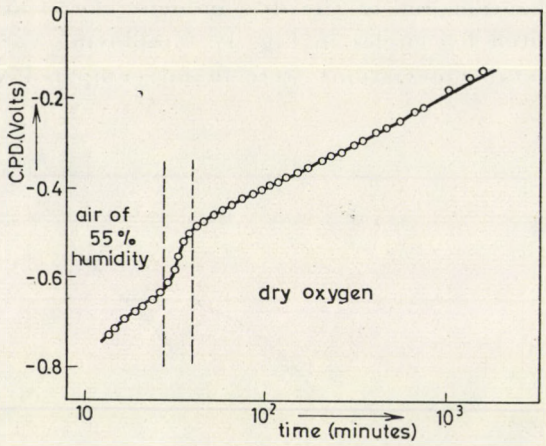


Fig. 4. C.P.D. changes of a freshly cleaved (010) surface vs time in humid air and dry oxygen

Discussion

As can be seen on the experimental curves taken during the stabilization process following the cleavage, the total magnitude of the C.P.D. changes, amounting to (1.3)—(1.4) volts, is surprisingly large. This fact indicates that there are drastic changes in surface structure during stabilization. According to the above-mentioned LEED measurements, oxygen atoms from lattice sites linking the second and third vanadium layers leave the surface during stabilization. The logarithmic law describing the time dependence of C.P.D. changes might be fitted with this supposition, though the correct correspondence needs further investigations. If the emission process plays role, it is probably connected with charge exchange, so our results concerning the effect of water molecules in the case of moist atmospheres might also be understood. The rate of stabilization of the C.P.D. grows with higher moisture content. According to our experiments, this rate does not depend on the kind of the ambient gas at the same pressure.

Our results show that gas transport near the surface also has an influence on the changes of C.P.D., i.e. it increases the rate of C.P.D. changes. (This may be seen on the portions of the curves in Figs. 1, 2 and 4 corresponding to the streaming-in of the gases.) This effect might be understood by the supposition that the streaming gas changes the concentrations of the reaction products in the surface region. To avoid the gas transport caused by the vibrating electrode, its amplitude was chosen about one order of magnitude less than the distance between sample and platinum electrode.

Further effects are under investigation, e.g. the temperature dependence of C.P.D., as an important problem from the point of view of catalysis.

Acknowledgement

The late Prof. A. Budó's sustained interest is gratefully acknowledged. Thanks are due to Dr. J. Łagowski (Institute of Physics of the Polish Academy of Sciences, Warsaw) for his help in the construction of the measuring equipment.

REFERENCES

1. H. Clark and D. J. Berets, Advances in Catalysis, Vol. IX., 204, 1956; J. D. Butler, Transactions of the Faraday Society, **56**, 1842, 1960.
2. L. Fiermans and J.Vennik, Suf. Sci., **9**, 187, 1968.
3. E. Gillis, Compt. Rend., **258**, 4765, 1964.
4. A. F. Ioffe, Physik der Halbleiter, Akademie Verlag, Berlin, 1960, p. 223.
5. A. Süli, I. Hevesi and J. Gyulai, Acta Phys. et Chem Szeged, **15** (to be published).

ИЗМЕРЕНИЯ КОНТАКТНОЙ РАЗНОСТИ ПОТЕНЦИАЛОВ НА ПОВЕРХНОСТИ (010) ПЯТИОКИСИ ВАНАДИЯ

И. ХЕВЕШИ, А. ШЮЛИ и Й. ДЬЮЛАИ

Резюме

Исследовались изменения контактной разности потенциалов между поверхностью (010) свежо расколенной пятиокиси ванадия и платиновым электродом при разных внешних условиях. Эксперименты показывают логарифмическую зависимость контактной разности потенциалов от времени стабилизации и свидетельствуют о важной роли влажности.

Acta Physica Academiae Scientiarum Hungaricae, Tomus 29 (1), pp. 85—90 (1970)

ON THE ANOMALOUS MULTIPLET SPLITTING OF THE TRIPLET TERMS OF THE ND MOLECULE

By

I. KOVÁCS and V. M. KORWAR*

DEPARTMENT OF ATOMIC PHYSICS, POLYTECHNICAL UNIVERSITY, BUDAPEST

(Received 17. II. 1970)

It is shown that the anomaly of the multiplet splitting observed in the $A\ ^3\Pi_i$ state of the ND molecule can be interpreted as the perturbation of the $A\ ^3\Pi_i$ state by the $^1\Pi$ state as well as by taking into account simultaneously the spin–spin interaction. The accurate value of the multiplet constant A has been determined for the level $v = 0$ of the state $A^3\Pi_i$.

1. Introduction

It was PANNETIER and GUENEBAUT [1] who first photographed some of the bands of the $(A^3\Pi_i - X^3\Sigma)$ system of ND under low dispersion and carried out their vibrational analysis. Recently, KRISHNAMURTHY and NARASIMHAM [2] have made a rotational analysis of the (0,0) band of this system. Also, KOPP et al. [3] have made partial analysis of the (0,0) and (1,1) bands.

KRISHNAMURTHY and NARASIMHAM found that the coupling constant A of the $A^3\Pi_i$ state of ND differed from that of NH and also that it was not constant, as it ought to be. They ascribe this to a possible inaccuracy in the assignment of the Q-branch lines and their satellites. It was therefore thought proper to re-examine theoretically the coupling constant for the $A^3\Pi_i$ state of ND on the same lines as by KOVÁCS [4] for the $A^3\Pi_i$ state of the NH molecule, and to study the multiplet splitting thoroughly.

2. The coupling constant A

As is known, multiplet Π-terms strictly belong to an intermediate case between Hund's cases (a) and (b). Hence throughout this treatment, the intermediate case has been considered to hold for the $^3\Pi_i$ state.

For the determination of the coupling constant the following relation obtained from BUDÓ's [5] formulae is made use of:

$$\frac{1}{4B^2}\{(F_3-F_1)-(H^c_{J+1}-H^c_{J-1})\}^2 = (Y-2)^2 - \frac{8}{3} + 4J(J+1), \qquad (1)$$

* On leave from Karnatak University, Dharwar, India.

where $Y = A/B$ (B = rot. constant), F_3, F_1 are the third and the first components, and H^c_{J+1} and H^c_{J-1}, the corresponding centrifugal corrections in the intermediate case computed from (see KOVÁCS [6])

$$\begin{aligned} H^c_N(J) &= S^2_{2,N} H^c_{2,2} + S^2_{1,N} H^c_{1,1} + S^2_{0,N} H^c_{0,0} + 2 S_{2,N} S_{1,N} H^c_{2,1} + \\ &+ 2 S_{1,N} S_{0,N} H^c_{1,0} + 2 S_{2,N} S_{0,N} H^c_{2,0}, \\ N &= J-1, J, J+1, \end{aligned} \tag{2}$$

where, further, the matrix elements H^c for Π state are given by

$$\begin{aligned} H^c_{2,2} &= -D\{[J(J+1)-3]^2 + 2[J(J+1)-2]\}, \\ H^c_{1,1} &= -D\{[J(J+1)+3]^2 - 12\}, \\ H^c_{0,0} &= -D\{[J(J+1)+1]^2 + 2J(J+1)\}, \\ H^c_{2,1} &= H^c_{1,2} = -2D\{J(J+1)-1\}\sqrt{2(J-1)(J+2)}, \\ H^c_{1,0} &= H^c_{0,1} = -2D\{J(J+1)+1\}\sqrt{2J(J+1)}, \\ H^c_{2,0} &= H^c_{0,2} = -2D\sqrt{(J-1)J(J+1)(J+2)}. \end{aligned} \tag{3}$$

D is centrifugal constant, and for the $S_{i,N}$ transformation matrix elements see later in Eq. (5). The results of the computations are tabulated in Table I.

Table I

J	A	J	A
2	—31.30	5	—33.30
3	—31.69	6	—33.02
4	—33.29	7	—33.21

As can be seen from the Table, A does not turn out to be a constant. Therefore, improvement in the constancy of A is sought by taking into consideration the spin—spin interaction and the spin—orbit interaction (perturbation by the $^1\Pi$ state) (see [4]). Eq. (1) will then be modified as

$$\begin{aligned} \frac{1}{4B^2}\{(F'_3 - F'_1) - \beta(S^2_{1,J+1} - S^2_{1,J-1}) - (H^c_{J+1} - H^c_{J-1})\}^2 = \\ = (Y-2)^2 - \frac{8}{3} + 4J(J+1), \end{aligned} \tag{4}$$

where F'_3 and F'_1 are the perturbed term values, and S are the transformation matrix elements given by (see KOVÁCS [6]), (for the $^3\Pi$ state)

$$S_{0,J-1}=\left[\frac{J(J+1)}{4C_1(J)}\right]^{1/2}u_1^+(J),\quad S_{1,J-1}=-\left[\frac{2(J-1)^2(J+1)^2}{C_1(J)}\right]^{1/2},$$

$$S_{2,J-1}=\left[\frac{(J-1)(J+2)}{4C_1(J)}\right]^{1/2}u_1^-(J)$$

$$S_{0,J}=\left[\frac{2J(J+1)}{C_2(J)}\right]^{1/2},\quad S_{1,J}=\left[\frac{(Y-2)^2}{C_2(J)}\right]^{1/2},\quad S_{2,J}=-\left[\frac{2(J-1)(J+2)}{C_2(J)}\right]^{1/2}$$

$$S_{0,J+1}=\left[\frac{J(J+1)}{4C_3(J)}\right]^{1/2}u_3^-(J),\quad S_{1,J+1}=\left[\frac{2J^2(J+2)^2}{C_3(J)}\right]^{1/2}, \tag{5}$$

$$S_{1,J+1}=\left[\frac{(J-1)(J+2)}{4C_3(J)}\right]^{1/2}u_3^+(J),$$

where

$$u_1^{\pm}(J)=[Y(Y-4)+4J^2]^{1/2}\pm(Y-2),$$
$$u_3^{\pm}(J)=[Y(Y-4)+4(J+1)^2]^{1/2}\pm(Y-2)$$

and for the inverted Π term

$$C_1(J)=Y(Y-4)(J+2)(J-1)+2(2J+1)(J+1)J(J-1),$$
$$C_2(J)=Y(Y-4)+4J(J+1),$$
$$C_3(J)=Y(Y-4)(J+1)J+2(2J+1)(J+2)(J+1)J,$$

and $\beta=\alpha-3\varepsilon$, where

$$\alpha=\frac{|H(^3\Pi_1{}^1\Pi_1)|^2}{\nu(^3\Pi\,{}^1\Pi)}$$

and ε is the constant of the spin—spin interaction.

The results of the computations are given in Table II.

Table II

J	A	J	A
2	—31.79	5	—33.73
3	—32.21	6	—33.68
4	—33.70	7	—33.84

Mean $A=-33.16$

A comparison of Tables I and II shows that, even after spin—spin and spin—orbit interactions have been taken into account, A does not assume a

constant value, the trend of its variation with J remaining the same. However, the set of A values in Table II is the true set as spin—spin and spin—orbit interactions, which have to be considered to explain the anomaly of the multiplet splitting, have been included while evaluating this set.

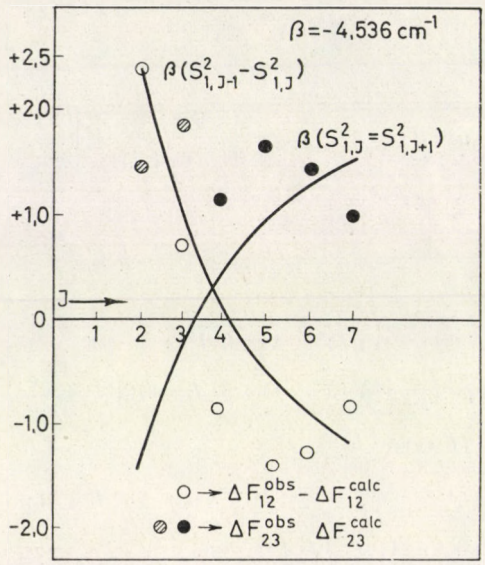


Fig. 1

3. Comparison between theory and observations

Without taking into account the spin—spin and spin—orbit interactions, there is discrepancy between observed and calculated multiplet splittings. This seems to be due to the removal of the $^3\Pi_1$ component from its original position due to these perturbations.

In order to see to what extent $^3\Pi_1$ deviates from its original position, taken as a function of the rotational quantum number, it is best to take the differences of the perturbed and the unperturbed distances of the neighbouring components. We have (for detailed explanation see KOVÁCS [6])

$$\Delta F_{12}^{\text{obs}} - \Delta F_{12}^{\text{calc}} = \beta(S_{1,J-1}^2 - S_{1,J}^2)\,, \tag{6}$$

$$\Delta F_{23}^{\text{obs}} - \Delta F_{23}^{\text{calc}} = \beta(S_{1,J}^2 - S_{1,J+1}^2)\,, \tag{7}$$

where $\Delta F_{ik}^{\text{calc}} = F_i^{\text{calc}} - F_k^{\text{calc}}$, F_i^{calc} and F_k^{calc} are computable from the well-known term formulae of BUDÓ. In Fig. 1 the right sides of (6) and (7) with $\beta = -4.536$ have been plotted against J. The left-sides have been shown by points.

4. Discussion

It is seen from Fig. 1 that there is some agreement, altough not very good, between experimental results and theoretical predictions; but two points, at $J = 2$ and $J = 3$ are far off their corresponding part of the theoretical curve. It was, therefore, thought worthwhile attempting to see if there were any possible perturbation caused by the $^1\Delta$ and $^1\Sigma$ terms in addition to the $^1\Pi$ term dealt with above. One can include such effects by writing as

$$\Delta F_{12}^{\text{obs}} - \Delta F_{12}^{\text{calc}} = \beta_\Sigma(S^2_{0,J-1} - S^2_{0,J}) + \beta(S^2_{1,J-1} - S^2_{1,J}) + \beta_\Delta(S^2_{2,J-1} - S^2_{2,J}),$$
$$\Delta F_{23}^{\text{obs}} - \Delta F_{23}^{\text{calc}} = \beta_\Sigma(S^2_{0,J} - S^2_{0,J+1}) + \beta(S^2_{1,J} - S^2_{1,J+1}) + \beta_\Delta(S^2_{2,J} - S^2_{2,J+1}),$$

where β_Σ and β_Δ are given by

$$\beta_\Sigma - \frac{|H(^3\Pi_0\,^1\Sigma)|^2}{\nu(^3\Pi\,^1\Sigma)}, \qquad \beta_\Delta = \frac{|H(^3\Pi_2\,^1\Delta_2)|^2}{\nu(^3\Pi\,^1\Delta)}.$$

For expressions for transformation matrix elements see Eq. (5) above. The values of β's, obtained by the technique of least-squares are:

$$\beta_\Sigma = -2.613, \qquad \beta = -4.329, \qquad \beta_\Delta = -1.132.$$

However, no better agreement between theory and observation was found.

5. Conclusion

Only after inclusion of spin—spin and spin—orbit interactions observed multiplet splitting can be explained. Otherwise there is large discrepancy between the observed and the calculated multiplet splittings. However, the coupling constant does not turn out to be constant even after inclusion of these interactions. As to the large discrepancy between the two sets of values, at $J = 2$, $J = 3$ and at $J = 4$ to $J = 7$, it may be that the measurements here, or as KRISHNAMURTHY and NARASIMHAM suggest, the assignment of J values to lines, may be in error.

Similarly deviations at the same J values ($J = 2$, 3) from one of the branches of the curve representing the spin—spin and spin—orbit interactions (shown by the two shaded circles in Fig. 1) are observed. This shows that there is probably error in the assignment of J values to lines.

Note added in proof. Recently new, more accurate measurements have heen published by BOLLMARK, KOPP and RYDH (Journ. Mol. Spectr. *34*, 487, 1970) extended to higher values the rotational quantum number. Now the recalculation of constants and of multiplet splittings using the new data is in progress and the results will be published later.

REFERENCES

1. G. PANNETIER and H. GUENEBAUT, Bull. Soc. Chim. France, **190**, 991, 1959.
2. G. KRISHNAMURTHY and N. A. NARASIMHAM, Proc. Ind. Acad. Sc., **57**, 50, 1968.
3. I. KOPP, M. KRONEKVIST and N. ALSUND, Arkiv. f. Fys., **30**, 9, 1965.
4. I. KOVÁCS, Acta Phys. Hung., **12**, 67, 1960.
5. Á. BUDÓ, Z. Phys., **96**, 219, 1935.
6. I. KOVÁCS, Rotational Structure in the Spectra of Diatomic Molecules, Akadémiai Kiadó, Budapest, and Adam Hilger Ltd., London, 1969, p. 71.

ОБ АНОМАЛЬНОМ МУЛЬТИПЛЕТНОМ РАСЩЕПЛЕНИИ ТРИПЛЕТНЫХ ТЕРМОВ МОЛЕКУЛЫ ND

И. КОВАЧ и В. М. КОРВАР

Резюме

Показывается, что аномалию мультиплетного расщепления, наблюдаемого в состоянии $A^3\Pi_i$ молекулы ND, можно интерпретировать возмущением состояния $A^3\Pi_i$ состоянием $^1\Pi$, а так же с одновременным принятием во внимание спин — спинового взаимодействия. Точное значение мультиплетной постоянной A определялось для уровня $v = 0$ состояния $A^3\Pi_i$.

Acta Physica Academiae Scientiarum Hungaricae, Tomus 29 (1), pp. 91—92 (1970)

COMMUNICATIO BREVIS

A NOTE ON THE OBSERVATION OF S° MESON

By

T. GÉMESY and G. SURÁNYI

CENTRAL RESEARCH INSTITUTE FOR PHYSICS, BUDAPEST

(Received 24. V. 1969)

In the search for the dubious S° meson first found by FELDMAN [1] in 1965, the γ-s emerging from the charge exchange interaction can be used in a xenon chamber experiment

$$\pi^+ + n \to p + X^\circ , \tag{1}$$

where the unknown particle X° decays into four photons which may form an S° resonance. An experiment using this method was performed by STRUGALSKI et al. [2, 3] at 2.34 GeV/c. However, there are many channels at this energy which give a proton and two π° in the final state having different effective masses. In order to use this experimental method of finding S° resonance one must rule out the possibility of the existence of a background channel, which could give a bump as a kinematic effect in the $\pi^\circ\pi^\circ$ effective mass distribution at about an energy of 720 MeV. The channel in question probably having a higher cross-section than the S° at this energy is

$$\pi^+ + n \to N^{*+} + \pi^\circ \to p + \pi^\circ + \pi^\circ . \tag{2}$$

In this letter we calculate the $\pi^\circ\pi^\circ$ effective mass distribution in the channel mentioned above. As has been experimentally and theoretically verified, this process goes via ϱ exchange, so the STODOLSKY—SAKURAI model [4] can be used. Let us define a coordinate system in the rest frame of N^{*+} so that the x and y axes should lie in the production plane, x is along the direction of the pion directly produced in Eq. (2), the z axis is perpendicular to the production plane. In this frame of reference the effective mass squared of $\pi_1^\circ \, \overset{\circ}{2}$ where π_1° denotes the pion given by the decay of N^{*+} can be easily evaluated:

$$M^2 = 2\left(m_{\pi^\circ}^2 + E_{\pi_1^\circ} \cdot E_{\pi_2^\circ} - p_{\pi_1^\circ} \cdot p_{\pi_2^\circ} \cdot \sin\Theta_{\pi_1} \cdot \cos\varphi_{\pi_1}\right), \tag{3}$$

where $E_{\pi_1^\circ}$, $E_{\pi_2^\circ}$, $p_{\pi_1^\circ}$, $p_{\pi_2^\circ}$ are the energies and momenta of π_1° and π_2°, $\Theta_{\pi_1^\circ}$ and $\varphi_{\pi_1^\circ}$ are the polar and azimuthal angles, respectively. According to the STODOLSKY—SAKURAI model the angular distribution of π_1° with respect to the normal of the production plane is

$$f(\Theta_{\pi_1^\circ},\ \varphi_{\pi_1^\circ}) = \frac{1}{8\pi}(1+3\cos\Theta_{\pi_1^\circ})$$

[5] and therefore the effective mass distribution is given by

$$f(M) = \frac{M}{4\pi}\int_0^{2\pi}\int_{-1}^{1}\delta\left(M^2 - 2(m^2\pi^\circ + E\pi_1^\circ E\pi_2^\circ - p\pi_1^\circ p\pi_2^\circ \cos\Theta_{\pi_1^\circ}\cos\varphi_{\pi_1^\circ})\right)\cdot$$
$$\cdot\,(1+3\cos^2\Theta_{\pi_1^\circ})\,d\cos\Theta_{\pi_1^\circ}\,d\varphi_{\pi_1^\circ} = \tag{4}$$
$$= \frac{M}{16\,p\pi_1^\circ\,p\pi_2^\circ}\left[5-3\left(\frac{2\,m\pi^\circ + 2\,E\pi_1^\circ E\pi_2^\circ - M^2}{2\,p\pi_1^\circ\,p\pi_2^\circ}\right)^2\right].$$

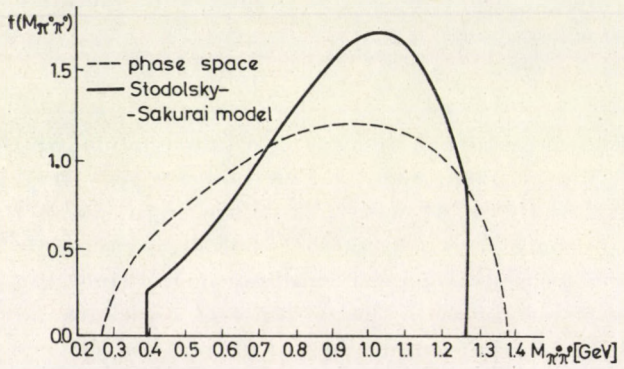


Fig. 1. The $M\pi^0\pi^0$ effective mass distribution for reaction 2 and the corresponding phase space distribution

Comparing this and the corresponding phase-space distribution (Fig. 1) one can conclude that the $\pi^+ n \to N^{*\,+}\pi^\circ$ channel does not affect the observation of the hypothetical S° resonance.

Completing this calculation we have made a series of Monte-Carlo calculations with other kinds of angular distributions which have resulted in the same conclusion.

REFERENCES

1. M. FELDMAN, Phys. Rev. Lett., **14**, 869, 1965.
2. Z. S. STRUGALSKI et al., Study of Neutral Bosons Decaying into π° Mesons and γ Quanta, to be published.
3. Z. S. STRUGALSKI et al., The ε° Meson, to be published.
4. L. STODOLSKY and J. J. SAKURAI, Phys. Rev. Lett., **11**, 90, 1963.
5. Lecture given by N. SCHMITZ at the 1965 Easter School for Physicists. CERN 65-24.

RECENSIONES

A. G. KULIKOVSZKIY and G. A. LJUBINOV: **Magnetohydrodynamics**

Addison — Wesley, Reading, Massachusetts, 1965, pp. 216

This book is a translation from Russian of Magnitnaya Gidrodinamika, published in Moscow in 1962 by the State Physics and Mathematics Press. The book does not deal with all the possible situations in which fluids or gases interact with electromagnetic fields and does not review any experimental data, but it presents a well-ordered sequence of problems by which the authors achieve a uniformity of presentation in this fast-moving field of physics.

In the first chapter the basic equations of electrodynamics and fluid dynamics, and the mixed magnetohydrodynamic equations are given. In Chapter Two the motion of an incompressible liquid is discussed. Chapter Three deals with simple wave structures and small disturbances in an ideal gas. Chapter Four is devoted to surfaces of discontinuity there, and the next chapters deal with its non-stationary and stationary motions. Chapter Seven discusses the stationary motion of a nonideal gas and, finally, the last chapter is devoted to the flow of a conducting fluid among magnetized bodies.

The clear presentation of the book makes it a sensitive exposition for any theoretical physicist interested in this modern branch of physics.

T. A. HOFFMANN

C. A. ROUSE: **Progress in High Temperature Physics and Chemistry**

Vol. 1, Pergamon Press, Oxford, 1967, pp. 242

The series of volumes of which this is the first brings together various theoretical, experimental and technological aspects of high temperature phenomena. This first volume includes articles of by S. G. BRUSH, B. H. ARMSTRONG, R. R. JOHNSTON, R. S. KELLY, H. E. DE WITT and S. G. BRUSH. The first article gives the general theories of the equation of the state of matter at high pressures and temperatures. This article provides a comprehensive presentation of the literature in this field. Then, theoretical calculations for the high-temperature low-density region are given, followed by those for the high-density low-temperature region. Finally, the thermodynamic description of high-pressure states is presented. An ample review of the literature concerning this field is given.

The second article gives the theoretical presentation of the opacity of high-temperature air. First, the occupation-number calculations are given, then the theory of atomic lir e transitions, and photoionization transitions. The last two chapters are devoted to an evaluation of opacity observations and the statistical mechanics of plasmas.

The whole volume provides a challenge for every theoretical physicist interested in high temperature physics.

T. A. HOFFMANN

K. PÁTER: **Lasers**

Iliffe Books Ltd, London, SNTL, Prague, 1967, pp. 288

This relatively small book tries to summarize the theory, practice and application of lasers in an extremely condensed way. The first chapter of the book deals with the general theory of emission and absorption, the second with the inversion of quantum systems and with stimulated emission. The third chapter deals with resonant cavities in the optical region and the next with noise and monochromaticity of coherent emission. The following chapters are devoted to the various physical forms of lasers, gas lasers, solid-state lasers, injection lasers and other types. The last four chapters are concerned with the applications of lasers in physics and optics, in communication and ranging, in treating and testing materials, and with biological and medical applications.

The book also gives some details of the theory of lasers, and is a useful aid for the experimental research worker in this field.

T. A. HOFFMANN

H. A. ELION: Laser Systems and Applications

Pergamon Press, Oxford, 1967, pp. 624

The first laser was announced in the first half of 1960. Since that time many lasers have been constructed and many improvements have been made. At the same time the application of lasers is becoming increasingly widespread. The application of lasers as high energy sources for welding and machining, for drilling, for chemical, photochemical, biological, and medical applications came together with their potential application as weapons. The spectrally pure light has enormous implications for photography and micrography, for spectroscopy itself and for plasma research. As a natural extension of microwaves, the laser radar techniques permitted the development of new methods for ranging and surveying and in general new trends in meteorology. As communications equipment the laser has opened new possibilities in space communication.

The book is a helpful tool for any field of laser application. The large NASA bibliography on lasers which extends to more that half of the volume is an extensive aid for any research worker in this field.

T. A. HOFFMANN

I. S. SHKLOVSKY: Supernovae

Translated from the Russian, John Wiley and Sons, London—New York—Sydney. 1968, 444 pages, with 124 figures. Interscience Monographs and Texts in Physics and Astronomy Vol. XXI. Price 25.000 US Dollars

This is the first comprehensive monograph on the supernovae which play a prominent part in the general picture of stellar and galactic evolution and in modern theories of the origin of primary cosmic rays. The task of the author was not easy, because this fascinating field of astrophysics is based on the application of the most diverse methods. The observational background is presented in considerable detail, particularly in respect to the Crab nebula, to which about one third of the book is devoted. As the book contains a fairly full coverage of work only up to the end of 1965, some parts of it are obsolescent.

The translation from Russian to English is very poor, with little knowledge of astronomical terminology and of the names of well-known astronomers. The numerical quantities given in this translation are also very often wrong.

L. DETRE

Interstellar Ionized Hydrogen

Edited by Y. TERZIAN. W. A. Benjamin, Inc. New York 1968, 774 pages, Price 15 US Dollars

A symposium on interstellar ionized hydrogen regions was held in Charlottesville, Virginia USA, between December 8 and 11, 1967. The symposium was organized by the National Radio Astronomy jointly with the Arecibo Ionospheric Observatory by a committee composed of W. E. HOWARD III., P. C. MEZGER, D. E. OSTERBROCK and Y. TERZIAN. This volume presents the proceedings of the symposium and includes 32 papers on the following topics: Observations related to regions of star formation, evolution of stars and HII regions, optical and radio observations of HII regions, the radio recombination lines of interstellar hydrogen, the electron temperature and large scale distribution of HII regions in the galaxy, and OH emission. The book was printed directly from a typescript prepared by the editors.

Physicists may be particularly interested in the problems connected with interstellar OH emission where a maser action must be present in space. Connected with the OH emission objects MEZGER discovered a new class of compact, high density HII regions with average electron densities of about 10^4 cm^{-3}, and diameters of less than 1.5 light years. The problems connected with the formation and evolution of stars in HII regions may also find a general interest among physicists.

L. DETRE

S. Borowitz: Fundamentals of Quantum Mechanics

XIV + 401 p., W. A. Benjamin, Inc., New York, Amsterdam, 1967

Der Untertitel des Buches lautet: Teilchen, Wellen und Wellenmechanik. Dieses in dem Untertitel angedeutete Programm wird vom Verfasser sehr konsequent und in einer leicht verständlichen Weise ausgearbeitet. Die ersten 7 Kapitel geben die klassischen Grundlegen, die zur Begründung der nachfolgenden 9 Kapiteln dienen, die eine komplette Wellenmechanik darstellen. Vom Leser wird sehr wenig vorausgesetzt, sogar einfache mathematische Hilfsmittel werden im Buch gebracht. Die vielen und vielseitigen sehr sorgsam durchgearbeiteten Beispiele sowie die am Ende jedes Kapitels stehenden zahlreichen Aufgaben werden den Leser zum Selbststudium anregen.

Meiner Ansicht nach ist das Buch eine ausgezeichnete Einführung in die Wellenmechanik, zu der man den Verfasser bestens beglückwünschen kann. Das Buch das auch für den Fachmann ein willkommenes Hilfswerk darstellt, kann besonders den Studierenden bestens empfohlen werden.

P. Gombás

D. R. Frankl: Electrical Properties of Semiconductor Surfaces

(International Series of Monographs on Semiconductors Vol. 7), XV + 310 p., Pergamon Press, Oxford, London, Edinburgh, New York, Toronto, Sydney, Paris, Braunschweig, 1967

Dies Buch gibt eine gute Darstellung der Physik der Oberfläche von Halbleitern. Es bringt auch eine Übersicht der Anwendung der Theorie und eine Kritik der vielseitigen Resultate. Neben vielen praktischen Anwendungen enthält es auch die Theorie der Oberflächenzustände auf einer idealen Oberfläche. Die nötigen Grundlagen sowie die Ausblicke auf die Theorie der Festkörper sind kurz gefasst. Vom Leser werden ziemlich ausführliche Kenntnisse der Theorie des festen Körpers vorausgesetzt. Das Buch kann sowohl dem Fachmann als den Studierenden auf diesem Gebiet bestens empfohlen werden.

P. Gombás

T. L. Loucks: Augmented Plane Wave Method

256 + XIV p., W. A. Benjamin, Inc., New York, Amsterdam, 1967. S 7.50

Das Ziel des Buches ist eine möglichst einfache Einführung in die Augmented Plane Wave-Methode zu geben. Der Verfasser des Buches ist der Ansicht, dass er in drei Etappen all das was ein Interessent auf diesem Gebiet benötigt, bringt. Dies scheint tatsächlich der Fall zu sein, nur scheint es mir, dass die Darstellungsweise des Stoffes auch einfacher sein hätte können.

Das Buch zergliedert sich in folgende Teile: 1 Übersicht und Kritik der Literatur der APW-Methode, 2. Theoretische Diskussion der APW-Methode, 3. Praktische Aspekte der APW-Methode, 4. Relativistische APW-Methode. Dem folgt ein Anhang mit 5 Abschnitten und die zitierte Literatur die keinesfalls auf Vollständigkeit Anspruch erhebt. Den Abschluss bilden Photokopien von Artikeln, die dem Verfasser in Bezug auf den behandelten Stoff als am wichtigsten erscheinen.

Beim Lesen des Buches bekommt man den Eindruck, dass das Buch ein bischen zu rasch geschrieben wurde, was natürlich auf Kosten der Gründlichkeit und einheitlichen Darstellung geht. Trotz diesem vielleicht nur dem Referenten erscheinenden Mangel kann das Buch all denen, die auf diesem Gebiet arbeiten mit gutem Gewissen empfohlen werden.

P. Gombás

Printed in Hungary

A kiadásért felel az Akadémiai Kiadó igazgatója — Műszaki szerkesztő: Farkas Sándor

A kézirat nyomdába érkezett: 1970. V. 7. — Terjedelem: 8,25 (A/5) ív, 30 ábra

70.70219 Akadémiai Nyomda, Budapest — Felelős vezető: Bernát György

The *Acta Physica* publish papers on physics, in English, German, French and Russian.
The *Acta Physica* appear in parts of varying size, making up volumes.
Manuscripts should be addressed to:

Acta Physica, Budapest 502, P. O. B. 24.

Correspondence with the editors and publishers should be sent to the same address.
The rate of subscription is $ 16.00 a volume.
Orders may be placed with "Kultúra" Foreign Trade Company for Books and Newspapers (Budapest I., Fő u. 32. Account No. 43-790-057-181) or with representatives abroad.

Les *Acta Physica* paraissent en français, allemand, anglais et russe et publient des travaux du domaine de la physique.
Les *Acta Physica* sont publiés sous forme de fascicules qui seront réunis en volumes.
On est prié d'envoyer les manuscrits destinés à la rédaction à l'adresse suivante:

Acta Physica, Budapest 502, P. O. B. 24.

Toute correspondance doit être envoyée à cette même adresse.
Le prix de l'abonnement est de $ 16.00 par volume.
On peut s'abonner à l'Entreprise du Commerce Extérieur de Livres et Journaux «Kultúra» (Budapest I., Fő u. 32. — Compte-courant No. 43-790-057-181) ou à l'étranger chez tous les représentants ou dépositaires.

«*Acta Physica*» публикуют трактаты из области физических наук на русском, немецком, английском и французском языках.
«*Acta Physica*» выходят отдельными выпусками разного объема. Несколько выпусков составляют один том.
Предназначенные для публикации рукописи следует направлять по адресу:

Acta Physica, Budapest 502, P. O. B. 24.

По этому же адресу направлять всякую корреспонденцию для редакции и администрации. Подписная цена — $ 16.00 за том.
Заказы принимает предприятие по внешней торговле книг и газет «*Kultúra*» (Budapest I., Fő u. 32. Текущий счет: № 43-790-057-181) или его заграничные представительства и уполномоченные.

INDEX

D. Berényi and *D. Varga:* The Details of the Critical Study of the Internal Bremsstrahlung Spectrum from ^{32}P. – *Д. Верени* и *Д. Варга:* Подробности критического изучения спектра внутреннего тормозного излиучения ^{32}P 1

G. Fáy: A Phenomenological Foundation of Quantum Logic. — *Г. Фаи:* Феноменологическое обоснование квантовой логики 27

J. Balázs and *B. Pődör*: On the Theory of Galvanomagnetic Effects in Semiconductors With Anisotropic Scattering. — *Й. Балаж* и *Б. Педер:* К теории гальваномагнитных явлений с анизотропным рассеянием 35

B. Rősner, Z. Bodó, T. Sebestyén and *B. Wohn*: Transmitted Phonon Drag Measurements in Ge. — *Б. Рэзнер, З. Бодо, Т. Шебештен* и *Б. Вон:* Измерение фононной тяги в Ge 45

I. Tamássy-Lentei: Potential Curves for One-Electron Heteronuclear Diatomic Systems in One-Centre Treatment. — *И. Тамаши-Лентеи:* Потенциальные кривые для одноэлектронных гетероядерных двухатомных систем в одноцентровом рассмотрении 67

J. Gyulai: Energy Distribution of Traps in GaP Crystals. — *Й. Дьюлаи:* Распределение энергии ловушек в кристаллах GaP 75

I. Hevesi, A. Süli and *J. Gyulai*: Contact Potential Difference Measurements on [010] Surfaces of Vanadium Pentoxide. — *И. Хевеши, А. Шюли* и *Й. Дьюлаи:* Измерения контактной разности потенциалов на поверхности [010] пятиокиси ванадия 79

I. Kovács and *V. M. Korwar*: On the Anomalous Multiplet Splitting of the Triplet Terms of the ND Molecule — *И. Ковач* и *В. М. Корвар:* Об аномальном мультиплетном расщеплении триплетных термов молекулы ND 85

COMMUNICATIO BREVIS

T. Gémesy and *G. Surányi*: A Note on the Observation of S^0 Meson 91

RECENSIONES

ACTA PHYSICA

ACADEMIAE SCIENTIARUM HUNGARICAE

ADIUVANTIBUS
L. JÁNOSSY, I. KOVÁCS, K. NAGY, A. SZALAY

REDIGIT
P. GOMBÁS

TOMUS XXIX FASCICULI 2—3

AKADÉMIAI KIADÓ, BUDAPEST
1970

ACTA PHYSICA

A MAGYAR TUDOMÁNYOS AKADÉMIA FIZIKAI KÖZLEMÉNYEI

SZERKESZTŐSÉG ÉS KIADÓHIVATAL: BUDAPEST V., ALKOTMÁNY UTCA 21.

Az *Acta Physica* német, angol, francia és orosz nyelven közöl értekezéseket a fizika tárgyköréből.

Az *Acta Physica* változó terjedelmű füzetekben jelenik meg: több füzet alkot egy kötetet.

A közlésre szánt kéziratok a következő címre küldendők:

Acta Physica, Budapest 502, P. O. B. 24.

Ugyanerre a címre küldendő minden szerkesztőségi és kiadóhivatali levelezés.

Megrendelhető a belföld számára az Akadémiai Kiadónál (Budapest V., Alkotmány utca 21. Bankszámla 05-915-111-46), a külföld számára pedig a „Kultúra" Könyv- és Hírlap Külkereskedelmi Vállalatnál (Budapest I., Fő u. 32. Bankszámla 43-790-057-181 sz.), vagy annak külföldi képviseleteinél és bizományosainál.

Die *Acta Physica* veröffentlichen Abhandlungen aus dem Bereich der Physik in deutscher, englischer, französischer und russischer Sprache.

Die *Acta Physica* erscheinen in Heften wechselnden Umfanges. Mehrere Hefte bilden einen Band.

Die zur Veröffentlichung bestimmten Manuskripte sind an folgende Adresse zu richten:

Acta Physica, Budapest 502, P. O. B. 24.

An die gleiche Anschrift ist auch jede für die Redaktion und den Verlag bestimmte Korrespondenz zu senden. Abonnementspreis pro Band: $ 16.00.

Bestellbar bei dem Buch- und Zeitungs-Aussenhandels-Unternehmen »Kultura« (Budapest I., Fő u. 32. Bankkonto Nr. 43-790-057-181) oder bei seinen Auslandsvertretungen und Kommissionären.

Acta Physica Academiae Scientiarum Hungaricae, Tomus 29 (2—3), pp. 97—106 (1970)

OXYGEN CONTENT DETERMINATION IN THIN SILICON SLICES

By

I. SZÉP and I. BÁRSONY

INDUSTRIAL RESEARCH INSTITUTE FOR ELECTRONICS "HIKI"
SEMICONDUCTOR LABORATORY, BUDAPEST

(Received 23. I. 1969)

A survey is given on the transmission spectrum minima due to different oxide bonds on the surface of and in the silicon crystal. Methods are described for the investigation of the oxygen content of thin silicon slices. The oxygen concentration values of a few samples are determined and the bulk absorption cross-sections of different SiO_2 groups are estimated.

1. Introduction

Silicon undergoes various chemical changes during certain technological procedures. One of these is the rise of oxygen content in the crystal. During treatments for a given time, the change in the oxygen content is obviously more pronounced the thinner the silicon slices. The manufacture of silicon-based semiconductor devices gave rise to problems which, in our opinion, are connected with the amount of oxygen bound in the silicon. Since thin silicon slices are used in the production of semiconductor devices it seems necessary to determine the oxygen content of these slices quantitatively. Two methods have been published for measuring the oxygen content of silicon: gas analysis by vacuum-fusion and infrared absorption spectroscopy. The latter was used in our experiments since it can be carried out quickly and is non-destructive.

2. Determination of the oxygen content by infrared absorption

During the growth process more or less oxygen can be incorporated in the silicon crystal, its quantity being influenced by the growth conditions [1]. The quantity of the dissolved oxygen increases if the silicon melt is in a quartz crucible or if the ambient gas contains oxygen. Especially the latter can play a considerable role since even a small quantity present increases the amount of oxygen dissolved in the silicon. If e.g. the ambient gas during growth is pure helium, the silicon contains practically no detectable oxygen, whereas if the oxygen content of the ambient gas amounts to about 10% or more, the oxygen content of the silicon reaches the maximum of the solid solubility.

By recrystallizing a crystal with a high oxygen content, the quantity of the dissolved oxygen can be reduced to a level where it is no longer detectable, provided that the oxygen content of the ambient gas (e.g. noble gases or hydrogen) does not exceed 1%.

The inhomogeneity of the oxygen concentration along the longitudinal axis is caused by temperature fluctuations. Their influence is, of course, more pronounced near the crystal surface than it is near the axis. The oxygen concentration is influenced by other factors besides the above parameters: i.e. the rate of rotation, the ratio between the crystal and the crucible diameter, the volume and surface of the melt wetting the wall of the crucibe and the duration of the wetting [1]. Pure silicon transmits infrared light at a wavelength above 1 nm. The infrared transmission spectrum shows different absorption peaks in the range of 6—25 μm. Some of these are induced by the impinging photons causing lattice vibration; the others are induced by the free carriers, i.e. by the impurities or the dopants. The spectrum also shows absorption peaks which are the superpositions of lines due to lattice vibrations and to certain impurities. Strong lattice vibration absorption peaks appear for instance at 6.9 μm and 11.3 μm.

The oxygen bound in silicon causes absorption maxima in several regions of the spectrum [2]. If the crystal contains oxygen, an absorption maximum always appears at 9.1 μm. This phenomenon is attributed to the oxygen bond in SiO_2 form. The SiO_2 formations in the crystal result in an absorption peak even at 20 μm which, however, is considerably lower than the former. Oxygen is seldom dissolved by silicon in the form of SiO; the absorption peak caused by SiO occurs at 10 μm.

If the silicon contains oxygen in the form of an oxide, the absorption spectrum changes. If the surface is covered by a thermal SiO_2 layer, two peaks appear, one at 9.15 and the other at 12.4 μm. If the SiO_2 layer is deposited pyrolitically on the surface, a shift of these peaks can be observed. They then appear at 9.25 μm and 12.3 μm [3]. The SiO layer on the surface shows a single absorption maximum at 9.3 μm. Thus, it is obvious that when preparing the sample for oxygen content determination of silicon it is essential to remove the oxide layer from the surface since its absorption peak at 9.15 μm would be superposed on the 9.1 μm absorption peak of the SiO_2 formation in the crystal.

Each of the various SiO_x modifications developed on the surface show characteristic but relatively weak absorption peaks. Table I shows the rarer oxide modifications and their absorption maxima.

The measurement of the absorption peaks is of special importance when the transition of these modifications into each other is to be studied: if, for instance, a phosphosilicate glass film is produced on the oxide surface, the peak at 9.1 μm characteristic for the SiO bond shifts towards lower wave-

lengths indicating that the quantity of the SiO_4-tetrahedron modifications increases [4].

The heat treatment of the crystal changes the absorption peaks of the different SiO_x modifications in the bulk. The effects of the heat treatment can be summarized as bringing about a change in the number of oxygen donors, the character of the SiO_x modifications and both the distribution and the number of dislocations [5]. According to FULLER [6] and KAISER [7] the

Table I

Absorption peaks of different SiO_x modifications

Si_2O_3 μm	SiO_4 μm	Si_2O_5 μm
9.6	9.35	9.35
	12.36	11.5
	20.8	19.6
	23.8	22.2
		24.4

number of the oxygen donor has its maximum at a heating temperature between 450—500 °C. Above this temperature their number gradually decreases. The donor distribution is inhomogeneous in the direction perpendicular to the axis, increasing towards the centre. For heat treatments at lower temperatures and at 1000 °C the absorption maxima characteristic for the different SiO_x formations change. A heat treatment at 1000 °C for 10 hours causes a decrease in the 9.1 μm peak to about a fifth of its original value. At the same time, control measurements by vacuum-fusion gas analysis do not show a decrease in oxygen content. So it is unquestionable, that, as a result of the heat treatment, some SiO_x modifications are transformed into one another and that, at a given temperature, the most stable modifications became dominant. The number of bonds developed is considerably influenced by the diffusion constant of the oxygen which increases proportionally with the temperature.

If the absorption spectrum does not show absorption peaks characteristic of the rarer SiO_x formations containing generally more oxygen, the oxygen content should be determined from the maximum at 9.1 μm. KAISER et al. [8] showed by absorption measurements on crystals free of oxide layers that this absorption peak is not a surface phenomenon but rather a bulk-effect, i.e. its presence is due to the oxygen content of the crystal bulk. Since they made their measurements on high purity silicon and the 9.1 μm absorption peak was fairly intensive, it seemed evident to suppose that this absorption maxi-

mum was not caused by the excitation of a bond between a certain impurity and oxygen but by that of silicon and oxygen. If the oxygen content in silicon is low this phenomenon may be interpreted according to the KAISER model as follows. The covalent bond between two neighbouring silicon atoms breaks up; the two silicon atoms bond with a previously interstitial oxygen atom so that they form an isosceles triangle with the 2 silicon atoms and the oxygen atom located in the vertices. The distance between the two neighbouring silicon atoms is equal to the lattice constant 2.33 Å. For this case the Si—O—Si angle at the vertex of the triangle is about 100°.

KAISER and KECK compared the infrared absorption results with those obtained by vacuum-fusion gas analysis and concluded that a linear correlation exists between the oxygen concentration values obtained by gas analysis and the absorption coefficient corresponding to the 9.1 μm infrared absorption peak. Taking into consideration that at 9.1 μm there also exists a lattice vibration absorption with a coefficient of about 0.8 cm^{-1} on which an absorption peak proportional to the oxygen concentration is superposed, its measurement allows for a quantitative analysis of the oxygen content in silicon. The sensitivity of this method increases with decreasing temperature. If the detection limit has to be increased e.g. down to 10^{16} atom/cm^3, which is considered as a rather low oxygen concentration, the measurements should be carried out at liquid air temperature.

Our oxygen concentration determinations were made at room temperature by the infrared absorption method, since the concentration values could also be measured in this temperature range.

3. Experimental

The infrared absorption spectra of silicon were measured using a Zeiss type UR-10 double-path infrared spectrophotometer. This allowed the continuous spectra in the 2—25 μm wavelength range to be measured.

Some experimental difficulties arose regarding the shape and adjustment of the sample and the determination of the beam path. An evaluable spectrum appears only if the path of the infrared beam through the bulk of the crystal is sufficiently long, since only a sufficiently great number of SiO_x formations with low surface absorption cross-section (about 10^{-8} cm^{-2}) can be used to give reliably "macroscopic" absorption results. Therefore, our measurements were made on samples differing in shape and size.

Since directly transmitted light is not sufficiently absorbed in a thin silicon slice, we tried to find solutions where the light path in the bulk would be longer without increasing the thickness of the slice.

Using total reflexion proved to be the best method. Its application in our measurements was reasonable from several points of view. Its main advan-

tage is that it is practically free of loss, since a ray arriving from an optically dense medium enters the less dense one to a very small extent. In practice the decrease in radiation intensity cannot be observed even if the medium of lower refractive index is strongly absorbing. In our particular case another advantage of the total reflexion method is that the refraction index of silicon is remarkably high and therefore the Brewster angle for total reflexion is small. Thus the phenomenon can be easily obtained.

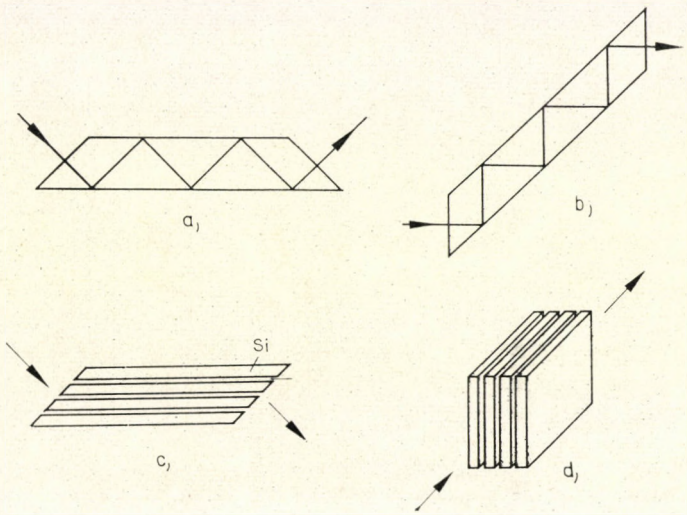


Fig. 1. Slices of different shape used for oxygen concentration determination

Taking into account that for light of a wavelength of 9 μm the reflexion index of silicon $n = 3.4$ the Brewster angle for the total reflexion comes to $\alpha \approx 17°$.

Considering that, especially for small penetration depths, we have a Si—SiO_2 interface rather than a silicon-air one, the relative refraction index n' is 2.25. Consequently $\alpha' \approx 26°$.

Since the lower the penetration depth i.e. the distance at which the electric field strength vector of the radiation decreases to $1/e$ times its initial value, the larger the angle of incidence, our samples were formed in each case so that the angle of incidence of the light beam reaching the total reflexion plane should be 45°. In this way, total reflexion and small penetration depth can both be obtained.

The shapes of the samples used in our measurements are shown in Fig. 1. For total reflexion the light path is $1/\sin \alpha$ times the original sample length. (In our case, it is about 1.5 times.) The sample shape of 1 mm thickness in Fig. 1/a is disadvantageous because the transmitted and the incident beams

diverge by 90°. Therefore, it can be deflected to the original direction (towards the entrance slit of the infrared spectrophotometer) only by two mirrors. Apart from the adjustment difficulties these mirrors would also introduce considerable absorption and polarization losses. Fig. 1/b shows a modification where the incident and transmitted beams are parallel: their shift is not significant enough to necessitate the application of re-deflecting mirrors. In order to obtain equal incidence angles of the subsequent reflexions and to avoid polarization within the sample, the opposite surfaces of the slice should be strictly parallel. This was effected by polishing them so that a size inaccuracy was attained about one order of magnitude lower than the wavelength of the light.

We succeeded in increasing the absorption cross-section considerably by using the arrangement shown in Fig. 1/c. In this case, the strict requirements concerning the different sizes caused problems only for slices thinner than 500 μm.

The arrangement for measuring slices thinner than 500 μm (about 200—300 μm) is shown in Fig. 1/d. It permits an increase in the absorption cross-section and, since there is no total reflexion, the requirement of parallel opposite surfaces is not so strict. A further advantage of these last two sample arrangements is that as the oxygen concentration is not being measured on a certain part of the slice, the value obtained is an average one characteristic of the whole slice.

The individual slices shown in Figs 1/c and 1/d are cemented with phthalate resin which is also used for polishing. Since we used the same fit for the polishing and for measurement in an unchanged form, any possible inaccuracy introduced by separating and re-fitting the slices was avoided which would have caused transmission loss. Control measurements proved that the 9.1 μm absorption maximum which was the principal point of the investigations was not completely unaffected by the adhesive and the glass substrate holder. Summing up what has been said, the measuring can be evaluated as follows: for the measurement of thin slices the specimen arrangement shown in Figures 1/a and 1/b could be well applied down to 1 mm, while that in Fig. 1/c down to 500 μm and that in Fig. 1/d down to 200 μm.

4. Determination of the oxygen concentration

The infrared absorption spectra of oxidized and non-oxidized slices with different resistivities and different thicknesses were measured. For example, in Fig. 2 the absorption spectra of an *n*-type non-oxidized silicon slice of 7.5 ohm cm resistivity and of 200 μm thickness are shown. The wavelengths in 100 cm^{-1} units are on the abscissa. The 9.1 μm/1120 cm^{-1} SiO_2 absorption

peak is clearly observable. The absorption maxima, naturally, correspond to the minima of the transmission curve. The oxygen concentration was calculated from the 9.1 μm peak using the following method [8].

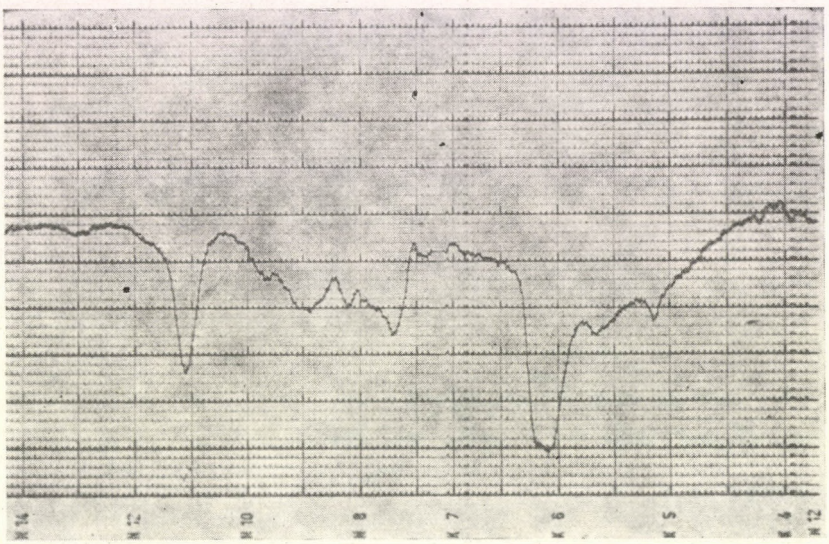


Fig. 2. Infrared absorption spectrum of a 220 μm thick silicon slice

Considering a simple, diatomic, harmonic oscillator, the area under the absorption maxima is

$$\int \alpha_\nu \, d_\nu = \frac{h\nu}{c} (B_{n,m} N_n - B_{m,n} N_m) , \tag{1}$$

where α_ν = absorption coefficient at ν frequency; c = light velocity in the silicon; N_n the number of the oscillators at the excitation level n, and N_m that at the excitation level m, $B_{n;m}$ and $B_{m;n}$ the Einstein absorption coefficients. The equation holds if we assume the charge distribution in the vibration oscillator to remain unchanged. At room temperature $h_\nu > kT$, therefore $N_n \gg N_m$, consequently

$$\int \alpha_\nu \, d_\nu = \frac{h\nu \, N_n \, B_{r;m}}{c} . \tag{2}$$

The value of the absorption coefficient in a material with a dielectric constant ε [9] is

$$B_{n;m} = \frac{\pi e^2 (n+1)(\varepsilon+2)^2}{3 \, \mu h\nu \cdot 9\varepsilon} , \tag{3}$$

where n is the refractive index of the material, μ the reduced mass of the vibration oscillators. After substituting for fundamental vibration ($n = 0$)

$$\int \alpha_\nu \, d_\nu = N_0 \frac{\pi e^2}{3 \mu c} \frac{(n^2+2)^2}{9 n}, \tag{4}$$

where N_0 is the number of the oscillators in the fundamental vibration. Approximating the area of the absorption peak by the product of the maximum absorption coefficient α_{max} and the half-width H, the number of the oscillators amounts to

$$N_0 = \frac{27 n \mu c}{(n^2+2)^2 \pi e^2} \alpha_{max} H. \tag{5}$$

Since each oxygen atom belongs to two oscillators, the number of the oxygen atoms is $N = N_0/2$. Only the maximum absorption coefficient α_{max} and the half-width H should be determined from the spectrum for the calculation of the oxygen concentration. The absorption peak coefficient can be calculated from the absorption law:

$$I = I_0 \, e^{-\alpha_{max} d}, \tag{6}$$

where I_0 is the incident, I the transmitted beam intensity, d the path length of the light through the material. It seemed to be more reasonable to substitute I_0 instead of the incident light intensity by the wavelength transmitted by the investigated substrate, since at this wavelength the spectrum has no absorption peak. It eliminates the error caused by the absorption loss eventually contributing to the 9.1 μm absorption peak. This method can be applied only if the reflectivity of silicon does not differ greatly for two incident light beams with different wavelengths. The difference between the two lights was less than 5% in our experiments. In the calculation the two intensity values and the half width of the 9.1 μm absorption maximum measured directly from the absorption spectrum were used.

Table II contains some characteristic data of several samples used in the measurements. The constants for the calculation were taken from the paper of KAISER [8]. However, we used the meanwhile modified and more accurate $n = 3.4$ value for the refraction index of silicon.

Since the 9.1 μm oxygen absorption peak is superimposed on the lattice vibration absorption with a coefficient of about 0.8 cm^{-1}, the maximum effective coefficient was used for the calculations, which is 0.8 cm^{-1} lower than the total absolute coefficient. The occlusions observed in the crystals were determined by X-ray measurements. It should be noted that the effective value of the minimum absorption coefficient should not exceed 7.2 cm^{-1}.

This corresponds to an oxygen concentration of about $2 \cdot 10^{18}$ cm^{-3}, i.e. the limit of solid solubility.

It could be concluded that between slices of various thickness produced from the same ingot, the difference in oxygen content would be small. Since the mechanical treatment cannot cause any considerable change in the oxygen

Table II

Oxygen concentration of different silicon slices

Characteristics of the slice				Absorption coefficient		Oxygen concentration	Remarks
No.	Type	Specific resistivity	Thickness	Total	Maximal effective		
		ohmcm	μm	cm^{-1}	cm^{-1}	$10^{17} \cdot$ cm^{-3}	
1	n	1.25	2000	3.3	2.5	4.88	
2	n	7.5	2000	4.08	3.28	6.40	Contains occlusions
3	n	7.7	220	4.0	3.2	6.25	Contains occlusions
4	n	5.2	250	2.05	1.25	3.41	After mechanical treatment
5	n	5.2	250	2.07	1.27	3.45	Oxidized, then oxide film removed

concentration, the observed small deviation proves that an appropriate process was found for the measurement of oxygen concentration in thin slices.

According to our recent results the conclusion seems to be well established that surface oxidization does not increase the oxygen concentration of the bulk within the measuring limits.

5. Absorption cross-section

BECKMAN determined the surface absorption cross-section of SiO_2 groups from the absorption spectra of SiO_2 films [10]. In his calculations he used the relation

$$\alpha_{max} = \alpha_0 N_{SiO_2}, \tag{7}$$

where N_{SiO_2} is the number of the SiO_2 groups and α_0 the cross-section of a single SiO_2 group. N_{SiO_2} is equal to half the number of oxygen atoms.

Hence, the absorption cross-section value of the SiO_2 groups contained in the oxide layer is

$$\alpha_0 \approx 1.1 \cdot 10^{-18} \text{ cm}^2. \tag{8}$$

Since we determined the number of SiO_2 groups located in the bulk and not on the surface, our results are suitable for a similar estimation of the bulk absorption cross-section of SiO_2 groups. According to Table I $\alpha_{max} = 3.2$; $N_{SiO_2} = 3.12 \cdot 10^{17}\,cm^{-3}$, the bulk absorption cross-section of the SiO_2 groups is:

$$\alpha_0 \approx 1.2 \cdot 10^{-17}\,cm^2. \tag{9}$$

Acknowledgments

Thanks are due to Mrs. E. Rózsa and to Dr. M. Szilágyi for their valuable assistance and discussions. We have to thank Dr. A. Kiss for his cooperation during the measurements.

REFERENCES

1. W. Kaiser and P. H. Keck, J. of Appl. Phys., **28,** 882, 1957.
2. G. W. Green et al., J. of Electronics and Control, **III,** 171, 1957.
3. W. A. Pliskin and H. S. Lehman, J. of Elchem. Soc., **112,** 1013, 1965.
4. W. A. Pliskin, Appl. Phys. Letters, **7,** 158, 1965.
5. Y. Yukimoto and H. Hori, Jap. J. of Appl. Phys., **6,** 1010, 1967.
6. C. S. Fuller et al., J. of Appl. Phys., **28,** 1427, 1957.
7. W. Kaiser, Phys. Rev., **105,** 1751, 1957.
8. W. Kaiser et al., Phys. Rev., **101,** 1264, 1956.
9. R. E. Richards and W. R. Burton, Trans. Faraday Soc., **45,** 874, 1949.
10. K. H. Beckman, Surf. Sci., **3,** 314, 1965.

ОПРЕДЕЛЕНИЕ СОДЕРЖАНИЯ КИСЛОРОДА В ТОНКИХ ПЛАСТИНКАХ КРЕМНИЯ

И. СЕЙП и И. БАРШОНЬ

Р е з ю м е

Рассматриваются минимумы инфракрасного трасмиссионного спектра различных бъемных и поверхностных кислородных связей кремния. Излагаются методы, исследоoания содержания кислорода в тонких пластинках кремния. Определяется значение вонцентраций кислорода в некоторых образцах и оценивается эффективное поперечное ечение объемной абсорпции групп SiO_2.

Acta Physica Academiae Scientiarum Hungaricae, Tomus 29 (2—3), pp. 107—116 (1970)

VIBRATION SPECTRA AND DEBYE TEMPERATURES OF TRANSITION METALS

By

S. K. SANGAL and P. K. SHARMA

PHYSICS DEPARTMENT, ALLAHABAD UNIVERSITY, ALLAHABAD, INDIA

(Received 23. I. 1969)

The vibration spectra and specific heats of three body-centred cubic transition metals, α-iron, tungsten and molybdenum have been calculated from BHATIA's model of electron-lattice interaction by considering second neighbour inter-ionic interactions. The force constants are determined from the experimental elastic constants and one measured frequency. The calculated specific heats are compared with the available experimental data by computing the equivalent Debye temperature as a function of temperature and the agreement with experiment is reasonably satisfactory.

I. Introduction

The theoretical study of the thermal properties of transition metals seems to have received very little attention in the past. However, during the last few years considerable attention has been paid to the experimental study of lattice vibrations in these metals by measuring the phonon dispersion relations from the observations of the momentum and energy changes in the inelastic scattering of slow neutrons. Detailed frequency-wave vector dispersion relations for normal modes of vibration travelling along the three symmetry directions of several transition metals are now available [1, 2]. This has stimulated considerable interest in the vibrational properties of these metals and attempts have been made to interpret the experimental results on the basis of Born — von Kármán force models.

The transition metals in the fifth and sixth columns of the periodic table have extremely interesting electronic and superconducting properties. They all have a body-centred cubic structure with one atom per unit cell similar to alkali metals. However, the interpretations of their thermal properties have been limited. The earlier computations of heat capacities of α-iron by CLARK [3], and SHARAN and TIWARI [4], of tungsten by FINE [5], SHARAN [6] and CLARK [3], and of molybdenum by SHARAN [6], and CLARK [3] do not show a satisfactory agreement with the experimental data at low temperatures. This is not surprising because these studies use models which consider limited inter-ionic interactions. In the case of the transition metals tungsten and molybdenum, it is found from neutron scattering experiments that the second neighbour force constants are of the same order as for first

neighbours. This suggests a long-range nature of interatomic interactions. Similar conclusions for α-iron have been obtained by CURIEN [7] from the analysis of his diffuse X-ray scattering measurements.

It is now well known that electrons in metals have a drastic influence on their lattice dynamical properties and these are responsible for the failure of the Cauchy relation. BHATIA [8] has propounded a model for studying the lattice vibrations in metals by considering the influence of electrons on ionic motion through the screening of the Coulomb interaction between metal ions. In this model, each element of the dynamic matrix is expressed as a sum of two terms contributed by electrons and ions, respectively. The electronic term is computed from the Thomas—Fermi model of the atom. The ionic part of the interaction is taken to be the first two terms in a Taylor expansion of the potential energy for the first nearest neighbours. The model has been found to give a reasonable description of lattice specific heats of many cubic metals [9]. It has recently been utilized to explain the temperature dependence of thermal expansion, Debye—Waller factors and transport properties of alkali and noble metals [10].

It would be desirable to consider a modification in BHATIA's model by considering the second nearest neighbour inter-ionic interactions. In this paper we present a modification of BHATIA's model by including the second neighbour ionic interactions. The theory is applied to obtain the vibration spectra and specific heats of three transition metals, α-iron, tungsten and molybdenum. The results of calculations are compared with available empirical data.

II. Theory

Proceeding in the usual way, the equation of motion can be written as [8]

$$\mathbf{e}M\omega^2 = 2\sum_n \left[\alpha_s \mathbf{e} + (\beta_s/a^2)(\mathbf{e}\cdot R^n)\,R^n\right]\left[\sin^2\frac{1}{2}(q\cdot R^n)\right]\times \times \frac{K_e(\mathbf{e}\cdot q)\,n^{-1}\,q}{1+K_e\,q^2/4\pi e^2\,n^2}\,, \tag{1}$$

where R^n is the equilibrium position vector of the nth atom, a half of the lattice constant, e the polarization vector, ω the angular frequency, q the phonon wave vector, n the electron number density and M the ionic mass. α_s and β_s are the first two derivatives of the potential energy for sth neighbour and the parameter K_e comes from the electronic part. BHATIA has considered the ionic interactions between the first nearest neighbours only. In a body-centred cubic structure, there are six second nearest neighbours having the position coordinates $a\,(\pm 2, 0, 0)$, $a\,(0, \pm 2, 0)$ and $a\,(0, 0, \pm 2)$. Summing the

series in Eq. (1) out to second nearest neighbours, we get for a nontrivial solution a 3×3 secular determinant for the determination of normal modes of vibration in a cubic metal. The expressions for the diagonal and non-diagonal elements of the matrix equation are given by

$$D_{ii}(q) = 8(\alpha_1+\beta_1)(1-C_1C_2C_3)+\alpha_2(S_1^2+S_2^2+S_3^2)+16\,\beta_2\,S_i^2+ \\ +\frac{4\,K_e\,a^3\,q_i^2}{1+K_e\,q^2/4\pi e^2\,n^2}\,,$$

$$D_{ij}(q) = 8\,\beta_1\,S_i\,S_j\,C_k+\frac{4\,K_e\,a^3\,q_i\,q_j}{1+K_e\,q^2/4\pi e^2\,n^2}\,, \qquad (2)$$

where $S_i = \sin(q_i\,a)$, $C_i = \cos(q_i\,a)$, q_i the ith Cartesian component of wave vector q, and α_1, β_1 and α_2, β_2 the first two derivatives of the potential energy for first and second nearest neighbours, respectively.

III. Calculation of parameters

The five parameters occurring in the theory can be connected with the elastic constants by going to the long wavelength limit. The required relations between the force constants and the elastic constants have been obtained by expanding the elements $D_{ij}(q)$ along the symmetry directions [100], [110] and [111] in powers of q_i retaining only quadratic terms and comparing the results with the Christoffel equation of elasticity. We assumed that the electronic parameter K_e is not modified by the inclusion of second neighbour interactions so that its value may be taken to be the same as in BHATIA's model i.e. C_{11}—C_{44}. Since the number of parameters to be determined are four, an additional relation is necessary to fix them. The additional relation is obtained from the experimentally observed frequency at the Brillouin zone boundary in the [110] transverse branch.

IV. Numerical computations

We have used the present theory to compute the vibration spectra and specific heats of three body-centred cubic transition metals, α-iron, tungsten and molybdenum. The computations are made by BLACKMAN's sampling technique [11]. In order to keep the labour of calculation within reasonable limit and yet to get a fairly large survey of frequencies, we have used an evenly spaced sample of 8000 wave vectors in the first Brillouin zone. From symmetry considerations, the vibration frequencies are calculated at nonequivalent points lying within the 1/48 irreducible sector of the Brillouin zone and weighted according to symmetrically equivalent points. Proper attention was given for

Table I

Values of constants used in the calculation

Metal	Elastic constants (10^{11} dynes/cm^2)			Lattice parameter (Å)	Ionic mass (a.m.u.)
	C_{11}	C_{12}	C_{44}		
α-iron	23.310	13.544	11.783	2.886	55.85
tungsten	52.327	20.453	16.072	3.160	183.86
molybdenum	44.077	17.243	12.165	3.141	95.95

Table II

Force constants for α-iron, tungsten and molybdenum

Metal	α_1	β_1	α_2	β_2	K_σ (10^{12} dynes/cm^2)
	(10^4 dynes/cm)				
α-iron	0.9012	0.9961	—0.0655	0	1.1527
tungsten	2.8410	0.2110	—0.1074	0	3.6255
molybdenum	2.6060	—0.1966	—0.1663	0	3.1912

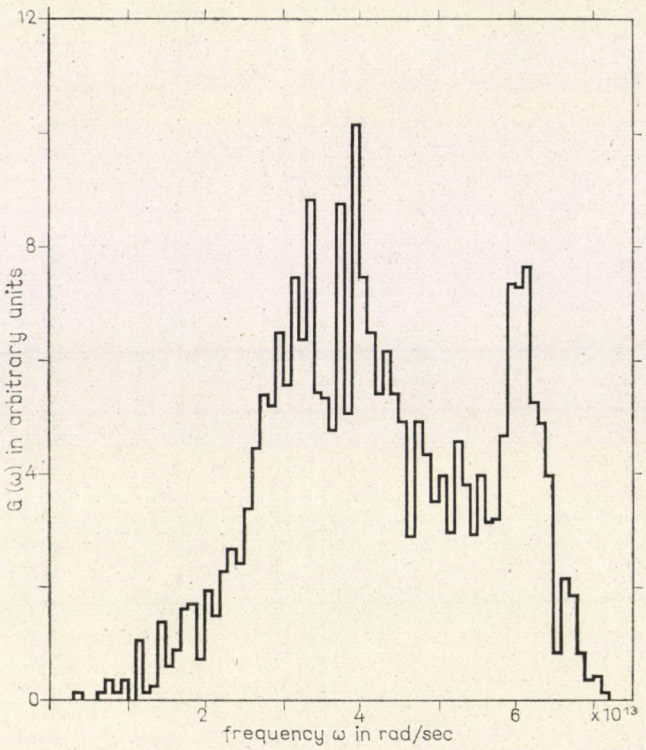


Fig. 1. The vibration spectra of α-iron

points lying on the surface, an edge or a corner of the Brillouin zone. The elastic constants and other relevant data for these metals needed in the calculation are listed in Table I. These elastic constants refer to room temperature. They are taken from the measurements of RAYNE and CHANDRASEKHAR [12] for α-iron, while those for tungsten and molybdenum are due to FEATHERSTON

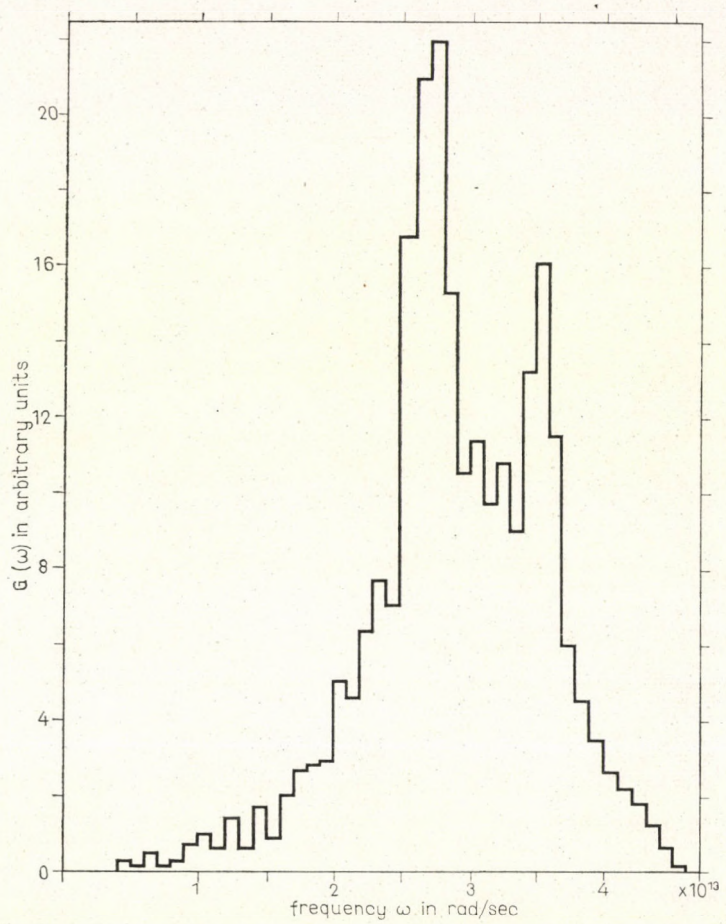


Fig. 2. The vibration spectra of tungsten

and NEIGHBOURS [13]. The values of the frequency at the zone boundary for the [110] transverse branch are taken from the work of LOW [14] for α-iron, from CHEN and BROCKHOUSE [15] for tungsten and from WOODS and CHEN [16] for molybdenum. The calculated values of the force constants from these input data are given in Table II.

The vibration spectra for α-iron, tungsten and molybdenum obtained from these force constants are shown in Figs. 1—3, respectively. These curves

have not been normalized and the units of $G(\omega)$ are arbitrary. Using these spectra, the specific heats at constant volume were calculated in the usual manner by numerical integration. The calculated specific heats are compared with the experimental data in terms of the equivalent Debye temperature Θ. The $\Theta - T$ curves for the three metals are shown in Figs. 4—6. For comparison, in these figures, we have also plotted the experimental data obtained at different temperatures.

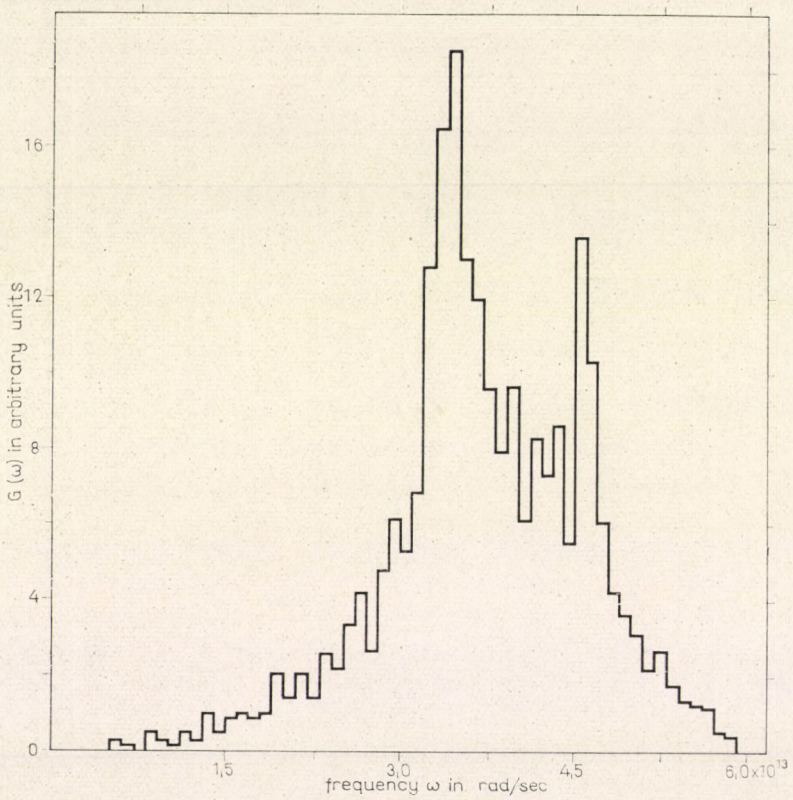


Fig. 3. The vibration spectra of molybdenum

V. Discussion

For convenience it is better to separate the discussion for the three metals.

(1) α-iron

The experimental data for the specific heats below 50 °K are taken from the work of DUYCKAERTS [17], while those above 50 °K are due to KELLEY [18]. The measurements of KELLEY are in broad agreement with those of EUCKEN and WERTH [19], and SIMON and SWAIN [20]. The experimental specific heats

have been plotted after correcting for the electronic and spin wave contributions. For this purpose the coefficients of the electronic and spin wave specific heat terms have been taken as 1.134×10^{-3} cal mol^{-1} deg^{-2} and $1.15 \times \times 10^{-5}$ cal mol^{-1} deg$^{-5/2}$, respectively, from the work of DIXON et al. [21].

It is seen from Fig. 4 that the agreement between theory and experiment is satisfactory in the middle temperature region. At low temperatures the experimental values are higher than the theoretical values, while above 120 °K

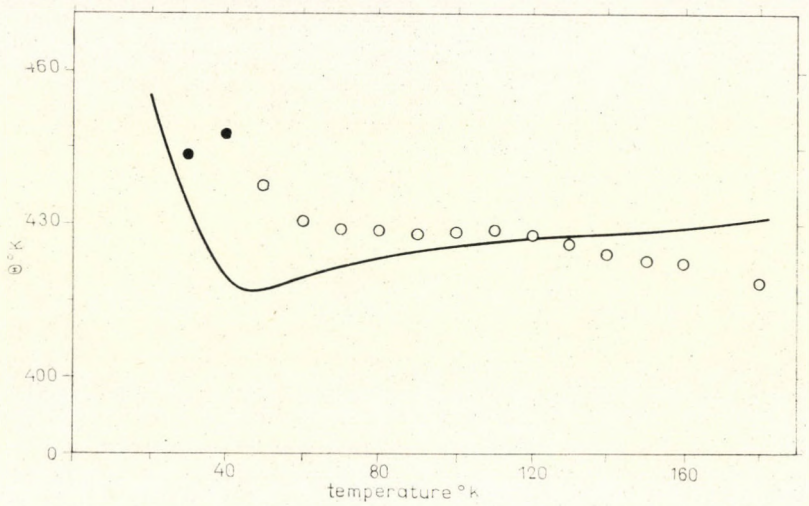


Fig. 4. The Debye temperature versus temperature curve for α-iron. The solid line represent our calculations. Experimental data are: ● DUYCKAERTS, ○ KELLEY

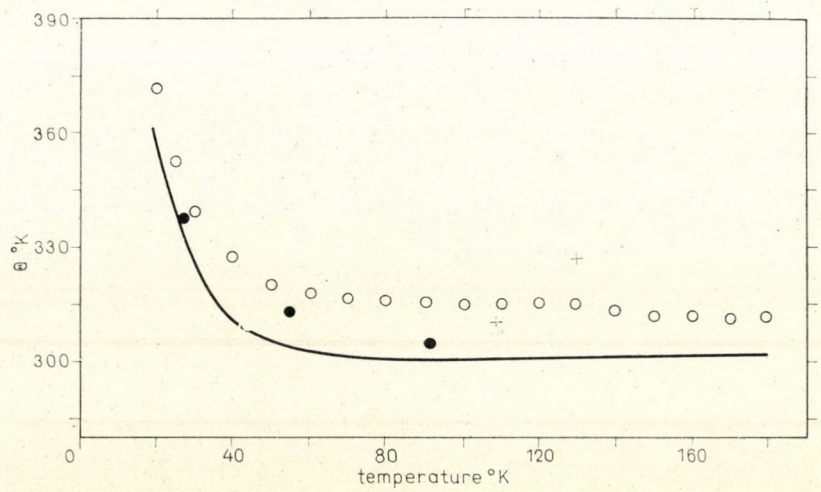


Fig. 5. Variation of Debye temperature of tungsten with temperature. The solid line is based on our computations. Experimental data are: ○ CLUSIUS and FRANZOSINI, ● LANGE, + ZWIKKER

the theoretical values are greater than experimental ones and the discrepancy increases with the rise of temperature. The discrepancies at lower and higher temperatures may be attributed to the neglect of temperature dependence of elastic constants and uncertainties in the electronic and spin wave contributions to the specific heat.

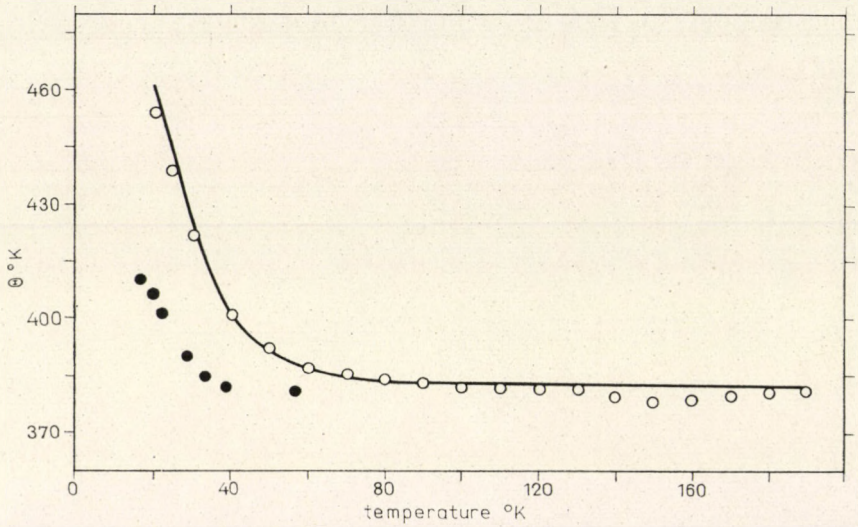


Fig. 6. The Debye temperature of molybdenum as a function of temperature. The solid curve depicts our calculations. Experimental data are: ○ CLUSIUS and FRANZOSINI, ● SIMON and ZEIDLER

(2) Tungsten

The heat capacities of tungsten have been measured by LANGE [22] between 26° and 91 °K and by ZWIKKER [23] above 100 °K. The more recent measurements of CLUSIUS and FRANZOSINI [24] are in approximate agreement with those of LANGE [22] and ZWIKKER [23]. The value of γ, the coefficient of the electronic specific heat term, reported by different workers varies within very wide limits. We have corrected the experimental specific heats with $\gamma = 0.27 \times 10^{-3}$ cal mol^{-1} deg^{-2} from the recent work of CLUSIUS and FRANZOSINI [24]. It will be seen from Fig. 5 that the calculated curve lies very close to the experimental Θ values. The difference between the observed and calculated Θ values never exceeds 4%.

(3) Molybdenum

The experimental data for the specific heats have been taken from the work of CLUSIUS and FRANZOSINI [24], and SIMON and ZEIDLER [25]. In this case the values of γ quoted by different workers are fairly consistent. We have

taken γ as 0.50×10^{-3} cal mol^{-1} deg^{-2} from CLUSIUS and FRANZOSINI [24] data. Fig. 6 shows that the calculated temperature variation of the Debye temperatures is in reasonably good agreement with experiments.

A survey of Figs. 4—6 shows that there is reasonably satisfactory agreement between theory and experiment by the inclusion of second neighbour interatomic interactions. The agreement is particularly good in the case of tungsten and molybdenum. BHATIA's model in the present form using three interatomic force constants gives a reasonable description of the thermal properties of transition metals.

It is worth while to mention here that the unionized free atoms of transition metals contain incomplete *d*-electronic shells. These are believed to be responsible for their large cohesive energies [26] and are expected to play an important role in the lattice dynamics of these metals. This is to be taken into account in studying the thermal properties of transition metals. However, its inclusion in lattice dynamical problems is extremely difficult owing to incomplete knowledge of the states of the valence electrons and their interaction with phonons.

Acknowledgements

The authors are grateful to the University Grants Commission, New Delhi for financial assistance. Part of the work was supported by the Department of Atomic Energy, Bombay.

REFERENCES

1. G. DOLLING and A. D. B. WOODS, in Thermal Neutron Scattering, edited by P. A. Egelstaff (Academic Press Inc., New York, 1965), p. 193.
2. B. N. BROCKHOUSE, in Phonons and Phonon Interactions, edited by T. A. Bak (W. A. Benjamin, Inc., New York, 1964), p. 221.
3. C. B. CLARK, Phys. Rev., **125,** 1898, 1962.
4. B. SHARAN and L. M. TIWARI, Phys. Status Solidi, **3,** 1408, 1963.
5. P. C. FINE, Phys. Rev., **56,** 355, 1939.
6. B. SHARAN, Phys. Status Solidi, **1,** 243, 1961.
7. H. CURIEN, Bull. Soc. Franc. Mineral Crystal, **75,** 197, 1952; Acta Cryst., **5,** 393, 1952.
8. A. B. BHATIA, Phys. Rev., **97,** 363, 1955.
9. A. B. BHATIA and G. K. HORTON, Phys. Rev., **98,** 1715, 1955; S. K. JOSHI and M. P. HEMKAR, J. Chem. Phys., **34,** 1458, 1961; Phys. Rev., **122,** 13, 1961; Physica, **27,** 793, 1961; M. P. HEMKAR and S. K. JOSHI, J. Phys. Soc. Japan, **17,** 754, 1962.
10. S. K. SANGAL and P. K. SHARMA, Acta Physica et Chemica, Hungary, **15,** 35, 1969. S. K. SANGAL, Ph. D. thesis, Agra University, Agra, India, 1968.
11. M. BLACKMAN, in Handbuch der Physik, edited by S. Flügge (Springer-Verlag, Berlin, 1958), Vol. 7, p. 325.
12. J. A. RAYNE and B. S. CHANDRASEKHAR, Phys. Rev., **122,** 1714, 1961.
13. F. H. FEATHERSTON and J. R. NEIGHBOURS, Phys. Rev., **130,** 1324, 1963.
14. G. G. E. LOW, Proc. Phys. Soc. (London), **79,** 479, 1962.
15. S. H. CHEN and B. N. BROCKHOUSE, Solid State Commun., **2,** 73, 1964.
16. A. D. B. WOODS and S. H. CHEN, Solid State Commun., **2,** 233, 1964.
17. G. DUYCKAERTS, Physica, **6,** 401, 1939.
18. K. K. KELLEY, J. chem. Phys. **11,** 16, 1943.
19. A. EUCKEN and H. WERTH, Z. anorg. allgem. Chem., **188,** 152, 1930.
20. F. SIMON and R. C. SWAIN, Z. Physik Chem., (Leipzig), **B28,** 189, 1935.

21. M. Dixon, F. E. Hoare, T. M. Holden and D. E. Moody, Proc. Roy Soc., **A285**, 561, 1965.
22. F. Lange, Z. Physik Chem. (Leipzig) **110**, 343, 1924.
23. C. Zwikker, Z. Physik, **52**, 668, 1928.
24. K. Clusius and P. Franzosini, Z. Naturforsch., **14A**, 99, 1959.
25. F. Simon and W. Zeidler, Z. Physik Chem., (Frankfurt) **123**, 387, 1962.
26. N. F. Mott, Rept. Progr. Phys., **25**, 218, 1962.

КОЛЕБАТЕЛЬНЫЕ СПЕКТРЫ И ТЕМПЕРАТУРА ДЭБАЯ ПЕРЕХОДНЫХ МЕТАЛЛОВ

С. К. САНГАЛ и П. К. ШАРМА

Р е з ю м е

По модели Бация взаимодействия электронов с решеткой с учетом междуионных взаимодействий вторых соседей определяются колебательные спектры и удельные теплоемкости трех объемноцентрированных кубических переходных металлов — железа, вольфрама и молибдена. Силовые константы определяются из опытных значений постоянных эластичности и измеренных частот колебаний. Вычисленные удельные теплоемкости сравниваются с имеющимися экспериментальными данными путем вычисления эквивалентной температуры Дэбая как функции температуры. Результаты удовлетворительно согласуются с экспериментальными данными.

Acta Physica Academiae Scientiarum Hungaricae, Tomus 29 (2—3), pp. 117—125 (1970)

THE INFLUENCE OF COBALT ON THE PHOTO-LUMINESCENCE OF SILVER-ACTIVATED ZnS : CdS PHOSPHORS CONTAINING NICKEL

By

M. S. EL-MANHARAWY

THE CANCER INSTITUTE, CAIRO UNIVERSITY, CAIRO, UAR

(Received 6. II. 1969)

The influence of cobalt inclusions in ZnS : CdS : Ag : Ni phosphors on their excitation and emission spectra, temperature-dependence of fluorescence and thermoluminescence has been studied. Increase in cobalt concentration seems to have no effect on the excitation and emission spectra. The temperature-dependence of fluorescence of phosphors containing 0%—0.065% cobalt has been measured over the temperature range of 77 °K to 600 °K. The observed changes in the activation energy for the quenching process with increase in cobalt concentration are attributed to the presence of deep electron traps. Thermoluminescence curves show peaks identified as due to chlorine, cadmium, cobalt and nickel impurities. The corresponding energy depths are 0.26 eV, 0.52 eV, 0.53 eV and 0.78 eV. A thermoluminescence peak with an energy depth of 1.09 eV has also been found. An attempt has been made to identify the origin of this peak.

Introduction

Impurity-activated zinc sulphide type phosphors with additional nickel, cobalt or iron impurities as "luminescence quenchers" have been investigated by many workers to study the fundamental luminescence mechanisms involved. It appears from the literature that most of the phosphors investigated contained only one type of quencher centre as the coactivator and no attempt was made to study the effect of introducing a second quencher centre together with the first. For instance, all the phosphors investigated by KLASENS and WISE [1]; GARLICK and GIBSON [2]; NAIL and his coworkers [3]; ROBERTS and WILLIAMS [4]; HOOGENSTRAATEN and KLASENS [5]; and HOOGENSTRAATEN [6] contained cobalt or nickel or iron as the luminescence quencher. The aim of this paper is to study the influence of cobalt inclusions on the photo-luminescence characteristics of ZnS : CdS : Ag : Ni phosphors.

It is known that when cobalt, nickel or iron is included in zinc sulphide type phosphors characteristic trapping levels with high recombination coefficients result. ARPIARIAN [7] and GERGELY [8] suggested that deep electron trapping states and/or, hole acceptor levels created by nickel or cobalt inclusions, are responsible for their quenching action. KRYLOVA [9] was the first to detect the thermal glow peak due to deep traps associated with cobalt impurity in zinc sulphide. This peak has a maximum at 383 °K for a warming

rate of 2 °K/sec. The system ZnS : Cu : Co has since been investigated by KLASENS and HOOGENSTRAATEN [5] who found that the usual thermoluminescence peak due to Cu in ZnS is quenched by the addition of Co, which suggests a retrapping process. HOOGENSTRAATEN [6] reported a value of 0.52 eV for the depth of the trap associated with cobalt and also found that the cobalts glow peak shifts to higher temperatures when either the cobalt concentration or the decay time of the glow is increased. The same author was unable to find the corresponding thermoluminescence peaks from samples containing nickel or iron but found sufficient indication that similar but much deeper trapping states are present. GARLICK and ELMANHARAWY [10] were recently able to detect a glow peak due to nickel impurity in silver-activated mixed crystals of zinc and cadmium sulphides by direct thermoluminescence measurements. This nickel glow peak has an energy depth of 0.78 eV and shifts regularly to lower temperatures with increase in either the cadmium content of the matrix lattice or the nickel impurity concentration.

Experimental techniques

Phosphors

All the phosphors, prepared in the presence of chlorine, were in powder form, with 41% ZnS, 59% CdS, 0.009% Ag, 0.00065% Ni and Co concentrations varying from 0% to 0.065%. This host lattice concentration is the threshold for the detection of the nickel glow peak by direct thermoluminescence measurements for reasons which will be published elsewhere [10].

Measurements

Conventional techniques were used for measuring excitation and emission spectra, temperature-dependence of fluorescence and thermoluminescence curves.

For measuring excitation spectra, light from a 50 watt tungsten lamp was chopped, scanned by a Barr and Stroud double prism monochromator equipped with calcium fluoride prisms, and then focused on the sample which was mounted in a cryostat. Emission from the sample was detected by a photomultiplier, amplified by an 800 C/sec tuned amplifier and finally recorded. Selected filters were placed in front of the photomultiplier to prevent any exciting light from reaching the detector. Measured spectra were corrected for the non-linear properties of the apparatus.

Emission spectra were measured by adapting the optical system so that emission from the sample after excitation by 3650 Å radiation from a mercury lamp, was focussed on the entrance slit of the monochromator. The intensity

of light passing through the monochromator was detected, amplified using the chopper disc system and recorded. Again, all measured spectra were corrected for the non-linear properties of the apparatus.

Temperature-dependence of fluorescence and thermoluminescence curvewere measured by mounting the phosphor in vacuum on the thermally insut lated cold finger of a cryostat. The temperature could be varied from 77 °K to 650 °K by means of liquid nitrogen and a heating element. A linear heating rate of 2.5 °K/sec was always maintained. Radiation from a mercury lamp fitted with a Chance OX1 filter was focussed on the phosphor surface and the emitted luminescence was focussed on a photomultiplier. The output signal was amplified by a d.c. amplifier and presented to a pen recorder.

The temperature of the phosphor was measured by a copper-constantan thermocouple and the generated e.m.f. was amplified and presented to a recorder which was synchronized with the first at the start of the experiment. The observed accuracy of the temperature readings was of the order of ± 3 °K. A solution of copper chloride and a Wratten 2E filter to reduce the intensity of emitted infra-red or reflected ultraviolet respectively, as well as a Kodak 22 optical filter appropriate to the spectrum, were introduced into the beam.

Results

(i) Excitation and emission spectra

Fig. 1 illustrates excitation spectra recorded at 77 °K and room temperature. Excitation can be seen to occur in the fundamental absorption band and in a second band of longer wavelength. It is obvious that the wavelength of maximum excitation efficiency is independent of the cobalt concentration. The spectra resemble those for ZnS : CdS : Ag and ZnS : CdS : Ag : Ni phosphors with the same host matrix lattice composition [10]. This indicates that the energy level structure with the silver impurity centres is not affected by the cobalt content. The decrease in excitation efficiency due to the increased quenching action with increase in cobalt concentration is also evident from the Figure.

Emission spectra recorded at 77 °K and room temperature are shown in Fig. 2. They agree quantitatively with previous results for ZnS : CdS : Ag and ZnS : CdS : Ag : Ni phosphors of similar host matrix lattice composition [10]. Thus, the introduction of cobalt has no influence on the spectral distribution of the silver emission band in these phosphors. No new emission due to cobalt or nickel could be found in the wavelength range of 3700 to 9000 Å. Again, the quenching action of cobalt is shown by the observed decrease in emission intensity as the cobalt concentration increases.

It is of interest to note the decrease in both the excitation efficiency and emission intensity in Figs. 1 and 2 with rise in temperature from 77 °K to room temperature. This is due to the well-known phenomenon of temperature-quenching of emission by positive hole migration, effective at elevated temperatures.

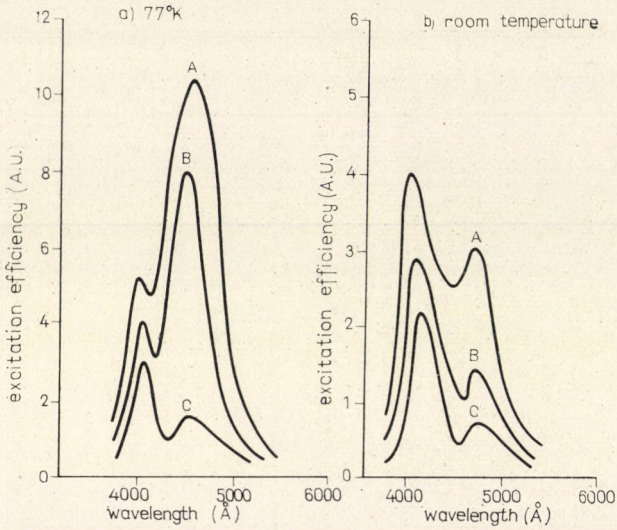


Fig. 1. Excitation spectra for 41% ZnS : 59% CdS : 0.009% Ag : 0.00065% Ni : x% Co phosphors; A) $x = 0$; B) $x = 0.0065$; C) $x = 0.0325$

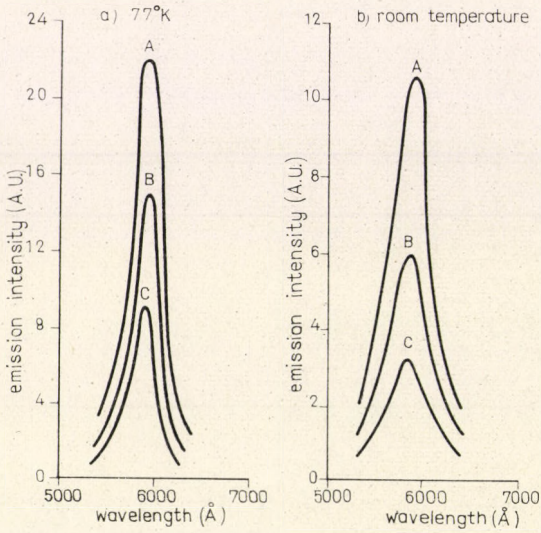


Fig. 2. Emission spectra for 41% ZnS : 59% CdS : 0.009% Ag : 0.00065% Ni : x% Co phosphors; A) $x = 0$%; B) $x = 0.0065$; C) $x = 0.0325$

(ii) Temperature-dependence of fluorescence

The curves showing the fluorescence intensity under steady excitation by 3650 Å radiation as a function of temperature are given in Fig. 3. While the maximum of each curve has been taken as 100, the relative intensities actually decrease with increase in cobalt concentration.

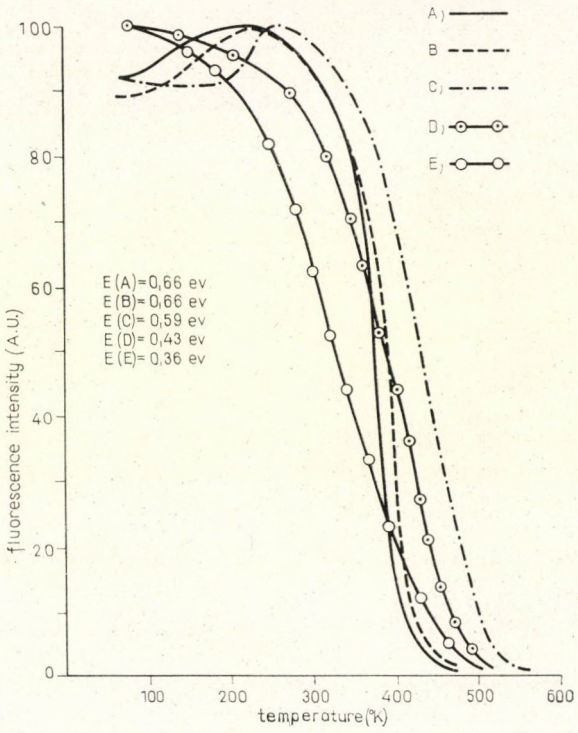


Fig. 3. Temperature-dependence of fluorescence curves for 41% ZnS : 59% CdS : 0.009% Ag : 0.00065% Ni : x% Co phosphors; A) $x = 0$; B) $x = 0.00013$; C) $x = 0.0013$; D) $x = 0.0325$; E) $x = 0.0650$

The curves follow the form of the equation suggested by KLASENS and WISE [1] which gives the fluorescence intensity, I, at a temperature, T, as:

$$I = \frac{I_0}{1 + C \exp(-E/KT)},$$

where: I_0 is the fluorescence intensity at low temperatures at which positive hole migration is negligible,

C is a constant,

K is Boltzmann's constant, and

E is the activation energy for the quenching process.

From the descending part of the temperature-dependence curve the activation energy, E, can be obtained from the slope of the straight line resulting when values of $(I_0/I - 1)$ are plotted logarithmically against $1/T$. For the cobalt-free phosphor, an activation energy of 0.66 eV was found by this method. It decreased gradually with increase in cobalt concentration, reaching a value of 0.36 eV for a cobalt concentration of 0.065%.

If such lowering of activation energy values were primarily due to the presence of cobalt, a shift of the silver emission band towards shorter wavelengths would be expected. No such shift was found, as is evident from the experimental results in Fig. 2. It is possible, however, that deep electron traps, known to be present in these phosphors and filled at low temperatures, are responsible for the changes observed. Undoubtedly, these electron traps affect the equilibrium between free electrons, holes and centres [1].

Since the number of deep electron traps is directly related to the cobalt concentration, it is therefore expected that more electrons will be trapped with increase in cobalt concentration. Consequently, fewer electrons will be available for recombination with empty silver centres to produce the observed fluorescence. This will cause a shift of the whole temperature-dependence curve, leading to a change in slope of the $\ln (I_0/I - 1)$ versus $1/T$ curve, from which the activation energy is calculated. This is in accordance with the work of HILL and KLASENS [11], who reported similar changes in slope of their curves with increase of cobalt concentration in ZnS : Ag : Co phosphors and attributed these changes to the presence of electron traps.

(iii) Thermoluminescence curves

Fig. 4. illustrates thermoluminescence curves for phosphors with different cobalt inclusions. Curve (A) for the cobalt-free phosphor exhibits three well-separated thermal glow peaks identified as specifically due to trapping states associated with chlorine, cadmium and nickel impurities. Their respective energy depths, estimated by using the variation of the heating rate method suggested by HOOGENSTRAATEN [6], are 0.26 eV, 0.52 eV and 0.78 eV. The energy depths of the chlorine and cadmium glow peaks are similar to those reported by HOOGENSTRAATEN in ZnS : CdS : Cu : Co phosphors, while that of the nickel glow peak is identical with that recorded by GARLICK and ELMANHARAWY [10] for ZnS : CdS : Ag : Ni phosphors.

With the gradual increase in cobalt concentration, the chlorine and cadmium glow peaks decrease in height, until at a cobalt concentration of 0.001% they disappear completely (curve B). This disappearance is attributed to the increased retrapping caused by the presence of cobalt and nickel. During the heating process, electrons released from the shallow trapping states due to chlorine and cadmium are retrapped into the deeper cobalt and nickel

trapping states. As the chlorine and cadmium glow peaks disappear, a glow peak appears at 310 °K. This new peak is identified as specifically due to trapping states associated with cobalt impurity. It has properties similar to those of the cobalt glow peak reported by HOOGENSTRAATEN [6] in ZnS : CdS : Cu : Co phosphors. The energy depth is 0.53 eV; it shifts to higher temperatures with increase in cobalt concentration; and it has the ability to retrap electrons from shallower trapping states during heating.

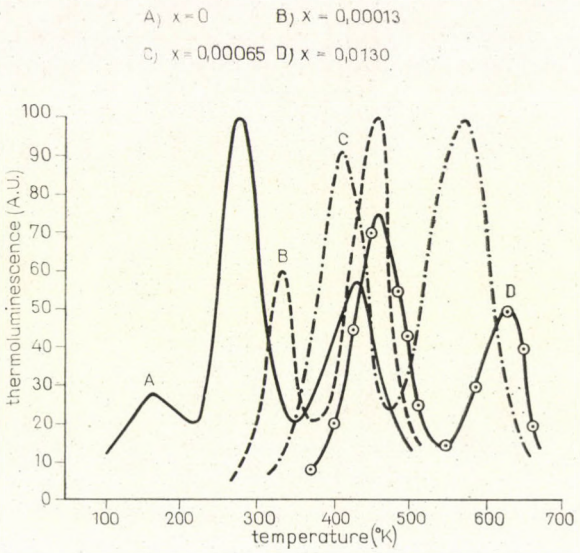


Fig. 4. Thermoluminescence curves for 41% ZnS : 59% CdS : 0.009% Ag : 0.00065% Ni : x% Co phosphors

Once the cobalt concentration reaches 0.0065%, the cobalt glow peak disappears while the nickel glow peak remains unaffected (Curve C). At the same time, a new glow peak with an energy depth of 1.09 eV appears at temperatures higher than 550 °K. This new peak is probably caused by the association of the activator (Ag) and coactivator (Co or Ni) centres. It is possible that at high impurity concentration, activator and coactivator centres associate and a pair of this type in which the activator centre is ionized by capturing a hole can act as an electron trap responsible for the new glow peak.

With further increase in cobalt concentration, the glow peak at temperatures higher than 550 °K decreases in height relative to that of the nickel glow peak (Curve D). There is no explanation for this observation at present, but a strong interaction between the various centres present is clearly evident.

It is interesting to mention that the glow colour is yellow at temperatures where the chlorine, cadmium and cobalt peaks appear. However, the emission colour changes to red at temperatures where the nickel glow peak appears. The colour of the very high temperature glow peak is also red.

Discussion and conclusions

It has been shown that the silver emission band in ZnS : CdS : Ag : Ni : Co phosphors is independent of the cobalt concentration, giving evidence that the energy level structure with the silver centres remains unaltered by the inclusion of the coactivators. This is in agreement with the SCHON [12], KLASENS [13] model, according to which the different centres of the activator and coactivator should have no influence on one another.

The form of the temperature-dependence curve is in accordance with the simple thermal quenching theory, though the activation energy for the quenching process changes with increase in cobalt concentration. These changes are primarily due to the presence of deep electron traps in the phosphors investigated.

The energy band gap in these phosphors is 2.79 eV, corresponding to a matrix lattice concentration of 41% ZnS : 59% CdS. From the emission spectra measurements, the silver level is 2.04 eV below the lower edge of the conduction band. When a trapped electron is freed on heating, the thermoluminescence colour resulting from its recombination, via the conduction band, with an empty silver centre should be yellow. While this was observed with the chlorine, cadmium and cobalt glow peaks, the colour of the nickel glow was red. It has been shown by GARLICK and ELMANHARAWY [10] that the nickel centres can provide an alternative level at which the recombination responsible for the glow occurs. A filled nickel trap which constitutes an effectively negative nickel centre may produce its own kind of activator level, like the silver activator centre, by lifting an occupied level from the valence band.

So far, it has not been possible to identify the exact origin of the glow peak appearing at temperatures higher than 550 °K. It is suggested that the association of centres at high impurity concentrations may give rise to this peak. Such a possibility has been considered by HOOGENSTRAATEN [6] in his extensive theoretical study of the association of centres, but this proposal still lacks quantitative elaboration. It is hoped that present conductivity and electron spin resonance measurements, feasible with these phosphors, may furnish additional knowledge of the nature of the impurities present and the luminescence mechanisms involved.

REFERENCES

1. H. A. KLASENS and M. E. WISA, J. Opt. Soc. Amer., **38**, 226, 1948.
2. G. F. J. GARLICK and A. F. GIBSON, J. Opt. Soc. Amer., **39**, 935, 1949.
3. W. R. NAIL, F. URBACH and D. PEARLMAN, J. Opt. Soc. Amer., **39**, 690, 1949.
4. S. ROBERTS and F. E. WILLIAMS, J. Opt. Soc. Amer., **40**, 516, 1950.
5. W. HOOGENSTRAATEN and H. A. KLASENS, J. Electrochem. Soc., **100**, 366, 1953.
6. W. HOOGENSTRAATEN, Philips Res. Rep., **13**, 515, 1958.

7. N. Arpiarian, J. Phys. Rad., **17**, 674, 1956.
8. G. Gergely, J. Phys. Rad., **17**, 679, 1956.
9. E. S. Krylova, Dok. Akad. Nauk. S.S.S.R., **64**, 495, 1949.
10. G. F. J. Garlick and M. S. Elmanharawy, "The Luminescence Mechanisms in ZnS : CdS : Ag : Ni Phosphors", to be published.
11. C. G. A. Hill and H. A. Klasens, J. Electrochem. Soc., **96**, 275, 1949.
12. M. Schon, Z. Naturf., **6**, 251, 1951.
13. H. A. Klasens, J. Electrochem. Soc., **100**, 72, 1953.

ВЛИЯНИЕ КОБАЛЬТА НА ФОТОЛЮМИНЕСЦЕНЦИЮ ФОСФОРОВ АКТИВИЗИРОВАННЫХ СЕРЕБРОМ И СОДЕРЖАЩИХ НИКЕЛЬ

М. С. ЭЛ-МАНХАРАВИ

Р е з ю м е

Изучаются влияние кобальта на спектры возбуждения и эмиссии, температурная зависимость флюоресценции и термолюминесценции фосфоров ZnS : CdS : Ag : Ni. Увеличение концентрации кобальта не оказывает влияния на спектры возбуждения и эмиссии. Измерялась температурная зависимость флуоресценции фосфоров, содержащих 0%—0,065% кобальта, в интервале температуры от 77°К до 600°К. Наблюдаемые изменения энергии активации при закалке и увеличении концентрации кобальта обусловлено наличием глубоких электронных ловушек. Появление пиков в термолюминесцентных кривых объясняется присутствием примесей хлора, кадмия, кобальта и никеля. Соответствующие глубины ям равны 0,26 эв, 0,52 эв, 0,53 эв и 0,78 эв. Найден также термолюминесцентный пик, соответствующий энергии глубины ямы 1,09 эв. Сделана попытка определить происхождение данного пика.

Acta Physica Academiae Scientiarum Hungaricae, Tomus 29 (2—3), pp. 127—141 (1970)

FINITE RANGE COULOMB STRIPPING IN (t, p) AND (He^3, n) REACTIONS

By

M. EL-NADI, A. OSMAN

FACULTY OF SCIENCE, CAIRO UNIVERSITY, CAIRO, UAR

and

T. H. RIHAN

ATOMIC ENERGY ESTABLISHMENT, CAIRO, UAR

(Received 11. V. 1969)

The theory of two-nucleon stripping reactions is considered, taking into account the Coulomb distortion and the finite-range effects at projectile energies below the Coulomb barrier. Applying the results to the reactions N^{14}(t, p)N^{16} and Be^9(He^3, n)C^{11} reliable agreement is observed with the experimental data especially in the forward direction.

1. Introduction

Recently, special attention has been directed to nuclear reactions, in which both the energies of the projectile and the outgoing particles are well below the Coulomb barrier [1—5]. The most striking feature of these reactions is the tendency of the angular distribution towards backward peaking. There are strong evidences that a direct interaction mechanism such as stripping takes place even in this low energy range. Coulomb stripping was first treated by TER-MARTIROSIAN [1] and BIEDENHARN et al. [2] in the case of deuteron stripping, assuming zero-range neutron—proton interactions. DAR et al. [3] have modified this theory by assuming finite-range interaction and applying some reasonable approximations. Lately, EL-NADI and RIHAN [4], and BUTTLE and GOLDFARB [5] have developed the Coulomb stripping theory in the general case of arbitrary cluster transfer.

On the other hand the two-nucleon stripping mechanisms considered by EL-NADI [6], NEWNS [7] and GLENDENNING [8] seem to give reliable fitting with the experimental data, when the projectile energy is above the Coulomb barrier.

The aim of the present work is to consider the two-nucleon stripping processes, when the energy of the projectile is well below the Coulomb barrier. An approximate treatment will be considered in which the projectile is assumed to be partially polarized so that the centre of mass coordinate may be replaced by the coordinate of the outgoing particle. This is the assumption introduced for (d, p) reactions by DAR et al. [3]. Using this approximation, a general

expression is derived in Section 2 for the two-nucleon stripping from a heavy projectile. In Section 3, an alternative method is given for the derivation of the differential cross-section for (t, p) reactions. In Section 4, a special case is considered in which the energy of the outgoing particle is above the Coulomb barrier, while that of the incident particle is below the barrier.

The results of this section could be applied to (He^3, n) reactions. Results and discussions are given in Section 5, where the results of the present calculations are compared with the experimental results of SCHWARTZ et al. [9] on N^{14}(t, p)N^{16} and DUGGAN et al. [10] on Be^9(He^3, n)C.

2. General consideration

Let us consider the reaction

$$A + T \rightarrow C + R ,$$

where A represents the projectile consisting of two nucleons (1) and (2) bound to a cluster (C) with relative angular momenta l_1 and l_2, respectively. R refers to the residual nucleus formed from the two nucleons bound to the target (T) with relative angular momenta l_{n1} and l_{n2}, respectively.

The transition matrix element for the two-nucleon stripping process may be given to a first approximation by [4]

$$T_{fi} = \langle \Phi_f^{(-)} | \{V_{1c} + V_{2c}\} | \psi_i^{(+)} \rangle . \tag{2.1}$$

From Fig. 1, it can be seen that:

$$\varrho = \mathbf{r}_2 + \frac{1}{2}\mathbf{r}_{12} ,$$

$$\mathbf{R} = \mathbf{r}_c + \frac{2m_n}{m_A}\mathbf{r}_2 + \frac{m_n}{m_A}\mathbf{r}_{12} .$$

When the charge of the cluster (C) is larger than that of the nucleons (1) and (2), the projectile (A) can be expected to be partially polarized by the target Coulomb field so that the cluster (C) will be on the farther side of the target (T) while the nucleons (1) and (2) will be nearer.* Assuming also the mass

* For the case of (He^3, n), one may assume that the two protons will be symmetrical with respect to the line joining the target nucleus and the neutron, so that, in this case, the replacement (2.2) may also be justified. The neutron in this case may, however, be nearer to the target nucleus.

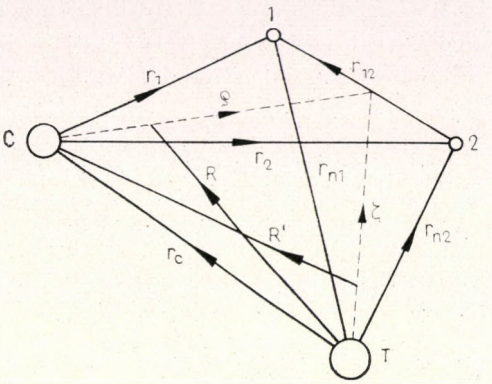


Fig. 1. Schematic diagram representing the two-nucleon stripping process

of the target nucleus to be much larger than the masses of the captured nucleons, one may introduce the approximations [4]

$$\psi_i^{(+)} = \Psi_{\mathbf{k}_i}^{(+)}(\mathbf{R}) \cdot X_i \approx \Psi_{\mathbf{k}_i}^{(+)}(\mathbf{r}_c) \cdot X_i \,,$$
$$\Phi_f^{(-)} = \Psi_{k_f}^{(-)}(\mathbf{R}') \cdot X_f \approx \Psi_{\mathbf{k}_f}^{(-)}(\mathbf{r}_c) \cdot X_f \,,$$

where $\Psi_{k_i}^{(+)}(r_c)$ and $\Psi_{k_f}^{(-)}(r_c)$ are the Coulomb wave functions describing the motion of the projectile in the initial state and the cluster (C) in the final state, respectively, but both with the argument $\mathbf{r}_c$,

$$\begin{aligned}\Psi_{\mathbf{k}_i}^{(+)}(\mathbf{r}_c) &= e^{-1/2\,\pi\eta_i}\,\Gamma(1+i\eta_i)\,e^{i\mathbf{k}_i\cdot\mathbf{r}_c}\,F\big(-i\eta_i, 1, i(k_i\,r_c - \mathbf{k}_i\cdot\mathbf{r}_c)\big)\,,\\ \Psi_{\mathbf{k}_f}^{(-)}(\mathbf{r}_c) &= e^{-1/2\,\pi\eta_f}\,\Gamma(1+i\eta_f)\,e^{-i\mathbf{k}_f\cdot\mathbf{r}_c}\,F\big(-i\eta_f, 1, i(k_f\,r_c + \mathbf{k}_f\cdot\mathbf{r}_c)\big)\,.\end{aligned} \tag{2.2}$$

$\mathbf{k}_i$ and $\mathbf{k}_f$ are the wave numbers of the incident and outgoing particles in the centre of mass system, respectively, X_i, X_f are the wave functions describing the internal motion in the initial and final channels, respectively.

These functions may be written in the following form, when one assumes that two nucleons from the projectile are transferred to the target nucleus:

$$\begin{aligned}X_i = \sum &\begin{Bmatrix} j_1 & j_2 & \sigma_1 & \sigma_2 & I_c \\ \mu_1 & \mu_2 & m_1 & m_2 & \mu_c \end{Bmatrix} \left(\frac{1}{2}\,\sigma_1\,l_1\,m_1|\,j_1\,\mu_1\right)\left(\frac{1}{2}\,\sigma_2\,l_2\,m_2|j_2\,\mu_2\right)\\ &(j_1\,\mu_1\,j_2\,\mu_2|j\,\mu_j)\,(j\,\mu_j\,I_c\,\mu_c|I_A\,\mu_A)\\ &\varphi_c(\zeta)\,\varphi_T(\eta)\,\varkappa_{1/2}^{\sigma_1}\,\varkappa_{1/2}^{\sigma_2}\,\varkappa_{I_c}^{\mu_c}\,\varkappa_{I_T}^{\mu' T}\\ &f_{l_1 m_1}(\mathbf{r}_1)\,f_{l_2 m_2}(\mathbf{r}_2)\,,\end{aligned}$$

and

$$\begin{aligned}X_f = \sum &\begin{Bmatrix} J_1 & J_2 & \sigma_1' & \sigma_2' & I_T \\ M_1 & M_2 & m_{n_1} & m_{n_2} & \mu_T \end{Bmatrix} \left(\frac{1}{2}\,\sigma_1'\,l_{n_1}\,m_{n_1}|J_1\,M_1\right)\left(\frac{1}{2}\,\sigma_2\,l_{n_2}\,m_{n_2}|J_2\,M_2\right)\\ &(J_1\,M_1\,J_2\,M_2|J\,M_J)\,(J\,M_J\,I_T\,\mu_T|I_R\,\mu_R)\\ &\varphi_c(\zeta)\,\varphi_T(\eta)\,\varkappa_{1/2}^{\sigma_1'}\,\varkappa_{1/2}^{\sigma_2'}\,\varkappa_{I_c}^{\mu_c'}\,\varkappa_{I_T}^{\mu_T}\\ &\Phi_{l_{n_1}\,m_{n_1}}(\mathbf{r}_{n1})\,\Phi_{l_{n_2}\,m_{n_2}}(\mathbf{r}_{n_2})\,,\end{aligned}$$

where the rotation $\Sigma\{\ \}$ is used to mean that the summation is performed over the indices included in the curled brackets. $\varkappa_\alpha^\beta$ is the spin wave function, φ_i the internal wave function of particle (i) and I_i and μ_i are the spin of particle (i) and its z-projection.

$$f_{l_1 m_1}(\mathbf{r}_1)\,,\ f_{l_2 m_2}(\mathbf{r}_2) \quad \text{and} \quad \Phi_{l_{n_1} m_{n_1}}(\mathbf{r}_{n_1}),\ \Phi_{l_{n_2} m_{n_2}}(\mathbf{r}_{n_2})$$

are the relative wave functions of the nucleons (1) and (2) in the projectile and residual nuclei, respectively.

The differential cross-section may be written as [4]:

$$\frac{d\sigma}{d\Omega} = \frac{\mathring{m}_i \mathring{m}_f}{(2\pi\hbar^2)^2}\,\frac{k_f}{k_i}\,\frac{1}{(2I_A+1)(2I_T+1)}\,\Sigma\left\{\begin{matrix}\mu_A\,\mu_T\\ \mu_C\,\mu_R\end{matrix}\right\}|T_{fi}|^2. \tag{2.3}$$

Expressing X_i and X_f in L—S coupling scheme and separating the functions for the relative and c.m. motion [13] one gets:

$$\begin{aligned} T_{fi} = \Sigma \left\{\begin{matrix} n_i\ N_i\ j_1\ j_2\ j\ l_1\ l_2\ l\ L\ \mathfrak{L}\ m\ M \\ n_f\ N_f J_1\ J_2\ J\ l_{n_1}\ l_{n_2}\ l_n\ L_n\ \mathfrak{L}_n\ m_n\ M_n \end{matrix}\right\} \mathring{\Theta}_{I_T J}(J_1 J_2)\,\Theta_{I_C j}(j_1 j_2) \\ T(J_1 J_2; \mathfrak{L}_n S)\,T(j_1 j_2; \mathfrak{L} S)\,\langle n_f l_n, N_f L_n; \mathfrak{L}_n | n_{f_1} l_{n_1}, n_{f_2} l_{n_2}; \mathfrak{L}_n\rangle \\ \langle n_i l, N_i L; \mathfrak{L} | n_1 l_1, n_2 l_2; \mathfrak{L}\rangle\,(l_n m_n L_n M_n | \mathfrak{L}_n \mathfrak{M}_n) \\ (\mathfrak{L}_n \mathfrak{M}_n S\sigma\,|\,J M_J)\,(J M_J I_T \mu_T\,|\,I_R \mu_R)\,(lm\,LM\,|\,\mathfrak{L}\mathfrak{M}) \\ (\mathfrak{L}\mathfrak{M} S\sigma\,|\,j\mu_j)\,(j\mu_j I_C \mu_C | I_A \mu_A)\,F^{\mathfrak{M}\mathfrak{M}_n}_{\mathfrak{L}\mathfrak{L}_n}, \end{aligned} \tag{2.4}$$

where $\langle nl, NL; \mathfrak{L}|n_1 l_1, n_2 l_2; \mathfrak{L}\rangle$ is the Talmi coefficient

$$\begin{aligned} F^{\mathfrak{M}\mathfrak{M}_n}_{\mathfrak{L}\mathfrak{L}_n} = \int \mathring{\vartheta}_{l_n m_n}(\mathbf{r}_{12})\,\{V_{1c}(\mathbf{r}_1)+V_{2c}(\mathbf{r}_2)\}\,U_{lm}(\mathbf{r}_{12}) \\ \Phi_{LM}(\varrho)\,\mathrm{d}\mathbf{r}_{12}\,\mathrm{d}\varrho\,\int \mathring{\Phi}_{L_n M_n}(\varrho+\mathbf{r}_c)\,\mathring{\Psi}^{(-)}(\mathbf{r}_c)\,\Psi^{(+)}(\mathbf{r}_c)\,\mathrm{d}\mathbf{r}_c\,. \end{aligned}$$

$U_{lm}(r_{12})$ and $\vartheta_{l_n m_n}(\mathbf{r}_{12})$ describe the relative motion of the two nucleons in the initial and final states, respectively, while $\Phi_{LM}(\varrho)$ and $\mathring{\Phi}_{L_n M_n}(\varrho + \mathbf{r}_c)$ describe the motion of their centre of mass in the projectile and residual nuclei, respectively. Now, choosing $\mathring{\Phi}_{L_n M_n}(\varrho + \mathbf{r}_c)$ to be of the form [12]:

$$\mathring{\Phi}_{L_n M_n}(\tau) = N(L_n, \ldots)\,\tau^{L_n - 1}\,e^{-\varkappa\tau}\,\mathring{Y}^{M_n}_{L_n}(\hat{\tau})$$

and using the expansion [13]

$$\begin{aligned} \tau^{L_n}\,\mathring{Y}^{M_n}_{L_n}(\boldsymbol{\tau}) = \sum_{\lambda\mu} (-)^{L_n-\lambda+M_n} \left(\frac{4\pi}{2\lambda+1}\right)^{1/2} \begin{pmatrix} 2L_n+1 \\ 2\lambda \end{pmatrix}^{1/2} \\ (r_c)^\lambda (\varrho)^{L_n-\lambda} (L_n - \lambda - (M_n+\mu)\,\lambda\mu | L - M_n) \\ Y^{-(M_n+\mu)}_{L_n-\lambda}(\hat{\varrho})\ Y^\mu_\lambda(\hat{\mathbf{r}}_c)\,, \end{aligned}$$

where

$$\boldsymbol{\tau} = \boldsymbol{r}_c - \boldsymbol{\varrho}\,; \quad \binom{X}{Y} = \frac{X!}{Y!\,(X-Y)!}\,.$$

One may write the integral $F_{\mathfrak{L}\mathfrak{L}_n}^{\mathfrak{M}\mathfrak{M}_n}$ in the form

$$F_{\mathfrak{L}\mathfrak{L}_n}^{\mathfrak{M}\mathfrak{M}_n} = C(L, L_n, \lambda, \nu, \varkappa)\, I(\nu, \Lambda, \Theta)\,, \tag{2.5}$$

where

$$C(L, L_n, \lambda, \nu, \varkappa) \int \mathrm{d}\varrho\, \mathrm{d}\mathbf{r}_{12}\, \varrho^{L_n-\lambda+2}\, \overset{*}{\vartheta}_{l_n m_n}(\mathbf{r}_{12}) \left\{V_{1c}(r_1)+V_{2c}(r_2)\right\} J_\nu(i\varkappa\varrho)\, U_{lm}(\mathbf{r}_{12})\, \Phi_{LM}(\varrho)\,. \tag{2.6}$$

is the factor containing the finite-range effects, and

$$I(\nu, \Lambda, \Theta) = \int \mathrm{d}\mathbf{r}_c\, h_\nu^{(1)}(i\varkappa r_c)\, r_c^\lambda\, \overset{*}{\Psi}^{(-)}(\mathbf{r}_c)\, \Psi^{(+)}(\mathbf{r}_c)\, Y_\Lambda^{m\Lambda}(\hat{\mathbf{r}}_c)\,. \tag{2.7}$$

The last integral (2.7) may be evaluated in the case of $\eta_i, \eta_f \gg 1$ by the saddle-point approximation, to give [4]

$$I(\nu, \Lambda, \Theta) = \frac{(i)^{-\nu}}{\varkappa}\,(-)^{\lambda+1}\, Y_\Lambda^{m\Lambda}(\hat{\mathbf{r}}_c) \left\{\frac{\mathrm{d}^\lambda}{\mathrm{d}\varkappa^\lambda}\, I_0\right\}, \tag{2.8}$$

where [1]

$$I_0 = 8\pi^2\,(\eta_i\,\eta_f)^{1/2}\, \exp\left\{-\pi\,(\eta_i+\eta_f)\right\} \frac{1}{(\boldsymbol{k}_i-\boldsymbol{k}_f)^2+\varkappa^2} \left\{\frac{(\varkappa-i\boldsymbol{k}_f)^2+k_i^2}{(\boldsymbol{k}_i-\boldsymbol{k}_f)^2+\varkappa^2}\right\}^{i\eta_f} \left\{\frac{(\varkappa-i\boldsymbol{k}_i)^2+k_f^2}{(\boldsymbol{k}_i-\boldsymbol{k}_f)^2+\varkappa^2}\right\}^{i\eta_i} \frac{F(-i\eta_f, -i\eta_i; |; -\zeta)}{1+\zeta}$$

$$\zeta = \frac{4\,k_i\,k_f}{(\boldsymbol{k}_i-\boldsymbol{k}_f)^2+\varkappa^2}\,\sin^2\frac{1}{2}\,\Theta\,. \tag{2.9}$$

Inserting (2.4), (2.5) and (2.8) into (2.3) one may write:

$$\frac{\mathrm{d}\sigma}{\mathrm{d}\Omega} = \frac{\overset{*}{m}_i\,\overset{*}{m}_f}{(2\pi\hbar^2)^2}\,\frac{k_f}{k_i}\,\frac{(2I_R+1)}{(2I_T+1)} \left|\sum_{a_1 a_2 a_3} \Sigma \begin{Bmatrix} n_i & n_f & j_1 & j_2 & j & l_1 & l_2 & l & L & \mathfrak{L} & \lambda \\ N_i & N_f & J_1 & J_2 & J & l_{n_1} & l_{n_2} & l_n & L_n & \mathfrak{L}_n & \nu \end{Bmatrix} \overset{*}{\Theta}_{I_T J}(J_1 J_2)\, \Theta_{l_0 j}(j_1 j_2)\, N(l_1, l_{n_1}, \ldots)\,(-)^{\nu+\lambda}\,(i)^{-\nu} \begin{pmatrix} 2L_n+1 \\ 2\lambda \end{pmatrix}^{1/2} \left\{(2a_1+1)\,(2a_2+1)\,(2a_3+1)\right\} \left\{(2\nu+1)\,(2L+1)\,(2\mathfrak{L}+1)\,(2L_n+1)\,(2\mathfrak{L}_n+1)\,(2L_n-2\lambda+1)\right\}^{1/2} T(J_1 J_2; \mathfrak{L}_n S)\, T(j_1 j_2; \mathfrak{L}\, S) \tag{2.10}$$

$$\langle n_f l_n, N_f L_n; \mathfrak{L}_n | n_{f_1} l_{n_1}, n_{f_2} l_{nf_2}; \mathfrak{L}_n \rangle \langle n_i l, N_i L; \mathfrak{L} | n_1 l_1, n_2 l_2; \mathfrak{L} \rangle$$

$$(L_0 L_n - \lambda_0 | \nu_0) \ (\lambda_0 \nu_0 | a_{30})$$

$$\begin{Bmatrix} J & a_1 & j \\ \mathfrak{L} & S & \mathfrak{L}_n \end{Bmatrix} \begin{Bmatrix} \lambda & \nu & a_3 \\ L & L_n & L_n - \lambda \end{Bmatrix} \begin{Bmatrix} l & L & \mathfrak{L} \\ L_n & a_2 & a_3 \end{Bmatrix} \begin{Bmatrix} l_n & L_n & \mathfrak{L}_n \\ \mathfrak{L} & a_1 & a_2 \end{Bmatrix}$$

$$C(L, L_n, \lambda, \nu, \varkappa) \left\{ \frac{\mathrm{d}^\lambda}{\mathrm{d}\varkappa^\lambda} I_0 \right\}^2 .$$

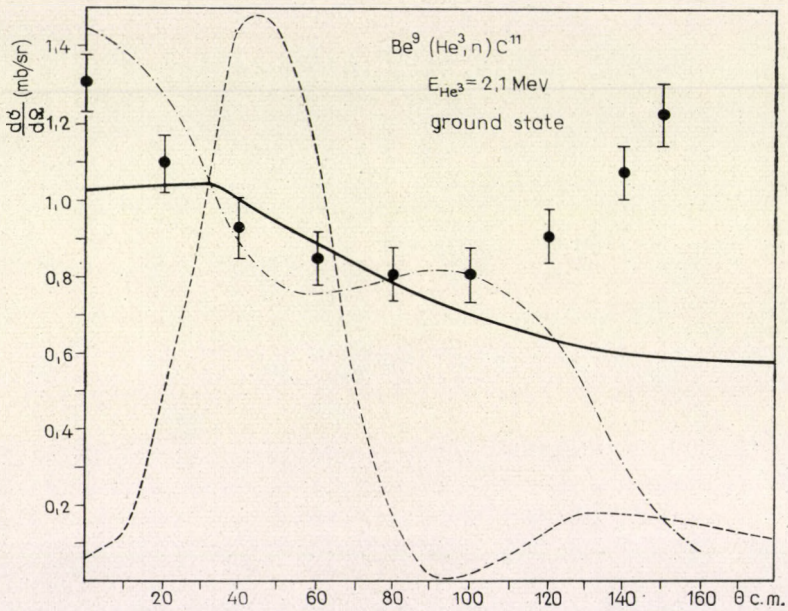


Fig. 2. The angular distribution of the ejected neutron leaving C^{11} nucleus in the ground state. The solid line corresponds to the present work, while the dashed-dotted line refers to the distorted wave calculations and the dashed line is the plane wave calculations. The experimental data are those of DUGGAN et al. [10]

This is the general expression for two nucleon stripping from a heavy projectile leading to the emission of an outgoing cluster C when the projectile energy is well below the Coulomb barrier, and the Q-value is very small so that the energy of the outgoing particle is below the corresponding Coulomb barrier.

3. The (t, p) reactions

For case of (t, p) reactions, one can give an alternative method for the derivation of an expression for the cross-section which will be equivalent to (2.10).

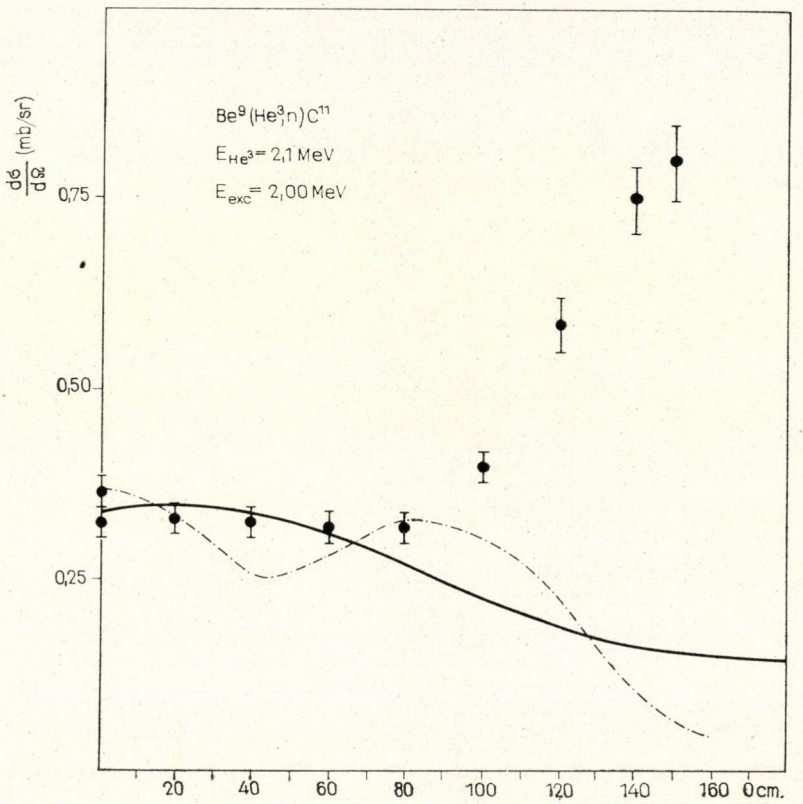


Fig. 3. The angular distribution of the ejected neutron leaving C^{11} nucleus in the first excited state. The solid line corresponds to the present work, while the dashed-dotted line refers to the distorted wave calculations. The experimental data are those of DUGGAN et al. [10]

Considering the triton to be composed of two neutrons, (1) and (2), and a proton (p), approaching the target (T), where the neutrons (1) and (2) will be captured to form the residual (nucleus) R leaving p as the outgoing particle.

Assuming the energy of the triton to be less than the Coulomb barrier, and the Q-value to be very small so as to keep the energy of the proton also

below the Coulomb barrier, one may write for the matrix-element for the reaction (t, p); using the expression (2.4)

$$T_{fi} = \sum \begin{Bmatrix} n\ j_1\ l_1\ M \\ N\ j_2\ l_2 \end{Bmatrix} \overset{*}{\Theta}_{I_T L}(j_1 j_2)\, T(j_1 j_2; L_0)\, \langle n_0, NL; L | \\ n_1 l_1, n_2 l_2; L\rangle\, (LM\, I_T\, \mu_T | I_R\, \mu_R)\, F, \tag{3.1}$$

where

$$F = \int \overset{*}{\Psi}{}^{(-)}(\mathbf{r}_p)\, \overset{*}{\vartheta}_0(\mathbf{r}_{12})\, \overset{*}{\Phi}_{LM}(\varrho + \mathbf{r}_p) \{V_{1p}(r_1) + V_{2p}(r_2)\} \\ U_0(\mathbf{r}_{12})\, \Phi_0(\varrho)\, \Psi^{(+)}(\mathbf{r}_p)\, \mathrm{d}\mathbf{r}_p\, \mathrm{d}\varrho\, \mathrm{d}\mathbf{r}_{12}. \tag{3.2}$$

Using Schrödinger's equation to eliminate the potentials $V_{1p}(r_1)$ and $V_{2p}(r_2)$ from (3.2), one gets [14]

$$F = \int \mathrm{d}\mathbf{r}_{12}\, \mathrm{d}\varrho\, \overset{*}{\vartheta}_0(r_{12}) \frac{\hbar^2}{4\overset{*}{m}} (\Delta_\varrho + 4\,\Delta_{r12} - \epsilon_0), \\ U_0(r_{12})\, \Phi_0(\varrho) \int \mathrm{d}\mathbf{r}_p\, \overset{*}{\Phi}(\varrho + \mathbf{r}_p)\, \overset{*}{\Psi}{}^{(-)}(\mathbf{r}_p)\, \Psi^{(+)}(\mathbf{r}_p).$$

If we expand $\overset{*}{\Phi}(\varrho + \mathbf{r}_p)$ in Taylor expansion in the form:

$$\overset{*}{\Phi}_L(\varrho + \mathbf{r}_p) = e^{\mathbf{e}\cdot\nabla_\Phi}\, \overset{*}{\Phi}_L(\mathbf{r}_p).$$

Expressing $\Phi_0(\varrho)$, $u_0(r_{12})$ and $\overset{*}{\vartheta}_0(r_{12})$ in the Gaussian form:

$$\Phi_0(\varrho) = N_1\, e^{-2\gamma_1 \varrho^2}, \\ U_0(r_{12}) = N_2\, e^{-1/2\,\gamma_1 r_{12}^2}, \\ \overset{*}{\vartheta}_0(r_{12}) = N_3\, e^{-\gamma_2 r_{12}^2},$$

one gets:

$$F = \frac{\hbar^2}{4\overset{*}{m}} N_1 N_2 N_3 \left(\frac{\pi}{2\gamma_1}\right)^{3/2} e^{\varkappa^2/(8\gamma_1)} \int \mathrm{d}r_{12}\, e^{-(1/2\,\gamma_1 + \gamma_2) r_{12}^2} \\ \{\varkappa^2 + \gamma_1^2 r_{12}^2 - \gamma_1 - \epsilon_0\}\, I_L(\theta). \tag{3.3}$$

Performing the integration over r_{12} and substituting the expression $I_L(\theta)$ [4] one gets:

$$F = \frac{\hbar^2}{4\overset{*}{m}} N_1 N_2 N_3 N_4 \left(\frac{\pi}{2\gamma_1}\right)^{3/2} e^{\varkappa^2/(8\gamma_1)} (-)^L \frac{1}{2} \pi^{1/2} \left(\frac{1}{2}\gamma_1 + \gamma_2\right)^{-3/2} \\ \left\{\frac{1}{2}\gamma_1^2 + \left(\frac{1}{2}\gamma_1 + \gamma_2\right)(\varkappa^2 - \gamma_1 - \epsilon_0)\right\} \frac{\partial^L}{\partial \varkappa^L} \{I_0\}\, \overset{*}{Y}{}_L^M(\hat{\mathbf{r}}_p). \tag{3.4}$$

Inserting (3.1) and (3.4) into (2.3) we get:

$$\frac{\mathrm{d}\sigma}{\mathrm{d}\Omega} = \frac{\overset{*}{m}_i \overset{*}{m}_f}{\overset{*}{m}^2} \frac{k_f}{k_i} \frac{(2I_R+1)}{(2I_T+1)} \pi^2 \frac{1}{2^{12}} \frac{1}{\gamma_1^3} e^{\varkappa^2/(4\gamma_1)} \left(\frac{1}{2}\gamma_1+\gamma_2\right)^{-3}$$

$$\left\{\frac{1}{2}\gamma_1^2+\left(\frac{1}{2}\gamma_1+\gamma_2\right)(\varkappa^2-\gamma_1-\epsilon_0)\right\}^2 \left| \sum \begin{Bmatrix} n & j_1 & l_1 & L \\ N & j_2 & l_2 & \end{Bmatrix} \right. \tag{3.5}$$

$$N_1 N_2 N_3 N_4 \overset{*}{\Theta}_{I_T L}(j_1 j_2)(-)^L \frac{1}{(2L+1)^{1/2}} T(j_1 j_2; L_0)$$

$$\langle n_0, NL; L | n_1 l_1, n_2 l_2; L\rangle \frac{\partial^L}{\partial x^L}\{I_0\}\Big|^2 .$$

4. Special case

For the purpose of comparing the present results with the experimental data, one may choose a simple case, in which the energy of the incident triton is below the Coulomb barrier and the Q-value is large such that the proton energy is above the Coulomb barrier in the final channel, the matrix-element will then be partially simplified.

In such case we shall approximate the wave function describing the relative motion in the entrance channel to be a Coulomb wave function, while in the exit channel we shall use a plane wave.

In other words in the integral:

$$A = \int \mathrm{d}\mathbf{r}\, \overset{*}{\Phi}_{LM}(\mathbf{r})\, \overset{*}{\Psi}^{(-)}(\mathbf{r})\, \Psi^{(+)}(\mathbf{r}) \tag{4.1}$$

one may take the following representation:

$$\Psi^{(+)}(\mathbf{r}) = e^{-1/2\,\pi\eta}\, \Gamma(1+i\eta)\, e^{ik_i \cdot r} F\big(-i\eta, 1, i(k_i r - \mathbf{k}_i \cdot \mathbf{r})\big), \tag{4.2}$$

$$\overset{*}{\Psi}^{(-)}(\mathbf{r}) = e^{-i\mathbf{k}_f \cdot \mathbf{r}}, \tag{4.3}$$

where k_i, k_f, η and $\overset{*}{m}_i$; have the same meaning as in Section 2.

$\overset{*}{\Phi}_{LM}(\mathbf{r})$ describes the motion of the proton outside the nucleus and will be taken in the form [13]:

$$\overset{*}{\Phi}_{LM}(\mathbf{r}) = N r^{L-1} e^{-\varkappa r} \overset{*}{Y}{}_L^M(\mathbf{r}). \tag{4.4}$$

Introducing (4.2), (4.3) and (4.4) into (4.1) one gets:

$$A = N e^{-1/2\,\pi\eta}\,\Gamma(1+i\eta)\int \mathrm{d}r\, r^{L-1}\, e^{-\varkappa r}\,\overset{*}{Y}(\hat{\mathbf{r}})\; e^{i\mathbf{q}\cdot\mathbf{r}}\, F\big(-i\eta, 1, i(kr-\mathbf{k}\cdot\mathbf{r})\big)\,, \tag{4.5}$$

where $\mathbf{k} = \mathbf{k}_i$ for simplicity $\mathbf{q} = \mathbf{k}_i - \mathbf{k}_f$.

Integrating over dr and then substituting it into (3.3) after integrating over $\mathrm{d}\mathbf{r}_{12}$ which may be introduced into (3.1), one gets:

$$T_{fi} = \sum \begin{Bmatrix} n & j_1 & l_1 & L & M \\ N & j_2 & l_2 & \lambda & \mu \end{Bmatrix} \Theta_{I_T L}(j_1 j_2)\, T(j_1 j_2; L_0)\, \langle n_0, NL;\, L|$$

$$n_1 l_1, n_2 l_2; L\rangle (-)^{I_T-\mu_T}\, \frac{(2I_R+1)^{1/2}}{(2L+1)^{1/2}}\, (I_R - \mu_R\, I_T\, \mu_T | L-M)\, \frac{\hbar^2}{4\overset{*}{m}}$$

$$N_1 N_2 N_3 N (\pi)^{7/2}\, (2)^{L-3/2}\, (i)^L\, (-)^{L-\lambda+M} \left(\frac{1}{2}\gamma_1^2 + \gamma_1\gamma_2\right)^{-3/2}$$

$$\left\{\frac{1}{2}\gamma_1^2 + \left(\frac{1}{2}\gamma_1 + \gamma_2\right)(\varkappa^2 - \gamma_1 - \epsilon_0)\right\} e^{\varkappa^2/(8\gamma_1)}\, e^{-1/2\,\pi\eta} \tag{4.6}$$

$$(\varkappa^2+q^2)^{-(L+1)}\, (2\lambda+1)^{-1/2} \begin{pmatrix} 2L+1 \\ 2\lambda \end{pmatrix}^{1/2} (q)^\lambda\, (k)^{L-\lambda}$$

$$\frac{\Gamma(L+1)\,\Gamma(1+i\eta)\,\Gamma(L-\lambda-i\eta)}{\Gamma(-i\eta)\,\Gamma(L+1-\lambda)}\, (L-\lambda-(M+\mu)\,\lambda\mu|L-M)$$

$$(1-z)^{i\eta-L}\, Y_{L-\lambda}^{-(M+\mu)}(\hat{\mathbf{k}})\; Y_\lambda^\mu(\hat{\mathbf{q}})\, F(-\lambda, 1+i\eta; L+1-\lambda; z).$$

Finally after summing over all projections and using (2.3), for the differential cross-section one may write the following expression:

$$\frac{\mathrm{d}\sigma}{\mathrm{d}\Omega} = \frac{\overset{*}{m}_i\,\overset{*}{m}_f}{\overset{*}{m}^2}\,\frac{k_f}{k_i}\,\frac{(2I_R+1)}{(2I_T+1)}\,(N_1 N_2 N_3 N)^2\,(\pi)^3 \left(\frac{1}{2}\gamma_1^2+\gamma_1\gamma_2\right)^{-3}$$

$$\left\{\frac{1}{2}\gamma_1^2 + \left(\frac{1}{2}\gamma_1+\gamma_2\right)(\varkappa^2-\gamma_1-\epsilon_0)\right\}^2 e^{\varkappa^2/4\gamma_1}\, e^{-\pi\eta}$$

$$\sum \begin{Bmatrix} n & N & j_1 & j_2 & l_1 & l_2 & L & \lambda \\ n' & N' & j_1' & j_2' & l_1' & l_2' & \mathfrak{L} & \lambda' \end{Bmatrix} (-)^{L+\mathfrak{L}} (2)^{2L-10} \dot{\Theta}_{I_T L}(j_1 j_2)$$

$$\Theta_{I_T L}(j_1' j_2') (2L+1)(2\mathfrak{L}+1) \begin{pmatrix} 2L \\ 2\lambda \end{pmatrix}^{1/2} \begin{pmatrix} 2L \\ 2\lambda' \end{pmatrix}^{1/2} (k)^{2L-\lambda-\lambda'}$$

$$(q)^{\lambda+\lambda'} (\varkappa^2+q^2)^{-2(L+1)}$$

$$\langle n_0, NL; L | n_1 l_1, n_2 l_2; L \rangle \langle n_0', N'L; L | n_1' l_1', n_2' l_2'; L \rangle \tag{4.7}$$

$$T(j_1 j_2; L_0) T(j_1' j_2'; L_0) \begin{Bmatrix} \lambda' & \lambda & \mathfrak{L} \\ L-\lambda & L-\lambda' & L \end{Bmatrix}$$

$$\begin{pmatrix} L-\lambda & L-\lambda' & \mathfrak{L} \\ 0 & 0 & 0 \end{pmatrix} \begin{pmatrix} \lambda & \lambda' & \mathfrak{L} \\ 0 & 0 & 0 \end{pmatrix} \frac{\Gamma(1+i\eta)\Gamma(1-i\eta)\Gamma(L-\lambda-i\eta)\Gamma(L-\lambda'+i\eta)}{\Gamma(-i\eta)\Gamma(+i\eta)}$$

$$z^{\lambda-L} z^{\lambda'-L} \frac{\mathrm{d}^{\lambda}}{\mathrm{d}z^{\lambda}} \left\{ z^L (1-z)^{i\eta-L+\lambda} \right\} \frac{\mathrm{d}^{\lambda'}}{\mathrm{d}\overset{*}{z}{}^{\lambda'}} \left\{ \overset{*}{z}{}^L (1-\overset{*}{z})^{-i\eta-L+\lambda'} \right\}$$

$$P_{\mathfrak{L}}(\cos\omega),$$

where we have used the following relation [15]:

$$F(-\lambda, 1+i\eta;\ L+1-\lambda;\ z) =$$
$$= \frac{z^{\lambda-L}(1-z)^{L-i\eta}\Gamma(L+1-\lambda)}{\Gamma(L+1)} \frac{\mathrm{d}^{\lambda}}{\mathrm{d}z^{\lambda}} \left\{ z^L (1-z)^{i\eta-L+\lambda} \right\},$$

since the hypergeometric wave function has the parameter which has positive integer values, which means that it will end after some definite terms.

5. Discussion and results

In the present work, we have found an analytic approximation for the two nucleon stripping process, based on some plausible approximations.

Comparison is made between the theoretical results (4.7) and some experimental data on the reaction $Be^9(He^3, n)C^{11}$ [10] (Figs. 2—5) and on the reaction $N^{14}(t, p)N^{16}$ [9] (Figs. 6 and 7). The incident energies are 2.1 MeV for

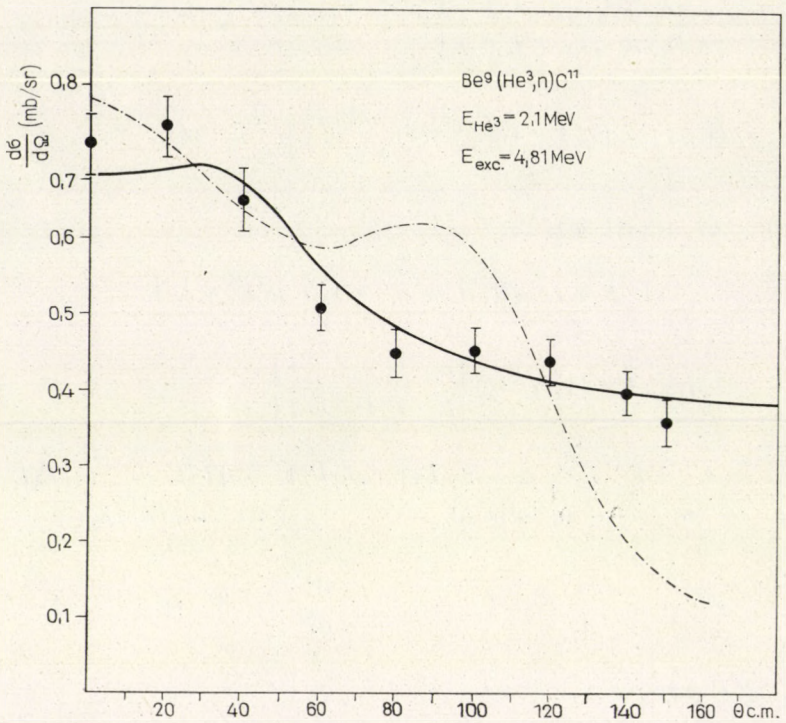


Fig 4. The angular distribution of the ejected neutron leaving C^{11} nucleus in the third excited state. The solid line corresponds to the present work, while the dashed-dotted line refers to the distorted wave calculations. The experimental data are those of DUGGAN et al. [10]

He^3 and 1.83 MeV for the tritons in the laboratory system, also the Q-values for the two reactions are 7.562 MeV and 5.242 MeV, respectively.

The dominant shell model configurations are predicted previously [17] for the considered levels of C^{11} and N^{16}.

Using the DWBA calculations [10], in the case of (He^3, n) reaction, the measured angular distributions are well described with angular momentum transfer of values $L = 2$ in the case of ground, first and third excited states, and with $L = 0$ for the unresolved fourth and fifth excited state. In the case of (t, p) reaction, the first and third excited states proceed with angular momentum transfer of $L = 1$.

In Figs. 2—7 the curves illustrate the Plane Wave Born approximation (dashed line) and the Distorted Wave Born approximation (dashed – dotted line) for these reactions. It may be observed that the effect of introducing the Coulomb interaction is to broaden the peaks and raise the magnitude of the angular

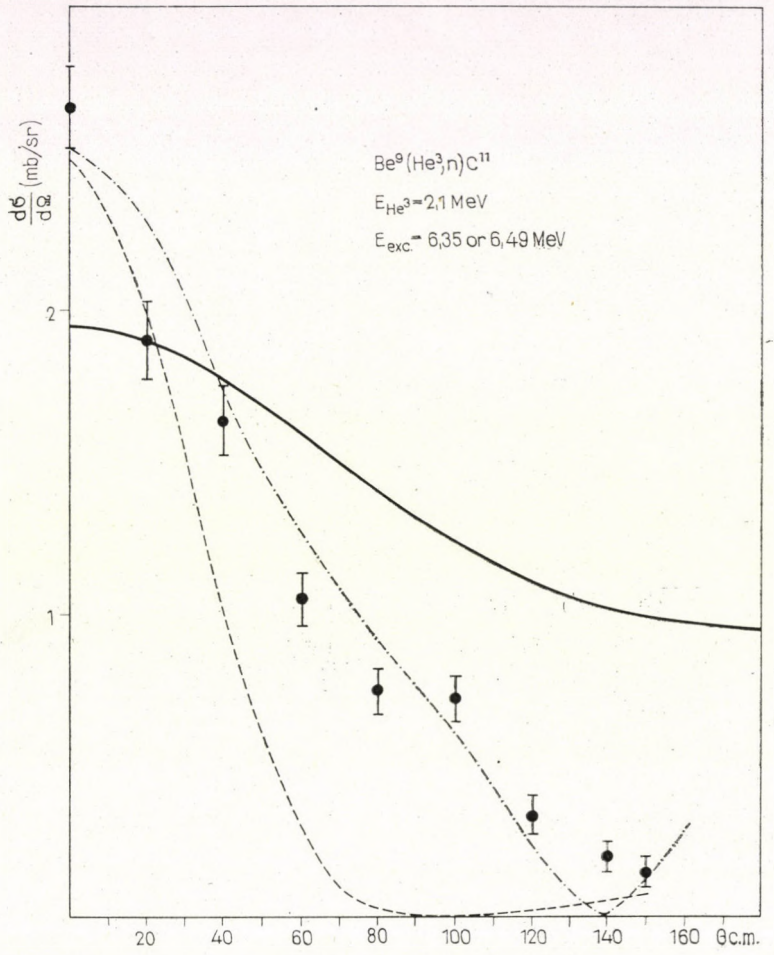


Fig. 5. The angular distribution of the ejected neutron leaving C^{11} nucleus in the unresolved fourth and fifth excited state. The solid line corresponds to the present work, while the dashed-dotted line refers to the distorted wave calculations and the dashed line is the plane wave calculations. The experimental data are those of DUGGAN et al. [10]

distribution at large angles. This is to be expected owing to Coulomb repulsion between the target nucleus and the projectile.

It may be observed that the agreement between the theoretical and experimental data are, in general, satisfactory.

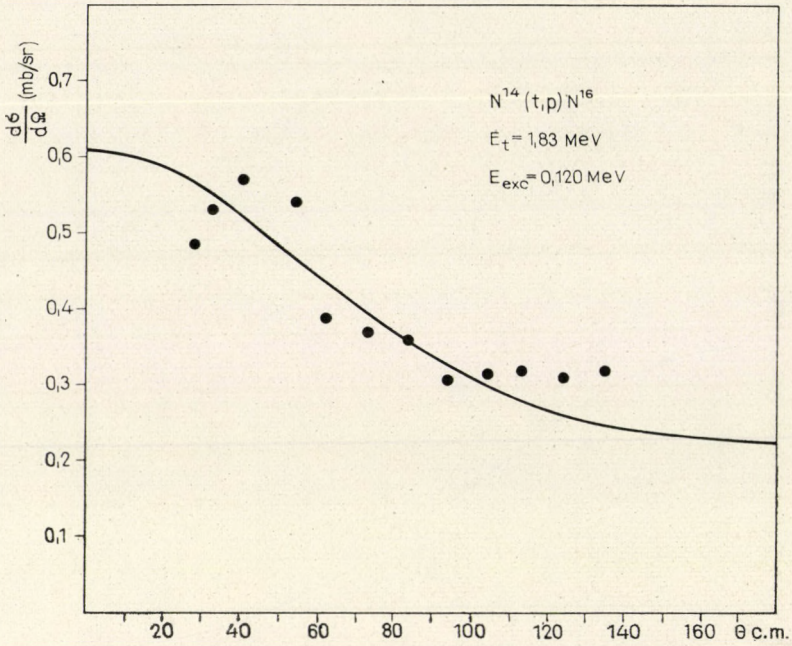


Fig. 6. **The angular distribution of the ejected proton leaving N^{16} nucleus in the first excited state. The solid line corresponds to the present work. The experimental data are those of SCHWARTZ et al. [9]**

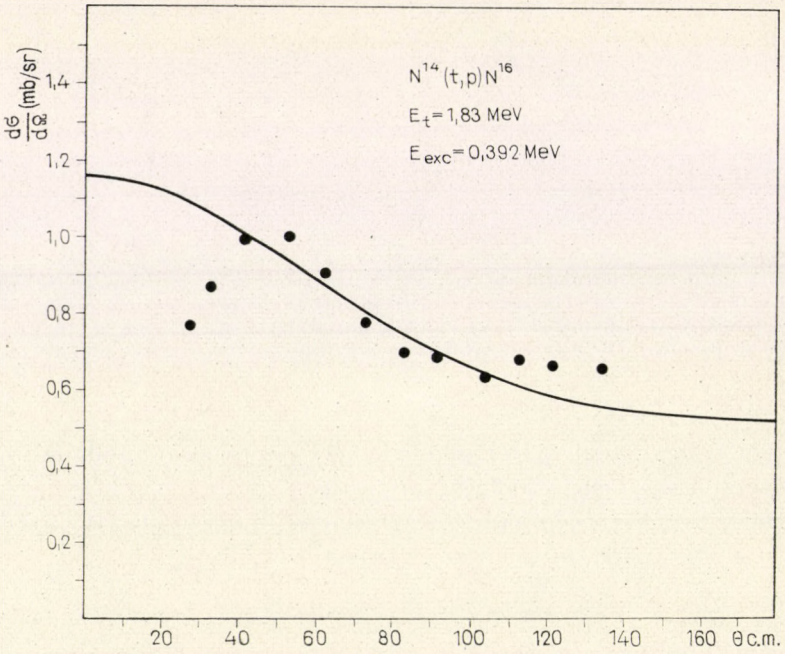


Fig. 7. **The angular distribution of the ejected proton leaving N^{16} nucleus in the third excited state. The solid line corresponds to the present work. The experimental data are those of SCHWARTZ et al. [9]**

REFERENCES

1. K. Ter-Martirosian, Soviet Physics JETP, **2**, 620, 1956.
2. L. C. Biedenharn, K. Boyer and M. Goldstein, Phys. Rev., **104**, 383, 1956.
3. A. Dar, A. De-Shalit and A. S. Reiner, Phys. Rev., **131**, 1732, 1963.
4. M. El-Nadi and T. H. Rihan, Proc. Phys. Soc., **87**, 119, 1966.
5. P. J. A. Buttle and L. J. B. Goldfarb, Proc. Phys. Soc., **83**, 701, 1964.
6. M. El-Nadi, Proc. Phys. Soc., **A70**, 62, 1957.
7. H. C. Newns, Proc. Phys. Soc., **76**, 489, 1960.
8. N. K. Glendenning, Nucl. Phys., **29**, 109, 1962.
9. R. B. Schwartz, H. D. Holmgren, L. M. Cameron and A. R. Knudson, Phys. Rev., **134**, B 577, 1964.
10. J. L. Duggan, P. D. Miller and R. F. Gabbard, Nucl. Phys., **46**, 336, 1963.
11. M. Moshinsky, Nucl. Phys., **13**, 104, 1959.
12. F. B. Morinigo, Phys. Rev., **134**, B 1243, 1964.
13. M. El-Nadi and H. Sherif, Nucl. Phys., **28**, 331, 1961.
14. M. E. Rose, "Elementary Theory of Angular Momentum" (John Wiley, New York), 1957.
15. I. N. Snaddon, "Special Functions of Mathematical Physics and Chemistry" (Interscience Publishers INC., New York), 1956.
16. A. Jucys, T. Levinson and V. Vanages, "Mathematical apparatus of the theory of angular momentum" (Vilnius, 1960).
17. J. P. Eliott and B. H. Flowers, Proc. Roy. Soc. (London), **A242**, 57, 1957.

КУЛОНОВСКАЯ РЕАКЦИЯ СРЫВА (t, p) и (He^3, n) С КОНЕЧНЫМ РАДИУСОМ ВЗАИМОДЕЙСТВИЯ

М. ЭЛ-НАДИ, А. ОСМАН и Т. Х. РИХАН

Резюме

Рассматривается теория двухнуклонной реакции срыва, с учетом эффектов кулоновского искажения и конечного радиуса при пристрельной энергии под кулоновским барьером. Применяя результаты для реакции N^{14}(t, p)N^{16} и Be^9(He^3, n)C^{11}, наблюдается соответствие с экспериментальными данными особенно в направлении падающего пучка.

Acta Physica Academiae Scientiarum Hungaricae, Tomus 29 (2—3), pp. 143—158 (1970)

CLUSTER TRANSFER REACTIONS AT LOW ENERGIES

By

M. EL-NADI, A. OSMAN

FACULTY OF SCIENCE, CAIRO UNIVERSITY, CAIRO, UAR

and

T. H. RIHAN

ATOMIC ENERGY ESTABLISHMENT, CAIRO, UAR

(Received 11. V. 1969)

The cluster transfer processes below the Coulomb barrier are investigated for arbitrary charges and angular momentum transfer, taking into account the finite range effects. An analytical expression for the differential cross-section is obtained and calculations are carried out for the Zr^{90}(d, p)Zr^{91} reaction. An analytical expression is also obtained for the differential cross-section for two cluster transfer reactions, and the results are compared with the data on the Al^{27}(He^3, p)Si^{29} reaction.

1. Introduction

Coulomb stripping reaction, since its first consideration by TER-MARTIROSIAN [1] and BIEDENHARN et al. [2] for (d, p) reactions, has been the subject of several recent works. At very low energies and small Q-values, the nuclear distorting fields may be ignored, and the only interactions in the entrance and exit channels will be mainly Coulombian. Therefore, the use of Coulomb distorted waves may give rise to reliable order of magnitude [3] for the stripping differential cross-section at low energies.

In the treatment by TER-MARTIROSIAN [1] and BIEDENHARN et al. [2], the zero-range approximation was adopted and the results were given for the case of large Coulomb parameters in the entrance and exit channels, using the saddle point approximation. Introducing a finite range interaction for (d, p) reaction and considering the deuteron polarizability, DAR et al. [4] were able to show that this leads to an increase in the order of magnitude of the differential cross-section. GOLDFARB [3] and BUTTLE and GOLDFARB [5, 6] have also estimated the correction for the finite range effects explicitly. EL-NADI and RIHAN [7] studied the general case of single particle transfer reactions and have shown that the finite range cross-section is larger than that corresponding to the case of the zero range; and that for values of the transferred angular momentum, different from zero, an additional angular dependent factor which also increases the cross-section at large angles appears in the expression for the cross-section.

The aim of the present work is to give an analytical expression for the differential cross-section of one and two cluster transfer reactions, taking the finite size of nuclei into consideration, following a method previously suggested by GRANT [8] for the (d, p) reaction. Two cases will be considered; first, when the Q-value of the reaction is small enough to keep the energy in the exit channel below the Coulomb barrier and, second, when the Q-value is large.

2. One cluster transfer reaction

Theory

Let us consider the stripping reaction

$$A\,(a + C) + T \rightarrow C + R\,(a + T)\,,$$

where the parentheses indicate bound states. One may assume that the particles a and C are bound with relative angular momentum l, while the particles a and T are bound with relative angular momentum L.

To describe this process the complete Hamiltonian H of the system, will be written in two alternative forms:

$$\begin{aligned} H &= H_i + V_i = (\hat{T}_a + \hat{T}_c + \hat{T}_T + V_{ac}) + (V_{aT} + {}_{cT}), \\ &= H_f + V_f = (\hat{T}_a + \hat{T}_c + \hat{T}_T + V_{aT}) + (V_{ac} + V_{cT})\,. \end{aligned}$$

where $\hat{T}_i$ is the kinetic energy operator of the particle (i), and V_{ij} is the interaction between the particles (i) and (j).

The initial Φ_i and final Φ_f non-interacting states of the system with plane waves for the relative motion, satisfy

$$(E - H_i)\,\Phi_i = 0 \text{ and } (E - H_f)\,\Phi_f = 0\,. \tag{1}$$

Then the transition amplitude may be given by [9]:

$$T_{fi} = \langle \psi_f^{(-)} | V_i | \Phi_i \rangle, \tag{2}$$

where $\psi_f^{(\pm)}$ is the ingoing wave solution of the complete Hamiltonian defined by:

$$\psi_f^{(\pm)} = \Phi_f + \frac{1}{E - H \pm i\epsilon} V_f \Phi_f. \tag{3}$$

Let us further introduce a partially interacting state $\varkappa_f^{(-)}$ according to:

$$\varkappa_f^{(-)} = \Phi_f + \frac{1}{E - H_f - i\epsilon} V_{cT}\, \varkappa_f^{(-)} \tag{4}$$

in terms of which $\psi_f^{(-)}$ may be written as:

$$\psi_f^{(-)} = \varkappa_f^{(-)} + \frac{1}{E-H-i\epsilon}(V_f - V_{cT})\,\varkappa_f^{(-)}. \tag{5}$$

From these equations, one may obtain the following expression for the transition amplitude:

$$T_{fi} = \langle \varkappa_f^{(-)} | V_{ac} | \psi_i^{(+)} \rangle\,, \tag{6}$$

where $\psi_i^{(+)}$ is the outgoing wave solution of the total Hamiltonian and may be written in the form:

$$\psi_i^{(+)} = \Phi_i + \frac{1}{E-H_i+i\epsilon} V_i\,\psi_i^{(+)}.$$

Then in the distorted wave Born approximation (DWBA), the matrix element (6) may be written in the form:

$$T_{fi}^{\text{D.W.B.}} = \langle \varkappa_f^{(-)} | V_{ac} | \varkappa_i^{(+)} \rangle, \tag{7}$$

where

$$\varkappa_i^{(+)} = \Phi_i + \frac{1}{E-H_i+i\epsilon} u_i \varkappa_i^{(+)}$$

and u_i is the distorting potential.

Now, when the projectile energy is well below the Coulomb barrier, one expects the long-range Coulomb forces to dominate. Consequently, $\varkappa_i^{(+)}$ may be represented by a Coulomb distorted wave function.

To obtain the expression of the wave function $\varkappa_i^{(+)}$, one may follow the method developed by GRANT [8] for the special case of (d, p) reactions.

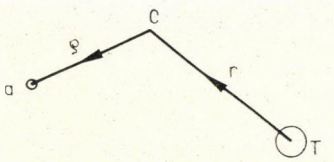


Fig. 1

Transforming to the variables r and ϱ (see Fig. 1) in the initial Hamiltonian H_i, one can obtain the following differential equation [10] for $\varkappa_i$:

$$\left[-\frac{\hbar^2}{2\mu_{cT}}\nabla_r^2 + \frac{\hbar^2}{m_c}\nabla_r\cdot\nabla_\varrho - \frac{\hbar^2}{2\mu_{cT}}\nabla_\varrho^2 + V_{ac}(\varrho) + \right.$$
$$\left. + \frac{z_a z_T e^2}{|r+\varrho|} + \frac{z_c z_T e^2}{r} - E\right]\varkappa_i = 0, \tag{8}$$

where μ_{ij} is the reduced mass of the particles (i) and (j), m_i is the mass of the particle (i). Neglecting spin complications, the solution of equation (1) can be given by (see Fig. 1):

$$\Phi_i = e^{i\mathbf{k}_i \cdot \left(\mathbf{r} + \frac{m_a}{m_A}\varrho\right)} \varphi_{lm}(\boldsymbol{\rho})\, \Phi_{I_a}^{\mu_a} \Phi_{I_c}^{\mu_c},$$

where φ_{lm} is the wave function of the relative motion of the particles (a) and (c) in the projectile (A), and $\Phi_{I_i}^{\mu_i}$ is the internal wave function of the particle (i).

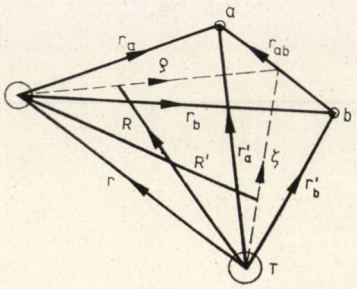


Fig. 2

One may now write the correct form of the wave function $\varkappa_i$ as:

$$\varkappa_i = \Phi_i\, \zeta(\mathbf{r}) + \mathfrak{J}(\mathbf{r}, \boldsymbol{\rho}), \tag{9}$$

where $\mathfrak{J}(\mathbf{r}, \boldsymbol{\rho})$ involve only states orthogonal to $\varphi_{lm}(\boldsymbol{\rho})$.

Introducing (9) into (8) and multiplying by $\overset{*}{\Phi}_i$ then integrating over ϱ, one can obtain the following equation for $\zeta(\mathbf{r})$:

$$\left[\nabla_r^2 + 2\,i\lambda \mathbf{k}_i \cdot \nabla_r - \frac{2\,\mu_{cT}\, z_A\, z_T\, e^2}{\hbar^2\, r} - \frac{2\,\mu_{cT}\, z_a\, z_T\, e^2}{\hbar^2} \cdot \right.$$

$$\left. \cdot \int \overset{*}{\varphi}_{lm}(\boldsymbol{\rho}) \left[\frac{1}{|\mathbf{r}+\boldsymbol{\rho}|} - \frac{1}{r}\right] \varphi_{lm}(\boldsymbol{\rho})\, d\boldsymbol{\rho}\right] \zeta(\mathbf{r}) = \tag{10}$$

$$= \int \overset{*}{\Phi}_i \left(\frac{2\,\mu_{cT}}{m_c} \nabla_r \cdot \nabla_\varrho + \frac{2\,\mu_{cT}}{\hbar^2} \frac{z_a\, z_T\, e^2}{|\mathbf{r}+\boldsymbol{\rho}|}\right) \mathfrak{J}(\mathbf{r}, \boldsymbol{\rho})\, d\boldsymbol{\rho},$$

where

$$\lambda = 1 - \frac{m_T\, m_a}{m_A\,(m_c + m_T)}.$$

An approximation to $\varkappa_i$ can now be obtained by neglecting the right hand side of Eq. (10).

Since $\mathcal{J}(\mathbf{r}, \varrho)$ contains states orthogonal to Φ_i, then such an approximation means that we ignore the effect of the dissociation of the projectile and its Coulomb excitation in the field of the target nucleus.

Then $\zeta(\mathbf{r})$ will be taken as the solution of:

$$\left[\nabla_r^2 + 2i\lambda \mathbf{k}_i \cdot \nabla_r - \frac{2\mu_{cT} z_A z_T e^2}{\hbar^2 r} - \frac{2\mu_{cT} z_a z_T e^2}{\hbar^2} \cdot \int \varphi_{lm}^*(\varrho) \left[\frac{1}{|\mathbf{r}+\varrho|} - \frac{1}{r}\right] \varphi_{lm}(\varrho)\, d\varrho\right] \zeta(\mathbf{r}) = 0. \tag{11}$$

The last term in equation (11) may, generally, be neglected in comparison with the third term, as the main contribution to the matrix element (7) due to the large Coulomb barrier comes from values of $r \geqslant R_t$, where R_t is the turning point, while the corresponding value of ϱ will be of the order of r_0 (the projectile radius) which is much less than R_t. Moreover, this term is divided by z_A in comparison with the third term.*

Consequently, one can finally write the following equation for $\zeta(r)$:

$$\left[\nabla_r^2 + 2i\lambda\, \mathbf{k}_i \cdot \nabla_r - \frac{2\nu k_i \eta_i}{r}\right] \zeta(\mathbf{r}) = 0, \tag{12}$$

the solution of which, with the appropriate boundary conditions is:

$$\zeta^{(+)}(\mathbf{r}) = e^{-1/2\,\pi\eta_i}\, \Gamma(1+i\eta_i)\, F\left(-i\eta_i, 1, i(k_i' r - \mathbf{k}_i' \cdot \mathbf{r})\right),$$

where $k_i' = \lambda\, k_i$ and $\nu = \mu_{CT}/\mu_{AT}$.

Therefore, we shall have the following approximate solution for $\varkappa_i^{(+)}$:

$$\varkappa_i^{(\pm)} \simeq \Phi_i\, \zeta^{(+)}(\mathbf{r}). \tag{13}$$

Turning now our consideration to $\varkappa_f^{(-)}$, let us consider the case when the Q-value of the reaction is small enough so that the energy in the final channel also remains below the Coulomb barrier. Hence one may also neglect the short-range nuclear force.

Therefore, in a similar manner, one may write the following approximation for $\varkappa_f^{(-)}$:

$$\varkappa_f^{(-)} \simeq \Phi_f\, \zeta^{(-)}(\mathbf{r}), \tag{14}$$

where

$$\zeta^{(-)}(\mathbf{r}) = e^{-1/2\,\pi\eta_f}\, \Gamma(1-i\eta_f)_1 F_1\left(i\eta_f, 1, -i(k_f' r + \mathbf{k}_f' \cdot \mathbf{r})\right),$$

$$k_f' = \lambda' k_f, \quad \lambda' = 1 - \frac{m_c\, m_a}{m_R\,(m_c + m_T)}, \quad \nu' = \frac{\mu_{cT}}{\mu_{cR}}$$

* This term can be neglected in the case of $l = 0$.

and (neglecting spin complications):

$$\Phi_f = e^{-i\mathbf{k}_f\cdot\left(\frac{m_T}{m_R}\mathbf{r}-\frac{m_a}{m_R}\varrho\right)}\varphi^R_{LM}(\mathbf{r}+\boldsymbol{\rho})\,\Phi^{\mu_a}_{I_a}\Phi^{\mu_T}_{I_T}.$$

Consequently for small Q-values, the stripping amplitude (7) can be written as:

$$\begin{aligned} T_{fi} = \sum \Theta(l,j)\,\overset{*}{\Theta}(L,J)\,(I_a\,\mu_a\,lm|j\mu)\,(j\mu I_c\,\mu_c|I_A\,\mu_A) \\ (I_a\,\mu_a\,LM|JU)\,(JUI_T\,\mu_T|I_R\,\mu_R)\,I^{mM}_{lL}, \end{aligned} \tag{15}$$

where

$$I^{mM}_{lL} = \int \mathrm{d}\boldsymbol{\rho}\, e^{iK\cdot\varrho}\,V(\varrho)\,\varphi_{lm}(\boldsymbol{\rho})\int e^{iq\cdot\mathbf{r}}\,\overset{*}{\varphi}_{LM}(\mathbf{r}+\varrho)\,\overset{*}{\zeta}^{(-)}(\mathbf{r})\,\zeta^{(+)}(\mathbf{r})\,\mathrm{d}\mathbf{r},$$

$$\mathbf{K} = \frac{m_a}{m_A}\mathbf{k}_i + \frac{m_a}{m_R}\mathbf{k}_f,$$

$$\mathbf{q} = \mathbf{k}_i - \frac{m_T}{m_R}\mathbf{k}_f,$$

and $\Theta(l,j)$ and $\overset{*}{\Theta}(L,J)$ are the corresponding spectroscopic factors.

Let $f^{(\pm)}_{\mathbf{k}'_i,\mathbf{k}'_f}$ be the correct distorted wave functions for Coulomb scattering by a point charge, i.e.:

$$f^{(+)}_{\mathbf{k}'_i}(\mathbf{r}) = e^{i\mathbf{k}'\cdot\mathbf{r}}\,\zeta^{(+)}(\mathbf{r}) \quad \text{and} \quad f^{(-)}_{\mathbf{k}'_f}(\mathbf{r}) = e^{ik'\cdot\mathbf{r}}\,\zeta^{(-)}(\mathbf{r}).$$

Then

$$I^{mM}_{lL} = \int \mathrm{d}\boldsymbol{\rho}\, e^{i\mathbf{K}\cdot\varrho}\,V(\varrho)\,\varphi_{lm}(\boldsymbol{\rho})\int e^{i\mathbf{Q}\cdot\mathbf{r}}\,\varphi_{LM}(\mathbf{r}+\boldsymbol{\rho})\,f^{(+)}_{\mathbf{k}'_i}(\mathbf{r})\,\overset{*}{f}^{(-)}_{\mathbf{k}'_f}(\mathbf{r})\,\mathrm{d}\mathbf{r},$$

where

$$\mathbf{Q} = \frac{m_C\,m_T}{m_A(m_c+m_T)}\mathbf{k}_i + \frac{m_a\,m_T}{m_P\,(m_c+m_T)}\mathbf{k}_f.$$

Now let us transform to the variables $\mathbf{r}+\boldsymbol{\rho} = \mathbf{r}_n$; $\boldsymbol{\rho} = \boldsymbol{\rho}$, and use the following approximations [11]:

$$\begin{aligned} f^{(+)}(\mathbf{r}_n-\boldsymbol{\rho}) &= e^{-\varrho\cdot\nabla_{r_n}} f^{(+)}(\mathbf{r}_n) \simeq e^{-i\mathbf{k}'_i\cdot\varrho}\,f^{(+)}(\mathbf{r}_n), \\ \overset{*}{f}^{(-)}(\mathbf{r}_n-\boldsymbol{\rho}) &= e^{-\varrho\cdot\nabla_n}\,\overset{*}{f}^{(-)}(\mathbf{r}_n) \simeq e^{i\mathbf{k}'_f\cdot\varrho}\,\overset{*}{f}^{(-)}(\mathbf{r}_n) \end{aligned} \tag{16}$$

(this approximation may be accepted as the main contribution comes from outside the nucleus. Therefore, we let the nabla operator act on the plane wave limit of $f^{(\pm)}$).

Thus, one may write:

$$I_{lL}^{mM} \simeq e^{-1/2\,\pi(\eta_i+\eta_f)}\,\Gamma(1+i\eta_i)\,\Gamma(1+i\eta_f)\int e^{i\varkappa\cdot\varrho}\,V(\boldsymbol{\rho})\,\varphi_{lm}(\boldsymbol{\rho})\,\mathrm{d}\boldsymbol{\rho}\int \mathrm{d}\mathbf{r}_n\,e^{i\mathbf{q}\cdot\mathbf{r}_n}\,\overset{*}{\varphi}_{LM}(\mathbf{r}_n)\;{}_1F_1\big(-i\eta_i,1,i(k_i'r_n-\mathbf{k}_i'\cdot\mathbf{r}_n)\big)\;{}_1F_1\big(-i\eta_f,1,i(k_f'r_n+\mathbf{k}_f'\cdot\mathbf{r}_n)\big), \tag{17}$$

where

$$\varkappa = \mathbf{k}_f - \frac{m_c}{m_A}\,\mathbf{k}_i .$$

Taking for $\overset{*}{\varphi}_{LM}(\mathbf{r}_n)$ the form [12]:*

$$\overset{*}{\varphi}_{LM}(\mathbf{r}_n) = N\,e^{-\beta r_n}\,r_n^{L-1}\,\overset{*}{Y}_L^M(\hat{\mathbf{r}}_n) .$$

With this choice I_{lL}^{mM} becomes [7]:

$$I_{lL}^{mM} \simeq N\,e^{-1/2\,\pi(\eta_i+\eta_f)}\,\Gamma(1+i\eta_i)\,\Gamma(1+i\eta_f)\,F_{lm}(\varkappa)\,(-)^L\left\{\frac{\partial^L}{\partial\beta^L}\,I_R\right\}, \tag{18}$$

where the function I_R is given in [13], and

$$F_{lm}(\varkappa) = \int \mathrm{d}\boldsymbol{\rho}\,e^{i\varkappa\cdot\varrho}\,V(\varrho)\,\varphi_{lm}(\boldsymbol{\rho}) .$$

If, however, the Q-value of the reaction is not small enough to keep the energy in the exit channel below the Coulomb barrier, one may approximate the wave function of the outgoing particle by a plane wave. With this approximation, the radial integral I_{lL}^{mM} will take the form:

$$\tilde{I}_{lL}^{mM} = Ne^{-1/2\,\pi\eta_i}\,\Gamma(1+i\eta_i)\,F_{lm}(\varkappa)\int \mathrm{d}\mathbf{r}_n\,r_n^{L-1}\,e^{-\beta r_n}\,e^{i\mathbf{q}\cdot\mathbf{r}_n}\,\overset{*}{Y}_L^M(\hat{\mathbf{r}}_n)\;{}_1F_1\big(-i\eta_i,1,i(k_1'r_n-\mathbf{k}_i'\cdot\mathbf{r}_n)\big). \tag{19}$$

Now from expression (15), for the differential cross-section one can get the following expression:

$$\frac{\mathrm{d}\sigma}{\mathrm{d}\Omega} = \frac{\mu_{AT}\,\mu_{CR}}{(2\,\pi\hbar^2)^2}\,\frac{k_f}{k_i}\,\frac{(2\,I_R+1)}{(2\,I_T+1)}\sum\begin{Bmatrix} j & J & l & L & m & M & b\\ j' & J' & l' & L' & m' & M' & \beta\end{Bmatrix}(-)^{L+L+l+l'+m'+M'+j+J+2I_a}\,\Theta(l,j)\,\overset{*}{\Theta}(L,J)\,\overset{*}{\Theta}(l',j')\,\Theta(L',J')\begin{Bmatrix} I_a & L' & J\\ L & I_a & b\end{Bmatrix}\begin{Bmatrix} I_a & l' & j\\ l & I_a & b\end{Bmatrix}(l'\,m'\,l-m|b\beta)(L'\,M'\,L-M|b\beta)\;\tilde{I}_{lL}^{mM}\,\overset{*}{\tilde{I}}{}_{l'L'}^{m'M'} . \tag{20}$$

* A combination of such terms may lead to a more exact function.

We shall now restrict ourselves to the case when $l = 0$. In this simple case the differential cross-section can be given by:

$$\frac{d\sigma}{d\tau} = \frac{\mu_{AT}\,\mu_{cR}}{(2\pi\hbar^2)^2}\,\frac{k_f}{k_i}\,\frac{(2I_R+1)}{(2I_T+1)}\sum_L |\Theta(l,j)|^2\,|\Theta(L,J)|^2$$

$$\frac{N^2(L)(4)^L(q^2)^L\,|\Gamma(L+1)|^2\,e^{-\pi\eta_i}\,|\Gamma(1+i\eta_i)|^2}{|\Gamma(-i\eta_i)|^2\,(\beta^2+q^2)^2}\,|F_{00}|^2$$

$$\sum_{\nu=0}^{L}\sum_{\nu'=0}^{L}\sum_{\Lambda}(-)^L\,\frac{\Gamma(\nu-i\eta_i)\,\Gamma(\nu'+i\eta_i)}{\Gamma(\nu+1)\,\Gamma(\nu'+1)}\begin{pmatrix}2L+1\\ 2\nu\end{pmatrix}^{1/2}\begin{pmatrix}2L+1\\ 2\nu'\end{pmatrix}^{1/2}$$

$$(2L+1)\left\{(2L-2\nu+1)(2L-2\nu'+1)\right\}^{1/2}P_\Lambda(\cos\omega)\left(\frac{k_i'}{q}\right)^{\nu+\nu'}$$

$$\left(\frac{1}{(q^2+\beta^2-2\mathbf{q}\cdot\mathbf{k}_i')^2+4\beta^2k_i'^2}\right)^L e^{2\eta_i\tan^{-1}}\,\frac{2\beta k_i'}{q^2-2\mathbf{q}\cdot\mathbf{k}_i'+\beta^2}$$

$$(\nu\,0\,\nu'\,0\,|\,\Lambda\,0)\,(L-\nu\,0\,L-\nu'\,0\,|\,\Lambda\,0)\begin{Bmatrix}\nu & L-\nu & L\\ L-\nu' & \nu' & \Lambda\end{Bmatrix}$$

$$F(-L+\nu,1+i\eta_i;\nu+1;z)\,F(-L+\nu',1-i\eta_i;\nu'+1;\bar{z}), \tag{21}$$

where

$$z = \frac{2\,\mathbf{q}\cdot\mathbf{k}_i+2\,i\beta k_i}{\beta^2+q^2}\,.$$

These results differ from those of MORINIGO [12], by an angular dependent factor in the exponential term. This factor will gradually increase in the forward and decrease in the backward direction.

Let us consider the reaction ^{90}Zr(d, p)^{91}Zr.

In this case we have $l = L = 0$ and consequently using Eq. (18) one may write:

$$I_{00} = Ne^{-1/2\,\pi(\eta_i+\eta_f)}\,\Gamma(1+i\eta_i)\,\Gamma(1+i\eta_f)\,F_{00}(\varkappa)\,I_R. \tag{22}$$

Now, let $\varphi_{00}(\varrho)$ be of the form:

$$\varphi_{00}(\varrho) = \bar{N}\,\frac{e^{-\lambda\varrho}}{\varrho}\,,$$

where $\bar{N}$ is a normalization coefficient, $\lambda = 2\,\mu_{pn}/\hbar^2\,\varepsilon$ and ε is the deuteron binding energy.

By eliminating the potential from the expression of $F_{00}(\varkappa)$ (using the Schrödinger equation describing the internal motion of the deuteron) one obtains:

$$F_{00}(\varkappa) = -\,\frac{\hbar^2}{2\,\mu_{pn}}\,\bar{N}\sqrt{4\pi}.$$

Therefore, in this case the differential cross-section may be written in the form (see Eq. (15)):

$$\frac{\mathrm{d}\sigma}{\mathrm{d}\Omega} \sim |I_R|^2 . \tag{23}$$

The significance of these results is indicated in the increase of the extracted spectroscopic factors obtained, which is consistent with the shell-model predictions.

3. Two-cluster transfer reactions

In this section, the two-cluster transfer reactions will be considered on the basis of the above formalism. For this purpose, let us consider the following reaction:

$$(a + b + C) + T \rightarrow C + (a + b + T) ,$$

where the parentheses also indicate bound states.

Following the same formalism as in Section 2, one gets the following expression for the matrix-element.

$$T_{fi}^{\mathrm{D.W.B.}} = \langle \varkappa_f^{(-)} | V_{ac} + V_{bc} | \varkappa_i^{(+)} \rangle . \tag{24}$$

If one again rewrites $\varkappa_i^{(+)}$ in the form:

$$\varkappa_i^{(+)} = \Phi_i \, \zeta(\mathbf{r}) + \mathfrak{J}(\mathbf{r}, \mathbf{r}_a, \mathbf{r}_b) , \tag{25}$$

(where $\mathfrak{J}(\mathbf{r}, \mathbf{r}_a, \mathbf{r}_b)$ may involve only states orthogonal to Φ_i), inserting it in the Schrödinger equation for $\varkappa_i$ (transformed to the new variables $\mathbf{r}$, $\mathbf{r}_a$ and $\mathbf{r}_b$), and multiplying by Φ_i^*, then integrating over $\mathbf{r}_a$ and $\mathbf{r}_b$; and then following the same procedure given in Section 2, one gets for $\zeta^{(+)}(\mathbf{r})$ and $\zeta^{(-)}(\mathbf{r})$ the same expressions in that section, except for λ and λ' given by:

$$\lambda = 1 - \frac{m_T (m_a + m_b)}{m_A (m_c + m_T)} \quad \text{and} \quad \lambda' = 1 - \frac{m_c (m_a + m_b)}{m_R (m_C + m_T)} .$$

Thus, with the same approximations, one may write the expression of the transition matrix-element in the form:

$$T_{fi} = \sum \begin{Bmatrix} n & n_f & j_a J_a j & l & L & \mathfrak{L} & S m & M \\ N & N_f & j_b J_b J & l_f & L_f & \mathfrak{L}_f & \sigma m_f & M_f \end{Bmatrix} \Theta_{I_c j}(j_a j_b) \, \Theta^*_{I_T J}(J_a J_b)$$
$$T(J_a J_b; \mathfrak{L}_f s) \, T(j_a j_b; \mathfrak{L} s) \, \langle nl, NL; \mathfrak{L} | n_a l_a, n_b l_b; \mathfrak{L} \rangle$$

$$\langle n_f l_f, N_f L_f; \mathfrak{L}_f | n_{af} l_{af}, n_{bf} l_{bf}; \mathfrak{L}_f \rangle (j\mu I_c \mu_c | I_A \mu_A)$$
$$(JU I_T \mu_T | I_R \mu_R) (\mathfrak{L}\mathfrak{M} s\sigma | j\mu) (\mathfrak{L}_f \mathfrak{M}_f s\sigma | JU)$$
$$(lm\, LM | \mathfrak{L}\mathfrak{M})(l_f m_f L_f M_f | \mathfrak{L}_f \mathfrak{M}_f)\, I_{\mathfrak{L}\mathfrak{L}_f}^{\mathfrak{M}\mathfrak{M}_f}, \tag{26}$$

where

$$I_{\mathfrak{L}\mathfrak{L}_f}^{\mathfrak{M}\mathfrak{M}_f} = \int \mathrm{d}\mathbf{r}_{ab}\, \mathrm{d}\boldsymbol{\rho}\, e^{i\mathbf{K}\cdot\boldsymbol{\rho}} \{V_{ac}(r_a)+V_{bc}(r_b)\} \vartheta_{lm}(\mathbf{r}_{ab})\, \overset{*}{\vartheta}_{l_f m_f}(\mathbf{r}_{ab})\, \Phi_{LM}(\boldsymbol{\rho}) \int \mathrm{d}\mathbf{r}\, e^{i\mathbf{Q}\cdot\mathbf{r}} \overset{*}{\Phi}_{L_f M_f}(\mathbf{r}+\boldsymbol{\rho})\, f^{(+)}(\mathbf{r}) \overset{*}{f}{}^{(-)}(\mathbf{r}) \tag{27}$$

with

$$\mathbf{K} = \frac{m_a+m_b}{m_A}\mathbf{k}_i + \frac{m_a+m_b}{m_R}\mathbf{k}_f,$$

and

$$\mathbf{Q} = \frac{m_T(m_a+m_b)}{m_A(m_c+m_T)}\mathbf{k}_i + \frac{m_T(m_a+m_b)}{m_R(m_c+m_T)}\mathbf{k}_f.$$

If one introduces the approximations (16), one obtains:

$$I_{\mathfrak{L}\mathfrak{L}_f}^{\mathfrak{M}\mathfrak{M}_f} = N e^{-1/2\pi\,(\eta_i+\eta_f)} \Gamma(1+i\eta_i)\, \Gamma(1+i\eta_f)\, F_{ll_fL}^{mm_fM}(\varkappa)(-)^{L_f}\left\{\frac{\partial^{L_f}}{\partial\beta^{L_f}} I_0\right\}. \tag{28}$$

where

$$\varkappa = \mathbf{k}_f - \frac{m_C}{m_A}\mathbf{k}_i.$$

I_0 is the TER-MARTIROSIAN amplitude, and

$$F_{ll_fL}^{mm_fM}(\varkappa) = \int \mathrm{d}\mathbf{r}_{ab}\, \mathrm{d}\boldsymbol{\rho}\, e^{i\varkappa\cdot\boldsymbol{\rho}} \{V_{ac}(r_a)+V_{bc}(r_b)\} \vartheta_{lm}(\mathbf{r}_{ab})\, \overset{*}{\vartheta}_{l_f m_f}(\mathbf{r}_{ab})\, \Phi_{LM}(\boldsymbol{\rho}). \tag{29}$$

Thus, introducing (28) into (26) and summing over all projections, for the differential cross-section, one gets the following expression:

$$\frac{\mathrm{d}\sigma}{\mathrm{d}\Omega} = \frac{m_i m_f}{(2\pi\hbar^2)^2}\frac{k_f}{k_i}\frac{(2I_R+1)}{(2I_T+1)} N^2 e^{-\pi(\eta_i+\eta_f)}\, \Gamma(1+i\eta_i)$$
$$\Gamma(1-i\eta_i)\, \Gamma(1+i\eta_f)\, \Gamma(1-i\eta_f)\Big| \sum \begin{Bmatrix} n & N & j_a & j_b & j \\ n_f & N_f & J_a & J_b & J \end{Bmatrix}$$
$$\begin{Bmatrix} l & L & \mathfrak{L} & S & a_2 & \mu & m & M & \alpha_2 \\ l_f & L_f & \mathfrak{L}_f & a_1 & a_3 & U & m_f & \alpha_1 & \alpha_3 \end{Bmatrix} (-)^{\alpha_1+\alpha_2+\alpha_3} \Theta_{I_c j}(j_a j_b)$$
$$\overset{*}{\Theta}_{I_T J}(J_a J_b)\, T(j_a j_b;\, \mathfrak{L}S)\, T(J_a J_b;\, \mathfrak{L}S)$$

$$\langle nl, NL; \mathfrak{L}|n_a l_a, n_b l_b; \mathfrak{L}\rangle \langle n_f l_f, N_f L_f; \mathfrak{L}_f|$$
$$n_{af} l_{af}, n_{bf} l_{bf}; \mathfrak{L}_f\rangle (-)^{L_f+S+a_1}(2a_1+1)(2a_2+1)(2a_3+1)$$
$$(2\mathfrak{L}+1)^{1/2}(2\mathfrak{L}_f+1)^{1/2} \begin{Bmatrix} j & a_1 & J \\ \mathfrak{L}_f & S & \mathfrak{L} \end{Bmatrix} \begin{Bmatrix} L & l & \mathfrak{L} \\ \mathfrak{L}_f & a_1 & a_2 \end{Bmatrix}$$
$$\begin{Bmatrix} L_f & l_f & \mathfrak{L}_f \\ l & a_2 & a_3 \end{Bmatrix} \begin{pmatrix} j & J & a_1 \\ -\mu & U & \alpha_1 \end{pmatrix} \begin{pmatrix} L & a_1 & a_2 \\ M & -\alpha_1 & \alpha_2 \end{pmatrix}$$
$$\begin{pmatrix} L_f & a_3 & a_2 \\ -M_f & \alpha_3 & -\alpha_2 \end{pmatrix} \begin{pmatrix} l_f & l & a_3 \\ -m_f & m & -\alpha_3 \end{pmatrix}$$
$$F_{ll_fL}^{mm_fM}(\varkappa) \frac{\partial^{L_f}}{\partial B^{L_f}} \{I_0\}\Big|^2. \tag{30}$$

(He^3, p) and (t, n) reactions

Here we shall consider the case when the energy of the incident He^3 and that of the outgoing proton are both well below the Coulomb barrier.

In this case $l = L = \mathfrak{L} = 0$ because $l_a = l_b = 0$ and $n_a = n_b = 0$ where the captured proton and neutron are in the S-state in the projectile, so that from (30) one can obtain the following expression for the differential cross-section

$$\frac{\mathrm{d}\sigma}{\mathrm{d}\Omega} = \frac{m_i^* m_f^*}{(2\pi\hbar^2)^2} \frac{k_f}{k_i} \frac{(2I_R+1)}{(2I_T+1)} N^2 \, e^{-\pi(\eta_i+\eta_f)} \Gamma(1+i\eta_i)\Gamma(1-i\eta_i)$$
$$\Gamma(1+i\eta_f)\,\Gamma(1-i\eta_f) \Big| \sum \begin{Bmatrix} n & J_a & J & l & \mathfrak{L} \\ N & J_b & S & L \end{Bmatrix} \sum_m \overset{*}{\Theta}_{I_T J}(J_a J_b)$$
$$T(J_a J_b; \mathfrak{L}S)(-)^{\mathfrak{L}+S} \langle nl, NL; \mathfrak{L}|n_a l_a, n_b l_b; \mathfrak{L}\rangle$$
$$\frac{(2\mathfrak{L}+1)^{1/2}}{(2S+1)^{1/2}} F_{lm}(\varkappa) \frac{\partial^L}{\partial \beta^L} \{I_0\}\Big|^2, \tag{31}$$

where l, L, $\mathfrak{L}$, n and N are introduced instead of l_f, L_f, $\mathfrak{L}_f$, n_f and N_f for simplicity only.

Special case

As an interesting example, one can consider the case when the Q-value of the reaction is so large that the energy of the outgoing proton (neutron) is above the Coulomb barrier. Then neglecting the Coulomb distortion in the final channel, Eq. (28) becomes:

$$\tilde{I}_{lL}^{mM} = e^{-1/2\,\pi\eta}\Gamma(1+i\eta) F_{lm}(\varkappa) \int \mathrm{d}\mathbf{r}_n \, e^{i\mathbf{q}\cdot\mathbf{r}_n}$$
$$\overset{*}{\Phi}_{LM}(\mathbf{r}_n)\, {}_1F_1(-i\eta, 1i(k'r_n - \mathbf{k}'\cdot\mathbf{r}_n)), \tag{32}$$

where

$$\mathbf{q} = \mathbf{k}_i - \frac{m_T}{m_R}\mathbf{k}_f$$

(and where l, L and $\mathfrak{L}$ are used instead of l_f, L_f and $\mathfrak{L}_f$, η also instaed of η_i and k' is used instead of k_i' for the sake of simplicity).

Taking for $\overset{*}{\Phi}_{LM}(\mathbf{r}_n)$ the MORINIGO [12] wave function and following the method adopted in the earlier Section 2, one obtains:

$$\begin{aligned}
\tilde{I}_{lL}^{mM} = \sum_{\lambda\mu_\lambda} & N(\pi)^{3/2}(i)^L(2)^{L+3}(-)^{L-\lambda+M}\left(\frac{1}{2\lambda+1}\right)^{1/2} \\
& \binom{2L+1}{2\lambda}^{1/2}(q)^\lambda(k')^{L-\lambda}(\beta^2+q^2)^{-(L+1)}(1-Z)^{i\eta-L} \\
& e^{-1/2\,\pi\eta}\,\frac{\Gamma(1+i\eta)\,\Gamma(L+1)\,\Gamma(L-\lambda-i\eta)}{\Gamma(-i\eta)\,\Gamma(L-\lambda+1)}\,F_l(\varkappa) \\
& {}_2F_1(-\lambda, 1+i\eta; L+1-\lambda; z)\,(L-\lambda-(M+\mu_\lambda)\,\lambda\mu_\lambda|\,L-M) \\
& Y_{L-\lambda}^{-(M+\mu_\lambda)}(\hat{\mathbf{k}}')\,Y_\lambda^{\mu_\lambda}(\hat{\mathbf{q}})\,\overset{*}{Y}_l^m(\hat{\mathbf{q}}),
\end{aligned} \tag{33}$$

where $F_l(\varkappa)$ is given in [13].

Introducing (33) into (26), then summing over all projections, the following expression for the differential cross-section is obtained:

$$\begin{aligned}
\frac{d\sigma}{d\Omega} = & \frac{m_i m_f}{(2\pi\hbar^2)^2}\,\frac{k_f}{k_i}\,\frac{(2I_R+1)}{(2I_T+1)}\,N^2\,\frac{\Gamma(1+i\eta)\,\Gamma(1-i\eta)}{\Gamma(-i\eta)\,\Gamma(+i\eta)}\,e^{-\pi\eta} \\
& \sum \begin{Bmatrix} n & N & J_a & J_b & J & l & L & \lambda & \mathfrak{L} & B \\ n' & N' & J_a' & J_b' & S & l' & L' & \lambda' & A & A \end{Bmatrix} \overset{*}{\Theta}_{I_T J}(J_a J_b)\,\Theta_{I_T J}(J_a' J_b') \\
& T(J_a J_b;\,\mathfrak{L}S)\,T(J_a' J_b';\,\mathfrak{L}S)\,\langle nl, NL;\,\mathfrak{L}|n_a l_a, n_b l_b;\,\mathfrak{L}\rangle \\
& \langle n' l', N' L'\mathfrak{L}|n_a' l_a', n_b' l_b';\,\mathfrak{L}\rangle\,(i)^L(-i)^{L'}(-)^A(2)^{L+L'} \\
& \frac{(2A+1)(2B+1)(2\Lambda+1)(2\mathfrak{L}+1)}{(2S+1)(2J+1)}\,(2l+1)^{1/2}(2l'+1)^{1/2}\binom{2L}{2\lambda}^{1/2}\binom{2L'}{2\lambda'}^{1/2} \\
& (q)^{\lambda+\lambda'}(k')^{L+L'-\lambda-\lambda'}(\beta^2+q^2)^{-(L+L'+2)}\,\Gamma(L-\lambda-i\eta) \\
& \Gamma(L'-\lambda'+i\eta)\,F_l(\varkappa)\,\overset{*}{F}_{l'}(\varkappa) \begin{Bmatrix} L-\lambda & \lambda & L \\ L'-\lambda' & \lambda' & L' \\ \Lambda & B & A \end{Bmatrix} \\
& \begin{Bmatrix} l & L & \mathfrak{L} \\ L' & l' & A \end{Bmatrix} \begin{pmatrix} L-\lambda & L'-\lambda' & \Lambda \\ 0 & 0 & 0 \end{pmatrix} \begin{pmatrix} \lambda & \lambda' & B \\ 0 & 0 & 0 \end{pmatrix} \begin{pmatrix} l & l' & A \\ 0 & 0 & 0 \end{pmatrix}
\end{aligned}$$

$$\begin{pmatrix} A & B & \Lambda \\ o & o & o \end{pmatrix} z^{\lambda-L}\, \overset{*}{z}{}^{\lambda'-L'}\, \frac{\mathrm{d}^{\lambda}}{\mathrm{d}z^{\lambda}} \left\{ z^{L} (1-z)^{i\eta-L+\lambda} \right\}$$

$$\frac{\mathrm{d}^{\lambda'}}{\mathrm{d}\overset{*}{z}{}^{\lambda'}} \left\{ \overset{*}{z}{}^{L'} (1-\overset{*}{z})^{-i\eta-L'+\lambda'} \right\} P_{\Lambda}(\cos\omega). \tag{34}$$

4. Discussion and results

The ratio between the result (23) and that obtained using TER-MARTIROSIAN's [1] results is shown in Fig. 3, while in Fig. 4 the ratio between ζ' and the corresponding ζ obtained by TER-MARTIROSIAN is shown. The data used in these calculations are according to GOLDFARB [3].

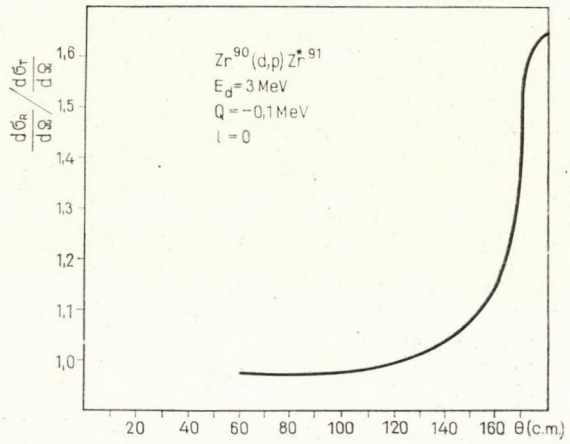


Fig. 3

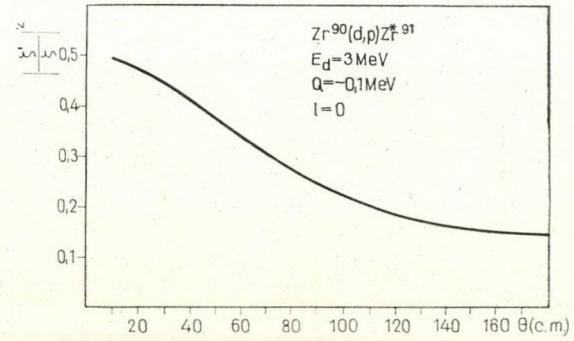


Fig. 4

For the purpose of numerical calculations in the case of the two cluster transfer process, one may consider (^{3}He, p) and (t, n) reactions. Comparison is made between the theoretical expression (34) and some experimental data on the reaction ^{27}Al(^{3}He, p)^{29}Si [14] for the ground, second and fourth excited

states of ^{29}Si (Figs 5, 6 and 7). The incident ^{3}He energy is 5 MeV in the laboratory system, and the Q-value for the reaction considered is 12.343 MeV.

For comparison, curves are drawn for the non-Coulomb plane wave Born approximation. The calculated angular distribution shows a forward peaking followed by a broad minimum at an angle of 150° in the ground state,

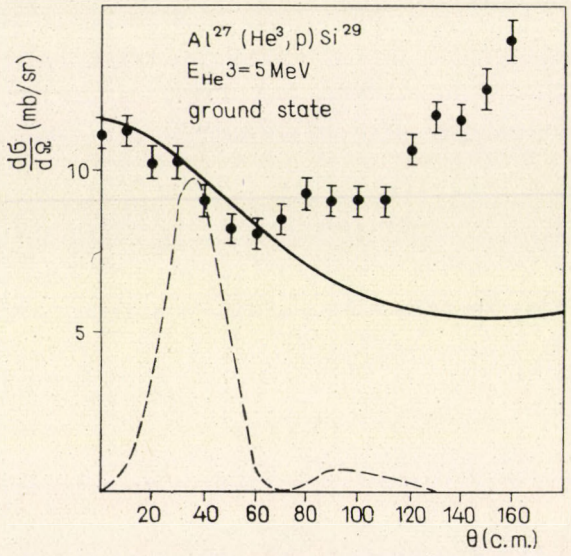


Fig. 5

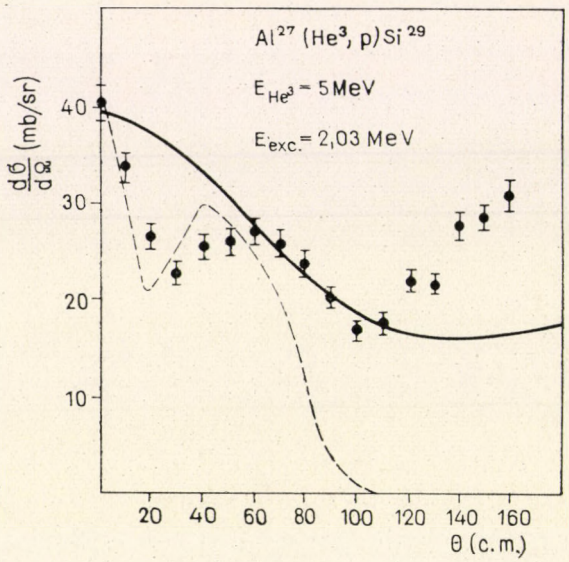


Fig. 6

140° in the second excited state and 120° in the fourth excited state. The magnitude of the differential cross-section in the backward direction increases with the increase of the excitation energy of ^{29}Si. Thus, the decrease in the energy of the outgoing proton so as to approach the value of the Coulomb barrier in the exit channel, shows two effects. First, a shift in the minimum

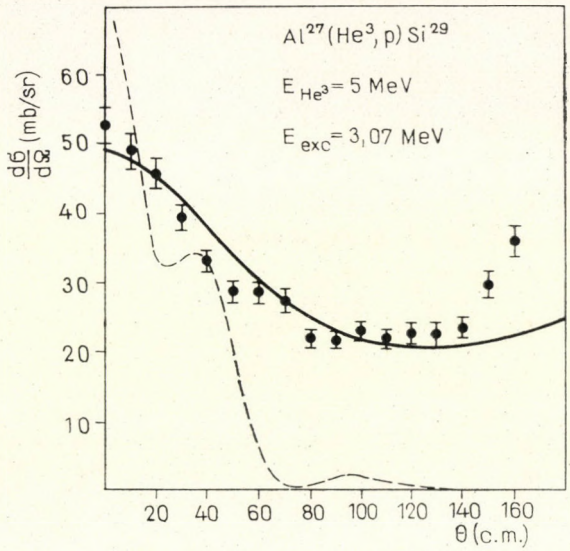


Fig. 7

towards the forward direction, and second, a gradual rise in the magnitude of the angular distribution in the backward direction. This may show that when the proton energy is well below the Coulomb barrier in the final channel, backward peaking for the angular distribution is observed, which agrees well with earlier works.

REFERENCES

1. K. Ter-Martirosian, Soviet Physics, JETP, **2,** 620, 1956.
2. L. C. Biedenharn, K. Boyer and M. Goldstein, Phys. Rev., **104,** 383, 1956.
3. L. J. B. Goldfarb, Nucl. Phys., **72,** 537, 1965.
4. A. Dar, A. De-Shalit and A. S. Reiner, Phys. Rev., **131,** 1732, 1963.
5. P. J. A. Buttle and L. J. B. Goldfarb, Phys. Soc., **83,** 701, 1964.
6. P. J. A. Buttle and L. J. B. Goldfarb, Nucl. Phys., **78,** 409, 1966.
7. M. El-Nadi and T. H. Rihan, Proc. Phys. Soc., **87,** 119, 1966.
8. I. P. Grant, Proc. Phys. Soc., **A68,** 244, 1955.
9. B. A. Lippmann and J. Schwinger, Phys. Rev., **79,** 469, 1950.
10. H. Margenau and G. M. Murphy, 1943 p. 395 "The Mathematics of Physics and Chemistry" (New York: Van Nostrand).
11. A. Y. Abul-Magd, M. El-Nadi and G. L. Vystosky, Nucl. Phys., **71,** 606, 1965.
12. F. B. Morinigo, Phys. Rev., **134,** B1243, 1964.
13. M. El-Nadi, A. Osman and T. H. Rihan, Acta Phys. Hung., **29,** 127, 1970. A. Osman, M. Sc. Thesis "Finite Range Coulomb Stripping Reactions" (Cairo University, 1967, Cairo, Egypt, U .A.R.).
14. S. Gorodetzky, G. Bassompierre et A. Gellmann, Nucl. Phys., **62,** 575, 1965.

РЕАКЦИИ ПРИ НИЗКИХ ЭНЕРГИЯХ С ПЕРЕДАЧЕЙ «КЛАСТЕРОВ»

М. ЭЛ-НАДИ, А. ОСМАН и Т. Х. РИХАН

Р е з ю м е

Исследуются процессы передачи кластеров под кулоновским барьером для произвольных зарядов и передачи момента количества движения, с учетом короткодействия взаимодействия. Получено аналитическое выражение для дифференциального поперечного сечения. Проведены вычисления для реакции $Zr^{90}(d, p)Zr^{91}$. Выведено также аналитическое выражение для дифференциального поперечного сечения для двухкластерных реакций. Результаты сравниваются с данными реакции $Al^{27}(He^3, p)Si^{29}$.

Acta Physica Academiae Scientiarum Hungaricae, Tomus 29 (2—3), pp. 159—165 (1970)

APPLICATION OF VARIATION-PERTURBATION THEORY TO THE STUDY OF THE INDUCTIVE EFFECT IN SATURATED MOLECULES BY THE METHOD OF GEMINALS II

HALOGEN-SUBSTITUTED HYDROCARBONS

By

R. G. NOUSRATOULLIN and I. Ts. LYAST

INSTITUTE FOR CHEMISTRY OF THE BASHKIRIAN BRANCH OF THE ACADEMY OF SCIENCES, UFA, USSR

(Received 18. IX. 1969)

An expression for the inductive effect potential obtained in paper [1] is simplified semi-empirically. The bond polarity parameter is introduced and the inductive effect of the substitution in the molecules CH_3X, C_2H_5X (X=F, Cl, Br) is considered. The dipole moments of the bonds and the populations on the atoms in these molecules are calculated.

1. Introduction

For understanding the nature of the inductive effects of the polar substitutes of chemical bonds it is necessary to know to what extent this influence is transmitted over chemical bonds. As was shown in a previous paper of this series [1] the inductive effect in saturated molecules can be considered on the basis of the variation-perturbation theory. The influence of the substitution in the spatially distant part of the molecule to the chemical bond can be taken into account electrostatically. The consideration of the substitution of atoms in the neighbouring bond is more important, but, ab initio calculations for this case are involved with well-known difficulties. From the point of view of the qualitative and semi-quantitative results, the simplification of the inductive potential leading to a clear physical and chemical interpretation is interesting.

In [1] the inductive potential was written in the following form:

$$\hat{u}_{\lambda\mu} = \hat{Q}_{\bar{\lambda}\nu'} - \hat{Q}_{\bar{\lambda}\nu} - 2\left(\frac{Z_{\nu'}}{r_{1,\nu'}} - \frac{Z_{\nu}}{r_{1,\nu}}\right), \tag{1}$$

where $\hat{Q}_{\bar{\lambda}\nu}$ is the operator including the operators of the Coulomb and exchange interactions between $\psi_{\lambda\mu}$ (12) and $\psi_{\bar{\lambda}\nu}$ (34) geminals [1—2] (Fig. 1). $Z_\nu/r_{1,\nu}$ is the operator of the interaction of electron "1" with nucleus "Z_ν".

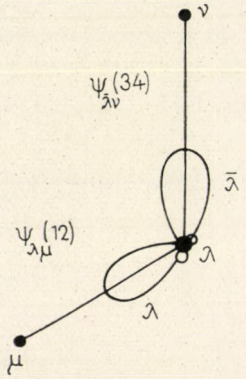


Fig. 1

Representing the geminal in the form of a bilinear expansion in terms of the one-electron basis functions $\{i\}$ the following expressions for the perturbed energy and coefficients of the expansion were obtained:

$$\epsilon^{(1)} = \sum_{i_1 \le i_2} \sum_{i_3 \le i_4} A^{(0)}_{i_1 i_2} A^{(0)}_{i_3 i_4} u\left[{}^{\lambda\mu\ \lambda\mu}_{i_1 i_2\ i_3 i_4}\right], \tag{2}$$

$$\epsilon^{(2)} = \sum \sum a_{i_1 i_2} A^{(0)}_{i_3 i_4} u\left[{}^{\lambda\mu\ \lambda\mu}_{i_1 i_2\ i_3 i_4}\right], \tag{3}$$

$$\sum_{i_1 \ge i_2}^{n-1} a_{i_1 i_2} \left\{ \mathcal{E}^{(0)}\left[{}^{\lambda\mu\ \lambda\mu}_{i_1 i_2\ i_3 i_4}\right] - E^{(0)}_{\lambda\mu} N\left[{}^{\lambda\mu\ \lambda\mu}_{i_1 i_2\ i_3 i_4}\right] \right\} = - \sum_{i_1 \ge i_2}^{n} A^{(0)}_{i_1 i_2} \left\{ u\left[{}^{\lambda\mu\ \lambda\mu}_{i_1 i_2\ i_3 i_4}\right] - \epsilon^{(1)} N\left[{}^{\lambda\mu\ \lambda\mu}_{i_1 i_2\ i_3 i_4}\right] \right\}, \tag{4}$$

here $u\left[{}^{\lambda\mu\ \lambda\mu}_{i_1 i_2\ i_3 i_4}\right]$ are the matrix elements of the perturbation operator (1), $\mathcal{E}^{(0)}\left[{}^{\lambda\mu\ \lambda\mu}_{i_1 i_2\ i_3 i_4}\right]$, $N\left[{}^{\lambda\mu\ \lambda\mu}_{i_1 i_2\ i_3 i_4}\right]$ are the matrix elements of the model energy operator and norm of the function $\psi^{(0)}_{\lambda\mu}(12)$.

$E^{(0)}_{\lambda\mu}$ is the energy of the unperturbed function $\psi^{(0)}_{\lambda\mu}(12)$. In the system of equations (4) one of the coefficients is supposed to be equal to zero (in the case of minimal basis $a_{12} = 0$). Also, the solution for an unperturbed system is supposed to be known.

2. Simplification of the inductive potential

Let us consider the simple case when the geminal is constructed only with the help of the atomic (hybrid) functions forming the valence bond " ":

$$\psi_{\bar{\lambda}\nu}(34) = A_{11}\,\bar{\lambda}(3)\,\bar{\lambda}(4) + A_{12}\left[\bar{\lambda}(3)\,\nu(4) + \bar{\lambda}(4)\,\nu(3)\right] + A_{22}\,\nu(3)\,\nu(4). \tag{5}$$

The chemical meaning of this expression is clear: the first and third terms are the ionic terms, the second term is the covalent one.

If one neglects the nonorthogonality of the geminals the expression for "Q" can be written in the form:

$$\hat{Q}_{\bar{\lambda}\nu}\varphi(1) = 4\int \frac{1}{r_{13}}[\psi_{\bar{\lambda}\nu}(34)]^2\, d(3)\, d(4)\, \varphi(1) - \\ - 2\int \frac{1}{r_{13}}\psi_{\bar{\lambda}\nu}(34)\,\psi_{\bar{\lambda}\nu}(41)\,\varphi(3)\, d(3)\, d(4)\,. \tag{6}$$

The terms of this expression are the Coulomb and exchange operators, respectively. In order to simplify the calculations of the Coulomb-exchange interactions it is convenient to use the generalized Mulliken's approximation to the operator "Q" [3]:

$$2\,\hat{Q}_{\bar{\lambda}\nu} = S_{\bar{\lambda}\nu}(\hat{Q}_{\bar{\lambda}\bar{\lambda}}+\hat{Q}_{\nu\nu})\,. \tag{7}$$

With this approximation, Eq. (6) becomes

$$\hat{Q}_{\bar{\lambda}\nu} = R_{\bar{\lambda}}\,\hat{Q}'_{\bar{\lambda}\bar{\lambda}}+R_{\nu}\,\hat{Q}'_{\nu\nu}\,, \tag{8}$$

where $R_{\bar{\lambda}}$ and R_{ν} have the meaning of the populations on the atomic orbitals "$\bar{\lambda}$" and "ν" forming the chemical bond and are expressed as:

$$R_{\bar{\lambda}} = \frac{1}{N}[A_{11}^2+A_{12}^2(1+S_{\bar{\lambda}\nu}^2)+3\,A_{11}\,A_{12}\,S_{\bar{\lambda}\nu}+A_{11}\,A_{22}\,S_{\bar{\lambda}\nu}^2+A_{12}\,A_{22}\,S_{\bar{\lambda}\nu}]\,, \tag{9}$$

$$R_{\nu} = \frac{1}{N}[A_{22}^2+A_{12}^2(1+S_{\bar{\lambda}\nu}^2)+A_{11}\,A_{12}\,S_{\bar{\lambda}\nu}^2+A_{11}\,A_{22}\,S_{\bar{\lambda}\nu}^2+3\,A_{12}\,A_{22}\,S_{\bar{\lambda}\nu}]\,, \tag{9'}$$

where "A" are the coefficients of the expansion (5) and "N" is the norm of the geminal $\psi_{\bar{\lambda}\nu}(34)$.

The operators "Q" have the following form:

$$\hat{Q}'_{\nu\nu}\varphi(1) = 4\int \frac{1}{r_{13}}[\nu(3)]^2\, d(3)\,\varphi(1) - 2\int \frac{1}{r_{13}}\nu(3)\,\varphi(3)\, d(3)\,\nu(1)\,. \tag{10}$$

The expression (8) can be rewritten in a more final form as:

$$2\,\hat{Q}_{\bar{\lambda}\nu} = (1-q_{\bar{\lambda}\nu})\,\hat{Q}'_{\bar{\lambda}\bar{\lambda}}+(1+q_{\bar{\lambda}\nu})\,\hat{Q}'_{\nu\nu} \tag{11}$$

where

$$q_{\bar{\lambda}\nu} = R_{\nu}-R_{\bar{\lambda}} = \frac{1}{N}[(A_{22}^2-A_{11}^2)+2\,A_{12}\,S_{\bar{\lambda}\nu}(A_{22}-A_{11})]\,. \tag{12}$$

The parameter "$q_{\bar{\lambda}\nu}$" can be termed as the bond polarity parameter and is the negative charge which in the bond "$\bar{\lambda}\nu$" is transferred from atom "λ" to atom "ν". In expression (12) the first term on the right is caused by the differences of the ionic contributions and the second term is connected with covalence and overlapping.

Taking into account the simplifications made, the inductive effect potential (1) can be written:

$$\hat{u}_{\lambda\mu} = \frac{1}{2}\left[(q_{\bar{\lambda}\nu} - q_{\bar{\lambda}\nu'})\,\hat{Q}'_{\bar{\lambda}\bar{\lambda}} + (1+q_{\bar{\lambda}\nu'})\,\hat{Q}_{\nu'\nu'} - (1+q_{\bar{\lambda}\nu})\,\hat{Q}^1_{\nu\nu}\right] - 2\left(\frac{Z_{\nu'}}{r_{1,\nu'}} - \frac{Z_\nu}{r_{1,\nu}}\right). \tag{13}$$

Under the influence of this potential an electronic displacement takes place along the chemical bond which leads to the change of the populations on the atomic orbitals forming the bond "$\lambda\mu$". To define the perturbed energy and the change of the populations it is necessary to find the matrix elements of the perturbation (13) on the basis of the functions belonging to the "$\lambda\mu$" bond. These expressions will depend on the polarity parameters "$q_{\bar{\lambda}\nu}$" and "$q_{\bar{\lambda}\nu'}$". The polarity parameter can be found from the condition that the calculated value of the molecule dipole moment should equal the corresponding experimental value. According to the vector model the total dipole moment of the molecule is represented as the sum of the dipole moment of the individual bonds. It can be easily shown that in our approximation the dipole moment of the "$\bar{\lambda}\nu$" bond is expressed as follows:

$$p_{\bar{\lambda}\nu} = (1-q_{\bar{\lambda}\nu})\,\delta_{\bar{\lambda}} + (1+q_{\bar{\lambda}\nu})\,\delta_\nu\,, \tag{14}$$

where $\delta_{\bar{\lambda}}$ and δ_ν are dipole moments of the atomic orbitals of bond with respect to its geometric centre.

The dipole moment of the bond "$\lambda\mu$" is equal to the sum of the dipole moments $p^{(0)}_{\lambda\mu}$ and $p_{\text{ind.}}$ caused by the substitution:

$$p_{\lambda\mu} = p^{(0)}_{\lambda\mu} + p_{\text{ind.}} \tag{15}$$

Induced dipole moment is defined by the coefficients obtained from the solution of the system of equations (4)

$$p_{\text{ind.}} = \sum_{i_1 \le i_2} \sum_{i_3 \le i_4} a_{i_1 i_2}\, A^{(0)}_{i_3 i_4}\, p\left[{}^{\lambda\mu\ \ \lambda\mu}_{i_1 i_2\ i_3 i_4}\right], \tag{16}$$

where

$$p\left[{}^{\lambda\mu\ \ \lambda\mu}_{i_1 i_2\ i_3 i_4}\right] = \int i_1(1)\, i_2(2)\,[Z(1)+Z(2)]\, i_3(1)\, i_4(2)\, d(1)\, d(2). \tag{17}$$

The process of the definition of the bond polarity parameter is iterative because of "$p_{\text{ind.}}$".

3. Halogen-substituted hydrocarbons

According to the above method the calculation of the influence of the substitution of the C—H and C—C bonds in the methane and ethane molecules was carried out. As the substitutes "v'" the atoms F, Cl, Br were taken with the Slater type functions $2p_\sigma$, $3p_\sigma$, $4p_\sigma$ which form the bond sp^3-hybrid orbital of the C-atom. (Note that the sp^3-orbital is orthogonal to the $(1s)_c$-orbital)

$$sp^3 = -0.1130(1s)_c + 0.5126(2s)_c + 0.8660(2p_\sigma)_c \,. \tag{18}$$

The exponential factors ζ of the AO forming the bonds C—X (X = F, Cl, Br) are taken according to Slater's rule: $\xi_{1s}^{(c)} = 5.7$, $\zeta_{2s,2p}^{(c)} = 1.625$, $\zeta_{2p}^{(F)} = 2.60$, $\zeta_{3p}^{(Cl)} = 2.033$, $\zeta_{4p}^{(Br)} = 1.90$. The exponential factor for the 1s hydrogen orbital is taken to be equal to $\xi_{1s}^{(H)} = 1.15$. The molecular integrals for the calculation of the matrix elements of perturbation were defined by the approximation of Slater orbitals by the series of Gaussian functions [4].

The dipole moments of the molecules CH_3X (X = F, Cl, Br) have the following values [5]:

$$CH_3F : p = 1.79 \text{ D}; \; CH_3Cl : p = 1.87 \text{ D}; \; CH_3Br : p = 1.80 \text{ D}.$$

The polarity parameters of the C—H bonds in methane and ethane are defined from formulas (9), (9′) and (12) using the results of [6] (see Table I). Then, the polarity of the C—X bond is calculated in the zero approximation according to the vector model. For the CH_3X molecule, for example, the polarity parameter of the C—X bond is equal to:

$$q_{c-x} = \frac{P_{\text{tot}} + p_{CH}^{(0)} + p_{\text{ind}} - (\delta_{\bar{c}} + \delta_x)}{\delta_x - \delta_{\bar{c}}} \,, \tag{19}$$

where $\delta_{\bar{c}}$ and δ_x are the atomic dipoles of the C—X bond.

Table I

Coefficients and energy of geminals in CH_4, C_2H_6 [6]

molecules / bonds		CH_4	C_2H_6
C—H	$A_{11}^{(0)}$	0.6486	0.6492
	$A_{12}^{(0)}$	1.0000	1.0000
	$A_{22}^{(0)}$	0.4083	0.4149
	$E^{(0)}$ a. u.	—1.9512	—1.9411
C—C	$A_{11}^{(0)}$		0.2133
	$A_{12}^{(0)}$		1.0000
	$A_{22}^{(0)}$		0.2133
	$E^{(0)}$ a. u.		—1.9400

Table II

Corrections to the coefficients and energy of geminals in CH_2X, C_2H_5X

molecules / bonds		CH_3F	CH_3Cl	CH_3Br	C_2H_5F	C_2H_5Cl	C_2H_5Br
C—H	a_{11}	0.0713	0.0441	0.0386	0.0701	0.0400	0.0293
	a_{22}	—0.0460	—0.0216	—0.0162	—0.0413	—0.0191	—0.0140
	$\varepsilon^{(1)}$ a. u.	—0.0922	—0.0646	—0.0522	—0.0911	—0.0608	—0.0502
C—C	a_{11}				0.0286	0.0160	0.0127
	a_{22}				—0.0215	—0.0125	—0.0121
	$\varepsilon^{(1)}$ a. u.				—0.0927	—0.0609	—0.0477

Table III

Polarity parameters and dipole moments of bonds

molecules / bonds		CH_4	CH_3F	CH_3Cl	CH_3Br	C_2H_6	C_2H_5F	C_2H_5Cl	C_2H_5Br
C—H	r	—0.0874	—0.1289	—0.1120	—0.1070	—0.0851	—0.1221	—0.1089	—0.0948
	p a. u.	0.6636	0.6107	0.6280	0.6385	0.6665	0.6132	0.6310	0.6412
C—X	q	—	0.3110	0.2519	0.1916	—	0.3110	0.2519	0.1916
	p a. u.	—	1.3150	1.3642	1.3472	—	1.3150	1.3642	1.3472
C—C	q	—	—	—	—	0.0000	—0.0212	—0.0120	—0.0080
	p a. u.	—	—	—	—	0.0000	0.0288	0.0163	0.0110

According to the calculations made the two iterations are sufficient for the self-consistent definition of the parameters "q". The results of the calculations are given in Tables II and III, where the corrections to the geminal of the C—H, C—C bonds and the polarity parameters, dipole moments of the bonds in CH_3X and C_2H_5X are shown. As is seen, the substitution of one hydrogen atom by the X atom leads to the charge transfer along the neighbouring C—H bond to the C atom and, to a decrease of the C—H bond dipole moment. The substitutes are placed in the inductive series

$$H < C < Br < Cl < F$$

which corresponds to known chemical concepts.

In conclusion the authors wish to thank Miss V. G. KASHITSINA for computing the integrals.

REFERENCES

1. R. G. Noustratoullin, Acta Phys. Hung., **24**, 163, 1968.
2. И. Ц. Ляст, Ж. структ. химии, **7**, 80, 1966.
3. J. M. Parks and R. G. Parr, J. Chem. Phys., **28**, 335, 1958.
4. И. Ц. Ляст, В. Г. Кашицына, Ж. структ. химии, **10**, 1133, 1969.
5. М. В. Волькенштейн, «Строение и физические свойства молекул», М., Изд-во АН СССР, 1955.
6. И. Ц. Ляст, Н. П. Пошюнайте, Ж. структ. химии (в печати).

ПРИМЕНЕНИЕ ВАРИАЦИОННОЙ ТЕОРИИ ВОЗМУЩЕНИЯ К ИЗУЧЕНИЮ ИНДУКТИВНОГО ЭФФЕКТА В НАСЫЩЕННЫХ МОЛЕКУЛАХ МЕТОДОМ ГЕМИНАЛЕЙ

II Галогенозамещенные углеводороды

Р. Г. НУСРАТУЛЛИН и И. Ц. ЛЯСТ

Резюме

Выражение для индуктивного потенциала, полученное ранее, упрощается введением полуэмпирического параметра полярности связи. Рассматривается индуктивный эффект замещения в молекулах CH_3X, C_2H_5X (X = F, Cl, Br). Вычислены дипольные моменты связей и заселенности на атомах

Acta Physica Academiae Scientiarum Hungaricae, Tomus 29 (2—3), pp. 167—181 (1970)

ON THE CORRESPONDENCE PRINCIPLE

By

G. FÁY

DEPARTMENT OF HISTORY AND PHILOSOPHY OF SCIENCE,
CHELSEA COLLEGE, UNIVERSITY OF LONDON, LONDON, ENGLAND*

(Received 30. IX. 1969)

Several concepts of possible "Correspondences" between quantum and classical mechanics will be defined and examined in what cases they can be satisfied.

Introduction

While classical mechanics cannot describe events in the microscopic world, quantum mechanics, it has been claimed, not only describes this world, but can also replace classical mechanics in the description of the macroscopic domain. If this claim is true then classical mechanics is deducible from quantum mechanics and we can find a method for this deduction in *general* [1]. The attraction of proving this claim true is great for both historians and philosophers of science — for historians because this would show a rational link in the scientific development missing at present; for philosophers because they would not have to tolerate any longer two inconsistent theories side by side.

Historically, the question of such a correspondence arose because the new (quantum) theory had to borrow names and concepts from the old (classical) theory. PLANCK in 1900 and BOHR in 1913 tried to justify their startling theoretical results by showing that, under appropriate conditions, quantum mechanics yields classical results [2]. The correspondence principle became a productive conceptual device for further development of the quantum theory [3].

In this article we will try to provide an answer to the question: In what cases do quantum and classical mechanics yield the same results in the description of nature. For this purpose we will find it necessary to define an "*Orbit-Probability Correspondence*" (an O-P Correspondence) and its various subclasses in order to create a language common to both theories within which the above question could be meaningfully formulated.

Examples will be given in which the subclasses of O-P Correspondence occur — or fail to occur — but no single uniform rule will be given which

* Present address: KGM ISZSZI, Budapest

determines whether correspondence occurs in any given case. Furthermore, we will propose a more general basis for a correspondence between the two mechanics — this will be called the *Logical Correspondence* (the L-Correspondence).

1. A suggested common language for the two mechanics — O-P Correspondence

The question of the relationship between the two theories has to be formulated more precisely because the two theories do not use the same language in the description of physical events; to get a sensible answer we must try and formulate a common language.

In order to develop such a language we must overcome three fundamental differences in their conceptual make-up:

1. Quantum mechanics is *essentially* a statistical theory while classical mechanics is not — in the sense that it can be reduced to a causal discipline [4].

2. Classical mechanics ascribes an orbit to a particle whereas quantum mechanics does not.

3. While quantum mechanics contains an *essential* constant (h) classical mechanics does not need *any particular* constant (e.g. g and γ are needed only in applications).

What we propose to do then is the following: We shall try to modify the conceptual framework of the two theories with respect to 1 and 2 above — so as to create a common language on the basis of which we shall try to define and establish a correspondence principle. Point 3 will be dealt with in a separate section.

This conceptual modification will be two-fold: it will introduce a kind of position probability into classical mechanics [4] and a kind of orbit into quantum mechanics, each term described in terms of classical and quantum mechanics, respectively. It will turn out that this can be done in more than one way.

What will this mean? Assuming we can fulfil our programme, this means that to every particle *both* theories ascribe a position probability:

$$W(x, t)$$

such that, given $W(x, 0)$ we can predict $W(x, t)$ for any $t > 0$. And, that to every particle *both* theories ascribe an orbit:

$$x(t)$$

such that, given $x(0)$ and $\dot{x}(0)$ we can predict $x(t)$ for any $t > 0$.

Probability is defined in quantum mechanics by:

$$W_q^{\psi}(x, t) = \psi(x, t)\, \psi^*(x, t)\,, \tag{1.1}$$

where $\psi(x, t)$ satisfies the time-dependent Schrödinger equation:

$$H\psi(x, t) = -\frac{h}{i}\frac{\partial\psi(x, t)}{\partial t} \quad (H \text{ is Hamiltonian}) \tag{1.2}$$

and ψ refers to the initial state, i.e. $\psi(x, 0)$.

Orbit is defined in classical mechanics by the Newton's equation of motion:

$$m\ddot{x}_c(t) = F \qquad (F \text{ is force}). \tag{1.3}$$

We will use the notation $x_c^S(t)$ where S refers to the initial classical mechanical state:

$$S = \{x(0), \dot{x}(0)\}. \tag{1.4}$$

Suppose then that we are in possession of a concept of quantum mechanical orbit $x_q(t)$, defined in quantum mechanical terms, and a classical mechanical position probability $W_c(x, t)$, defined in classical mechanical terms. Now we can define a correspondence principle, an *Orbit-Probability Correspondence*, as follows:

Definition 1.1: We say that an O-P correspondence occurs between the classical mechanical state S and the quantum mechanical state ψ if

(O) $\qquad x_q^{\psi}(t) = x_c^S(t) \qquad$ for any $t > 0$,

(P) $\qquad W_q^{\psi}(x, t) = W_c^S(x, t) \qquad$ for any x and for any $t > 0$.

As we can see, the O-P correspondence consists of two parts: an orbit (O-) and a probability (P-) correspondence. The O-correspondence is suggested by the EHRENFEST theorem [5], while P-correspondence comes naturally out of NEUMANN's work [6]. This correspondence gives a particle *at the same time* an orbit and a position probability, both defined in mechanical and classical sense.

The reason why we introduce them jointly is that from a statistical point of view the expectation value for the orbit gives an incomplete description of of the relevant physical event, and, as we shall see later, one way to introduce "orbit" into quantum mechanics is via its expectation value.

As we suggested earlier, there is more than one way of defining an O-P correspondence. In fact we will suggest *two* ways for defining orbit in quantum

mechanics and *one* way for defining probability in classical mechanics. This means that we can define *two* O-P correspondences. The next section considers the first of the two possibilities. It should be said here that both are of "*predictive type*" in the sense that, given the orbit and probability at $t = 0$, we can calculate them for $t > 0$. Later on another type of correspondence will be introduced (Chapter 6).

2. Ehrenfest orbit for quantum mechanics and probability for classical mechanics

For *historical* reasons [7] it is interesting to introduce a quantum mechanical orbit as follows:

Definition 2.1:

$$x_q^{\psi}(t) = \bar{x}(t) ,$$

where $\bar{x}(t)$ is the expectation value of the coordinate x in the state $\psi(x, t)$.

The expectation value of a function $f(x)$ is by definition:

$$\bar{f}(x) = \int_{-\infty}^{+\infty} \psi(x, t)\, f(x)\, \psi^*(x, t)\, dx .$$

It is very important to realise that in general $\bar{f}(x) \neq f(\bar{x})$; only in the case when $f(x)$ is linear are the two functions equal [8].

The orbit introduced by the definition 2.1 we shall call "EHRENFEST orbit", since its concept is closely related to EHRENFEST's theorem [9].

We shall now introduce the following theorem:

Theorem 2.1: If the force $F(x)$ is linear then the orbit $\bar{x}$ satisfies the following equation:

$$m\ddot{\bar{x}} = F(\bar{x}),$$

i.e. we get Newton's equation of motion.

It is again important to realise that if $F(x)$ is not linear then the right-hand side of the theorem should be replaced by $\bar{F}(x)$, which is different from $F(\bar{x})$ and the equation is no longer analogous to that of NEWTON [10].

When $F(x)$ is linear then EHRENFEST's theorem is valid and we have the following theorem:

Theorem 2.2: If the force $F(x)$ is of the form $F(x) = ax + b$, where a, b are constants then to every classical mechanical state S there belongs a quantum mechanical state ψ such that

$$x_q^{\psi}(t) = x_c^{S}(t) \text{ for any } t \geqslant 0 . \tag{2.1}$$

Proof: If a classical state is given i.e. if $x(0)$ and $\dot{x}(0)$ are given, then we can construct the following quantum mechanical state:

$$\psi(x, 0) = \begin{cases} 1/\lambda_0 \exp\left[2\pi i \dfrac{x - x(0) + \lambda_0/2}{\lambda_0}\right] & \text{if } -\lambda_0/2 \leqslant x - x(0) \leqslant \lambda_0/2, \\ 0 \text{ otherwise,} \end{cases} \tag{2.2}$$

where $\lambda_0 = h/m\dot{x}(0)$ is the de Broglie wavelength of a particle with momentum $m\dot{x}(0)$. For ψ given by (2.1) we get:

$$x_q^{\psi}(0) = \bar{x}(0) = \int_{-\infty}^{+\infty} \psi(x, 0)\, x\psi^*(x, 0)\, dx = 1/\lambda_0 \int_{x(0)-\lambda_0/2}^{x(0)+\lambda_0/2} x \cdot 1 \cdot dx = x(0).$$

Let $\psi(x, t)$ denote the solution of the Schrödinger equation belonging to the initial conditions (see 2.1). Let ϱ denote the operator belonging to the momentum p. For $\dot{x}_q^{\psi}(0)$ we have:

$$\begin{aligned} \dot{x}_q^{\psi}(0) &= \left[\frac{\partial}{\partial t} x_q^{\psi}(t)\right]_{t=0} = \left[\frac{\partial \bar{x}}{\partial t}\right]_{t=0} = [1/m\, \bar{p}]_{t=0} \\ &= 1/m \int_{-\infty}^{+\infty} \psi(x, t)\, [p\psi(x, t)]^*\, dx \\ &= \dot{x}(0). \end{aligned}$$

Since here Newton's equation is linear, our result that at $t = 0$ $x_q^{\psi}(t) = x_c^S(t)$ and $\dot{x}_q^{\psi}(t) = \dot{x}_c^S(t)$ ensures that for any $t > 0$ these equations are valid.

This means that we can assign a quantum mechanical orbit to a mechanical state S. Of course, the chosen ψ must be normalised and satisfy the hermiticity condition for the momentum operator p. It is easy to show that these conditions are satisfied by $\psi(x, 0)$ given by (2.2).

Conversely, given an initial quantum mechanical state $\psi(x, 0)$ we can define:

$$x(0) = \int_{-\infty}^{+\infty} \psi(x, 0)\, x\psi^*(x, 0)\, dx,$$

and

$$\dot{x}(0) = 1/m \int_{-\infty}^{+\infty} \psi(x, 0)\, [p\psi(x, 0)]^*\, dx.$$

Then the classical state $S = \{x(0), \dot{x}(0)\}$ will clearly satisfy (2.1).

This then establishes an orbit correspondence between classical and quantum mechanics. The initial state, given by (2.2) has a simple statistical meaning as we can see by the graph of the corresponding density function $W_q^{\psi}(x, 0)$.

Since de Broglie wavelength λ_0 of a classical particle is of extremely small order (for example, if $m = 1$ g, $\dot{x} = 1$ cm/sec, $\lambda_0 = 6 \cdot 10^{-27}$ cm) the

shape of the function $W_q^{\psi}(x, 0)$ is extremely sharp. Practically the statistical uncertainty arising from the statistical character of $W_q^{\psi}(x, 0)$ is ignorable for all future times t.

We shall call the O-P correspondence in which the orbit part is introduced by the theorem 2.2 *Ehrenfest Correspondence*. We shall next show that the probability part of this correspondence cannot be satisfied in general (see definition 1.1).

First of all we shall take the classical mechanical concept for the simultaneous density function x_0 and p_0 at $t = 0$ and we shall denote it by:

$$W_c^s(x_0, p_0) \,. \tag{2.3}$$

Then, for $t > 0$, we shall use the well-known transformation formula for the probability density function as follows:

If the probability density of the co-ordinate and momentum at $t = 0$ is

$$W_c^s(x_0, p_0)$$

and x_0 and p_0 depend on time, according to the solution of Newton's equation

$$\begin{aligned} x &= x(t) = f(x_0, p_0, t) \,, \\ p &= p(t) = g(x_0, p_0, t) \,, \end{aligned} \tag{2.4}$$

then the probability density of the coordinate and momentum at $t > 0$ will be given by:

$$W_c^s(x, p, t) = W_c^s[x_0(x, p), p_0(x, p)] \frac{\partial(x_0, p_0)}{\partial x \, \partial p} \,, \tag{2.5}$$

where $x_0(x, p)$ and $p_0(x, p)$ are the solutions of the equations (2.4) and

$$\frac{\partial(x_0, p_0)}{\partial x \, \partial p} = \begin{vmatrix} \dfrac{\partial x_0(x, p)}{\partial x} & \dfrac{\partial x_0(x, p)}{\partial p} \\ \dfrac{\partial p_0(x, p)}{\partial x} & \dfrac{\partial p_0(x, p)}{\partial p} \end{vmatrix} \tag{2.6}$$

which is the Jacobi determinant for the pair of functions x_0, p_0.

Using (2.5), i.e. the probability density function for $t = 0$, we introduce the position probability density function as follows:

$$W_c^s(x, t) = \int_{-\infty}^{+\infty} W_c^s(x, p, t) \, dp \tag{2.7}$$

and the question is now: What is the relationship between $W_c^s(x, t)$ defined by (2.7) and $W_q^\psi(x, t)$ given in equation (1.1)? For only if we can find the conditions under which they are equal can we complete our task of finding a possible correspondence between the two mechanics.

Our next theorem shows that this is, however, in general not possible, because the probability in (2.7) cannot in general satisfy the P-part of the definition (1.1). In fact we find that demanding the identity of the probabilities is too strong. In the next section we will demand the indentity of dispersions, which is a weaker demand, and try to find conditions under which this will work.

3. Dispersion correspondence

If we are given an orbit concept for both quantum and classical mechanics and we are given dispersions as well, then we can define an O-D correspondence which is weaker than the original O-P correspondence [11]. We have the following definition.

Definition 3.1: An O-D correspondence occurs between the classical mechanical state S and the quantum mechanical state ψ if the following two conditions are satisfied:

$$\text{(O)} \qquad x_c^s(t) = x_q^\psi(t) \quad \text{for} \quad t > 0\,,$$

$$\text{(D)} \qquad \Delta_c^s(t) = \Delta_q^\psi(t) \quad \text{for} \quad t > 0\,,$$

where the symbol Δ means *dispersion* in the usual statistical way.

Consider now the following theorem:

Theorem 3.1: For a harmonic oscillator the O-D correspondence occurs if and only if the following conditions are satisfied:

$$1.\ \Delta x_q(0)\,(m \cdot w)^2 + \Delta^2 p_c(0) = 2\,(m \cdot w)^2\,[B^2 - \overline{x_q^2}(0)]\,,$$

$$2.\ \overline{x_c(0)\,p_c(0)} = \overline{x_c(0) \cdot p_c(0)}\,,$$

$$3.\ \Delta_c x(0) = \Delta_q x(0)\,,$$

where m is the mass of the oscillator, $w = \sqrt{k/m}$, k is the force constant,

$$B_\psi^2 = \sum_{n=0} |(\psi_m, \psi)|^2\,(\psi_n, x^2\,\psi_n)\,,$$

ψ_n is the n-th eigenfunction, $(\,,\,)$ denotes the scalar product, — denotes the expectation value.

Proof: The classical orbit for the harmonic oscillator is given by

$$x(t) = x(0)\cos wt - \frac{p(0)}{mw}\sin wt \tag{3.1}$$

and

$$p(t) = -x(0)\, mw \sin wt - p(0)\cos wt\,. \tag{3.2}$$

Combining the equations (3.1) and (3.2) using the transformation formula (2.4) and using the probability density function given by (2.6) we get:

$$\begin{aligned}\Delta_c^2 x(t) = \overline{x_c^2}(t) - \overline{x_c}^2(t) &= \int_{-\infty}^{+\infty} x^2 W_c(x,t)\,dx - \left[\int_{-\infty}^{+\infty} x\, W_c(x,t)\,dx\right]^2 \\ &= \Delta_c^2 x(0)\cos^2 wt + \frac{1}{m^2 w^2}\Delta_c^2 p(0)\sin^2 wt - \\ &- \frac{1}{mw}\left[\overline{x(0)\,p(0)} - \overline{x(0)}\cdot\overline{p(0)}\right]\sin^2 wt.\end{aligned} \tag{3.3}$$

Consider now the solution of the time-dependent Schrödinger equation for the harmonic oscillator [11]:

$$\psi(x,t) = \sum_{n=0}^{\infty} e^{-i/\bar{h}\varepsilon_n}\psi_n(x)\,(\psi_n(x),\psi)\,, \tag{3.4}$$

where

$$\psi_n(x) = A_n H_n\left(\frac{x}{l_0}\right)e^{-x^2/2l_0} \tag{3.5}$$

$$A_n = |\sqrt{\pi}\, l_0\, 2^n\, n!|^{-1/2},\; l_0 = \left(\frac{\bar{h}^2}{mk}\right)^{1/4},\; \varepsilon_n = \frac{w\bar{h}}{2}(2n+1), \tag{3.6}$$

$$H_n(x) = (-1)^n\, e^{x^2}\frac{d^n}{dx^n}(e^{-x^2})\,, \tag{3.7}$$

the n-th Hermite polynomial.

From (3.4)—(3.7) we get by routine but rather tedious computation:

$$\Delta_q^2 x(t) = A\cos 2wt - B_\psi^2 + x_q^2(t)\,, \tag{3.8}$$

where

$$A = \sum_{n+0}^{\infty} a_{n+2}\, a_n (x^2)_{n+2,n} + a_{n-2}\, a_n (x^2)_{n-2,n}\,,$$

$$a_i = \begin{cases}(\psi_i,\psi) & \text{if} \quad i \geqslant 0\,,\\ 0 & \text{if} \quad i < 0\,,\end{cases}$$

$$(x^2)_{i,k} = \begin{cases} l_0^2/4\sqrt{i(k+1)} & \text{if} \quad i > k \geqslant 0,\\ 0 & \text{if} \quad i < \text{ or } \quad k < 0,\\ l_0^2/4\sqrt{k(i+1)} & \text{if} \quad 0 \leqslant i < k.\end{cases}$$

Putting $t = 0$ in the equation (3.8) we get:

$$A = \Delta_q^2 x(0) - B_\psi^2 + x_q^2(0),$$

whence with 3.3 and 3.8, the difference between the quantum and classical dispersions is as follows:

$$\begin{aligned}\Delta_q^2 x(t) - \Delta_q^2 x(t) = {} & [\Delta_q^2 x(0) - \Delta_c^2 x(0)] \cos^2 wt - \\ & - \frac{1}{(mw)^2} [\Delta_q^2 x(0)\,(mw)^2 + \Delta^2 p_c(0) - \\ & - 2\,mw\,(B_\psi^2 - x_q^2(0)) \sin^2 wt - \\ & - \frac{1}{mw} [\overline{x(0)\,p(0)} - \overline{x(0)}\;\overline{p(0)}] \sin 2\,wt\end{aligned}$$

from which the theorem 3.1 follows.
Now, condition 3 is realistic since it just gives the initial conditions.

condition 2 physically means that there is no statistical correlation between coordinate and momentum at $t = 0$.

condition 1 is difficult to interpret physically, at least *we* could not give it an interpretation.

Theorem 3.1 shows that O-D and therefore O-P correspondence does not occur in general but that O-D can occur — provided the conditions 1—3 are satisfied.

We shall next consider another way of introducing orbit into quantum mechanics. This will not give us an O-P correspondence that always works, of course, since the same probability considerations apply again. But we feel it is nevertheless worth considering.

4. Hamilton—Jacobi correspondence

We have the following definition:

Definition 4.1: An H-J-P correspondence occurs between the quantum mechanical state ψ and classical state S if

(H—J)
$$x_q^\psi(t) = x_x^S(t) \quad \text{for } t > 0 \text{ and}$$

$$x_q^\psi(t) = i\bar{h}/2 \int_0^t \frac{\partial}{\partial x} \left(\ln \frac{\psi^*}{\psi} \right) dt + x_q^\psi(0)$$

(P) $$W_q^{\psi}(x,t) = W_c^{s}(x,t) \text{ for any } x \text{ and for any } t > 0.$$

The orbit as defined above is called a *Hamilton—Jacobi orbit* [12]. Clearly, H-J-P correspondence is a special case of O-P.

The reason why we want to define the quantum mechanical orbit in this way is because we can write:

Theorem 4.1: $m\ddot{x}_q^{\psi}(t) = -\partial V_q/\partial x$ which is again Newton's equation of motion.

Here

$$V_q^{\psi} = V + \frac{\bar{h}^2}{2m}\left[\frac{\psi^{*\prime\prime}(x,t)}{\psi(x,t)} + \frac{\psi^{\prime\prime}(x,t)}{\psi(x,t)}\right]$$

and

$$\psi^{\prime\prime}(x,t) = \frac{\partial^2}{\partial x^2}\psi(x,t)\,,$$

$$\psi^{*\prime\prime}(x,t) = \frac{\partial^2}{\partial x^2}\psi^{*}(x,t)\,.$$

Proof:

$$m\ddot{x}_q^{\psi}(t) = m\frac{i}{2}\frac{\bar{h}}{m}\frac{\partial}{\partial t}\left[\frac{\partial}{\partial x}\ln\frac{\psi^{*}(x,t)}{\psi(x,t)}\right]$$

$$= \frac{i\bar{h}}{2}\frac{\partial}{\partial x}\left[\frac{\dot{\psi}^{*}(x,t)}{\psi^{*}(x,t)} - \frac{\dot{\psi}(x,t)}{\psi(x,t)}\right]$$

$$= \frac{i\bar{h}}{2}\frac{\partial}{\partial x}\left[\frac{i/\bar{h}H\psi^{*}(x,t)}{\psi^{*}(x,t)} - \frac{i/\bar{h}\,H\psi(x,t)}{\psi(x,t)}\right]$$

$$= -\frac{1}{2}\frac{\partial}{\partial x}\left|2V + \frac{h^2}{2m}\left(\frac{\psi^{*\prime\prime}(x,t)}{\psi^{*}(x,t)} + \frac{\psi^{\prime\prime}(x,t)}{\psi(x,t)}\right)\right|$$

$$= -\frac{\partial V_q^{\psi}}{\partial x}\,.$$

In the definition 4.1 the value of $x_q^{\psi}(0)$ was not defined and therefore it can be chosen arbitrarily.

The question is now: Under what conditions is $x_q^{\psi}(t) = x_c^{s}(t)$ for $t > 0$? The necessary conditions are (1) that the force is linear, (2) that either A or B hold where A and B are given by:

A $$\begin{cases} x_q^{\psi}(0) = x_c^{s}(0), \\ \dot{x}_q^{\psi}(0) = \dot{x}_c^{s}(0), \end{cases}$$

(B) $$\left[\frac{i\bar{h}}{2m}\frac{\psi^{*\prime}(x,t)}{\psi^{*}(x,t)} - \frac{\psi^{\prime}(x,t)}{\psi(x,t)}\right]_{t=0} = \dot{x}_c^{s}(0)$$

and (3) that $V_q^{\psi} = V$. Given these we can have an H-J correspondence.

Conditions (1) to (3), of course, do not guarantee the complete H-J-P correspondence. In fact one can find a $\psi(x, t)$ satisfying A and satisfying [12]

$$W_c^S(x, 0) = W_q^\psi(x, 0)$$

with

$$W_c^S(x, t) \neq W_q^\psi(x, t) .$$

Incidentally, we have the following theorem:

Theorem 4.2: Let $x_q^\psi(t)$ denote a Hamilton—Jacobi orbit. Then A and B are equivalent.

Proof:

$$\dot{x}_q^\psi(0) = \frac{i\bar{h}}{2m} \frac{\partial}{\partial x} \left[\ln \frac{\psi^*(x, t)}{\psi(x, t)} \right]_{t=0}$$

$$= \frac{i\bar{h}}{2m} \left[\frac{\psi'^*(x, t)}{\psi^*(x, t)} - \frac{\psi'(x, t)}{\psi(x, t)} \right]_{t=0}$$

$$= \dot{x}_c^S(0) .$$

It is worth pointing out that the condition $V_q^\psi = V$ itself does not guarantee any orbit-correspondence [14]. One might think that as $h \to 0$, V_q^ψ becomes V. This is, however, not the case.

For example, if ψ is the initial state given in the proof of theorem 2.2 see p. 171), then

$$V_q^\psi = V + \frac{1}{2m} \dot{x}^2(0) \neq V \quad \text{if} \quad \dot{x}(0) \neq 0 .$$

In other words, it may happen that V does not contain h at all and still no correspondence to occur! This brings us naturally to consider the third fundamental difference between classical and quantum mechanics (see p. 167).

But before we go on let us consider once again the preceding pages. We have tried to follow our programme outlined on p. 167, i.e. we have created a possible common language between the classical and quantum mechanics in the sense that we have introduced a concept of orbit into the quantum and the concept of probability into the classical mechanics. We have then tried to establish an Orbit-Probability correspondence between them, that is we have tried to find the conditions under which:

$$x_q^\psi(t) = x_c^S(t) \qquad \text{for any } t > 0$$

and

$$W_q^\psi(x, t) = W_c^S(x, t) \text{ for any } x \text{ and for any } t > 0.$$

We found that such a correspondence does not hold in general but only in some very special cases. It would be desirable to see the logical connections between the two subcases of O-P correspondence. We, however, cannot establish any connection.

5. Planck's constant and the problem of correspondence

Quantum and classical mechanics remain different even if we introduce a common language between them — because we cannot establish an O-P correspondence.

It is traditional among physicists to believe that the process by which one can regain classical from quantum mechanics is the limiting process $h \to 0$ or rather $(h|k) \to 0$ where k is a quantity of the same dimensions as h [15]. Our example on the previous page suggests, however, that this is not always the case.

Nevertheless it may happen that a formula can be derived in quantum mechanics which does not contain h and that the same formula can be derived from classical mechanics [16]. Larmor's theorem is a well-known example of such a case:

$$\vec{\omega} = -\frac{q}{2mc}\vec{B},$$

where $\vec{\omega}$ is the angular velocity of the precession of a charged particle in a magnetic field $\vec{B}$, q is the charge of the particle, m its mass and c is the velocity of light.

Instead of considering the process $h \to 0$ as the bridge between the two mechanics, we would like to suggest another principle of correspondence. It will cover a limited area of intersection between the two. Our conjecture is this.

It seems to us that it should be possible in principle to derive every quantum (or classical) mechanical formula from classical (or quantum) mechanics provided that every physical quantity occurring in the formula is definable in classical (or quantum) mechanical terms but does not contain h in the case of a quantum mechanical formula.

6. Logical correspondence

We feel, however, that there is a more fundamental way of comparing the two theories: by considering their respective probability fields.

Each probability field contains well-defined algebraic structure of events. The two are different: classical mechanics uses the classical (Kolmogorov's) probability field whereas quantum mechanics uses its own probability field.

The two also have some common features:

1. *Events* (on the set of which a probability is defined) can be interpreted in the same way, namely both kinds of events are of the following form: "A physical quantity R has one of its possible values in the interval $[a, b]$ in a given state" [17].

2. Algebraic *operations* such as: negation (or complement) of an event; conjunction of two events; disjunction of two events, can be defined on the set of either kind of events.

These two kinds of events can be characterised in a very perspicuous algebraic way. The question of correspondence can be formulated then as follows: What kind of alterations should be made on the quantum mechanical set of events in order to obtain the classical set? Such a correspondence we will call Logical Correspondence (L-correspondence).

The "logical" part of the name comes from the fact that events can also be called "propositions" and sets of events with the above mentioned algebraic operations "a logic" [18].

Let us first see how these sets of events can be characterised algebraically in each case.

In the classical case the set of events is a Bolean σ-algebra. In other words a σ-complete complemented distributive lattice [19].

In the quantum mechanical case the set of events makes a non-distributive but uniquely orthocomplemented (orthomodular) lattice isomorphic to the lattice of all subspaces of a denumerably infinite-dimensional Hilbert space.

According to the definition of events and to the rules of quantum mechanics to every event there belongs a Hermitian linear operator. Because of the non-Bolean character of the quantum mechanical set of events, two such events a and b cannot in general be related classically, in the sense that

$$a = (a \cap b) \cap (a \cup b') \text{ holds [20]}, \tag{6.1}$$

where $\cap$, $\cup$, $'$, are the symbols for conjunction, disjunction and complementation, respectively.

We shall formulate the definition of L-correspondence as follows:

Definition 6.1: Let us consider a pair of classical and quantum mechanical states S and ψ. Let us consider a pair of physical events a_c^s and b_c^s classically as follows:

$$\begin{aligned} a_c^s &: \quad \alpha_a < A_c^s \leqslant \beta_a, \\ b_c^s &: \quad \alpha_b < B_c^s \leqslant \beta_a, \end{aligned} \tag{6.2}$$

where α and β are numbers, A_c^s and B_c^s physical quantities defined classically by the initial state S.

Let a_q^ψ, b_q^ψ be the quantum mechanical interpretation of the pair of events a_c^s and b_c^s in a way analogous to (6.2).

We say that a *logical correspondence* occurs between S and *with respect to* a given pair of events a and b if

$$a_q^\psi = (a_q^\psi \cap b_q^\psi) \cup (a_q^\psi \cap b_q^{\psi'}). \tag{6.3}$$

The set of quantum mechanical events such that every pair of its elements satisfies (6.3) makes a Bolean algebra, i.e. behaves like a classical mechanical set of events [22].

Example in which (6.3) holds can be found in C. PIRON's doctoral thesis. (See [20].)

Instead of drawing conclusions we stress the open character of the question of correspondence between the two theories.

Acknowledgements

The contents of this article developed from some lectures delivered by the author to the Quantum Mechanics seminar at the Department of History and Philosophy of Science, Chelsea College, in the Spring Term of 1969.

I am indebted to Dr. H. R. POST, Head of the Department, for suggesting the problem, and to the audience of the seminar, especially Professor J. TAYLOR (University of Colorado) and Professor R. SCHLEGEL (University of Michigan) for the inspiring discussions.

Finally, I wish to express my gratitude to Mrs. B. HOARE, a Research Student of the Department, who read the manuscript and who supplied many useful suggestions.

REFERENCES

1. C. f., N. BOHR, Atomic Theory and the Description of Nature, Cambridge, Univ. Press. 1934, p. 35.
2. M. PLANCK, "Über irreversible Strahlungsvorgänge", Annalen der Physik, **1**, 69, 1900. N. BOHR, "On the constitution of atoms and molecules", Philosophical Magazine, **26**, 1, 1913.
3. For a good account of the historical development of quantum theory see M. JAMMER, "The Conceptual Development of Quantum Mechanics", McGraw-Hill, New York, 1966.
4. J. VON NEUMANN, Mathematical Foundations of Quantum Mechanics, University Press, Princeton, 1955, p. 208. An interesting aspect of this approach can be found in M. BORN's article: Vorhersagbarkeit in der klassischen Mechanik, Z. Phys., **153**, 372, 1958.
5. P. EHRENFEST, Z. Phys., **45**, 455, 1927.
6. See [4].
7. See [5].
8. Many textbooks overlook this point. See e.g. BOHM, Quantum Theory, Prentice Hall Inc., U.S.A., 1961, p. 134.
9. See [5].
10. For this remark I am indebted to Prof. J. TAYLOR, Imperial College.
11. This correspondence is closely related to the *spread of the wave-function*, see e.g. A. MESSIAH: Quantum Mechanics I, North Holland, Amsterdam, 1965, p. 218.
12. See N. ROSEN: Am. J. Phys., **32**, 377, 1964; and N. ROSEN: Am. J. Phys., **32**, 537, 1964.
13. See [12].
14. See [12].
15. See [12].
16. See for example E. MERZBACHER: Quantum Mechanics, John Wiley & Sons, New York—London 1962, p. 285; and K. R. SYMAN, Mechanics, Addison-Wesley, Reading, Mass. 1957, p. 244.

17. See [4] p. 206.
18. See G. Birkhoff and J. von Neumann, "The Logic of Quantum Mechanics", Ann. Math., **37,** 823, 1936.
19. See [18].
20. This relation between a and b is called a compatibility relation or commensurability relation. It has been investigated in detail by many authors. For the relevant references see J. M. Jauch's excellent book: Foundations of Quantum Mechanics, Addison-Wesley, London 1968.
21. See [20].
22. See [20].

О ПРИНЦИПЕ СООТВЕТСТВИЯ

Г. ФАИ

Р е з ю м е

Определяются некоторые трактовки возможных «соответствий» между квантовой и классической механиками и рассматриваются случаи, при которых они могут быть удовлетворены.

Acta Physica Academiae Scientiarum Hungaricae, Tomus 29 (2—3), pp. 182—192 (1970)

OPTICAL REFLECTION OF V_2O_5 SINGLE CRYSTALS

By

I. HEVESI and B. KARVALY

INSTITUTE OF EXPERIMENTAL PHYSICS, JÓZSEF ATTILA UNIVERSITY, SZEGED

(Received 1. X. 1969)

Reflection measurements were made on vanadium pentoxide single crystals of (010(orientation, in the wavelength region 380 nm to 800 nm. Optical constants were calculated on the basis of reflection spectra obtained with linearly polarized light in || and ⊥ positions of polarization (the electric vector **E** being parallel to the crystallographic axes *a* and *c*). The results confirmed the values of the refractive index obtained from our transmission measurements in the region of weak absorption (550 nm to 800 nm), as well as the conclusions concerning the shape of the absorption edge. On the other hand, the measurements gave numerical values of the refractive index at shorter wavelengths and allowed some conclusions to be drawn for regions of anomalous dispersion.

1. Introduction

Optical properties of V_2O_5 single crystals have been dealt with in our earlier papers [1—3]. The measurements described there were chiefly concerned with the shape of the fundamental absorption edge (in the spectral range from ~500 nm to 550 nm) and with the determination of the optical constants (refractive index and absorption index) in the region of weak absorption (~550 nm to 800 nm), based upon measurement of the transmission of very thin split crystal plates. Measurements of diffuse reflectance confirmed information about the position of the absorption edge and about the band gap width [4]. The measurements of regular reflectivity described in the present paper support the results of the investigations mentioned above and provide further quantitative data on the refractive and absorption index in the region of shorter wavelengths.

Measurements concerning regular reflection on V_2O_5 single crystals have been published by KENNY, KANNEWURF and WHITMORE [5]. Their investigations were limited to the spectral region between 550 nm and 750 nm and their results, obtained with polarized light at normal incidence, show relatively great deviations. It may be due to this fact that they did not give refractive indices based on their measurements of reflectivity.

Our present investigations extended the reflection measurements towards shorter wavelengths down to 380 nm, thus including the spectral region of the fundamental absorption edge. On the other hand, the greater accuracy

of the measurements allowed the refractive indices to be determined in the neighbourhood of the fundamental absorption edge and made it possible to study the dependence of the reflectivity on the angle of polarization. Furthermore, combination of our reflection measurements with earlier data on transmission enabled us to calculate absorption coefficients down to 450 nm.

2. Measurement of reflection

Reflection measurements were performed on crystal plates of (010) orientation, 2 to 3 nm thick and of 1—2 cm^2 surface area, prepared as described in [1]. Reflection spectra were measured in two specific positions of the crystal plate, the electric vector **E** of the linearly polarized light incident perpendicularly on the sample being parallel to the crystallographical *c* axis or parallel to the *a* axis, i.e. normal to the *c* axis (designed as positions $\parallel$ and $\perp$, respectively). In the spectral range of our investigations, the crystal plates were non-transparent, and presented an optically perfect surface; thus the reflection could be considered as originating totally from the front surface of the crystal plate. It should be remarked here that the authors of [5] used thinner crystals, which allowed reflection and transmission measurements to be made with the same crystal. It can be supposed that the deviations in their results may be ascribed partly to interference effects in crystals of that thickness (to be dealt with in a further paper).

2.1. Apparatus for reflection measurements

A diagram of the apparatus used in our measurements is shown in Fig. 1. The auto-collimating plane grating monochromator of a single beam spectrophotometer, Type OPTICA MILANO CF4, was used as monochromator (M), a Hilger polarizing filter (PF) being placed between its exit slit and the reflection attachment. The polarizing filter could be adjusted with a precision of 1°, by means of a scale on its mounting. The double prism (DP I and II) consisted of two right-angle isosceles triangles of different size, each of which could be adjusted and fixed in the desired position around an axis perpendicular to the plane of Fig. 2. The light beam issuing from the monochromator (solid line), after passing the polarizing filter and the double prism, impinged on the sample (S) or on the reference standard brought into the light path (the latter, not shown in the figure, consisted of an electrolytically precipitated gold mirror), then, after reflection, the light beam (broken line) was projected by the prism II to the photomultiplier (PH), EMI Type 9558 A. The intensity of the photocurrent was measured with a ZEISS "Skalen-Galvanometer" having a sensitivity of $4 \cdot 10^{-10}$ Amp. per scale division.

2.2. Principle of measurement

In connection with the accuracy of the measurements with the double prism apparatus it had to be examined (a) to what extent perpendicular incidence can be obtained by the double prism attachment, taking into account the dispersion by the material of the prisms, and (b) whether the measured quotient of the light fluxes reflected from the sample and from the gold reference standard is in accordance with, or deviates only negligibly from, the true relative reflectivity of the sample compared with the reflectivity of a gold mirror.

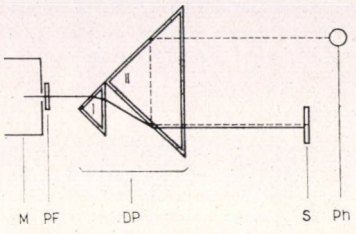


Fig. 1. Diagram of the apparatus for reflection measurements

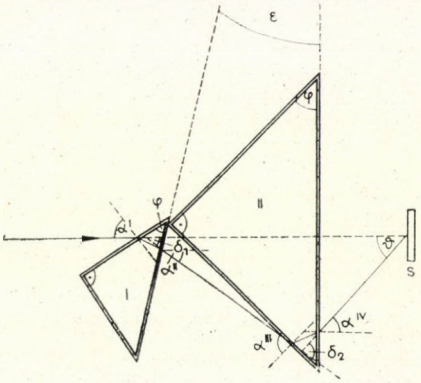


Fig. 2

Let us suppose that the base of prism II is parallel with the surface of the sample and that of the reference standard on which measurements are made and that both surfaces are perpendicular to the light beam issuing from the monochromator. Then, as can be seen from Fig. 2, the following relations will hold

$$\begin{aligned} \delta_1 &= \alpha^{\mathrm{I}} + \alpha^{\mathrm{II}} - \varphi \,, \\ \delta_2 &= \alpha^{\mathrm{III}} + \alpha^{\mathrm{IV}} - \varphi \,, \\ \delta_2 &= \delta_1 + \vartheta \,. \end{aligned} \tag{1}$$

As is easily seen, the angle ϑ enclosed by the surface normal and the light beam incident on the sample (for the sake of clearness the light paths are drawn considerably distorted in the Figure) can be made sufficiently small by suitably changing the value of $\delta_2 - \delta_1$ i.e. the angle enclosed by the bases of prisms I and II. Thus, the requirement of normal incidence can be met. On the other hand, with respect to the relations (1) and Snell's law, elementary calculation leads to the relation

$$\frac{d\alpha^{\mathrm{I}}}{dn} = \frac{1}{\sqrt{2 - n^2}} \tag{2}$$

The change with wavelength of the refractive index n of the prisms being negligible in the spectral range considered, it results from (2) that the changes in ϑ (and, in consequence of the reversibility of the light beams, also in α^{I}) can also be neglected (e.g. for $n = 1.4$ the change in refractive index $dn = 0.01$ would result in a correction $d\alpha^{\mathrm{I}} = 0.05°$, which is considerably less than the error resulting from the divergence of the light beam).

As shown by the following considerations, the relative reflectivity of the sample can be determined by measuring the light flux reflected from the sample and from the reference standard. Let the light flux incident on the refracting surface of prism

II be designed by I_0, the external reflectivity of the refracting surfaces (1) and (2) (see Fig. 3) by r_1 and r_2, the internal reflectivity of these surfaces by r_1' and r_2', respectively. From the light flux $I_0(1-r_1)(1-r_2')$ incident on the sample, the fraction $RI_0(1-r_1)(1-r_2')$ will be reflected, whereas the fraction $RI_0(1-r_1)(1-r_2')^2(1-r_2)r_1^2$ reaches the photomultiplier. At the same time also the fraction $I_0(1-r_1)r_1'r_2'(1-r_2')$ of the light flux $I_0(1-r_1)r_2'$ reflected by the refracting surface (2) will contribute to the light flux incident on the photomultiplier, so that the response of the detector will be proportional to the light flux $I_R = I_0(1-r_1)\,1-r_2')\,r_1^2[(1-r_2')(1-r_2)R + r_2']$.

Thus, the quotient of the light fluxes reflected from the sample of reflectivity R and from the standard of reflectivity R_0 gives the measured relative reflectivity R_m. The relation between the latter and the true relative reflectivity R/R_0 can be expressed, with insignificant omissions, as follows:

$$R_m = \frac{R}{R_0} + \frac{r_2'}{(1-r_2)(1-r_2')R_0}\,\frac{R_0-R}{R_0}\,. \tag{3}$$

In our case, $r_2 = r_2'$ (the incidence of the light emerging from the prism and of that coming from the sample being perpendicular with very good approximation) and, with $n = 1.4$, $r_2 = 0.028$, i.e.

$$R_m = \frac{R}{R_0} + 0{,}03\,\frac{R_0-R}{R_0^2}\,,$$

it can be seen that the resulting error of the measurements is not more than $\sim 1\%$ even in the worst case (when $R_0 - R$ is relatively great).

3. Results and discussion

In Fig. 4 the reflection spectra $R(\lambda)$ determined for $\parallel$ and $\perp$ polarizations are represented by open and filled circles, respectively. It can be seen from both well-separated curves that whereas the reflectivity shows a slow increase in the range of weak absorption (550 nm to 800 nm), a remarkable increase is to be observed in the range of fundamental absorption (below 550 nm), each curve presenting two maxima, not far from each other. The maxima for $\parallel$ polarization are to be found at about 430 nm and 495 nm, the value of the latter being higher; for $\perp$ polarization the maxima are situated at about 435 nm and 480 nm, but here the maximum at the shorter wavelength is higher. For comparison, Fig. 4 also contains the reflection coefficients calculated from the refractive indices given in [1] for $\parallel$ and $\perp$ polarizations (open and filled triangles, respectively). The agreement between the measured values and those calculated from the refractive index is very good.

The dependence of reflectivity on the angle of polarization is shown in Fig. 5 (solid line). The points for $\alpha = 0°$ and $\alpha = 90°$, both marked with filled circles, represent the values or $\parallel$ and $\perp$ polarizations, respectively. The curves measured at different wavelengths are similar to each other and to the curves showing the dependence of the transmission $T(\alpha)$ on the angle of polarization (3). Similarly as the curves for $T(\alpha)$, those for $R(\alpha)$ can be well approximated with a curve calculated from the formula

$$R(\alpha) = R^{\perp} + (R^{\parallel} - R^{\perp})\cos^2\alpha\,, \tag{4}$$

(where $R^{\parallel}$ and $R^{\perp}$ mean the reflectivity 0° anat $\alpha = \mathrm{d}\,\alpha = 90°$). The values of $R(\alpha)$ calculated from Eq. (4) at intervals of 10 degrees (marked with open triangles) are fitted by a curve (broken line) in Fig. 5. Most of the systematical deviations between the curves and points of measurement may be due to errors of some degrees in adjusting the $\parallel$ and $\perp$ positions of polarization. This is sup-

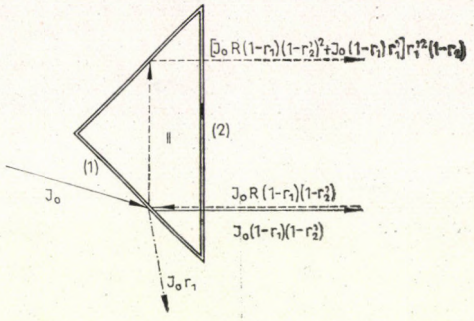


Fig. 3

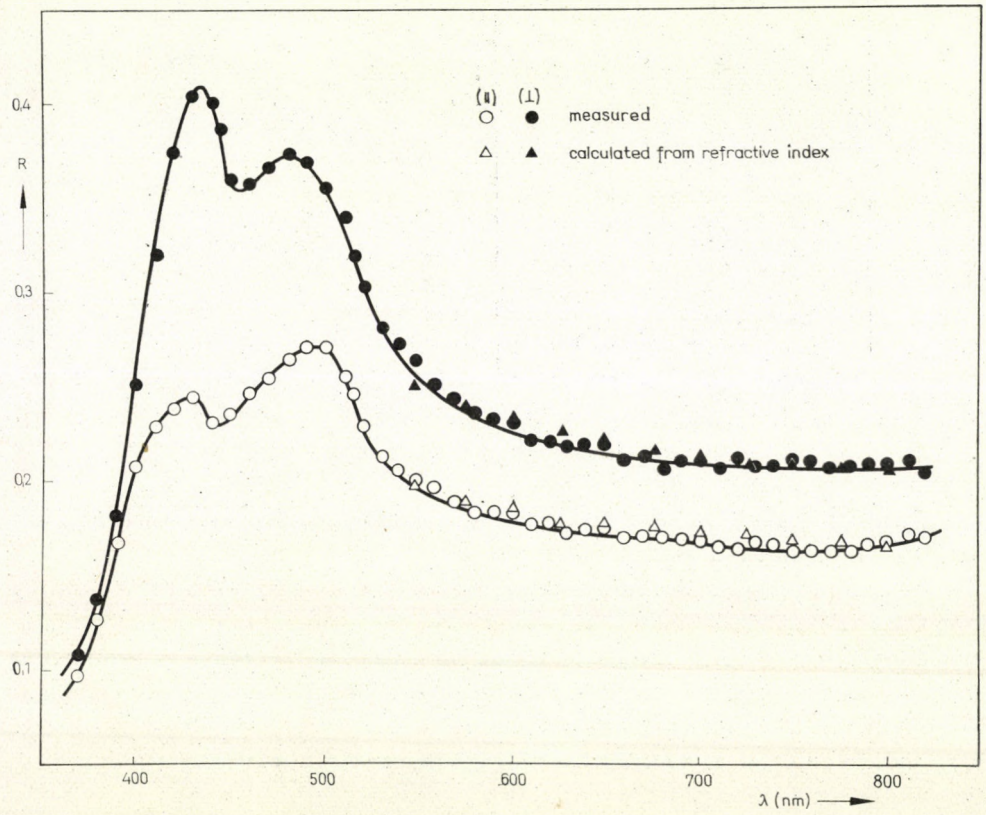


Fig. 4. Refraction spectra of V_2O_5 single crystals for $\parallel$ and $\perp$ polarization, calculated from refractive index (see [1]) and measured

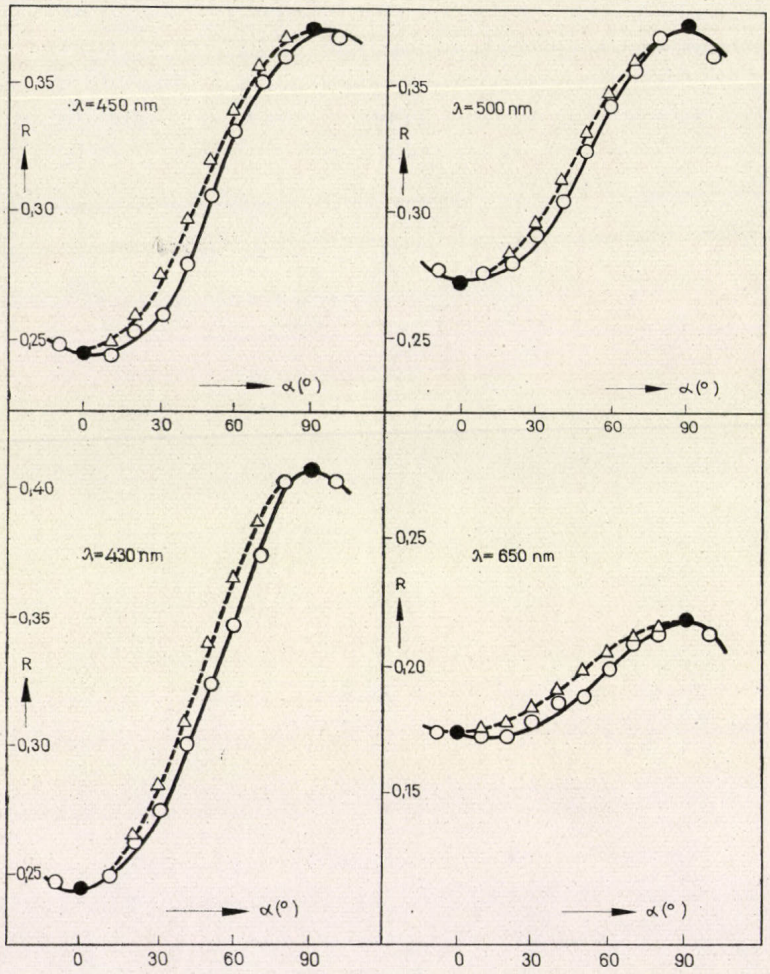


Fig. 5. Dependence of reflectivity of V_2O_5 single crystals on angle of polarization at different wavelengths (○ measured, △ calculated)

ported by the fact that the calculated curves can be well fitted to the points of measurement by a shift of about 5 degrees.

From the reflection curves $R(\lambda)$ the refractive index n and absorption index k were calculated in the wavelength region between 450 nm and 800 nm; for shorter wavelengths (down to about 380 nm), in the range of anomalous dispersion, an estimate for the probable course of the curves $n(\lambda)$ and $k(\lambda)$ is given from the analysis of the curves $R(\lambda)$.

The values of the refractive index calculated from the relation

$$R = \frac{(n-1)^2 + k^2}{(n+1)^2 + k^2} \tag{5}$$

for weak absorption (neglecting k) are plotted in Fig. 6 for both polarizations (open and filled triangles, respectively). Combining the above reflection measurements with earlier transmission measurements, it can be shown on the basis of the relation

$$T_a = \frac{(1-R)^2 e^{-Kd}}{1-R^2 e^{-2Kd}}, \tag{6}$$

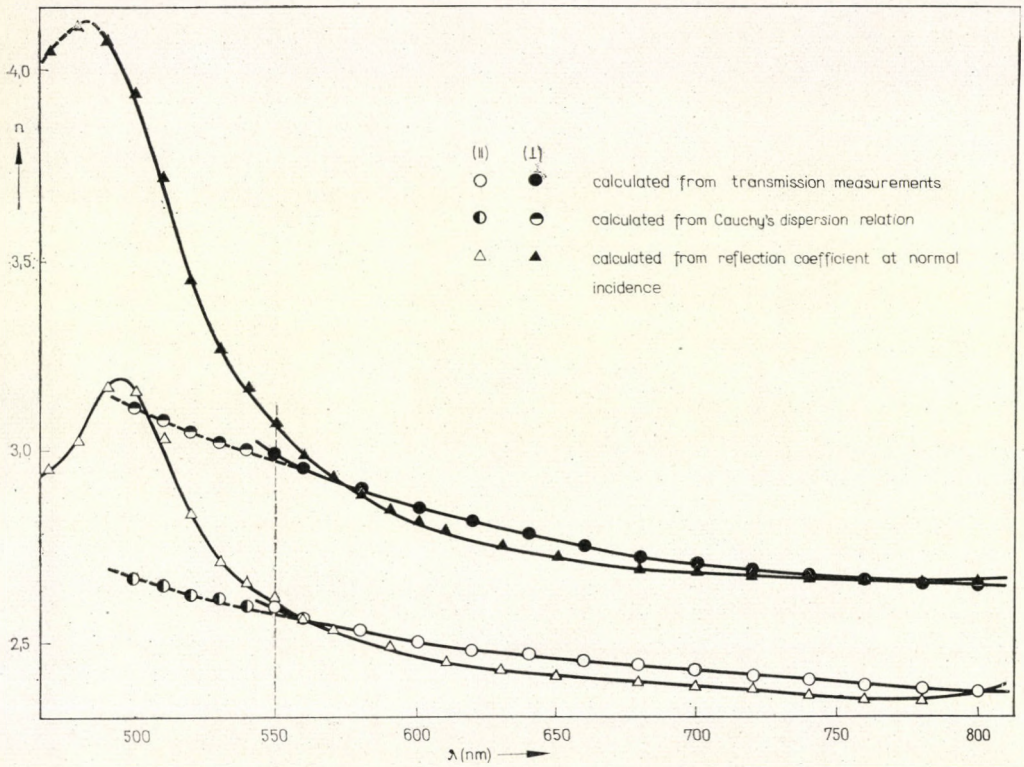


Fig. 6. Refractive indices of V_2O_5 single crystals for || and ⊥ polarization

(where T_a means the mean transmission, d the thickness of the crystal plate and K the absorption coefficient) that k^2 in Eq. (5) can be neglected up to 450 nm for || polarization and up to 480 nm for ⊥ polarization. The values of the refractive index at different wavelengths for both polarizations, calculated in this way, can be compared with the values obtained earlier [1] on the basis of the interference structure of the transmission curves for thin crystal plates, (see the Table and Fig. 6). The Table also contains the values of the refractive index at 670.8 nm (Li) and at 589.3 nm (Na) taken from [6] and [7]. It can be seen from the Table that the greatest deviation does not exceed 4%. The steep increase of the $n(\lambda)$ curves at wavelengths below 550 nm indicates that

the regularity of normal dispersion to be found at greater wavelengths is altered in this region. The curves $n(\lambda)$ calculated from Cauchy's dispersion relation

$$n = A + B/\lambda^2 \tag{7}$$

for the wavelength region 500 nm to 550 nm are also shown in Fig. 6. The constants A and B were determined as mean values calculated for 10 correlated values of n and λ, taken from our earlier $n(\lambda)$ curves for $\parallel$ and $\perp$ polarizations (1).

Table I

Refractive indices of V_2O_5 single crystals for $\parallel$ and $\perp$ polarization ($n^{\parallel}$ and $n^{\perp}$, respectively)

(nm)	Calculated from transmission measurements of HEVESI [1]		Calculated from reflection measurements (present work)		Data of KING and SUBER [7]		Data of Глазырин and Фотиев [6]	
	$n^{\parallel}$	$n^{\perp}$	$n^{\parallel}$	$n^{\perp}$	$n^{\parallel}$	$n^{\perp}$	$n^{\parallel}$	$n^{\perp}$
800	2.37	2.65	2.37	2.67				
750	2.39	2.67	2.35	2.66				
700	2.43	2.71	2.38	2.68				
670.8	2.44	2.73	2.40	2.70	2.45	2.70		
650	2.45	2.77	2.41	2.72				
589.3	2.51	2.88	2.48	2.84	2.55	2.89	2.53	2.84
560	2.56	2.96	2.56	2.98				
550	2.59	2.99	2.61	3.06				
540			2.65	3.16				
530			2.71	3.26				
520			2.82	3.45				
510			3.03	3.72				
500			3.15	3.94				
490			3.16	4.07				
480			3.11					
470			3.02					
460			2.95					
450			2.85					

As can be seen from the Figure, the curves calculated from reflection measurements fit well with those calculated from Cauchy's formula in the region above 550 nm. It should be remarked that KENNY, KANNEWURF and WHITEMORE [5], in their calculations, used values of R extrapolated on the basis of Cauchy's formula for reflection for wavelengths less than 550 nm. This does not seem to be justified according to our above results; it did not,

however, cause essential deviations in the value of k, as the errors in R or n due to uncertainties in k are of secondary importance for high values of k.

As mentioned above, by combining the results of reflection measurements with our earlier data about transmission, it was possible to extend the calculation of absorption indices with Eq. (6) to shorter wavelengths than before [3]. The results obtained for the dependence of k on photon energy, in accordance with earlier suggestions, support the finding that, proceeding towards higher energies, the shape of the absorption edge follows the course corresponding to the mechanism of direct-forbidden band-band transition, whereas at lower energies it obeys Urbach's rule.

On the basis of our reflection measurements, it seems possible to make reasonable suppositions about the course of the curves $n(\lambda)$ and $k(\lambda)$ at wavelengths shorter than 450 nm and 480 nm for $\parallel$ and $\perp$ polarizations, respectively, and their influence on reflection spectra. It immediately follows from our experiments that the curve $n(\lambda)$ for $\parallel$ polarization shows a maximum near 490 nm, where also the reflection curve has its long wave maximum (see Fig. 6 and Table). A similar situation seems to be probable at $\perp$ polarization, though it was not possible to calculate the refractive index for this case down to the same wavelengths as for $\parallel$ polarization.

The maxima of the $n(\lambda)$ curves and the decreasing tendency of the curves in the region of higher energies suggest the appearance of anomalous dispersion in this region. With increasing absorption the weight of the effect of the decreasing refractive index on reflection also decreases, whereas the still increasing absorption index begins to have a determining effect. Qualitative considerations suggest that the minima of the reflection curves and the subsequent maxima at shorter wavelengths may also be interpreted with the above suppositions. The steep decrease in the reflection curves around 400 nm could be attributed to a decrease in the absorption index and to the role of the refractive index, which here again begins to become dominant.

The above suggestions concerning the course of $n(\lambda)$ and $k(\lambda)$ need further corroboration which can be expected from reflection and transmission measurements in the region of higher photon energies and from a determination of the optical constants n and k by means of a Kramers—Kronig analysis. An account of investigations in this field will be given later.

The authors are indebted to the late Prof. A. Budó, Director of the Institute, for his interest in these investigations.

REFERENCES

1. I. Hevesi, Acta Phys. Hung., **23,** 75, 1967.
2. Z. Bodó and I. Hevesi, phys. stat. sol., **20,** K45, 1967.
3. I. Hevesi, Acta Phys. Hung., **23,** 415, 1967.
4. I. Hevesi, Acta Phys. et Chem. Szeged, **13,** 39, 1967.

5. N. Kenny, C. R. Kannewurf and D. H. Whitemore, J. Phys. Chem. Solids, **27**, 1237, 1966.
6. М. П. Глазырин и А. А. Фотиев, Кристаллография, **9**, 506, 1964.
7. B. W. King and L. L. Suber, J. Am. Ceram. Soc., **38**, 306, 1955.

ОПТИЧЕСКОЕ ОТРАЖЕНИЕ МОНОКРИСТАЛЛОВ V_2O_5

И. ХЕВЕШИ и Б. КАРВАЛЬ

Р е з ю м е

Проводились измерения отражения монокристаллов пятиокиси ванадия ориентированных по (010) в интервале длин волн от 380 нм до 800 нм. Из спектров отражения, полученных линейно поляризованным светом с $\parallel$ и $\perp$ поляризациями (электрический вектор E параллелен к кристаллографическим осям a и c соответственно), вычислялись оптические постоянные. Результаты подтверждают значения коэффициента преломления, полученные из наших трансмиссионных измерений в области слабой поглощеиии (550 нм—800 нм), а также выводы касающиеся формы края поглощении. С другой стороны, измерены значения коэффициента преломления при более коротких длинах волн и поэтому стало возможным сделать некоторые выводы об областях аномальной дисперсии.

Acta Physica Academiae Scientiarum Hungaricae, Tomus 29 (2—3), pp. 193—202 (1970)

COLLECTIVE VIBRATIONS OF THE STATISTICAL NUCLEAR MODEL

By

E. BALÁZS

RESEARCH GROUP FOR THEORETICAL PHYSICS
OF THE HUNGARIAN ACADEMY OF SCIENCES, BUDAPEST

(Received 3. X. 1969)

The collective vibrations of ^{90}Zr are calculated by applying the statistical nuclear model and the Bloch—Jensen theory. The results allow us to give a theoretical interpretation of the experimentally observed resonances in the quasi-elastic photon scattering on ^{90}Zr.

1. Introduction

The application of the statistical (or Thomas—Fermi) method for nuclei was first proposed by GOMBÁS [1]. The basic idea is the following: the nucleus is divided into volume elements and we assume that each volume element dv can be treated as a piece of nuclear matter. The energy $U(\varrho_n, \varrho_p)\, dv$ is associated with the volume element dv where $U(\varrho_n, \varrho_p)$ is the energy per unit volume as a function of the neutron and proton densities in nuclear matter. This function contains the Fermi kinetic energy and the interaction energy of the nucleons.

Several methods have been developed for studying nuclear matter. The simplest is to construct a phenomenological expression for $U(\varrho_n, \varrho_p)$ as has been done by SKYRME [2], and BERG and WILETS [3].

GOMBÁS [1] used a pure exchange effective interaction between the nucleons,

$$V_{\text{eff}} = J(r)\left[-\frac{1}{3} + \frac{2}{3}P^{\sigma} - \frac{2}{3}P^{\tau} - \frac{4}{3}P^{\sigma}P^{\tau}\right], \tag{1.1}$$

and thus achieved saturation automatically. In his work specific analytic forms for $J(r)$ were chosen, and it was shown that the best fit to the experimental data of nuclei could be achieved by using Gaussian type radial part [4]:

$$J(r) = -\gamma e^{-(r/r_0)^2}, \tag{1.2}$$

where

$$r_0 = \frac{\hbar}{M_\pi C} = 1{,}355\ \text{F}, \gamma = 98{,}45\ \text{MeV}. \tag{1.3}$$

Using this phenomenological effective interaction an analytic expression can be derived for the energy density $U(\varrho_n, \varrho_p)$. (See Eq. (84) of [1].)

In recent years the theory of nuclear matter has made great progress. The BRUECKNER—GOLDSTONE method [5] describes the strong correlation between two nucleons at short distances. Binding energy and density have been calculated in fair agreement with experiment by SPRUNG and BHARGAVA [6]. Using these results BETHE [7] developed a statistical theory for finite nuclei. This work is based on realistic nuclear forces and the energy expression is derived from first principles without using any phenomenological procedure.

All the above theories are concerned with the static equilibrium state of nuclei. In this paper we generalize the statistical model to non-equilibrium states and determine the collective vibrations of spherical nuclei. In Section 2 we give the hydrodynamic equations of motion of nuclear matter. This hydrodynamic description was first used by BLOCH and JENSEN [8] for an electron gas. A similar calculation was carried out by KISDI [9] for nuclear matter but his work is restricted to the case when neutrons and protons move together. Our description does not contain this restriction so that our hydrodynamic equations of motion correspond to a two-component fluid in which the neutrons and protons move independently.

In Section 3 a hydrodynamic description is applied to the determination of collective vibrational modes of small amplitudes. The modes in which neutrons move against protons have particular interest, because these modes can be considered as the giant dipole resonances of nuclei [10].

In Section 4 the collective vibrations of GOMBÁS's statistical model of ^{90}Zr are treated and the results are discussed in Section 5.

2. Hydrodynamic equations of motion of nuclear matter

In the hydrodynamic description of nuclear matter the density distributions

$$\varrho_n(r, t) \text{ and } \varrho_p(r, t) \tag{2.1}$$

and velocity distributions

$$v_n(r, t) \text{ and } v_p(r, t) \tag{2.2}$$

characterize its state. We assume that the velocities can be derived from velocity potentials as follows

$$v_n = \operatorname{grad} w_n(r, t) \text{ and } v_p = \operatorname{grad} w_p(r, t) . \tag{2.3}$$

The task of the hydrodynamic treatment of nuclear matter is to determine the densities and velocity potentials as functions of space and time. The equations of motion are derived from the variational principle

$$\delta \int_{t_0}^{t} L dt = 0 , \tag{2.4}$$

where L is the Lagrangian of nuclear matter composed of neutrons and protons:

$$\begin{aligned} L = & M \int \varrho_n \left\{ \frac{\partial w_n}{\partial t} + \frac{1}{2} (\operatorname{grad} w_n)^2 \right\} dw + \\ & + M \int \varrho_p \left\{ \frac{\partial w_p}{\partial t} + \frac{1}{2} (\operatorname{grad} w_p)^2 \right\} dw + \\ & + \int U(\varrho_n, \varrho_p) \, dw + \frac{e^2}{2} \int \varrho_p \varphi_p \, dv . \end{aligned} \tag{2.5}$$

Here M denotes the nucleon mass and φ_p is the Coulomb potential of proton density distribution,

$$\varphi_p(r, t) = \int \frac{\varrho_p(r', t)}{|r - r'|} dr' . \tag{2.6}$$

The above expression for L is the generalization of Bloch—Jensen's Lagrangian for nuclear matter.

The equations of motion can be obtained by varying L with respect to the densities and velocity potentials. The variation of the densities gives the following equations of motion

$$\begin{aligned} & M \left\{ \frac{\partial w_n}{\partial t} + \frac{1}{2} (\operatorname{grad} w_n)^2 \right\} + \frac{\partial u}{\partial \varrho_n} = 0 , \\ & M \left\{ \frac{\partial w_p}{\partial t} + \frac{1}{2} (\operatorname{grad} w_p)^2 \right\} + \frac{\partial u}{\partial \varrho_p} + e^2 \varphi_p = 0 , \end{aligned} \tag{2.7}$$

and the variation of L with respect to the velocity potentials results in the well-known continuity equations

$$\begin{aligned} & \frac{\partial \varrho_n}{\partial t} + \operatorname{div} (\varrho_n \operatorname{grad} w_n) = 0 , \\ & \frac{\partial \varrho_p}{\partial t} + \operatorname{div} (\varrho_p \operatorname{grad} w_p) = 0 . \end{aligned} \tag{2.8}$$

3. The static equilibrium state and the vibrational modes

The static equilibrium state is characterized by time-independent density distributions

$$\varrho_n(r) \text{ and } \varrho_p(r) \tag{3.1}$$

and by vanishing velocities, i.e. by space-independent velocity potentials,

$$w_n(t) \text{ and } w_p(t). \tag{3.2}$$

Substituting Eqs. (3.1) and (3.2) into the equations of motion it can be seen that the continuity equations (2.8) are satisfied identically and (2.7) gives

$$\begin{aligned} -M\frac{dw_n}{dt} &= \frac{\partial U}{\partial \varrho_n}, \\ -M\frac{dw_p}{dt} &= \frac{\partial U}{\partial \varrho_p} + e^2\varphi_p. \end{aligned} \tag{3.3}$$

Since the left sides of Eqs. (3.3) depend only on t, and the right sides depend only on r, both sides must be equal constants called ε_n and ε_p, respectively. Thus (3.3) shows that the velocity potentials depend linearly on t,

$$\begin{aligned} w_n(t) &= w_{n0} - \frac{\varepsilon_n}{M}t, \\ w_p(t) &= w_{p0} - \frac{\varepsilon_p}{M}t, \end{aligned} \tag{3.4}$$

and the densities have to satisfy the following equations

$$\begin{aligned} \frac{\partial U}{\partial \varrho_n} - \varepsilon_n &= 0, \\ \frac{\partial U}{\partial \varrho_p} + e^2\varphi_p - \varepsilon_p &= 0. \end{aligned} \tag{3.5}$$

The density equations (3.5) are the Thomas—Fermi equations for nuclei. It can be easily seen that these equations can be derived from the minimum principle of nuclear energy

$$E = \int U(\varrho_n, \varrho_p)\, dv + \frac{e^2}{2}\int \varphi_p \varrho_p\, dv = \min \tag{3.6}$$

with the restrictions

$$\int \varrho_n \, dw = N, \quad \int \varrho_p \, dv = Z. \tag{3.7}$$

Instead of solving the Thomas—Fermi equations (3.5) we determine the densities from (3.6) and (3.7) by using Ritz's variational method. In first approximation the nucleus is considered to be of homogeneous density distributions, i.e.:

$$\begin{aligned} &\varrho_n(r) = \frac{3N}{4\pi R^2}, \quad \varrho_p(r) = \frac{3Z}{4\pi R^3} \quad \text{if} \quad r < R, \\ &\varrho_n(r) = 0, \qquad \varrho_p(r) = 0 \qquad \text{if} \quad r > R, \end{aligned} \tag{3.8}$$

where R is the nuclear radius and is considered as a parameter of variation.

Now let us turn to the vibrational states of nuclei. The amplitudes of vibrations are assumed to be small quantities. Therefore,

$$\varrho_n = \varrho_{n0} + \eta_n, \quad \varrho_p = \varrho_{p0} + \eta_p, \quad \varphi_p = \varphi_{p0} + \psi_p \tag{3.9}$$

can be written, where ϱ_{n0}, ϱ_{p0} and φ_{p0} are the densities and the Coulomb potential in the static equilibrium and η_n, η_p, ψ_p are small perturbations. Of course η_p and ψ_p are connected by the relation

$$\psi_p(r) = \int \frac{\eta_p(r')}{|r - r'|} \, dv'. \tag{3.10}$$

Putting (3.9) into the equations of motion (2.7) we get in first order

$$\begin{aligned} &M \frac{\partial w_n}{\partial t} + \left(\frac{\partial^2 U}{\partial \varrho_n^2} \right)_0 \eta_n + \left(\frac{\partial^2 U}{\partial \varrho_n \, \partial \varrho_p} \right)_0 \eta_p = 0, \\ &M \frac{\partial w_p}{\partial t} + \left(\frac{\partial^2 U}{\partial \varrho_n \partial \varrho_p} \right)_0 \eta_n + \left(\frac{\partial^2 U}{\partial \varrho_p^2} \right) \eta_p + e^2 \psi_p = 0. \end{aligned} \tag{3.11}$$

Here the index 0 refers to the static equilibrium case and all the terms containing higher powers or products of η_n, η_p, ψ_p, w_n and v_p are neglected.

Substituting (3.9) into the continuity equations (2.8) and assuming the equilibrium densities to be constant as in (3.8) we get

$$\begin{aligned} &\frac{\partial \eta_n}{\partial t} + \varrho_{n0} \, \Delta w_n = 0, \\ &\frac{\partial \eta_p}{\partial t} + \varrho_{p0} \, \Delta w_p = 0, \end{aligned} \tag{3.12}$$

where the equilibrium densities are given by

$$\varrho_{n0} = \frac{3N}{4\pi R^3}, \quad \varrho_{p0} = \frac{3Z}{4\pi R^3} \tag{3.13}$$

and R corresponds to the minimum of the energy E.

The elimination of the velocity potentials w_p and w_n from Eqs. (3.11) and (3.12) yields

$$\begin{aligned} &\frac{\partial^2 \eta_n}{\partial t^2} - \lambda_{nn} \Delta\eta_n - \lambda_{np} \Delta\eta_p = 0, \\ &\frac{\partial^2 \eta_p}{\partial t^2} - \lambda_{pn} \Delta\eta_n - \lambda_{pp} \Delta\eta_p + \omega_c^2 \eta_p = 0, \end{aligned} \tag{3.14}$$

where the constants λ_{nn}, λ_{np}, λ_{pn}, λ_{pp} and ω_c^2 denote the following quantities

$$\begin{aligned} &\omega_c^2 = 4\pi e^2 \varrho_{p0}/M, \\ &\lambda_{nn} = \frac{\varrho_{n0}}{M}\left(\frac{\partial^2 U}{\partial \varrho_n^2}\right)_0, \quad \lambda_{np} = \frac{\varrho_{n0}}{M}\left(\frac{\partial^2 U}{\partial \varrho_n \partial \varrho_p}\right)_0, \\ &\lambda_{pn} = \frac{\varrho_{p0}}{M}\left(\frac{\partial^2 U}{\partial \varrho_n \partial \varrho_p}\right)_0, \quad \lambda_{pp} = \frac{\varrho_{p0}}{M}\left(\frac{\partial^2 U}{\partial \varrho_p^2}\right)_0 \end{aligned} \tag{3.15}$$

and the Poisson equation $\Delta\psi_p = -4\pi\eta_p$ has been used.

We look for the solution of Eqs. (3.14) by substituting

$$\begin{aligned} \eta_n &= A_n y(r)\, Y_{lm}(\vartheta, \varphi)\, e^{i\omega t}, \\ \eta_p &= A_p y(r)\, Y_{lm}(\vartheta, \varphi)\, e^{i\omega t}, \end{aligned} \tag{3.16}$$

where A_n and A_p are constant amplitudes and Y_{lm} is the well-known spherical harmonics.

Putting (3.16) into (3.14) we get

$$\begin{aligned} &\omega^2 A_n y(r) + (\lambda_{nn} A_n + \lambda_{np} A_p)\left(y''(r) + \frac{2}{r} y'(r) - \frac{l(l+1)}{r^2} y(r)\right) = 0, \\ &(\omega^2 - \omega_c^2) A_p y(r) + (\lambda_{pn} A_n + \lambda_{pp} A_p)\left(y''(r) + \frac{2}{r} y'(r) - \frac{l(l+1)}{r^2} y(r)\right) = 0. \end{aligned} \tag{3.17}$$

These equations are satisfied only if

$$y''(r) + \frac{2}{r} y'(r) - \frac{l(l+1)}{r^2} y(r) = -\alpha^2 y(r) \tag{3.18}$$

and

$$\left(\lambda_{nn} - \frac{\omega^2}{\alpha^2}\right) A_n + \lambda_{np} A_p = 0,$$
$$\lambda_{pn} A_n + \left(\lambda_{pp} - \frac{\omega^2 - \omega_c^2}{\alpha^2}\right) A_p = 0. \tag{3.19}$$

In order to solve (3.18) the dimensionless variable $x = \alpha r$ is introduced. Hence (3.18) is transformed to the form

$$\frac{d^2y}{dx^2} + \frac{2}{x}\frac{dy}{dx} + \left(1 - \frac{l(l+1)}{x^2}\right) y = 0. \tag{3.20}$$

Its solution has the form

$$y = \frac{C}{\sqrt{x}} J_{l+1/2}(x), \tag{3.21}$$

where $J_{l+1/2}(x)$ denotes the ordinary Bessel function and C is an arbitrary constant.

The deformation of the nuclear surface can be neglected because of the large surface tension, hence the radial velocities on the surface can be taken to zero:

$$\left(\frac{\partial w_n}{\partial r}\right)_{r=R} = \left(\frac{\partial w_p}{\partial r}\right)_{r=R} = 0, \tag{3.22}$$

where R is the nuclear radius in the equilibrium state.

Differentiating (3.11) with respect to r and putting $r = R$ we are led to the following boundary conditions:

$$\left(\frac{\partial \eta_n}{\partial r}\right)_{r=R} = \left(\frac{\partial \eta_p}{\partial r}\right)_{r=R} = 0. \tag{3.23}$$

With these conditions the relation

$$lJ_{l+1/2}(x_l) - x_l J_{l+3/2}(x_l) = \tag{3.24}$$

is obtained, where $x_l = \alpha R$.

For each l Eq. (3.24) has a set of roots. The smallest positive roots of (3.24) are given in Table I. Using these values we can calculate the parameter α for different modes by the relation.

$$\alpha = \frac{x_l}{R}. \tag{3.25}$$

Table I

l	0	1	2
x_l	4.49	2.08	3.34

Now we turn to the system of equations (3.19). This is a homogeneous algebraic system for A_n and A_p. This can be solved only if the determinant of the system equals zero, i.e.:

$$\left(\lambda_{nn} - \frac{\omega^2}{\alpha^2}\right)\left(\lambda_{pp} - \frac{\omega^2 - \omega_c^2}{\alpha^2}\right) - \lambda_{np}\lambda_{pn} = 0. \tag{3.26}$$

From Eq. (3.26) the values of ω, i.e. the different energies $\hbar\omega$ of different modes of vibrations can be calculated. The ratios of amplitudes A_n and A_p can be obtained from (3.19). A little consideration shows that for a given value of α, (3.26) has two positive roots, i.e. two real values of ω are obtained.

4. Collective vibrations of Gombás's model

As an illustrative example let us consider the vibrations of GOMBÁS's model. First the static equilibrium state with homogeneous density distributions is determined. The nuclear binding energy can be obtained by multiplying the energy density (86) of [1] by the volume of the nucleus.

$$\begin{aligned} E(R) = {} & 28{,}86\, A^{5/3}\left(1 + \frac{5}{9}n^2\right)\frac{1}{R^2} + 0{,}8639\,\frac{A^2}{4}(1-n^2)\frac{1}{R} - \\ & + 1{,}579\, R^3\left[6\sqrt{\pi}\,\omega^3\,\Phi(\omega) + (6\omega^2 - 12)\,e^{-\omega^2} - 18\,\omega^2 + 12 + \right. \\ & \left. + \frac{1}{3}n^2\left\{6\,\omega^2 - 4\,\omega^4 - e^{-\omega^2}(2\omega^4 + 6\omega^2)\right\}\right]. \end{aligned} \tag{4.1}$$

Here A is the mass number, $n = (N - Z)/A$ is the relative neutron excess and ω denotes the following quantity

$$\omega = 1{,}355\left(\frac{9\pi A}{8}\right)^{1/3}\frac{1}{R}. \tag{4.2}$$

In (4.1) and (4.2) the nuclear radius is measured in 1 F $= 10^{-13}$ cm units and the energy is given in MeV. It should be mentioned that for the sake of simplicity GOMBÁS's energy density formula has been expanded in terms of the

relative neutron excess n and the expansion has been cut at terms containing n^2.

By varying R in (4.1) a minimum for E can be obtained. This minimum value of E is the binding energy of the nucleus and the value of R related to this minimum is the nuclear radius in equilibrium state. In the case of ^{90}Zr the results are

$$E = -784.3 \text{ MeV}, \quad R = 4.322 \text{ F}. \tag{4.3}$$

The experimentally observed binding energy is $E = -784.292$ MeV [11]. The agreement between the two values is excellent.

In order to determine the collective vibrations first one has to calculate the characteristic constants (3.15) using the equilibrium parameters (4.3). Putting the numerical results into (3.19) and (3.26) the vibrational modes are obtained. The results are shown in Table II.

Table II

	0		1		2	
α^2	1.0793		0.23162		0.59723	
$\hbar\omega$	4.279	11.02	2.062	9.452	3.327	11.48
An/Ap	6.094	−0.1919	26.67	−0.04393	13.17	−0.08881

5. Discussion

The results in Table II clearly demonstrate that if all nucleons move together ($A_n/A_p > 0$), the energy of the vibration is significantly smaller than in the case when protons move against neutrons. This result is in good agreement with the statement of [10].

The quasi-elastic photon scattering measurements on ^{90}Zr [12] give well defined peaks at the energies 9.1 MeV, 10.4 MeV, 11.5 MeV. The agreement between our results and those measured experimentally suggests that we can interpret the above mentioned peaks as different modes of vibrations of the nucleus calculated on the basis of the above model.

The author is highly indebted to Prof. Dr. P. Gombás for suggesting the problem and for his kind interest during the work.

REFERENCES

1. P. Gombás, Acta Phys. Hung., **1**, 329, 1952.
2. T. H. R. Skyrme, Phil. Mag., **1**, 1043, 1956.
3. R. A. Berg and L. Wilets, Phys. Rev., **101**, 201, 1956.
4. P. Gombás and D. Kisdi, Acta Phys. Hung., **17**, 261, 1964.

5. K. A. Brueckner and C. A. Levinson, Phys. Rev., **97**, 1344, 1955; K. A. Brueckner, Phys. Rev., **97**, 1353, 1955; J. Goldstone, Proc. Roy. Soc. (London), **A293**, 265, 1957.
6. P. N. Bhargava and D. W. L. Sprung, Ann. Phys. (N. Y.) **42**, 222, 1967.
7. H. A. Bethe, Phys. Rev., **167**, 879, 1968.
8. F. Bloch, Zs. für Phys., **81**, 363, 1935; H. Jensen, Zs. für Phys., **106**, 620, 1937; P. Gombás, Handb. d. Phys. 36, Springer Verlag, Berlin, Göttingen, Heidelberg, 1958.
9. D. Kisdi, Acta Phys. Hung., **8**, 387, 1958.
10. G. E. Brown, Collective Motion and the Application of Many Body Techniques, Proceedings of the International School of Physics "Enrico Fermi" XXIII, Varenna, Italy. Acad. Press, New York and London, 1963.
11. A. H. Wapstra, Handb. d. Phys. 38/1, Springer Verlag, Berlin, Göttingen, Heidelberg, 1958.
12. P. Axel et al., Phys. Rev. Letts., **10**, 299, 1963.

КОЛЛЕКТИВНЫЕ КОЛЕБАНИЯ В СТАТИСТИЧЕСКОЙ ЯДЕРНОЙ МОДЕЛИ

Э. БАЛАЖ

Р е з ю м е

Применением статистической ядерной модели и теории Блоха-Йенсена вычисляются коллективные колебания ^{90}Zr. Результаты позволяют дать теоретическую интерпретацию экспериментально наблюдаемых резонансов в квази-эластичном рассеянии фотонов на ^{90}Zr.

Acta Physica Academiae Scientiarum Hungaricae, Tomus 29 (2—3), pp. 203—220 (1970)

INVESTIGATIONS ON THE CONNECTIONS BETWEEN THE BULK ABSORPTION AND DIFFUSE REFLECTANCE SPECTRA OF POWDERED SOLIDS

Part II

By

B. KARVALY and F. PINTÉR

INSTITUTE OF EXPERIMENTAL PHYSICS, JÓZSEF ATTILA UNIVERSITY, SZEGED

(Received 8. X. 1969)

Comparative experimental investigations concerning the validity of the most important connections between absorption and diffuse reflectance spectra were made on two didymium glass powder samples of 7.3 and 12.2 μ particle size. According to our investigations, the best estimates of the true absorption coefficient of glass powders can be obtained on the basis of BODÓ's and ANTONOV-ROMANOVSKY's theories, whereas JOHNSON's and MELAMED's theories do not lead to satisfactory results for powder samples of the particle sizes used in our work. A qualitative interpretation of the divergences is attempted.

§ 1. Introduction

The laws of absorption and propagation of radiation in strongly scattering media, such as powders, both luminescent and non luminescent, suspensions, papers, textile materials, etc. are little known, except for some special cases. Therefore, only approximative data on the shape of the absorption band and the value of the absorption coefficient are available. In order to clarify these problems, which call for great attention both from the scientific and the industrial point of view, investigations have been made by various authors, without, however, leading to a satisfactory solution [1—7].

The aim of most researches was to give connections between the diffuse reflectance spectra and the true absorption spectra defined on the basis of the LAMBERT—BEER law. The results available in the literature show that, for the time being, the diffuse reflectance spectra are the most suitable basis for estimating the absorption spectra of powdered solids. In consideration of the relatively numerous theories elaborated [2—7], which are, however, founded on essentially different suppositions, it seemed justifiable to make comparative experimental investigations on the efficiency of some theories published in recent years. These investigations appeared all the more necessary as the various authors in their research work used samples of greatly different particle sizes varying from 5.5 μ to 650 μ, produced by different methods, and, therefore, their results are not suitable for a comparison of the theories with respect to validity and accuracy.

§ 2. Experimental methods and results

In our spectroscopical investigations on diffuse reflectance a selective didymium filter glass, ZEISS BG 35, rich in absorption bands in a relatively small spectral range, was used. The transmission spectrum of the carefully cleaned plane-parallel glass plate was measured with a recording spectrophotometer, OPTICA MILANO CF 4 DR. In the range between 400 nm and 620 nm a practically constant band width of 3.2 Å was secured with the use of an elliptical tungsten lamp (TUNGSRAM, 12 V, 100 W).

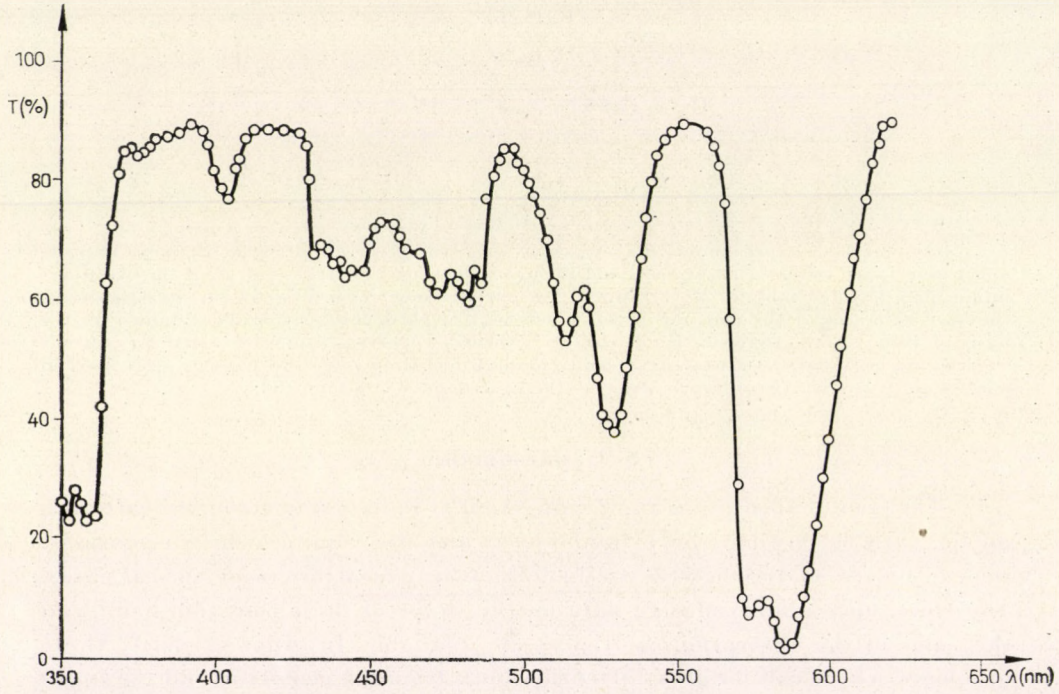


Fig. 1. Transmission spectrum of didymium glass (Zeiss BG 35)

The true absorption spectrum of the didymium glass has been calculated from the transmission spectrum (Fig. 1), taking into account the losses due to reflection, with the following relation

$$k(\lambda) = \frac{1}{d} \ln \frac{(1-r)^2}{\tau_m(\lambda)} . \tag{1}$$

In this expression $k(\lambda)$ is the true (bulk) absorption coefficient and $\tau_m(\lambda)$ the measured transmittance at wavelength λ, d the thickness of the plane-parallel glass plate, and the reflection coefficient r depends on the mean refractive index n as follows: $r = [(n-1)/(n+1)]^2$, where n can be considered as constant in the range of measurements (in our case $n = 1.55$). The maximal error of the true absorption coefficient calculated from Eq. (1) does not exceed ± 0.15 cm^{-1}, even in the worst case, and the relative error is not greater than 5%. The choice of the didymium glass permitted inferences in several relations to be drawn.

After the transmission measurements, glass powder fractions of 7.3 and 12.2 μ mean particle size (see Fig. 2) were prepared from the filter glass BG 35 by the method described in [8].

To measure the diffuse reflectance spectra, the spectrophotometer was provided with a double beam reflectance attachment containing an ULBRICHT sphere of 15 cm diameter.

The reference MgO standard sample consisted of a fresh MgO layer of 1 mm thickness, smoked on a 2 mm thick MgO layer bound with carboxy-methyl-cellulose [9]. The geometry of the reflectance attachment secured perpendicular incidence and diffuse observation. During the reflectance measurements the band width was practically identical with that mentioned in connection with the measurement of transmission spectra.

The absolute diffuse reflectance spectra of the didymium glass powder samples have been calculated with the reflectance data for MgO given by BENFORD, LLOYD and SCHWARZ [10]. The diffuse reflectance spectra obtained in this way are shown in Fig. 3.

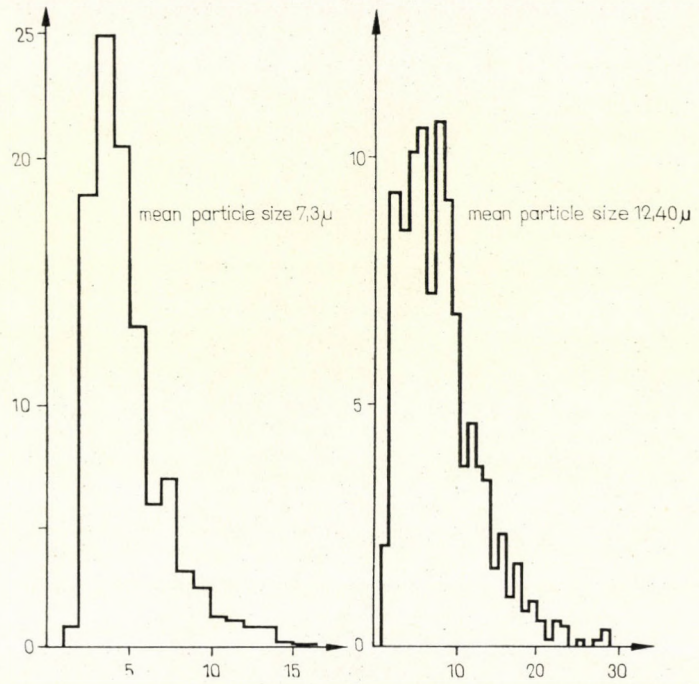


Fig. 2. Histograms of particle size of powdered didymium glass samples (1 scale division = 5/3 μ)

A crucial factor in the reflectance measurements is the accuracy of the diffuse reflectance of MgO. We have, however, to remember that the relevant data of different authors show differences of 1—2% [10—13], and, therefore, our results, similarly to those mentioned, imply an incertainty of this order.

On the basis of the diffuse reflectance spectra of the didymium glass powder samples it can be stated that the diffuse reflectance spectra show a pronounced dependence on particle size, as also found by other authors [2, 3, 14], and the spectra for two different particle sizes can be practically brought into coincidence by vertical shifting. This points to the fact that the reflectance spectra, despite their remarkable dependence on particle size,

are not sufficiently sensitive to changes in particle size, at least if the differences are not essentially greater than those between our samples.

If we admit that the reflectance spectra depend on the optical thickness of the particle $k(\lambda) \cdot l$ (where l means the particle size), which is a fundamental supposition of most theories [2—7], then similar statements can be made for the changes in absorption, too. This seems to be supported by a comparison

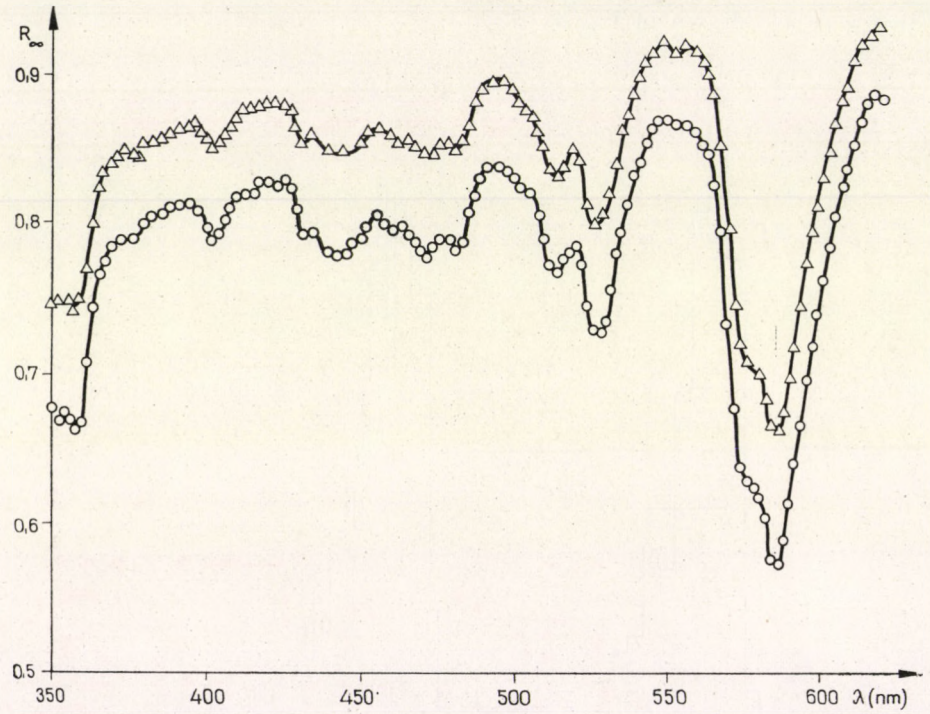


Fig. 3. Diffuse reflectance spectra of powdered didymium glass. △ — diffuse reflectance spectrum of powdered didymium glass of 7.3 μ particle size; ○ — diffuse reflectance spectrum of powdered didymium glass of 12.40 μ particle size

between the normalized absorption spectrum $k(\lambda)/k_{\max}$ and the diffuse reflectance spectra, both shown in Fig. 3, and further by the fact that the reflectance spectra are much less pronounced than the transmission and true absorption spectra; it is remarkable that the reflectance spectra become flatter towards the range of shorter wavelengths.

Finally, we have to make a very essential remark. According to KORTÜM and OELKRUG [15] the transmission and diffuse reflectance spectra can be brought into congruence by using an appropriate scale. It is evident, however, that there can be no question of such a coincidence in our case, the quotient of neighbouring maxima and minima being different in both spectra. This

contradiction between KORTÜM's results and ours can be ascribed to the fact that the authors mentioned supported their statements by absorption measurements made on samples which had a single broad absorption band and, therefore, they could not observe that in the case of structured spectra the ratios of intensity of the different bands in the spectrum, and that steeply ascending bands, lying very near to each other (see the range from 570 nm to 590 nm in Fig. 3), cannot be resolved in the reflectance spectra. These considerations seem to be supported by the fact that the single bands of both spectra can be acceptably fitted; the scales to be used as well as the degree of coincidence, however, depend also on the steepness of the bands (e.g. it is not possible to fit twin-bands of the transmission and reflectance spectra).

§ 3. Discussion

In the following we deal with a detailed study of the true absorption spectra, calculated from the diffuse reflectance spectra shown in Fig. 1 on the basis of SCHUSTER—KUBELKA—MUNK's theory[1] as well as BODÓ's, JOHNSON's, ANTONOV-ROMANOVSKY's and MELAMED's theories.

3.1. Discussion of the results obtained on the basis of Schuster—Kubelka—Munk's theory

According to calculations not detailed here [14], the following relation holds for the effective absorption coefficient k^*, the scattering coefficient s and diffuse reflectance R_∞ of a powder layer of infinite thickness:

$$\frac{k^*}{s} = \frac{(1 - R_\infty)^2}{2R_\infty} = f(R_\infty). \tag{2}$$

This permits k^* to be calculated by measuring R_∞ and s, and, in principle, the true absorption coefficient k of the material of the powder particles to be determined if the proportionality between k^* and k is known.

In our calculations it has been supposed, as usual, that the scattering coefficient s is independent of the wavelength and is constant for a given sample. Thus the quotient $(k^*/s)(k/s)_{\max}$ of the values of k/s calculated from Eq. (2) is, in principle, independent of the particle size and identical with the relative absorption spectrum $k(\lambda)/k_{\max}$. The results of our calculations as shown in Fig. 4, allow the following statements to be made.

[1] Theoretically it is to be expected that the true (bulk) absorption spectrum and the absorption spectra calculated from diffuse reflectance will be in accordance, but for a constant factor explicitly not determined.

The relative absorption spectra calculated from the diffuse reflectance spectra can be acceptably fitted to the data obtained from transmission measurements. However, the relative absorption spectra of our powder samples show a pronounced dependence on particle size, which is unexpected and cannot be theoretically interpreted. It is surprising that a relatively better

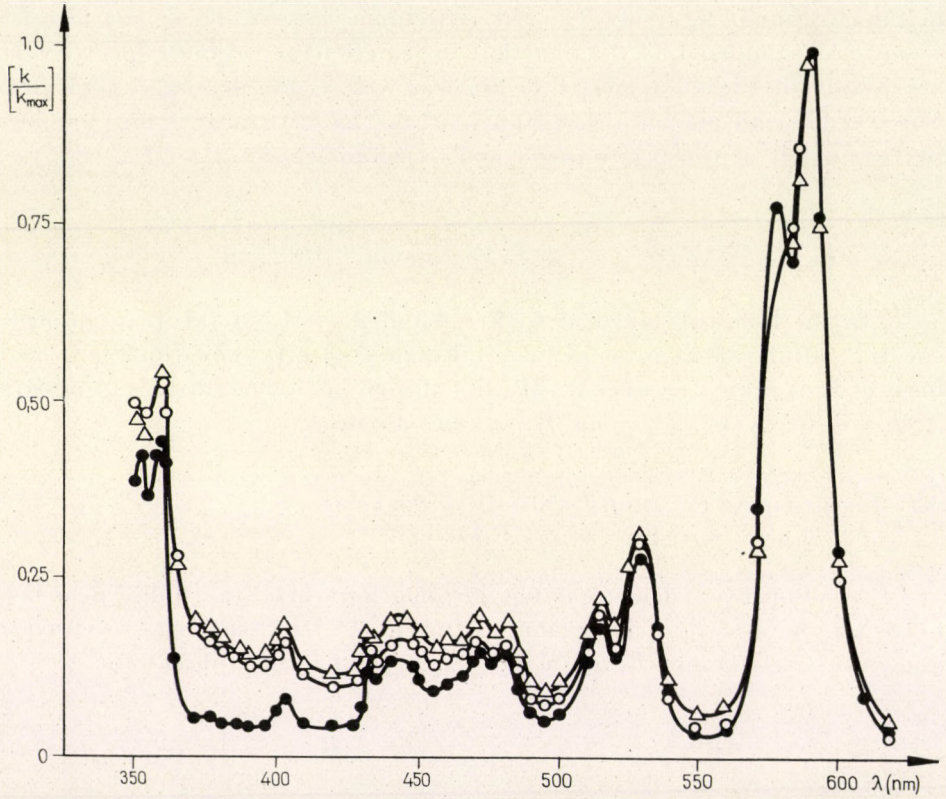


Fig. 4. Relative absorption spectra of didymium glass. ● — relative true (bulk) absorption spectrum; △ — relative absorption spectrum of powdered glass of 7.3 μ particle size; ○ — relative absorption spectrum of powdered glass of 12.40 μ particle size (△ and ○ calculated from diffuse reflectance according to KUBELKA—MUNK's theory)

accordance can be found with samples of larger particle size (12.2 μ). In the range of relatively weak absorption (relative values less than 0.1) higher deviations were found for both particle sizes. This can be attributed partly to the increased weight of uncertainties in the reflectance measurements and partly to the greater role of the multiple internal reflections inside the particles which is more probable in the case of weak absorption. The truth of the latter supposition seems to be supported by the fact that the quotients of the values k^*/s calculated from Eq. (2) and the true absorption coefficients k belonging

to the same wavelengths show a remarkable regular dependence on the wavelength (Fig. 5), contrary to the constant value to be expected from SCHUSTER—KUBELKA—MUNK's theory and KORTÜM's investigations on thin scattering layers [15]. It seems from what has been said above that, in the range of relatively weak absorption (less than 1 cm^{-1}, according to our transmission measurements), the degree of approximation of SCHUSTER—KUBELKA—MUNK's theory for the propagation of radiation in a powder sample is less satisfactory than is generally supposed. The well observable similarity of the dependence on wavelength of the quotient $(k^*/s)/k(\lambda)$ shown in Fig. 5 to the true absorption spectrum indicates that the absorption coefficient plays some role in the results, in spite of the quotient form. (It seems probable that the effective absorption



Fig. 5. Quotient of k^*/s and the true (bulk) absorption coefficient k. △ — for 7.3 μ particle size; ○ — for 12.40 μ particle size

coefficient k^*, instead of being linear in k, involves a higher power of k). Therefore, apart from other difficulties, Eq. (2) gives, even in principle, an acceptable estimate of $k(\lambda)$ only if the consequences of multiple internal reflections can be neglected.

Presumably also, the increase of the refractive index and, consequently, changes in the scattering coefficient s may contribute to the divergences of the absorption spectra calculated from the diffuse reflectance spectra and from the true absorption spectrum which increase with decreasing wavelength (Fig. 4).

3.2. *Discussion of the results obtained on the basis of Bodó's theory*

According to Bodó's theory [2, 3] the following relation is to be found between the diffuse reflectance R_∞ of a powder layer of infinite thickness, the mean particle size l and the true absorption coefficient k of the particles:

$$k = \frac{1}{2l} \ln \frac{(1-r)^2 + 2r(1-2r-r^2) f(R_\infty) - (r^2+r^4)}{(1-r)^2 - 2rf(R_\infty)}, \tag{3}$$

where $f(R_\infty) = (1 - R_\infty)^2/2R_\infty$, and r means the reflection coefficient of the particle surface, supposed to be independent of the wavelength of radiation. According to Bodó's concept, r can be estimated from the relation

$$\lim_{kl \to \infty} R_\infty = r. \tag{4}$$

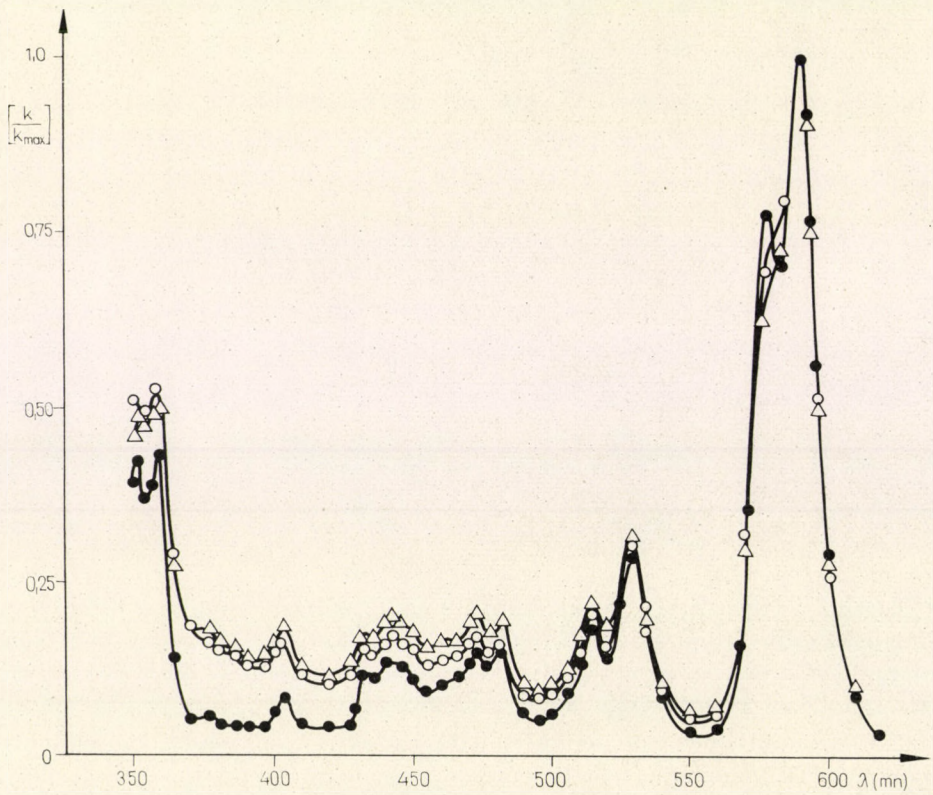


Fig. 6. Relative absorption spectra of didymium glass. ● — relative true (bulk) absorption spectrum; △ — relative absorption spectrum of powdered glass of 7.3 μ particle size; ○ — relative absorption spectrum of powdered glass of 12.40 μ particle size (△ and ○ calculated from diffuse reflectance according to Bodó's theory)

Investigations concerning this theory seem to be of some importance because BODÓ's original investigations were limited to some discrete wavelengths; his evaluations being based on measurements on relatively numerous samples of different particle sizes. Therefore, the applicability of the theory in the case of a few powder samples cannot be assessed on the basis of his

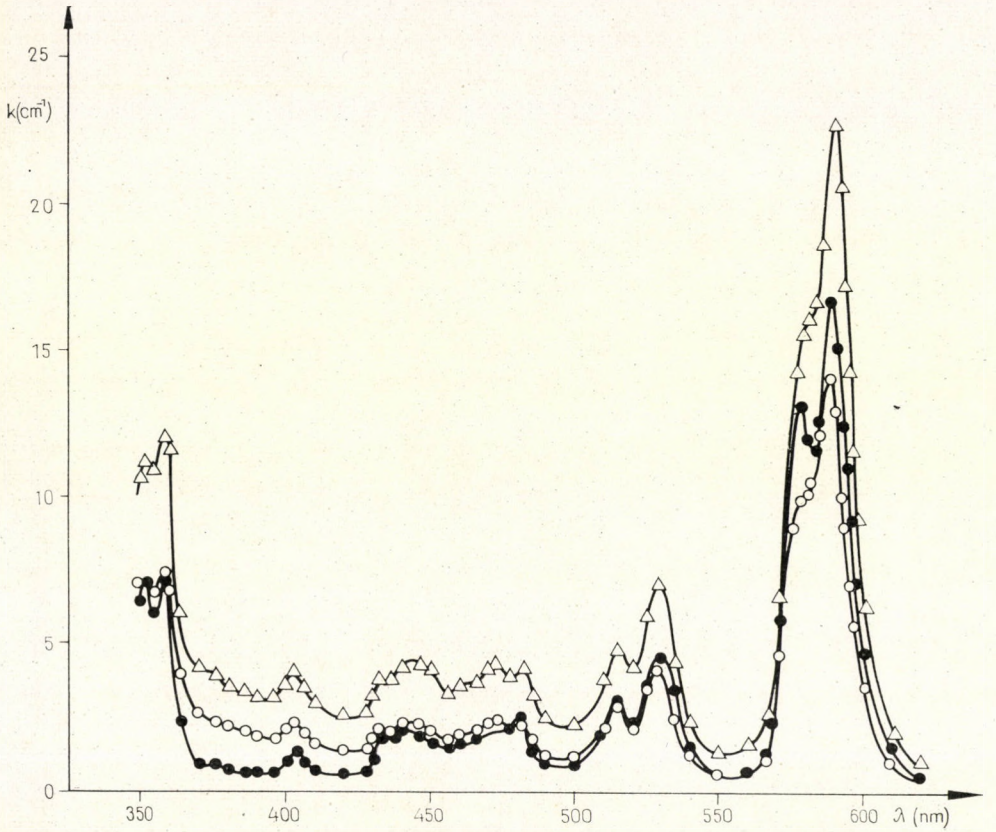


Fig. 7. Absorption spectra of didymium glass. ● — true (bulk) absorption spectrum. △ — absorption spectrum of powdered glass of 7.3 μ particle size; ○ — absorption spectrum of powdered glass of 12.40 μ particle size (△ and ○ calculated from diffuse reflectance according to BODÓ's theory)

original paper. According to our experiences, the estimation of r from Eq. (4) in the case of only two powder samples of different and relatively small particle sizes gives rise to uncertainties, the consequences of which are uncontrollable. Therefore, we used r calculated from FRESNEL's formula for perpendicular incidence with a mean refractive index $n = 1.55$ ($r = 0.045$). With this value, k was obtained from Eq. (3), knowing R_∞ and the microscopically measured value of l. The relative absorption spectra and the true absorption spectra, both calculated from diffuse reflectance, are shown in Figs. 6 and 7.

The shapes of the relative absorption spectra, obtained from transmission and diffuse reflectance spectra are in qualitative agreement and their structure is also similar. In the relative absorption spectra calculated from diffuse reflectance spectra of powder samples some dependence on the particle size is found which becomes more pronounced for weak absorption and shorter wavelengths. The absorption bands in the spectra calculated from reflectance are somewhat broader than those obtained from transmission. The quantitative efficiency of the theory can be assessed from Fig. 7. It can be seen that in the short wavelength region of the spectra, where the true absorption is weak (1—2 cm^{-1}), the absorption calculated from diffuse reflectance is essentially higher, the deviations amounting to 50—300%. It is remarkable that the rate of deviation markedly increases with decreasing wavelength for both samples (see the wavelength region from 400 nm, to 450 nm). The relative deviation shows a decrease in the region between 450 nm and 500 nm, but it essentially increases for very low (≤ 1 cm^{-1}) absorption values. In the wavelength interval from 500 nm to 550 nm the values obtained with powder samples of larger particle size are nearly identical with those calculated from transmission and, in a small region, they are even somewhat lower. In the case of the sample of 7.3 μ the calculated values are higher by not more than 35% compared with the true absorption coefficient. In the spectral region between 550 nm and 620 nm the values of bulk absorption are higher, without exception, than those of powder samples. The two bands between 575 nm and 590 nm could not be separated in the reflectance spectra (see Fig. 1). Therefore, they appear distorted in the absorption spectra, as well. Around the maximum, the results concerning the sample of smaller particle size are higher than the true values, whereas for the other sample they are lower. This feature does not change essentially up to the long wavelength end of the spectrum.

The fact that a deviation of 35% maximum is found in the regions of higher absorption values (from 4 cm^{-1}) means that, for glass powder samples of refractive index $n = 1.55$, the absorption coefficient of the powder sample calculated from the diffuse reflectance can be estimated within a limit of error of 35%.

3.3. Discussion of the results obtained on the basis of Johnson's theory

JOHNSON [4] gives the following relation between the parameters of a single particle (the particle size l, the true absorption coefficient $k(\lambda)$ and the reflection coefficient of the particle surface r, defined by FRESNEL's formula for perpendicular incidence in the form: $r = 1.5[(n-1)/(n+1)]^2$) and the diffuse reflectance of the powder sample of infinite thickness:

$$R_\infty = r\left[1+2\,\frac{e^{y\ln(1-r)-2kl}}{2\,kl-\ln(1-r)}\right], \tag{5}$$

where y can be calculated from the equation

$$\frac{(1-r)^{y-1}}{y} = \frac{1}{2} + \frac{1}{4}r + \frac{1}{6}r^2 + \ldots . \tag{6}$$

The relative and true absorption spectra calculated with Eqs. (5) and (6) are shown in Figs. 8 and 9, respectively.

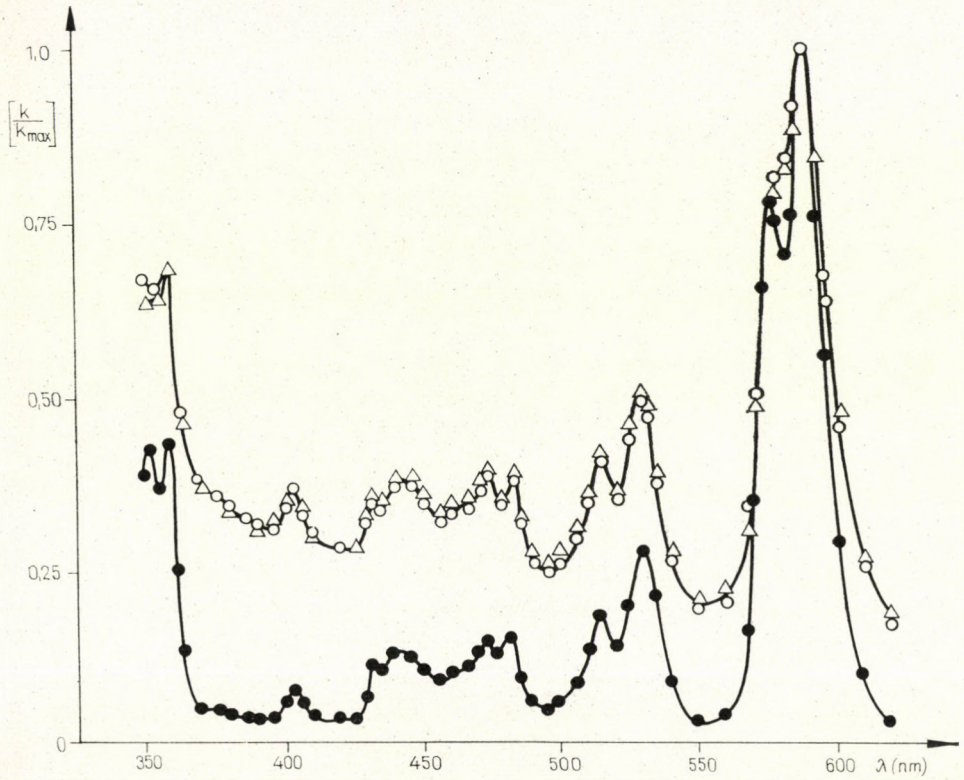


Fig. 8. Relative absorption spectra of didymium glass. ● — relative true (bulk) absorption spectrum; △ — relative absorption spectrum of powdered glass of 7.3 μ particle size; ○ — relative absorption spectrum of powdered glass of 12.40 μ particle size (△ and ○ calculated from diffuse reflectance according to JOHNSON's theory)

According to Fig. 8, the position and the shape of the relative absorption spectra calculated from diffuse reflectance is found to be in agreement with that obtained from transmission measurements, but both spectra appear distorted as to the values of maxima and minima. It is remarkable that the particle size has only little influence on the results, which means (with respect to Fig. 9) that the theory seems unsuitable for describing the effects of relatively small changes in absorption and particle size. This also follows from

theoretical considerations as well as from the excessive divergences obtained in the relative absorption spectra.

As can be seen from Fig. 9, the numerical values of the true absorption coefficients calculated according to this theory are higher by nearly an order of magnitude than those obtained from transmission measurements. Thus,

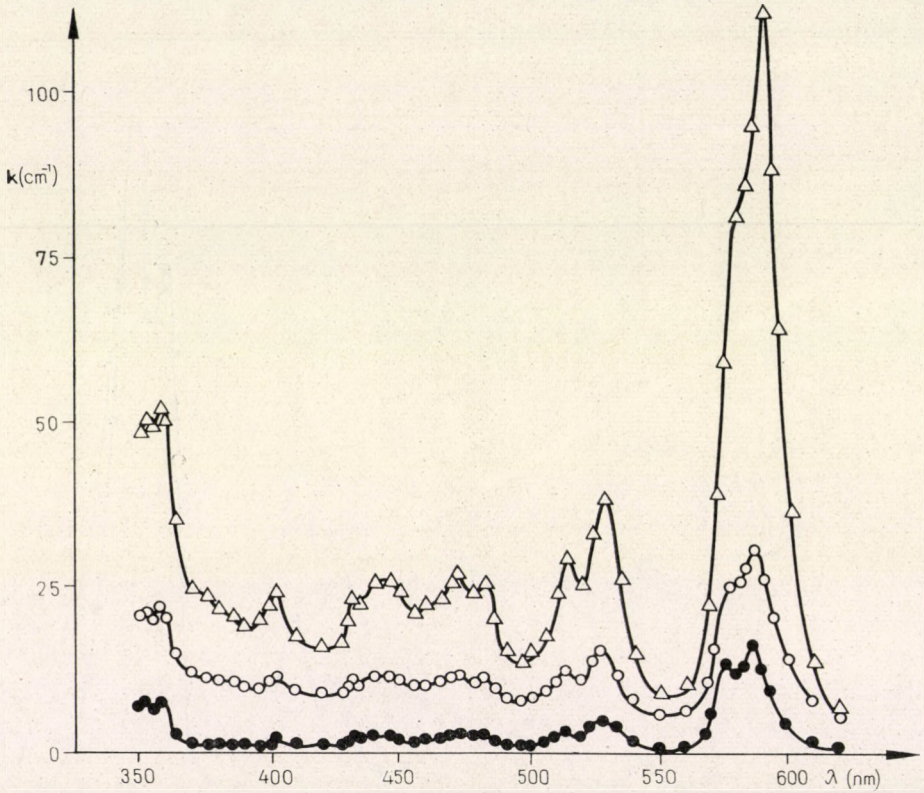


Fig. 9. Absorption spectra of didymium glass. ● — true (bulk) absorption spectrum; △ — absorption spectrum of powdered glass of 7.3 μ particle size; ○ — absorption spectrum of powdered glass of 12.40 μ particle size (△ and ○ calculated from diffuse reflectance according to JOHNSON's theory)

in the case of relatively small particle sizes, such as those used in the present investigations, the theory cannot be applied even for estimating the true absorption coefficient from diffuse reflectance data. (In the case of larger particles and higher absorption the approximation given by the theory is much better, as shown in [16].)

3.4. Discussion of the results obtained with Antonov-Romanovsky's theory

ANTONOV-ROMANOVSKY's paper [5], essentially by combining SCHUSTER—KUBELKA—MUNK's and BODÓ's theories, described the connection between

absorption and diffuse reflectance spectra for materials of low refractive index with the following formula:

$$k = \frac{1}{2l} \ln \frac{(1-r)^2+2r(1-2r)\,f(R_\infty)}{(1-r)^2-2rf(R_\infty)}\,, \tag{7}$$

in which the meaning of the symbols is the same as earlier.

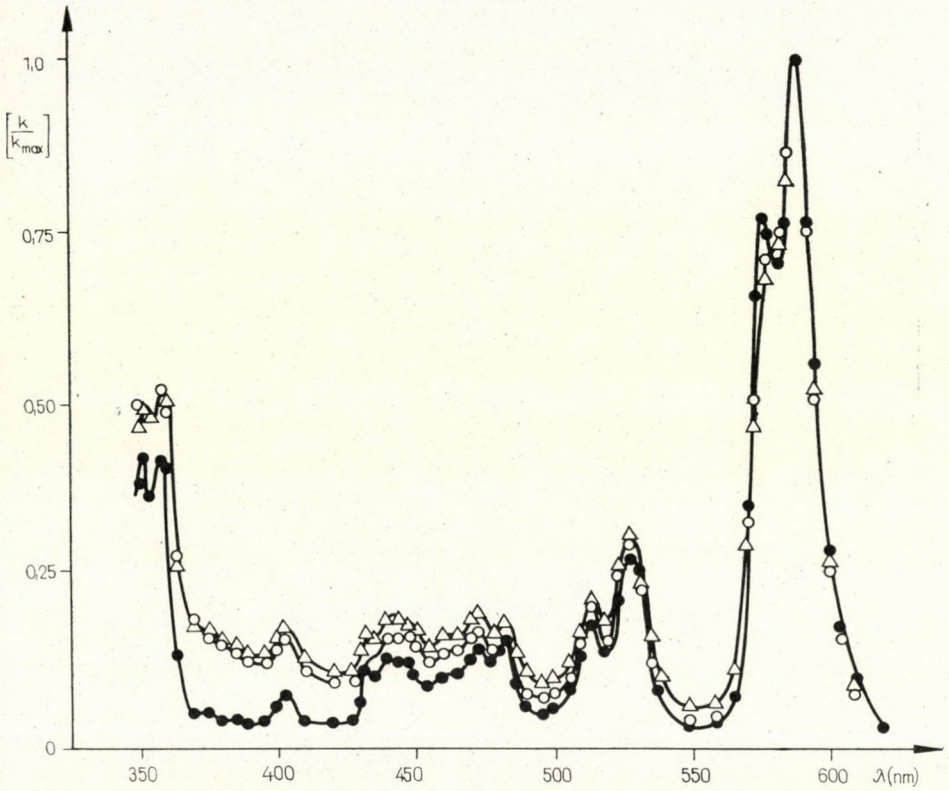


Fig. 10. Relative absorption spectra of didymium glass. ● — relative true (bulk) absorption spectrum; △ — relative absorption spectrum of powdered glass of 7.3 μ particle size; ○ — absorption spectrum of powdered glass of 12.40 μ particle size (△ and ○ calculated relative from diffuse reflectance according to ANTONOV-ROMANOVSKY's theory)

On the basis of the relative absorption spectra $k(\lambda)k_{\max}$ and the absolute bulk absorption spectra calculated with Eq. (7) and plotted in Figs. 10 and 11, essentially the same statements can be made as under 3.2, but with the addition that, according to our results, it seems possible to estimate the numerical value of the bulk absorption coefficients with somewhat higher accuracy (within an error of $\pm 30\%$) than with the use of BODÓ's theory. The uncertainties arising from errors in the measurement of the particle size are, however, too great for attributing major importance to this increased accuracy. On the

basis of the theory it is also possible, in principle, to estimate the scattering coefficient s and the ratio $k/k(\lambda)$ in SCHUSTER—KUBELKA—MUNK's theory with the aid of the connections

$$s = \frac{1}{l}\,\frac{2r}{1+r} \quad \text{and} \quad \frac{k^*}{k} = \frac{1-r}{1+r}\,. \tag{8}$$

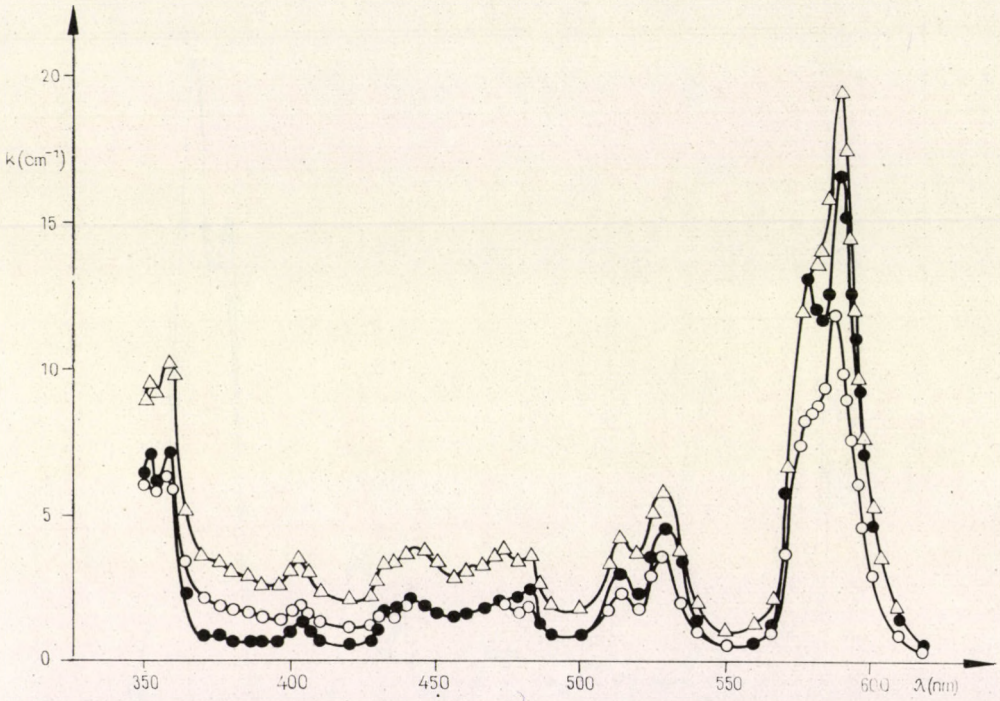


Fig. 11. Absorption spectra of didymium glass. ● — true (bulk) absorption spectrum; △ — absorption spectrum of powdered glass of 7.3 μ particle size; ○ — absorption spectrum of powdered glass of 12.40 μ particle size (△ and ○ calculated from diffuse reflectance according to ANTONOV-ROMANOVSKY's theory)

The following values for s were obtained with our samples:

$$s \approx 118 \text{ cm}^{-1} \text{ for } 7.3\ \mu \text{ particle size,}$$
$$s \approx 71 \text{ cm}^{-1} \text{ for } 12.2\ \mu \text{ particle size;}$$

whereas the quotient k^*/k was 0.90 independent of the particle size. Comparing these results with the measurements of KORTÜM et al. [15], these values calculated on the basis of ANTONOV-ROMANOVSKY's theory do not seem to be acceptable even as approximations.

The estimation of k^*/k suggested in the above form cannot be considered as satisfactorily corresponding to physical reality, as a value at least greater than l is to be expected even from SCHUSTER—KUBELKA—MUNK's theory,

which is to be considered as very approximative. Indeed, according to experiments of KORTÜM and OELKRUG [15] a value between 2.7—2.9, independent of the wavelength, results for this quotient.

As a conclusion, the estimation of the true absorption coefficient with ANTONOV-ROMANOVSKY's theory does not give essentially better results than those based on BODÓ's concept, and the estimates proposed for s and $k^*/k(\lambda)$ are not consistent with experimental results. Of course, this cannot be ascribed merely to ANTONOV-ROMANOVSKY's model, but also to the approximative character of SCHUSTER—KUBELKA—MUNK's original theory.

ANTONOV-ROMANOVSKY's theory concerning particles of irregular shape has not been discussed here, this case being of very little probability for refractive index $n = 1.55$.

3.5. Discussion of the results obtained with Melamed's theory

MELAMED [7], after a relatively complicated deduction, gives the following connection between the diffuse reflectance R_∞ of a powder layer of infinite thickness and optical and geometrical parameters of a single powder particle:

$$R_\infty = 2\,ur_e + \frac{(1-2\,ur_e)\,(1-R_\infty\,r_e)\,uT}{(1-R_\infty\,r_e)-(1-u)\,(1-r_e)\,TR_\infty}\,, \tag{9}$$

where

$$u = \frac{u_0}{1-(1-2\,u_0)\,T}\,,$$

where $u_0 = 0.284$ is a geometrical factor, r_e means the external diffuse reflection factor of the particle surface and T is defined by the relation

$$T = \frac{(1-r_i)\,M}{1-r_i\,M}\,.$$

Here r_i is the internal diffuse reflection factor of the particle surface and M can be expressed with the particle size l and the true absorption coefficient in the following form:

$$M = \frac{2}{(kl)^2}\,[1-(kl+1)\,e^{-kl}]\,.$$

The relative and the true absorption spectra obtained with Eq. (8) are plotted in Figs. 12 and 13, respectively. According to Fig. 12 MELAMED's theory also gives a qualitatively true picture of the changes in absorption, and the relative values of the maxima and minima show an acceptable agreement with those obtained from transmission measurements in the range of not too

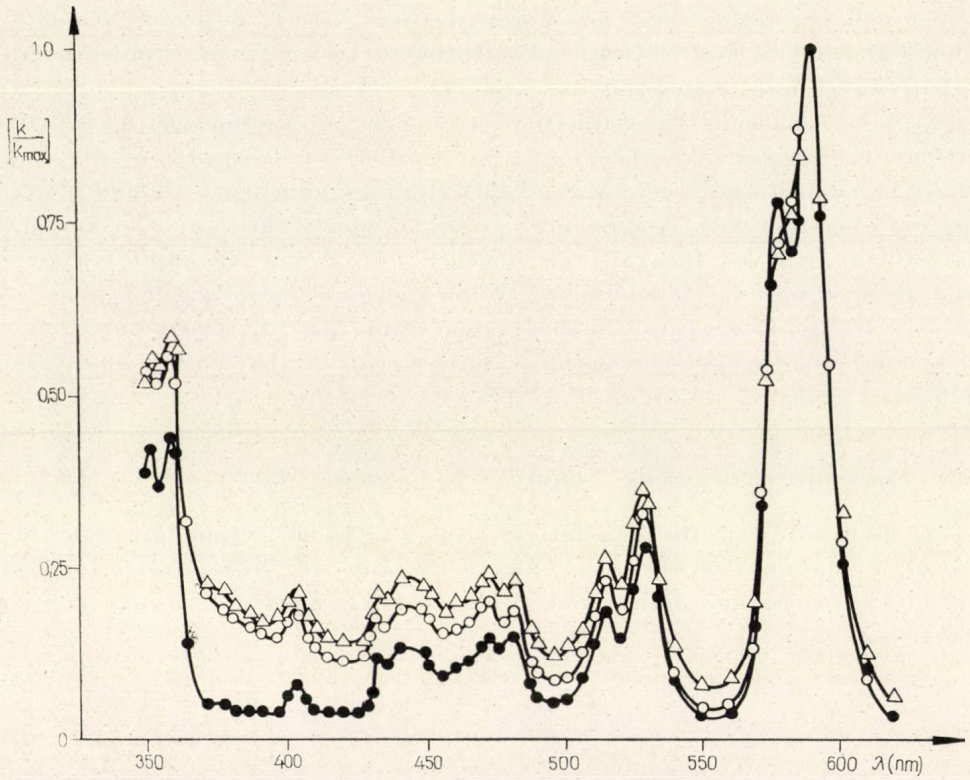


Fig. 12. Relative absorption spectra of didymium glass. ● — relative true (bulk) absorption spectrum; △ — relative absorption spectrum of powdered glass of 7.3 μ particle size; ○ — relative absorption spectrum of powdered glass of 12.40 μ particle size (△ and ○ calculated from diffuse reflectance according to MELAMED's theory)

low absorption. The divergences are, however, essentially higher than in the case of SCHUSTER—KUBELKA—MUNK's, BODÓ's and ANTONOV-ROMANOVSKY's theories, though essentially less than those of the values obtained with JOHNSON's model.

The quantitative results for k (Fig. 13) are generally higher by a factor about 4—5 than those obtained from transmission measurements; this may be attributed to the emphasized role of the internal reflection in the deduction of Eq. (8) [16]. This supposition seems to be confirmed by the fact that, with decreasing particle sizes, the absorption coefficients calculated from diffuse reflectance show increasing deviations from each other as well as from the absorption values calculated from transmission. Thus, it can be stated that MELAMED's theory in its present form does not give adequate estimates of the true (bulk) absorption coefficient of powder samples of relatively small particle sizes, as e.g. those used in our investigations.

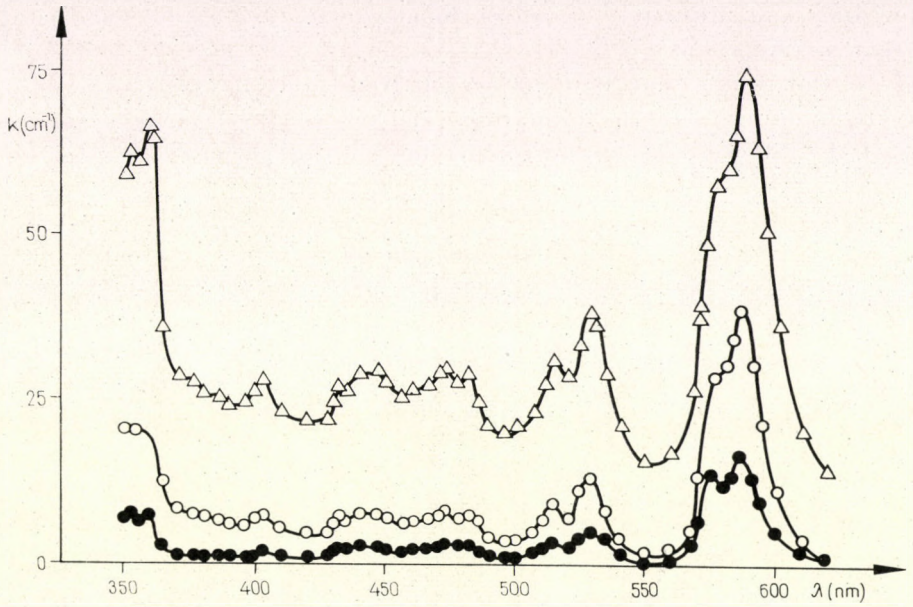


Fig. 13. Absorption spectra of didymium glass. ● — true (bulk) absorption spectrum; △ — absorption spectrum of powdered glass of 7.3 μ particle size; ○ — absorption spectrum of powdered glass of 12.40 μ particle size (△ and ○ calculated from diffuse reflectance according to MELAMED's theory)

§ 4. Conclusions

Comparative experimental investigations were made with didymium glass powder samples of 7.3 μ and 12.2 μ particle size, approximating those of the usual crystal phosphors, in order to clarify the connections between the most important theories concerning the relations between the true absorption spectra and diffuse reflectance spectra. On the basis of the experimental results, the following statements can be made:

1. A close connection exists between the bulk transmission and diffuse reflectance spectra of powdered solids, with the refinement that the corresponding bands of the transmission and diffuse reflectance spectra can be fitted ot each other by using a suitable scale.

2. The particle size of the powder sample has a definite influence on the diffuse reflectance spectrum; so, the diffuse reflectance spectra are essentially defined by the effective thickness of the particles of powder sample, the absorption coefficient and the position of the respective spectral band.

3. In the case of glass powder samples with relatively small particle size, the true absorption coefficient can be estimated within an error of $\pm 35\%$ on the basis of BODÓ's and ANTONOV-ROMANOVSKY's theories, whereas

JOHNSON's and MELAMED's theories do not seem to be applicable without further investigations.

4. Our results show that further partly theoretical, partly experimental investigations are necessary to mark off and to extend the range of applicability of the different models. Investigations for this purpose are in progress.

Acknowledgement

The authors' gratitude is due to the late Prof. Dr. Á. BUDÓ, Director of the Institute for the interest he showed in this work during the last period of his life. Thanks are due to Prof. Dr. I. KETSKEMÉTY for stimulating interest and valuable remarks during the work.

LITERATURE

1. P. KUBELKA and F. MUNK, Z. Techn. Phys., **12,** 593, 1931.
2. Z. BODÓ, Acta Phys. Hung., **1,** 135, 1951.
3. Z. BODÓ, MTA III. Oszt. Közl., **2,** 239, 1952.
4. P. D. JOHNSON, JOSA, **42,** 978, 1952.
5. В. В. Антонов-Романовский, ЖЭТФ, **26,** 459, 1954.
6. О. П. Гирин, В. И. Степанов, ЖЭТФ, **27,** 467, 1954.
7. N. T. MELAMED, J. Appl. Phys., **34,** 560, 1963.
8. B. KARVALY and F. PINTÉR, Silikattechnik (Berlin), **21,** 7, 1970.
9. H. KROCHMANN, private communication.
10. F. BENFORD, S. LLOYD and G. P. SCHWARZ, JOSA, **38,** 445, 1948; JOSA, **38,** 964, 1948.
11. E. E. K. MIDDLETON and C. L. SANDERS, JOSA, **41,** 419, 1951.
12. P. A. TELLEX and J. R. WALDRON, JOSA, **45,** 19, 1955.
13. K. SHIBATA, JOSA, **47,** 172, 1957.
14. G. KORTÜM, Reflexionsspektroskopie, Springer-Verlag, Berlin—Heidelberg—New York, 1969.
15. G. KORTÜM and D. OELKRUG, Naturwissenschaften, **53,** 600, 1966.
16. B. KARVALY, Acta Phys. Hung., **28,** 381, 1970.

ИССЛЕДОВАНИЯ О ВЗАИМОСВЯЗИ МЕЖДУ СПЕКТРАМИ ИСТИННОГО (МАССИВНОГО) ПОГЛОЩЕНИЯ И ДИФФУЗНОГО ОТРАЖЕНИЯ ПОРОШКООБРАЗНЫХ ВЕЩЕСТВ

Часть II

Б. КАРВАЛЬ и Ф. ПИНТЭР

Резюме

Проводились экспериментальные проверки найболее важных соотношений между спектрами истинного (массивного) поглощения и диффузного отражения в случае порошков дидимиевого стекла с размерами частиц 7,3 и 12, 2 μ. Что касается наших исследований, найлучшая оценка для коеффициента истинного (массивного) поглощения в случае порошков стекла получилась по теории Бодо и Антонов-Романовского, в то время как теории Джонсона и Меламеда не дали удовлетворительные результаты для порошкообразных веществ с размерами частиц, встречающимися в нашей работе. Излагается попытка дать качественное объяснение расходимостей.

Acta Physica Academiae Scientiarum Hungaricae, Tomus 29 (2—3), pp. 221—228 (1970)

INVESTIGATIONS ON CONNECTIONS BETWEEN FLUORESCENCE POLARIZATION AND FOREIGN QUENCHING IN VISCOUS SOLUTIONS

By

L. SZALAY and Z. VÁRKONYI

INSTITUTE OF EXPERIMENTAL PHYSICS, JÓZSEF ATTILA UNIVERSITY, SZEGED

(Received 9. X. 1969)

The degree of polarization of fluorescence in aqueous glycerol solutions of trypaflavine quenched by rhodamine B has been studied in the concentration range $6 \cdot 10^{-5}$ to $2 \cdot 10^{-3}$ mole/l of quencher, viscosities between 0.01 to 20 Poise and temperatures from 0°C to 50°C. PERRIN—LEVSHIN's relation of rotational depolarization has been found valid. The molar volume of trypaflavine derived from this relation was found to increase with increasing quencher concentration and viscosity. This has been explained by a rearrangement of the solvent layer around the excited molecule. The dependence of the molar volume on the mean lifetime of excitation permits conclusions on the kinetics of formation of the solvation shell.

Introduction

Dynamic foreign quenching exerts a considerable effect on the degree of polarization of fluorescence in solutions.

The degree of polarization p decreases with decreasing viscosity η_v and increasing temperature T, i.e. with increasing T/η_v [1]. This decrease has been ascribed to thermal rotation of the particles capable of fluorescence in the excited state. On the basis of Einstein's theory of Brownian rotation of molecules for excitation with linearly polarized light, supposing exponential decay of fluorescence and spherical form of fluorescent particles, the well known PERRIN—LEVSHIN formula of rotational depolarization has been obtained:

$$\frac{1}{p} - \frac{1}{3} = \left(\frac{1}{p_0} - \frac{1}{3}\right)\left(1 + \frac{RT\tau}{V\eta_v}\right), \tag{1}$$

where p_0 means the limiting polarization, V the molar volume of the fluorescent particle together with its solvation shell, τ the lifetime, and R the gas constant.

According to Eq. (1) the function $1/p = f(1/\eta_v)$ is linear if the other quantities are constant. Experimental results, however, do not always yield straight lines; the deviation from the straight line appears to be more significant particularly in the case of lower viscosities. This has been ascribed by several authors to a deviation of the decay from the exponential law, or to the fact that the luminescent particles cannot be considered as being of spherical form. These suppositions are, however, not sufficient to give a

satisfactory explanation (see [2]). JABŁÓŃSKI [3] obtained a formula of rotational depolarization which accounts for the deviation mentioned above by taking into consideration the so-called torsional vibration.

GÁTI and SZALAY [4] showed for aqueous glycerol solutions that a deviation from the straight was found because the depolarizing effect of secondary fluorescence had not been taken into account by earlier authors. However, even after correcting for this effect, deviations from linearity were found for some solutions (e.g. in the case of glycerol solution of trypaflavine).

As is well known, in the case of dynamic quenching besides changes in the fluorescence yield of the solution also the degree of polarization of fluorescence can be altered. If the quenching obeys the exponential law, there will be linearity between the relative yield and the relative mean lifetime of the excited state [5]: $\eta/\eta_0 = \tau/\tau_0$. Thus, Eq. (1) takes the following form:

$$\left(\frac{1}{p} - \frac{1}{3}\right) = \left(\frac{1}{p_0} - \frac{1}{3}\right)\left(1 + \frac{RT}{\eta_v V}\frac{\eta}{\eta_0}\tau_0\right), \tag{2}$$

where η_0 and τ_0 denote the yield and the lifetime of the unquenched solution, respectively.

According to Eq. (2) linearity between $1/p$ and η/η_0 will exist for non-absorbing quenchers, if the depolarizing effect of initial quenching can be neglected, or if the quenching has a dynamic character (see e.g. [6], [7]). HEVESI [8] studied the validity of the PERRIN—LEVSHIN formula in detail for some quenched aqueous glycerol dye solutions. He found that in practice it is permissible to calculate with an exponential law of quenching. Namely, the experimental error in determining the parameters of Eq. (1) is considerably higher than the possible error arising from the assumption of exponential quenching. For a glycerol solution of fluorescein quenched by potassium iodide a linear relation between $1/p$ and η/η_0 was found, if initial quenching was not taken into account. It was further shown by HEVESI [8] that in viscous solutions quenched by foreign quenchers the function $1/p = fT/\eta_v$ is not linear. He found that omitting the effect of initial quenching, i.e. assuming an exponential decay, the relation

$$\frac{1}{P} = \frac{1}{p_0} + \left(\frac{1}{p_0} - \frac{1}{3}\right)\frac{A}{V}\frac{T}{\eta_v}\frac{1}{1 + B\dfrac{T}{\eta_v}c} \tag{3}$$

holds instead of Eq. (1) and Eq. (2). The parameters A and B can be determined from molecular characteristics. If $c = 0$, i.e. in the absence of dynamic quenching, this formula takes the form of Eq. (1). If $c \neq 0$, $1/p$ is a non-linear

function of T/η_v and yields a curve concave from below, which is in accordance with experimental results.

In this paper we studied the degree of polarization of fluorescence in aqueous glycerol solutions quenched by foreign absorbing substances.

Composition of the systems

Experimental methods

In the experiments aqueous and aqueous glycerol solutions, with 60% and 90% glycerol containing trypaflavine and rhodamine B were used. The measurements were carried out with solutions at 273, 298 and 323 °K temperature. With a constant trypaflavine concentration of 1.25×10^{-4} mole/l, the concentration of the quencher (rhodamine B) was varied between 6.25×10^{-5} mole/l and 2×10^{-3} mole/l. Changing the viscosity of the solutions as above the dependence of the degree of polarization on quenching and on viscosity was investigated in the viscosity range from 0.01 P to 20 P. Only the degree of polarization of fluorescence emitted by the donor (trypaflavine) was measured. The degree of polarization was measured with a polarization spectrofluorimeter constructed by VIZE [12]. The true degree of polarization corrected for secondary fluorescence was determined from the directly measured degree of polarizations by the methods of BUDÓ and KETSKEMÉTY [9] and GÁTI and SZALAY [4], respectively. The lifetimes τ_0 of unquenched solutions used in the calculations were determined with the formula of STRICKLER and BERG [13]. The decay times of quenched solutions were obtained from the relation $\tau = \tau_0\eta/\eta_0$. The relative yield η/η_0 was determined by the method described in [15].

The viscosity of the solutions was measured with a Hoeppler viscosimeter, and the refractive index with an Abbe refractometer. Constant temperature of solutions was maintained with a Hoeppler ultrathermostat.

Results of measurement. Discussion

In Fig. 1 the dependence of p on quencher concentration is shown for three solutions of different viscosity at constant temperature, and the same in Fig. 2 for a solvent of given composition at three different temperatures. The results obtained with parameters not shown in the Figures were similar.

From the results published in [14], a linear relation between $1/p$ and η/η_0 has been found (Fig. 3). This means that the effect of initial quenching can be practically neglected, i.e. the decay of luminescence can be considered as exponential with very good approximation also in quenched solutions.

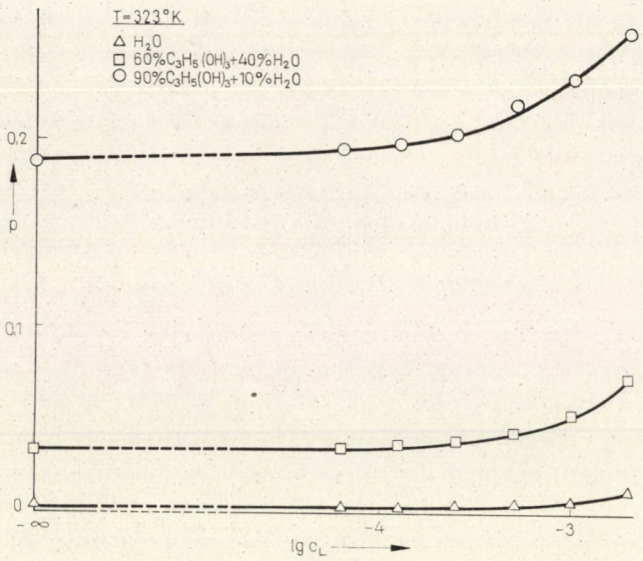


Fig. 1

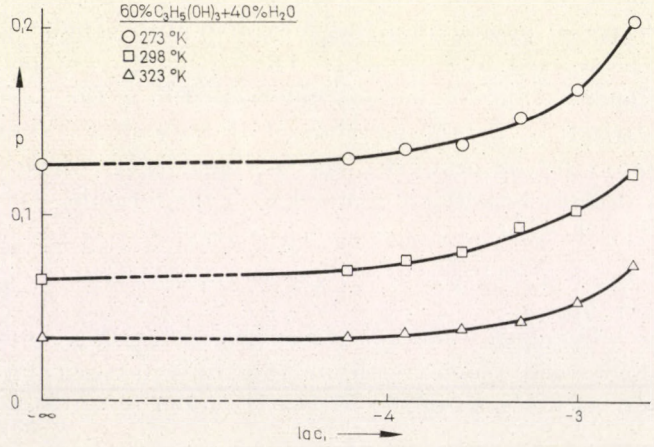


Fig. 2

The linearity holds only if T/η_v in Eq. (1) is constant. In Fig. 4 the dependence of $1/p$ on T/η_v is shown. Linearity is not fulfilled and curves slightly concave from below are obtained, similarly as in HEVESI's results [14].

This result may be due to the fact that τ and/or V is not constant. Plotting the values of $1/p$ as a function of $T/\eta_v\tau$ (Fig. 5), a straight line is obtained with good approximation; consequently the value of V was constant for a given quencher concentration. V can be determined from the slope of the straight line. The physically acceptable values of V obtained in this way are listed in Table I.

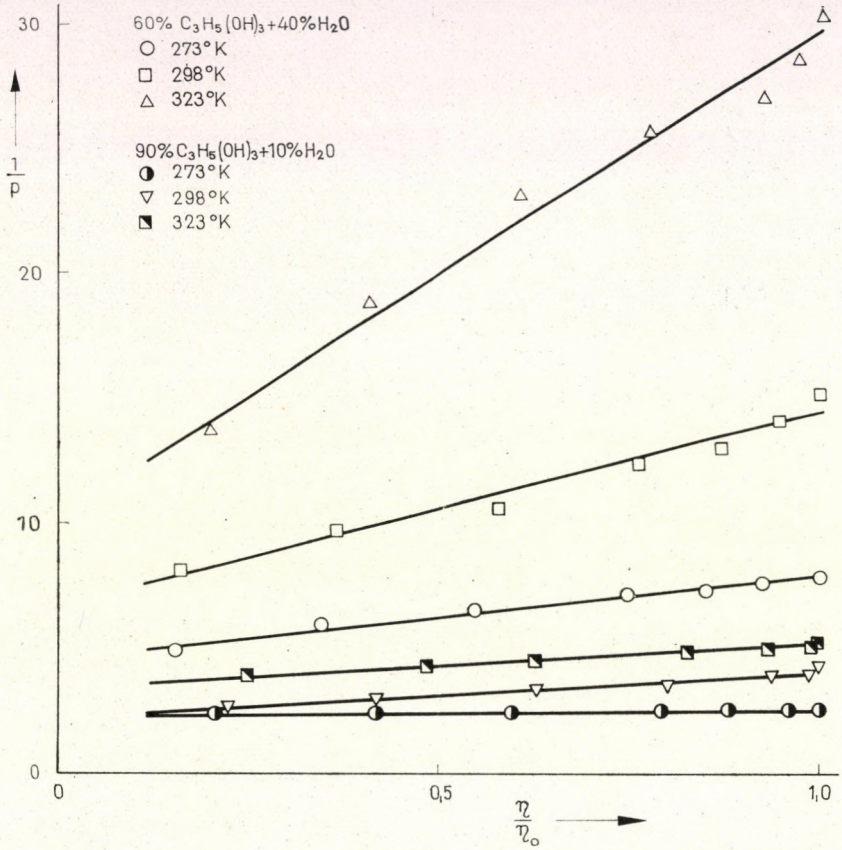

60% $C_3H_5(OH)_3$+40%H_2O
273°K
298°K
323°K
90%$C_3H_5(OH)_3$+10%H_2O
273°K
298°K
323°K
$\frac{1}{p}$
30
20
10
0
0
0,5
1,0
$\frac{\eta}{\eta_0}$

Fig. 3

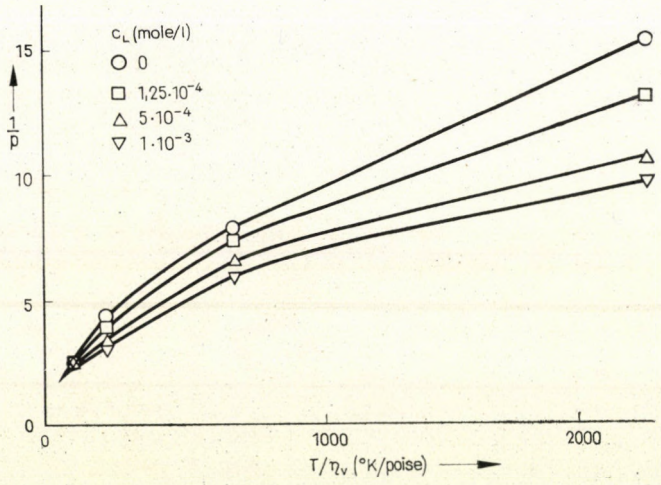

c_L(mole/l)
0
$1{,}25\cdot10^{-4}$
$5\cdot10^{-4}$
$1\cdot10^{-3}$
$\frac{1}{p}$
15
10
5
0
0
1000
2000
T/η_v (°K/poise)

Fig. 4

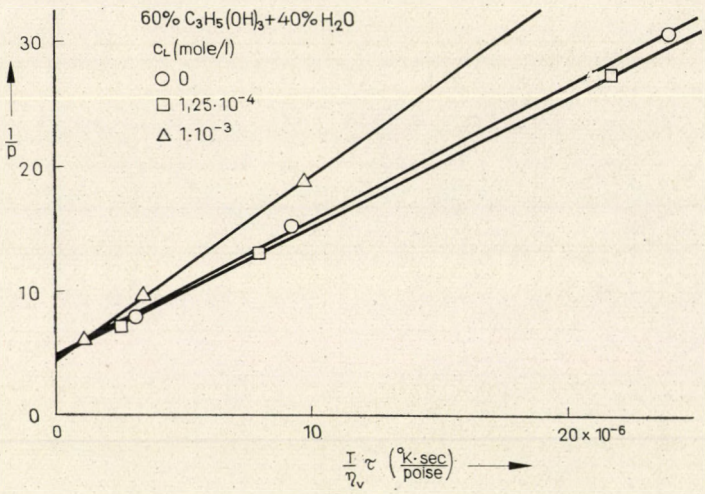


Fig. 5

For aqueous solutions (as a consequence of greater errors in determining p) the straight line seemed less well-defined. Therefore, aqueous solutions were not further studied in this respect. According to SZALAY [10] V decreases with increasing viscosity. Later BAUER [11] obtained the same results. A comparison of our values obtained with 60% and 90% glycerol solutions confirms these findings. It can be seen, however, that the values of V, within the same series of the solution, depends on the concentration of the quencher. This dependence is understable if V is the volume of the molecule including the solvation shell existing in the instant of excitation. The change of the dipole moment in the instant of excitation entails a rearrangement of the solvation shell. In a solution of low viscosity this rearrangement can be accomplished by the instant of emission, whereas in solutions of high viscosity the building

Table I

C_L mole/l	60% glycerol		90% glycerol	
	τ mean 10^{-9} sec	V cm^3	τ mean 10^{-9} sec	V cm^3
0	4,42	525,26	3,93	313,85
$6{,}25.10^{-5}$	4,19	360.08	3,85	270,05
$1{,}25.10^{-4}$	3,90	333,05	3,60	242,14
$2{,}5.10^{-4}$	3,37	290,82	3,18	214,46
5.10^{-4}	2,56	233,22	2,44	188,96
1.10^{-3}	1,66	173,20	1,74	137,79
2.10^{-3}	0,76	100,00	0,90	74,26

up of the solvation shell may not be completed during the lifetime of the excited state. This may be the reason for the fact that a molar volume of 525 cm^3 was obtained for 60% glycerol unquenched solutions against only 314 cm^3 in 90% glycerol unquenched solutions.

In case of equal viscosity, the molar volume will decrease with increasing quencher concentration, because the stronger the quenching the shorter is the mean life time of the excited state and, thus, the building up of the solvation shell around the excited molecule will be less complete by the instant of emission in quenched solutions.

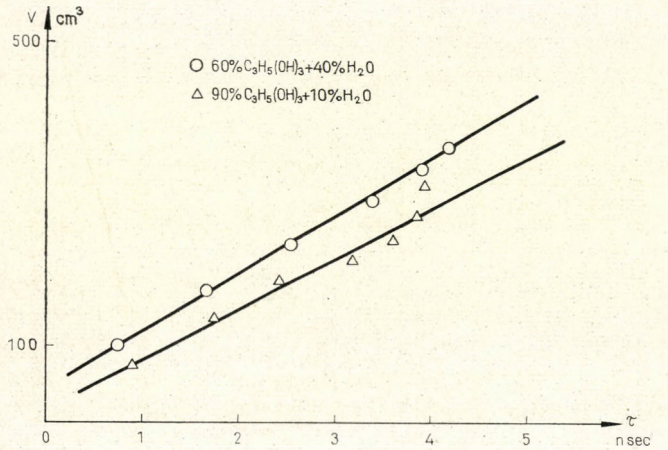


Fig. 6

If this concept is acceptable conclusions can be drawn concerning the building up of the solvation shell from the dependence of V on quencher concentration. In Table I the lifetimes τ of the excited states for different quencher concentrations are also listed. (These are mean values of the lifetimes for three different temperatures; the maximal deviations from the mean value did not exceed 8%. The relation shown in Fig. 6 is obtained by plotting V as a function of τ. Apart from the points belonging to the greatest value of τ the volume of the solvation shell increases linearly with time (the lifetime of the excited state). The straight line shown with a solid line has been calculated by the least square method from the points of measurement shown in the Figure. The building up of V, beginning from the moment of excitation evidently cannot be a linear function of time, because the extrapolation of the straight lines for $\tau = 0$ would give too small molar volumes (20 to 50 cm^3) for the trypaflavine molecule without solvation shell. Further, it can be understood that the slope of the straight line $V = V(\tau)$ for the solvent of less viscosity (the upper straight line in Fig. 6) must be greater than for the solvent

of higher viscosity. Namely, this slope indicates the rate of formation of the solvation shell and this should evidently be greater in a less viscous medium.

As is to be seen from the above, the effect of foreign quenching on the degree of polarization of fluorescence allows inferences to be drawn upon the kinetics of formation of the solvation shell, and from a knowledge of this kinetics interesting data about the values of microviscosity and local viscosity can be expected with further considerations.

Acknowledgement

Thanks are due to the late Prof. Á. BUDÓ, Director of the Institute of Experimental Physics, Member of the Hungarian Academy of Sciences, for his help in this work during the last period of his life.

REFERENCES

1. S. I. VAVILOV and V. L. LOVSHIN, Z. Phys., **16**, 135, 1923.
2. F. PERRIN, Acta Phys. Polon., **5**, 335, 1936.
3. A. JABŁOŃSKI, Bull. Acad. Polon., **8**, 259, 1961.
4. L. GÁTI and L. SZALAY, Acta Phys. et Chem. Szeged, **4**, 90, 1958.
5. V. L. LOVSHIN and S. I. VAVILOV, Zs. Phys., **48**, 397, 1928.
6. S. I. VAVILOV and A. N. SEVCHENKO, Dokl. Akad. Nauk SSSR. **3**, 274, 1936.
7. A. N. SEVCHENKO, Trudi GOI, **14**, 65, 1941.
8. J. HEVESI, Thesis, Szeged, 1965.
9. Á. BUDÓ and I. KETSKEMÉTY, Acta Phys. Hung., **14**, 167, 1962.
10. L. SZALAY, Thesis, Szeged, 1964.
11. R. K. BAUER, Acta Phys. Polon., **33**, 441, 1968.
12. L. VIZE, Acta Phys. et Chem. Szeged, **15**, I—II. 1969.
13. S. I. STRICKLER and R. A. BERG, J. Chem. Phys., **37**, 814, 1962.
14. J. HEVESI, Acta Phys. et Chem. Szeged, **8**, 16, 1962.
15. Z. VÁRKONYI, Acta Phys. et Chem. Szeged, **15**, 19, 1969.

ИССЛЕДОВАНИЯ СООТНОШЕНИЙ МЕЖДУ ФЛУОРЕСЦЕНТНОЙ ПОЛЯРИЗАЦИЕЙ И ПОСТОРОННИМ ПОГАСИТЕЛЕМ В ВИСКОЗНЫХ РАСТВОРАХ

Л. САЛАИ и З. ВАРКОНИ

Резюме

Изучалась степень поляризации флуоресценции вводяных глицерольных растворах грапафлавина, погашенного родамином В, в области концентрации погасителя от 6. 10^{-5} до 2. 10^{-3} моль/l, вязкости от 0,01 до 20 пуаз и температуры от 0°C до 50°C. Соотношение Перрена-Левшина для ротационной деполяризации оказывается верным. Молярный объем грипафлавина, определенный, по вышеуказанному соотношению увеличивается с увеличением концентрации погасителей и вязкости. Это объясняется перегруппировкой слоя растворителя около возбужденной молекулы. Зависимость молярного объема от среднего времени жизни возбуждения дает возможность сформулировать вывод о кинетике образования сольватационной оболочки.

Acta Physica Academiae Scientiarum Hungaricae, Tomus 29 (2—3), pp. 229—237 (1970)

PENETRATION OF ELECTROMAGNETIC WAVES INTO PLASMA

By

R. M. GUPTA and N. L. VARMA

DEPARTMENT OF PHYSICS, UNIVERSITY OF RAJASTHAN, JAIPUR—4, INDIA

(Received 9. X. 1969)

LANDAU studied the longitudinal field penetration into a semi-bounded plasma considering specularly reflecting electrons at the boundary. KURILKO and POPOV and then GORMAN examined the same problem considering a fraction 'p' of all incident electrons reflecting specularly and the remaining portion diffusely. Lastly, MASON treated the same problem at length and gave solutions for specular and diffuse reflections. Here the problem of penetration of transverse electromagnetic waves into a semi-bounded plasma has been formulated. We have studied specular reflection of electrons and applied these results to discuss the anomalous skin effect.

Introduction

LANDAU [1] studied the penetration of an external longitudinal electric field into a semi-bounded plasma. KURILKO and POPOV [2], GORMAN [3] and MASON [4] extended the study of field penetration when a fraction of the electrons is reflected specularly and the remaining electrons are reflected diffusely.

Here, we are interested in the problem of the penetration of transverse electromagnetic waves at a plane conducting boundary in the field-free plasma. We have considered ions to provide a uniform, smeared out positive charge background. Vlasov's equation for electrons and Maxwell's field equation are taken as the basic equations for the problem. For simplicity, we shall assume the equilibrium distribution to be isotropic in velocity space. In this case there is no coupling between the transverse and longitudinal waves, because the linear system of equations reduces to three separate sets of essentially one-dimensional equations after integration over two velocity components.

Here we have examined the problem of penetration of transverse electromagnetic waves into a semi-bounded field-free plasma. We have formulated the problem considering a fraction 'p' of electrons reflecting specularly at the boundary and the remaining fraction reflecting diffusely with a Maxwellian distribution. The semi-bounded plasma is replaced with an equivalent plasma filling the full-space and divided at $z = 0$ by a plane conducting boundary. We have calculated the electric field when all the electrons are reflected specularly. For field calculations we have used Hilbert transforms and half-range Fourier transforms.

Basic equations

The Vlasov equation is used for collisionless plasma and is combined with Maxwell's field equations to study electromagnetic waves. The electron distribution is given by a single particle function $f(r, v, t)$ and is separated into two parts as,

$$f(r, v, t) = n_0 f_0(v) + f_1(r, v, t)\,, \tag{1}$$

where n_0 and f_0 refer to the equilibrium state and $f_1(r, v, t)$ is the small deviation from the equilibrium. In the absence of the static electric and magnetic fields, the Vlasov equation reduces to

$$\frac{\partial f_1}{\partial t} + V \cdot \frac{\partial f_1}{\partial r} + \frac{n_0 e}{m}\left\{E(r, t) + \frac{V \times B(r, t)}{C}\right\} \cdot \frac{\partial f_0}{\partial V} = 0\,. \tag{2}$$

Maxwell's equations are

$$\begin{aligned} \nabla \times B &= \frac{4\pi}{C} j + \frac{1}{C}\frac{\partial E}{\partial t}\,, & \nabla \cdot B &= 0\,, \\ \nabla \times E &= -\frac{1}{C}\frac{\partial B}{\partial t}\,, & \nabla \cdot E &= 4\pi\varrho\,, \end{aligned} \tag{3}$$

where E and B are the electric and magnetic field strengths. $\varrho(r, t)$ and $j(r, t)$ are the charge and current densities, respectively, and are defined as follows:

$$\varrho(r, t) = e \int f_1(r, V, t)\, dV, \quad j(r, t) = e \int V f_1(r, V, t)\, dV\,. \tag{4}$$

If we consider the wave propagation along the z-axis, then the following reduced distribution functions are defined

$$\begin{aligned} f_x(z, v_z, t) &= \iint v_x f_1(z, V, t)\, dv_x\, dv_y\,, \\ f_y(z, v_z, t) &= \iint v_y f_1(z, V, t)\, dv_x\, dv_y\,, \\ f_z(z, v_z, t) &= \iint f_1(z, V, t)\, dv_x\, dv_y. \end{aligned} \tag{5}$$

Now the linearized Vlasov's equation (2) is multiplied by v_x, v_y and 1, respectively and then integrating over v_x and v_y components of velocity. The resultant equations are combined with relevant components from Maxwell's equations. We finally obtain the following three different sets of equations.

Set I

$$\frac{\partial f_x}{\partial t} + v_z \frac{\partial f_x}{\partial z} - \frac{n_0 e}{m} E_x F(v_z) = 0,$$

$$\frac{\partial E_x}{\partial t} = -C\,\frac{\partial B_y}{\partial_z} - 4\pi e\int f_x(z, v_z, t)dv_z, \tag{6}$$

$$\frac{\partial B_y}{\partial t} = -C\,\frac{\partial E_x}{\partial z},$$

where

$$F(v_z) = \iint f_0(V)\,dv_x\,dv_y \tag{7}$$

is an even, non-negative function of v_z; it decreases monotonically for $v_z > 0$ and is normalised to unity. This set involves the x-component of the electric field.

Set II

$$\frac{\partial f_y}{\partial t} + v_z\frac{\partial f_y}{\partial z} - \frac{n_0 e}{m}E_y F(v_z) = 0,$$

$$\frac{\partial E_y}{\partial t} = C\,\frac{\partial B_x}{\partial z} - 4\pi e\int f_y(z, v_z, t)\,dv_z, \tag{8}$$

$$\frac{\partial B_x}{\partial t} = C\,\frac{\partial E_y}{\partial z}.$$

This involves only the E_y component.

Set III

$$\frac{\partial f_z}{\partial t} + v_z\frac{\partial f_z}{\partial z} + \frac{n_0 e}{m}E_z\frac{dF(v_z)}{dv_z} = 0,$$

$$\frac{\partial E_z}{\partial z} = 4\pi e\int f_z(z, v_z, t)\,dv_z. \tag{9}$$

This involves only E_z. Now there are three reduced problems. The first two sets correspond to transverse electromagnetic waves with different direcsions of polarization, and the third set to the longitudinal plasma waves. The ast set of equations has been studied extensively by MASON [4]. Here we hall discuss only transverse waves.

Formulation of the problem

Sets I and II form equivalent problems for transverse electromagnetic waves and here we shall restrict ourselves to the first set of equations only· The semi-bounded plasma is replaced with an equivalent plasma filling the full-space and divided at $z = 0$ by a plane conducting boundary. This is insu-

lated from the plasma medium and electrons are reflected with fractional accommodation. An external signal is generated at the boundary so as to create the fields $E \exp(-i\omega t)$ and $\pm B \exp(-i\omega t)$ at $z = 0^{\pm}$. The signal penetrates the entire plasma in accordance with Maxwell's equations, and the linearized Vlasov equation. The fundamental equations of the problem are,

$$\begin{aligned} &\frac{\partial f_x}{\partial t} + v_z \frac{\partial f_x}{\partial z} - \frac{n_0 e}{m} E_x F(v_z) = 0, \\ &\frac{\partial E_x}{\partial t} = -C \frac{\partial B_y}{\partial z} - 4\pi e \int f_x(z, v_z, t)\, dv_z, \\ &\frac{\partial B_y}{\partial t} = -C \frac{\partial E_x}{\partial z}. \end{aligned} \tag{10}$$

Here fields vary with time as $\exp(-i\omega t)$ and we put

$$f_x(z, v_z, t) = g(z, v_z)\, e^{-i\omega t}. \tag{11}$$

The suffixes on fields are omitted onwards for convenience. The exponential time dependence is true throughout. Here we propose to find $E(z > 0)$.

The half-range Fourier transform 'plus transforms' are defined as follows:

$$g_+(v_z, k) = \int_0^\infty g(v_z, z)\, e^{-ikz}\, dz$$

and

$$A_+ = \int_0^\infty A(z)\, e^{-ikz}\, dz, \tag{12}$$

where $A(z)$ stands for field components. Now, we have

$$\int_0^\infty \frac{\partial g}{\partial z} e^{-ikz}\, dz = ikg_+ - g(v_z, 0^+)$$

and

$$\int_0^\infty \frac{\partial A}{\partial z} e^{-ikz}\, dz = ikA_+ - A(0^+). \tag{13}$$

Similarly 'minus transforms' are obtained from corresponding integrals over the range $z < 0$. The 'plus transforms' are obviously analytic for $I_m(k) < 0^-$ and non-analytic for $I_m(k) > 0^-$, while the minus transforms are non-analytic for $I_m(k) < 0^+$.

Applying Fourier transforms to the field equations in the set of equations (10), where suffixes have been dropped for convenience, we get,

$$ikE_{\pm}\left(\cup - \frac{C^2}{\cup}\right) = \mp K_{\pm} + 4\pi j_{\pm}, \tag{14}$$

where

$$\cup = \frac{\omega}{k},$$

$$K_+ = \frac{C^2}{\cup} E(0) + CB(0), \tag{15}$$

$$K_- = \frac{C^2}{\cup} E(0) - CB(0)$$

and

$$j_\pm = e\int_{-\infty}^{\infty} g_\pm \, dv_z \,. \tag{16}$$

In the absence of perturbed fields, equation (14) yields,

$$4\pi J_\pm = \pm K_\pm \,, \tag{17}$$

The first equation of the set of equations (10) is multiplied by e, then making use of Eq. (11), and taking Fourier transforms, it yields on simplification:

$$j_\pm = \frac{\pm N(k, 0^\pm) + \dfrac{\varepsilon(k) J\pm}{\cup^2 - C^2}}{1 + \dfrac{\varepsilon(k)}{\cup^2 - C^2}} \,, \tag{18}$$

where

$$N(k, 0^\pm) = \int_{-\infty}^{\infty} \frac{e v_z g(v_z, 0^\pm)}{(-i\omega + ikv_z)} \, dv_z \,.$$

$$\varepsilon(k) = \frac{i}{k} \cup \omega_p^2 \int_{-\infty}^{\infty} \frac{F(v_z)}{(-i\omega + ikv_z)} \, dv_z$$

and

$$\omega_p^2 = \frac{4\pi e^2 n_0}{m} \,.$$

The boundary condition at $z = 0$ is $g(v_z > 0) = g(-v_z)$. At boundary $z = 0^+$, the fractional accommodation and particle flux conservation requires,

$$g(v_z, 0^+) = \begin{cases} -(1-p) \dfrac{n_0 s^-(0^+)}{C_0} F(v_z) + pg(-v_z, 0^+) & \text{for } v_z > 0 \\ g(v_z, 0^+) & \text{for } v_z < 0 \end{cases} \tag{19}$$

where

$$C_0 = \int_0^{\infty} v_z F(v_z) \, dv_z$$

and

$$n_0 s^-(0^+) = \int_{-\infty}^{\infty} v_z g(v_z, 0^+) \, dv_z \,.$$

Similarly at the boundary $z = 0^-$, we evaluated $g(v_z, 0^-)$. The substitution of these values in the expression for $N(k, 0^{\pm})$ in Eq. (18), gives,

$$N(k, 0^{\pm}) = \mp(1-p)\, S_{\mp}(0)\, I_{\pm}(k) + pS_{\pm}(k) + S_{\mp}(k). \tag{20}$$

Here

$$I_+(k) = -I_-(k) = -\frac{i\omega}{C_0}\int_0^{\infty} \frac{v_z F(v_z)}{(-i\omega + ikv_z)}\, dv_z, \tag{21}$$

$$S_-(k) = -S_+(-k) = \int_{-\infty}^{0} \frac{ev_z\, g(v_z, 0^+)}{(-i\omega + ikv_z)}\, dv_z, \tag{22}$$

such that

$$S_-(0) = \frac{en_0\, s^-(0^+)}{(-i\omega)}.$$

We have used the fact that $g(v_z, 0^+) = g(-v_z, 0^-)$ in the definition of $s_{\pm}(k)$.

Using equations (14) to (22), we get,

$$E_+(k) = \frac{iUk_+ - 4\pi iU\{-(1-p)\, S_-(0)\, \hat{I}_+(k) + pS_+(k) + S_-(k)\}}{kD(k)}, \tag{23}$$

$$E_-(k) = \frac{-iUk_- - 4\pi iU\{-(1-p)\, S_+(0)\, \hat{I}_-(k) - pS_-(k) - S_+(k)\}}{kD(k)}, \tag{24}$$

where

$$D(k) = U^2 - C^2 + \varepsilon(k). \tag{25}$$

Now $E(z>0)$ can be obtained in two ways. First we have to apply the inverse Fourier transform to Eq. (23), in that case the source transforms $S_{\pm}(k)$ have to be known. But these source transforms depend on the return distribution to the boundary, $g(v_z \lessgtr 0, 0^{\pm})$. Secondly a suitable combination of E_+ and E_- has to be inverse Fourier transformed where the unknown contribution of the $S_{\pm}(k)$ terms to the electric field are cancelled.

We have defined the functions $D(k)$, $I_{\pm}(k)$ and $S_{\pm}(k)$ for real k. To consider the gradual growth of the external fields we assume a vanishingly small imaginary part of ω. The study of the analytic behaviour of these functions in the remainder of the k plane is very essential to find the field $E(z > 0)$. MASON [4] has defined similar functions in connection with the penetration of the plasma wave field and discussed the analytic behaviour of the functions for a large values of z. We have observed that the analytic behaviour of the functions defined here is exactly the same as those defined by MASON [4] and, therefore, we omit discussion here.

Specular reflection

In the case of specular reflection, the total number of electrons are reflected and there is no diffuse reflection, i.e., $p = 1$.

Now adding E_+ and E_-, we have,

$$\tilde{E} = E_+ + E_- = \frac{2iCB(0) \cup}{kD(k)} . \tag{26}$$

The $S_\pm(k)$ cancel in Eq. (26) and after applying inverse Fourier transform for $z > 0$, we obtain,

$$E(z > 0, p = 1) = \frac{iCB(0)}{\pi} \int_{-\infty}^{\infty} \cup \frac{e^{ikz}}{kD(k)} dk . \tag{27}$$

The integral in equation (27) passes below the E_+ pole at $k = 0$ and above the E_- pole there. It can be written in more explicit form as,

$$E(z > 0) = \frac{iCB(0)}{\pi} \left[\int_0^{\infty} \cup \frac{e^{ikz}}{kD(k)} dk + \int_{-\infty}^{0} \cup \frac{e^{ikz}}{kD^*(k)} dk \right], \tag{28}$$

where $D^*(k)$ is the complex conjugate of $D(k)$.

The above equation can also be written as,

$$E(z > 0) = \frac{i\omega CB(0)}{\pi} \int_{-\infty}^{\infty} \left[\omega^2 - {}^2 Ck^2 - \omega\omega_p^2 \int_{-\infty}^{\infty} \frac{F(v_z)}{(\omega - kv_z + i\sigma)} dv_z \right]^{-1} e^{ikz} dk , \tag{29}$$

where σ is the vanishingly small imaginary part of ω.

For $\omega > \omega_p$, the term in the brackets in equation (29) has real zeros at $\pm k = \omega / \pm U_t$ and this follows from the definition of $D(k)$ and $D^*(k)$. For this case we have,

$$\omega^2 - C^2 k^2 - \omega\omega_p^2 p \int \frac{F(v_z)}{(\omega - kv_z)} dv_z = 0 . \tag{30}$$

The refractive index $n(\omega)$ for all frequencies can be defined as

$$n = \frac{Ck}{\omega} .$$

We have observed from Maxwell's equations that the electric and magnetic fields are continuous at $z = 0$. The electric and magnetic fields in

the vacuum can be written as follows

$$E(z) = B(0)\,\frac{e^{i\omega z/C} + R_C\, e^{i\omega z/C}}{1-R_C}\,,$$
$$B(z) = B(0)\,\frac{e^{i\omega z/C} - R_C\, e^{-i\omega z/C}}{1-R_C}\,, \qquad z<0\,, \tag{31}$$

where R_C is the reflection coefficient which can be evaluated from the value of surface impedance Z. For the evaluation of surface impedance it is not necessary to know the explicit form of $g(z, v_z)$.

Since

$$Z = \frac{4\pi}{C}\,\frac{E(0)}{B(0)}\,, \tag{32}$$

so that

$$R_C = \frac{Z - 4\pi/C}{Z + 4\pi/C}\,. \tag{33}$$

Anomalous skin effect

Let us first consider that

$$\omega^2 - C^2k^2 - \omega\omega_p^2 \int \frac{F(v_z)}{(\omega - kv_z + i\sigma)}\, dv_z = k^2\, D(k) \quad \text{for } k>0$$
$$= k^2 D^*(k) \quad \text{for } k<0 \tag{34}$$

For $\omega > \omega_p$ the electromagnetic waves are undamped for large values of z. From Eq. (29), we obtain the electric field asymptotically for a large value of z:

$$E(z) \sim -2\omega_c\, B(0) \cdot \left[\frac{\partial\{k^2\, D(k)\}}{\partial k}\bigg|_{k=\,\omega/U_t}\right]^{-1} \cdot e^{i\omega z/U_t}\,. \tag{35}$$

Making use of equations (31) and (35) transmission coefficient T_C can be defined as follows:

$$\frac{T_C}{1-R_C} = -2\omega_C \left[\frac{\partial\{k^2\, D(k)\}}{\partial k}\bigg|_{k=\,\omega/U_t}\right]^{-1}\,. \tag{36}$$

Acknowledgements

The authors are greatly indebted to Professor P. L. BHATNAGAR for encouragement and helpful suggestions. They are also grateful to Dr. K. C. SHARMA for many useful discussions.

REFERENCES

1. L. D. Landau, J. Phys. U.S.S.R., **10**, 25, 1946.
2. V. I. Kurilko and V. A. Popov, Zh. Tekh. Fiz., **36**, 466, 1966 (Sov. Phys. Tech. Phys., **11**, 344).
3. D. Gorman, Phys. Fluids, **10**, 2502, 1967.
4. R. J. Mason, J. Maths. Phys. **9**, 868, 1968.

ПРОНИКНОВЕНИЕ ЭЛЕКТРОМАГНИТНЫХ ВОЛН В ПЛАЗМУ

Р. М. ГУПТА и Н. Л. ВАРМА

Р е з ю м е

Ландау изучая проникновение продольного поля в полуограниченную плазму-рассматривая отражающие электроны находящиеся у границы. Курилко и Попов, а также Горман исследовали эту же самую проблему, рассматривая часть «p» падающих электронов, отражающей зеркально, а остальную часть отражающей диффузно. Наконец данная проблема подробно изучалась Масоном, кто дал решения для зеркального и диффузного отражений. В данной работе сформулируется проблема проникновения поперечных электромагнитных волн в полуограниченную плазму. Исследовалось зеркальное отражение электронов, излагается применение полученных результатов к изучению аномального скин-эффекта.

Acta Physica Academiae Scientiarum Hungaricae, Tomus 29 (2—3), pp. 239—241 (1970)

ANGULAR ANISOTROPY OF FISSION FRAGMENTS IN TERNARY FISSION OF ^{235}U AND ^{238}U INDUCED BY 14 MeV NEUTRONS

By

I. KOVÁCS, L. NAGY and I. VINNAY

CENTRAL RESEARCH INSTITUTE FOR PHYSICS, BUDAPEST

(Received 23. X. 1969)

The angular anisotropy of fission fragments of ^{235}U and ^{238}U with respect to the direction of 14 MeV neutrons was found to be larger in ternary than in binary fission.

The angular anisotropy of fission fragments in ternary fission with the emission of long-range α-particles has been studied by several authors [1—5]. RAMANNA et al. [1] reported that in the ternary fission of ^{238}U induced by 14 MeV neutrons, the angular distribution of fragments is peaked at 90°. GILLET et al. [4] found the distribution to be approximately isotropic, while ATNEOSEN et al. [2] obtained with 17.5 MeV protons nearly identical forward-peaking distributions for the fragments of binary and ternary fission. The angular distribution of fragments in the fission of ^{235}U induced by 3 MeV neutrons was found by HATTANGADI et al. [3] and NADKARNI [5] to have a maximum at 90°.

In the present work the fission fragments and long-range α-particles were detected by semiconductor detectors of 225 mm^2 area (Fig. 1). The D_α detector counted the α-particles in a nearly 2π solid angle; the detectors D_0 and D_{90} counted the fission fragments in the ranges $0° \pm 35°$ and $90° \pm 35°$, respectively, relative to the neutron beam axis. The fissile material of about 2 mg/cm^2 thickness and 180 mm^2 area was deposited on 9.7 mg/cm^2 stainless steel backing which was sufficient to stop the fission fragments and the α-particles of the natural α-decay of uranium. The divergence of the neutron beam at the target was about $\pm 17°$.

The electronic discrimination for long-range α-particles was set at about 4.5 MeV. In the fission channels a relatively high discrimination threshold of about 30 MeV was applied which resulted in detecting only the pulses produced by fission fragments. The number of ternary fissions was obtained from the coincidence counts between D_α and one of the fission detectors, after correcting for chance coincidences. Each channel width of the four coincidence units was 100 ns. The chance to true coincidence rate was about equal to unity.

Table I shows the results of the measurements; N_t^0 and N_t^{90} are the number of ternary fissions the fragments of which were detected at angles 0° and 90°, respectively; $N_t^0/N_b^0 = R_0$ and $N_t^{90}/N_b^{90} = R_{90}$ are the ternary to binary ratios at the specified angles. The ratio R_0/R_{90} is insensitive to the inhomogeneities of the fissile layer, the non-uniformity of the neutron beam

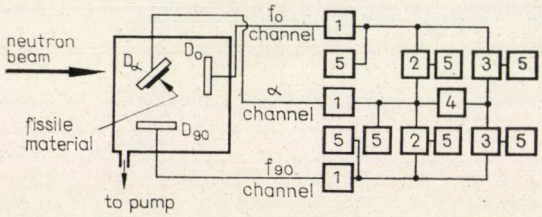


Fig. 1. Schematic diagram of detector geometry and electronic system: 1 — amplifier and discriminator; 2 — coincidence unit; 3 — coincidence unit for chance coincidences; 4 — delay line of 2 μs; 5 — scaler

Table I

Nuclide	E_n	N_t^0	N_t^{90}	R_0/R_{90}
^{235}U	Therm.	2045	2239	0.96 ± 0.04
^{235}U	14 MeV	1918	1271	1.18 ± 0.06
^{238}U	14 MeV	632	435	1.17 ± 0.11

and the inaccuracies of the geometry. For checking the experimental equipment as a whole, the R_0/R_{90} ratio was measured also in thermal runs, in which the neutrons were thermalized with the help of a paraffin block. Within the limits of error, the measured value is equal to unity.

The fragments of binary fission for neutrons of about 14 MeV are known to show a forward-peaked angular distribution. In the present measurements the angular distribution of fission fragments in ternary fission of ^{235}U was found to be also forward-peaked and the anisotropy to be even higher than for binary fission. For ^{238}U the distribution exhibits a slightly forward-peaking tendency, similar to that obtained in [2]. These results are in qualitative agreement with those already reported in [6].

Calculations in terms of the statistical model for the anisotropy of fission fragments [7] give

$$W_0/W_{90} = 1 + I_m^2/8K_0^2,$$

where K_0 is the average value of the projection of the angular momentum on the nuclear symmetry axis, and I_m is the maximum value of the angular momentum. Considering this relation, present results suggest that in the nuclear states from which ternary fission takes place K_0 is less than in those leading to binary fission.

REFERENCES

1. R. Ramanna, K. G. Nair and S. S. Kapoor, Phys. Rev., **129,** 1350, 1963.
2. R. A. Atneosen, T. D. Thomas and G. T. Garvey, Phys. Rev., **139,** B307, 1965.
3. V. A. Hattangadi, T. Methasiri, D. M. Nadkarni, R. Ramanna and P. N. Rama Rao, Proceedings of the Symposium on the Physics and Chemistry of Fission, Vienna, 1965, Vol. II, p. 397.
4. A. Gillet, Thu Phong Doan, C. Carles and R. Chastel, Compt. Rend., **262,** 296, 1966.
5. D. M. Nadkarni, Nucl. Phys., **A112,** 241, 1968.
6. I. Kovács, L. Nagy, T. Nagy and I. Vinnay, KFKI Közlemények, **16,** 325, 1968.
7. I. Halpern and V. M. Strutinsky, Proc. 2nd U.N. Int. Conf. on the Peaceful Uses of Atomic Energy, Geneva, 1958, Vol. 15, p. 408.

УГЛОВАЯ АНИЗОТРОПИЯ ОСКОЛКОВ ДЕЛЕНИЯ В ТРОЙНОМ ДЕЛЕНИИ ^{235}U И ^{238}U, ВЫЗВАННАЯ НЕЙТРОНАМИ 14 МЭВ

И. КОВАЧ, Л. НАДЬ и И. ВИННАИ

Резюме

Угловая анизотропия осколков деления ^{235}U и ^{238}U по отношению направления нейтронов с энергией 14 МЭВ оказалась большей в тройном делении по сравнению с наблюдаемой в двойном делении.

Acta Physica Academiae Scientiarum Hungaricae, Tomus 29 (2—3), pp. 243—249 (1970)

THE COLLECTIVE EFFECT OF PARAMAGNETIC AND DIAMAGNETIC IMPURITIES ON THE TEMPERATURE OF SUPERCONDUCTING TRANSITION

By

I. KIRSCHNER, A. STARK

DEPARTMENT FOR ATOMIC PHYSICS, ROLAND EÖTVÖS UNIVERSITY, BUDAPEST

and

I. I. FALKO

M. GORKI UNIVERSITY, KHARKOV, USSR

(Received 4. XI. 1969)

We calculate the dependence of the transition temperature and its derivative with respect to pressure on the concentration of both paramagnetic and diamagnetic impurities. It is shown that the assumption of a Lifshitz singularity in the density of normal single-electronic states results in a good agreement of theoretical predictions with experimental data.

Introduction

It is well known that two mechanisms have been suggested to explain the effect of diamagnetic impurities on the transition temperature: a decrease of anisotropy in electronic interaction [1] and a change in the nature of the Fermi surface topology [2]. The influence of paramagnetic impurities was explained theoretically by A. A. ABRIKOSOV and L. P. GORKOV [3] with no regard to the possibility of a modification in the topology of Fermi surface by adding impurities.

In our work we examine the collective effect of paramagnetic and diamagnetic impurities on the transition temperature when there is a Lifshitz singularity in the density of normal single-electronic states. It is shown that the effects of paramagnetic impurities can be completely eliminated by the subsequent addition of diamagnetic impurities.

Derivation of the basic equations

We represent the Hamiltonian of our system in the form

$$\hat{H}^e+\hat{H}^d+\hat{H}^p \equiv -\frac{1}{2}\sum_{\alpha,\beta}\int \lambda\psi_\alpha^+(\vec{r})\,\psi_\beta^+(\vec{r})\,\psi_\beta(\vec{r})\,\psi_\alpha(\vec{r})\,d\vec{r}+$$

$$+\sum\sum\int \psi_\alpha^+(\vec{r})\,u_{1d}(\vec{r}-\vec{r}_{jd})\,\psi_\alpha(\vec{r})\,d\vec{r}+ \qquad (1)$$

$$+\sum_{\alpha,\beta}\sum_{j_p}\int \psi_\alpha^+(\vec{r})\,[u_{1p}(\vec{r}-\vec{r}_{jp})\,\delta_{\alpha\beta}+u_{2p}(\vec{r}-\vec{r}_{jp})\cdot(\vec{s}\,\vec{\sigma})_{\alpha\beta}]\,\psi_\beta(\vec{r})\,.$$

Here $\hat{H}^e$ is a general interaction between electrons, λ effective interaction potential, $\hat{H}^d$ and $\hat{H}^p$ interaction between electrons and diamagnetic or paramagnetic atoms, respectively, sum over j_p and j_d implies summation over all paramagnetic and diamagnetic impurity atoms, respectively, $\vec{s}$ moment of a paramagnetic atom, $\vec{\sigma}$ the Pauli spin matrices and u_{kl} interaction potentials.

Using matrices [2]

$$\hat{\tau}_1=\begin{pmatrix}\hat{O} & \hat{I}\\ \hat{I} & \hat{O}\end{pmatrix},\quad \hat{\tau}_2=i\begin{pmatrix}\hat{O} & -\hat{I}\\ \hat{I} & \hat{O}\end{pmatrix},\quad \hat{\tau}_3=\begin{pmatrix}\hat{I} & \hat{O}\\ \hat{O} & -\hat{I}\end{pmatrix},$$

$$\vec{\sigma}=\begin{pmatrix}\hat{\sigma}_p & \hat{O}\\ \hat{O} & \hat{\sigma}_p\end{pmatrix},\ \hat{U}=\begin{pmatrix}\hat{I} & \hat{O}\\ \hat{O} & \hat{I}\end{pmatrix},\ \hat{\sigma}_2=\begin{pmatrix}\hat{\sigma}_{p_2} & \hat{O}\\ \hat{O} & \hat{\sigma}_{p_2}\end{pmatrix}=i\begin{pmatrix}0 & -1 & 0 & 0\\ 1 & 0 & 0 & 0\\ 0 & 0 & 0 & -1\\ 0 & 0 & 1 & 0\end{pmatrix} \tag{2}$$

and four-component creation-annihilation operators [4]

$$\Psi(\vec{r})=\begin{pmatrix}\Psi_\uparrow(\vec{r})\\ \Psi_\downarrow(\vec{r})\\ \Psi_\uparrow^+(\vec{r})\\ \Psi_\downarrow^+(\vec{r})\end{pmatrix};\quad \Psi^+(\vec{r})=\{\psi_\uparrow^+(\vec{r}),\,\psi_\downarrow^+(\vec{r}),\,\psi_\uparrow(\vec{r}),\,\psi_\downarrow(\vec{r})\} \tag{3}$$

we can rewrite $\hat{H}^d+\hat{H}^p$ in the form

$$\hat{V}=\sum_{jd}\Psi^+(\vec{r}_{jd})\,u_{1d}\,\hat{\tau}_3\,\Psi(\vec{r}_{jd})+\sum_{jp}\Psi^+(\vec{r}_{jp})[u_{1p}\,\hat{\tau}_3+u_{2p}\,\vec{\alpha}\,\vec{s}_{jp}]\Psi(\vec{r}_{jp})\,, \tag{4}$$

where

$$\vec{\alpha}=\frac{\hat{U}+\hat{\tau}_3}{2}\,\vec{\sigma}+\frac{\hat{U}-\hat{\tau}_3}{2}\,\hat{\sigma}_2\,\vec{\sigma}\,\hat{\sigma}_2\,. \tag{5}$$

We assumed a zero-range interaction between electrons and impurity atoms

$$V(\vec{r})=\sum_{jd}u_{1d}\,\delta(\vec{r}-\vec{r}_{jd})+\sum_{jp}u_{1p}\,\delta(\vec{r}-\vec{r}_{jp})+\sum_{jp}u_{2p}\,\delta(\vec{r}-\vec{r}_{jp})\cdot(\vec{s}_{jp}\,\vec{\sigma}_p). \tag{6}$$

We introduce the 4×4 matrix Green's function [2]

$$g_{\alpha\beta}(1,1')=\begin{pmatrix}\hat{G}(1,1') & \hat{F}(1,1')\\ F^+(1,1') & \hat{G}^{tr}(1,1')\end{pmatrix}=\frac{1}{i}\,\langle\hat{\tau}\Psi_\alpha(1)\,\Psi_\beta(1')\rangle, \tag{7}$$

$$\alpha,\beta=1,2,3,4,$$

where $\langle \ldots \rangle$ stands for both a statistical average and an average over positions and spin directions of paramagnetic and diamagnetic impurities, $\hat{\tau}$ is Wick's operator.

Using standard methods we easily obtain an equation for the Fourier component of the matrix Green's function

$$g_\nu^{-1}(\vec{p}) = \xi_\nu \hat{U} - \varepsilon_{\vec{p}}\,\hat{\tau}_3 - \Delta - \frac{\Gamma_n \pi}{m p_F}\,\hat{\tau}_3 \int \frac{d^3\vec{p}}{(2\pi)^3}\, g_\nu(\vec{p})\,\hat{\tau}_3 - \\ - \frac{1}{3}\,\frac{\pi}{m p_F}\,\Gamma_s\,\vec{\alpha} \int \frac{d^3\vec{p}}{(2\pi)^3}\, g_\nu(\vec{p})\,\hat{\tau}_3 \vec{\alpha}\,, \tag{8}$$

where ν is an odd integer, $\xi_\nu = i\,\pi\nu\,T$, T absolute temperature, $\varepsilon_{\vec{p}}$ electronic energy measured from the Fermi surface, $\hat{\Delta} = \Delta\,\hat{\tau}_1\hat{\sigma}_2$, Δ is a real quantity,

$$\Gamma_n = \frac{1}{\pi}\, m p_F [n_d |u_{1d}|^2 + n_p\,|u_{1p}|^2 \equiv \Gamma_{nd} + \Gamma_{np}$$

and

$$\Gamma_s = \frac{1}{\pi}\, m p_F\, n_p \langle s_j(s_j+1)\rangle\, |u_{2p}|^2$$

are the rates for normal and spin-flip scattering for an electron at the Fermi surface, p_F = Fermi momentum, m electronic mass, n_d and n_d density of diamagnetic and paramagnetic impurities, respectively, $\langle s_j(s_j+1)\rangle$ is an average over $\vec{s}^2$.

To solve Eq. (8) we assume that

$$g_\nu^{-1}(\vec{p}) = \tilde{\omega}(\xi_\nu)\,\hat{U} - \tilde{\varepsilon}_{\vec{p}}(\xi_\nu)\,\hat{\tau}_3 + \hat{\Delta}(\xi_\nu)\,\hat{\tau}_1\hat{\sigma}_2. \tag{9}$$

Determination of the transition temperature

Replacing (9) into (8) we obtain a system of equations for the determination of the unknown functions $\tilde{\omega}(\xi_\nu)$, $\tilde{\varepsilon}_{\vec{p}}(\xi_\nu)$, $\tilde{\Delta}(\xi_\nu)$. If $T = T_k$, then $\tilde{\Delta}(\xi_\nu) = \Delta = 0$. The method of their calculation is similar to that of [2]. Taking into account the low concentration of impurities, we get the next equation for T_k in an approximation of first order

$$-\lambda\, Im \int \frac{d\omega}{\pi} \int d\varepsilon\; th\,\frac{\omega}{2T_k}\, \nu(\varepsilon+\varepsilon_F)\, \frac{\omega + i\,\dfrac{\Gamma_n+\Gamma_s}{2}}{(\omega+i\,\Gamma_s)\left[\left(\omega+i\,\dfrac{\Gamma_n+\Gamma_s}{2}\right)^2 - \varepsilon^2\right]} = 1, \tag{10}$$

where $\nu(\varepsilon + \varepsilon_F)$ is the density of normal single-electronic states and ε is measured from the Fermi surface.

In the case when there is a change in the nature of the Fermi surface topology [5]

$$\nu(\varepsilon) = \nu_0(\varepsilon) + \delta\nu(\varepsilon) \tag{11}$$

we shall consider the generation of an electronic group, and therefore

$$\delta\nu(\varepsilon) = A\sqrt{\varepsilon - \varepsilon_k}\,\Theta(\varepsilon - \varepsilon_k)\,,$$

$$A = \frac{m_1\sqrt{2\,m_3}}{2\,\pi^2}\,, \tag{12}$$

where $\Theta(x)$ is unity for $x > 0$ and zero for $x < 0$, m_1 and m_3 are the principal elements of effective mass tensor.

We assume that

$$\varepsilon_F = \varepsilon_F^0 + \gamma_d\,\Delta Z_d\,\Gamma_{nd} + \gamma_p\,\Delta Z_p\,\Gamma_{np}, \tag{13}$$

where ΔZ_d and ΔZ_p is the difference in the valence of the atoms of the metal and atoms of diamagnetic and paramagnetic impurities, respectively, γ_d and γ_p are numerical constants of order unity.

Since we have the next equation for

$$\lambda\,\nu_0(\varepsilon_F^0)\,\mathrm{Re}\int_0^{\omega_D} d\omega\,\frac{th\,\dfrac{\omega}{2T_k}}{\omega + i\Gamma_s} - \lambda A\,\mathrm{Re}\int_0^{\omega_D} d\omega\,\frac{th\,\dfrac{\omega}{2T_k}}{\omega + i\Gamma_s}\left(\sqrt{\alpha - \omega} - \sqrt{\alpha^* + \omega}\right) = 1, \tag{14}$$

where

$$\alpha = \alpha_d\,\Delta Z_d\,\Gamma_{nd} + \alpha_p\,\Delta Z_p\,\Gamma_{np} - i\,\frac{\Gamma_n + \Gamma_s}{2} + \varepsilon_F^0 - \varepsilon_k\,,$$

$$\alpha^* = \alpha_d\,\Delta Z_d\,\Gamma_{nd} + \alpha_p\,\Delta Z_p\,\Gamma_{np} + i\,\frac{\Gamma_n + \Gamma_s}{2} + \varepsilon_F^0 - \varepsilon_k\,.$$

In agreement with the experimental situations we consider the case

$$\frac{|\alpha|}{2\,T_k} \leq 1\,, \quad \frac{\Gamma_s}{2\,T_k} \leq 0{,}1$$

at a fixed concentration of paramagnetic impurities. The second part of Eq. (14) is expanded into a power series. We have

$$\int_0^{\omega_D} d\omega\,\frac{th\,\dfrac{\omega}{2\,T_k}}{\omega + i\Gamma_s}\left[(\alpha - \omega)^{1/2} - (\alpha^* + \omega)^{1/2}\right] =$$

$$= (2\,T_k)^{1/2}\left\{\int_0^{\omega_D/2T_k} d\omega\,\frac{th\,\omega}{\omega + i\Gamma_s/2\,T_k}\left[i\omega^{1/2} - \frac{i\alpha}{4T_k\,\omega^{1/2}} - \omega^{1/2} -\right.\right.$$

$$-\frac{\alpha^*}{4T_k\omega^{1/2}}+\dots\Big]+\int_0^{|\alpha|/2T_k} d\omega\,\frac{th\,\omega}{\omega+i\Gamma_s/2\,T_k}\Big[\Big(\frac{\alpha}{2T_k}\Big)^{1/2}-$$
$$-\frac{\omega}{2\left(\frac{\alpha}{2\,T_k}\right)^{1/2}}-\Big(\frac{\alpha^*}{2\,T_k}\Big)^{1/2}-\frac{\omega}{2\left(\frac{\alpha^*}{2\,T_k}\right)^{1/2}}+\dots\Big]- \tag{15}$$
$$-\int_0^{|\alpha|/2T_k} d\omega\,\frac{th\,\omega}{\omega+i\Gamma_s/2\,T_k}\Big[i\omega^{1/2}-\frac{i\alpha}{4\,T_k\,\omega^{1/2}}-\omega^{1/2}-\frac{\alpha^*}{4\,T_k\,\omega^{1/2}}\Big]\Big\}.$$

Leaving only the terms of first order with respect to $\Gamma_s/2\,T_k$ we obtain after simple calculation the following result

$$\frac{\Delta T_k}{T_k^0}=a(\Gamma_s)-\frac{A}{\nu_0(\varepsilon_F^0)}\Big\{\frac{\mathrm{Re}\,\alpha^{1/2}\,|\alpha|^{1/2}}{T_k}-\frac{\mathrm{Im}\,\alpha^{1/2}\,\Gamma_s}{2\,T_k}+$$
$$+2\,\Gamma_s^{1/2}+\frac{|\alpha|^{3/2}}{3\,T_k}+\frac{\mathrm{Im}\,\alpha-\mathrm{Re}\,\alpha}{2\,(2\,T_k)^{1/2}}\Big[C-2\Big(\frac{|\alpha|}{2\,T_k}\Big)^{1/2}+ \tag{16}$$
$$+\frac{3}{\sqrt{2}}\arctan\Big(\Big(\frac{2\,|\alpha|}{\Gamma_s}\Big)^{1/2}-1\Big)+\frac{3}{\sqrt{2}}\,\frac{\pi}{4}\Big]-$$
$$-2\,\Gamma_s^{1/2}\Big[\frac{1}{2\sqrt{2}}\arctan\Big(\Big(\frac{2\,|\alpha|}{\Gamma_s}\Big)^{1/2}-1\Big)+\frac{\pi}{8\sqrt{2}}-$$
$$-\frac{1}{4\sqrt{2}}\ln\frac{|\alpha|+\sqrt{2}\,|\alpha|^{1/2}\,\Gamma_s^{1/2}+\Gamma_s}{|\alpha|-\sqrt{2}\,|\alpha|^{1/2}\,\Gamma_s^{1/2}-\Gamma_s}\Big]\Big\},$$

where $a(\Gamma_s)$ is due to the first part of Eq. (14) as a result of the ABRIKOSOV—GORKOV theory, and $2<C=\mathrm{const}<2.5$.

As a next step we shall calculate the dependence of T_k on the pressure P at a zero concentration of paramagnetic impurities. The derivation of T_k with respect to pressure leads to the relation

$$\frac{dT_k}{dP}(\Gamma_{nd})=C'\big(\omega_d,\nu_0(\varepsilon_F^0)\big)+\frac{A}{\nu_0(\varepsilon_F^0)}\,\frac{d\varepsilon_F^0}{dP}\Big[\frac{CT_k^{1/2}}{2\sqrt{2}}-\frac{|\alpha|^{1/2}}{2}- \tag{17}$$
$$-\frac{|\mathrm{Re}\,\alpha|+|\alpha|}{2\,\mathrm{Re}\,\alpha^{1/2}}-\frac{|\mathrm{Re}\,\alpha|}{|\alpha|}\Big(\mathrm{Re}\,\alpha^{1/2}-\frac{|\alpha|}{2}+\frac{\mathrm{Re}\,\alpha-\mathrm{Im}\,\alpha}{4\,|\alpha|^{1/2}}\Big)\Big].$$

These results are in good agreement with experimental data [6], [7], [8].

Appendix

We show for a pure superconductor that $\Delta = \lambda F(1, 1)$ is the energy gap. We determine the Green's function

$$\begin{aligned} G_{\alpha\beta}(x, x') &= -i\langle\hat{\tau}\psi_\alpha(x)\,\psi_\beta^+(x')\rangle\,, \\ \psi_\alpha(x) &= e^{iHt}\,\psi_\alpha(\vec{x}, 0)\,e^{-iHt}\,, \\ x &= \vec{x}, t\,. \end{aligned} \tag{A(1)}$$

If we neglect the effects of scattering of particles by one another we obtain the next equation for the Green's function, using Wick's theorem

$$\begin{aligned} &\left(i\frac{\partial}{\partial t} + \frac{\nabla^2}{2m} + \mu\right) G(x-x') + \Delta F^+(x-x') = \delta(x-x')\,, \\ &\left(-i\frac{\partial}{\partial t} + \frac{\nabla^2}{2m} + \mu\right) F^+(x-x') - \Delta^* G(x-x') = 0\,, \end{aligned} \tag{A(2)}$$

where

$$\begin{aligned} F^+_{\alpha\beta}(x, x') &= -i\langle\tau\psi_\alpha^+(x)\,\psi_\beta^+(x')\rangle, \\ F_{\alpha\beta}(x, x') &= -i\langle\tau\psi_\alpha(x)\,\psi_\beta(x')\rangle, \\ \Delta &= \lambda F(0^+)\,,\ \Delta^* = \lambda F^+(0^+) \end{aligned} \tag{A(3)}$$

and μ is chemical potential.

In a similar way we derive the equation for $F(x, x')$. The complete system of equations we represent in the following compact matrix form

$$\begin{pmatrix} i\frac{\partial}{\partial t} + \frac{\nabla^2}{2m} + \mu & \Delta \\ -\Delta^* & -i\frac{\partial}{\partial t} + \frac{\nabla^2}{2m} + \mu \end{pmatrix} \times \begin{pmatrix} G(x-x') & F(x-x') \\ F^+(x-x') & -G(x'-x) \end{pmatrix} = \delta(x-x')\,. \tag{A(4)}$$

Using Fourier transformation

$$g(x-x') = iT\sum_\nu \int \frac{d^3\vec{p}}{(2\pi)^3}\, g_\nu(\vec{p})\, e^{i\vec{p}(\vec{r}-\vec{r}') - i\xi_\nu(t-t')}, \tag{A(5)}$$

where $\xi_\nu = i\,\pi\nu\,T$ and ν is an odd integer, we get the following relation for the Fourier components of Eq. A (4)

$$\begin{aligned} (\xi_\nu - \varepsilon_{\vec{p}})\,G_\nu(\vec{p}) + \Delta F_\nu^+(\vec{p}) &= 1\,, \\ (\xi_\nu - \varepsilon_{\vec{p}})\,F_\nu^+(\vec{p}) + \Delta^* G_\nu(\vec{p}) &= 0\,. \end{aligned} \tag{A(6)}$$

Hence,

$$G_\nu(\vec{p}) = -\frac{\xi_\nu + \varepsilon_{\vec{p}}}{\varepsilon_{\vec{p}}^2 + \Delta^2 - \xi_\nu^2}, \quad F_\nu^+(\vec{p}) = \frac{\Delta^*}{\varepsilon_p^2 + \Delta^2 - \xi_\nu^2}. \qquad \text{A(7)}$$

Therefore, it is shown that Δ is in fact the energy gap.

REFERENCES

1. D. Markovitz and L. P. Kadanoff, Phys. Rev., **131,** 564, 1963.
2. I. I. Falko, V. G. Bariakhtar and V. I. Makarov, JETP, **49,** 1858, 1965.
3. A. A. Abrikosov and L. P. Gorkov, JETP, **39,** 1781, 1960.
4. L. P. Kadanoff and I. I. Falko, Phys. Rev., **136,** A 1170, 1964.
5. I. M. Lifshitz, JETP, **38,** 1569, 1960.
6. B. G. Lazarev, L. S. Lazareva, V. I. Makarov, T. A. Ignateva, JETP, **46,** 829, 1964.
7. B. G. Lazarev, L. S. Lazareva, V. I. Makarov, JETP, **43,** 2311, 1962.
8. M. F. Merriam, S. M. Liu, D. P. Seraphim, Phys. Rev., **136,** A 17, 1964.

СОВМЕСТНОЕ ВЛИЯНИЕ ПАРА- И ДИАМАГНИТНЫХ ПРИМЕСЕЙ НА ТЕМПЕРАТУРУ СВЕРХПРОВОДЯЩЕГО ПЕРЕХОДА

И. КИРШНЕР, А. ШТАРК и И. И. ФАЛЬКО

Резюме

Выводится зависимость температуры перехода и её производной по давлению от концентрации пара- и диамагнитных примесей. Показано, что предположение об особенности в плотности одноэлектронных состояний приводит к хорошему согласию теоретических предсказаний с опытными данными.

Acta Physica Academiae Scientiarum Hungaricae, Tomus 29 (2—3), pp. 251—265 (1970)

COMPLEX POLES, CUTS, INDEFINITE METRIC AND UNITARITY

By

K. L. NAGY

INSTITUTE FOR THEORETICAL PHYSICS OF THE ROLAND EÖTVÖS UNIVERSITY, BUDAPEST

(Received 11. XI. 1969)

In connection with LEE—WICK's electrodynamics, unitarity problems are discussed on exactly soluble models with complex ghosts.

1. Recently T. D. LEE and G. C. WICK [1—4] proposed that an indefinite metric field theory, when only complex ghosts are allowed, might yield a completely finite, probabilistically interpretable field theory. It is seen that causality is certainly violated, but by fixing some parameters appropriately this violation cannot be observed experimentally. At the same time (physical) unitarity is stated to be held. This is the point we wish to discuss here.

It is well known that indefinite metric field theories in general do not give a unitary S-matrix. Some ways out of this difficulty have been proposed by HEISENBERG (see e.g. [5]), FROISSART [6], BOGOLJUBOV [7], SUDARSHAN [8], YOKOYAMA [9], SHIMODAIRA [10], etc. Another possibility also arises when only complex ghosts are present. Let us suppose that in a theory the Hamiltonian possesses the following eigenstate structure: For real eigenvalues all eigenstates $|E, \text{phys}\rangle$ are physical with $+1$ norms. Beside these there should be complex eigenvalues belonging to non-physical states $|E_c\rangle$ and then these vectors form a complete system. Then, the theory is probabilistically interpretable. An extremely simple proof runs as follows [11]. Let us consider a physical "in" state and analyze it in terms of "out" states. Because of the supposed completeness

$$|E, \text{phys; in}\rangle = \Sigma\, a(u)\, |E, \text{phys; out}\rangle + \Sigma\, b(u)\, |E_c\rangle . \tag{1}$$

By applying $H - E$ on both sides it follows that $b(u) = 0$, so that $\Sigma\, a^*(u)a(u) = +1$ preserving interpretability. If we pay some attention to degeneracy and to the fact that we are in the continuous spectrum nothing can be wrong with this argument.

In [1—4] it is supposed that complex eigenvalues appear in complex conjugate pairs. Since this fact concerns us from the point of view of interpretability, let us settle this question first.

A state vector space H with indefinite metric is a linear space with a scalar product fulfilling all the axioms for the scalar product, except $\langle A \mid A\rangle > 0$. If there exists at least one vector $\mid A\rangle \neq 0$, $\langle A \mid A\rangle = 0$, orthogonal also to all the other vectors, H is called a vector space with degenerate metric. Now this case can be excluded. Let us suppose we have a state with $\langle A \mid B\rangle = 0$ for all $\mid B\rangle$ including $\mid A\rangle$. Then in relevant physical quantities like $\langle 0 \mid \varphi(x)\,\psi(y) \mid 0\rangle$ after substituting a complete system in the middle, because of orthogonality $\mid A\rangle$ does not give any contribution. $\mid A\rangle$ is not a ghost which, just by definition, through its possible mysterions action here and there we may meet, but an unobservable state. Therefore the degenerate case may be omitted.

In each state vector space with an indefinite metric it is easy to prove that for an Hermitian operator over the space (in the physical literature it is called pseudohermitian) the following are fulfilled:

$$\bar{P} = \langle A \mid P \mid A\rangle = \text{real}\,, \tag{2}$$

$$(p^* - p)\langle p \mid p\rangle = 0\,, \tag{3}$$

$$(p_1^* - p_2)\langle p_1 \mid p_2\rangle = 0\,, \quad \text{if} \quad (P - p_i)\mid p_i\rangle = 0\,. \tag{4}$$

We must investigate whether it is possible for a Hermitian operator, let us say the Hamiltonian, to have a complex eigenvalue without its complex conjugate pair. Suppose that $p = a + ib$, $b \neq 0$ is such a single eigenvalue. From Eq. (3) for each eigenstate $\langle p \mid p\rangle = 0$, and from Eq. (4) it is orthogonal to all the eigenstates with other eigenvalues. Let us suppose we have a degenerate eigenvalue problem. Therefore, $\mid p\rangle_1$ and $\mid p_2\rangle$ are also eigenstates to p. Then for all α, β $\mid\rangle = \alpha \mid p_1\rangle + \beta \mid p_2\rangle$ is also an eigenstate. Therefore $\langle\mid\mid\rangle = 0$. Since α and β are arbitrary, ${}_1\langle p \mid p\rangle_2 = 0$. Therefore, in a field theory with a non-degenerated metric, when the eigenvectors of a Hermitian operator form a complete system, the possibility of a complex eigenvalue, without its complex conjugate pair is excluded.

In a vector space with indefinite metric, even in a finite dimensional space it is not certain whether the eigenvectors of a Hermitian operator form a complete system. But then a dipole or multipole ghost situation appears. The interpretability of such a theory must be, and has been, frequently investigated [5, 6, 11]. Even in this case the dipole ghost must belong to a real eigenvalue. Then,

$$\bar{H} = \langle A \mid H \mid A\rangle$$

is real (H pseudohermitian) for each state. With

$$|A\rangle = \alpha\,|E\rangle + \beta|D\rangle\,,$$

$$\bar{H} = \alpha^*\,\beta E\,\langle E|D\rangle + \beta^*\,\alpha E\,\langle D|E\rangle + \beta^*\,\beta(E\,\langle D|D\rangle + \lambda\,\langle D|E\rangle)\,.$$

If $\alpha = 0$, the sum of the third and fourth terms is real, therefore for all α, β

$$(\alpha^* \beta \langle E|D\rangle + C.C.)\, E = \text{real}.$$

Because of the non degenerated metric $\langle E \mid D\rangle \neq 0$, so E must be real. The case of two diple ghosts to complex conjugated eigenvalues is of course not excluded. Therefore, let us accept, in accordance with [1—4], that the eigenvalues of the physical variables (esp. the Hamiltonian) appear in complex conjugate pairs; $E_c^+ = (E_c^-)^*$ with the eigenvectors $\mid E_c^+\rangle$, $\mid E_c^-\rangle$, respectively.

But then a situation required by (1) hardly seems to be realizable. Namely, let us suppose that in the one particle sector Eq. (1) is satisfied, with $\mid E_c^+\rangle \neq 0$, $\mid E_c^-\rangle \neq 0$. In elementary particle physics it is generally accepted that the length of the interaction among particles is short enough to allow factorized in-going and out-going states. Then states like $\mid E_c^+\rangle \times$ $\times \mid E_c^-\rangle$ appear e.g. in the two particle sector with the real eigenvalue $E_c^+ + E_c^-$. On the other hand such states take away from the norm of the (physical) in-going state, therefore the physical S-matrix ceases to be unitary. Against this simple argument there stand two facts; one must consider the interplay of more than one physical variable (namely the four momenta), and also that the scattering eigenstates belong to the continuous spectrum. Concerning the first problem we discuss some models; concerning the second we remark beforehand that in (1) the Σ sign possesses only a symbolic meaning. One gets even then an interpretable theory when, in developing the physical "in" state, we find

$$|E, \text{phys. in}\rangle = \Sigma a(u)|E, \text{phys; out}\rangle + \Sigma c(u)|E, \text{non phys; out}\rangle\,, \qquad (5)$$

E is always real, but the set of $\mid E$, non phys.$\rangle$ states appearing in (5) are of zero measure.

2. Actually one might say that model theories where some relevant particles are considered to be infinitely heavy (i.e. without three momenta) violate (physical) unitarity. Let us elucidate this with a simple argument in the Lee model complex ghost case. Here unitarity survives, of course, in the $N - \Theta$, $N - 2\Theta$, ... $N - n\Theta$, sectors. Consider, however, the scattering 3Θ on $2N$. The initial energy eigenvalue is then real. In the end state then besides the state $\mid 2N, 3\Theta\rangle$ complex ghost V-particle packets $\mid E_c^+\rangle$ around the point let us say x_1, $\mid E_c^-\rangle$ around the point x_2, + one Θ packet may appear, and conversely. Since the eigenvalues E_c^+, E_c^- are complex conjugated the total energy is real. The superposition of these states

$$C_1|E_c^+(x_1)\,, E_c^-(x_2)\,, \Theta\rangle + C_2\,|E_c^+(x_2)\,, E_c^-(x_1)\,, \Theta\rangle$$

both having zero norm but not being orthogonal may give any positive or negative squared norm different from zero. Violation of unitarity was indeed

proved here by a direct calculation in a paper by S. TANAKA [12] where ideas similar to [1—4] were first proposed. The same was also shown in [13, II]. These papers have been devoted just to find some trick to avoid this difficulty. In [13, I] two versions of the model were treated. One is the original one with

$$\varrho_{1,2}(\omega) = 2\sqrt{\frac{\omega}{|k|}} f(k) \begin{cases} \sin |k| \dfrac{L}{2} \\ \\ \cos |k| \dfrac{L}{2} \end{cases} .$$

Taking this literally, unitarity should hold for all L. This is not so (c.f. also [13, I] p. 4). For example for $L = 0$ where no physical standing wave bound state might occur this is explicitly seen from (4.15). The second version takes $\varrho_1^2 = \varrho^2(\omega)$, $\varrho_2^2 = \varrho^2(\omega)\,(1 + \alpha)$. With this choice the stable state which would lead to the violation of unitarity indeed moves off the real axis in the $N, N' - 2\Theta$ sector. This, however, only transfers the non-unitarity into the sector $2N, 2N' - 4\Theta$. The price was to introduce some new feature, a new parameter. This also refers to [13, II]. Let us show here the violation of unitarity on a most simple model of such a type.

Consider the model with the Hamiltonian $H = H_0 + H_1$,

$$\begin{aligned} H_0 &= m_v \psi_v^* \psi_v + m_N \psi_N^* \psi_N + \int w(k)\, a^*(k)\, a(k)\, d^3k + MA^* B + M^* B^* A\,, \\ H_1 &= -\int (8\pi\omega)^{-1/2} \left(\psi_v^* a(k)\, \psi + \psi^* a^*(k)\, \psi_v\right) d^3k\,, \\ \psi &= g\psi_N + g_1 A + g_2 B,\ \omega = \sqrt{k^2 + m_\Theta^2}\,,\ M = m + i\Gamma, \end{aligned} \tag{6}$$

and for the commutators we prescribe

$$\begin{gathered} [\psi_v, \psi_v^*] = [\psi_{N1}\, \psi_N^*] = [A, B^*] = [B, A^*] = 1\,, \\ [a(k), a^*(k')] = \delta(k - k')\,. \end{gathered} \tag{7}$$

All the other commutators vanish. With this choice, to the original Lee model we have adopted the non-physical fields A and B in the above form. From our point of view the presence of a cut-off is quite irrelevant. Therefore, in expressions containing $g - s$ from H_1 everywhere $(2\omega)^{-1/2} \to f(\omega)$ is understood; $f(\omega)$ is an appropriate cut-off function. Then m_Θ, m_v, m_N, m, Γ and $g - s$ are finite real numbers. The solution of (6) and (7) is constructed as usual on a vacuum state $|0\rangle$ defined by

$$a|0\rangle = \psi_v|0\rangle = \psi_N|0\rangle = A|0\rangle = B|0\rangle = 0,\ \langle 0|0\rangle = 1\,.$$

A most simple check gives:

$$H\,|0\rangle = (H - m_N)\,\psi_N^*\,|0\rangle = (H-\omega)\,a^*(k)\,|0\rangle = \\ = (H-M)\,A^*\,|0\rangle = (H-M^*)\,B^*\,|0\rangle = 0\,, \tag{8}$$

i.e. the real vacuum N, Θ particle states are the corresponding bare ones, and for A and B a complex ghost situation occurs, with

$$|E_c^+\rangle = A^*\,|0\rangle,\ |E_c^-\rangle = B^*\,|0\rangle,\ \langle E_c^+|E_c^+\rangle = \langle E_c^-|E_c^-\rangle = 0,\ \langle E_c^+|E_c^-\rangle = 1\,, \tag{9}$$

the state vector space is a space with indefinite metric, of course. In the following we put $m_N = 0$.

Let us investigate first the $N - \Theta$ scattering sector. Here a general state possesses the form

$$|E\rangle = \left(\alpha\psi_v^* + \psi_N^* \int \varphi(k)\,a^*(k)\,d^3k + \right. \\ \left. + A^* \int \varphi_1(k)\,a^*(k)\,d^3k + B^* \int \varphi_2(k)\,a^*(k)\,d^3k\right)|0\rangle\,, \tag{10}$$

with the norm

$$\langle E|E\rangle = \alpha^*\,\alpha + \int \varphi^*\,\varphi\,d^3k + \int (\varphi_1^*\,\varphi_2 + \varphi_2^*\,\varphi_1)\,d^3k\,. \tag{11}$$

The eigenvalue equation $H\,|\,E\rangle = E\,|\,E\rangle$ gives immediately

$$(\omega - E)\,\varphi = (8\pi\omega)^{-1/2}\,\alpha g\,, \\ (\omega + M - E)\,\varphi_1 = (8\pi\omega)^{-1/2}\,\alpha g_1\,. \\ (\omega + M^* - E)\,\varphi_2 = (8\pi\omega)^{-1/2}\,\alpha g_2\,, \\ (m_v - E)\,\alpha = \int (8\pi\omega)^{-1/2}\,(g\varphi + g_1\,\varphi_2 + g_2\,\varphi_1)\,d^3k\,.$$

For the physical $N - \Theta$ scattering, a plane wave appears only in $\varphi(k)$, $E(k)$ real, $E = \sqrt{k_0^2 + m_\Theta^2}$; since only s-wave scattering occurs

$$\varphi = k_0^{-1}\,(4\pi)^{-1/2}\,\delta(k - k_0) + \alpha g (8\pi\omega)^{-1/2}\,(\omega - E \mp i\varepsilon)^{-1}, \\ \varphi_1 = \alpha g_1 (8\pi\omega)^{-1/2}\,(\omega + M - E)^{-1}\,, \\ \varphi_2 = \alpha g_2\,(8\pi\omega)^{-1/2}\,(\omega + M^* - E)^{-1}, \\ h\,(E \pm i\,\varepsilon)\ \alpha_{\substack{\text{out} \\ \text{in}}}(E) = g\,k_0\,(2\,E)^{-1/2}, \tag{12}$$

$$h(z) = m_v - z - g^2 \int \frac{k^2\,dk}{2\,\omega(\omega - z)} - \\ - g_1\,g_2 \int \frac{k^2\,dk}{2\,\omega}\left[\frac{1}{\omega + M - z} + \frac{1}{\omega + M^* - z}\right]. \tag{13}$$

One might notice here also the main role of the indefinite metric. With $g^2 = -g_1 g_2$, $h(z)$ is less divergent even without cut off. From (12) and (13) the S-matrix is

$$S = e^{2i\delta(E)} = 1 + i\pi(2E)^{-1/2} g\alpha_{\text{out}} = 1 + \frac{i\pi g^2 k_0}{h(E+i\varepsilon)},$$

which is unitary. It exhibits beside the physical cut two further cuts parallel to the real axis starting from $m_\Theta + m \pm i\Gamma$ on the physical sheet. These cuts are direct consequences of the one particle complex ghosts $|E_c^+\rangle$, $|E_c^-\rangle$. The function $h(z)$ also contains a pole (or poles) corresponding to the real V-particle. This behaviour is, so far, quite typical for such theories and nothing is wrong with the interpretability.

Taking into account the simple structure of H and which was said before, violation of unitarity can be expected in the $2N - \Theta$ sector first. Here a general state is

$$\begin{aligned} |E\rangle = [&(\alpha\varphi_N^* + \alpha_1 A^* + \alpha_2 B^*)\psi_v^* + \int \{\psi_N^* \psi_N \Phi(k) + \\ &+ A^* \psi_N^* \Phi_1(k) + B^* \psi_N^* \Phi_2(k) + A^* A^* \Phi_3(k) + \\ &+ A^* B^* \Phi_4(k) + B^* B^* \Phi_5(k)\} a^*(k)\, d^3 k]\, |0\rangle . \end{aligned} \tag{14}$$

From the eigenvalue equation $H|E\rangle = E|E\rangle$ one gets nine equations; three of these are, e.g.

$$\begin{aligned} (2m_N + \omega - E)\Phi(k) &= (8\pi\omega)^{-1/2} \alpha g , \\ (M + M^* + \omega - E)\Phi_4(k) &= (\alpha_1 g_2 + \alpha_2 g_1)(8\pi\omega)^{-1/2}, \\ (m_v + m_N - E)\alpha &= \int (8\pi\omega)^{-1/2} (2g\Phi + g_1\Phi_2 + g_2\Phi_1)\, d^3 k . \end{aligned} \tag{15}$$

Again for the physical $2N - \Theta$ scattering (s wave) a Dirac δ appears only in $\Phi(k)$, and a straightforward calculation gives the S-matrix

$$S = e^{2i\delta(E)} = 1 + i\pi(2E)^{-1/2} g\alpha_{\text{out}} = 1 + \frac{2\, i\pi g^2 k_0}{g(E+i\varepsilon)},$$

$$g(z) = \text{Det}\begin{vmatrix} A & B & C \\ D & E & F \\ G & H & I \end{vmatrix} \cdot \left(\text{Det}\begin{vmatrix} E & F \\ H & I \end{vmatrix}\right)^{-1},$$

$$\begin{aligned} A(z) &= m_v + m_N - z - 2g^2 J(m_N, m_N; z) - \\ &\quad - g_1 g_2 [J(m_N, M; z) + J(m_N, M^*; z)], \\ E(z) &= m_v + M - z - 2 g_1 g_2 J(M, M; z) - g^2 J(m_N, M; z) - \\ &\quad - g_1 g_2 J(M, M^*; z), \; I(z) = E(M \leftrightarrows M^*; z), \end{aligned}$$

$$B(z) = -gg_2 J(m_N, M; z), \quad C(z) = -gg_1 J(m_N, M^*; z),$$
$$D(z) = -gg_1 J(m_N, M; z), \quad F(z) = -g_1^2 J(m, M^*; z),$$
$$G(z) = -gg_1 J(m_N, M^*; z), \quad H(z) = -g_2^2 J(M, M^*; z),$$
$$J(x, y; z) = \int \frac{k^2\, dk}{2\omega(x+y+\omega-z)}.$$

$g(z)$ now possesses four complex cuts starting from $m_N + m + m_\Theta \pm i\,\Gamma$, $m_N + m_\Theta + 2(m \pm i\,\Gamma)$ and S is explicitly seen not to be unitary above $2\,m + m_\Theta$. The reason, obviously, is the appearance of the non physical A and B particle pair with real total energy in the end state.

Next we deal with the fact that the introduction of three momenta might change the situation considerably.

3. Unitarity in [3] was explicitly studied in several graphs of some models with $f\psi^m\Phi^n$ type of interactions. We list them.

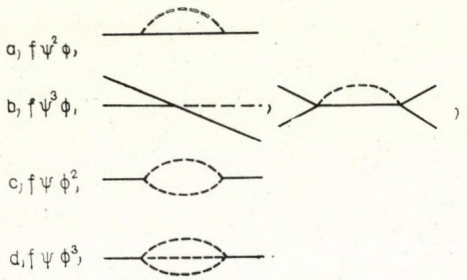


Fig. 1

Violation of (physical) unitarity might occur first in these models when two non physical boson lines appear in the end state. Thus, e.g. for

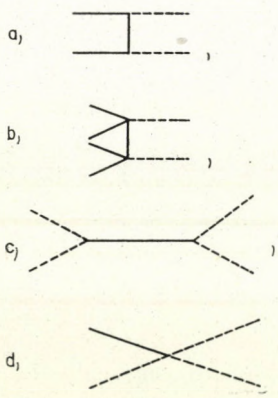


Fig. 2

When we wish to study only the scattering of physical particles these diagrams have to be doubled. Then violation of unitarity appears as un unwanted branch point on the real axis. Thus,

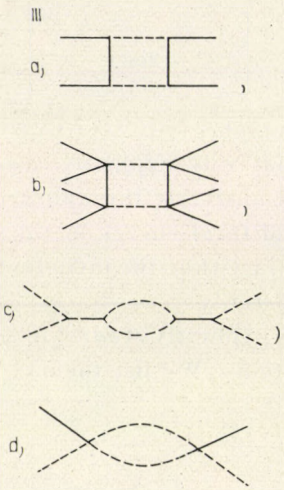


Fig. 3

are interesting diagrams. III. a) was studied by COLEMAN and GLASHOW [14] and in [3] the interesting case I. c). Both of these calculations show that if we first take the centre of mass system and calculate the S-matrix here, unitarity is violated, while in any other system unitarity survives. How this happens formally is clearly seen from [3], [4] and [14]. Here we show it avoiding any reference to any perturbation method, which seems us to be most important, on exactly soluble models for the cases III. c) and d). In connection with the indefinite metric calculations we use the η-less formalism [5, 11]; otherwise, we take H_0 from [3] (cf. Appendix).

4. We treat the model defined by the Hamiltonian $H = H_0 + H_1$,

$$\begin{aligned} H_0 &= \int v(k)\,\psi^*(k)\,\psi(k)\,d^3k + \int v_1(k)\,a_1^*(k)\,a_1(k)\,d^3k + \\ &+ \int v_2(k)\,a_2^*(k)\,a_2(k)\,d^3k + \int \omega(k)\,b^*(k)\,c(k)\,d^3k + \\ &+ \int \omega^*(k)\,c^*(k)\,b(k)\,d^3k\,, \end{aligned} \tag{16}$$

$$v(k) = \sqrt{k^2+\mu^2}\,,\ v_i(k) = \sqrt{k^2+m_i^2}\,,\ \omega(k) = \sqrt{k^2+M^2}\,,$$

k denotes the three-momentum, μ^2, m_i^2 real, M^2 complex. ψ, a_i are three physical fields, b and c describes particles with complex conjugated M^2.

$$H_1 = g \iint \{\psi^*(k)\,[f_1(q,k)\,a_1(q)\,a_2(k-q) + \\ + f_2(q,k)\,c(q)\,b(k-q)] + \\ + \psi(k)\,[f_1^*(q,k)\,a_1^*(q)\,a_2^*(k-q) + \\ + f_2^*(q,k)\,c^*(q)\,b^*(k-q)]\}\,d^3k\,d^3q\,. \tag{17}$$

The commutation relations are

$$[\psi(k), \psi(k')]_{+(\text{or}-)} = [a_1(k), a_1^*(k')] = [a_2(k), a_2^*(k')] = \\ = [c(k), b^*(k')[= [b(k), c^*(k')] = \delta(k-k')\,, \tag{18}$$

all the other commutators vanish. It simply follows

$$H|0\rangle = \big(H - v_i(k)\big)\,a_i^*(k)|0\rangle = \big(H-\omega(k)\big)\,b^*(k)|0\rangle = \big(H-\omega^*(k)\big)\,c^*(k)|0\rangle\,.$$

$|\,0\rangle$ is defined by

$$a_i|0\rangle = \psi|0\rangle = b|0\rangle = c|0\rangle = 0\,,\quad \langle 0|0\rangle = 1\,.$$

With

$$|k;\omega(k)\rangle = b^*(k)|\,0\rangle\,,\ |k;\omega^*(k)\rangle = c^*(k)|0\rangle\,,$$
$$\|\|k;\omega(k)\rangle\| = \|\|k,\omega^*(k)\rangle\| = 0,\quad \langle k,\omega|k',\omega^*\rangle = \delta(k-k')$$

a complex ghost one-particle pair of the total H appeared. Newt we turn to the real ψ-particle (a_1, a_2 scattering) sector. Here an exact eigenstate possesses the form

$$|E\rangle = [\int \varphi(k)\,\psi^*(k)\,d^3k + \iint \Phi_1(q_1,q_2)\,a_1^*(q_1)\,a_2^*(q_2)\,d^3q_1\,d^3q_2 + \\ + \iint \Phi_2(q_1,q_2)\,c^*(q_1)\,b^*(q_2)\,d^3q_1\,d_3q_2]\,|0\rangle\,, \tag{19}$$

with the norm

$$\langle E'|E\rangle = \int \varphi^{*\prime}(k)\,\varphi(k)\,d^3k + \iint \Phi_1'^*(q_1,q_2)\,\Phi_1(q_1,q_2)\,d^3q_1\,d^3q_2 + \\ + \iint \Phi_2'^*(q_2,q_1)\,\Phi_2(q_1,q_2)\,d^3q_1\,d^3q_2\,. \tag{20}$$

Notice that the last term is not positive definite, as it must be in indefinite metric. From $H\,|\,E\rangle = E\,|\,E\rangle$ one obtains

$$\big(v(k)-E\big)\,\varphi(k) = -g\int [f_1(q,k)\,\Phi_2(q,k-q) + f_2(q,k)\,\Phi_1(k-q,q)]\,d^3q \\ \big(v_1(q_1)+v_2(q_1)-E\big)\,\Phi_1(q_1,q_2) = -g\varphi(q_1+q_2)\,f_1^*(q_1,q_1+q_2)\,, \\ \big(\omega^*(q_1)+\omega(q_2)-E\big)\,\Phi_2(q_1,q_2) = -g\varphi(q_1+q_2)\,f_2^*(q_1,q_1+q_2)\,. \tag{21}$$

For the physical a_1, a_2 scattering with in-going or outgoing waves

$$\Phi_1(q_1,q_2) = \delta(q_1-q_1^0)\,\delta(q_2-q_2^0) - \frac{g\varphi_{\mp}(q_1+q_2)\,f_1^*(q_1,q_1+q_2)}{v_1(q_1)+v_2(q_2)-E\mp i\varepsilon}\,,$$

$$\Phi_2(q_1, q_2) = -\frac{g\varphi_\mp(q_1+q_2) f_2^*(q_1, q_1+q_2)}{\omega^*(q_1)+\omega(q_2) - E \mp i\varepsilon},$$

$$\left(v(k) - E - g^2 \int \frac{|f_1(q,k)|^2 d^3q}{v_1(q)+v_2(k-q)-E\mp i\varepsilon} - \right. \tag{22}$$

$$\left. - g^2 \int \frac{f_2(q,k) f_2^*(k-q,k)\, d^3q)}{\omega^*(k-q)+\omega(q)-E\mp i\varepsilon}\right) \varphi_\mp(k) = -gf_1(q_1^0, k)\delta(k-q_1^0-q_2^0),$$

$$E = \sqrt{q_1^{02}+m_1^2} + \sqrt{q_2^{02}+m_2^2}.$$

Defining

$$h(k,z) = v(k) - z - g^2 \int \frac{|f_1(q,k)|^2 d^3q}{v_1(q)+v_2(k-q)-z} - \tag{23}$$

$$- g^2 \int \frac{f_2(q,k) f_2^*(k-q,k)\, d^3q}{\omega^*(k-q)+\omega(q)-z},$$

the real ψ particle energy eigenvalues are given by

$$h(k, E) = 0.$$

Notice that $h^*(k,z) = h(k,z^*)$ for real k. From (20), for the scattering states (19), (22), a tedious but straightforward calculation gives

$$\langle q_1^{0\prime}, q_2^{0\prime}, E'; \overset{\text{in}}{\text{out}} | q_1^0, q_2^0, E; \overset{\text{in}}{\text{out}} \rangle = \delta(q_1^{0\prime} - q_1^0)\,\delta(q_2^{0\prime} - q_2^0),$$

and the S-matrix is

$$\langle q_1^{0\prime}, q_2^{0\prime}, E'; \text{out} | q_1^0, q_2^0, E; \text{in} \rangle = \delta(q_1^{0\prime} - q_1^0)\,\delta(q_2^{0\prime} - q_2^0) -$$

$$- 2\,i\pi\delta(q_1^{0\prime}+q_2^{0\prime}-q_1^0-q_2^0)\,\delta(E'-E)\,A.$$

$$A = \frac{g^2 f_1(q_1^0, q_1^0+q_2^0)\, f_1^*(q_1^{0\prime}, q_1^0+q_2^0)}{h(q_1^0+q_2^0, E+i\varepsilon)}. \tag{24}$$

A through h contains the integral

$$g^2 \int \frac{|f_1(q, q_1^0+q_2^0)|\, d^3q}{v_1(q)+v_2(q_1^0+q_2^0-q) - E - i\varepsilon},$$

which gives the physical cut, and also the integral

$$g^2 \int \frac{f_2(q, q_1^0+q_2^0)\, f_2^*(q_1^0+q_2^0-q, q_1^0+q_2^0)\, d^3q}{\omega^*(q_1^0+q_2^0-q)+\omega(q)-E-i\varepsilon}. \tag{25}$$

When we now fix

$$q_1^0+q_2^0=0\,,$$

$\omega^*(-q)+\omega(q)$ is real for all q; the factor $i\varepsilon$ is relevant and the corresponding integral exhibits the non-physical cut showing that (the physical) unitarity is violated. When, however, $q_1^0+q_2^0\neq 0$ the integral is well defined [3, 4] without $i\varepsilon$ since points in q space for which the integrand is singular are lying on a circle giving a zero contribution to the three dimensional integration. Consequently, unitarity holds. A quite similar calculation gives for interaction d) with

$$\begin{aligned}H_1=g\iiint\{&\psi^*(k)\,a_1^*(q_1)\,[f_1(k,q_1,q_2)\,a_2(q_2)\,a_3(k+q_1-q_2)+\\&+f_2(k,q_1,q_2)\,c(q_1)\,b(k+q_1-q_2)]+\\&+\psi(k)\,a_1(q_1)\,[f_1^*(k,q_1,q_2)\,a_2^*(q_2)\,a_3^*(k+q_1-q_2)+\\&+f_2^*(k,q_1,q_2)\,c^*(q_1)\,b^*(k+q_1-q_2)]\}\,d^3k\,d^3q_1\,d^3q_2\,,\end{aligned}$$

that the exactly second order S-matrix for the physical ψ, a_i scattering contains an integral like (25) with the same consequences.

Before we turn away from the safe ground of explicit formulae we point out that Eq. (21) possesses another linearly independent scattering state non-physical solution with

$$\begin{aligned}\Phi_1(q_1,q_2)&=-\frac{g\varphi_\pm(q_1+q_2)\,f_1^*(q_1,q_1+q_2)}{v_1(q_1)+v_2(q_2)-E\mp i\varepsilon}\,,\\ \Phi_2(q_1,q_2)&=\delta(q_1-q_1^0)\,\delta(q_2-q_2^0)-\frac{g\varphi_\pm(q_1+q_2)\,f_2^*(q_1,q_1+q_2)}{\omega^*(q_1)+\omega(q_2)-E\mp i\varepsilon}\,,\end{aligned}\tag{26}$$

$$h(k,E\pm i\varepsilon)\,\varphi_\pm(k)=-g f_2(q_2^0,k)\,\delta(k-q_1^0-q_2^0)\,,$$

$$E=\sqrt{q_1^{02}+M^{*2}}+\sqrt{q_2^{02}+M^2}\,.\tag{27}$$

Since these types of solutions contain incident plane waves for non-physical particles the corresponding states will be denoted by

$$|q_1^0,q_2^0,E;\text{ non phys; in, out}\rangle\,.\tag{28}$$

From (27) E is real only if $q_1^{02}=q_2^{02}$.

Again, the S-matrix for physical $\to$ non- physical transitions can be calculated. In the centre of mass system this gives

$$\begin{aligned}\langle q_1^{0\prime},q_2^{0\prime},E';\text{ non phys; out}|q_1^0,q_2^0,E;\text{ in}\rangle&=\\=-2\,i\pi\delta(q_1^{0\prime}+q_2^{0\prime})\,\delta(E'-E)\,B\,,&\\ B=\frac{g^2 f_1(q_1^0,0)\,f_2(q_2^0,0)}{h(0,E+i\varepsilon)}\,,&\end{aligned}\tag{29}$$

since from momentum conservation, E' remains always real. Opening of this channel was indicated by the cut of the centre of mass physical amplitude. For the case $q_1^0 + q_2^0 \neq 0$ a situation described under (5) emerges. Namely (29) with $q_1^0 + q_2^0 = p$ contains factors with $(\sqrt{q_1^{0\prime 2} + M^{*2}} + \sqrt{(p - q_1^{0\prime})^2 + M^2} - E \pm i\varepsilon)^{-1/2}$, E real. When the total rate of production of non physical particles is calculated one integrates over $d^3q_1^{0\prime}$. This brings us back exactly to what was said under (25) and (5).

5. All these results show that Lorentz covariance is violated. This means that if we take the Hamiltonian from [2] or (16) literally, violation — non violation phenomena can be understood only in a fixed frame. For "head on" collisions non-physical particles are produced; for others not. These concepts are obviously frame dependent, whereas production rates are not. Here, two questions arise. First where is Lorentz invariance actually violated (cf. Appendix and [15]) and second, just requiring an invariance postulate perhaps this prescription might suggest a definite alternative. To the second question there seems to be no definite answer. Namely we might say: One must calculate the amplitude in the centre of mass system first (COLEMAN—GLASHOW) and then transform the results in any other system (unitarity violation), or one must calculate everything with $p \neq 0$ (LEE), and define the case $p = 0$ as $p \to 0$ (unitarity survives). At least for these scatterings both prescriptions give an invariant S-matrix [14], [3] (cf., however, also [15]). Are there, then, independently of covariance some arguments in favour of either of these prescriptions? There is nothing else left but the known fact that in reality, the scattering of wave packets is related to a matrix element such as (24). According to F. KÁROLYHÁZY a close examination of the scattering of wave packets leads to LEE's prescription. The reason is essentially that in the spectrum of momenta of the incident packet, $p = 0$ is a point of zero measure.

6. In a paper by CUTKOSKY et al. [15] in order to obtain a non analytic but unitary S-matrix another prescription was proposed: Let us calculate the S-matrix in the usual way (e.g: in the centre of mass system) but let the masses of the non-physical particles have different imaginary parts.

$$M_1 - M_2 = i\delta \,. \tag{30}$$

After everything has been calculated (including $\varepsilon \to 0$) $\delta \to 0$. From a field theoretical point of view (30) means that the bare Hamiltonian is not even pseudo-hermitian. It would be interesting to investigate this possibility in each order (cf. [15] p. 18). At the end we might feel that LEE—WICK's electrodynamics gives a certain solution to the old problem of finite quantum field theories. Which is best among the rival ideas [1—10] remains to be decided in the future.

Appendix

Here we wish to show how one gets the Hamiltonian (16) using the η-less formalism, and touch the problem where Lorentz invariance is lost.

Let us suppose that we have two real fields Φ_1 and Φ_2 with a bilinear interaction. Φ_2 is a field quantized in the usual way, Φ_1 leads to indefinite metric. For our purpose we choose the Lagrangian (m, γ real)

$$L = \frac{1}{2}\left(\frac{\partial \Phi_1}{\partial x_\mu}\right)^2 - \frac{1}{2}\left(\frac{\partial \Phi_2}{\partial x_\mu}\right)^2 - (\Phi_2 - \Phi_1)\frac{m^2}{2} - \gamma m \Phi_1 \Phi_2 . \tag{A I}$$

Since from this

$$[\Phi_2(r,t), \dot{\Phi}_2(r',t)] = -[\Phi_1(r,t), \dot{\Phi}_1(r',t)] = i\delta(r-r') \tag{A II}$$

all the other commutators vanish. By the usual procedure one can build up the bare Fock space $\{F_0\}$ which is a vector space with indefinite metric for $\gamma = 0$

$$\langle N_1', N_2' | N_1, N_2 \rangle = (-1)^{N_1} \delta(N_1' - N_1)\, \delta(N_2' - N_2) .$$

In this space the theory is obviously represented in a covariant way; all the Lorentz generators are unitary (pseudo-unitary) operators over this space. Now let us take $\gamma = (\text{real}) \neq 0$.

It is easy to see that the linear transformation

$$\Phi_1 = \frac{i}{\sqrt{2}}(C - B), \quad \Phi_2 = \frac{1}{\sqrt{2}}(B + C), \tag{A III}$$

or inversely

$$C = \frac{1}{\sqrt{2}}(\Phi_2 - i\Phi_1), \quad B = \frac{1}{\sqrt{2}}(\Phi_2 + i\Phi_1)$$

brings the Lagrangian to the following diagonal form

$$L = -\frac{1}{2}\left(\frac{\partial B}{\partial x_\mu}\right)^2 - \frac{1}{2}\left(\frac{\partial C}{\partial x_\mu}\right)^2 - \frac{1}{2}(m^2 + i\gamma m) B^2 - \frac{1}{2}(m^2 - i\gamma m) C^2 , \tag{AIV}$$

with (either directly or from (A II), (A III))

$$[B(r,t), \dot{B}(r',t)] = [C(r,t), \dot{C}(r',t)] = i\delta(r - r') , \tag{A V}$$

all the other commutators vanish. From (A III)

$$B^* = C, \quad C^* = B, \tag{A VI}$$

and the field equations are

$$(\Box - M^2)\, B = (\Box - M^{2*})\, C = 0\,,$$
$$M = m^2 + i\,\gamma\, m\,. \tag{A VII}$$

Just as in the ordinary case (A III) cannot be represented as a unitary transformation over $\{F_0\}$. From this comes, in part, the problem of invariance. In [3] it is proposed that for any given Lorentz frame the corresponding conjugate momenta of the fields to B and C are to be defined as usual, and B, C, P_B, P_C expanded in three dimensional Fourier series with three real momenta k and complex normalizing factors $(\omega(k) = \sqrt{k^2 + M^2})$, $\omega(k)^{-1/2}$, $\omega^*(k)^{-1/2}$. Notice that from (A VI)

$$B(r) = \frac{1}{(2\pi)^{3/2}} \int \frac{d^3 k}{\sqrt{2\,\omega(k)}} \left(b(k)\, e^{ikr} + c^*(k)\, e^{-ikr}\right),$$
$$C(r) = \frac{1}{(2\pi)^{3/2}} \int \frac{d^3 k}{\sqrt{2\omega^*(k)}} \left(c(k)\, e^{ikr} + b^*(k)\, e^{-ikr}\right).$$

Then one gets (16), and through the expansion coefficients b, c, b^*, c^* the real particle Fock space $\{F\}$ can be built up. This procedure is not invariant; not all of the Lorentz generators are represented on $\{F\}$. A particle possessing real k, complex ω in a given frame turns out in another frame with complex four momenta.

We are greatly indebted to Professors F. KÁROLYHÁZY, G. MARX and G. PÓCSIK for most valuable discussions.

REFERENCES

1. T. D. LEE and G. C. WICK, Nucl. Phys., **B9**, 209; **B10**, 1, 1969.
2. T. D. LEE, A Possible Way to Remove Divergence Difficulties in Physics. Proceedings of the 1969 Topical Conference on Weak Interactions, CERN, 1969.
3. T. D. LEE, A Relativistic Complex Pole Model with Indefinite Metric. Preprint, to be published in Memorial Volume in honour of Gregor Wentzel. The University of Chicago Press, 1969.
4. T. D. LEE and G. C. WICK, Concerning the Preprint, "Unitarity Troubles in Lee-Wick Electrodynamics" by COLEMAN and GLASHOW, CERN preprint, 1969.
5. W. HEISENBERG, Introduction to the Unified Field Theory of Elementary Particles. Wiley and Sons Ltd, London, 1967.
6. M. FROISSART, Suppl. Nuovo Cimento, **14**, 197, 1959.
7. N. BOGOLIUBOV, Proceedings of the 1958 International Conference on High Energy Physics, CERN, p. 129, 1958.
8. E. C. G. SUDARSHAN, Phys. Rev., **133 B**, 487, 1964; Indefinite Metric and Nonlocal Field Theories, preprint of Syracuse University, No. SU-1206—131, 1967.

9. K. YOKOYAMA, Progr. Theor. Phys., **27**, 373, 1962.
10. H. SHIMODAIRA, Nucl. Phys., **17**, 486, 1960.
11. K. L. NAGY, State Vector Spaces with Indefinite Metric in Quantum Field Theory. Akadémiai Kiadó, Budapest, 1966.
12. S. TANAKA, Progr. Theor. Phys., **29**, 104, 1963.
13. O. NACHTMANN, On the Two Baryon Sectors of Soluble Models with Indefinite Metric I, II, CERN preprints No. TH 1028, 1033, 1969.
14. S. COLEMAN and S. L. GLASHOW, Unitarity Trouble in Lee-Wick Electrodynamics, Harvard University preprint, Cambridge, 1969.
15. R. E. CUTKOSKY, P. V. LANDSHOFF, D. J. OLIVE and J. C. POLKINGHORNE, A Non-Analytic S-Matrix, Preprint of the DAMTP, University of Cambridge, No 25, 1969.

КОМПЛЕКСНЫЕ ПОЛЮСЫ, РАЗРЕЗЫ, НЕОПРЕДЕЛЕННАЯ МЕТРИКА И УНИТАРНОСТЬ

К. Л. НАДЬ

Р е з ю м е

Обсуждаются проблемы унитарности в электродинамике Ли-Вика в случае модели, имеющей точное решение с комплексными состояниями.

Acta Physica Academiae Scientiarum Hungaricae, Tomus 29 (2—3), pp. 267—278 (1970)

ÜBER DIE GRUNDLAGEN DER STATISTISCHEN THEORIE DES ATOMKERNS

Von

P. GOMBÁS

PHYSIKALISCHES INSTITUT DER UNIVERSITÄT FÜR TECHNISCHE WISSENSCHAFTEN, BUDAPEST

und

FORSCHUNGSGRUPPE FÜR THEORETISCHE PHYSIK DER UNGARISCHEN AKADEMIE DER WISSENSCHAFTEN, BUDAPEST

und

D. KISDI

FORSCHUNGSGRUPPE FÜR THEORETISCHE PHYSIK DER UNGARISCHEN AKADEMIE DER WISSENSCHAFTEN, BUDAPEST

(Eingegangen: 21. I. 1970)

Es werden die Grundlagen der statistischen Theorie der Atomkerne bei Zugrundelegung eines allgemeinen Ausdruckes für die gegenseitige Wechselwirkung der Nukleonen entwickelt, die dem heutigen Stand unserer Kenntnisse entspricht.

§ 1. Einleitung

Eine statistische Theorie der Atomkerne wurde schon vor fast 20 Jahren von einem von uns beiden entwickelt, wobei jedoch für die zwischen den Nukleonen wirkenden Kräfte Ausdrücke vorausgesetzt wurden, die dem heutigen Stand unseres Wissens nicht mehr entsprechen [1]. Die damals entwickelte Theorie hat heute nur mehr höchstens einen halbempirischen Wert, indem man die dort zwischen den Nukleonen wirkenden Kräfte als halbempirische Kräfte betrachten kann.

Das Ziel der vorliegenden Arbeit ist die Grundlagen der statistischen Theorie der Kerne und zwar unter Voraussetzung von internuklearen Kräften, die dem heutigen Stand unseres Wissens entsprechen, zu entwickeln.

§ 2. Grundlagen

Das Hauptziel der statistischen Theorie der Kerne ist die Bestimmung der Nukleonenverteilung und der Energie eines Kerns in der stabilen Gleichgewichtslage. Dies geschieht auf Grund des Energieminimumsprinzips in der Weise, dass man die Energie E des Kerns als Funktion der Neutronendichte ϱ_n und Protonendichte ϱ_p ermittelt und aus der Funktion $E(\varrho_n, \varrho_p)$ diejenigen

Dichteverteilungen bestimmt, für die E ein Minimum aufweist. Für ϱ_n und ϱ_p bestehen die folgenden Nebenbedingungen

$$\int \varrho_n \, dv = N \quad \text{und} \quad \int \varrho_p \, dv = Z \,, \tag{1}$$

wo N die Anzahl der Neutronen, Z die der Protonen im Kern und dv das Volumenelement bezeichnen.

Die Energie eines Kerns setzt sich aus 3 Haupt-Anteilen zusammen: aus der kinetischen Energie der Nukleonen, aus der von den nuklearen Kräften resultierenden Wechselwirkungsenergie der Nukleonen und aus der elektrostatischen Wechselwirkungsenergie der Protonen. Mit diesen Energieanteilen wollen wir uns im Nachstehenden einzeln befassen.

§ 3. Die kinetische Energie der Nukleonen

Die kinetische Energie E_k des Kerns setzt sich aus der kinetischen Energie E_k^n der Neutronen und E_k^p der Protonen additiv zusammen. Man hat also

$$E_k = E_k^n + E_k^p. \tag{2}$$

Die kinetische Energie der Neutronen gestaltet sich folgendermassen

$$E_k^n = \int_\Omega \left(\frac{1}{3} \varkappa_F \varrho_n^{5/3} - \varkappa_1 \varrho_n^{4/3} \frac{1}{r} + \varkappa_2 \varrho_n \frac{1}{r^2} - \varkappa_3 \frac{1}{r^5} \right) dv + \\ + \frac{2}{3} \varkappa_F \int \varrho_n^{5/3} \, dv + \varkappa_w \int \frac{(\operatorname{grad} \varrho_n)^2}{\varrho_n} \, dv \,,$$

wo r die Entfernung vom Koordinatenursprung bezeichnet und die Konstanten die folgende Bedeutung haben:

$$\left.\begin{aligned} \varkappa_F &= \frac{3}{10} (3\pi^2)^{2/3} \frac{\hbar^2}{M} \,, & \varkappa_w &= \frac{1}{8} \frac{\hbar^2}{M} \,, \\ \varkappa_1 &= \frac{1}{8} (3\pi^2)^{1/3} \frac{\hbar^2}{M} \,, \quad \varkappa_2 = \frac{1}{24} \frac{\hbar^2}{M} \,, \quad \varkappa_3 &= \frac{1}{5760\,\pi^2} \frac{\hbar^2}{M} \,. \end{aligned}\right\} \tag{4}$$

Das erste Integral auf der rechten Seite in (3) gibt die radiale Fermische kinetische Energie der Neutronen mit Berücksichtigung einer Korrektion [2], die die sogenannte radiale kinetische Selbstenergie der Nukleonen (die auch im letzten Integral enthalten ist) ausschaltet. Dieses erste Integral ist nur auf den Raumteil Ω auszudehnen, in welchem der Integrand positiv, d. h., wo

$$(3\pi^2 \varrho_n)^{1/3} \geqq \frac{1}{2r} \tag{5}$$

ist. Das zweite Integral representiert die azimutale kinetische Energie der Nukleonen und das letzte Integral die Weizsäckersche kinetische Inhomogenitätskorrektion.

Ein ganz ähnlicher Ausdruck gilt für die kinetische Energie der Protonen E_k^p mit dem Unterschied, dass in diesem ϱ_p statt ϱ_n steht.

§ 4. Die elektrostatische Wechselwirkungsenergie der Protonen

Die elektrostatische Wechselwirkungsenergie E_{el} der Protonen im Kern setzt sich aus der gewöhnlichen elektrostatischen Wechselwirkungsenergie E_c der Protonen und der Austauschenergie E_a der Protonen zusammen. Man hat also

$$E_{el} = E_c + E_a \,, \tag{6}$$

wo sich E_c und E_a folgendermassen gestalten

$$E_C = \frac{1}{2} \iint \frac{e^2}{r_{12}} \varrho_p(\mathfrak{r}_1)\, \varrho_p(\mathfrak{r}_2)\, d\mathfrak{v}_1\, d\mathfrak{v}_2 \,, \tag{7}$$

$$E_A = -\varkappa_a \int \varrho_p^{4/3}\, d\mathfrak{v} \tag{8}$$

mit

$$\varkappa_A = \frac{3}{4} \left(\frac{3}{\pi}\right)^{1/3} e^2. \tag{9}$$

§ 5. Die internuklearen Kräfte

Zur Berechnung der aus den zwischen den Nukleonen wirkenden Kräften resultierenden Energie des Kerns müssen wir uns zunächst mit diesen Kräften befassen. Ein sehr allgemeiner Ausdruck für die potentielle Energie dieser Kräfte ist der folgende [3]

$$V = V_{\text{central}} + V_{\text{spin-orbit}} + V_{\text{tensor}}, \tag{10}$$

in welchem V_{central} die zentrale Wechselwirkungsenergie der Nukleonen, $V_{\text{spin-orbit}}$ die aus der Wechselwirkung des Spin- und Bahnmomentes der Nukleonen resultierende Energie und V_{tensor} die aus den Tensorkräften entstehende Energie darstellt.

Der allgemeine Ausdruck für die zentrale Wechselwirkungsenergie lautet folgendermassen

$$V_{\text{central}} = V_W + V_B P_\sigma - V_H P_\tau - V_M P_\sigma P_\tau. \tag{11}$$

Hier bezeichnet P_σ und P_τ den Vertauschungsoperator für die Spine bzw für die Ladungen von zwei Nukleonen, die man mit den Paulischen Matrizen folgendermassen darstellen kann:

$$P_\sigma = \frac{1}{2}(1+\vec{\sigma}_1\vec{\sigma}_2) \quad \text{und} \quad P_\tau = \frac{1}{2}(1+\vec{\tau}_1\vec{\tau}_2). \tag{12}$$

Die Wechselwirkungsenergien V_W, V_B, V_H und V_M sind Funktionen der gegenseitigen Entfernung r der beiden wechselwirkenden Nukleonen; sie können aber auch noch von dem relativen Impuls p und dem relativen Impulsmoment L der beiden Nukleonen abhängen, es ist also

$$\begin{aligned} &V_i = V_i(r, p, L)\,, \\ &(i = W, B, H, M)\,. \end{aligned} \tag{13}$$

Die aus der Spin-Bahn-Wechselwirkung resultierende Energie hat folgende Gestalt

$$V_{\text{spin-orbit}} = [V_{LSO}+V_{LSE}P_\tau]\cdot(\vec{L}, \vec{S})\,, \tag{14}$$

wo

$$\vec{L} = [\mathfrak{r}, \mathfrak{p}] \tag{15}$$

den relativen Drehimpuls und

$$\vec{S} = \frac{1}{2}(\vec{\sigma}_1 + \vec{\sigma}_2) \tag{16}$$

den resultierenden Spin der beiden Nukleonen bezeichnen. Die Wechselwirkungspotentiale V_{LSO} und V_{LSE} können geradeso wie (13) wieder Funktionen von r, p und L sein.

Schliesslich geben wir noch den allgemeinen Ausdruck für die Tensorkräfte an. Dieser ist der folgende

$$\begin{aligned} V_{\text{tensor}} = {} & (V_{TRO} + V_{TRE}P_\tau)\cdot[3(\vec{\sigma}_1, \mathfrak{r})(\vec{\sigma}_2, \mathfrak{r}) - r^2(\vec{\sigma}_1, \vec{\sigma}_2)] + \\ & + (V_{TPO} + V_{TPE}P_\tau)\cdot[3(\vec{\sigma}_1, \mathfrak{p})(\vec{\sigma}_2, \mathfrak{p}) - p^2(\vec{\sigma}_1, \vec{\sigma}_2)] + \\ & + (V_{TLO} + V_{TLE}P_\tau)\cdot[3(\vec{\sigma}_1, \vec{L})(\vec{\sigma}_2, \vec{L}) - L^2(\vec{\sigma}_1, \vec{\sigma}_2)]. \end{aligned} \tag{17}$$

Die Wechselwirkungsenergien V_{TRO}, V_{TRE}, V_{TPO}, ... können auch hier geradeso wie die in den Ausdrücken (11) und (14) stehenden entsprechenden Wechselwirkungsenergien wieder Funktionen von r, p und L sein.

§ 6. Berechnung der aus den internuklearen Kräften resultierenden Wechselwirkungsenergie

Nachdem wir im vorangehenden Paragraphen den allgemeinen Ausdruck der internuklearen Kernkräfte besprochen haben, können wir nun die aus diesen Kräften resultierende Wechselwirkungsenergie der Nukleonen berechnen. Diese Energie gibt in der Hartree—Fockschen Näherung der bekannte nachstehende Ausdruck

$$E = \frac{1}{2} \sum_{\alpha=1}^{A} \sum_{\beta=1}^{A} \{(\alpha\beta|V|\alpha\beta) - (\alpha\beta|V|\beta\alpha)\}, \tag{18}$$

in welchem die Matrixelemente die folgende Bedeutung haben

$$(\alpha\beta|V|\gamma\delta) = \int \psi_\alpha^*(x_1)\, \psi_\beta^*(x_2)\, V(x_1, x_2)\, \psi_\gamma(x_1)\, \psi_\delta(x_2)\, dx_1\, dx_2. \tag{19}$$

In diesem Ausdruck bezeichnet $\psi_\alpha(x)$ die Hartree—Focksche Wellenfunktion des α-ten Nukleons und x steht statt dem Ortsvektor $\mathfrak{r}$ der Spinvariable und der Isotopen-Spin-Variable. Die Summation ist in (18) auf alle Nukleonen $A = N + Z$ zu erstrecken.

Der Energieausdruck (18) des Kerns vereinfacht sich wesentlich, wenn man einen Kern in Betracht zieht, in welchem sich die Nukleonen paarweise in Quantenzuständen befinden, die sich nur in der entgegengesetzten Spinrichtung der Nukleonen unterscheiden. In solchen Kernen heben sich nämlich bei der quantenmechanischen Mittelbildung die aus dem Spin resultierenden Glieder im Energieausdruck auf; die Glieder der Spin-Bahn-Wechselwirkung, sowie die aus den Tensorkräften resultierenden Glieder, die den Spin enthalten, fallen durch die Mittelbildung weg, wie sich dies durch eine elementare Rechnung leicht zeigen lässt. Die aus den zentralen Wechselwirkungskräften resultierende Energie vereinfacht sich also für diese Kerne folgendermassen:

$$E = E_{np} + E_{nn} + E_{pp}, \tag{20}$$

wo E_{np} die aus der Neutron-Proton-, E_{nn} die aus der Neutron-Neutron-, und E_{pp} die aus der Proton-Proton-Wechselwirkung resultierende Energieanteile bezeichnen und sich folgendermassen gestalten

$$E_{np} = 4 \sum_{l=1}^{N/2} \sum_{k=1}^{Z/2} \left\{ \left(kl \left| V_W + \frac{1}{2} V_B \right| kl \right) + \left(kl \left| V_M + \frac{1}{2} V_H \right| lk \right) \right\}, \tag{21}$$

$$E_{nn} = 2 \sum_{l_1 \neq l_2 = 1}^{N/2} \left\{ \left(l_1 l_2 \left| V_W + \frac{1}{2} V_B - V_H - \frac{1}{2} V_M \right| l_1 l_2 \right) + \right.$$
$$\left. + \left(l_1 l_2 \left| V_M + \frac{1}{2} V_H - V_B - \frac{1}{2} V_W \right| l_2 l_1 \right) \right\}, \tag{22}$$

$$E_{pp} = 2 \sum_{k_1 \neq k_2 = 1}^{Z/2} \left\{ \left(k_1 k_2 \left| V_W + \frac{1}{2} V_B - V_H - \frac{1}{2} V_M \right| k_1 k_2 \right) + \right.$$
$$\left. + \left(k_1 k_2 \left| V_M + \frac{1}{2} V_H - V_B - \frac{1}{2} V_W \right| k_2 k_1 \right) \right\}. \tag{23}$$

Eine wesentliche Vereinfachung bedeutet, dass die in den Ausdrücken (21), (22) und (23) stehenden Matrixelemente nur mehr von den Ortskoordinaten abhängen; sie haben folgende Gestalt

$$(kl\,|V_i|\,mn) = \int \varphi_k^*(\mathfrak{r}_1)\, \varphi_l^*(\mathfrak{r}_2)\, V_i(\mathfrak{r}_1 - \mathfrak{r}_2)\, \varphi_m(\mathfrak{r}_1)\, \varphi_n(\mathfrak{r}_2)\, d\boldsymbol{v}_1\, d\boldsymbol{v}_2\,, \tag{24}$$

wo $\varphi_k(\mathfrak{r})$ den nur vom Ort abhängigen Anteil der Eigenfunktion des k-ten Neutrons bzw. Protons bezeichnet.

Wir wollen nun den Fall ausführlicher untersuchen, in welchem die Wechselwirkungsenergien V_i ($i = W, B, H, M$) statt (13) nur von der gegenseitigen Entfernung r der beiden Nukleonen abhängen, d. h. V_i die folgenden Funktionen sind $V_i = V_i(r)$. In diesem Falle werden in (24) die V_i Ortsfunktionen, die mit den Eigenfunktionen $\varphi(\mathfrak{r})$ vertauschbar sind. Wenn wir zur Abkürzung die folgenden Bezeichnungen einführen

$$\left.\begin{aligned} V_a(r) &= V_W + \frac{1}{2} V_B\,, & V_c(r) &= V_W + \frac{1}{2} V_B - V_H - \frac{1}{2} V_M\,, \\ V_b(r) &= V_M + V_H\,, & V_d(r) &= V_M + \frac{1}{2} V_H - V_B - \frac{1}{2} V_W\,, \end{aligned}\right\} \tag{25}$$

dann kann man die Energieausdrücke (21), (22) und (23) in folgender Form schreiben

$$E_{np} = \iint V_a(\mathfrak{r}_{12})\, \varrho_p(\mathfrak{r}_1)\, \varrho_p(\mathfrak{r}_2)\, d\boldsymbol{v}_1\, d\boldsymbol{v}_2 + \iint V_b(\mathfrak{r}_{12})\, \eta_p^*(\mathfrak{r}_1, \mathfrak{r}_2)\, \eta_n(\mathfrak{r}_1, \mathfrak{r}_2)\, d\boldsymbol{v}_1\, d\boldsymbol{v}_2, \tag{26}$$

$$E_{nn} = \frac{1}{2} \iint V_c(\mathfrak{r}_{12})\, \varrho_n(\mathfrak{r}_1)\, \varrho_n(\mathfrak{r}_2)\, d\boldsymbol{v}_1\, d\boldsymbol{v}_2 + \frac{1}{2} \iint V_d(\mathfrak{r}_{12}) |\eta_n(\mathfrak{r}_1, \mathfrak{r}_2)|^2\, d\boldsymbol{v}_1\, d\boldsymbol{v}_2\,, \tag{27}$$

$$E_{pp} = \frac{1}{2} \iint V_c(\mathfrak{r}_{12})\, \varrho_p(\mathfrak{r}_1)\, \varrho_p(\mathfrak{r}_2)\, d\boldsymbol{v}_1 d\boldsymbol{v}_2 + \frac{1}{2} \iint V_d(\mathfrak{r}_{12}) |\eta_p(\mathfrak{r}_1, \mathfrak{r}_2)|^2\, d\boldsymbol{v}_1\, d\boldsymbol{v}_2. \tag{28}$$

Hier bedeutet ϱ_n bzw. ϱ_p die quantenmechanische Dichtefunktion der Neutronen bzw. Protonen; es ist also

$$\varrho_n(\mathfrak{r}) = 2\sum_{l=1}^{N/2} |\varphi_k(\mathfrak{r})|^2 \quad \text{und} \quad \varrho_p(\mathfrak{r}) = 2\sum_{k=1}^{Z/2} |\varphi_k(\mathfrak{r})|^2 . \tag{29}$$

η_n und η_p sind die den Neutronen bzw. Protonen entsprechenden Dichtematrizen

$$\eta_n(\mathfrak{r}_1, \mathfrak{r}_2) = 2\sum_{l=1}^{N/2} \varphi_l(\mathfrak{r}_1)\,\varphi_l^*(\mathfrak{r}_2) , \tag{30}$$

$$\eta_p(\mathfrak{r}_1, \mathfrak{r}_2) = 2\sum_{k=1}^{Z/2} \varphi_k(\mathfrak{r}_1)\,\varphi_k^*(\mathfrak{r}_2) . \tag{31}$$

Diese Dichtematrizen gehen für grosse gegenseitige Entfernung $|\mathfrak{r}_1 - \mathfrak{r}_2|$ der Nukleonen rasch gegen Null, demzufolge die zweiten Integrale in den Energieausdrücken (26), (27) und (28) die Wechselwirkung mit kurzer Reichweite repräsentieren.

Die gesamte Wechselwirkungsenergie E der Nukleonen zerfällt also in zwei Anteile: in einen Anteil E_{long}, der aus der Wechselwirkung mit grosser Reichweite entsteht und in einen Anteil E_{short}, der aus der Wechselwirkung mit kurzer Reichweite resultiert

$$E = E_{\text{long}} + E_{\text{short}} , \tag{32}$$

$$E_{\text{long}} = \iint \Big\{ V_a(r_{12})\,\varrho_p(\mathfrak{r}_1)\,\varrho_n(\mathfrak{r}_2) + \\ + \frac{1}{2} V_c(r_{12})[\varrho_p(\mathfrak{r}_1)\,\varrho_p(\mathfrak{r}_2) + \varrho_n(\mathfrak{r}_1)\,\varrho_n(\mathfrak{r}_2)] \Big\}\, d\nu_1\, d\nu_2, \tag{33}$$

$$E_{\text{short}} = \iint \Big\{ V_b(r_{12})\,\eta_p^*(\mathfrak{r}_1, \mathfrak{r}_2)\,\eta_n(\mathfrak{r}_1, \mathfrak{r}_2) + \\ + \frac{1}{2} V_d(r_{12})\,[|\eta_p(\mathfrak{r}_1, \mathfrak{r}_2)|^2 + |\eta_n(\mathfrak{r}_1, \mathfrak{r}_2)|^2] \Big\}\, d\nu_1\, d\nu_2 . \tag{34}$$

Im Falle der elektrostatischen Wechselwirkung der Protonen ist die Wechselwirkungsenergie langer Reichweite mit der elektrostatischen Coulombschen Wechselwirkungsenergie E_{Coul} der Protonen und die Wechselwirkungsenergie kurzer Reichweite mit der aus der elektrostatischen Wechselwirkung resultierenden Austauschenergie E_{A} der Protonen identisch.

§ 7. Berechnung der Kernenergie

Der Energieanteil E_{long} ist ein aus den Dichtefunktionen ϱ_n und ϱ_p aufgebautes einfaches Integral. Wesentlich komplizierter ist die Sachlage beim Energieanteil E_{short}, der nach (34) auch die nicht-diagonalen Elemente der Dichtematrix enthält.

Im Falle einer statistischen Behandlung des Kerns zieht man die Wechselwirkung kurzer Reichweite in der Weise in Betracht, dass man zunächst die Energie E_{short} für ein Nukleonengas im Volumen Ω als Funktion von ϱ_n und ϱ_p berechnet und dann den Kern in Volumenelemente dv aufteilt und zwar in der Weise, dass man die Nukleonen in jedem Volumenelement als ein Nukleonengas von konstanter Dichte betrachten kann; die Gesamtenergie des Kerns setzt sich dann als Summe der Energien der einzelnen Volumenelemente zusammen.

In einem kräftefreien Volumen Ω ist die Verteilung der Nukleonen konstant und die Wellenfunktionen der Nukleonen sind ebene Wellen. Die Wellenfunktion des k-ten Nukleons gestaltet sich also folgendermassen

$$\varphi_k(\mathfrak{r}) = \frac{1}{\sqrt{\Omega}} e^{-i/\hbar\,(\mathfrak{p}_k,\mathfrak{r})}, \tag{35}$$

wo $\mathfrak{p}_k$ den Impuls des k-ten Nukleons bezeichnet.

Die Dichte der Nukleonen erhält man durch die Summierung der Beträge dieser Wellenfunktionen. Wenn man die Summierung wie üblich durch eine Integration ersetzt, so erhält man z. B. für die Neutronendichte ϱ_n im Volumen Ω

$$\varrho_n = 2\sum_{k=1}^{N/2}\left|\frac{1}{\sqrt{\Omega}} e^{i/\hbar\,(\mathfrak{p}_k,\mathfrak{r})}\right|^2 = \frac{2}{\Omega}\sum_{k=1}^{N/2} 1 = \frac{2}{\Omega}\,\frac{\Omega}{(2\pi\hbar)^3}\int_0^{p_{\mu n}} 4\pi p^2\,dp = \frac{p_{\mu n}^3}{3\pi^2\hbar^3}\,, \tag{36}$$

wo p den Impulsbetrag und $p_{\mu n}$ den maximalen Wert dieses Betrages, d. h. den Betrag des maximalen Impulses der Neutronen bezeichnet. Für diesen letzteren ergibt sich aus (36) der Zusammenhang

$$p_{\mu n} = (3\pi^2\hbar^3\varrho_n)^{1/3}. \tag{37}$$

Ganz ähnlich erhält man im Falle von Protonen

$$p_{\mu p} = (3\pi^2\hbar^3\varrho_p)^{1/3}. \tag{38}$$

Die Dichtematrix der Neutronen gestaltet sich mit den ebenen Wellen als Eigenfunktionen folgendermassen

$$\eta_n(\mathfrak{r}_1, \mathfrak{r}_2) = 2 \sum_{k=1}^{N/2} \frac{1}{\Omega} e^{i/\hbar\,(\mathfrak{p}_k, \mathfrak{r}_{12})} = \frac{2}{\Omega} \cdot \frac{\Omega}{(2\pi\hbar)^3} \int e^{i/\hbar\,(\mathfrak{p}, \mathfrak{r}_{12})}\, d^3\mathfrak{p}\,. \tag{39}$$

Nach Durchführung der Integration über die Winkelvariablen erhält man

$$\eta_n(\mathfrak{r}_1, \mathfrak{r}_2) = \frac{1}{\pi^2 \hbar^3} \int_0^{p_{\mu n}} \frac{\sin\left(\frac{p r_{12}}{\hbar}\right)}{\frac{p r_{12}}{\hbar}} 4\pi p^2\, dp\,. \tag{40}$$

Die Integration lässt sich hier einfach durchführen und ergibt folgendes Resultat

$$\eta_n(\mathfrak{r}_1, \mathfrak{r}_2) = \frac{p_{\mu n}^3}{3\pi^2 \hbar^3} D\left(\frac{p_{\mu n} r_{12}}{\hbar}\right) = \varrho_p D\left(\frac{p_{\mu n} r_{12}}{\hbar}\right), \tag{41}$$

wo D die Funktion

$$D(u) = \frac{3(\sin u - u \cos u)}{u^3} \tag{42}$$

bezeichnet.

Für die Dichtematrix der Protonen erhält man den zu (42) analogen Ausdruck

$$\eta_p(\mathfrak{r}_1, \mathfrak{r}_2) = \varrho_p D\left(\frac{p_{\mu p} r_{12}}{\hbar}\right). \tag{43}$$

Mit Hilfe der Formeln für die Dichtematrizen lässt sich die aus den Kräften mit kurzer Reichweite resultierende Energie E_{short} für ein Nukleonengas mit konstanter Dichte berechnen. Nach Einsetzen von (41) und (43) in (34) ergibt sich

$$\begin{aligned} E_{\text{short}} = \iint \Bigg\{ & V_b(r_{12})\, \varrho_n \varrho_p\, D\left(\frac{p_{\mu n} r_{12}}{\hbar}\right) D\left(\frac{p_{\mu p} r_{12}}{\hbar}\right) + \\ & + \frac{1}{2} V_d(r_{12}) \left[\varrho_n^2 D^2\left(\frac{p_{\mu n} r_{12}}{\hbar}\right) + \varrho_p^2 D^2\left(\frac{p_{\mu p} r_{12}}{\hbar}\right) \right] \Bigg\} d\boldsymbol{v}_1\, d\boldsymbol{v}_2\,. \end{aligned} \tag{44}$$

Bei der Berechnung dieses Integrals ist es zweckmässig als Integrationsvariable die relative Koordinate

$$\mathfrak{r} = \mathfrak{r}_1 - \mathfrak{r}_2 \equiv \mathfrak{r}_{12} \tag{45}$$

und die Schwerpunktskoordinate

$$\mathfrak{R} = \frac{1}{2}(\mathfrak{r}_1 + \mathfrak{r}_2) \tag{46}$$

je zweier Nukleonen einzuführen. Da der Integrand von der Schwerpunktskoordinate $\mathfrak{R}$ unabhängig ist, bedeutet die Integration über $\mathfrak{R}$ eine Multiplikation mit Ω.

Wenn man statt der Energie E_{short} die entsprechende Energiedichte

$$U_{\text{short}} = \frac{E_{\text{short}}}{\Omega}$$

einführt, so gelangt man für ein Nukleonengas mit konstanter Dichte zu folgendem Endergebnis

$$\begin{aligned} U_{\text{short}}(\varrho_n, \varrho_p) = \varrho_n \varrho_p \int_0^\infty V_b(r)\, D\left(\frac{p_{\mu n}\, r}{\hbar}\right) D\left(\frac{p_{\mu p}\, r}{\hbar}\right) 4\pi r^2\, dr + \\ + \frac{1}{2}\varrho_n^2 \int_0^\infty V_d(r)\, D^2\left(\frac{p_{\mu n}\, r}{\hbar}\right) 4\pi r^2\, dr + \\ + \frac{1}{2}\varrho_p^2 \int_0^\infty V_d(r)\, D^2\left(\frac{p_{\mu p}\, r}{\hbar}\right) 4\pi r^2\, dr . \end{aligned} \tag{47}$$

Die Energie E_{short} eines Kerns mit inhomogener Nukleonendichte erhält man gemäss den weiter oben Gesagten folgendermassen

$$E_{\text{short}} = \int U_{\text{short}}\big(\varrho_n(\mathfrak{r}), \varrho_p(\mathfrak{r})\big)\, dv . \tag{48}$$

Hiermit sind wir im Besitz aller Formeln, die man zur Berechnung der Energie eines Kerns benötigt.

Der in der Theorie der Kerne grundlegende Ausdruck der Energie eines Kerns als Funktion der Dichten ϱ_n und ϱ_p hat also folgende Gestalt

$$E = (E_F + E_W + E_G) + (E_{\text{long}} + E_{\text{short}}) + (E_{\text{Coul}} + E_A) . \tag{49}$$

Die Glieder in der ersten Klammer auf der rechten Seite dieses Ausdruckes enthalten die kinetische Energie des Kerns, die Glieder in der zweiten Klammer auf der rechten Seite repräsentieren die aus den Kernkräften entstehende Wechselwirkungsenergie der Nukleonen und schliesslich die beiden Glieder in der letzten Klammer auf der rechten Seite geben die elektrostatische Coulombsche Energie und Austauschenergie der Protonen.

Die einzelnen Energieanteile haben die folgende Gestalt:

$$E_F = \varkappa_F \int (\varrho_n^{5/3} + \varrho_p^{5/3})\, dv , \tag{50}$$

$$E_W = \varkappa_w \int \left[\frac{(\text{grad}\, \varrho_n)^2}{\varrho_n} + \frac{(\text{grad}\, \varrho_p)^2}{\varrho_p}\right] dv , \tag{51}$$

$$E_G = -\int [g(\varrho_n) + g(\varrho_p)]\, dv\,, \tag{52}$$

wo die Funktion g die nachstehende Bedeutung hat

$$\left.\begin{aligned} g(\varrho_n) &= \frac{1}{2}\varkappa_F \varrho_n^{5/3}, \qquad \text{für} \qquad r \leqq \frac{\hbar}{2p_{\mu n}}, \\ g(\varrho_n) &= \varkappa_1 \varrho_n^{4/3}\frac{1}{r} - \varkappa_2 \varrho_n \frac{1}{r^2} + \varkappa_3 \frac{1}{r^5}, \quad \text{für} \quad r \geqq \frac{\hbar}{2p_{\mu n}}. \end{aligned}\right\} \tag{53}$$

$$E_{\text{long}} = \iint \left\{ V_a(r_{12})\, \varrho_n(\mathfrak{r}_1)\, \varrho_p(\mathfrak{r}_2) + \frac{1}{2} V_c(r_{12})[\varrho_n(\mathfrak{r}_1)\, \varrho_n(\mathfrak{r}_2) + \varrho_p(\mathfrak{r}_1)\, \varrho_p(\mathfrak{r}_2)] \right\} dv_1\, dv_2\,, \tag{54}$$

$$E_{\text{short}} = \int U_{\text{short}}(\varrho_n, \varrho_p)\, dv\,, \tag{55}$$

$$E_{\text{Coul}} = \frac{1}{2}\iint \frac{e^2}{r_{12}} \varrho_p(\mathfrak{r}_1)\, \varrho_p(\mathfrak{r}_2)\, dv_1\, dv_2\,, \tag{56}$$

$$E_A = -\varkappa_A \int \varrho_p^{4/3}\, dv\,. \tag{57}$$

§ 8. Einiges zur Berechnung des Energieminimums

Aus dem Energieausdruck des Kerns hat man nun noch das Energieminimum zu bestimmen. Dies kann am einfachsten mit einem Variationsverfahren geschehen und zwar z. B. auf folgender Weise. Man setzt für ϱ_n und ϱ_p Funktionen an, die die Randbedingungen erfüllen und die einige Variationsparameter enthalten, die aus der Minimumsforderung der Energie bestimmt werden. Man ist natürlich bestrebt einen Ansatz zu finden, der mit möglichst wenigen Variationsparametern zum Ziel führt, d. h. eine rasche Konvergenz ergibt. Solche Ansätze dürften unserer Ansicht nach z. B. die folgenden beiden sein

$$\varrho_n(r) = \varrho_{n0}\, e^{-a_n^2 r^2}\left(1 + \frac{1}{3} c_n\, r^2\right), \quad \varrho_p(r) = \varrho_{p0}\, e^{-a_p^2 r^2}\left(1 + \frac{1}{3} c_p\, r^2\right),$$

sowie

$$\varrho_n(r) = \frac{\varrho_{n0}}{1 + e^{(r-a_n)/c_n}}, \qquad \varrho_p(r) = \frac{\varrho_{p0}}{1 + e^{(r-a_p)/c_p}},$$

wo ϱ_{n0} und ϱ_{p0} Normierungskonstanten bezeichnen, die aus den Gleichungen (1) festgelegt werden und a_n, a_p, c_n sowie c_p Variationsparameter sind, die aus der Minimumsforderung der Energie bestimmt werden.

LITERATUR

1. P. Gombás, Acta Phys. Hung., **I,** 329, 1952; P. Gombás, Acta Phys. Hung., **II,** 223, 1952; P. Gombás, E. Mágori, B. Molnár u. É. Szabó, Acta Phys. Hung., **IV,** 267, 1955; P. Gombás, P. Szépfalusy u. E. Mágori, Acta Phys. Hung., **VII,** 251, 1957; P. Gombás, Fortschritte der Physik, **5,** 159, 1957.
2. P. Gombás, Annalen der Physik, **12,** 255, 1953. Man vgl. auch in Flügges Handb. d. Physik Artikel von P. Gombás, **36,** Springer Verlag, Berlin, 1956.
3. M. A. Preston, Physics of the Nucleus, S. 114, Addison-Wesley Publishing Comp., Inc., Reading, Massachusetts, Palo Alto, London, 1962.

ОБ ОСНОВАХ СТАТИСТИЧЕСКОЙ ТЕОРИИ АТОМНЫХ ЯДЕР

П. ГОМБАШ и Д. КИШДИ

Резюме

Введением общего выражения взаимодействия нуклонов развивается статистическая теория атомных ядер, которая соответствует нынешнему состоянию наших знаний.

Acta Physica Academiae Scientiarum Hungaricae, Tomus 29 (2—3), pp. 279—295 (1970)

THEORETICAL STUDY OF SPACE-CHARGE-LIMITED (SCL) CURRENTS AND ITS APPLICATION TO ZnS SINGLE CRYSTALS

By

J. BALÁZS and Z. BODÓ

RESEARCH INSTITUTE FOR TECHNICAL PHYSICS
OF THE HUNGARIAN ACADEMY OF SCIENCES, BUDAPEST

(Received 22. I. 1970)

In this paper a general treatment of SCL currents is given for wide band-gap crystals containing several trapping levels. Thick samples have been studied thus carrier diffusion can be neglected. The temperature dependence of the $I—V$ characteristics is analysed.

An exact solution of the problem was found without neglecting the free and trapped electron density for thermal equilibrium (hitherto in the literature this has been neglected). In this case the mathematical treatment proved to be simpler even for a crystal containing two deep and one shallow trap levels.

Experimental results obtained on ZnS single crystals were analysed and interpreted.

1. Introduction

In the last 15 years the investigation of SCL currents has become one of the most useful methods for semi-insulators and semiconductors with a wide energy gap. These investigations may provide us with information of the depth and density of the traps, and the distribution of the charges, and other physical properties.

The first fundamental work was done by LAMPERT, SMITH and ROSE [1—3]. Their experimental and theoretical work called attention to the effectiveness of this method. In the course of time the theory of SCL currents developed by taking into account the role of the traps and that of the carrier diffusion. Thus, it became more complete than MOTT and GURNEY's model [4] for the case of a perfect insulator. The treatment of an entirely general case is hindered, by calculation difficulties, but in the majority of cases occurring in practice it is possible to make simplifications, and omissions.

It was shown by WRIGHT and others [5—9] that for a description of the contacts and their vicinity, carrier diffusion has to be taken into account. Its influence is negligible in samples thicker than 10 μm. The fact that the influence of carrier diffusion is often negligible, accounts for the wide applicability of LAMPERT's diffusionless model [1]. ENGLISH and DREWS [10] extended LAMPERT's model of a one-trap level to the case of a two-trap level.

In this paper, a general treatment of SCL currents is given for wide band-gap crystals containing several trapping levels. Thick samples have been

studied, so carrier diffusion could be neglected. The temperature dependence of the I—V characteristics has been analysed.

An exact solution of the problem was found without neglecting the free and trapped electron density for thermal equilibrium (hitherto in the literature this has been neglected). In this case the mathematical treatment proved to be simpler even for a crystal containing two deep and one shallow trap levels (see F1. case).

In our Laboratory ZnS single crystals of several hundred μm thickness have been studied. The temperature dependence (290—410 °K) of I—V characteristics have been determined. They exhibited an SCL character. In the literature few data are available ([11], [12]) for SCL currents in ZnS.

Two activation energy values have been obtained on the basis of the different temperature dependence of the ohmic and quadratic regions of the I—V characteristics. Such studies have been carried out by SCHMIDLIN and ROBERTS [13] on HgS and GaP.

From the analysis of a two-level theoretical model with certain values of parameters the measured and calculated I—V characteristics could be well fitted.

2. Theoretical model

Basic assumptions:

a) An n-type insulator material with wide band-gap with negligible free-hole concentration.

b) The contacts are ohmic (injecting majority carriers).

c) One-dimensional geometric arrangement (ξ coordinate).

d) In comparison with the thickness of the crystal, that of the layer on the surface, where the diffusion current is dominant, could be neglected. (At $\xi = 0$ the following boundary conditions can be applied: $\Phi = 0$, $d\Phi/d\xi = 0$, where Φ is the potential; Fig. 1.)

e) $E_1', E_2', \ldots, E_f'$ are shallow levels of discrete energy values in the band-gap (energy values are measured from the bottom of the conduction band), which are above the equilibrium Fermi-level (F_0) even on the surface, so it is impossible to fill them completely. $E_1, E_2, \ldots, E_k$ are deep levels of discrete energies which may be filled up under the influence of an external voltage (current flows) and thus the quasi-Fermi-level might also rise above them. However, the deep levels that can be considered as completely filled up, even in the inside region of the material in the temperature region considered even in the absence of any external field are not taken into account (see e.g. the case C later). Thus, the separation of the shallow levels from the deep ones takes place according to the localization on the surface. In this case the material of the contacts is important too.

f) The local thermodynamic equilibrium is valid at all points. Thus, the same quasi-Fermi-level $F(\xi)$ is valid for all energy levels. Neither the probability of trapping and escape, nor the mobility of the carriers is changed by the electric field.

g) In thermodynamic equilibrium the concentration of the electrons at the levels are given by: $E_c : n_0$ (free electron concentration); $E_1' : n_{10}'$, $\ldots$, $E_f' : n_{f0}'$; $E_1 : n_{10}, \ldots, E_k : n_{k0}$. In the case of current flow these quantities are $n(\xi), n_1'(\xi), \ldots, n_f'(\xi)$ and $n_1(\xi), \ldots, n_k(\xi)$.

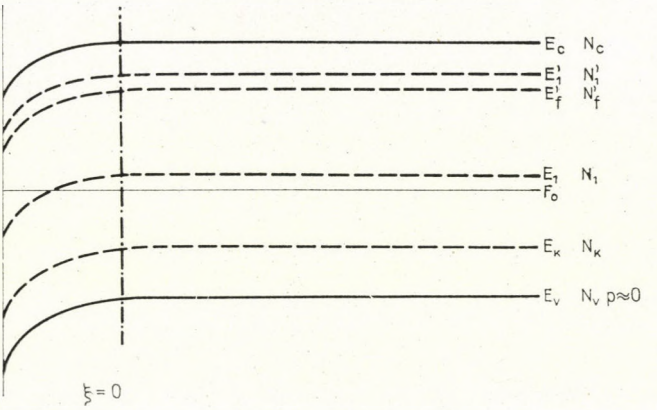


Fig. 1. The band picture

If the particle current and the mobility of the electrons are i and μ_n, respectively, then

$$i = n\mu_n \frac{d\Phi}{d\xi}; \quad n = \frac{i}{\mu_n \, d\Phi/d\xi} . \tag{1}$$

Investigating the stationary case the particle current i does not depend on the coordinate ξ. Applying further the Poisson-equation

$$\frac{d^2\Phi}{d\xi^2} = \frac{e}{\varepsilon}\left[(n-n_0) + \sum_{j=1}^{f}(n_j'-n_{j0}') + \sum_{r=1}^{k}(n_r-n_{r0})\right]. \tag{2}$$

Since

$$\begin{aligned} n_0 &\approx N_c \, e^{-\frac{E_c-F_0}{kT}}; \quad n_{j0}' \approx N_j' \, e^{-\frac{E_j'-F_0}{kT}}, \\ n &\approx N_c \, e^{-\frac{E_c-F(\xi)}{kT}}; \quad n_j' \approx N_j' \, e^{-\frac{E_j'-F(\xi)}{kT}}. \end{aligned} \tag{3}$$

Thus

$$n_j' \approx \frac{n_{j0}'}{n_0} n .$$

But

$$n_{r_0} = \frac{N_r}{1+\exp\left(\frac{E_r - F_0}{kT}\right)} .$$

Hence

$$n_r = \frac{N_r}{1+\exp\left(\frac{E_r - F(\xi)}{kT}\right)} = \frac{N_r}{\frac{n_0}{n}\frac{N_r - n_{r0}}{n_{r_0}} + 1} \tag{4}$$

by solving the following non-linear differential equation with the boundary conditions $\Phi(0) = 0$ and $d\Phi/d\xi|_{\xi=0} = 0$, Φ can be determined.

$$\frac{d^2\Phi}{d\xi^2} = \frac{e}{\varepsilon}\left[\frac{i}{\mu_n \frac{d\Phi}{d\xi}} - n_0 + \frac{i\sum_{j=1}^{f} n'_{j0}}{\mu_n \frac{d\Phi}{d\xi} n_0} - \sum_{j=1}^{f} n'_{j0} + \right.$$
$$\left. + \sum_{r=1}^{k} \frac{N_r}{\frac{N_r - n_{r0}}{n_{r_0} i} n_0 \mu_n \frac{d\Phi}{d\xi} + 1} - \sum_{r=1}^{k} n_{r_0}\right] . \tag{5}$$

It is to be remarked that LAMPERT assumed $n_0 \approx 0$, $n'_{j0} \approx 0$, $n_{r0} = 0$. Later on it can be seen that taking into account these terms, too, the calculation is simplified.

Let us introduce the dimensionless variables I, V and x, defined by the following equations:

$$I = \frac{i}{I_0}; \quad V = \frac{\Phi}{V_0}; \quad x = \frac{\xi}{L}; \tag{6}$$

where

$$I_0 = \frac{8e}{9\varepsilon} n_0 M \mu_n L; \quad V_0 = \frac{8e}{9\varepsilon} ML^2; \tag{7}$$

L is the length of the sample (the distance between the electrodes) and

$$M = n_0 + \sum_{j=1}^{f} n'_{j0} . \tag{8}$$

Further

$$R(x) = \frac{V(x)}{I}; \quad \frac{dR}{dx} = \dot{R} = \frac{n_0}{n}; \quad \frac{d^2R}{dx^2} = \ddot{R}, R(1) = \frac{V}{I} . \tag{9}$$

Then the differential equation (5) can be written as

$$\frac{8I}{9}\ddot{R} = \frac{1-\dot{R}}{\dot{R}} + \frac{1-\dot{R}}{M}\sum_{r=1}^{k}\frac{N_r - n_{r_0}}{\frac{N_r - n_{r_0}}{n_{r_0}}\dot{R}+1}. \tag{10}$$

This equation has to be solved with the initial conditions $R(0) = 0$; $\dot{R}(0) = 0$. If $I \to 0$, $\dot{R} \to 1$ and $I \to \infty$, $\dot{R} \to 0$, therefore $0 < \dot{R} < 1$.

Since in Eq. (10) every term after the Σ notation is positive, each zero-place of the expression (10), regarded as an algebraic equation, is negative except for $\dot{R} = 1$. Generally this is an equation of $(k+1)$-th degree with $k+1$ roots: $1, -\alpha_1, -\alpha_2 \ldots -\alpha_k$.

$$-\frac{9}{8I}\frac{1}{\ddot{R}} = \delta + \sum_{j=1}^{k}\frac{\beta_j}{\dot{R}+\alpha_j} + \frac{\beta_0}{\dot{R}-1}. \tag{11}$$

The quantities $\alpha_1, \alpha_2, \ldots, \alpha_k$ and $\delta, \beta_0, \beta_1, \ldots \beta_k$ can be obtained from Eq. (10). Except for some simple cases this expression can be solved only numerically but it can easily be seen that

$$\delta = \frac{M}{M + \sum_{r=1}^{k} n_{r_0}}, \tag{12}$$

$$\beta = \frac{M}{M + \sum_{r=1}^{k} n_{r_0}\left(1 - \frac{n_{r_0}}{N_r}\right)}, \tag{13}$$

$$\sum_{j=1}^{k}\frac{\beta_j}{\alpha_j} = \beta_0 - \delta, \tag{14}$$

$$\sum_{j=1}^{k}\frac{\beta_j}{\alpha_j^2} = 1 - \beta_0. \tag{15}$$

The integral of Eq. (11) can be solved in a parametric form with $\dot{R} = t$

$$\begin{aligned} -\frac{9x}{8I} &= \delta t + \sum_{j=1}^{k}\beta_j \ln\left(1+\frac{t}{\alpha_j}\right) + \beta_0 \ln(1-t), \\ -\frac{9R(x)}{8I} &= \frac{\delta t^2}{2} - \sum_{j=1}^{k}\alpha_j\beta_j \ln\left(1+\frac{t}{\alpha_j}\right) + \beta_0 \ln(1-t) + \left(\sum_{j=k}^{k}\beta_j + \beta_0\right)t. \end{aligned} \tag{16}$$

Applying Eqs. (9) and (14)

$$I = -\frac{9}{8}\frac{1}{\delta t + \left[\delta + \sum_{j=1}^{k}\frac{\beta_j}{\alpha_j}\right]\ln(1-t) + \sum_{j=1}^{k}\frac{\beta_j}{\alpha_j}\left[\beta_j \ln\left(1+\frac{t}{\alpha_j}\right)\right]}, \tag{17}$$

$$V = I\frac{\frac{\delta t^2}{2} - \sum_{j=1}^{k}[\alpha_j\beta_j\ln(1+t/\alpha_j)] + \left[\delta + \sum_{j=1}^{k}\frac{\beta_j}{\alpha_j}\right]\ln(1-t) + \left[\sum_{j=1}^{k}\beta_j + \delta + \sum_{j=1}^{k}\frac{\beta_j}{\alpha_j}\right]t}{\delta t + \left[\delta + \sum_{j=1}^{k}\frac{\beta_j}{\alpha_j}\right]\ln(1-t) + \sum_{j=1}^{k}\left[\beta_j\ln\left(1+\frac{t}{\alpha_j}\right)\right]}.$$

The asymptotic behaviour for low and high I can be determined. If $t \to 1$, then $I \to 0$, $V \sim I$, Ohm's law. But if $t \to 0$ then $I \to \infty$, $V \sim \sqrt{I}$; this is the quadratic law. The transitional region between these two limits is given by intermediate t values.

For levels below the Fermi-level even in the case of thermal equilibrium $(N_r - n_{r0})/n_{r0} < 1$. At these levels (e.g. $r = l+1, l+2, \ldots, l+m$) the first terms of the denominator of Eq. (10) can be neglected, i.e. instead of Eq. (10) we can write:

$$\frac{8I}{9}\ddot{R} = \frac{1-\dot{R}}{\dot{R}} + \frac{1-\dot{R}}{M}P + \frac{1-\dot{R}}{M}\sum_{r=1}^{l}{}' \frac{N_r - n_{r0}}{\frac{N_r - n_{r0}}{n_{r0}}\dot{R}+1}, \tag{18}$$

where

$$P = \sum_{r=l+1}^{l+m}(N_r - n_{r0}). \tag{19}$$

This means that the constant term contained in an equation of type (11) is missing.

$$-\frac{9}{8I\ddot{R}} = \sum_{j=1}^{l+1}\frac{\beta_j}{\dot{R}+\alpha_j} + \frac{\beta_0}{\dot{R}-1}. \tag{20}$$

It can be seen that

$$\beta_0 = \frac{M}{M+P+\sum_{r=1}^{l}{}' n_{r0}\left(1+\frac{n_{r0}}{N_r}\right)}, \tag{21}$$

$$\sum_{j=1}^{l+1}\frac{\beta_j}{\alpha_j} = \beta_0, \tag{22}$$

$$\sum_{j=1}^{l+1}\frac{\beta_j}{\alpha_j^2} = 1 - \beta_0 \tag{23}$$

relations are valid.

Now the solution is

$$I = -\frac{9}{8}\,\frac{1}{\left[\sum_{j=1}^{l+1}\frac{\beta_j}{\alpha_j}\right]\ln(1-t)+\sum_{j=1}^{l+1}\beta_j\ln\left(1+\frac{t}{\alpha_j}\right)}\,,$$

$$V = I\,\frac{\left[\sum_{j=1}^{l+1}\frac{\beta_j}{\alpha_j}\right]\ln(1-t)-\sum_{j=1}^{l+1}\left[\alpha_j\beta_j\ln\left(1+\frac{t}{\alpha_j}\right)\right]+\left[\sum_{j=1}^{l+1}\left(\beta_j+\frac{\beta_j}{\alpha_j}\right)\right]t}{\left[\sum_{j=1}^{l+1}\frac{\beta_j}{\alpha_j}\right]\ln(1-t)+\sum_{j=1}^{l+1}\beta_j\ln\left(1+\frac{t}{\alpha_j}\right)}\,. \qquad (24)$$

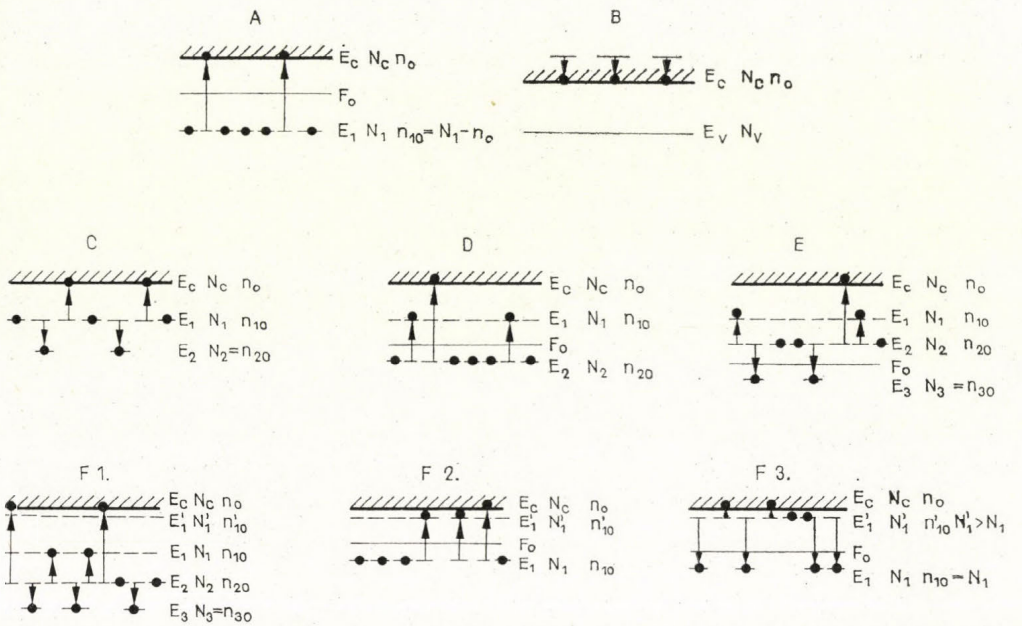


Fig. 2. Conditions of special cases. A. $f = 0, l = 0, m = 1$; B. $f = 0; k = 0$; C. $f = 0, k = 1$; D. $f = 0, l = 1, m = 1$; E. $f = 0, k = 2$; F1. $f = 1, k = 2$; F2. $f = 1, l = 0, m = 1$; F3. $f = 1, k = 0$

The asymptotes are equal to those of Eq. (17). In special cases I and V have been determined in parametric form. Using the above introduced notations the basic assumptions for the investigated cases and the calculated I—V characteristics are presented and interpreted. The conditions of special cases are shown in Fig. 2.

A) Deep donor ($f = 0$, $l = 0$, $m = 1$).

Now $l = 0$ in Eq. (18) and $P = M = n_0$. Therefore $\beta_0 = 1/2$, $\alpha_1 = 1$, $\beta_1 = 1/2$ and thus

$$I = -\frac{9}{4}\,\frac{1}{\ln(1-t^2)}\,, \qquad (25)$$

$$V = I \frac{t + \frac{1}{2}\ln(1-t) - \frac{1}{2}\ln(1+t)}{\frac{1}{2}\ln(1-t^2)} .$$

Here the I—V characteristics can be expressed

$$V = I + \frac{8}{9} I^2 \ln\left(1 + \sqrt{1 - e^{-9/4I}}\right) - \frac{8}{9} I^2 \sqrt{1 - e^{-9/4I}} . \tag{26}$$

In Fig. 3. ln (ei) is plotted against ln $\Phi(L)$. The temperature dependence of the mobility is neglected. The limit of validity of Ohm's law can be determined by the intersection of ohmic and quadratc regions. If $L = 10^{-1}$ cm, the cross-section 10^{-2} cm^2, $\varepsilon = 10^{-12}$ Asec/Vcm and $\mu_n = 10^2$ cm^2/Vsec, Table I shows these values for materials of different resistivity.

B) Fictive insulator ($f = 0$, $k = 0$).

In Eq. (10) $k = 0$, $M = n_0$, so $\beta_0 = 1$, $\delta = 1$.

$$I = -\frac{9}{8} \frac{1}{t + \ln(1-t)}; \qquad V = I \frac{t^2/2 + t + \ln(1-t)}{t + \ln(1-t)} . \tag{27}$$

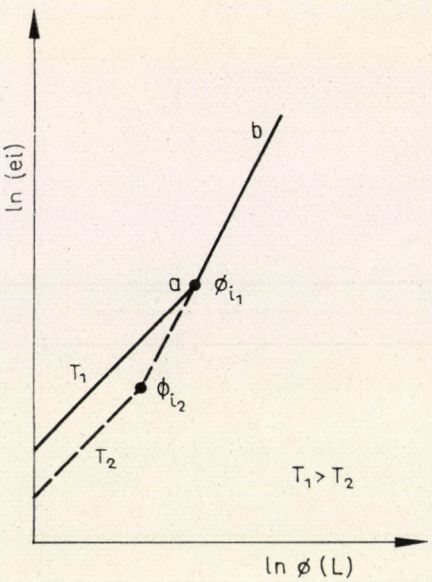


Fig. 3. I—V characteristics A case

a: $ei = \frac{e\mu_n \Phi N_c}{L} \exp\left(-\frac{E_c - F_0}{kT}\right) = \frac{e\mu_n n_0}{L}\Phi$; b: $ei = \frac{9}{8}\frac{\varepsilon\mu_n}{L^3}\Phi^2$;

Φ_i the potential of the point of intersection $\Phi_i = \frac{8eL^2}{9\varepsilon} n_0$

It is impossible, however, to give an explicit expression for this case, but in Fig. 4. it is apparent that there is almost no difference between the numerically determined cases A and B.

C) Deep donor and deeper acceptor ($f = 0$, $k = 1$). k equals 1 because the deeper acceptor level is practically completely filled up, i.e. for this level in Eq. (10) not only the condition $(N_r - n_{r0})/n_{r0} \ll 1$ is valid but also $N_r - n_{r0} \approx 0$. In this case the only role of the level N_2 is the condition $n_{10} = N_1 - n_0$ looses its validity. (In Fig. 2 this can be seen from the condition

Table I

The limit of validity of Ohm's law

ϱ [Ωcm]	σ_{n_0} [A/Vcm]	Φ_i [V]	i_i [A]
1	1	10^8	10^7
10^4	10^{-4}	10^4	10^{-1}
10^8	10^{-8}	1	10^{-9}
10^{12}	10^{-12}	10^{-4}	10^{-17}

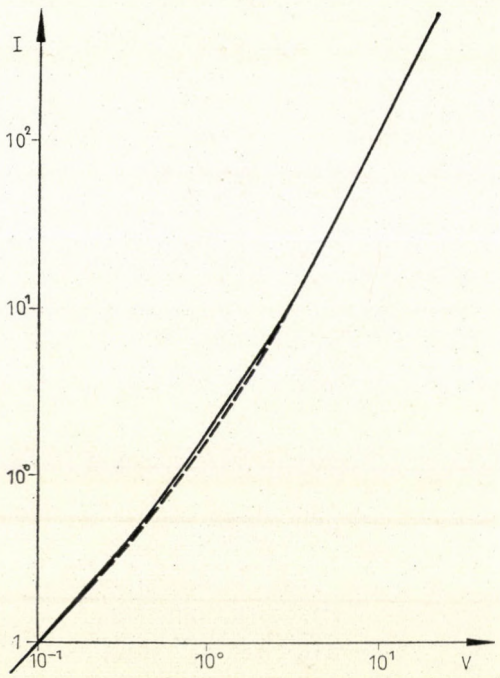


Fig. 4. $I-V$. characteristics
Full line A case, dashed line B case

$N_2 = n_{20}$. Similar situation is in the cases E, F1 and F3 too.) This is the case treated by LAMPERT as an insulator having one discrete trapping level [1], used the parameter $\lambda = (n_0 + n_{10})/n$. In our calculations $t = n_0/n = 1$ is always a root of the algebraic equation to be solved.

The solution contains still two further parameters. It seems to be suitable to choose the following parameters.

$$C = \frac{n_{10}}{M} = \frac{n_{10}}{n_0}; \quad d = \frac{n_{10}}{N_1 - n_{10}} = \frac{n_{10}}{p_{10}}. \tag{28}$$

If $N_2 = 0$ then $c = d$. If $d \to \infty$ the solution tends towards the case A, and if $d \to 0$, it tends towards the case B. As we have seen in Fig. 4 these cases are almost equal, so if $0 < d < \infty$ every solution might not strongly differ from case A. If $d \to 0$ this corresponds to case A, where the Fermi-level gradually sinks and at last the electrons escape at the donor level, i.e. the donor level is ionized. Our result can be summarized as follows: For insulators having only one donor level the shape of the I—V characteristics hardly depends on the position of the Fermi-level (i.e. on the temperature, and if so, only through μ_n).

If $c < 1$, the solution corresponds to the case B independently of the d values. That is, if the equilibrium electron concentration of the N_1 traps is low compared to the free electron concentration, they do not affect the characteristics [14].

Essential changes occur only if $c \gg 1$ and $c \gg d$. Now the two following essential cases exist: $d \ll 1$ and $d \geqslant 1$ (Figs. 5 and 6). It can be seen that in both cases a region steeper than the quadratic one appears. This is the so called "trap filled limit" (TFL) belonging to that level which can be well determined if the region is very steep.

The quadratic region following Ohm's law disappears if $d \geqslant 1$ whereas in case of $d \ll 1$ it shows a strong temperature dependence (Fig. 5) with an activation energy $E_c - E_1$. The limit of validity of Ohm's law increases with the ratio

$$\frac{\text{equilibrium electron concentration at the level}}{\text{equilibrium conduction electron concentration}}.$$

D) Deep acceptor and deeper donor ($f = 0$, $l = 1$, $m = 1$). Case C is practically regained.

E) Between two deep acceptors a deep donor ($f = 0$, $k = 2$).

In this case the parameters are the following:

$$c_1 = \frac{n_{10}}{n_0}; \quad c_2 = \frac{n_{20}}{n_0}; \quad d_1 = \frac{n_{10}}{p_{10}}; \quad d_2 = \frac{n_{20}}{n_0}. \tag{29}$$

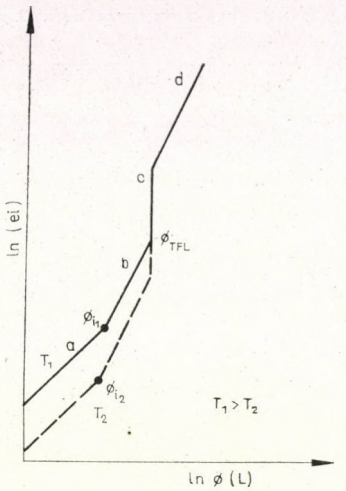


Fig. 5. $I-V$ characteristics C case if $c \gg 1$, $d \ll 1$.

a: $ei = \frac{e\mu_n n_0}{L} \Phi$; b: $ei = \frac{9\varepsilon\mu_n}{8L^3} \frac{N_c}{N_1} \exp\left(-\frac{E_c - E_1}{kT}\right) = \frac{9\varepsilon\mu_n}{8L^3} \Phi^2 \frac{n_0}{n_{10}}$

c: $\Phi_{TFL} = \frac{8eL^2}{9\varepsilon}(N_1 - n_{10}) \approx \frac{8eL^2}{9\varepsilon} N_1$; d: $ei = \frac{9\varepsilon\mu_n}{8L^3}\Phi^2$; $\Phi_i = \frac{8eL^2}{9\varepsilon} n_{10}$

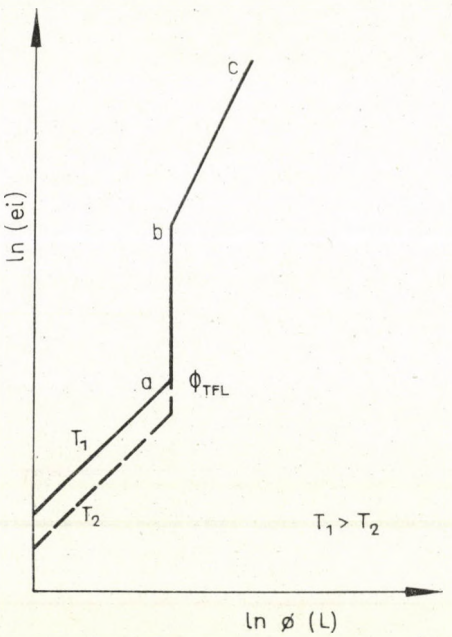


Fig. 6. $I-V$ characteristics C case if $c \gg 1$, $d \geq 1$.

a: $ei = \frac{e\mu_n n_0}{L} \Phi$; b: $\Phi_{TFL} = \Phi_i = \frac{8eL^2}{9\varepsilon} N_1$; c: $ei = \frac{9\varepsilon\mu_n}{8L^3} \Phi^2$

The solution is given by Eq. (17). Its result is of interest if

$$c_2 \gg c_1 \gg 1\,; \quad 1 \gg d_2 \gg d_1\,; \quad c_1 d_2 \gg c_2 d_1 \tag{30}$$

(see Fig. 7).

The most important conclusion is that the activation energy of each quadratic region determines the trap energy value going with it in the band-gap.

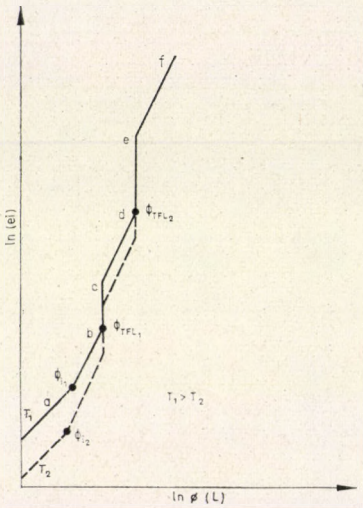


Fig. 7. I—V characteristics E case if $c_2 \gg c_1 \gg 1, 1 \gg d_2 \gg d_1$, $c_1 d_2 \gg c_2 d_1$

a: $ei = \dfrac{e\,\mu_n\,n_0}{L}\,\Phi$; b: $ie = \dfrac{9\,\varepsilon\mu_n}{8\,L^3}\,\Phi^2\,\dfrac{N_c}{N_2}\exp\left(-\dfrac{E_c - E_2}{kT}\right) = \dfrac{9\,\varepsilon\mu_n}{8\,L^3}\,\Phi^2\,\dfrac{n_0}{n_{20}}$;

c: $\Phi_{TFL_1} = \dfrac{8\,eL^2}{9\varepsilon}\,N_2$ d: $ie = \dfrac{9\varepsilon\mu_n}{8L^3}\,\Phi^2\,\dfrac{N_c}{N_1}\exp\left(-\dfrac{E_c - E_1}{kT}\right) = \dfrac{9\varepsilon\mu_n}{8L^3}\,\Phi^2\,\dfrac{n_0}{n_{10}}$;

e: $\Phi_{TFL_2} = \dfrac{8eL^2}{9\varepsilon}\,N_1$; f: $ie = \dfrac{9\varepsilon\mu_n}{8L^3}\,\Phi^2$; $\Phi_i = \dfrac{8eL^2}{9\varepsilon}\,n_{20}$

F) The influence of a shallow trap.

1. $f = 1$, $k = 2$, i.e. shallow acceptor and between the two deep acceptors a deep donor.

2. Shallow acceptor and deep donor $f = 1$, $l = 0$, $m = 1$.

3. Shallow donor and deep acceptor $f = 1$, $k = 0$.

It is characteristic to all three cases that the last quadratic region depends on the temperature through the activation energy $E_c - E_1'$. These cases differ from cases E, A and B only for this reason and further that in cases 2 and 3 the limit of validity increases with the ratio n_{10}'/n_0.

As the most important results of our theoretical investigation the following might be stated:

1. For a pure insulator of high resistivity Ohm's law is valid only within the unmeasurable potential limit Φ_i. If the band gap contains any trap level, Φ_i increases with the ratio

$$\frac{\text{equilibrium electron concentration at the level}}{\text{equilibrium conduction electron concentration}} .$$

This region is followed by a SCL one.

2. From the temperature dependence of the quadratic region of the I—V characteristics the activation energy and the position of the trap level can be determined. By this method the location of the trap levels has been determined in HgS, GaP, Se and CdS, [13], [15] and [16].

If several separable temperature dependent quadratic regions occur, it is possible to determine the position of the trap levels. Further, with the help of TFL regions also the trap concentrations can be determined [1].

In principle, more information can be obtained if the measurements are carried out at a lower temperature, but the low values of the current limit the measurements.

It is to be remarked that in several cases of parameter choice the TFL region proved to be indistinct (in the relationship $I \sim V^n$, the exponent n was 3—5 instead of 8—10). This was found in several authors' experiments [6], [10], [12], [15]. This uncertainty of the TFL causes the discrepancies occurring in the determination of trap concentrations and, therefore, it is important to treat the results provided by TFL with caution [14]—[17].

3. Experimental

In this paper experimental results and their interpretation, obtained on two samples, are presented in detail.

The I—V characteristics of ZnS single crystals were determined between 290—410 °K. The two types of crystals studied were grown by chemical transport reaction in our Institute. The undoped cubic crystals were grown in a closed system at 850—900 °C using I_2, whereas the heavily stacking faulted cubic ones doped with Mn were grown at 1200—1300 °C transported by HCl in an open system.

The samples were platelets of several hundred microns thickness. Indium contacts were deposited in "sandwich" arrangement. The measurements were carried out in the dark and in 10^{-5} torr vacuum, in order to eliminate surface conduction [12]. The method was checked by samples supplied with guard ring contacts [18], and the results proved to be satisfactory.

The samples were mounted on teflon. The d.c. measurements were carried out in the current region 10^{-14}—10^{-5} A and in the voltage region 10^{-1}—

10^3 V. The sample holder chamber was carefully screened. The current was measured with a Victoreen Dynamic Capacitor Electrometer, Model 475A, and the voltage was supplied by batteries. Before every measurement the samples were kept at about 140 °C for 1—1.5 hours since according to our experience, in this way the samples regained their initial state. Each point of the I—V characteristics was read off at ten minutes time intervals, whereas the stationary equilibrium state had been practically achieved. The temperature of the samples was stabilized within ± 1 °C.

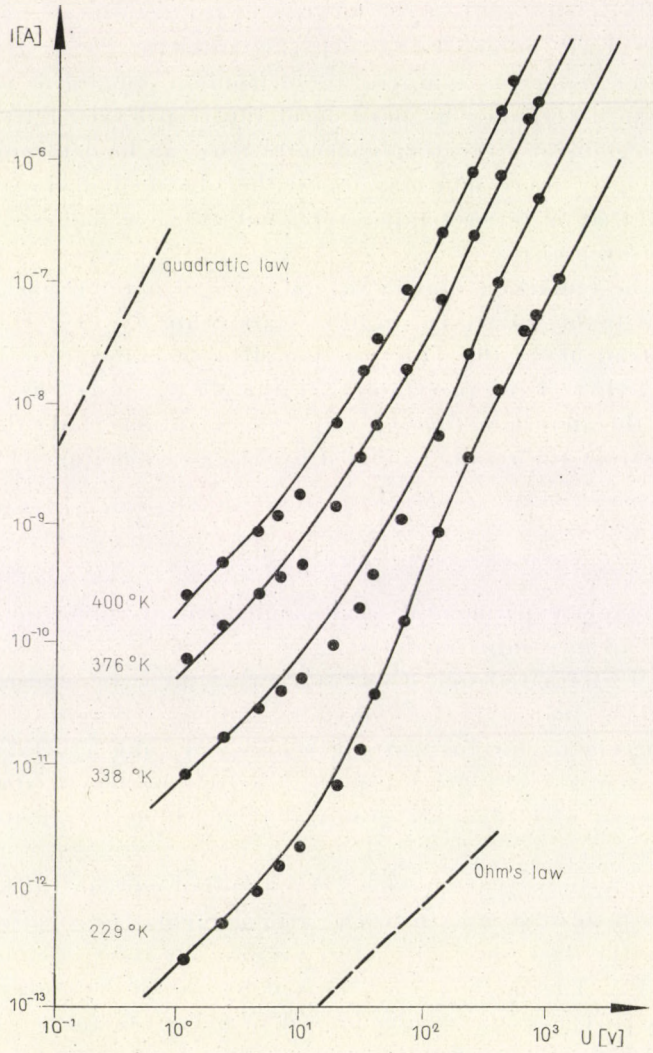


Fig. 8a. Fitting of experimental and theoretical I—V characteristics. Full lines: calculated characteristics; points: measured values. a) undoped sample

4. Results and discussion

The experimental I—V characteristics can be interpreted by the theory of SCL currents. On the basis of the sign of the thermoelectric power the samples are n-type. From the temperature dependence of the ohmic region of the characteristics and from the quadratic region following the steeper region, respectively, the activation energy has been determined. It was found that 0.66 (0.67) eV arises from the first region and 0.45 (0.46) eV from the

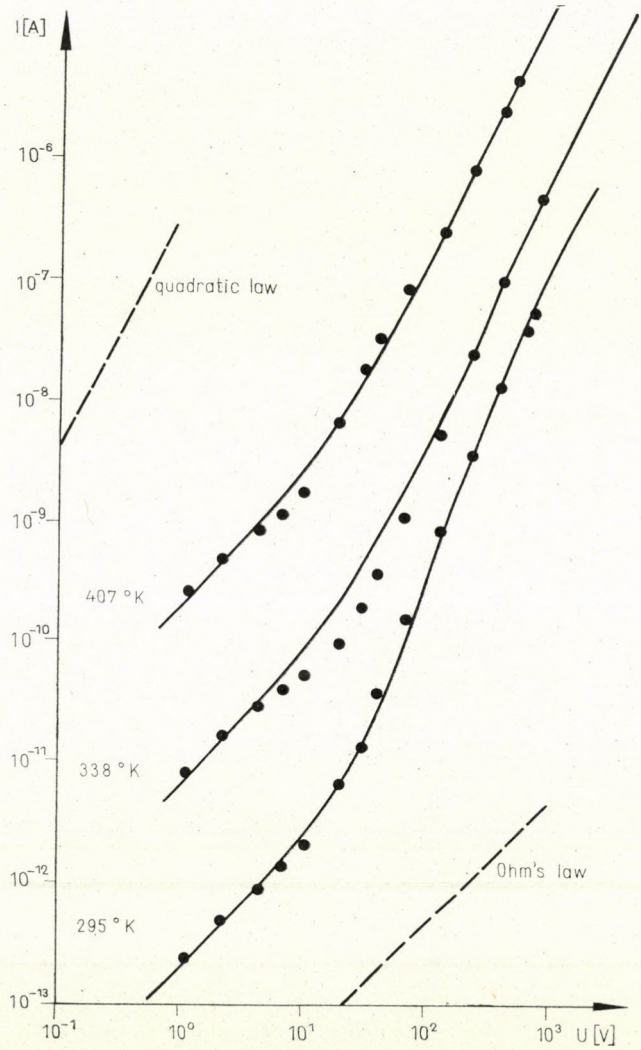


Fig. 8b Fitting of experimental and theoretical I—V characteristics. Full lines: calculated characteristics; points: measured values. b) sample doped with Mn

latter one in the case of an undoped sample (and for the Mn doped sample). These energy values can be interpreted with the help of the foregoing model.

The activation energy 0.45 (0.46) eV characterises a trap level below the conduction band. The interpretation of the other activation energy is more problematic. In the works of SCHMIDLIN and ROBERTS [13] the model of two dominant levels has been treated excluding the special case when the Fermi-

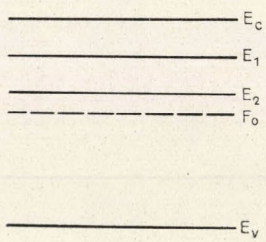


Fig. 9. Energy scheme of the investigated ZnS single crystals

Table II

The obtained energy values for ZnS crystals

Energy	Undoped samples	Samples doped with Mn
$E_C - E_1$	0.45 eV	0.46 eV
$E_C - E_2$	≈0.79 eV	≈0.79 eV
$E_C - E_{F_*}$	0.82 (299 °K)	0.83 (295 °K)
$E_C - E_{F_0}$	0.88 (400 °K)	0.89 (407 °K)

level has happened to fall within a few times kT of any level. In our case the second level fell within a few times kT of the Fermi-level, thus the corresponding equations of [13] were not applicable for the determination of the position of that level. Therefore it was determined directly on the basis of the temperature dependence of the Fermi-level. Following SHOCKLEY's designation [19] we measured F_0^* as second activation energy (0.66 (0.67) eV) where $F_0^* = F_0 - T(dF_0/dT)$. For both kinds of crystals the experimental and theoretical curves could be well fitted assuming the trap depth $E_2 = 0.79$ eV (Fig. 8). Thus the following energy scheme (Fig. 9) was obtained, and the corresponding energy values are given in Table II.

As can be seen, the two most important statements of the theoretical model — concerning the extension of the limit of validity of Ohm's law and the determining role of the activation energy of the quadratic region — are proved. We have to emphasize that the value obtained directly for the energy E_1 is accurate while that obtained indirectly for E_2 is less accurate.

The authors thank Dr. G. Gergely for helpful discussions. They are also indebted to Mr. I. Bertóti, Mr. P. Kovács, Mrs. Dr. M. Somogyi and Mr. J. Hagyó for producing and preparing the crystals.

REFERENCES

1. M. A. Lampert, Phys. Rev., **103,** 1648, 1956.
2. A. Rose, Phys. Rev., **97,** 1538, 1955.
3. M. A. Lampert, A. Rose and R. W. Smith, J. Phys. Chem. Sol., **8,** 464, 1958.
4. N. F. Mott and R. W. Gurney, Electronic Processes in Ionic Crystals, Oxford Clarendon Press, 1940.
5. G. T. Wright, Sol. Stat. El., **2,** 165, 1961.
6. D. J. Page, A. A. Kayali and G. T. Wright, Proc. Phys. Soc., **80,** 1133, 1962.
7. D. J. Page, Sol. Stat. Elect., **9,** 255, 1966.
8. R. H. Tredgold and G. G. Roberts, J. Phys. Chem. Sol., **25,** 1349, 1964.
9. M. A. Lampert and F. Edelman, J. Appl. Phys., **35,** 2971, 1964.
10. A. C. English and R. E. Drews, Sci. Electr., **9,** 1, 1963.
11. W. Ruppel, Helv. Phys. Acta, **31,** 311, 1958.
12. J. Balázs, Acta Phys. Hung., **25,** 413, 1968.
13. F. W. Schmidlin and G. G. Roberts, Phys. Rev. Letts., **20,** 1173, 1968; G. G. Roberts and F. W. Schmidlin, Phys. Rev., **180,** 785, 1969.
14. Ю. С. Рябинкин, ФТТ **6,** 2989, 1964.
15. H. P. D. Lanyon and W. E. Spear, Proc. Phys. Soc., **77,** 1157, 1961.
16. R. Bube, J. Appl. Phys., **33,** 1733, 1962.
17. G. A. Marlor and J. Woods, Proc. Phys. Soc., **81,** 1013, 1963.
18. M. J. Russ, J. Appl. Phys., **34,** 1831, 1963.
19. W. Shockley, Electrons and Holes in Semiconductors, D. van Nostrand Comp. Inc., 1950, p. 471.

ТЕОРЕТИЧЕСКОЕ ИЗУЧЕНИЕ ТОКА ОГРАНИЧЕННОГО ПРОСТРАНСТВЕННЫМ ЗАРЯДОМ (ТОПЗ) И ЕГО ПРИМЕНЕНИЕ К ИЗУЧЕНИЮ МОНОКРИСТАЛЛОВ ZnS

Й. БАЛАЖ и З. БОДО

Резюме

В данной работе дается общее изложение тока ограниченного пространственным зарядом для кристаллов с широкой запрещенной зоны, содержащих несколько прилипаний уровней. Так как изучались толстые образцы диффузией носителей можно пренебречь. Анализируется температурная зависимость вольт-амперной характеристики.

Найдено точное решение проблемы без пренебрежения плотностью свободных и захваченных ловушками электронов в случае термического равновесия (до сих пор в литературе этим эффектом пренебрегали). В этом случае математический формализм оказался более простым даже в случае кристалла, содержащего один мелкий и два глубоких уровней прилипаний.

Анализируются и интерпретируются экспериментальные результаты, полученные на монокристалле ZnS.

Acta Physica Academiae Scientiarum Hungaricae, Tomus 29 (2–3), pp. 297–300 (1970)

COMMUNICATIO BREVIS

SOME REMARKS ON CORRECTIONS CONCERNING ENERGY TRANSFER PROCESSES IN LUMINESCENT MIXED SOLUTIONS

By

J. Dombi

INSTITUTE OF EXPERIMENTAL PHYSICS, JÓZSEF ATTILA UNIVERSITY, SZEGED

(Received 2. X. 1969)

1. In a paragraph of the discussion in our paper [1] we suggested some corrections to the formula used by Rozman et al. for the experimental determination of the quantum yield of non-radiative energy transfer [2, 3]. Rozman, in a letter to the Editor,[1] answered our suggestions concerning his formula for evaluating the quantum yield of non-radiative energy transfer from experimental results, with the aid of transfer-efficiency. Therefore, after revising our respective considerations, we wish to make some modification concerning Eq. (29) in [1], as follows. (The symbols to be used are the same as in [1], so we shall not repeat the definitions.)

The formula given by Rozman for the connection between the quantum yield η_t of non-radiative energy transfer and the efficiency T_{12} (see Eq. (23)

[1] In the following we give the full text of Rozman's letter: "Уважаемый Редактор! В статье Й. Домби, опубликованной в Вашем журнале (**25,** 287, 1968), предложено исправление метода экспериментального определения квантового выхода безизлучательного переноса энергии, использованного в наших работах. Именно с целью сохранения соотношений (23) и (24) предлагается заменить (25) формулой (29). Однако легко видет, что (29) не соответствует тому правильному словесному определению η_t, которое дано Домби на стр. 304.

В самом деле, в соотствии с физическим смыслом величин можно записать

$$\eta_1 = \frac{K_e}{K_e + K_i + K_t}$$

$$\eta_t = \frac{K_t}{K_e + K_i + K_t}$$

где K_e, K_i и K_t—константы скоростей испускания фотона, безизлучательной конверсии и переноса энергии к акцептору ($K_t = 0$ при $[A] = 0$). Отсюда получаем

$$\eta_t = 1 - \frac{\eta_1}{\eta_{10}}$$

т. е. формулу (25). И. М. Розман"

in [1]), in the limiting case, when the radiative energy transfer can be considered as practically equal to zero with decreasing layer-thickness of the mixed solution, will take the following form:

$$T_{12} = \eta_t \,, \tag{1}$$

where

$$T_{12} = \frac{I_{21}/I_{22} - \alpha_{21}}{\alpha_{11}} \,, \quad \eta_t = 1 - \frac{\eta_1}{\eta_{10}} \,. \tag{2) and (3)}$$

To check the validity of Eq. (1) for this case, let η_t and T_{12} be expressed with the probability of the elementary processes in the molecules.

2. In the rather frequent case when there is no overlap between the absorption spectrum $k_1(\lambda)$ of the donor and the emission spectrum $f_2(\lambda)$ of the acceptor ($a_1 = 0$), and if — as supposed by ROZMAN — the quenching effect of the acceptor on the fluorescence of the donor can be neglected ($w_2 = 0$), then, for total absorption, the first equation of Eq. (3) in [1] can be written as follows:

$$(E_{\lambda 0}\, \alpha_{11}\, \eta_1^* - s_1\, n_1 - b_1\, n_1 - a_2\, n_1)\, dV\, dt = 0 \,. \tag{4}$$

Thus,

$$n_1 = \eta_1^* \frac{E_{\lambda 0}\, \alpha_{11}}{s_1 + b_1 + a_2} \,. \tag{5}$$

Using this value of n_1 in the expression of the quantum yield η_1 of donor fluorescence, we obtain

$$\eta_1 = \frac{s_1\, \eta_1}{E_{\lambda 0} \alpha_{11}} = \eta_1^* \frac{s_1}{s_1 + b_1 + a_2} \,. \tag{6}$$

If $c_2 = 0$, then $\eta_1 = \eta_{10}$ and $a_2 = 0$. Therefore,

$$\eta_{10} = \eta_1^* \frac{s_1}{s_1 + b_1} = \eta_1^*\, \eta_{1m} \,. \tag{7}$$

From Eqs. (6) and (7), we obtain for η_t defined in Eq. (3)

$$\eta_t = \frac{a_2}{s_1 + b_1 + a_2} \,. \tag{8}$$

This expression is identical with that given in ROZMAN's letter.

3. If the mixed solution is excited by light of wavelength λ_1 which is mainly absorbed by the donor, the part of the fluorescence quanta I_{21} emitted by the acceptor will originate from acceptor molecules which have directly

absorbed the exciting light; their number will be $E_{\lambda 10}\,\alpha_{21}$ and that of the emitted photons, $E_{\lambda 10}\,\alpha_{21}\,\eta_2(\lambda_1)$. From the excited molecules of the donor, the exciting energy of n_r molecules will be transferred by non-radiative processes. If $w_2 = 0$, as supposed, then n_r molecules of the acceptor will get into the excited state, and $n_r\,\eta_{2m}$ fluorescence photons emitted by them will furnish another part of I_{21}. Therefore,

$$I_{21} = E_{\lambda 10}\,\alpha_{21}\,\eta_2(\lambda_1) + n_r\,\eta_{2m}\,. \tag{9}$$

If the wavelength λ_2 of the exciting light is absorbed only by the acceptor, the number I_{22} of the fluorescence quanta emitted by the acceptor will be, again for total absorption,

$$I_{22} = E_{\lambda 20}\,\eta_2(\lambda_2)\,. \tag{10}$$

I_{21} and I_{22} mean the fluorescence intensities obtained with the same exciting light flux, and thus $E_{\lambda 10} = E_{\lambda 20} = E_{\lambda 0}$. If we suppose that $\eta_2(\lambda_1) = \eta_2(\lambda_2)$, then, from Eqs. (9) and (10)

$$\frac{I_{21}}{I_{22}} = \alpha_{21} + \frac{n_r\,\eta_{2m}}{E_{\lambda 0}\,\eta_2(\lambda_2)}\,. \tag{11}$$

We obtain from Eqs. (2), (10) and (11) for the efficiency

$$T_{12} = \frac{n_r\,\eta_{2m}}{\alpha_{11}\,E_{\lambda 0}\,\eta_2(\lambda_2)} = \frac{n_r}{E_{\lambda 0}\,\alpha_{11}\,\eta_2^*(\lambda_2)}\,. \tag{12}$$

As can be seen from, Eq. (4), $n_r = a_2 n_1$, and so with the use of Eq. (5) it follows from Eq. (12) that

$$T_{12} = \frac{\eta_1^*(\lambda_1)}{\eta_2^*(\lambda_2)}\,\frac{a_2}{s_1 + b_1 + a_2}\,. \tag{13}$$

4. Comparison of Eqs. (8) and (13) shows that the value of η_t defined by Eq. (3) has to be multiplied by $\eta_1^*(\lambda_1)/\eta_2^*(\lambda_2)$ to obtain T_{12}, i.e. Eq. (1) will be correct only when instead of the definition given by ROZMAN, η_t is defined as follows:

$$\eta_t = \frac{\eta_1^*(\lambda_1)}{\eta_2^*(\lambda_2)}\left(1 - \frac{\eta_1}{\eta_{10}}\right) = \frac{\eta_1^*(\lambda_1)}{\eta_2^*(\lambda_2)}\,(1 - S)\,. \tag{14}$$

Consequently, the relation for η_t suggested in Eq. (29) of our paper [1] has to be modified according to Eq. (14); furthermore, as results from Eq. (17) in [1], using the relation $\eta^*(\lambda) = \eta(\lambda)/\eta_m$ and the above Eq. (14), the equation

$$\eta_t = A \frac{\eta_1(\lambda_1)}{\eta_2(\lambda_2)} \tag{15}$$

will be the correct expression instead of Eq. (30) in [1].

REFERENCES

1. J. DOMBI, Acta Phys. Hung., **25**, 287, 1968.
2. I. M. ROZMAN, Optics and Spectrosc., **10**, 354, 1961.
3. E. A. ANDREESTHEV, C. F. KILIN, I. M. ROZMAN and B. I. SHIROKOV, Izv. Akad. Nauk. S.S.S.R., Ser. Fiz., **27**, 533, 1963.

RECENSIONES

V. L. Arnold and A. Avez: Ergodic Problems of Classical Mechanics

The Mathematical Physics Monograph Series, W. A. Benjamin, Inc. New York 1968. pp. 286

The book is designed to introduce the reader to the new presentation and to the new results of the ergodic theory as applied to differential geometry and classical mechanics. After an introductory chapter on dynamical systems (written to define terminology) the ergodic properties are summarized. Then the theory is shown to work in applications to unstable and stable systems (e.g. geodesic flows of compact Riemannian manifolds with negative curvature, stability within integrable systems).

The general framework in which the authors give this really concise survey provides an excellent insight into the multilateral applicability and importance of this branch of mathematical physics. The material is presented in such a way that the book should be used with much profit by students in the first or second year graduate course, independently of their main professional interest (mathematicians, physicists, astronomers, etc.). An extensive bibliographical survey is also given.

I. Abonyi

István Kovács: Rotational Structure in the Spectra of Diatomic Molecules

Akadémiai Kiadó, Budapest, Adam Hilger Ltd., London and American Elsevier Publishing Company, New York, 1969 pp. 320

The rotational fine structure of the band spectra gives the most detailed information on the electronic structure of diatomic molecules. Theoretical investigation of this topic started in the early days of quantum theory. Two-thirds of the paper have been published in the last twenty years, and the author of the book has made a substantial contribution in the clarification of ideas about the rotational structure of diatomic molecules. The book makes references to 218 papers and the present volume comprises the results up to the end of 1966.

The main chapters of the volume are as follows:

Preface
Introduction
General remarks on observed spectra

1. Foundations of a theory of diatomic molecules
   1.1. Wave equation and its approximate solution
   1.2. Interactions of the electron spin
   1.3. Matrix elements arising from the terms neglected on the separation of the wave equation
   1.4. Perturbation matrix of the centrifugal term
   1.5. Perturbation calculation
2. Multiplet term formulas
   2.1. Spin multiplets and Λ-type doubling
   2.2. L-multiplets
3. Intensity distribution in rotational bands
   3.1. General remarks
   3.2. Intensity distribution among spin multiplets of the same multiplicity
   3.3. Intensity distribution among spin multiplets of different multiplicity
   3.4. Intensity distribution for L-multiplets

4. Perturbations in the spectra
4.1. General theory of perturbations
4.2. Perturbations among states of the same multiplicity
4.3. Perturbations among states of different multiplicity
4.4. Methods for the determination of the constants of perturbing molecular terms

References
Author Index
Subject Index

The investigation of the detailed rotational structure in the spectrum of the diatomic molecules is a field of many scientists because of its theoretical and practical importance. The determination of many atomic, molecular and nuclear data became possible through the investigation of the spectra of diatomic molecules. Its practical importance may be understood by considering the fact that the most important constituents of the atmosphere of the earth are diatomic molecules.

Not all the material in this monograph has previously appeared in print. The author has made detailed investigations to make the book self-consistent. Many of the multiplet formulae and the intensity distribution formulae are the results of his recent investigations.

This monograph can be read by anyone with some knowledge of basic quantum mechanics. Some understanding of elementary theory of angular momentum and basic models of diatomic molecules is necessary.

The book will be a useful guide for experimental and theoretical research workers who wish to work on the structure of rotational spectra of diatomic molecules. It may be helpful not only to physicists and chemists working on spectroscopy, but also to astronomers and those working on models of the atmospheres of the earth and stars.

R. GÁSPÁR

G. VARSÁNYI: Vibrational Spectra of Benzene Derivatives

Akadémiai Kiadó, Budapest and Academic Press, New York and London, 1969. pp. 430

Whereas in the case of diatomic molecules, owing to their single possible normal vibration, it is mainly the study of the rotational structure of spectra that leads to a better understanding of the internal molecular structure, in the case of polyatomic molecules, owing to the larger number of normal vibrations, the study of vibrational structure already provides interesting information on their structure and composition. The most important tools to study the vibrational structure are infrared and Raman spectra, which have already been applied extensively and efficiently to the structural investigations of intricate organic molecules for a long time. Of the organic molecules, benzene and its derivatives play an important role in organic chemistry, and such compounds are used as starting materials in many factories producing dyes, pharmaceutical preparations, explosives and industrial chemicals. The very same substances also have special importance from the point of view of theoretical chemistry, and the applicability of quantum mechanics for chemical problems was proved on the examples of these compounds. In recent years many books and monographs have appeared about the theory of vibrational spectra. This, however, is the first monograph dealing with the problems of the vibrational spectra of benzene and its derivatives. The extensive literature dealing with the vibrational spectra of benzene derivatives and their assignments has been compiled for about 30 years. A survey of this literature can be found in the third part of the present book. So that the book should be useful not only for physicists and researchers familiar with theoretical spectroscopy, but also for consultation by chemists concerned with structure elucidation, the author's aim was to present in the first part of the book the absolutely necessary fundamentals needed for a comprehension of part three. For the sake of completeness it was necessary to insert the second part of an entirely theoretical character written by S. SZŐKE. This part, however, may be regarded as largely independent of the third part, and can be understood by itself. In the third part, the author has succeeded in deducing general rules for the interpretation of frequencies which depend on the masses of substituents and their orientation with

respect to the ring and to one an other. With the help of these rules, an easily perceptible and qualitative interpretation is given for the frequencies. Such a systematic and detailed analysis of the vibrational spectra of substituted benzenes has not been treated in the literature so far, and the present work constitutes the first success along these lines. The author has compiled the list of all important studies that have dealt with this great and difficult problem, and presents the spectra of compounds containing single and multiple carbon, oxygen, and sulphur bonds in the side chains. This book will be useful not only for chemists using the vibrational spectra for structure elucidation and to solve analytical problems: physicists and chemists dealing with the theoretical calculations of vibrational spectra will find a copious and systematic source of information in this book.

I. Kovács
Department of Atomic Physics
Polytechnical University, Budapest

J. Yvon: Correlations and Entropy in Classical Statistical Mechanics

International Series of Monographs in Natural Philosophy, Vol. 21.; Translated from the French by H. S. H. Massey; Edited by D. ter Haar; Pergamon, Oxford, 1969; XX + 183 pages

Having in mind his senior undergraduate and graduate students of physics, the author discusses in this volume methods of classical statistical mechanics employed in the study of entropy, together with a description of the correlations connected with the approximation methods of classical statistical mechanics. First, probability densities and their evolution are defined followed by a treatment of the occupation of states, the cumulant method, molecular disorder and mixtures. By introducing the concept of statistical entropy and its evolution in different cases, the canonical laws of thermodynamic equilibrium and thermal quilibrium in the case of identical point molecules are discussed in detail. Finally, the fine structure in thermal equilibrium, phase changes, and thermal waves in fluids are investigated. The last chapter is devoted to the connection between entropy and heat, i.e., the H-theorem, the statistical entropy densities and thermal entropy. This monograph is based on the author's lectures at the University of Paris. Both its subject and its method of treatment make it of particular value to readers interested in an introduction to the applications of classical statistical mechanics to problems of entropy.

J. I. Horváth

L. D. Landau and E. M. Lifshitz: Mechanics

Vol. 1. of Course of Theoretical Physics; Translated from the Russian by J. B. Sykes and J. S. Bell; 2nd ed.; Pergamon, Oxford, 1969; VII + 165 pages

The first volume of the famous "Course of Theoretical Physics" by Landau and Lifshitz is devoted to the foundation of classical mechanics. As in the other volumes of this Course the authors' exposition makes no use of the historical approach, but from the very beginning it is based on the most general principles: Galileo's principle of relativity and Hamilton's principle of least action. The conservation laws of mechanics are, e.g., derived direct from the symmetry properties of space, time and the Lagrangian. In dealing with the integration of the equations of motion especially Keppler's problem is treated in detail. Then, collisions between particles, the theory of small oscillations, the motion of a rigid body, finally the canonical formalism of classical mechanics are investigated.

No extensive revision of the book was necessary for the second English edition, but a few additional comments and problems have been inserted in various places.

J. I. Horváth

S. DRAKE and I. E. DRABKIN: Mechanics in Sixteenth-Century in Italy, Selections from Tartaglia, Benedetti, Guido Ubaldo and Galileo Galilei

The University of Wisconsin Press, Madison, Milwaukee and London, 1969, S. 12.50

Physics, and especially mechanics, in the sixteenth century is marked by the transition from medieval to modern scientific thought, so its study is crucial to an understanding of intellectual history. This anthology of treatises on mechanics translated and adapted by Prof. S. DRAKE and I. E. DRABKIN illuminates some important conceptual developments during this period.

NICCOLO TARTAGLIA in parts of his Nova Scientia and Quesiti et Inventioni applies principles of mechanics to ballistics and balances. GIOVANNI BATTISTA BENEDETTI criticizes the traditional approaches to physical problems, GUIDO UBALDO discusses simple machines in his Mechanicorum Liber, GALILEO GALILEI's contribution "Dialogue of Motion" and "Memoranda on Motion" remained unpublished until the nineteenth century.

After an introduction of sixteenth-century mechanics S. DRAKE and I. E. DRABKIN present translations of these selections and annotate them including diagrams from the originals making them fully accessible to modern physicists. This beautiful book can be recommended to everybody who is interested in the mechanics of the Sixteenth-Century.

P. GOMBÁS

Y. TAKAHASHI: An Introduction to Field Quantization

International Series of Monographs in Natural Philosophy, Vol. 20.
Pergamon Press, Oxford, London, Edinburgh, New York, Toronto, Sidney, Paris, Braunschweig, 1969.

This book, written by one of the leading physicists in this field who has contributed many papers to this subject, gives an excellent introduction to relativistic quantum field theory. The Hamiltonian formalism is abandoned and the book is based on the Heisenberg equation of motion. It contains the following chapters: I. Introduction, II. Non-relativistic fields, III. Relativistic Free Fields, IV. Some Aspects of Linear Field Equations, V. Quantization of Relativistic Free Fields, VI. Transformation of Field Operators, VII. An Explicit Construction of Wave Functions, VIII. Interacting Fields. In the Appendix mostly mathematical problems are discussed.

This book can be recommended as a text book for graduate students; the material is so arranged that the formulae can be used very easily.

P. GOMBÁS

INDEX

I. Szép and *I. Bársony:* Oxygen Content Determination in Thin Silicon Slices. — *И. Сейп* и *И. Баршонь:* Определение содержания кислорода в тонких пластинках кремния 97

S. K. Sangal and *P. K. Sharma:* Vibration Spectra and Debye Temperatures of Transition Metals. — *С. К. Сангал* и *П. К. Шарма:* Колебательные спектры и температура Дэбая переходных металлов 107

M. S. El-Manharawy: The Influence of Cobalt on the Photo-Luminescence of Silver-Activated ZnS : CdS Phosphors Containing Nickel. — *М. С. Эл-Манхарави:* Влияние кобальта на фотолюминесценцию фосфоров активизированных серебром и содержащих никель 117

M. El-Nadi, A. Osman and *T. H. Rihan:* Finite Range Coulomb Stripping in (t, p) and (He^3, n) Reactions. — *М. Эл-Нади, А. Осман* и *Т. Х. Рихан:* Кулоновская реакция срыва (t, p) и (He^3,n) с конечным радиусом взаимодействия 127

M. El-Nadi, A. Osman and *T. H. Rihan:* Cluster Transfer Reactions at Low Energies — *М. Эл-Нади, А. Осман* и *Т. Х. Рихан:* Реакции при низких энергиях с передачей «кластеров» 143

R. G. Nousratoullin and *I. Ts. Lyast:* Application of Variation-Perturbation Theory to the Study of the Inductive Effect in Saturated Molecules by the Method of Geminals II. Halogen-Substituted Hydrocarbons. — *Р. Г. Нусратуллин* и *И. Ц. Ляст:* Применение вариационной теории возмущения к изучению индуктивного эффекта в насыщенных молекулах методом геминалей II. Галогенозамещенные углеводороды 159

G. Fáy: On the Correspondence Principle. — *Г. Фаи:* О принципе соответствия 167

I. Hevesi and *B. Karvaly:* Optical Reflection of V_2O_5 Single Crystals. — *И. Хевеши* и *Б. Карваль:* Оптическое отражение монокристаллов V_2O_5 183

E. Balázs: Collective Vibrations of the Statistical Nuclear Model. — *Э. Балаж:* Коллективные колебания в статистической ядерной модели 193

B. Karvaly and *F. Pintér:* Investigations on the Connections between the Bulk Absorption and Diffuse Reflectance Spectra of Powdered Solids II. — *Б. Карваль* и *Ф. Пинтэр:* Исследования о взаимосвязи между спектрами истинного (массивного) поглощения и диффузного отражения порошкообразных веществ II 203

L. Szalay and *Z. Várkonyi:* Investigations on Connections between Fluorescence Polarization and Foreign Quenching in Viscous Solutions. — *Л. Салаи* и *З. Варкони:* Исследования соотношений между флуоресцентной поляризацией и посторонним погласителем в вискозных растворах 221

R. M. Gupta and *N. L. Varma:* Penetration of Electromagnetic Waves into Plasma. — *Р. М. Гупта* и *Н. Л. Варма:* Проникновение электромагнитных волн в плазму 229

I. Kovács, L. Nagy and *I. Vinnay:* Angular Anisotropy of Fission Fragments in Ternary Fission of ^{235}U and ^{238}U Induced by 14 MeV Neutrons. — *И. Ковач, Л. Надь* и *И. Виннаи:* Угловая анизотропия осколков деления в тройном делении ^{235}U и ^{238}U вызванная нейтронами 14 МэВ 239

I. Kirschner, A. Stark and *I. I. Falko:* The Collective Effect of Paramagnetic and Diamagnetic Impurities on the Temperature of Superconducting Transition. — *И. Киршнер, А. Штарк* и *И. И. Фалко:* Совместное влияние пара и диамагнитных примесей на температуру сверхпроводящего перехода 243

K. L. Nagy: Complex Poles, Cuts, Indefinite Metric and Unitarity. — *К. Л. Надь:* Комплексные полюсы, разрезы, неопределенная метрика и унитарность 251

P. Gombás und *D. Kisdi:* Über die Grundlagen der statistischen Theorie des Atomkerns. — *П. Гомбаш* и *Д. Кишди:* Об основах статистической теории атомных ядер 267

J. Balázs and *Z. Bodó:* Theoretical Study of Space-Charge-Limited (SCL) Currents and its Application to ZnS Single Crystals. — *Й. Балаж* и *З. Бодо:* Теоретическое изучение тока ограниченного пространственным зарядом (топз) и его применение к изучению монокристаллов ZnS 279

COMMUNICATIO BREVIS

J. Dombi: Some Remarks on Corrections Concerning Energy Transfer Processes in Luminescent Mixed Solutions 297

RECENSIONES 361

PHYSIK UND CHEMIE DER KRISTALLOBERFLÄCHE

Vortragstagung vom 8. bis 11. Oktober 1966 in Halle (Saale)

Vorbereitet von Prof. Dr. H. BETHGE (Halle/S.), Prof. Dr. W. KLEBER (Berlin) und Prof. Dr. A. NEUHAUS (Bonn)

Herausgegeben von Prof. Dr. Dr. J.-H. SCHARF, Halle/S.

(Nova Acta Leopoldina. Neue Folge. Suppl. 1)

1968. VI, 446 Seiten mit 220 Abbildungen

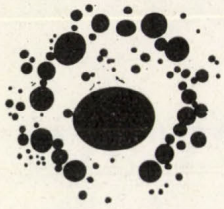
Kunstleder 53,— M

Auf dem Gebiete der Kristallforschung begegnen sich Physik, Chemie, Mineralogie und physikalische Chemie. Der große Aufschwung, den die Grenzflächenphysik und Grenzflächenchemie genommen haben, hängt in erster Linie zusammen mit der Entwicklung neuer experimenteller Techniken, so z. B. der Beherrschung des Hochvakuums. Die Thematik der Tagung bringt das Neueste und reicht von Atomanordnungen in Kristalloberflächen über Kristallwachstum und Adsorption bis zur Katalyse hin.



Bestellungen an den Buchhandel erbeten

JOHANN AMBROSIUS BARTH LEIPZIG



Journal of Aerosol Science

Chairman of the Editorial Board
C. N. DAVIES
London School of Hygiene and Tropical Medicine London

It has been known for some time that there exists a genuine need for a publication handling original papers on all aspects of aerosol science. For too long aerosol research results have been published in a diversity of specialist journals, often of an applied nature. The importance of the subject is obvious and accepted; basic theoretical and experimental work demands independent treatment.

The desired forum has now been created by the publication of the JOURNAL OF AEROSOL SCIENCE, a new, high level journal dealing solely with aerosol research.

This international journal allows for the publication of original papers on all aspects of the subject. These include basic aerosol formation; processes and reactions; nucleation; chemistry; optics; mechanics; electrostatics; analysis; electromagnetic, acoustic and nuclear radiations; diffusion processes; mobility; condensation and evaporation; heat motion; energy distribution; forces of attraction and repulsion; turbulence; coagulation; deposition; biological action in man and animals; microscopy and electron microscopy; instrumentation.

Applied scientists, engineers and doctors who use aerosol techniques will find the journal invaluable for keeping up with modern developments. Its fundamental approach and presentation of results in the most general form will appeal to students and research workers.

Papers submitted for publication in the JOURNAL OF AEROSOL SCIENCE will be subjected to constructive criticism by identified referees who will discuss them with the authors as far as is required. All submissions to this new journal are welcomed and should be sent to one of the members of the Editorial Board.

Published quarterly — first issue January 1970

Annual subscription:	£12.00	$30.00	A$26.00
Two Years:	£21.60	$54.00	A$47.00
Single Issues:	£ 3.50	$ 9.00	A$ 8.00

Please write to Dept. ED (t) for an inspection copy and information on related journals.



PERGAMON PRESS
HEADINGTON HILL HALL
OXFORD OX3 0BW ENGLAND

Solutions of the Simplified Self-consistent Field for all Atoms of the Periodic System of Elements from $Z = 2$ to $Z = 92$

BY P. GOMBÁS AND T. SZONDY

The text of these tables is in English and German. It contains the solutions in two approximations of the simplified self-consistent field, worked out by one of the authors, for all electron states of the atoms from $Z = 2$ to $Z = 92$. In the second approximation the eigenfunctions are obtained in a simple way in analytical form which are represented explicitly for all electron states. This is the most important result of this work since the analytical representation of the eigenfunctions of the self-consistent field has up to now been undertaken only in a few works.

In English and German · Approx. 80 pages · 17 × 25
Cloth

1828

AKADÉMIAI KIADÓ

PUBLISHING HOUSE OF THE HUNGARIAN ACADEMY OF SCIENCES

BUDAPEST

Dr. M. FRANK und Dr. W. STOLZ

FESTKÖRPERDOSIMETRIE IONISIERENDER STRAHLUNG

283 Seiten mit 97 Abbildungen und 28 Tabellen. 14,7×21.5 cm. 1969
In Leinen 39,– M

INHALT:

EINFÜHRUNG · THEORETISCHE GRUNDLAGEN DER DOSIMETRIE · INTEGRIERENDE FESTKÖRPERDOSIMETRIE · SZINTILLATIONSDOSIMETRIE · DOSIMETRIE DURCH STRAHLENINDUZIERTE LEITFÄHIGKEITSÄNDERUNG IN FESTKÖRPERN

Mit der raschen Weiterentwicklung von Wissenschaft und Technik haben sich auch die Anwendungsmöglichkeiten durchdringender Strahlungen wesentlich erweitert, und es ergab sich zwangsläufig die Notwendigkeit, die Meßmethoden der Strahlungsdosis zu verbessern. In der vorliegenden Monographie werden die verschiedenen Verfahren der Festkörperdosimetrie nebst ihren Anwendungsmöglichkeiten beschrieben. Die Festkörpermethoden haben gegenüber der Ionisations- und Filmdosimetrie wesentliche Vorteile.

BSB B. G. TEUBNER VERLAGSGESELLSCHAFT

LEIPZIG

Printed in Hungary

A kiadásért felel az Akadémiai Kiadó igazgatója — Műszaki szerkesztő: Farkas Sándor

A kézirat nyomdába érkezett: 1970. VII. 15. — Terjedelem: 19 (A/5) ív, 68 ábra

71.70155 Akadémiai Nyomda, Budapest — Felelős vezető: Bernát György

The *Acta Physica* publish papers on physics, in English, German, French and Russian.

The *Acta Physica* appear in parts of varying size, making up volumes.

Manuscripts should be addressed to:

Acta Physica, Budapest 502, P. O. B. 24.

Correspondence with the editors and publishers should be sent to the same address.

The rate of subscription is $ 16.00 a volume.

Orders may be placed with "Kultúra" Foreign Trade Company for Books and Newspapers (Budapest I., Fő u. 32. Account No. 43-790-057-181) or with representatives abroad.

Les *Acta Physica* paraissent en français, allemand, anglais et russe et publient des travaux du domaine de la physique.

Les *Acta Physica* sont publiés sous forme de fascicules qui seront réunis en volumes.

On est prié d'envoyer les manuscrits destinés à la rédaction à l'adresse suivante:

Acta Physica, Budapest 502, P. O. B. 24.

Toute correspondance doit être envoyée à cette même adresse.

Le prix de l'abonnement est de $ 16.00 par volume.

On peut s'abonner à l'Entreprise du Commerce Extérieur de Livres et Journaux «Kultúra» (Budapest I., Fő u. 32. — Compte-courant No. 43-790-057-181) ou à l'étranger chez tous les représentants ou dépositaires.

«*Acta Physica*» публикуют трактаты из области физических наук на русском, немецком, английском и французском языках.

«*Acta Physica*» выходят отдельными выпусками разного объема. Несколько выпусков составляют один том.

Предназначенные для публикации рукописи следует направлять по адресу:

Acta Physica, Budapest 502, P. O. B. 24.

По этому же адресу направлять всякую корреспонденцию для редакции и администрации. Подписная цена — $ 16.00 за том.

Заказы принимает предприятие по внешней торговле книг и газет «*Kultúra*» (Budapest I., Fő u. 32. Текущий счет: № 43-790-057-181) или его заграничные представительства и уполномоченные.

Reviews of the Hungarian Academy of Sciences are obtainable at the following addresses:

ALBANIA
Drejtorija Qändrone e Pärhapjes dhe Propagandimit tä Librit
Kruga Konferenca e Päzes
Tirana

AUSTRALIA
A. Keesing
Box 4886, GPO
Sydney

AUSTRIA
GLOBUS
Höchstädtplatz 3
A-1200 Wien XX

BELGIUM
Office International de Librairie
30, Avenue Marnix
Bruxelles 5
Du Monde Entier
5, Place St. Jean
Bruxelles

BULGARIA
HEMUS
11 pl Slaveikov
Sofia

CANADA
Pannonia Books
2, Spadina Road
Toronto 4, Ont.

CHINA
Waiwen Shudian
Peking
P. O. B. 88

CZECHOSLOVAKIA
Artia
Ve Směčkách 30
Praha 2
Poštovní Novinová Služba
Dovoz tisku
Vinohradská 46
Praha 2
Mad'arská Kultura
Václavské nám. 2
Praha I
SLOVART A. G.
Gorkého
Bratislava

DENMARK
Ejnar Munksgaard
Nörregade 6
Copenhagen

FINLAND
Akateeminen Kirjakauppa
Keskuskatu 2
Helsinki

FRANCE
Office International de Documentation et Librairie
48, rue Gay Lussac
Paris 5

GERMAN DEMOCRATIC REPUBLIC
Deutscher Buch-Export und Import
Leninstraße 16
Leipzig 701
Zeitungsvertriebsamt
Fruchtstraße 3—4
1004 Berlin

GERMAN FEDERAL REPUBLIC
Kunst und Wissen
Erich Bieber
Postfach 46
7 Stuttgart S.

GREAT BRITAIN
Blackwell's Periodicals
Oxenford House
Magdalen Street
Oxford
Collet's Subscription Import Department
Denington Estate
Wellingsborough. Northants.
Robert Maxwell and Co. Ltd.
4—5 Fitzroy Square
London W. I

HOLLAND
Swetz and Zeitlinger
Keizersgracht 471—487
Amsterdam C.
Martinus Nijhof
Lange Voorhout 9

INDIA
Hind Book House
66 Babar Road
New Delhi I

ITALY
Santo Vanasia
Via M. Macchi 71
Milano
Libreria Commissionaria Sansoni
Via La Marmora 45
Firenze

JAPAN
Kinokuniya Book-Store Co. Ltd.
826 Tsunohazu 1-chome
Shinjuku-ku
Tokyo
Maruzen and Co. Ltd.
P. O Box 605
Tokyo-Central

KOREA
Chulpanmul
Phenjan

NORWAY
Tanum-Cammermeyer
Karl Johansgt 41—43
Oslo I

POLAND
RUCH
ul. Wronia 23
Warszawa

ROUMANIA
Cartimex
Str. Aristide Briand 14—18
Bucureşti

SOVIET UNION
Mezhdunarodnaya Kniga
Moscow G—200

SWEDEN
Almquist and Wiksell
Gamla Brogatan 26
S—101 20 Stockholm

USA
F. W. Faxon Co. Inc.
15 Southwest Park
Westwood Mass. 02090
Stechert Hafner Inc.
31. East 10th Street
New York, N. Y. 10003

VIETNAM
Xunhasaba
19, Tran Quoc Toan
Hanoi

YUGOSLAVIA
Forum
Vojvode Mišića broj 1
Novi Sad
Jugoslovenska Knjiga
Terazije 27
Beograd

ACTA PHYSICA

ACADEMIAE SCIENTIARUM HUNGARICAE

ADIUVANTIBUS
L. JÁNOSSY, I. KOVÁCS, K. NAGY, A. SZALAY

REDIGIT
P. GOMBÁS

TOMUS XXIX FASCICULUS 4

AKADÉMIAI KIADÓ, BUDAPEST
1970

ACTA PHYS. HUNG.

ACTA PHYSICA

A MAGYAR TUDOMÁNYOS AKADÉMIA FIZIKAI KÖZLEMÉNYEI

SZERKESZTŐSÉG ÉS KIADÓHIVATAL: BUDAPEST V., ALKOTMÁNY UTCA 21.

Az *Acta Physica* német, angol, francia és orosz nyelven közöl értekezéseket a fizika tárgyköréből.

Az *Acta Physica* változó terjedelmű füzetekben jelenik meg: több füzet alkot egy kötetet.

A közlésre szánt kéziratok a következő címre küldendők:

Acta Physica, Budapest 502, P. O. B. 24.

Ugyanerre a címre küldendő minden szerkesztőségi és kiadóhivatali levelezés.

Megrendelhető a belföld számára az Akadémiai Kiadónál (Budapest V., Alkotmány utca 21. Bankszámla 05-915-111-46), a külföld számára pedig a „Kultúra" Könyv- és Hírlap Külkereskedelmi Vállalatnál (Budapest I., Fő utca 32. Bankszámla 43-790-057-181 sz.), vagy annak külföldi képviseleteinél és bizományosainál.

Die *Acta Physica* veröffentlichen Abhandlungen aus dem Bereich der Physik in deutscher, englischer, französischer und russischer Sprache.

Die *Acta Physica* erscheinen in Heften wechselnden Umfanges. Mehrere Hefte bilden einen Band.

Die zur Veröffentlichung bestimmten Manuskripte sind an folgende Adresse zu richten:

Acta Physica, Budapest 502, P. O. B. 24.

An die gleiche Anschrift ist auch jede für die Redaktion und den Verlag bestimmte Korrespondenz zu senden. Abonnementspreis pro Band: $ 16.00.

Bestellbar bei dem Buch- und Zeitungs-Aussenhandels-Unternehmen »Kultúra« (Budapest I., Fő u. 32. Bankkonto Nr. 43-790-057-181) oder bei seinen Auslandsvertretungen und Kommissionären.

Acta Physica Academiae Scientiarum Hungaricae, Tomus 29 (4), pp. 305—307 (1970)

ON THE SYMMETRY PROPERTIES OF THE EQUATION OF MOTION

By

N. D. SEN GUPTA

TATA INSTITUTE OF FUNDAMENTAL RESEARCH, BOMBAY 5, INDIA

(Received 3. V. 1969)

The object of this paper is to obtain the restrictions on the form of the force functions of a system of particles due to the covariance of the equation of motion with respect to the Euclidean group.

1. Introduction

In a recent paper KNAPECZ [1] has investigated the restriction on the form of the force functions of the dynamic law of a system of point particles due to the validity of the Euclidean invariance. The discussion was confined to the case of motion of a system of particles in a plane, because of the limitation of the method used, namely that of functional equations. If instead of introducing finite transformations which naturally leads to functional equations, one considers infinitesimal transformations one is led to linear differential equations which are much easier to investigate; further, restriction to motion in a plane is no longer a restriction. The analytical problem is, essentially, to find the general form of the vectors which are functions of basic vectors, namely the position and velocities of the particles. The general problem of the nature of tensors which are functions of vectors has been studied by the author [2]. In that paper the invariance group considered is the orthogonal group.

The object of this short paper is to extend the method used in [2] to the Euclidean group by adding translation to the rotation. The problem of pure rotation has been investigated in detail in [2], without any restriction on the number of vectors involved so long as all of them are finite. Our discussion here will be directed exclusively to the additional conditions to be imposed due to the translational invariance.

2. The dynamic problem

Let x_i^λ be the ith co-ordinate of the λth particle. The Greek superscripts refer to the particle indices which may be N in number and the Latin subscripts refer to the space coordinates, $i = 1, 2, 3$. The corresponding component

of the velocity is represented by $v_i^\lambda = dx_i^\lambda/dt$. So that the equations of motion are

$$\frac{dx_i^\lambda}{dt} = F_i^\lambda(x,\ v)\,, \tag{1}$$

x and v stand for the entire set of particle coordinates and velocities. The effect of the operation of an infinitesimal element of the Euclidean group on x_i^λ and v_i^λ are given by

$$x'^\lambda_i = \sum_i (\delta_{ij} + e_{ij})\, x_j^\lambda + \tau_i \tag{2}$$

and

$$v_i'^\lambda = \sum_i (\delta_{ij} + e_{ij})\, v_j^\lambda\,. \tag{3}$$

The summation over Latin indices are from 1, 2, 3. There are six parameters, three τ_i for translation and three e_{ij} for rotation, which are antisymmetric,

$$e_{ij} + e_{ji} = 0. \tag{4}$$

In order that Eqs. (1) are covariant with respect to the transformation (2) and (3), $F_i^\lambda(x,v)$ should satisfy

$$F_i'^\lambda = F_i^\lambda(x_j^\mu + \sum_k e_{jk}\, x_k^\mu + \tau_j,\, v_j^\nu + \sum_k e_{ik}\, v_k^\nu) = F_i^\lambda(x, v) + \sum_j e_{ij} F_j^\lambda(x, v)\,. \tag{5}$$

Since e_{ij} and τ_k are independent infinitesimal parameters the differential equations for F_i^λ, are given by

$$\sum_\mu \left\{\left(x_k^\mu \frac{\partial}{\partial x_j^\mu} - x_j^\mu \frac{\partial}{\partial x_k^\mu}\right) + \left(v_k^\mu \frac{\partial}{\partial v_j^\mu} - v_j^\mu \frac{\partial}{\partial v_k^\mu}\right)\right\} F_{i_1}^\lambda = F_{i_1}^\lambda - F_{i_3}^\lambda \tag{6}$$

and

$$\sum_\mu \frac{\partial F_{i_1}^\lambda}{\partial x_j^\mu} = 0\,, \tag{7}$$

where i_1, i_2, i_3 are any cyclic permutations of 1, 2, 3. The summations with Greek indices are over the number of particles, e.g. $\mu = 1, 2, \ldots .N$.

3. The nature of the force function

The nature of the solution of Eq. (6) in general for tensors of any rank has already been discussed in [2]. Here, we shall mention the results. The only additional restriction on F_i^λ are the three Eqs. (7) for $j = 1, 2, 3$, the most

general solution of which is any function of $x_j^\mu - x_j^\nu$. Thus they restrict only the explicit dependence on the co-ordinates. Hence the most general form of F_i^λ is

$$F_i^\lambda(x, v) = \sum_\varphi v_i^\varphi A^{\lambda\varphi} + \sum_{\mu,\nu} (x_i^\mu - x_i^\nu) B^{\lambda\mu\nu} + \\ + \sum_{j,k,\mu,\nu} \varepsilon_{ijk} \left\{ v_j^\mu v_k^\nu C^{\lambda\mu\nu} + \sum_\theta (x_j^\mu - x_j^\nu) v_k^\theta D^{\lambda\mu\nu\theta} + \right. \\ \left. + \sum_{\theta,\varphi} (x_j^\mu - x_j^\nu)(x_k^\theta - x_k^\varphi) E^{\lambda i\mu\nu\theta\varphi} \right\}; \tag{8}$$

(ε_{ijk} is totally antisymmetric with $\varepsilon_{123} = 1$).

The coefficients

$$A^{\lambda\varphi}, B^{\lambda\mu\nu}, C^{\lambda\mu\nu}, D^{\lambda\mu\nu\theta} \quad \text{and} \quad E^{\lambda\mu\nu\theta\Phi}$$

are functions of the scalars

$$\sum_i (x_i^\mu - x_i^\nu)(x_i^\theta - x_i^\varphi), \quad \sum_i (x_i^\mu - x_i^\nu) v_i^\theta, \quad \sum_i v_i^\theta v_i^\varphi .$$

The expressions (8) for the force functions are a little different from those of HOUTAPPLE, VAN DAM and WIGNER [3], where velocities also appear only as differences, since the invariance group considered there is the Galilei group, supplemented by the fact that time does not appear explicitly.

REFERENCES

1. G. KNAPECZ, Acta Phys. Hung. **23,** 203, 1967.
2. N. D. SEN GUPTA, Annali di Matematica pura ed Applicata, (IV), **58,** 45, 1965.
3. R. M. F. HOUTAPPEL, H. VAN DAM and E. P. WIGNER, Rev. Mod. Phys., **37,** 595, 1965.

О СВОЙСТВАХ СИММЕТРИИ УРАВНЕНИЯ ДВИЖЕНИЯ

Н. Д. СЕН ГУПТА

Резюме

Предмет данной работы — получить ограничения на форму силовых функций системы частиц, которые обусловлены ковариантностью уравнения движения по отношению группы Евклида.

Acta Physica Academiae Scientiarum Hungaricae, Tomus 29 (4), pp. 309–317 (1970)

PUNCH PROBLEM OF TRANSVERSELY ISOTROPIC MATERIAL FOR A HALF-SPACE WITH MIXED THERMAL CONDITIONS

By

ABDUL MAJED MOLLA

DEPARTMENT OF MATHEMATICS, ULUBERIA COLLEGE, HOWRAH, W. B., INDIA

(Received 17. VI. 1969)

In this paper stresses and displacement components have been calculated for a transversely isotropic frictionless half-space when the temperature field and the normal displacement component are prescribed within a circular region of radius 'a' while the remaining stress-free surface is radiating in accordance with Newton's law. The solutions of both the thermal and the elastic problems are obtained in terms of the solution of a Fredholm integral equation of the second kind.

Introduction

MAHALANABIS [1] discussed the problem of smooth frictionless half-space of transversely isotropic material when the temperature is prescribed over a circular portion of its free surface and the remainder radiates in accordance with Newton's law. The solution was obtained in terms of the solution of the Fredholm integral equation of the second kind by using COOKE's [2] result.

This paper deals with the Punch problem of a frictionless half-space of a transversely isotropic material when the temperature field and the normal displacement component are prescribed within a circular region of radius 'a', the remainder stress free surface radiates in accordance with Newton's law (constant of proportionality being $k_1 > 0$).

The solutions of both thermal and elastic problems involve dual integral equations. The solutions of both thermal and elastic problems are obtained in terms of the solutions of Fredholm integral equations of the second kind by using COOKE's [2] result.

Method of solution

Let us consider the frictionless boundary of the semi-infinite transversely isotropic elastic medium to be the plane $z = 0$, the z-axis being directed into the medium.

In the steady state thermal problem, the temperature field at any point satisfies the partial differential equation

$$\nabla^2 T = 0, \quad \nabla^2 \equiv \frac{\partial^2}{\partial r^2} + \frac{1}{r}\frac{\partial}{\partial r} + k^2 \frac{\partial^2}{\partial z^2} \tag{1}$$

with the boundary conditions

$$\left.\begin{aligned} \frac{\partial T}{\partial Z} &= k_1 (T - T_1), \quad r > a \\ T &= T_0 (r/a), \qquad r < a \end{aligned}\right\} \text{on } z = 0. \tag{2}$$

The solution of (1) can be assumed as

$$T = \int_0^\infty \alpha A(\alpha) \cdot e^{-\alpha z/k} \cdot J_0(\alpha r)\, d\alpha, \tag{3}$$

where $Jn\,(\alpha r)$ is the Bessel function of order n.

From the boundary conditions (2) using (3) and also substituting

$$\alpha a = n, \; r/a = e, \tag{4}$$

we obtain

$$\left.\begin{aligned} &\int_0^\infty g(n)\, J_0(ne)\, dn = 0, \qquad \varrho > 1 \\ &\int_0^\infty G(n)\, g(n)\, J_0(ne)\, d\eta = 1/k \left\{T_0(e) - T_1\right\}, \; \varrho < 1 \end{aligned}\right\}, \tag{5}$$

where

$$G(n) = \frac{1}{n + kk_1 a},$$

$$g(n) = \frac{n}{ka^2} \left\{A(n/a) \cdot (n + kk_1 a) - 2\pi kk_1 \cdot T_1 a \delta(n/a)\right\}.$$

Putting $a = 1$, $k = y_2$, $\nu = 0$, $\alpha = -y_2$ in Cooke's [2] results, we obtain the solution of dual integral equation (5) as

$$g(n) = \frac{2n}{\pi} \int_0^1 f(t) \cos nt\, dt, \tag{6}$$

where

$$\left.\begin{aligned} &f(x) - \frac{2kk_1 a}{\pi} \int_0^1 k_2(x, t) f(t)\, dt = T(x), \quad 0 \leq x \leq 1, \\ &k_2(x, t) = \int_0^\infty \frac{1}{n + kk_1 a} \cos nt \cos nx\, dn, \end{aligned}\right. \tag{7}$$

and

$$I(x) = \frac{1}{k} \int_0^1 \frac{t}{\sqrt{1 - t^2}} \left\{T_0(xt) - T_1 + xtT_0'(xt)\right\} dt.$$

Now $A(\alpha)$ is known from (6) and, thus, the temperature field can be determined from (5) with the aid of (6) and (7).

The well-known stress-strain relations in a transversely isotropic material can be written as,

$$\begin{aligned}
\widehat{rr} &= c_{11}\, e_{rr} + c_{12}\, e_{\theta\theta} + c_{13}\, e_{zz} - b_1\, T, \\
\widehat{\theta\theta} &= c_{12}\, e_{rr} + c_{11}\, e_{\theta\theta} + c_{13}\, e_{zz} - b_1\, T, \\
\widehat{zz} &= c_{13}(e_{rr} + e_{\theta\theta}) + c_{33}\, e_{zz} - b_2\, T, \\
\widehat{rz} &= c_{44}\, e_{rz},
\end{aligned} \tag{8}$$

where

$$\begin{aligned}
b_1 &= (c_{11} + c_{12})\, \alpha_1 + c_{13}\, \alpha_2\,, \\
b_2 &= 2\, c_{13}\, \alpha_1 + c_{33}\, \alpha_2\,,
\end{aligned}$$

and c_{11}, c_{12} etc. are elastic constants and α_1, α_2 are the coefficients of linear expansion of the solid.

The strain components in terms of displacements are

$$e_{rr} = \frac{\partial u}{\partial r}\,, \quad e_{\theta\theta} = \frac{u}{r}\,, \quad e_{zz} = \frac{\partial \omega}{\partial z}\,, \quad e_{rz} = \frac{\partial u}{\partial z} + \frac{\partial \omega}{\partial r}\,. \tag{9}$$

The equations of equilibrium are given (TIMOSHENKO [4]) as

$$\begin{aligned}
&\frac{\partial}{\partial r}(\widehat{rr}) + \frac{\partial}{\partial z}(\widehat{rz}) + \frac{1}{r}(\widehat{rr} - \widehat{\theta\theta}) = 0\,, \\
&\frac{\partial}{\partial r}(\widehat{rz}) + \frac{\partial}{\partial z}(\widehat{zz}) + \frac{1}{r}(\widehat{rz}) = 0\,.
\end{aligned} \tag{10}$$

Substituting the values of stress components (8) and the strain components (9) in (10), we obtain

$$\begin{aligned}
&c_{11}\left(\frac{\partial^2 u}{\partial r^2} + \frac{1}{r}\frac{\partial u}{\partial r} - \frac{u}{r^2}\right) + c_{44}\frac{\partial^2 u}{\partial z^2} + (c_{13} + c_{44})\frac{\partial^2 w}{\partial r\, \partial z} = b_1 \frac{\partial T}{\partial r}\,, \\
&c_{44}\left(\frac{\partial^2 w}{\partial r^2} + \frac{1}{r}\frac{\partial w}{\partial r}\right) + c_{33}\frac{\partial^2 w}{\partial z^2} + (c_{13} + c_{14})\frac{\partial}{\partial z}\left(\frac{\partial u}{\partial r} + \frac{u}{r}\right) = b^2 \frac{\partial T}{\partial z}\,.
\end{aligned} \tag{11}$$

Let us assume

$$\begin{aligned}
u &= \frac{\partial}{\partial r}(\Phi + \overline{T}) \\
w &= \frac{\partial}{\partial z}(\lambda\Phi + \mu\overline{T})\,,
\end{aligned} \tag{12}$$

where Φ and $\overline{T}$ are functions of r and z, λ and μ are Lame's constants.

Eqs. (11) are satisfied if

$$c_{11}\left(\frac{\partial^2 \Phi}{\partial r^2}+\frac{1}{r}\frac{\partial \Phi}{\partial r}\right)+\{c_{44}+\lambda(c_{13}+c_{44})\}\frac{\partial^2 \Phi}{\partial z^2}=0\,,$$
$$c_{11}\left(\frac{\partial^2 \bar{T}}{\partial r^2}+\frac{1}{r}\frac{\partial \bar{T}}{\partial r}\right)+\{c_{44}+\mu(c_{13}+c_{44})\}\frac{\partial^2 \bar{T}}{\partial z^2}=b_1 T\,, \tag{13}$$

and

$$(c_{13}+c_{44}+\lambda c_{44})\left(\frac{\partial^2 \Phi}{\partial r^2}+\frac{1}{r}\frac{\partial \Phi}{\partial r}\right)+\lambda c_{33}\frac{\partial^2 \Phi}{\partial z^2}=0\,,$$
$$(c_{13}+c_{44}+\mu c_{44})\left(\frac{\partial^2 \bar{T}}{\partial r^2}+\frac{1}{r}\frac{\partial \bar{T}}{\partial r}\right)+\mu c_{33}\frac{\partial^2 \bar{T}}{\partial z^2}=b_2 T\,. \tag{14}$$

Let us suppose,

$$\bar{T}=\int_0^\infty B(\alpha)\cdot \alpha A(\alpha)\, e^{-\alpha z/k}\cdot J_0(\alpha r)\, d\alpha\,, \tag{15}$$

where $B(\alpha)$ is a function of α only and will be obtained from the equations of equilibrium.

Inserting the values of T and $\bar{T}$ from (3) and (15) in the second equations of (13) and (14), we obtain

$$\alpha^2 B(\alpha)\ [\{c_{44}+\mu\,(c_{13}+c_{44})\}-c_{11}k^2]=b,\ k^2, \tag{16}$$
$$\alpha^2 B(\alpha)\ [\mu\, c_{33}-k^2\,(c_{13}+c_{44}+\mu c_{44})]=b_2 k^2\,. \tag{17}$$

Eqs. (16) and (17) are simultaneously satisfied if

$$\alpha^2 B(\alpha)=\frac{k^2\,[b_1(c_{33}-k^2\,c_{44})-b_2(c_{13}+c_{44})]}{[(c_{44}-k^2\,c_{11})\,(c_{33}-k^2\,c_{44})+k^2\,(c_{13}+c_{44})^2]}=P(\text{say})=\text{constant}. \tag{18}$$

The solutions of the equations of equilibrium are obtained in terms of two stress functions Φ_1, Φ_2 and the expressions for the stresses and displacement components can be written (SHARMA [3]) as

$$\widehat{rr}=\left(c_{11}\frac{\partial^2}{\partial r^2}+c_{12}\frac{1}{r}\frac{\partial}{\partial r}\right)(\Phi_1+\Phi_2+\bar{T})+$$
$$+\,c_{13}\frac{\partial^2}{\partial z^2}(\lambda_1\Phi_1+\lambda_2\Phi_2+\mu\bar{T})-b_1 T,$$
$$\widehat{\theta\theta}=\left(c_{12}\frac{\partial^2}{\partial r^2}+c_{11}\frac{1}{r}\frac{\partial}{\partial r}\right)(\Phi_1+\Phi_2+\bar{T})+$$
$$+\,c_{13}\frac{\partial^2}{\partial z^2}(\lambda_1\Phi_1+\lambda_2\Phi_2+\mu\bar{T})-b_1 T\,,$$

$$\widehat{zz} = c_{13}\left(\frac{\partial^2}{\partial r^2} + \frac{1}{r}\frac{\partial}{\partial r}\right)\Phi_1+\Phi_2+\bar{T}) + \tag{19}$$

$$+ c_{33}\frac{\partial^2}{\partial z^2}(\lambda_1\Phi_1+\lambda_2\Phi_2+\mu\bar{T}) - b_2 T,$$

$$\widehat{rz} = c_{44}\frac{\partial^2}{\partial r\,\partial z}[(1+\lambda_1)\Phi_1+(1+\lambda_2)\Phi_2+(1+\mu)\bar{T}],$$

$$u = \frac{\partial}{\partial r}(\Phi_1+\Phi_2+\bar{T}),$$

$$w = \frac{\partial}{\partial z}(\lambda_1\Phi_1+\lambda_2\Phi_2+\mu\bar{T}),$$

where Φ_1 and Φ_2 are the solutions of

$$\left(\frac{\partial^2}{\partial r^2} + \frac{1}{r}\frac{\partial}{\partial r} + \nu_i^2\frac{\partial^2}{\partial z^2}\right)\Phi_i = 0, \quad (i = 1, 2) \tag{20}$$

ν_1^2, ν_2^2 being the roots of the quadratic equation

$$c_{11}c_{44}\nu^4 + (2c_{13}c_{44} - c_{11}c_{33} + c_{13}^2)\nu^2 + c_{33}c_{44} = 0. \tag{21}$$

The values of λ that is λ_1, λ_2 correspond to the values of ν_1^2, ν_2^2, respectively, and

$$\mu = \frac{b_1 k^2(c_{13}+c_{44})+b_2(c_{44}-k^2 c_{11})}{b_1(c_{33}-k^2 c_{44}) - b_2(c_{13}+c_{44})} \tag{22}$$

and

$$\frac{\lambda(c_{13}+c_{44})+c_{44}}{c_{11}} = \frac{\lambda c_{33}}{\lambda c_{44}+c_{14}+c_{44}} = \nu^2. \tag{23}$$

As solutions of Eq. (20), let us assume

$$\Phi_1 = \int_0^\infty \alpha C(\alpha)\, e^{-\alpha z/\nu_1}\cdot J_0(\alpha r)\, d\alpha, \tag{24}$$

$$\Phi_2 = \int_0^\infty \alpha D(\alpha)\, e^{-\alpha z/\nu_2}\cdot J_0(\alpha r)\, d\alpha,$$

where $C(\alpha)$ and $D(\alpha)$ are functions of α only and are to be determined from the elastic boundary conditions. Now inserting the values of Φ_1, Φ_2, T and $\bar{T}$ from (24), (3) and (15) in Eqs. (19), we get

$$\widehat{rr} = (c_{11}-c_{12})\int_0^\infty \frac{\alpha^2}{r}\{C(\alpha)\,e^{-\alpha z/\nu_1}+D(\alpha)\,e^{-\alpha z/\nu_2}+$$

$$= B(\alpha)\,A(\alpha)\,e^{-\alpha z/k}\}J_1(\alpha r)\,d\alpha + \int_0^\infty \alpha^3\left\{\left(\frac{\lambda_1 c_{13}}{\nu_1^2}-c_{11}\right)C(\alpha)\,e^{-\alpha z/\nu_1}+\right.$$

$$+\left(\frac{\lambda_2 c_{13}}{\nu_2^2}-c_{11}\right)\cdot D(\alpha)\cdot e^{-\alpha z/\nu_2}+$$

$$\left.+\,B(\alpha)\,A(\alpha)\cdot\left(\frac{\mu c_{13}}{k^2}-c_{11}\right)e^{-\alpha z/k}\right\}J_0(\alpha r)\,d\alpha -$$

$$-\,b_1\int_0^\infty \alpha A(\alpha)\,e^{-\alpha z/k}\cdot J_0(\alpha r)\,d\alpha\,,$$

$$\widehat{\theta\theta} = (c_{12}-c_{11})\int_0^\infty \frac{\alpha^2}{r}\{C(\alpha)\,e^{-\alpha z/\nu_1}+D(\alpha)\,e^{-\alpha z/\nu_2}+$$

$$+\,B(\alpha)\,A(\alpha)\,e^{-\alpha z/k}\}J_1(\alpha r)\,d\alpha +$$

$$+\int_0^\infty \alpha^3\left\{\left(\frac{\lambda_1 c_{13}}{\nu_1^2}-c_{12}\right)C(\alpha)\cdot e^{-\alpha z/\nu_1}+\left(\frac{\lambda_2 c_{13}}{\nu_2^2}-c_{12}\right)D(\alpha)\cdot e^{-\alpha z/\nu_2}+\right.$$

$$\left.+\,B(\alpha)\,A(\alpha)\cdot\left(\frac{\mu c_{13}}{k^2}-c_{12}\right)e^{-\alpha z/k}\right\}J_0(\alpha r)\,d\alpha -$$

$$-\,b_1\int_0^\infty \alpha A(\alpha)e^{-\alpha z/k}J_0(\alpha r)\,d\alpha\,, \qquad (25)$$

$$\widehat{zz} = \int_0^\infty \alpha^3\left\{\left(\frac{\lambda c_{33}}{\nu_1^2}-c_{13}\right)C(\alpha)\cdot e^{-\alpha z/\nu_1}+\left(\frac{\lambda_2 c_{33}}{\nu_2^2}-c_{13}\right)D(\alpha)\,e^{-\alpha z/\nu_2}+\right.$$

$$\left.+\,B(\alpha)\,A(\alpha)\left(\frac{\mu c_{33}}{k^2}-c_{13}\right)e^{-\alpha z/k}\right\}J_0(\alpha r)\,d\alpha -$$

$$-\,b_2\int_0^\infty \alpha A(\alpha)\,e^{-\alpha z/k}J_0(\alpha r)\,d\alpha\,,$$

$$\widehat{rz} = c_{44}\int_0^\infty \alpha^3\left\{\frac{1+\lambda_1}{\nu_1}C(\alpha)\,e^{-\alpha z/\nu_1}+\frac{1+\lambda_2}{\nu_2}D(\alpha)\,e^{-\alpha z/\nu_2}+\right.$$

$$\left.+\,\frac{1+\mu}{k}B(\alpha)\,A(\alpha)\,e^{-\alpha z/k}\right\}J_1(\alpha r)\,d\alpha\,,$$

$$u = -\int_0^\infty \alpha^2\{C(\alpha)\,e^{-\alpha z/\nu_1}+D(\alpha)\,e^{-\alpha z/\nu_2}+B(\alpha)\,A(\alpha)\,e^{-\alpha z/k}\}J_1(\alpha r)\,d\alpha\,,$$

$$w = -\int_0^\infty \alpha^2\left\{C(\alpha)\cdot\frac{\lambda_1}{\nu_1}\cdot e^{-\alpha z/\nu_1}+D(\alpha)\cdot\frac{\lambda_2}{\nu_2}e^{-\alpha z/\nu_2}+\right.$$

$$\left.+\,B(\alpha)\,A(\alpha)\,e^{-\alpha z/k}\right\}J_0(\alpha r)\,d\alpha\,.$$

To solve the elastic problem, we assume the following boundary conditions on the plane $z = 0$,

$$\begin{aligned} w &= f(r/a), \qquad r < a, \\ \widehat{zz} &= 0, \qquad r > a, \\ \widehat{rz} &= 0, \qquad 0 \leq r \leq \infty. \end{aligned} \tag{26}$$

From (26) using (25), we obtain

$$\frac{1+\lambda_1}{\nu_1} C(\alpha) + \frac{1+\lambda_2}{\nu_2} D(\alpha) + \frac{1+\mu}{k} B(\alpha) A(\alpha) = 0, \tag{27}$$

$$\begin{aligned} \int_0^\infty \alpha^3 \Big\{ \Big(\frac{\lambda_1 c_{33}}{\nu_1^2} - c_{13} \Big) C(\alpha) + \Big(\frac{\lambda_2 c_{33}}{\nu_2^2} - c_{13} \Big) D(\alpha) + \\ + B(\alpha) A(\alpha) \Big(\frac{\mu c_{33}}{k^2} - c_{13} \Big) \Big\} J_0(\alpha r) \, d\alpha = 0, \quad r > a, \end{aligned} \tag{28}$$

and

$$\begin{aligned} \int_0^\infty \alpha^2 \Big\{ \frac{\lambda_1}{\nu_1} C(\alpha) + \frac{\lambda_2}{\nu_2} D(\alpha) + B(\alpha) A(\alpha) \frac{\mu}{k} \Big\} J_0(\alpha r) \, d\alpha = \\ = - f(r/a), \quad r < a. \end{aligned} \tag{29}$$

From (27), (28) and (29), we obtain

$$\begin{aligned} \int_0^\infty \alpha^3 \Big[\Big\{ \Big(\frac{\lambda_1 c_{33}}{\nu_1^2} - c_{13} \Big) - \Big(\frac{\lambda_2 c_{33}}{\nu_2^2} - c_{13} \Big) \frac{\nu_2}{\nu_1} \cdot \frac{1+\lambda_1}{1+\lambda_2} \Big\} C(\alpha) + \\ + \Big\{ \Big(\frac{\mu c_{33}}{k^2} - c_{13} \Big) - \Big(\frac{\lambda_2 c_{33}}{\nu_2^2} - c_{13} \Big) \frac{k}{\nu_1} \cdot \frac{1+\mu}{1+\lambda_2} \Big\} B(\alpha) A(\alpha) \Big] \times \\ \times J_0(\alpha r) \, d\alpha = 0, \quad r > a \end{aligned} \tag{30}$$

and

$$\begin{aligned} \int_0^\infty \alpha^2 \Big[\frac{\lambda_1 - \lambda_2 \nu_2}{\nu_1 \nu_2 (1+\lambda_2)} \cdot C(\alpha) + \Big(\frac{\mu}{k} - \frac{k}{\nu_1} \cdot \frac{\lambda_2}{\nu_2} \cdot \frac{1+\mu}{1+\lambda_2} \Big) B(\alpha) A(\alpha) \Big] \times \\ \times J_0(\alpha r) \, d\alpha = - f(r/a), \qquad r < a. \end{aligned} \tag{31}$$

Using the substitutions (4) in (30) and (31), we obtain the following dual integral equations,

$$\begin{aligned} &\int_0^\infty \psi(n) J_0(ne) \, dn = 0, && e > 1, \\ &\int_0^\infty \chi(n) \psi(n) J_0(ne) \, dn = 1/a \{ f_1(e) - f(e) \}, && e < 1 \end{aligned} \tag{32}$$

where

$$\psi(n) = \frac{n^3}{a^4}\left[\left\{\left(\frac{\lambda_1 c_{33}}{\nu_1^2} - c_{13}\right) - \left(\frac{\lambda_2 c_{33}}{\nu_2^2} - c_{13}\right)\frac{\nu_2}{\nu_1}\cdot\frac{1+\lambda_1}{1+\lambda_2}\right\} C(n/a) + \right.$$

$$\left. + \left\{\left(\frac{\mu c_{33}}{k^2} - c_{13}\right) - \frac{k}{\nu_1}\,\frac{1+\mu}{1+\lambda_2}\left(\frac{\lambda_2 c_{33}}{\nu_2^2} - c_{13}\right)\right\} B(n/a)\, A(n/a)\,,\right.$$

$$C(n/a) = \frac{a^4 n^{-3}\psi(n) - \Delta_1 B(n/a)\, A(n/a)}{\Delta_2}$$

$$\Delta_1 = \left(\frac{\mu c_{33}}{k^2} - c_{13}\right) - \frac{k}{\nu_1}\,\frac{1+\mu}{1+\lambda_2}\left(\frac{\lambda_2 c_{33}}{\nu_2^2} - c_{13}\right),$$

$$\Delta_2 = \left\{\left(\frac{\lambda_1 c_{33}}{\nu_1^2} - c_{13}\right) - \frac{\nu_2}{\nu_1}\,\frac{1+\lambda_1}{1+\lambda_2}\left(\frac{\lambda_2 c_{33}}{\nu_2^2} - c_{13}\right)\right.,$$

$$\chi(n) = n^{-1}\cdot\frac{(x_1 - \lambda_2\nu_2)}{\nu_1\nu_2(1+\lambda_2)\,\Delta_2}\,,$$

$$f_1(e) = \int_0^\infty n^2 a^{-3}\left\{\frac{(\lambda_1 - \lambda_2\nu_2)}{\nu_1\nu_2(1+\lambda_2)}\cdot\frac{\Delta_1}{\Delta_2} - \right.$$

$$\left. - \left(\frac{\mu}{k} - \frac{k}{\nu_1}\cdot\frac{\lambda_2}{\nu_2}\cdot\frac{1+\mu}{1+\lambda_2}\right)\right\} B(n/a)\, A(n/a)\, J_0(ne)\cdot ds\,.$$

Putting

$$a = \left[\frac{c_{33}\{\lambda_1\nu_2(1+\lambda_2) - \lambda_2\nu_1(1+\lambda_1)\} - \nu_1\nu_2 c_{13}\{\nu_1(1+\lambda_2) - \nu_2(1+\lambda_1)\}}{(\lambda_1 - \lambda_2\nu_2\nu_2)\,\nu_1}\right],$$

$k = y_2$, $\nu = 0$, $\alpha = -y_2$ in COOKE's [2] result, we obtain the solution of (32) as

$$\psi(n) = \frac{2n}{\pi}\int_0^1 F(t)\cos nt\, dt\,, \tag{33}$$

where

$$F(x) + \frac{2}{\pi}\int_0^1 k_3(x,t)\, F(t)\, dt = I,(x)\,, \quad 0 \leq x \leqq 1\,,$$

$$k_3(x,t) = \frac{\{\lambda_1 - \lambda_2\nu_2 - \nu_1\nu_2(1+\lambda_2)\,\Delta_2\}}{\nu_1\nu_2(1+\lambda_2)\,\Delta_2} \times \int_0^\infty \cos nt\cos n_x\, dn \tag{34}$$

and

$$I_1(x) = \frac{1}{a}\int_0^1 \frac{1}{\sqrt{1-t^2}}\left\{f_1(xt) - f(xt) + xt\left(f_1'(xt) - f'(xt)\right)\right\} dt\,.$$

Now $C(\alpha)$ and $D(\alpha)$ are known from (33) and (27). Thus all the stresses and displacement components are completely determined from (25) with the aid of (6), (18), (27) and (33).

Acknowledgement

In conclusion, I convey my heartful thanks to Dr. R. K. MAHALANABIS, Department of Mathematics, Jadavpur University, Calcutta-32, India for his kind help in preparing this paper.

REFERENCES

1. R. K. MAHALANABIS, Bull. Cal. Math. Soc. (in press) 1966.
2. J. C. COOKE, Qrt. Jl. Mech. Appl. Math. 106, 1956.
3. B. SHARMA, Jour. of Appl. Mech., **23**, 1956.
4. S. TIMOSHENKO and J. N. GOODIER, Theory of Elasticity, Second Edn., McGraw-Hill Book Co. Inc., p. 234. (1951).

ПРОБЛЕМА УДАРНОЙ ВОЛНЫ В ПОПЕРЕЧНО ИЗОТРОПНОМ МАТЕРИАЛЕ, ЗАПОЛНЯЮЩЕМ ПОЛУПРОСТРАНСТВО СО СМЕШАННЫМИ ТЕРМИЧЕСКИМИ УСЛОВИЯМИ

А. М. МОЛЛА

Р е з ю м е

В данной работе определяются компоненты напряжения и смещений в случае полупространства, без трения и обладающего поперечной изотропией, при условии, что в круговой области с радиусом a заранее заданы температурное поле и нормальная составляющая смещения, в то время как остальная, свободная от напряжения поверхность излучает согласно закону Ньютона. Решения как термической, так и эластичной проблем получены в форме решения интегрального уравнения второго порядка Фредхолма.

Acta Physica Academiae Scientiarum Hungaricae, Tomus 29 (4), pp. 319–329 (1970)

АНАЛОГИЧЕСКИЕ ЧЕРТЫ МАТРИЦЫ ЭНТРОПИИ И МАТРИЦЫ ПРОВОДИМОСТИ

И. КИРШНЕР
КАФЕДРА АТОМНОЙ ФИЗИКИ, УНИВЕРСИТЕТ ИМ. Л. ЭТВЕША, БУДАПЕШТ

(Поступило 24. VII. 1969)

Термодинамическая матрица энтропии g и матрица проводимости L невзаимозаменяемы, однако между ними можно обнаружить некие аналогии. В данной статье при помощи теории вероятности показано математическое происхождение этих матриц, связь их с переходной вероятностью к их физический смысл. Кроме этого исследованы макроскопические следствия аналогии g и L матриц и указано на то, что эта аналогия, в первую очередь, проявляется в описании принципа статической стабильности.

Введение

В термодинамике необратимых процессов отклонение от состояния равновесия характеризуется α-параметрами,

$$\alpha_i = \frac{x_i - (x_i)_0}{x_{n+1}}, \quad i = 1, 2, \ldots, n, \tag{1}$$

где x_i i-товая экстенсивная величина, $(x_i)_0$ ее значение в равновесном состоянии, а x_{n+1} объем или масса исследуемой системы. Соответственно α_i плотности или удельные данные, исходные точки шкал которых относятся к состоянию равновесия. В этой же самой шкале α-параметр энтропии можно представить как функцию остальных:

$$\alpha_s = \alpha_s(\alpha_1, \alpha_2, \ldots, \alpha_n) \tag{2}$$

при помощи которых общие термодинамические силы задаются соотношением

$$X_i = \frac{\partial \alpha_s}{\partial \alpha_i} - \left(\frac{\partial \alpha_s}{\partial \alpha_i}\right)_0.$$

С другой стороны из члена второго порядка разложения в ряд

$$g_{ik} = -\left(\frac{\partial^2 \alpha_s}{\partial \alpha_i \, \partial \alpha_k}\right)_0 = -\left(\frac{\partial^2 \alpha_s}{\partial \alpha_k \, \partial \alpha_i}\right)_0 = g_{ki} \tag{3}$$

дается квадратичная, симметричная и позитивно определенная матрица n-ого порядка $g = g[g_{ik}]$, которая находится с общими силами в соотношении вида

$$X_i = -\sum_k g_{ik}\,\alpha_k\,, \tag{4}$$

где X и α векторы, а само уравнение действительно во втором приближении.

Если в системе одновременно существуют несколько разнородных сил и «токов», то соотношение между ними [1] выражается уравнением проводимости

$$\dot{\alpha}_i = \sum_k L_{ik}\,X_k\,, \tag{5}$$

где $L = L[L_{ik}]$ матрица также само n-ого порядка, квадратичная, симметричная и позитивно определенная.

При помощи этих величин необратимое изменение энтропии $\Delta\alpha_s$ и производительность энтропии σ примут выражение:

$$\Delta\alpha_s = -\frac{1}{2}\sum_{i,k} g_{ik}\,\alpha_i\,\alpha_k = \frac{1}{2}\sum_i X_i\,\alpha_i \tag{6}$$

и

$$\sigma = \Delta\dot{\alpha}_s = \sum_{i,k} L_{ik}\,X_i\,X_k = \sum_i \dot{\alpha}_i\,X_i = -\sum_{i,k} g_{ik}\,\dot{\alpha}_i\,\alpha_k\,. \tag{7}$$

Фигурирующие в этих уравнениях матрицы g и L невзаимозаменяемы [2]

$$gL \neq Lg, \tag{8}$$

и поэтому между ними не может существовать функциональная зависимость.

Попов [3], стремьясь к механической аналогии предположил, что и основное уравнение необратимых процессов можно записать в виде уравнения Ньютона:

$$X = -\ddot{\alpha}. \tag{9}$$

Путем интегрирования этого уравнения, при помощи довольно сложных математических вычислений, получил связь между g и L матрицами. На инкорректность этого предположения первым обратил внимание Фэньеш [4]. Рассмотрим, к чему приводит предположение (9). Путем дифференцирования уравнения проводимости (5), в матричной форме, можно определить простое соотношение между X и $\ddot{\alpha}$, если в полученное уравнение

$$\ddot{\alpha} = L\dot{X}$$

подставим выражение

$$\dot{X} = -g\,LX.$$

При этом путем сведения этих двух дается, что

$$\ddot{\alpha} = -Lg\,LX,$$

или

$$X = -L^{-1}g^{-1}L^{-1}\ddot{\alpha}.$$

Сравнивая это с условием Попова (9), получим уравнение

$$L^{-1}g^{-1}L^{-1} = U,$$

где U единичная матрица. В конечном счете это уравнение дает соотношение между g и L, по которому

$$L = g^{-1/2}. \tag{10}$$

Этот результат ирреальный, потому что исключает возможность сингулярности g, или к нулевому значению матрицы энтропии принадлежит бесконечное значение матрицы пороводимости, что часто не осуществляется. Поэтому (10) не представляет физическое взаимодействие.

Причины подобия по теории вероятности

Опыты, однако, показывают, что между характерными свойствами и прекращением некоторых особенностей этих двух матриц имеется определенная параллельность. К этим относятся в одинаковой мере позитивно определенный характер g и L, симметричность или исчезновение этих же самых свойств в адекватных случаях.

Проверим, что кроме опыта какие теоретические основания имеют эти сходства.

Пусть в точке r физической системы в момент времени t плотности экстенсивных величин будут $\varrho_1, \varrho_2, \ldots, \varrho_n = \{\varrho\}$. Отклонение от состояния равновесия характеризуется параметрами $\alpha_1, \alpha_2, \ldots, \alpha_n = \{\alpha\}$. Установление этого состояния случайное и ее вероятность будет

$$f = f(\varrho, t), \tag{11}$$

которая задана безусловными плотностями вероятности, определенные в пространстве состояния $\varrho_1, \varrho_2, \ldots, \varrho_n$ и нормирована на единицу

$$\int f(\varrho, t)\; d^n\varrho = 1, \tag{12}$$

где

$$d^n \varrho = d\varrho_1 \cdot d\varrho_2 \ldots d\varrho_n .$$

Начальное состояние при $t = 0$ характеризуется плотностями $\varrho_{10}, \varrho_{20}, \ldots, \varrho_{n0} = \{\varrho_0\}$, с вероятностью возникновения $f = f(\varrho_0)$. Далее, от состояния в момент времени $t = 0$ к состоянию в момент времени $t' = t$ переводит однородный стохастический процесс. Вероятность перехода при этом $F = F(\varrho|\varrho_0; t)$, и так

$$f(\varrho, t) = \int F(\varrho|\varrho_0; t)\, f(\varrho_0)\, d^n \varrho_0 . \tag{13}$$

Ожидаемая скорость изменения i-товой плотности в точке r

$$\langle v_i(\varrho_0)\rangle = \lim_{t\to 0} \frac{1}{t} \int (\varrho_i - \varrho_{i0})\, F(\varrho|\varrho_0; t)\, d^n \varrho ,$$

где интеграл означает ожидаемое смещение состояния. Смещение всегда является результатом макроскопического конвективного потока: к точке r текут части тела, находящиеся в различных состояниях. Если макроскопический поток не возникает, тогда

$$\langle v_i \rangle = 0 .$$

Однако с точки зрения термодинамики необратимых процессов кондуктивный поток и при этом может возникнуть. В таких случаях необходимо ввести понятие новой величины, тензора дисперсии:

$$a_{ik}(\varrho_0) = \frac{1}{2} \lim_{t\to 0} \frac{1}{t} \int (\varrho_i - \varrho_{i0})(\varrho_k - \varrho_{k0})\, F(\varrho|\varrho_0; t)\, d^n \varrho . \tag{14}$$

Используя уравнения Кольмогорова [5], именно при $\langle v_i \rangle = 0$, приняв во внимание какой угодно (во времени неоднородный) случай, то для начальных данных будем иметь

$$-\frac{\partial F}{\partial t_0} = \sum_{i,k} a_{ik} \frac{\partial^2 F}{\partial \varrho_{i0}\, \partial \varrho_{k0}} , \tag{15}$$

и для данных, относящихся ко конечному состоянию

$$\frac{\partial F}{\partial t_0} = \sum_{i,k} \frac{\partial^2 (a_{ik} F)}{\partial \varrho_i\, \partial \varrho_k} . \tag{16}$$

Умножив (16) на $f(\varrho_0)$ и интегрируя по ϱ_0, получим

$$\frac{\partial f}{\partial t} = \sum_{i,k} \frac{\partial^2 (a_{ik} f)}{\partial \varrho_i\, \partial \varrho_k} = \mathrm{div}_\varrho \nabla_\varrho a f . \tag{17}$$

Если считать выражение

$$h = -k \ln f \tag{18}$$

«сигнальной энтропией», тогда

$$\frac{\partial h}{\partial t} = -k \frac{1}{f} \frac{\partial f}{\partial t} = -\frac{k}{f} \operatorname{div}_\varrho \nabla_\varrho af,$$

где k постоянная и так

$$\frac{\partial h}{\partial t} + k \operatorname{div}_\varrho \left(\frac{1}{f} \nabla_\varrho af \right) = -\frac{k}{f^2} (\nabla_\varrho f, \nabla_\varrho af), \tag{19}$$

что имеет вид уравнения типа непрерывности. В точке r значение пространственной плотности макроскопической энтропии совпадает с ожидаемым значением $\langle \varrho_s \rangle$:

$$\langle \varrho_s(r, t) \rangle = \int fh \, d^n \varrho = -k \int f \ln f \, d^n \varrho, \tag{20}$$

что нечто другое, как действительное значение плотности энтропии.

Объяснение свойств L и g матрицы дают именно эти уравнения. Из (19) видно, что L_{ik} соответствует тензор дисперсии a_{ik}, элементы которых (и так и элементы L) являются функционалами переходной вероятности. Так как тензор дисперсии позитивно определенный, то из этого следует и позитивная определенность матрицы проводимости.

Семидефинитный характер $L_{ii} = 0 \leftrightarrow a_{ii} = 0$ соответствует такому состоянию, когда распределение по ϱ_i точечное (детерминистическое) по которому могло бы существовать только одно состояние с одной вероятностью. В таких случаях, естественно, статистика не имела бы места, однако такой случай никогда не встречается. При очень резком, но неточечном распределении a_{ii}, и этому соответственно и L_{ii}, имеют очень малые величины.

Далее, при $i \neq k$, $a_{ik} \leftrightarrow L_{ik}$ измеряет вероятностную зависимость ϱ_i и ϱ_k. Так, если ϱ_i и ϱ_k независимые вероятные переменные, тогда $a_{ik} = 0 \leftrightarrow L_{ik} = 0$, $i \neq k$, и при этом L диагональная, и перекрестные эффекты не возникают.

Матрица g дается из второй производной плотности энтропии $\langle \varrho_s \rangle$. Сама ϱ_s зависит от ожидаемых значений $\langle \varrho_i \rangle$, как от граничных значений, и так

$$g_{ik} = -\frac{\partial^2 \langle \varrho_s \rangle}{\partial \langle \varrho_i \rangle \, \partial \langle \varrho_k \rangle} \tag{21}$$

из чего видно, что позитивная определенность матрицы g является следствием уравнения (20). Значение интеграла тогда будет максимальное когда

$f(\varrho)$ постоянная, или, если ее график наиболее плоский (рис. 1 и 2). Практически имеет место последний случай, потому что вспомогательные условия (например законы сохранения) в общем препятсвуют равномерному распределению.

В конечном счете причина аналогичного поведения g и L матриц заключается в том, что оба являются функционалами одного и того же вероятностного распределения. Из этого следует, что в специальных случаях одновременно могут стать нерегулярными, именно тогда, когда F внезапно изменяет свое значение.

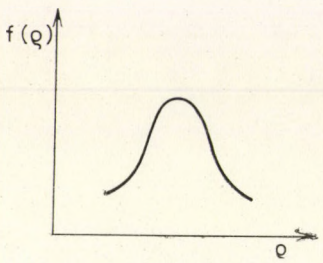


Рис. 1

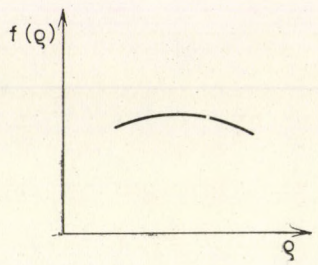


Рис. 2

Параллельность, однако, незакономерная так как, с одной стороны, эти две матрицы являются разными функционалами переходных вероятностей, с другой стороны они приобретают позитивно определенный характер по разным причинам.

Описанные выше рассуждения показывают, что элементы L матрицы само по себе не могут вызвать неустойчивость термодинамического состояния и вместе с тем, быть может, фазовое превращение. Причиной этого является то, что матрица дисперсии ни в коем случае не может быть индефинитная. Для поддержания стабильности при значении $g_{ii} = 0$ необходимо чтобы в соответствующем порядке было бы $L_{ii} \to \infty$, что означает бесконечную дисперсию и в действительности не всегда осуществляется. Встречающиеся в некоторых случаях бесконечно-большие значения коэффициента проводимости может вызвать в крайнем случае только нейтральное равновесие.

Феноменологические следствия

Состояние исследуемой системы и любой момент времени однозначно определяется заданием α_i или X_i. В состоянии статического равновесия значения всех α_i и X_i равны нулю, в прочем зависят от времени. Отклонение от состояния равновесия возникает при возбуждении некоторой помехи α или X.

По отношению к величине неравновесных параметров возникающих в результате помех можно установить количественные соотношения, которые могут быть истолкованы как статические стабилизационные критерии.

Сначала исследуем самый простой случай с двумя переменными. На том основании, что общие силы являются однородными линейными функциями α — параметров, по формуле (4):

$$\begin{aligned} -X_1 &= g_{11}\alpha_1 + g_{12}\alpha_2, \\ -X_2 &= g_{21}\alpha_1 + g_{22}\alpha_2 \end{aligned} \tag{22}$$

для которых действительно, что $D_g = g_{11}g_{22} - g_{12}^2 > 0$, $g_{11} > 0$ и $g_{22} > 0$. Найдя решение α_1 и α_2 из (22), X_1 можно выразить как функции α_1 и X_2, далее X_2 как функции α_2 и X_1:

$$\begin{aligned} -X_1 &= \frac{g_{11}g_{22}-g_{12}^2}{g_{22}}\alpha_1 - \frac{g_{12}}{g_{22}}X_2 = \frac{D_g}{g_{22}}\alpha_1 - \frac{g_{12}}{g_{22}}X_2, \\ -X_2 &= \frac{g_{11}g_{22}-g_{21}^2}{g_{11}}\alpha_2 - \frac{g_{21}}{g_{11}}X_1 = \frac{D_g}{g_{11}}\alpha_2 - \frac{g_{21}}{g_{11}}X_1. \end{aligned} \tag{23}$$

А соответствующим дифференцированием можно найти те силы, которые возбуждаются α-параметрами

$$\begin{aligned} \left|\frac{\partial X_1}{\partial \alpha_1}\right|_{x_1} &= g_{11} - \frac{g_{12}^2}{g_{22}} = \frac{D_g}{g_{22}} = \left|\frac{\partial X_1}{\partial \alpha_1}\right|_{\alpha_2} - \left|\frac{\partial X_1}{\partial \alpha_2}\right|_{\alpha_1}^2 \cdot \left|\frac{\partial \alpha_2}{\partial X_2}\right|_{x_1}, \\ \left|\frac{\partial X_2}{\partial \alpha_2}\right|_{x_1} &= g_{22} - \frac{g_{21}^2}{g_{11}} = \frac{D_g}{g_{11}} = \left|\frac{\partial X_2}{\partial \alpha_2}\right|_{\alpha_1} - \left|\frac{\partial X_2}{\partial \alpha_1}\right|_{\alpha_2}^2 \cdot \left|\frac{\partial \alpha_1}{\partial X_1}\right|_{\alpha_1}, \end{aligned} \tag{24}$$

где величины, фигурирующие в индексах — также само и в дальнейших формулах — равны нулю.

В виду того, что на правой стороне уравнений (24) оба члена положительны, следует, что

$$\begin{aligned} \left|\frac{\partial X_1}{\partial \alpha_1}\right|_{\alpha_2} &> \left|\frac{\partial X_1}{\partial \alpha_1}\right|_{x_2} > 0 \\ \left|\frac{\partial X_2}{\partial \alpha_2}\right|_{\alpha_1} &> \left|\frac{\partial X_2}{\partial \alpha_2}\right|_{x_1} > 0, \end{aligned} \tag{25}$$

а последнее нечто иное, как статический стабилизационный критерий. На основании (22) и (23) можно вычислить также и величины сил для разных типов помех:

при $\alpha_1 \neq 0$ и $\alpha_2 = 0$ $\quad -X_1 = g_{11}\alpha_1,$

$$\begin{aligned}
&\text{пни} \quad \alpha_1 \neq 0 \quad \text{и} \quad X_2 = 0 \qquad -X_1 = \frac{D_g}{g_{22}}\alpha_1, \\
&\text{при} \quad \alpha_2 \neq 0 \quad \text{и} \quad \alpha_1 = 0 \qquad -X_2 = g_{22}\alpha_2, \\
&\text{при} \quad \alpha_2 \neq 0 \quad \text{и} \quad X_1 = 0 \qquad -X_2 = \frac{D_g}{g_{11}}\alpha_1.
\end{aligned} \tag{26}$$

Далее на основании (6) даются четыре вида необратимых изменений энтропии, существующие как меры помех:

$$\begin{aligned}
\Delta\alpha_s &= \frac{1}{2}X_1\alpha_1 = -\frac{1}{2}g_{11}\alpha_1^2, \\
\Delta\alpha_s &= \frac{1}{2}X_1\alpha_1 = -\frac{1}{2}\frac{D_g}{g_{22}}\alpha_1^2, \\
\Delta\alpha_s &= \frac{1}{2}X_2\alpha_2 = -\frac{1}{2}g_{22}\alpha_2^2, \\
\Delta\alpha_s &= \frac{1}{2}X_2\alpha_2 = -\frac{1}{2}\frac{D_g}{g_{11}}\alpha_2^2,
\end{aligned} \tag{27}$$

где знак минус символизирует именно отклонение от положения равновесия [6].

В общем случае [7], если возможное число взаимодействий n, и соответственно этому может существовать n-ое число α-параметров или сил, то отклонение от равновесного состояния можно произвести путем возбуждения некоторого α-параметра (например α_1) или силы (например X_1). Помеха α_1 в теле индуцирует силу X_1, как меру удаления от равновесия. Это начальное состояние может осуществиться при фиксированном $\alpha_1 \neq 0$ n-различным образом, а значение возникающей X_1 силы удовлетворяет следующему ряду неравенств

$$|X_1|_{\alpha_2,\ldots,\alpha_n} > |X_1|_{x_2,\alpha_3,\ldots,\alpha_n} > |X_1|_{x_2,x_3,\alpha_4,\ldots,\alpha_n} > \cdots > |X_1|_{x_2,\ldots,x_n}. \tag{28}$$

По этому возбужденная помехой $\alpha_1 \neq 0$ сила $X_1 \neq 0$ тем больше, чем меньше число тех значений параметров α_i которые имеют значения отличные от нуля в результате помехи.

Эта теорема означает, что если считать мерой помехи $\alpha_1 \neq 0$ возбужденную ею силу $X_1 \neq 0$ и если допустить возбуждение и других параметров α_i, то сбитое состояние тем менее будет отличаться от равновесного, чем больше параметров $\alpha_i \neq \alpha_1$ помогают принимать помеху.

Естественно, возможно и двойственность ряда неравенства (28). Если первичная помеха возникает при возбуждении некоторой силы X_i (пусть

будет именно сила X_1), то последнее индуцирует такое α_1, для которого при фиксированном $X_1 \neq 0$:

$$|\alpha_1|_{x_2,\ldots,x_n} > |\alpha_1|_{\alpha_2,x_3,\ldots,x_n} > |\alpha_1|_{\alpha_2,\alpha_3,x_4,\ldots,x_n} > \ldots > |\alpha_1|_{\alpha_2,\ldots,\alpha_n}. \tag{29}$$

Эти неравенства не имеют динамический характер, и относятся только к получению помехи и к соответствующим начальным состояниям и не касаются процесса затухания самой помехи.

К сбитому состоянию, естественно, относится иная энтропия, как к равновесному. На основании (6) видно, что изменение энтропии идет в направлении возростания ряда неравенств (28) и (29). Поэтому и изменение энтропии можно отнести к тем свойствам, которые характеризуют отклонение от равновесия.

Сказанные выше, в случае двух переменных, очевидно можно сформулировать следующим образом:

1. С помехой $\alpha_1 \neq 0$ одновременно индуцируется сила X_1 и если с этим одновременно вступает и другой параметр α_2, то сила X_1 будет меньше, чем если возбуждением силы X_2 препятствовать появлению α_2.

2. Одновременно с сбиением $X_1 \neq 0$ индуцируется параметр α_1 и вместе с этим одновременно возникает сила X_2, посредством которой значение α_1 меньше, чем если $\alpha_2 \neq 0$.

Для определенных состояний изменения во времени характеризуются уравнениями (5) и (7), которые формально подобны к уравнениям (4) и (6). На этом основании можно было бы предположить что вместо соотношений (4) и (6) применяя (5) и (7) прийдем к действительному закону стабильности динамического характера. Однако это не так. Динамические формулы (5) и (7) также само характеризуют только начало изменения состояния, возникновение динамизма, в конечном счете само начальное состояние, но не дают никакой информации о дальнейшем формировании начавшегося процесса.

Однородная линейная форма уравнений проводимости, далее позитивно определенный характер и симметричность L матрицы, на основании рассуждений подобных выше, для $\dot{\alpha}_1$ и $\dot{\alpha}_2$ потоков индуцированных силами X_1 и X_2 приводят к соотношениям, подобных к (25):

$$\begin{aligned} |\dot{\alpha}_1|_{x_2} &> |\dot{\alpha}_1|_{\dot{\alpha}_2} > 0\,, \\ |\dot{\alpha}_2|_{x_1} &> |\dot{\alpha}_2|_{\dot{\alpha}_1} > 0\,. \end{aligned} \tag{30}$$

Далее, подобно (26) и (27) выражения потоков, возникающих при различных помехах, будут:

$$\text{если} \qquad X_1 \neq 0 \quad \text{и} \quad X_2 = 0\,, \quad \text{то} \quad \dot{\alpha}_1 = L_{11} X_1\,,$$

$$\begin{aligned}
&\text{если} \quad X_1 \neq 0 \quad \text{и} \quad \dot{\alpha}_2 = 0\,, \quad \text{то} \quad \dot{\alpha}_1 = \frac{D_L}{L_{22}} X_1\,, \\
&\text{если} \quad X_2 \neq 0 \quad \text{и} \quad X_1 = 0\,, \quad \text{то} \quad \dot{\alpha}_2 = L_{22} X_2\,, \\
&\text{если} \quad X_2 \neq 0 \quad \text{и} \quad \dot{\alpha}_1 = 0\,, \quad \text{то} \quad \dot{\alpha}_2 = \frac{D_L}{L_{11}} X_2\,,
\end{aligned} \tag{31}$$

а соответствующие типы производительности энтропии:

$$\begin{aligned}
\sigma &= \dot{\alpha}_1 X_1 = L_{11} X_1^2\,, \\
\sigma &= \dot{\alpha}_1 X_1 = \frac{D_L}{L_{22}} X_1^2\,, \\
\sigma &= \dot{\alpha}_2 X_2 = L_{22} X_2^2\,, \\
\sigma &= \dot{\alpha}_2 X_2 = \frac{D_L}{L_{11}} X_2^2\,,
\end{aligned} \tag{32}$$

где $D_L = L_{11}L_{22} - L_{12}^2 > 0$, $L_{11} > 0$ и $L_{22} > 0$.

В общем, если X_1 считать первичной помехой, то при определенном исходном значении X_1 возможно что исходные значения остальных сил и потоков будут равны нулю. Значения потоков $\dot{\alpha}_1 \neq 0$, относящихся к различным осуществимым возможностям, из-за позитивно определенный характер матрицы L, подобно к (29), характеризуется рядом неравенств

$$|\dot{\alpha}_1|_{x_2,\ldots,x_n} > |\dot{\alpha}_1|_{\dot{\alpha}_2,x_3,\ldots,x_n} > |\dot{\alpha}_1|_{\dot{\alpha}_2,\dot{\alpha}_3,x_4,\ldots,x_n} > \ldots > |\dot{\alpha}_1|_{\dot{\alpha}_2,\ldots,\dot{\alpha}_n}. \tag{33}$$

По этому возникающий при возбуждении X_1, начальный поток $\dot{\alpha}_1$ тем больше, чем число других возникающих сил будет меньше. Другими словами это означает, что возникающий поток будет тем больше, чем число термодинамических степеней свободы (независимых интенсивных параметров) на которых распределяется внесенная помеха, будет меньше.

Естественно, справедлива и дуальность. Данный поток $\dot{\alpha}_1 \neq 0$ индуцирует такую начальную силу X_1, значение которой тем больше, чем меньше число тех других потоков, которые имеют возможность на участие в этом:

$$|X_1|_{\dot{\alpha}_2,\ldots,\dot{\alpha}_n} > |X_1|_{x_2,x_3,\ldots,\dot{\alpha}_n} > |X_1|_{x_2,x_3,\dot{\alpha}_4,\ldots,\dot{\alpha}_n} > \ldots > |X_1|_{x_2,\ldots,x_n}. \tag{34}$$

Подобно раннему и ряд неравенств (34) можно истолковать так, что сила $X_1 \neq 0$ вызванная потоком $\dot{\alpha}_1 \neq 0$ уже заранее будет меньшей (большей) соответственно тому, что первичный поток α_1 вступит во взаимодействие с чем большим (меньшим) числом остальных потоков и образует перекрестные эффекты.

Отклонение от состояния равновесия можно характеризовать и возникшейся производительностью энтропии. Т. е., чем больше мгновенное значение производительности энтропии, относящейся к начальному состоянию, тем больше отклонение системы от состояния равновесия в момент помехи. С другой стороны на основании (7) видно, что производительность энтропии возростает (убывает) в направлении возростания (убывания) соответствующего ряда неравенств.

При интерпретации проверенных случаев нужно подчеркнуть, что всегда имеются в виду помехи а также и индуцированные величины в какой-то данный момент времени, а о самом динамизме процесса не может быть и речи. Следовательно, динамические интерпретации в литературе [8], [9], [10] не обоснованные. Первичная помеха и возникшая при этом величина относятся к одному и тому же моменту времени и между ними имеет место совершенная одновременность. По этому соотношения (28) и (29), (33) и (34) однозначно носят статический характер, существование которых обеспечивается позитивно определенностью и симметричностью g и L матриц.

Эти рассуждения показывают, что g и L играют подобную роль и ведут себя аналогично с точки зрения обеспечивания статической стабильности.

Из равновесных (4) и (6), динамических (5) и (7) законов можно сделать тот вывод, что они относятся только к определенному начальному состоянию именно к тому моменту времени, когда система претерпевает помеху. Само установление нового равновесия, а также и процессы вызывающие это, характеризуются совместно уравнениями (4)—(6) и (5)—(7).

ЛИТЕРАТУРА

1. L. Onsager, Phys. Rev., **37**, 405, 1931; **38**, 2265, 1931.
2. S. R. de Groot, Thermodynamics of Irreversible Processes, North-Holland P. C., Amsterdam, 1952.
3. К. Попов, ЖЭТФ, **28**, 257, 1955.
4. И. Фэньеш, ЖЭТФ, **35**, 1039, 1958.
5. A. Rényi, Valószínűségszámítás, (Tankönyvkiadó, Budapest, 1934).
6. I. Fényes, Termosztatika és Termodinamika, Műszaki Könyvkiadó, Budapest, 1968.
7. I. Kirschner, Magy. Fiz. Folyóirat, **17**, 71, 1969.
8. M. Planck, Ann. Phys., **19**, 759, 1934.
9. T. Ehrenfest-Afanasjeva, G. L. de Haas-Lorentr, Physica, **2**, 743, 1935.
10. H. B. Callen, Thermodynamics, Wiley, New-York, London, 1960.

ANALOGOUS FEATURES OF THE ENTROPY AND CONDUCTIVITY MATRICES

I. KIRSCHNER

Abstract

The thermodynamic entropy matrix g and the conductivity matrix L are not interchangeable, but several sorts of analogy can be found between them. In this paper the mathematical derivation of these matrices, by means of the probability theory, their connection with the transition probability and their physical meaning will be examined. Further, the macroscopic consequences of the analogous features of g and L will be discussed and it will be shown that they appear, primarily, in the description of the static stability principle.

Acta Physica Academiae Scientiarum Hungaricae, Tomus 29 (4), pp. 331—339 (1970)

A METHOD FOR THE SPECTROPHOTOMETRIC INVESTIGATION OF ABSORPTION AND FLUORESCENCE EMISSION IN MEDIA OF EXTREMELY WEAK ABSORPTION

By

I. KETSKEMÉTY and L. KOZMA

INSTITUTE OF EXPERIMENTAL PHYSICS, JÓZSEF ATTILA UNIVERSITY, SZEGED

(Received 1. VIII. 1969)

An integrating cuvette for studying the absorption and fluorescence spectra of weakly absorbing media as well as their yield function and decay time is described and the methods of measurement are outlined. Experimental results show that the methods can be used for solutions of concentrations down to 10^{-8} mole/l. In spherical integrating cuvettes of some centimetres diameter the mean path lengths of the light according to calculation and fluorimetric measurements are found to be 2 to 3 metres.

§ 1. In measuring absorption spectra of media of extremely weak absorption, a cuvette of great length, or shorter ones provided with mirror systems are used to increase the path length [1, 2]. Though investigations on the fluorescence of such media can be made more easily by assembling the emitted light with mirrors [3], the range of spectrophotometric investigations of fluorescence with the methods used hitherto has rarely been extended to regions of absorption coefficients $k(\nu) < 10^{-3}$ cm^{-1}. Spectrophotometric investigations in weakly absorbing but scattering media can be based on formulae of various authors [4]. These methods, however, do not generally permit an easy determination of the quantities to be measured. The aim of the present paper is to describe an experimental method for the determination of absorption and emission spectra, luminescence yield, and decay time of solutions, gases, aerosols, suspensions (scattering media) with relative ease and suitable accuracy, down to absorption coefficients of 10^{-4} cm^{-1}.

§ 2. With our method a spherical cuvette G (see Fig. 1) made of quartz or glass and coated on this exterior surface with diffusely reflecting material (e.g. magnesium oxide) is completely filled with the sample. On the reflective coating of G the relatively small areas e and o are left free. If $k(\nu)r < 10^{-2}$, then according to our experiments the light of frequency ν and intensity N_e entering G through e will produce there a radiation field which can be considered, with good approximation, as a homogeneous and isotropic photon gas of density n_ν.[1] Thus for n_ν

$$\frac{4\pi}{3} r^3 \frac{dn_\nu}{dt} = N_e - N_a - N_r - N_m \tag{1}$$

[1] N_e in photons/sec; n_ν in photons/cm^3.

will hold, where N_a, N_r and N_m mean the rate of change in the number of photons in G, due to absorption in the medium, non-complete reflection, and to the escape of photons through the uncoated areas of the reflecting surface, respectively. It is clear that, $N_a = 4\pi/3\, r^3\, n_\nu c n^{-1} k(\nu)$, $N_r = \pi r^2 c n^{-1} n_\nu (1-R_\nu)$,

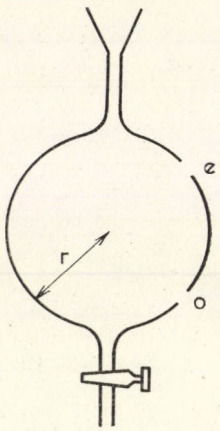


Fig. 1

and $N_m = 1/4\, mcn^{-1} n_\nu$, where c is the velocity of light, n the refractive index of the medium, and R_ν the reflectance of the coating. It follows from Eq. (1) that

$$n_\nu = \frac{nN_e/V}{ck(\nu) + \frac{3}{4r} c(1-R_\nu) + \frac{3}{16\pi r^3} mc}; \tag{2}$$

m means the sum of the uncoated areas on the surface of G, and V is the volume of the sphere.

§ 3. The determination of the absorption coefficient of solutions is carried out as follows. The sphere G is filled first with the solvent, then with the solution and the intensities N_{o0} and N_o of the light[2] emerging through o or the corresponding photocurrents I_0 and I of a photomultiplier are measured with a constant value of N_e. As the intensity of the light emerging through o is proportional to the density of the photon gas in G, we have from Eq. (2)

$$k(\nu) = A\left(\frac{I_0}{I} - 1\right), \tag{3}$$

where the value of A, characteristic of the sphere G, is

$$A = \frac{3}{4r}(1-R_\nu) + \frac{3}{16\pi r^3} m. \tag{4}$$

[2] In photons/sec.

For gases and aerosols I_0 and I mean the photocurrents measured with an empty cuvette and with a cuvette filled with the absorbing material, respectively.

§ 4. The determination of the fluorescence spectrum is based upon the following considerations. If the medium is luminescent, then, as a result of the presence of the photon gas of frequency ν, a luminescence photon gas will also be produced, which will be homogeneous and isotropic for sufficiently low values of the absorption coefficient (see above). Let the density of the luminescence photon gas be denoted by n', its spectral distribution by $f^*(\nu')$. It is easy to see that for n' the relation

$$\left(\frac{d}{dt}n'\right) Vf^*(\nu')\,d\nu' = [N_f f(\nu') - N_{fr}(\nu') - N_{fm}(\nu') - cn'Vf^*(\nu')\,k(\nu')]\,d\nu' = 0 \quad (5)$$

holds, where N_f means the total number of the luminescence photons produced during unit time, $f(\nu')$ the true spectral distribution of luminescence, and $d\nu'$ a small frequency interval of the emission spectrum. The second term in the square brackets of Eq. (5) takes into account the rate of change in number of photons due to incomplete reflection, the third that due to escape through the uncoated areas of the surface, while the fourth term denotes the decrease of the luminescence light caused by reabsorption in G. It should be remarked in connection with Eq. (5) that *a)* in principle, N_f should involve the secondary, tertiary, etc. luminescence photons excited by reabsorbed luminescence light, and *b)* that the secondary, tertiary etc. luminescence light has not necessarily the same true luminescence spectrum $f(\nu')$ as the primary emission due to the exciting light of frequency ν (for miscellaneous solutions see [5]).

In the following it has been assumed throughout that the spectral effect of secondary luminescence can be neglected. This supposition seems to be acceptable, e.g. in the case of sufficiently diluted fluorescent solutions containing only one kind of fluorescent material. In this case the remarks made under *a)* and *b)* can be ignored and then the relation $N_f = N_a\,\eta(\nu)$ will hold, where $\eta(\nu)$ is the absolute fluorescence yield of the solution at exciting frequency ν. In the following our considerations will be restricted to the fluorescence of the highly diluted solutions mentioned above.

For the terms in Eq. (5), taking into account the decrease in the number of fluorescence photons caused by incomplete reflection and by escape through the uncoated surface of area m, the following relations hold:

$$N_{fm}(\nu') = \frac{1}{4} mn' f^*(\nu') \frac{\tau}{n}, \quad (6)$$

$$N_{fr}(\nu') = \pi r^2 n' f^*(\nu) (1 - R_{\nu'}) \frac{c}{n}. \quad (7)$$

From Eqs. (5—7) we obtain the following equation for the true fluorescence spectrum:

$$f(\nu') = \frac{n' cf^*(\nu')}{n N_a \eta(\nu)} \left[\frac{m}{4} + \pi r^2 (1 - R_{\nu'}) + \frac{4\pi}{3} r^3 k(\nu') \right] \tag{8}$$

which allows the true spectrum $f(\nu)$ to be calculated from the normalized spectrum $f^*(\nu)$ of the fluorescence light observed through o.

§ 5. Eq. (8) also makes it possible to determine the yield. Namely, n' is given by the spectral intensity $N_{f0}(\nu') = 1/4\, on' f^*(\nu')\, c/n$ escaping through o, and N_a is known (see § 2). However, this method of determining the absolute quantum yield involves inevitable errors because, *a)* the measurement of the photon flux escaping through o into the solid angle 2π is rather difficult[3], and *b)* the measurement of the yield is perturbed by secondary fluorescence, even if the latter can be neglected in measuring the emission spectrum. Using the above equations we obtain for the absolute quantum yield

$$\eta(\nu) = \left[\int_0^\infty N_{fm}(\nu')\, d\nu' \left(1 + \frac{4\pi r^2 (1 - R_{\nu'})}{n} \right) + \frac{4V}{m} \int_0^\infty N_{fm}(\nu')\, k(\nu')\, d\nu' \right] \times$$

$$\times \frac{k(\nu) + \frac{3}{4r}(1 - R_{\nu'}) + \frac{3m}{16\pi r^3}}{N_e k(\nu)} \tag{9}$$

and for the relative quantum yield $\eta^*(\nu)$, if f is independent of ν, the simple relation

$$\eta^*(\nu) = \text{const.} \frac{k(\nu) + \frac{3}{4r}(1 - R_\nu) + \frac{3}{16\pi r^3}}{N_e k(\nu)} \cdot N_{fm}(\nu'). \tag{10}$$

In Eq. (10) ν' is a frequency at which the reabsorption has no observable effect. Considering that for using Eq. (10) it is necessary to know $N_{fm}(\nu')$ only apart from a constant factor, to determine $\eta^*(\nu)$ it will be sufficient to measure the intensity of the fluorescence light emerging through o in an arbitrary solid angle. It is much easier to perform this latter measurement.

§ 6. The formulae to be used for determining the decay time of fluorescence with the aid of the integrating sphere G can be obtained with the following considerations. Let us suppose that beside the exciting light of stationary intensity N_e a light flux of modulated intensity $N'(t) = N' \sin \omega t$ ($N' < N_e$) enters through o. Let the light passing through o be monochromatic and of

[3] E.g. the exterior surface of the sphere G in the neighbourhood of o should be brought into optical contact with a liquid in order to eliminate total reflection.

frequency ν. For studying the decay time, the exciting and the fluorescence photon gas, both of constant density, produced by the flux N_e in G, are unimportant. Therefore, they will be neglected in our further calculations (though this will result in negative densities and fluxes appearing in our equations). If G contains a diluted fluorescent solution described in § 4, then, instead of Eq. (1), we have to write

$$\frac{dn_\nu}{dt} = N \sin \omega t - n_\nu \frac{c}{n} k(\nu) - \frac{3}{4r} \frac{c}{n} (1-R_\nu) n_\nu, \tag{11}$$

where $N = N'/V$. In Eq. (11) the losses due to the escape through the uncoated surface of area m have not been taken into account; this simplification has no influence on our present considerations. From Eq. (11) we obtain for the time dependent part of the density of the photon gas in G

$$n_\nu \propto \sin \omega(t-\tau'); \tag{12}$$

where τ' is a time delay for which, by simple calculation, we obtain

$$\tau' = \frac{1}{\omega} \arctan \frac{\omega n}{ck(\nu) + \frac{3c}{4r}(1-R)}. \tag{13}$$

The intensity of the light leaving G through the aperture o being proportional to the density of the photon gas in G with good approximation, τ' can be measured by the fluorimetric determination of the intensity modulation of the light entering G and emerging from it.

For the time dependent part of the density n' of the fluorescence photon gas in the case of modulated excitation, we can write

$$V \frac{dn'}{dt} = N_f - N_{fr}, \tag{14}$$

where the influence of reabsorption has been neglected; N_f means the number of the fluorescence photons emitted in G during unit time, and N_{fr} the number of those absorbed on the wall because of incomplete reflection. For N_{fr} the relation

$$N_{fr} = n' \frac{c}{n} (1-R') \pi r^2 \tag{15}$$

will hold similarly to that given for $N_{fr(\nu')}$; and N_f is given, in the case of the considered exponential decay of the solution, by

$$N = \frac{1}{\tau} \eta V \frac{c}{n} k(\nu) \int_0^\infty n e^{-t'/\tau} n_\nu(t-t')\, dt', \tag{16}$$

where τ is the decay time to be determined. From Eqs. (12)—(16) we obtain with simple but cumbersome calculations

$$n'(t) = \text{const. } \sin \omega(t - \tau' - \tau'' - \tau). \tag{17}$$

Here, τ'' can be calculated as follows:

$$\tau'' = \frac{1}{\omega} \arctan \frac{\omega n}{c(1-R')\frac{3}{4r}}. \tag{18}$$

The decay time τ can be determined in practice by measuring the time delay $\tau' + \tau'' + \tau$ in Eq. (17) with a fluorimeter and subtracting from this the mean life time of the exciting photons and fluorescence photons, τ' and τ'', given by Eqs. (13) and (18), respectively.

§ 7. Concerning the use in practice of the relationships explained hitherto we have to make the following remarks. According to our experiences the integrating cuvette need not necessarily be of spherical shape; in the case of an irregular shape of the cuvette the relations of the preceding paragraphs can be used, of course with adequate modifications concerning the meaning of the symbols for the dimensions of the cuvette. So e.g. the constant A in Eq. (3) cannot be immediately calculated with Eq. (4) for an irregularly shaped cuvette. Instead, a suitable empirical constant has to been substituted for r. In other words, A has to be calculated from Eq. (3) using a medium of known absorption coefficient. Moreover, it is advisable to consider r and R as empirical constants, because in our considerations in § 2—6 an ideal case has been assumed in which the finite thickness of the glass or quartz wall of the cuvette had no effect. In reality, the wall always behaves as a "light pipe"; in consequence of repeated total reflections in the wall, the photon gas will be subject to losses through the wall of the feed and exit pipes for the liquid.

It has been assumed in § 2 that G has a diffusely reflecting exterior coating. Our experiments showed that this condition is not indispensable: the photon gas produced in the cuvette will be homogeneous and isotropic with good approximation also if the coating consists of a regularly reflecting metal layer, e.g. of silver.

§ 8. In order to check the applicability of the method dealt with, numerous spectrophotometric measurements were performed. The arrangement used is shown in Fig. 2. The light of the source Q (incandescent lamp or high pressure Xe or Hg lamp) falls through the monochromator M_1 upon the area e of G. The photomultiplier Ph_1 irradiated with the light reflected by the semi-transparent plate P was used to control the intensity of the entering light. The light leaving G at o reaches the photomultiplier Ph_2 through the monochroma-

tor M_2. (When investigating the absorption, M_1 and M_2 have to be adjusted to the same wave length; for measuring the emission spectrum the adjustment of M_1 is constant, that of M_2 has to be varied.) The monochromator M_2 is indispensable even in absorption measurements, if the investigated medium exhibits fluorescence, because the measurement would be disturbed by the fluorescence light leaving G.

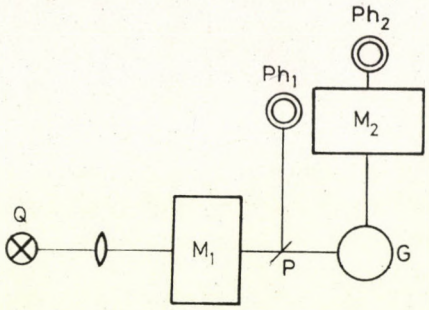


Fig. 2

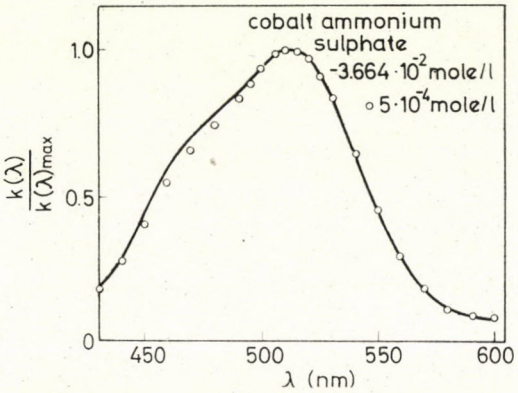


Fig. 3

To illustrate the results of our absorption measurements with the arrangement described above, the absorption spectrum of an aqueous cobalt ammonium sulphate solution of $5 \cdot 10^{-4}$ mole/l concentration is shown in Fig. 3. In this Figure the little circles denote our experimental data, and the full curve the absorption spectrum given for a solution of $3{,}66 \cdot 10^{-2}$ mole/l concentration in the literature [6]. (Temperature of measurement: 27.5 °C). The data of the spherical cuvette used in the measurements: $r = 3.9$ cm; the quality of the glass wall: Jena Molybdenum Uviol Glass; material of the reflecting coating: magnesium oxide. In order to obtain the molar decadic extinction coefficient found in the literature for cobalt ammonium sulphate, the value $A = 4.1 \cdot \cdot 10^{-3}$ had to be assigned to G.

In Fig. 4 the results of our investigations concerning the spectral distribution of fluorescence are illustrated by the spectrum of an aqueous fluorescein solution of $5 \cdot 10^{-8}$ mole/l concentration measured with the arrangement and integrating sphere described. The little circles show the distribution as a function of wavelength; the emission spectrum of a solution of $1 \cdot 10^{-4}$ mole/l concentration is represented by the full curve. (Temperature of measurement: 25 ± 2 °C.

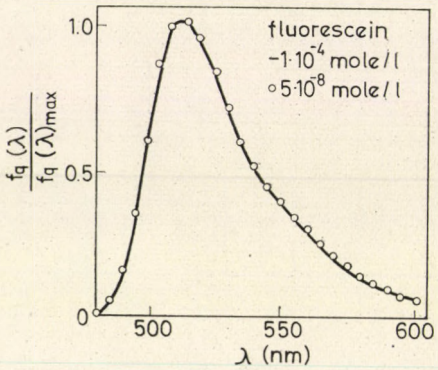


Fig. 4

The correction for reabsorption of the experimental fluorescence spectrum was made using Eq. (8). In applying this formula, however, it is not necessary to know the accurate values of m, r, and R. Namely, it can easily be seen that the equation

$$f(\nu) = C \frac{I_0}{I} f^*(\nu) \tag{19}$$

is equivalent to Eq. (8). Here C is a normalizing factor, while I and I_0 mean the intensities belonging to the frequency ν', which were defined in § 3 in connection with the measurement of absorption.

Our experiments concerning the determination of the yield function $\eta(\nu)$ and of the decay time τ with the aid of the integrating sphere, which, beside other results, supported the respective formulae, will be dealt with in a following paper. Concerning the fluorimetric measurements with the sphere, we wish only to remark that our results supported the relation derived from Eq. (13)

$$\tau' \approx \frac{4rn}{3c\,(1-R)} \tag{20}$$

for the solvent. According to this formula the photons entering the sphere G through e have a path length of 1 to 3 metres in the mean, even if the radius of the sphere is not more than a few centimetres.

The authors wish to express their gratitude to the late Prof. Á. Budó, Director of the Institute, for valuable discussions during the last period of his life.

REFERENCES

1. A. A. Shishlovskii, Prikladnaia Fizicheskaia Optika, FIZMATGIZ, Moscow, 1961.
2. V. L. Levshin, Metodi Spectralnovo Analiza, Izd. Mosk. Universiteta, Moscow, 1962.
3. C. F. Ravilious, R. T. Farrar and S. H. Liebson, J. Opt. Soc. Amer., **44**, 238, 1954.
4. B. Karvaly, Acta Phys. Hung., in press.
5. I. Ketskeméty, Acta Phys. Hung., **10**, 429, 1959.
6. G. Kortüm, Kolorimetrie-Photometrie und Spektroskopie, 3. Aufl., Springer, Berlin, 1955.

МЕТОД ДЛЯ СПЕКТРОФОТОМЕТРИЧЕСКОГО ИЗУЧЕНИЯ ПОГЛОЩЕНИЯ И ФЛУОРЕСЦЕНТНОГО ИЗЛУЧЕНИЯ СЛАБО ПОГЛОЩАЮЩИХ СРЕД

И. КЕЧКЕМЕТИ и Л. КОЗМА

Резюме

Описано интегрирующая кювета и экспериментальные методики, которые можно проводить с ней для измерения спектра поглощения и испускания, квантового выхода и времени затухания слабо поглощающих сред. Экспериментальные результаты показывают, что эти методы можно использовать до концентраций 10^{-8} моль/л. В случае интегрирующих кювет, имеющих диаметры несколько *см*, средний свободный пробег фотонов по флуориметрическими измерениями и по расчётными данными 2—3 метра.

Note added in proof. Most detailed experimental results will be published elsewhere (Acta Phys. et Chem., Szeged, **16**, 7, 1970).

Acta Physica Academiae Scientiarum Hungaricae, Tomus 29 (4), pp. 341—357 (1970)

УГЛОВАЯ АНИЗОТРОПИЯ ДЕЛЕНИЯ ЯДЕР НЕЙТРОНАМИ И СТРУКТУРА БАРЬЕРА

Х. Д. АНДРОСЕНКО, С. Б. ЕРМАГАМБЕТОВ, Г. Н. СМИРЕНКИН, Д. Л. ШПАК
ФИЗИКО-ЭНЕРГЕТИЧЕСКИЙ ИНСТИТУТ, ОБНИНСК, СССР

и

И. КОВАЧ
ЦЕНТРАЛЬНЫЙ ИНСТИТУТ ФИЗИЧЕСКИХ ИССЛЕДОВАНИЙ, БУДАПЕШТ

(Поступило 21. XI. 1969)

Сообщаются результаты измерений угловых распределений осколков деления Th^{232}, U^{238}, Np^{237}, Pu^{238}, Pu^{240}, Pu^{242}, Am^{241} нейтронами. Исследования производились на электростатических генераторах ФЭИ. Главное внимание уделено изучению околопороговой области энергий возбуждения. Полученные экспериментальные данные не укладываются в рамки традиционного описания вероятности деления, но получают удовлетворительное объяснение с помощью представлений о двугорбом барьере. В связи с обсуждением результатов выполненных измерений затронуты вопросы о квазистационарных состояниях ядра во второй яме, о структуре барьеров, о четно-нечетных различиях вероятности деления и энергетической щели ядра при больших деформациях.

Введение

Угловая анизотропия разлета осколков деления является следствием преимущественной ориентации углового момента ядра $\bar{J}$ относительно пучка бомбардирующих частиц и неоднородности распределения проекций момента K на ось симметрии (направления разделения). Реализующийся спектр $f(\kappa)$ зависит от энергии возбуждения в переходном состоянии $E^* = E - E_f$ и способа возбуждения, определяющего доступный набор угловых моментов. Специальный интерес представляет область малых E^*, когда ядро холодное и в делении участвует небольшое число переходных квантовых состояний — каналов деления [1, 2]. С дискретностью спектра нижайших каналов деления связывается появление сложной структуры в энергетической зависимости угловых распределений осколков $W(\Theta)$, вблизи порога, наблюдаемого в сечении σ_f.

Исследования околопорогового деления ядер обнаружили ряд качественных эффектов, свидетельствующих о плодотворности идей модели каналов деления. Наиболее важными представляются результаты изучения четно-четных делящихся ядер, применительно к которым данная модель, использующая для спектра каналов деления аналогию со спектрами возбужденных равновесных состояний, ведет к конкретным следствиям. Ожидаемая квантовая структура барьера была наблюдена при изучении фотоделения [3] и реакций типа (d, pf) [4, 5].

Однако, более подробные эксперименты и детальный количественный анализ энергетической зависимости угловой анизотропии [6—10] выявили неполноту традиционного описания деления ядер вблизи порога [1, 2]. Объяснение ряда свойств и явлений, не укладывающихся в рамки общепринятой концепции Н. Бора-Уилера—О. Бора, в том числе и угловой анизотропии, стало возможным благодаря пересмотру представлений о форме барьера деления. В 1967 г. Струтинским [11] были осуществлены расчеты потенциальной энергии деформации ядра с учетом оболочечных эффектов, показавшие значительные отступления формы барьера деления от параболической, которая мотивировалась моделью жидкой капли. Согласно [11], реальный барьер деления в обычно используемом одномерном представлении имеет форму кривой с двумя максимумами. Физические идеи, связанные с новыми представлениями о форме барьера и квазистационарными состояниями в яме между максимумами [12, 13], дали начало так называемой модели двугорбого барьера деления.

Настоящая работа посвящена исследованию актуальных вопросов, связанных с угловой анизотропией и структурой барьера деления. Экспериментальная часть работы включает в себя некоторые результаты измерений, выполненных в последние годы с моноэнергетическими нейтронами на электростатических генераторах ФЭИ. Большинство представленных данных получено с помощью трековой методики. Здесь мы не ставим перед собой задачу детального описания экспериментов и их результатов — это будет сделано позднее. Цель настоящего сообщения — продемонстрировать недостаточность традиционного описания угловой анизотропии деления и обсудить возможность его уточнения на основе модели двугорбого барьера.

I. Экспериментальные результаты и следствия

A. Деление Th^{232} (n, f) *вблизи порога*

Результаты измерений сечения деления σ_f [14] и угловых распределений осколков $W(\Theta)$ представлены на рис. 1 и 2. Кривые на рис. 2 — $W(\Theta) = \sum_{n=0}^{3} a_{2n} P_{2n}(\cos\Theta)$, где $P_{2n}(\cos\Theta)$ — полиномы Лежандра, рассчитаны с помощью метода наименьших квадратов. Данные об угловой анизотропии $W(0°)/W(90°)$ изображены на вставке к рис. 1, где они сравниваются с результатами других измерений [8, 15, 16]. Угловые распределения, измеренные разными авторами [15, 16], согласуются между собой хуже, чем данные об угловой анизотропии.

Задачей данного эксперимента было получение подробной информации о σ_f и $d\sigma_f(\Theta)/d\Omega \sim W(\Theta)$ для каналового анализа. Идентификация преобладающих каналов деления κ^{π} и восстановление энергетической зависимости

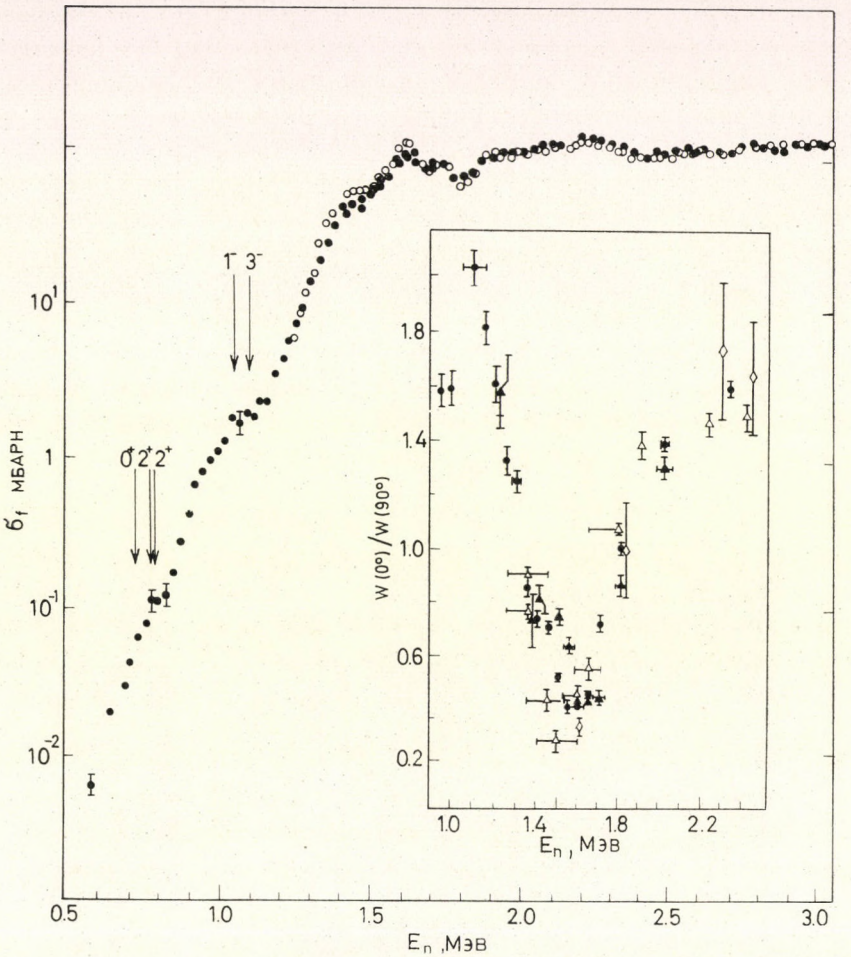


Рис. 1. Зависимость сечения деления Th^{232} от энергии нейтронов E_n : — ● [14], ○ — данные Атласа нейтронных сечений. На вставке — угловая анизотропия ● — настоящая работа, △ — [8], △, ◇ — [15]

проницаемости барьеров $P_{k\pi}(E_n)$ производились, как обычно, путем эмпирического подбора таких квантовых характеристик, которые бы обеспечивали согласие расчета

$$\frac{d\sigma_f(\Theta, E_n)}{d\Omega} \approx \frac{\lambda^2(E_n)}{4} \sum_{J,K,\pi} (2J+1)\, T_l^J(E_n)\, \frac{P_{K\pi}(E_n)\cdot \gamma_{jK}}{\sum\limits_{l',j',m} T_{l'}^{j'}(E_n - E_m)} \cdot W_{JK}(\Theta) \qquad (1)$$

с экспериментом. В выражении (1)(I) мы пренебрегли в знаменателе делительной Γ_f и радиационной Γ_γ ширинами по сравнению с нейтронной шириной $\Gamma_n \sim \sum\limits_{l',j',m} T_{l'}^{j'}(E_n - E_m)$; λ — длина волны нейтрона; $T_{l'}^{j'}$ — оптические коэф-

фициенты проницаемости нейтронов [17]; $\pi = (-1)^I$, индекс m — нумерует уровни ядра-мишени; γ_{JK} — учитывает зависимости проницаемости барьера деления от полного углового момента J в соответствии с обычно принимаемым предположением, что различия $P_{K\pi}$ для разных J сводятся к вычитанию энергии вращения $E_{\text{rot}} = \hbar^2/2J\,[J(J+1) - K(K+1)]$ из энергии, концентрирующейся в делительных степенях свободы (в расчетах принималось $\hbar^2/2J = 4$ кэв).

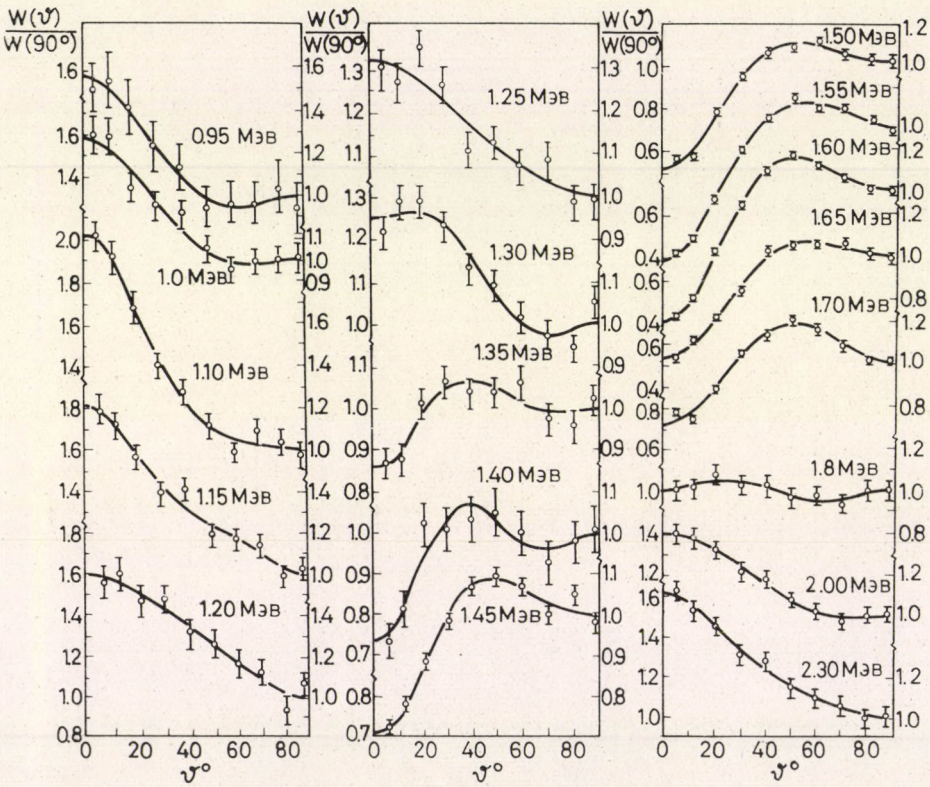


Рис. 2. Угловые распределения осколков деления Th^{232} нейтронами

Классическая схема каналового анализа [2] состоит в отыскании высоты $E_f^{K\pi}$ и параметра кривизны $\hbar\omega_{K\pi}$, связанных с $P_{K\pi}(E_n)$ известным соотношением Хилла-Уилера для параболического барьера

$$P_{K\pi}(E_n) = \left[1 + \exp\left(2\pi\,\frac{E_f^{K\pi} - E_n - B_n}{\hbar\omega_{K\pi}}\right)\right]^{-1}, \qquad (2)$$

где B_n — энергия связи нейтрона. Такие расчеты были осуществлены для реакций Th^{232}(n, f) [16] и U^{234}(n, f) [18], однако они не дают детального описания хода $\sigma_f(E_n)$, так как выражение (2) монотонно зависит от E_n и игно-

рирует резонансные явления, отмеченные в [6, 7]. В настоящей работе анализ производился способом, предложенным Воротниковым [6], в котором никаких ограничений на энергетическую зависимость $P_{K\pi}(E_n)$ не накладывается.

Отметим наиболее важные результаты анализа.

а) При всех E_n удается добиться согласия расчета $W(\Theta)$ с опытом в пределах коридора экспериментальных ошибок, используя лишь две-три комбинации доминирующих состояний K^π. Основной качественной чертой реализующегося спектра K_π является резкое изменение в узком интервале энергий $E_n \sim 0{,}1-0{,}2$ Мэв роли отдельных состояний (вступление и исчезновение), что свидетельствует о нерегулярном «резонансном» поведении $P_{K\pi}(E_n)$, не согласующемся с (2).

б) Идентификации даже преобладающих каналов деления свойственна неоднозначность. Не удается определить четность состояний $K = 1/2$, вносящих значительный вклад при всех изученных энергиях; трудно различить состояния $K^\pi = 3/2^+$ и $5/2^-$, $5/2^+$ и $7/2^-$, соответственно. По этой причине на рис. 3 приводятся два варианта результатов анализа для $K^\pi = 1/2^+$ (а) и $1/2^-$ (б), а на каждом из этих рисунков в отдельных областях E_n — по две возможности $P_{K\pi}$, дающих примерно одинаковое согласие с опытом (пунктирная и сплошная кривые). Источником ошибок может явиться также неопределенность параметра $\hbar^2/2J$. Однако, в отсутствии детальной информации об уровнях ядра-мишени выше 1,2 Мэв идентификация K^π, (но не абсолютная величина $P_{K\pi}$) нечувствительна.

в) Благоприятным обстоятельством является тот факт, что к неопределенности идентификации квантовых характеристик каналов некритичен главный результат анализа: наличие резонансов $P_{K\pi}(E_n)$ с шириной порядка 0,1 Мэв. Нерегулярности $\sigma_f(E_n)$ в районе 1,1 и 1,6 Мэв связаны с резонансами $P_{1/2\pi}$ и $P_{3/2\pi}$, соответственно; привлекавшееся прежде традиционное объяснение конкуренцией нейтронной ширины [2] в этих случаях неприемлемо. Величина $P_{1/2\pi}(0)$, полученная путем экспоненциальной экстраполяции к $E_n = 0$, сильно расходится с проницаемостью, оцененной по сечению деления Th^{232} тепловыми нейтронами [19]. Последняя примерно в тысячу раз превосходит экстраполированное значение [14]. Этот факт показывает, что нерегулярное изменение проницаемости барьера сохраняется в глубоко подбарьерной области возбуждений. Наиболее яркая картина резонансных эффектов $P(E)$ наблюдена в работе [20].

Б. Деление U^{238}, Np^{237}, Pu^{238}, Pu^{240}, Pu^{242}, Am^{241} *нейтронами*

Измерение угловых распределений осколков деления U^{238}, Pu^{240}, Pu^{242} выполнены преимущественно в околопороговой области энергий нейтронов, для Np^{237}, Pu^{238}, Am^{241} — вплоть до порогоа (n, nf) — реакции. Коэффициент

угловой анизотропии $A=W(0°)/W(90°)-1$ для пяти ядер-мишеней изображен на рис. 4. Для трех из них Pu^{238} ($\approx 85\%$), Pu^{240} ($\approx 93\%$) и Pu^{242} ($\approx 95\%$) точность измерений в подпороговой области лимитировалась изотопными примесями.

Общим свойством исследованных ядер является практически полное отсутствие каналовых эффектов в угловом распределении осколков. Полу-

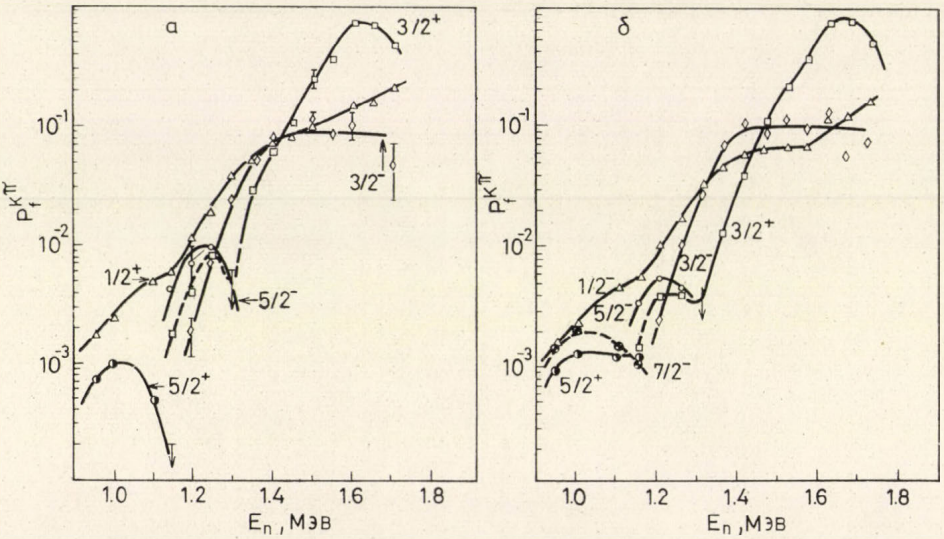


Рис. 3. Зависимость проницаемости барьера деления Th^{232} (n, f) от энергии нейтронов E_n для различных квантовых состояний ядра K^π : (а) — в предположении, что четность каналов $K = 1/2$ положительна, (δ) — отрицательна (см. текст)

ченные для изотопов Np, Pu, Am угловые распределения при всех энергиях в том числе и под порогом, хорошо описываются простым выражением

$$\frac{W(\Theta)}{W(90°)} = 1 + A\cos^2\Theta. \tag{3}$$

Соответствие анизотропной части $W(\Theta)$, квадратичной зависимости от $\cos\Theta$ при достаточных возбуждениях обычно рассматривается как признак статистического распределения K [27]:

$$f(K) \sim \exp\left(-\frac{K^2}{2K_0^2}\right). \tag{4}$$

Для описания $W(\Theta)$, в этом случае широко используется соотношение статистической теории

$$W(\Theta) \sim \sin^{-3}\Theta \int_0^{P\sin^2\Theta} x^{1/2} e^{-x} I_0(x)\, dx = \sin^{-3}\Theta \cdot \Phi(P\sin^2\Theta) \tag{5}$$

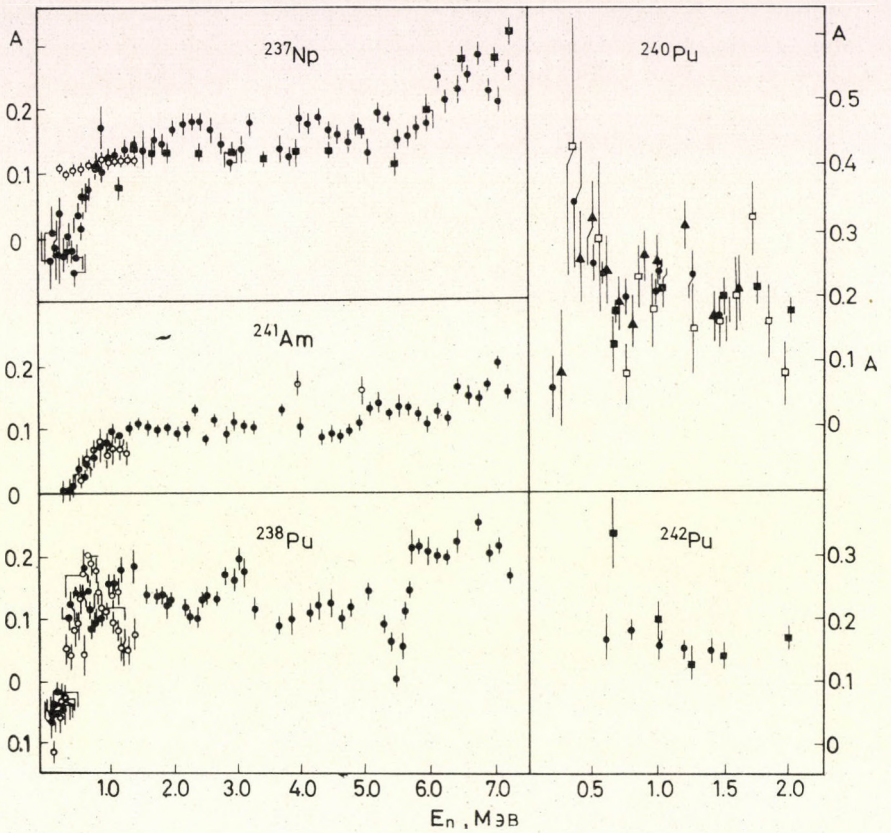


Рис. 4. Зависимость коэффициента угловой анизотропии деления от энергии нейтронов для ядер — мишеней Np^{237}: ○ — [22]; Am^{241}: ○ — [23]; Pu^{238}: ○ — [24]; Pu^{240}: ■ — [26], □ — [25], △ — [8]; Pu^{242}: □ — [26]. Для всех ядер: ● — данные настоящей работы

при малом

$$p = \frac{\langle J^2 \rangle}{2K^2},$$

т. е. малой анизотропии, переходящее в (3). У обсуждаемых ядер $A \lesssim 0{,}2$.

Тем не менее, соответствие экспериментальных данных с $W(\Theta)$ соотношению (3) в реакции (n, f) без дополнительного анализа нельзя рассматривать как достаточный признак распределения (4). Дело в том, что зависимость (3) выполняется при любом спектре каналов для малых энергий $E_n \lesssim 0{,}5$ Мэв, когда в сечении образования составного ядра доминируют волны с $l \leq 1$. Лишь вклад более высоких угловых моментов приводит к отступлениям от (3).

Убедимся на примере Pu^{238} (n, f), что экспериментальные угловые распределения осколков нельзя объяснить, привлекая малое число состояний

K^π. Эта реакция еще интересна и тем, что для нее в работе [24] был выполнен каналовый анализ, приведший к противоположному выводу. Согласно [24], деление Pu^{238} нейтронами имеет порог при $E_n \approx 0{,}8—1{,}0$ Мэв и происходит до 1,5 Мэв преимущественно через два типа состояний $K^\pi = 1/2^-$ и $3/2^-$. На рис. 5 полученные нами экспериментальные распределения сравниваются с расчетом, производившемся по схеме, использованной выше при анализе

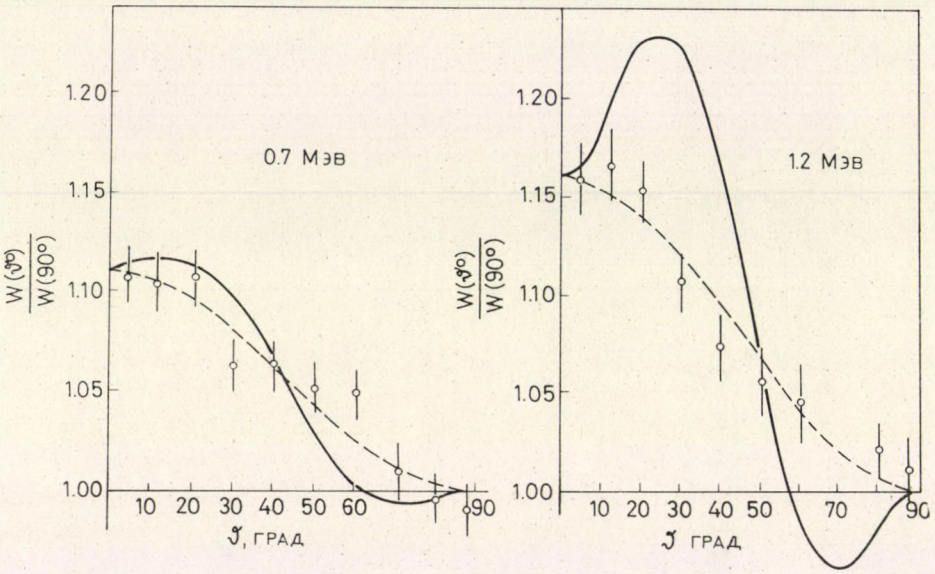


Рис. 5. Угловые распределения осколков при делении Pu^{238} нейтронами: ○ — [9], кривые — расчет (см. текст)

реакции Th^{232} (n, f). Иные простые комбинации K^π дают еще большее расхождение с опытом.

Яркая демонстрация участия в делении тяжелых ядер вблизи порого большого числа состояний была получена при изучении реакции U^{238} (n, f) [9]. Коэффициент угловой анизотропии согласуется с данными Лэмфира [8] и достигает 0,6. В этом случае приближение (Z) не является удовлетворительным и для проверки гипотезы (4) необходимо пользоваться выражением (5). Наиболее интересная часть экспериментальных данных изображена на рис. 6 в компактном представлении, использующем согласно (5), что

$$\frac{W(0°)}{W(\Theta)} = \frac{2}{3}\,\frac{(p\sin^2\Theta)^{3/2}}{\Phi(p\sin^2\Theta)} \tag{6}$$

зависит от единственного параметра $x = p\sin^2\theta$. Правая часть (6), как показано на рис. 6, при $p \lesssim 1$ с хорошей точностью линейно зависит от x. Таким

образом, деление U^{238} (n, f) под порогом на 0,5—0,7 Мэв происходит так, как если бы в нем принимало участие значительное число каналов.

Резкое изменение характера и зависимости от энергии углового распределения осколков при увеличении числа нуклонов на несколько единиц в области, где свойства равновесных ядер изменяются мало, удивительно. Никаких ограничений по A и Z на реализацию каналовых эффектов для ядер с одинаковой четностью числа нуклонов модель О. Бора не накладывает. И в самом деле, результаты экспериментов по фотоделению [28] показывают, что каналовые эффекты в угловых распределениях осколков и в случае тяжелых ядер не исчезают во-все, а лишь смещаются в область возбуждений примерно на 1 Мэв ниже высоты барьера, наблюдаемой в сечении деления.

Интерес представляет также немонотонный характер энергетической зависимости угловой анизотропии при значительных возбуждениях, где справедливость статистического описания не вызывает сомнения. Определенная из данных об угловой анизотропии на рис. 4 энергетическая зависимость $K_0^2(E^*)$ для составных ядер — нечетно-нечетного Np^{238} и нечетного Pu^{239} — на рис. 7 сравнивается с аналогичной зависимостью для четно-четного ядра Pu^{240}, делящегося в реакциях Pu^{239} (n, f) [29, 30]. Энергия возбуждения в первых двух случаях вычислена как разность $E_n - E_{nf}$, где E_{nf} — энергия нейтронов, при которой наблюдается порог в сечении деления.

Наличие ступенчатой структуры в ходе $K_0^2(E^*)$ Pu^{240} в работе [4] и ряде последующих [5, 30] было истолковано как следствие энергетической щели 2Δ в спектре внутренних возбуждений. Основываясь на оценке скачка K_0^2

$$\delta K_0^2 = 2\langle K_p^2\rangle = \frac{N(N+1)}{3} \approx 20 \tag{7}$$

связанного с разрывом пары нуклонов, авторы [4] для переходного состояния получили величину $\Delta_f \approx 1{,}3$ Мэв, почти вдвое превосходящую равновесное значение $\Delta_0 \approx 0{,}7$ Мэв. В (7) $\langle K_p^2\rangle$ равное значению K_0^2 для одной неспаренной частицы, оценено как среднее по всем одночастчным уровням последней незаполненной оболочки с полным квантовым числом $N = 7—8$. Анализ энергетической зависимости $K_0^2(E^*)$ в более широкой области возбуждений до 30 Мэв привел Гриффина [29] к заключению, что критическая энергия фазового перехода E_{Kp}^* из сверхтекучего состояния в ферми-газовое составляет примерно 19 Мэв, что также соответствует аномально высокому значению $\Delta_f \approx 1{,}2$ Мэв.

В дальнейшем интерпретация скачкообразной зависимости $K_0^2(E^*)$ при низких возбуждениях и надежность определения Δ_f, E_{Kp}^* и $\langle K_p^2\rangle$ были подвергнуты сомнению [31, 32]. Пересмотр анализа [29] привел в работе [32] к существенно более низким значениям $E_{Kp}^* = 9{,}5 \pm 3$ Мэв и $\Delta_f = 0{,}77 \pm$ $\pm$ 0,15 Мэв, близким к равновесным. K_0^2, как следует из рис. 7, при $E^* \to 0$

(Np^{238} и Pu^{239}) стремится к значениям, соответствующим $\langle K_p^2 \rangle \approx 5$, а не 10, как по оценке (7) (см. также [30]). Из рис. 7 видно, что уменьшение $\langle K_p^2 \rangle$ вдвое при значительном разбросе разных данных о K_0^2 для Pu^{240} ведет к большей неопределенности установления величины Δ_f. Наконец, из-за наличия ступенчатой структуры $K_0^2(E^*)$ у Np^{238} и Pu^{239}, спектр переходных состояний

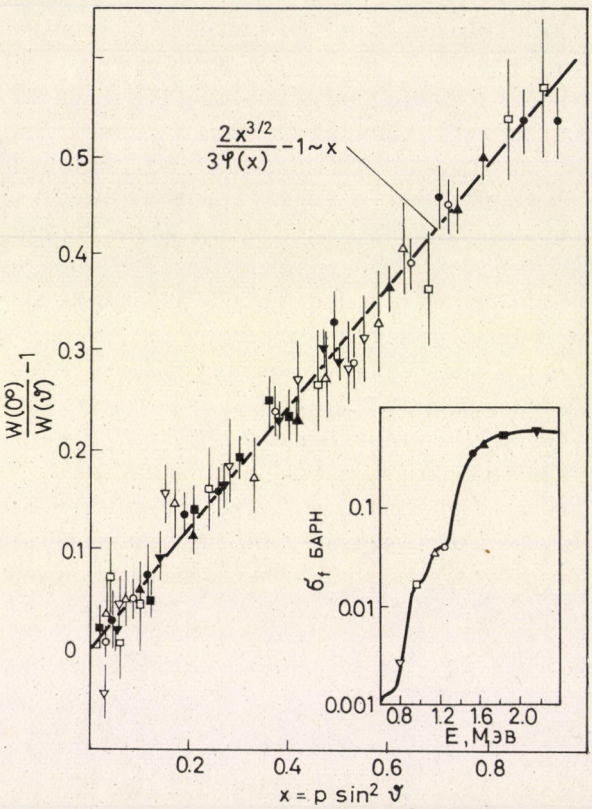


Рис. 6. Сопоставление экспериментальных данных ○ $W(\Theta)\,N^{238}$ с выражением (5) статистической теории угловых распределений осколков деления (см. текст). На вставке — энергетическая зависимость сечения деления $\sigma_g(E_k)N^{238}$ нейтронами. Обозначения: ○ — 1,25 Мэв, ● — 1,55 Мэв, ▲ — 1,65 Мэв, ▽ — 0,8 Мэв, — — 0,95 Мэв; ▽ — 1,15 Мэв, □ — 1,85 Мэв, ▽ — 2,2 Мэв

которых не имеет энергетической щели, неочевидной становится сама возможность определения Δ_f по величине скачка δK_0^2 (7).

Отказ от предположения об аномальной величине энергетической щели делает необходимым переосмысливание физической природы четно-нечетных различий для барьеров деления. Во многих работах, в особенности, посвященных систематизации экспериментальных данных о периодах спонтанного деления и высоте барьеров, различия четных и нечетных ядер связываются с разностью энергетических поверхностей в переходном и равновесном

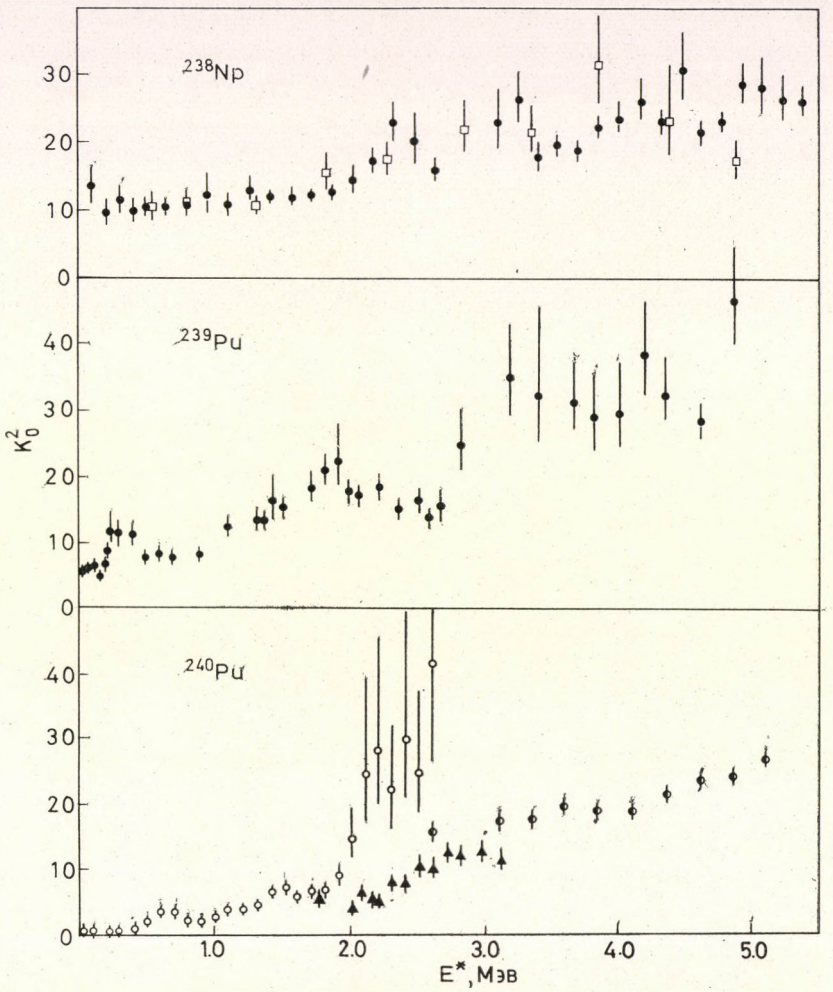


Рис. 7. Зависимость параметра K_0^2 от энергии возбуждения E^* для делящихся ядер Np^{238} Pu^{239}, Pu^{240}. На нижнем рисунке: ○ — [5], ◐ — [29], ▲ — [30]

состояниях, т. е. $\Delta_f - \Delta_0$. Примеры таких систематик [33] представлены на рис. 8. В них использованы значения E_f, как определенные для четно-четных делящихся ядер из каналового анализа угловой анизотропии деления в (d, pf) и (γ, f) — реакциях [5, 10] (см. ниже таблицу I), для нечетных и нечетно-нечетных — из порога, наблюдаемого в сечениях деления нейтронами. Расстояние между двумя ветвями зависимости Γ_n/Γ_f от $(E_f - B_n)$ из статистических соображений может быть оценено как $\Delta_f + \Delta_0$. Оно согласно рис. 8б составляет приерно 2 Мэв. Как эта величина, так и расщепление E_f на рис. 8а соответствуют предположению о значительной разности $\Delta_f - \Delta_0$, соста-

вляющей в среднем 0,5—0,7 Мэв. Однако, это широко распространенное объяснение четно-нечетных значений E_f противоречиво, поскольку в рамках предположения о значительной разнице Δ_f и Δ_0 должно было бы наблюдаться расщепление данных рис. 8а и 8б у нечетных и нечетно-нечетных ядер на величину $\Delta_f - \Delta_0$, а оно отсутствует (см. подробнее [33]).

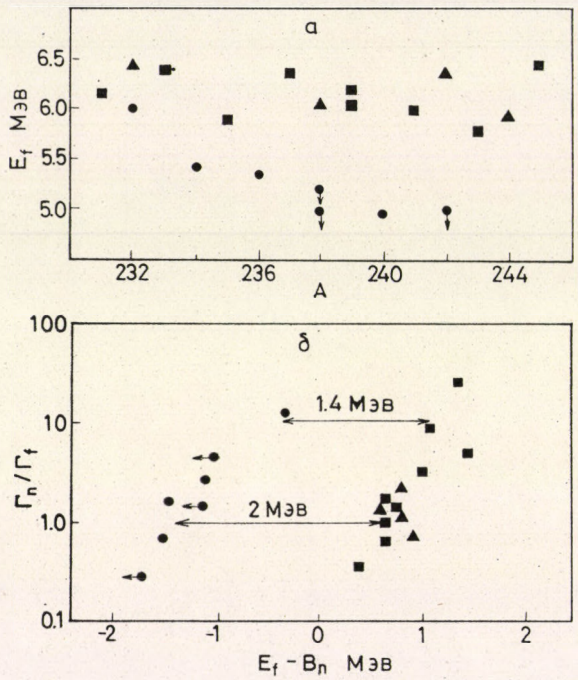


Рис. 8. а) Пороги вынужденного деления четно-четных — ●, нечетных — ■ и нечетно-нечетных — ▲ ядер. б) Отношение средних нейтронной и делительной ширин в зависимости от разности $E_f - B_n$. Обозначения те же, что и для а)

Таким образом, вопрос о природе четно-нечетных различий барьеров деления не может быть решен с помощью гипотезы о возрастании энергетической щели с деформацией ядра, но остается также открытым, если принять $\Delta_f \approx \Delta_0$.

II. Интерпретация

Перечислим наиболее существенные результаты обсуждения представленных экспериментальных данных.

1. В энергетической зависимости проницаемости барьера наблюдаются отступления от экспоненциального монотонного хода в виде резонансов. Положения резонансов $P_{K\pi}$, соответствующие разным квантовым характеристикам K^π, не совпадают.

2. С увеличением числа нуклонов в узкой области масс делящихся ядер каналовые эффекты вблизи наблюдаемого в сечении порога исчезают, смещаясь в подпороговую область энергий.

3. Выдвинут ряд аргументов против гипотезы о значительной разнице в энергетической щели в переходном и равновесном состояниях. Однако, отказ от этого предположения не устраняет трудности объяснения четно-нечетных различий в барьерах деления.

Круг явлений, не укладывающихся в традиционную картину деления, значительно шире и выходит за рамки вопросов, связанных с угловой анизотропией разлета осколков (спонтанно-делящиеся изомеры, группировка резонансов сечения деления медленными нейтронами). Для их объяснения весьма плодотворной оказалась модель двугорбого барьера [12, 13]. Согласно [12], переходное состояние во второй яме (между максимумами A и B) подобно обычному компаунд-состоянию ядра равновесной формы. Если вероятность диссипации энергии коллективного движения в нуклонные степени свободы велика, то ядро, прежде чем разделиться, будет дважды претерпевать эволюцию перехода внутренней энергии в энергию деформации. В этом смысле реакция деления может рассматриваться как двухступенчатый процесс. Эта качественно новая особенность и является источником обсуждаемых эффектов.

Наличие квазистационарных уровней во второй яме приводит к тому, что проницаемость барьера, в отличие от монотонной функции (2), в окрестности уровней изменяется резонансным образом [12, 13]. Кроме резонансов с шириной A 0,1 Мэв типа тех, которые реализуются при делении Th^{232} быстрыми нейтронами, в сечении деления медленными нейтронами наблюдается группировка сильных и слабых резонансов — структура с шириной резонансов огибающей порядка 0,01—0,1 кэв расстоянием между резонансами порядка 0,1—10 кэв. Согласно [12], первые связываются с вибрационными состояниями, вторые — с состояниями внутреннего возбуждения.

Первоначально резонансы первого типа пытались относить к состояниям в первой яме [7, 34], однако, соображения о диссипации колебательной энергии во внутренние степени свободы эту возможность поставили под сомнение [12, 13]. Для обсуждения данного вопроса, по-видимому, весьма существенна принадлежность резонансов проницаемости к определенной комбинации K^π (см. рис. 3). Если вибрационные состояния связывать с первой ямой, то для объяснения этого факта придется привлечь слишком сильное предположение о сохранении K в продолжение всей эволюции делящегося ядра.

Положения резонансов с разными K^π не обнаруживают регулярной структуры, расстояние между ними во многих случаях (рис. 3) значительно меньше ожидаемого для вибрационных состояний ($\sim \hbar\omega \approx 0{,}5 - 1$ Мэв). Этот факт, по-видимому, свидетельствует о том, что резонансы $P_{K\pi}$ для раз-

ных комбинаций K^π следует относиться к вибрационным состояниям в разных ямах, иначе говоря, о наличии расщепления кривых потенциальной энергии деформации в зависимости от квантовых характеристик в соответствии с основной идеей модели О. Бора. Квазистационарные состояния во второй яме благодаря резонансному изменению $P_{K\pi}(E)$ играют значительную роль в развитии каналовых эффектов при делении ядер.

Исчезновение каналовых эффектов в угловой анизотропии деления вблизи порога, наблюдаемого в сечении, при увеличении числа нуклонов в делящемся ядре, согласно [12], связано с изменением структуры двугорбого барьера: уменьшением максимума B и углублением ямы между максимумами. Допустим, следуя [12], что яма на барьере достаточно глубока, и ядро в ней живет достаточно долго по сравнению с характерным периодом миграции величины K. В этом предположении ядро «забывает» о квантовых состояниях, в которых оно находилось при прохождении первого барьера A, и дальнейшее развитие процесса деления будет определяться спектром состояний на барьере B.

Очевидно, что в случае $E_{fB} \gtrsim E_{fA}$ будет осуществляться традиционная ситуация: разнообразие форм $W(\Theta)$ и значительный масштаб изменения угловой анизотропии вблизи наблюдаемого порога деления. В противоположном случае $E_{fB} < E_{fA}$, может возникнуть принципиально новая картина, так как наблюдаемый в сечении порог определяется высотой большого из барьеров, т. е. E_{fA}, а реализующийся спектр каналов деления — энергией возбуждения в критической точке B. При достаточной разнице $\delta_{AB} = E_{fA} - E_{fB} > 0$ каналовые эффекты в угловых распределениях осколков будут проявляться в существенно подбарьерной области энергий. При этом около порога плотность каналов деления может быть уже значительной, так что на опыте будет реализоваться распределение K, близкое к статистическому.

Экспериментальная картина изменений $W(\Theta)$ и $A(E)$ в рассмотренных в настоящей работе случаях удовлетворительно согласуются с этим описанием.

Значения δ_{AB}, в таблице I, полученные из анализа данных по фоторделению [28], согласуются с оценками, полученными из анализа группировки резонансов сечения деления Np^{237} и Pu^{240} медленными нейтронами [35]. Отметим, что обсуждаемое явление — смещение каналовых эффектов в угловой анизотропии в подбарьерную по сечению деления область энергий, — по-видимому, наблюдается также в исследованиях реакций типа (d, pf). Экспериментальные данные [4, 5] показывают, что максимум угловой анизотропии, за который ответственны состояния $K = 0$, находится в области $E < B_n$, где делимость ядер $\sigma_f/\sigma_C \approx \Gamma_f/\Gamma_\gamma \ll 1$. Для объяснения этого парадокса авторы [5] допускают, по нашему мнению, слишком сильное предположение, что радиационная ширина Γ_γ примерно на порядок превосходит значения, наблюдаемые при $E \approx B_n$ в (n, γ) — реакциях.

В рамках изложенных представлений модели двугорбого барьера деления можно также понять природу четно-нечетных различий E_f, представленных на рис. 8. Поскольку данные о высоте барьеров деления, определенные из энергетических зависимостей угловой анизотропии (четно-четные ядра) и сечения деления (нечетные и нечетно-нечетные ядра) относятся к различным барьерам B и A, соответственно, при анализе четно-нечетных различий E_f необходимо учитывать разность δ_{AB}. Расщепление E_f на рис. 8а именно и соответствует этой величине, уменьшающейся, как и в таблице I, в сторону более легких делящихся ядер. Расстояние между ветвями семейства $\Gamma_n/\Gamma_f = f(E_f - B_n)$ для тяжелых ядер ($\Gamma_n/\Gamma_f < 1$) включает в себя $\delta_{AB} = 2$ Мэв $- (\Delta_f + \Delta_0) \approx 0{,}6$ Мэв при $\Delta_f \approx \Delta_0 \approx 0{,}7$ Мэв. Для легких ядер ($\Gamma_n/\Gamma_f \gg 1$), как показано на рис. 8б, это расстояние уменьшается до $\Delta_f + \Delta_0 \approx 1{,}4$ Мэв, согласуясь с $\delta_{AB} \approx 0$.

Таблица I

Разность высот барьеров деления δ_{AB} по данным реакции (γ, f) [28]

ядро	δ_{AB}[Мэв]
Th^{232}	0*
U^{238}	0,4
Pu^{238}	0,7
Pu^{240}	0,9
Pu^{242}	0,9

* Значения характеристики, приведенные в таблице, следует рассматривать, как оценки, имеющие точность $\sim 0{,}2$ Мэв.

Отметим, в заключение, еще одно обстоятельство, касающееся описания вероятности деления в целом. Свойства угловых распределений осколков показывают, что, кроме каналовых эффектов, связанных с квазистационарными состояниями во второй яме, при делении реализуются каналовые эффекты в старом смысле, т. е. обусловленные расщеплением состояний на барьере B. При этом отсчет числа каналов, определяющих вероятность деления, следует вести от барьера B, а не от дна второй ямы, как можно было бы ожидать, исходя из роли квазистационарных состояний. Данное предположение подтверждает величина K_0^2 при энергиях, близких к порогу: K_0^2 для четно-четных ядер по мере приближения к барьеру B стремится к нулю, а для нечетных — к одночастичному значению (рис. 7). Пример расчета сечения деления Pu^{240} быстрыми нейтронами в этом предположении, позволяющем получить удовлетворительное описание экспериментальных данных в околопороговой области энергий, приведен в работе [35].

Авторы выражают глубокую благодарность П. Л. Капице, А. И. Лейпунскому В. М. Струтинскому за интерес к исследованиям и М. К. Голубевой и Н. Е. Федоровой за большой труд по просмотру стеклянных детекторов, широко использовавшихся в измерениях.

ЛИТЕРАТУРА

1. A. Bohr, Int. Conf. Peaceful Uses Atomic Energy, (Proc. Conf. Geneva, 1955) **2**, UK New York 151, 1955.
2. J. A. Wheeler, «Fast Neutron Physics», Part II (J. B. Marion, J. L. Fowler, Eds.) Intersci. Publ., New York, v. **II**, 2051, 1963.
3. Н. С. Работнов, Г. Н. Смиренкин, А. С. Солдатов, Л. Н. Усачев, С. П. Капица, Ю. М. Ципенюк, Physics and Chemistry of Fission (Proc. Symp. Salzburg 1955) I, IAEA, Vienna 135, 1965.
4. H. C. Britt, W. R. Gibbs, J. J. Griffin, R. H. Stones, Phys. Rev. Lett., **11**, 343, 1963; Phys. Rev., **139**, B354, 1965.
5. H. C. Britt, F. A. Rickey, W. S. Hall, Rep. IA-DC-9562, 1968.
6. П. Е. Воротников, С. М. Дубровина, Г. Н. Отрошенко, В. А. Шигин, Ядерная физика, **5**, 295, 1967, П. Е. Воротников, Ядерная физика, **7**, 1228, 1968.
7. J. E. Lynn, Nuclear Data for Reactors (Proc. Symp. Paris), **2**, IAEA, Vienna, 89, 1967.
8. R. W. Lamphere, Physics and Chemistry of Fission (Proc. Symp. Salzburg 1965) I, IAEA, 63, 1965.
9. Х. Д. Андросенко, Г. Н. Смиренкин, Письма ЖЭТФ, **8**, 181, 1968; Д. Л. Шпак, Г. Н. Смиренкин, Письма ЖЭТФ, **8**, 545, 1968; **9**, 196, 1969.
10. С. П. Капица, Н. С. Работнов, Г. Н. Смиренкин, А. С. Солдатов, Л. Н. Усачев, Ю. М. Ципенюк, Письма ЖЭТФ, **9**, 128, 1969.
11. V. M. Strutinsky, Nucl. Phys., **A95**, 420, 1968.
12. V. M. Strutinsky, S. Bjornholm, Int. Symp. Nucl. Structure, Dubna, 1968.
13. J. E. Lynn, Int. Symp. Nucl. Structure, Dubna, 1968.
14. С. Б. Ермагамбетов, В. Ф. Кузнецов, Г. Н. Смиренкин, Ядерная физика, **5**, 257, 1967.
15. R. L. Henkel, J. E. Brolley, Phys. Rev., **103**, 1292, 1956; S. Lo Nigro, C. Milone, Nucl. Phys., **A96**, 617, 1967.
16. A. N. Behkami, J. H. Roberts, W. Loweland, J. R. Huizenga, Nucl. Phys., **A118**, 65, 1968.
17. С. Б. Ермагамбетов, В. Е. Колесов, В. Г. Нестеров, Г. Н. Смиренкин, А. С. Тишин, Ядерная физика, **8**, 704, 1968.
18. A. N. Behkami, J. H. Roberts, W. Loweland, J. R. Huizenga, Phys. Rev., **171**, 1267, 1968.
19. Е. И. Корнеев, В. С. Скобкин, Г. Н. Флоров, ЖЭТФ, **37**, 41, 1959.
20. J. Pedersen, B. D. Kuzminov, Phys. Lett., **29B**, 176, 1969.
21. Б. М. Гохберг, Г. А. Отрощенко, В. А. Шигин, ДАН, **128**, 1157, 1959.
22. J. E. Simmons, R. L. Henkel, Phys. Rev., **120**, 198, 1960.
23. П. Е. Воротников, С. М. Дубровина, Г. А. Отрощенко, В. А. Шигин ДАН, **169**, 314, 1966.
24. П. Е. Воротников, С. М. Дубровина, Г. А. Отрощенко, В. А. Шигин, Ядерная физика, **3**, 479, 1966,
25. В. Г. Нестеров, Г. Н. Смиренкин, И. И. Бондаренко. Атомная энергия **10**, 620, 1961.
26. J. E. Simmons, R. B. Perkins, R. L. Henkel, Phys. Rev., **137**, B809, 1965.
27. В. М. Струтинский, Атомная энергия, **2**, 508, 1957.
28. С. П. Капица, Н. С. Работнов, Г. Н. Смиренкин, А. С. Солдатов, Л. Н. Усачев, Ю. М. Ципенюк, Письма, ЖЭТК, **9**, 128, 1959.
29. J. J. Griffin, Phys. Rev., **132**, 2204, 1963.
30. J. R. Huizenga, A. N. Behkami, J. W. Meadows, E. D. Klema, Phys. Rev., **174**, 1539, 1968.
31. В. М. Струтинский, В. А. Павлинчук, Physics and Chemistry of Fission (Proc. Symp. Salzburg 1965) I, IAEA, Vienna, 127, 1965.
32. Г. Н. Смиренкин, В. Г. Нестеров, А. С. Тишин, Ядерная физика, **6**, 921, 1967.
33. A. V. Ignatyuk, G. N. Smirenkin, Phys. Lett., **29B**, 159, 1969.
34. Б. Т. Гейликман, Ядерная физика, **9**, 535, 1969.
35. Е. Гай, А. В. Игнатюк, Н. С. Работнов, Г. Н. Смиренки, Доклад на 2-ой Симпозиум по физике и химии деления, Вена, 1969.

ANGULAR ANISOTROPY OF NUCLEAR FISSION BY NEUTRONS AND THE BARRIER STRUCTURE

H. D. ANDROSENKO, S. B. ERMAGAMBETOV, G. N. SMIRENKIN, D. L. SHPAK and I. KOVÁCS

Abstract

The authors report on measurements of the angular distribution of fragments produced in the neutron-induced fission of ^{232}Th, ^{238}U, ^{237}Np, ^{238}Pu, ^{240}Pu, ^{242}Pu and ^{241}Am target nuclei. Particular attention is paid to excitation energies near the threshold. The experimental data do not fit the traditional picture of fission probability, but can be satisfactorily explained in terms of double-humped barrier concepts. In discussing the results of the measurements, the authors touch on the quasi-stationary states of the nucleus in the second valley, the structure of barriers, even — odd differences in fission probability, and the question of the penetration probability at certain energies in the case of highly deformed nuclei.

Acta Physica Academiae Scientiarum Hungaricae, Tomus 29 (4), pp. 359—364 (1970)

CALCULATION OF ELECTRON SCATTERING ON THE BASIS OF THE STATISTICAL ATOM MODEL IN WHICH THE ELECTRONS ARE GROUPED ACCORDING TO THE PRINCIPAL QUANTUM NUMBER

By

A. DOBAY-SZEGLETH

PHYSICAL INSTITUTE OF THE UNIVERSITY FOR TECHNICAL SCIENCES, BUDAPEST

(Received 2. XII. 1969)

The paper is concerned with atomic form factor calculations based on the statistical atom model in which the electrons are grouped according to the principal quantum number and considers the role of the various shells in scattering.

To our present knowledge the most important method used for the calculation of the internal structure of atoms is the Hartree-Fock self-consistent field method. However, to carry out such a calculation, even if an electronic computer is used, requires much effort and is very time-consuming. Therefore it is of very great importance that GOMBÁS suggested a simplified self-consistent field method the accuracy of which is almost identical with that of Hatree-Fock calculations, while at the same time the calculations are much simpler. This method will be briefly described below.

The electrons of the atom are grouped into shells corresponding to the principal quantum numbers, i.e. K, L, M, . . . shells characterized by the principal quantum numbers $n = 1, 2, 3, \ldots$, respectively. The wave functions of the electrons of the n-th shell are taken to be identical and the radial part of the wave is denoted by $f_n(r)$. This wave function must, of course, satisfy the usual boundary conditions, so it must vanish for $r = 0$ and $r = \infty$ and it must be a normalized function.

$$\int_0^\infty f_n^2(r)\, dr = 1\,. \tag{1}$$

If there are N_n electrons in the n-th shell, the radial electron density of this shell is

$$D_n(r) = N_n f_n^2(r)\,. \tag{2}$$

Our aim is to build up the total energy of the atom as an expression of these wave functions $f_n(r)$. The energy of the electrons in the n-th shell includes the following terms:

$E_i^{(n)}$ is the radial kinetic self-energy, which is absolutely exact, $E_g^{(n)}$ is due to the non-classical interaction resulting from the Pauli exclusion prin-

ciple valid between the electrons of the n-th shell on the one hand, and the electrons below the n-th shell, on the other. This non-classical energy has been determined by GOMBÁS by the methods of the statistical atom model [1].

$E_{\varphi}^{(n)}$ is the azimuthal energy of the electrons of the n-th shell,

$E_{k}^{(n)}$ is the interaction energy of the electrons in the n-th shell and the atom,

$E_{e}^{(n)}$ is the total interaction energy of the electrons of the n-th shell.

The total energy of the atom is:

$$E[f_1, f_2, \ldots] = \sum_n (E_i^{(n)} + E_g^{(n)} + E_{\varphi}^{(n)} + E_k^n + E_e^{(n)}) . \tag{3}$$

The wave functions $f_n(r)$ are determined from the requirement that the total energy be minimal. In searching for the minimum the auxiliary condition (1) must naturally be taken into account.

A very simple method to find the wave functions is to use the Ritz method.

The wave function is assumed in the following form:

$$f_n^{(r)} = A_n r^{\varkappa_n} e^{-\lambda_n r}, \tag{4}$$

where A_n is a normalization constant, for which from (1) the expression

$$A_n = \sqrt{\frac{(2\lambda_n)^{2\varkappa_n+1}}{\Gamma(2\varkappa_n+1)}} \tag{5}$$

is obtained; $\varkappa_n$ and λ_n are variational parameters, calculated from the minimum condition of the total energy. The results for the Ar atom are given below.

n	$\varkappa_n$	λ_n
1	1.0	18.515
2	2.0	6.560
3	3.0	2.405

The total energy of the atom is found to be —527.00 atomic units, while the experimental value is —525.4. The agreement is excellent.

As is known for the treatment of the scattering of high energy electrons on atoms it is essentially the form factor

$$F(\varkappa) = 4\pi \int_0^{\infty} \frac{\sin(\varkappa r)}{\varkappa r} \varrho(r)\, r^2\, dr \tag{6}$$

that has to be calculated.

As

$$4\pi\varrho(r)r^2 = D(r) \tag{7}$$

the radial density is

$$F(\varkappa) = \int_0^\infty D(r)\frac{\sin(\varkappa r)}{\varkappa r}\,dr. \tag{8}$$

Knowing the radial density we have to calculate only the integral in (8). The calculations are based on the atom model described in the foregoing. In this atom model the electrons are grouped according to the principal quantum number, and so information can be obtained on the contribution of each electron shell to the construction of the form factor of the atom.

In this model the radial electron density is the sum of the contributions of the respective shells:

$$D(r) = \sum_n D_n(r). \tag{9}$$

The radial density of the n-th shell is obtained as the square of the radial wave function multiplied by the number N_n of the electrons in the shell

$$D_n(r) = N_n f_n^2(r). \tag{10}$$

Thus the form factor (10) becomes as follows:

$$F(\varkappa) = \sum_n N_n \int_0^\infty f_n^2(r)\frac{\sin \varkappa r}{\varkappa r}\,dr. \tag{11}$$

The integrals occurring here can be calculated for the wave functions $f_n(r)$ in an elementary way.

Introducing the notation

$$I_n = \int_0^\infty f_n^2(r)\frac{\sin \varkappa r}{\varkappa r}\,dr \tag{12}$$

we obtain

$$I_n = \frac{(2\lambda_n)^{2\varkappa_n+1}}{\varkappa(2\varkappa_n)!}(2\varkappa_n-1)!\,\frac{\sin[2\varkappa_n \arctan \varkappa/2\lambda_n]}{[(2\lambda_n)^2+\varkappa^2]^{\varkappa_n}}. \tag{13}$$

The form factor $F(\varkappa) = \sum_n N_n I_n$ has been calculated in particular for the Ar and Kr atoms. The Ar atom is built up of 3 electron shells, characterized by the principal quantum numbers $n = 1, 2, 3 \ldots$, respectively. The occupation numbers are $N_1 = 2$, $N_2 = 8$, $N_3 = 8$. The form factor of Ar is shown in Fig. 1,

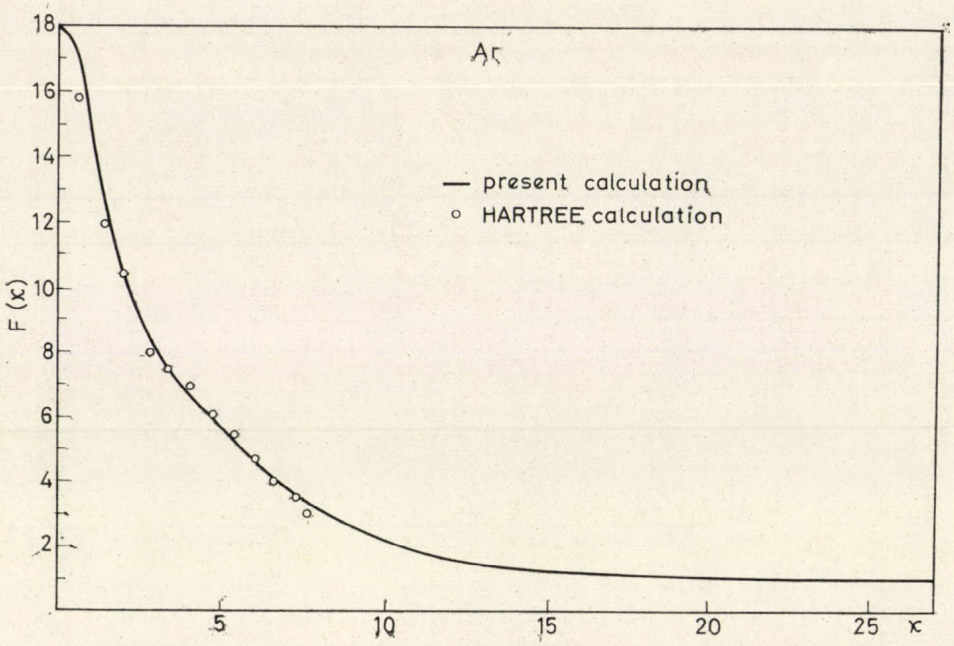


Fig. 1. Form factor of the Ar atom

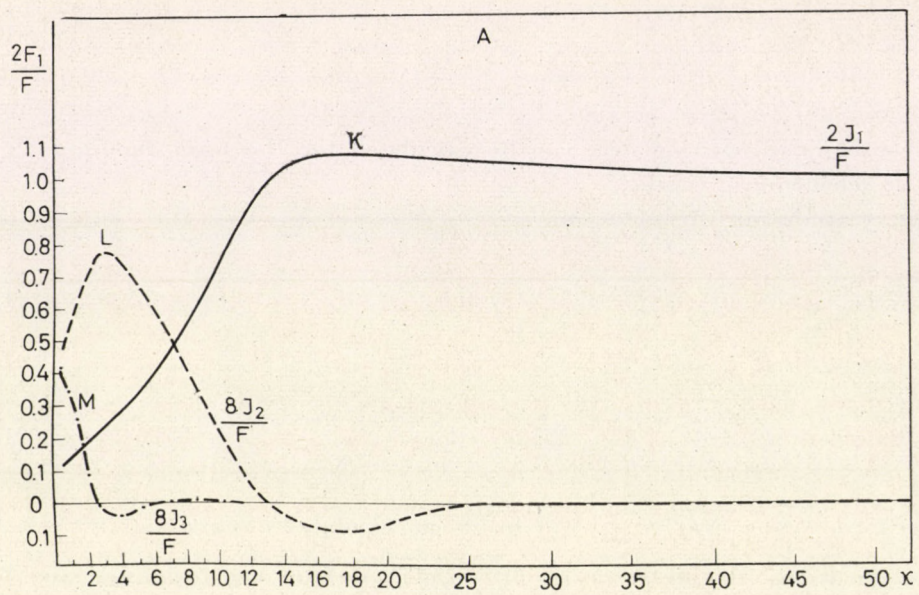


Fig. 2. Form factors of the individual shells as compared to the total form factor for the Ar atom

where $\varkappa$ is plotted on the abscissa in atomic units. For comparison the form factor obtained from the Hartree calculation is also shown [2].

It can be stated that the agreement is very excellent, both regarding the shape of the curve and the quantitative values. In Fig. 2 the form factors of the respective shells are shown as compared with the overall form factors. From the Figure it appears to what extent the respective electron shells con-

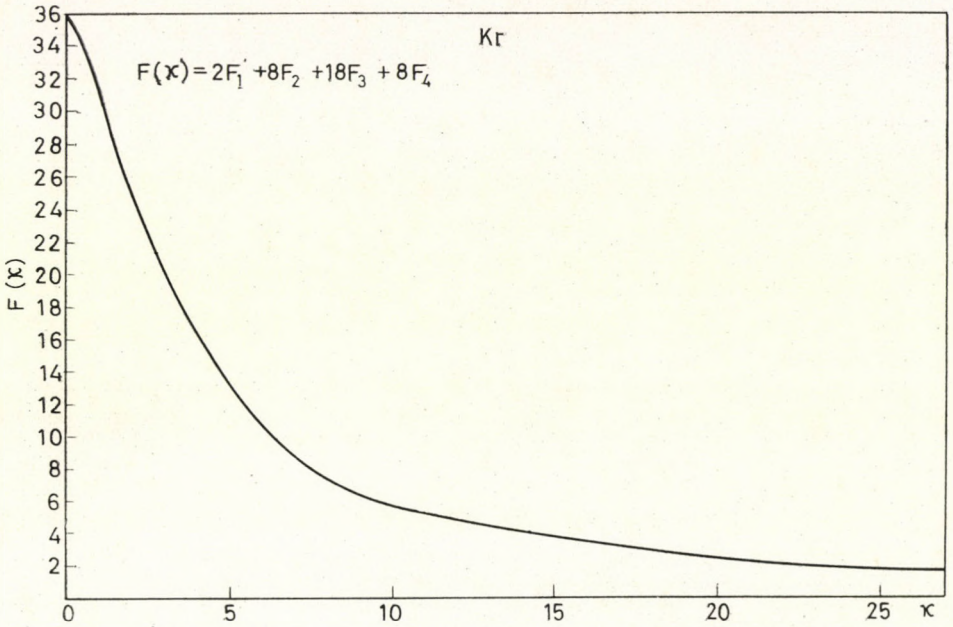


Fig. 3. Form factor of the Kr atom

tribute to the form factor of the atom. It can be seen that for very small $\varkappa$ the contribution of each electron shell is proportional to the number of electrons, i.e. the contribution of the K shell is 1/9th, and that of both the L and the M shell is 4/9th. With increasing $\varkappa$ ($\varkappa \approx 4/a_0$), the contribution of the central L shell is the most significant and, finally, for very large $\varkappa$ ($\varkappa \approx 25/a_0$) practically only the innermost K shell makes a contribution. As $\varkappa$ is proportional to the change of the angular momentum of the scattered electron, our results can be formulated in such a way that electrons scattered very strongly are scattered mainly on the innermost K shell, while the outer L and M shells are responsible for the scattering of electrons subject to smaller deviation.

Similar calculations have been carried out for the Kr atom. Here the number of electron shells is four ($n = 1, 2, 3, 4$). The occupation numbers are as follows: $N_1 = 2$, $N_2 = 8$, $N_3 = 8$, $N_4 = 8$. The results are shown in Figs. 3

and 4. Fig. 3 represents the total form factor, and Fig. 4 the relative contributions of the respective shells. It can be seen that for large x values, i.e. for strong scattering, it is mainly the innermost K shell which is decisive, and the weaker the scattering the more important is the role of the outer electron shells in the formation of scattering. The reason why we consider the above results

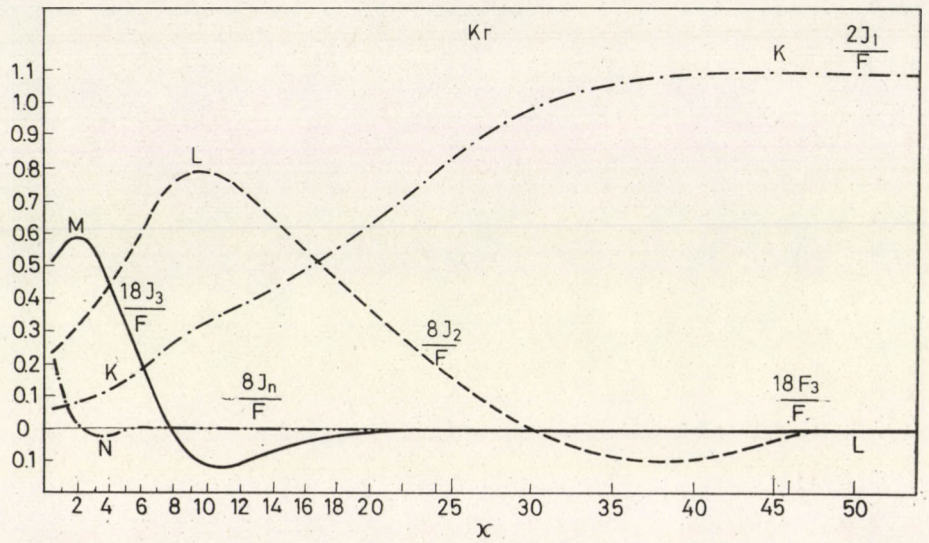


Fig. 4

very valuable is that, to our knowledge, the relative contributions of the respective electron shells have not yet been investigated in the literature.

The author is indebted to Prof. P. Gombás for valuable advice and help.

REFERENCES

1. P. Gombás, Pseudopotentiale, Chapter 16, Springer-Verlag, Wien — New York, 1967.
2. Landolt-Börnstein, Zahlenwerte und Funktionen, Band I, Teil 1.

РАСЧЕТ РАССЕЯНИЯ ЭЛЕКТРОНОВ ПО СТАТИСТИЧЕСКОЙ МОДЕЛИ АТОМА, В КОТОРОЙ ЭЛЕКТРОНЫ СГРУППИРОВАНЫ ПО ГЛАВНОМУ КВАНТОВОМУ ЧИСЛУ

А. ДОБАИ-СЕГЛЕТ

Р е з ю м е

Работа содержит вычисления формфактора атома, проводимые по статистической модели, в которой электроны сгруппированы по главному квантовому числу. Исследуется роль елотдьных оболочек в формировании картины рассеяния.

Acta Physica Academiae Scientiarum Hungaricae, Tomus 29 (4), pp. 365—371 (1970)

EXPERIMENTAL STUDY OF THE $^{24}Mg(d, p)^{25}Mg$ REACTION IN THE ENERGY RANGE 650—500 keV

By

L. MESKÓ, B. SCHLENK and A. VALEK

INSTITUTE OF NUCLEAR RESEARCH OF THE HUNGARIAN ACADEMY OF SCIENCES, DEBRECEN

(Received 22. XII. 1969)

Angular distributions and absolute cross-sections of the groups p_0, p_1, p_2, p_3 and p_4 from the reaction $^{24}Mg(d,p)^{25}Mg$ have been measured in the range $E_d = 650$—500 keV with a semiconductor detector on a natural Mg target. The angular distributions are asymmetrical about 90°, their shapes vary strongly with deuteron energy and the groups p_1 and p_2 have the largest cross-sections. The experimental data have been analysed in terms of Legendre polynomials.

Introduction

The $^{24}Mg(d,p)^{25}Mg$ reaction has been studied by several authors. The results of previous investigations at low deuteron energies ($E_d \leq 5$ MeV) may be summarized as follows:

In the range of energies between 0.7 and 1.7 MeV GROTDAL and NYBØ [1] found strong fluctuations in the excitation functions of groups p_0—p_4. The explanation of those results was given by NYBØ et al. [2] based on ERICSON's fluctuation theory, assuming some contribution from direct interactions.

From 1.2 to 2.5 MeV, OMAR et al. [3] measured the angular distributions and excitation functions of seven proton groups. The measured excitation functions showed some resonance-like behaviour. The shapes of the angular distributions varied considerably with the bombarding energy. The results were interpreted by interference between the compound and the direct interaction mechanism.

Over the range $E_d = 2$—4 MeV, LEE et al. [4] measured the angular distributions as well as the excitation functions of groups p_0—p_4 and attempted to determine the ratio of the direct reaction to the compound nuclear process.

Excitation functions for p_0—p_4 groups were measured by GALLMANN et al. [5] at three angles in the energy range 2.8—6.1 MeV and the results were analysed on the basis of ERICSON's fluctuation theory.

The aim of the present work was to extend the investigations carried out so far on the $^{24}Mg(d,p)^{25}Mg$ reaction towards lower bombarding energies well below the Coulomb barrier in order to gain experimental data for the reaction mechanism of certain proton groups. Accordingly, we have measured the

angular distributions and the absolute cross-sections of the groups p_0, p_1, p_2, p_3 and p_4 from the reaction $^{24}Mg(d,p)^{25}Mg$ in the energy range 650—500 keV. The experimental data have been analysed in terms of Legendre polynomials.

Experimental apparatus and method

Deuterons were accelerated by the cascade generator of ATOMKI, Institute of Nuclear Research, Debrecen, Hungary. The high voltage of the cascade generator was measured to 1% accuracy by a rotary-type voltmeter calibrated with (p, γ) resonances on ^7Li, ^{19}F and ^{27}Al. After passing through a 12° magnetic analyser and collimator system, the ion beam hit the target placed in the centre of the target chamber used for angular distribution measurements [6].

A thin layer of Mg with natural isotopic composition evaporated on a Cu foil of about 0.3 mg/cm^2 thickness was used as a target. The determination of target thickness was carried out by measuring the shift of the 340 keV resonance line of the reaction $^{19}F(p,\alpha\gamma)$. The Mg layer was evaporated from a point source, under suitable geometrical conditions simultaneously on Cu backings and Cu backings covered with a thin layer of CaF_2 (approx. 5 μg/cm^2). These targets were used to measure the shift of the 340 keV resonance line of the reaction $^{19}F(p,\alpha\gamma)$, due to the energy loss of protons in the Mg layer. From the value of the shift the number of target atoms could be determined by using data dE/dx from [7]. The thickness of the target varied from 35 to 45 keV.

The ion current was measured by a current integrator connected to the Faraday cup.

The angular distributions of the proton groups were measured with an ORTEC SBCJ-25-300 semiconductor detector which could be rotated from 0° to 155°. Another semiconductor detector of the same type, mounted in the target chamber at an angle of 90° was used as a monitor. A 3 mg/cm^2 Al foil placed in front of the detectors absorbed the scattered deuterons. After passing through charge-sensitive pre-amplifiers, main amplifiers and an electronic mixing unit, the pulses of the detectors were analysed with a NTA 512 pulse-height analyser. The application of the electronic mixing unit [8] permitted the simultaneous recording of the respective portions of the two independent detector spectra with the 512-channel analyser. This procedure ensured precise monitoring even in the course of the lengthy measurements required by the low cross-sections.

Fig. 1 shows a typical spectrum recorded at $E_d = 650$ keV and at $\Theta_{lab} = 105°$. The spectrum of the measuring detector is recorded in channels 170—512; that of the monitor detector in channels 0—140. The p_0, p_1 and p_2 groups

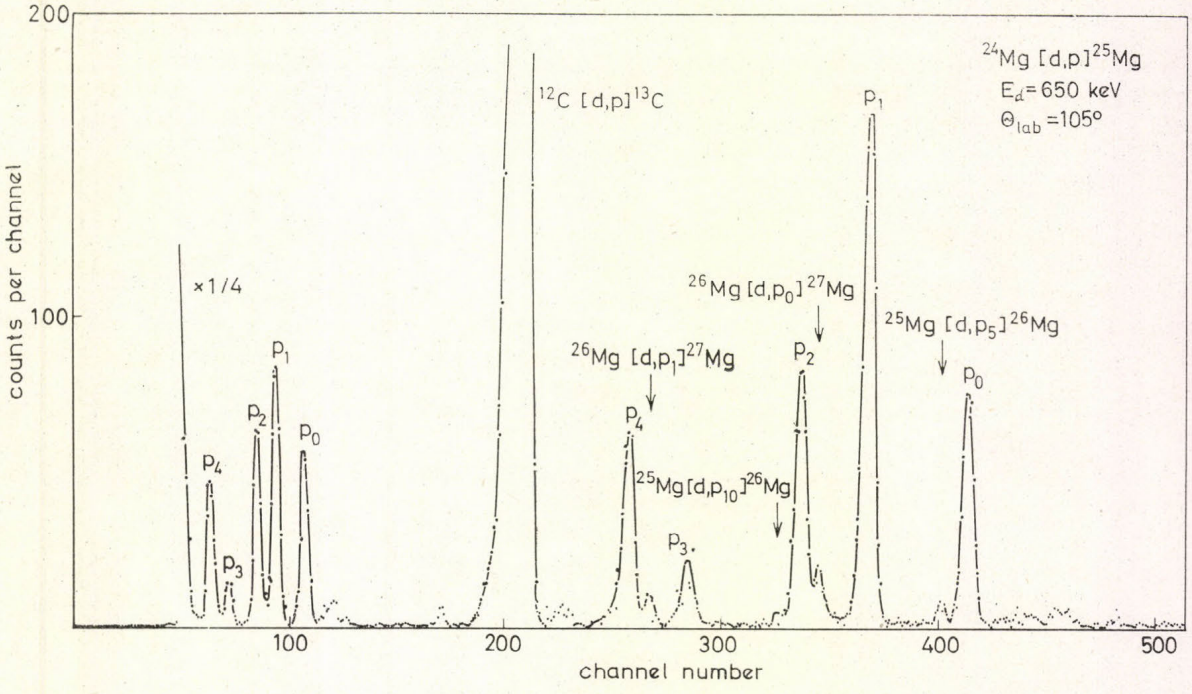


Fig. 1. A typical energy spectrum of protons from the reaction ^{24}Mg(d,p)^{25}Mg. The spectrum of the monitor detector is recorded in channels 0—140; that of the measuring detector in channels 170—512

of the monitor spectrum could easily be separated from the background and were used for monitoring purposes.

In the course of the measurements, first the relative angular distributions of the various proton groups were determined at a bombarding ion current intensity of 0.8—0.9 μA. Then, the absolute differential cross-sections of the proton groups were measured at an angle $\Theta_{lab} = 90°$ and the relative angular distributions were standardized to those values. During the run of the absolute measurements the bombarding ion current was reduced to 0.4 μA and the constancy of target thickness was checked.

Results and discussion

Figs. 2 and 3 show the results of angular distribution measurements in a centre-of-mass frame of reference at various bombarding energies. The errors indicated in connection with experimental angular distributions refer to the

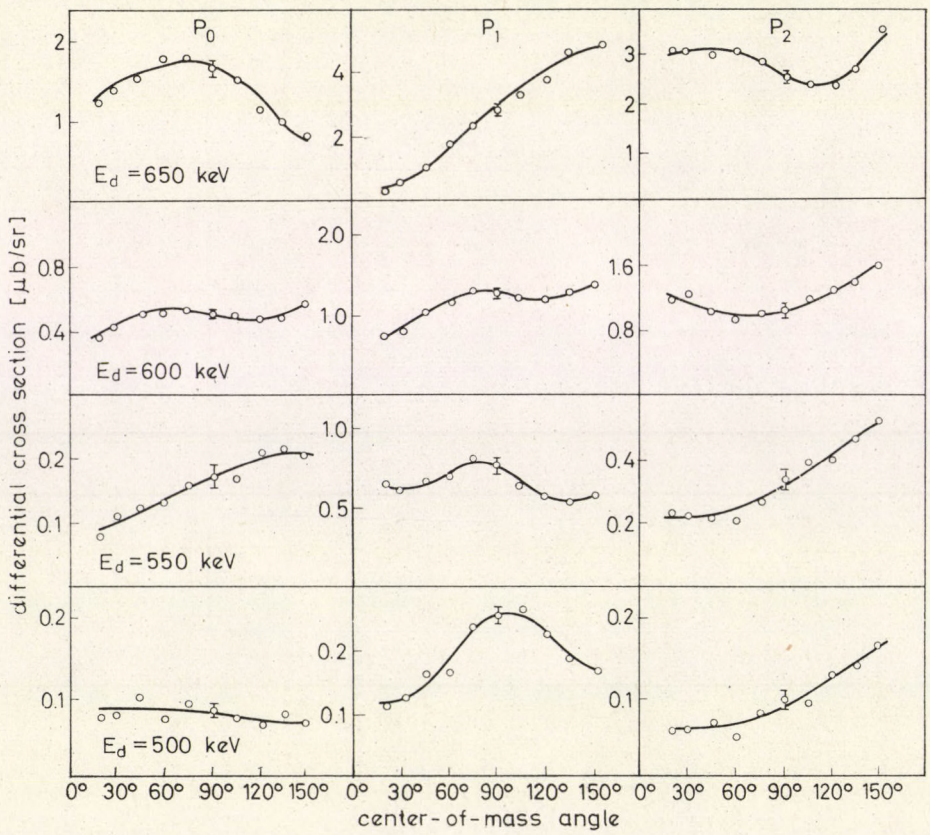


Fig. 2. Differential cross-sections of proton groups p_0, p_1 and p_2 from the reaction $^{24}Mg(d,p)^{25}Mg$

reproducibility errors of the measurements and evaluation. The errors of the absolute cross-section values mainly due to the inaccuracy of the target thickness determination are estimated in general to be about 35%. The lines in the Figures are the least-squares fits of the experimental points to the series of Legendre polynomials. The angular distributions were analysed up to P_l giving an acceptable χ^2. Table I contains the A_1/A_0, A_2/A_0 etc. coefficients with errors and the calculated χ^2 values.

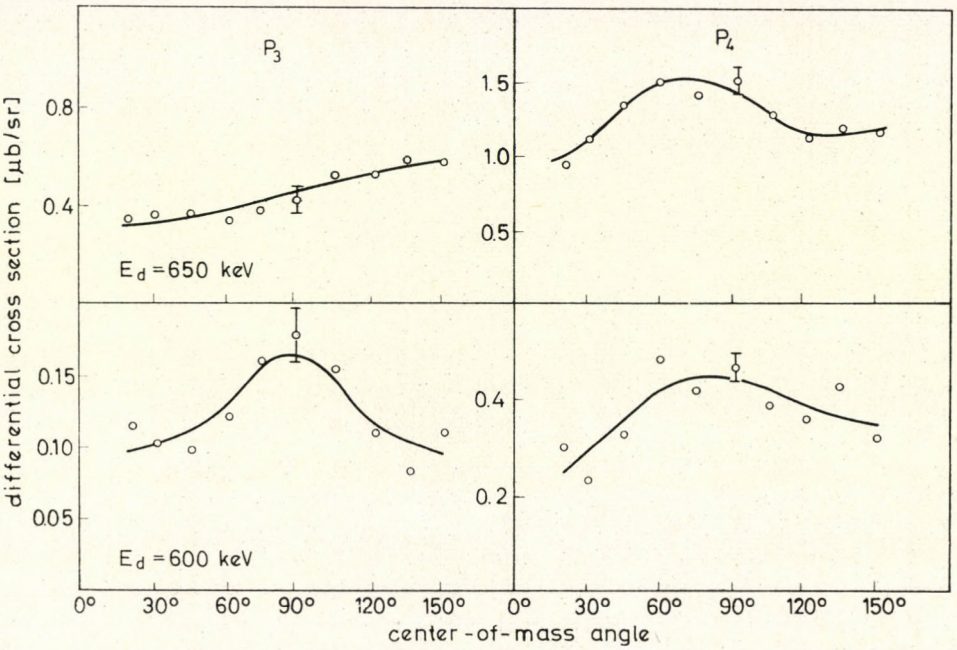


Fig. 3. Differential cross-sections of proton groups p_3 and p_4 from the reaction $^{24}Mg(d,p)^{25}Mg$

As can be seen from the results the angular distributions are asymmetrical about 90°, their shapes vary strongly with deuteron energy and the groups p_1 and p_2 have the largest cross-sections. All these features are in good agreement with the earlier results [1, 3, 4].

In the deuteron energy range studied here the excitation energy of the compound nucleus ^{26}Al is about 12.5 MeV. The ERICSON fluctuation analysis carried out at a little higher excitation energies [1, 4] has led to an average resonance width $\Gamma = 20$—50 keV but the average level spacings D should be smaller than that value. Accordingly, the condition $\Gamma \geq D$ for the existence of ERICSON fluctuations seems to be satisfied for the present energy range, too. Therefore, it may be assumed, in agreement with earlier results obtained at

Table I

Coefficients of the Legendre polynomials

$$\frac{d\sigma}{d\Omega} = \sum_{l=0}^{n} A_l P_l(\cos\Theta)$$

	E_d(keV)	A_1/A_0	A_2/A_0	A_3/A_0	A_4/A_0	χ^2
P_0	650	0.26±0.03	−0.38±0.04			2.14
	600	−0.08±0.02	−0.02±0.03	−0.21±0.03		0.42
	550	−0.38±0.04	−0.09±0.06			0.91
	500	0.10±0.06				0.89
P_1	650	−0.86±0.03	−0.04±0.04			4.74
	600	−0.19±0.02	−0.12±0.03	−0.20±0.04		1.28
	550	0.10±0.02	−0.16±0.03	−0.15±0.04	0.18±0.05	0.73
	500	−0.16±0.04	−0.45±0.06	0.09±0.07	0.11±0.09	1.41
P_2	650	0.03±0.02	0.21±0.03	−0.21±0.03		0.48
	600	−0.22±0.02	0.27±0.03			0.66
	550	−0.51±0.04	0.15±0.05			1.15
	500	−0.58±0.05	0.22±0.07			1.78
P_3	650	−0.31±0.04				0.78
	600	0.05±0.10	−0.38±0.13			4.09
P_4	650	0.04±0.02	−0.19±0.04	−0.21±0.05		0.74
	600	−0.04±0.07	−0.29±0.11	−0.11±0.13		5.81

higher bombarding energies, that the strong changes in the shape of the angular distributions with the bombarding energy predominantly originate from fluctuations of the ERICSON type. Nevertheless, some contribution of direct processes to the given reaction mechanism could not be excluded in the energy region considered here.

REFERENCES

1. T. GROTDAL and K. NYBØ, Physica Norvegica, **1**, 221, 1964.
2. K. NYBØ, T. GROTDAL and I. SINGSTAD, Physica Norvegica, **2**, 33, 1966.
3. H. M. OMAR, I. I. ZALOUBOVSKY, M. H. S. BAKR, R. ZAGHLOUL and V. J. GONTCHAR, Nucl. Phys., **56**, 97, 1964.
4. S. M. LEE, Y. HIRATATE, K. MIURA, S. KATO and S. MORITA, Nucl. Phys., **A122**, 97, 1968.
5. A. GALLMANN, P. WAGNER and P. E. HODGSON, Nucl. Phys., **88**, 675, 1966.
6. B. SCHLENK, I. PAPP and L. MESKÓ, Atomki Közl., **8**, 232, 1966.
7. C. F. WILLIAMSON, J. P. BOUJOT and J. PICARD, CEA-R3042, 1966.
8. B. SCHLENK and A. VALEK, Atomki Közl., **9**, 393, 1967.

ИССЛЕДОВАНИЕ ЯДЕРНОЙ РЕАКЦИИ $^{24}Mg(d, p)^{25}Mg$ В ОБЛАСТИ ЭНЕРГИИ 650—500 кэв

Л. МЕШКО, В. ШЛЕНК и А. ВАЛЕК

Р е з ю м е

С помощью полупроводниковых детекторов на металлической Mg мишени с естественным составом изотопов определены угловые распределения и эффективное поперечное сечение ядерной реакции $^{24}Mg(d, p)^{25}Mg$ в области энергии 650—500 Кэв. Измерения проводились в случае групп p_0, p_1 и p_2 при четырех, а в случае групп p_3 и p_4 — при двух различных значениях бомбардирующей энергии. Угловые распределения не симметричны относительно 90°, вид их очень сильно меняется с изменением бомбардирующей энергии, с наибольшим значением эффективного поперечного сечения обладают группы p_1 и p_3. Анализ экспериментальных угловых распределений производится с помощью полиномов Лежандра.

Acta Physica Academiae Scientiarum Hungaricae, Tomus 29 (4), pp. 373–378 (1970)

A GHOSTLESS LEE MODEL*

By

J. CUNNINGHAM

DEPARTMENT OF APPLIED MATHEMATICS, UNIVERSITY COLLEGE OF NORTH WALES, BANGOR, U. K.

(Received 31. III. 1970)

A static model in which a point nucleon may emit an infinite number of light relativistic bosons is constructed. By suitable choice of coupling constants the model may be made free from ghost states.

1. Introduction

The LEE model [1] is studied principally for the insight which it gives into the methods of relativistic field theory. Although, being a static model, it is merely pseudo relativistic it provides a solvable field theoretic framework in which to test the techniques which one proposes to use in sophisticated relativistic theories which do not admit exact solutions.

One of the main difficulties of LEE's model is the occurrence of states of negative norm, so-called ghost states [2, 3]. If one modifies LEE's model in such a way as to make it invariant under Galilean transformations a ghostless LEE model may be constructed [4] but, of course, in such a model one must surrender further features of relativistic theory such as mass non conservation. If one modifies LEE's model in such a way as to make it relativistically invariant one destroys its essential simplicity and enters the realm of non-local field theory [5]. In this paper the ghost problem is studied along the lines indicated by RUIJGROK and VAN-HOVE [6, 7, 8]. However, the device used by these authors, namely that after a specified number of boson emissions the static nucleon reverts to its original state, is not made in this paper: instead a sequence of coupling constants which tends monotonically to zero is defined in such a way that when the number of coupling constants becomes infinite ghost states are automatically forbidden even in the case of a point nucleon [9].

* An earlier version of this paper was presented by the author as a lecture at University of Wales Colloquium in Applied Mathematics, 1968, and has been reported by Md. Safar Ali in M. Sc. thesis, Wales, 1968, unpublished.

2. The model

Consider the Hamiltonian

$$H = H_0 + H_I + \delta H, \tag{1}$$

with

$$H_0 = m \sum_{n=1}^{\nu+1} \psi_n{}^* \psi_n + \sum_{k} \omega a^* a\,, \tag{2}$$

$$H_I = -\sum_{n=1}^{\nu} \sum_{\mathbf{k}} \frac{g_n F_\nu(\omega)}{\sqrt{(2\omega\Omega)}} \{\psi_n^* \psi_{n+1} a + \psi_{n+1}^* \psi_n a^*\}, \tag{3}$$

$$\delta H = -\sum_{n=1}^{\nu} \delta m_n \psi_n^* \psi_n\,, \tag{4}$$

$$\omega^2 = \mu^2 + \mathbf{k}^2, \tag{5}$$

where ψ_n^* and $a^* = a^*(\mathrm{k})$ are respectively creation operators for the nth state of the static nucleon whose physical mass (for every value of n) is m and for the boson of mass μ whose momentum is k; the quantity Ω is the volume of periodicity, the numbers g_n (real for Hermitian H) are coupling constants, the function $F_\nu(\omega)$ is a "cut-off", and δm_n denotes the usual mass renormalisation constant for the nth nucleon state.

The normalised state vector corresponding to the $(r + N)$th *bare* nucleon state containing N bosons of momenta $\mathrm{k}_1, \mathrm{k}_2, \ldots, \mathrm{k}_N$ is

$$\frac{1}{\sqrt{N!}} \Big| r, N> = \frac{1}{\sqrt{N!}} \psi_{r+N}^* a^*(\mathbf{k}_1)\, a^*(\mathbf{k}_2) \ldots a^*(\mathbf{k}_N) \Big| 0, 0>, \tag{6}$$

where $|0,0>$ denotes the vacuum state.

An unnormalised state vector corresponding to the physical rth nucleon state is

$$|\mathbf{r}> = |\,r, 0> + \sum_{N=1}^{\nu-r+1} \sum_{\mathbf{k}_1, \mathbf{k}_2, \ldots, \mathbf{k}_N} \Phi_r^N(\mathbf{k}_1, \mathbf{k}_2, \ldots, \mathbf{k}_N) |r, N>. \tag{7}$$

If

$$H|\mathbf{r}> = (m + \omega_r)|\mathbf{r}>, \tag{8}$$

then

$$\omega_r + \delta m_r = \frac{-g_r}{\sqrt{(2\Omega)}} \sum_{\mathbf{k}} \omega^{-1/2} F_\nu(\omega)\, \Phi_r^1(\mathbf{k}) \tag{9}$$

and

$$\Phi_r^N(\mathbf{k}_1, \mathbf{k}_2, \ldots, \mathbf{k}_N) = \frac{-1}{\sqrt{(2\Omega)^N}} \frac{1}{N!} \prod_{i=1}^{N} \omega^{-1/2} (\omega_i - \omega_r)^{-1} F_\nu(\omega_i)\, g_{r+i-1} \tag{10}$$

for $N \geq 1$. Thus

$$\omega_r + \delta m_r = \frac{-g_r^2}{2\Omega} \sum_{\mathbf{k}} \omega^{-1}(\omega - \omega_r)^{-1} F_\nu^2(\omega) . \tag{11}$$

Now the mass renormalisation constant δm_r is determined by the condition that $\omega_r = 0$ satisfies the eigenvalue equation (8). Therefore

$$\delta m_r = \frac{-g_r^2}{2\Omega} \sum_{k} \omega^{-2} F_\nu^2(\omega) . \tag{12}$$

The renormalisation constant $Z_2(r)$ is determined by normalising the physical rth nucleon state $|\mathbf{r}\rangle$ $(\omega_r = 0)$

$$Z_2^{-1}(r) = 1 + \frac{1}{2\Omega} \sum_{N=1}^{\nu-r+1} \frac{1}{N!} \sum_{\mathbf{k}_1, \mathbf{k}_2, \ldots, \mathbf{k}_N} \prod_{i=1}^{N} \omega_i^{-3} F_\nu^2(\omega_i) g_{r+i-1}^2 \tag{13}$$

$$= 1 + \sum_{N=1}^{\nu-r+1} \frac{1}{N!} (g_r g_{r+1} \ldots g_{r+N-1})^2 L_\nu^N , \tag{14}$$

where

$$L_\nu = \frac{1}{2\Omega} \sum_{k} \omega^{-3} F_\nu^2(\omega), \tag{15}$$

which diverges logarithmically in the case $F_\nu(\omega) = 1$.

3. Ghosts

Let us now inquire whether there exist solutions $\omega_r \neq 0$ of the eigenvalue equation (8). Such states, if they exist, we shall call ghost states [2]. We may manipulate equation (11) using equation (12) to obtain

$$\omega_r \left\{ 1 + \frac{g_r^2}{2\Omega} \sum_{k} \frac{F_\nu^2(\omega)}{\omega^2(\omega - \omega_r)} \right\} = 0 . \tag{16}$$

If now we consider a model in which the unrenormalised coupling constants are related by a formula

$$g_r^2 = \lambda_{r,\nu} g_\nu^2, \quad 1 \leq r \leq \nu, \tag{17}$$

where $g_r \geq g_{r+2}$, $r = 1, 2, \ldots, \nu - 1$, and $\lambda_{\nu,\nu} = 1$, then we may rewrite Eq. (18) as

$$\omega_r \left\{ 1 + \frac{g_\nu^2 \lambda_{r,\nu}}{2\Omega} \sum_{k} \frac{F_\nu^2(\omega)}{\omega^2(\omega - \omega_r)} \right\} = 0 . \tag{18}$$

The renormalised coupling constants G_r are given by the formulae

$$G_r = Z_2^{1/2}(r) Z_2^{-1/2}(r+1) g_r, \quad 1 \leq r < \nu \tag{19}$$

$$G_\nu = Z_2^{1/2}(\nu) g_\nu \tag{20}$$

and satisfy

$$G_r^2 = \lambda_{r,\nu} \left\{ \frac{Z_2(r)}{Z_2(r+1)\, Z_2(\nu)} \right\} G_\nu^2, \quad 1 \leq r < \nu. \tag{21}$$

Thus Eq. (18) becomes

$$\omega_r \left\{ 1 + \frac{G_\nu^2 \lambda_{r,\nu}}{2\,\Omega Z_2(\nu)} \sum_{\mathbf{k}} \frac{F_\nu^2(\omega)}{\omega^2(\omega - \omega_r)} \right\} = 0 . \tag{22}$$

But

$$Z_2^{-1}(r) = 1 + \sum_{N=1}^{\nu-r+1} \frac{1}{N!} (g_\nu^2 L_\nu)^N \lambda_{r,r} \lambda_{r+1,\nu} \ldots, \lambda_{r+N-1,\nu}$$

and (23)

$$Z_2^{-1}(\nu) = 1 + g_\nu^2 L_\nu$$

$$= 1 + Z_2^{-1}(\nu) G_\nu^2 L_\nu, \tag{24}$$

so that

$$Z_2(\nu) = 1 - G_\nu^2 L_\nu. \tag{25}$$

The roots $\omega_r \neq 0$ satisfying equation (8) are therefore given by

$$H(\omega_r) = 0, \tag{26}$$

where

$$H(\omega_r) = Z_2(\nu) + \frac{G_\nu^2 \lambda_{r,\nu}}{2\Omega} \sum_{\mathbf{k}} \frac{F_\nu^2(\omega)}{\omega^2(\omega - \omega_r)} . \tag{27}$$

Now

$$H'(\omega_r) = \frac{G_\nu^2 \lambda_{r,\nu}}{2\Omega} \sum_{\mathbf{k}} \frac{F_\nu^2(\omega)}{\omega^2(\omega - \omega_r)^2} \tag{28}$$

$$> 0$$

and

$$H(-\infty) = Z_2(\nu). \tag{29}$$

Thus below the threshold $\omega_r < \mu$ there can be no second root of Eq. (8) unless $Z_2(\nu) \leq 0$.

Now in the case of LEE's model $\nu = 1$ and it is clear that in the point nucleon case ($F_\nu(\omega) = 1$) $Z_2(\nu) = -\infty$; only by choosing $F_\nu(\omega)$ such that $F_\nu(\omega) \to 0$ as $\omega \to \infty$ sufficiently rapidly to prevent the divergence of L_ν can the ghost problem be avoided.

However, in our case, it is hoped that, by choosing $\lambda_{r,\nu}$ suitably, $G_\nu^{-2} \to \infty$ sufficiently rapidly with ν that $Z_2(\nu) > 0$ for sufficiently large ν. We shall suppose that, in our model, as $\nu \to \infty$, $F_\nu(\omega) \to 1$, i.e., that we are dealing in the case $\nu = \infty$ with point nucleons.

4. Exorcision

If the condition $Z_2(\nu) > 0$ for the exclusion of ghost states is to be satisfied for sufficiently large values of ν it follows from equation (25) that, asymptotically for large ν,

$$G_\nu^{-2} \sim \lambda_\nu^{-1} L_\nu, \tag{30}$$

where

$$\lambda_\nu = 0(1), \tag{31}*$$

with

$$\lim_{\nu \to \infty} \lambda_\nu = \lambda, \quad 0 \leq \lambda < 1. \tag{32}$$

Then, for sufficiently large values of ν, say $\nu \geq \nu_0$, it follows that

$$1 \geq Z_2(\nu) > 0 \tag{33}$$

and

$$Z_2(\infty) = 1 - \lambda, \quad 0 \leq \lambda < 1. \tag{34}$$

Now the behaviour of G_ν^{-2} is fixed by our choice $\lambda_{r,\nu}$ through, say, Eq. (21): if, asymptotically, for large ν, $G_\nu^{-2} \sim \lambda_\nu^{-1} L_\nu$ then it follows from Eq. (21) that

$$\lambda_\nu \sim \frac{G_r^2 L_\nu}{G_r^2 L_\nu + \lambda_{r,\nu} Z_2(r)/Z_2(r+1)}, \tag{35}$$

so that whether or not criterion (31) is satisfied depends critically on the behaviour of the ratio $Z_2(r)/Z_2(r+1)$. It follows from Eq. (23) that

$$\begin{aligned} Z_2^{-1}(r) \geq 1 + \sum_{N=1}^{\nu-r} \frac{1}{N!} (g_\nu^2 L_\nu)^N \lambda_{r+1,\nu} \lambda_{r+2,\nu} \ldots \lambda_{r+N,\nu} + \\ + \frac{1}{(\nu-r+1)!} (g_\nu^2 L_\nu)^{\nu-r+1} \lambda_{r,\nu} \lambda_{r+1,\nu} \ldots \lambda_{\nu,\nu} > \\ > Z_2^{-1}(r+1), \end{aligned} \tag{36}$$

since $\lambda_{r,\nu} \geq \lambda_{r+1,\nu}$ for all r. Thus it is evident that

$$0 \leq \frac{Z_2(r)}{Z_2(r+1)} \leq 1 \tag{37}$$

* The symbol $0(x)$ denotes a term of order x at most.

equality being possible only for infinite ν. Thus it is necessary that

$$\frac{\lambda_{r,\nu} Z_2(r)}{Z_2(r+1)} \to \infty \tag{38}$$

as $\nu \to \infty$ at least as rapidly as L_ν in order that criterion (31) be satisfied.

Then a sufficient condition to ensure the absence of ghost states is that

$$\lim_{\nu\to\infty} \left\{ \frac{Z_2(r)}{Z_2(r+1)} \right\} > 0 , \quad \lambda_{r,\nu}^{-1} = 0(L_\nu^{-1}) . \tag{39}$$

It is clearly possible to choose suitable $\lambda_{r,\nu}$. For example if

$$\lambda_{r,\nu} = \nu - r + 1, \tag{40}$$

then

$$\frac{Z_2(r)}{Z_2(r+1)} \sim 1 - \frac{G_r^2 L_\nu}{\nu - r + 1} . \tag{41}$$

REFERENCES

1. T. D. Lee, Phys. Rev., **95**, 1929, 1954.
2. G. Kallen and W. Pauli, Dan. Mat. Pys. Medd., **30**, No. 7, 1955.
3. W. Heisenberg, Nucl. Phys., **4**, 532, 1957.
4. J. M. Levy-Leblond, Commun. Math. Phys., **4**, 145, 1967.
5. G. Wataghin, Nuovo Cimento, **9**, 519, 1959.
6. T. W. Ruijgrok and L. Van-Hove, Physica, **22**, 880, 1956.
7. T. W. Ruijgrok, Physica, **24**, 185, 205, 1958 and **25**, 357, 1959.
8. L. Van-Hove, Physica, **25**, 369, 1959.
9. This possibility was suggested to the author by D. B. Fairlie in a conversation about 1960

МОДЕЛЬ ЛИ БЕЗ ПРИЗРАЧНЫХ СОСТОЯНИЙ

ДЖ. КАНИНГЭМ

Р е з ю м е

Разработана статистическая модель, в которой точечный нуклон способен излучать бесконечное число легких релятивистских бозонов. Соответсвующим выбором констант связи модель станет свободней от призрачных состояний.

Acta Physica Academiae Scientiarum Hungaricae, Tomus 29 (4), pp. 379—381 (1970)

A DIFFERENTIAL APPROACH TO HIGH ENERGY BEHAVIOUR OF FEYNMAN AMPLITUDES

By

J. CUNNINGHAM

DEPARTMENT OF APPLIED MATHEMATICS, UNIVERSITY COLLEGE OF NORTH WALES, BANGOR, U. K.

(Received 31. III. 1970)

Asymptotic behaviour for the 'box' scattering diagram is determined using partial differential equations for the amplitude rather than the usual integral representations.

1. Introduction

The asymptotic behaviour of the box diagram amplitude has previously been evaluated by several different methods, the 'k-space' method, the 'd-line' method, the 'Mellin transform' method (see, e.g., EDEN et al. [1], which is a definitive account of the analytic properties of collision amplitudes, and RISK [2] which reviews in great detail the perturbative approach to high energy behaviour). All these methods are based directly on integral representations for the amplitude and the Mellin transform technique has been used successfully to study infinite sums of perturbative amplitudes.

Starting from the Feynman parameter representation for perturbative amplitudes DE ALFARO et al. [3] have derived sets of coupled partial differential equations for the amplitudes. In particular GIFFON [4] has set up the relevant equations for the box diagram and used them to locate Landau singularities and discuss absorbtive parts. In this paper we shall simply point out that the asymptotic behaviour of this amplitude may also be deduced.

2. Equations

The box diagram amplitude $F(s,t)$ satisfies the differential equations

$$\frac{\partial}{\partial t}(\Delta F) = -\Delta^{-1} \sum_{\substack{m,p=1 \\ m \neq p}}^{4} \frac{\binom{m}{3}\binom{mp}{m1}}{\binom{m}{m}} Fmp, \tag{1}$$

$$\frac{\partial}{\partial s}(\Delta F) = -\Delta^{-1} \sum_{\substack{m,p=1 \\ m \neq p}}^{4} \frac{\binom{m}{4}\binom{mp}{m2}}{\binom{m}{m}} Fmp\,, \tag{2}$$

where, for the case of equal mass particles,

$$\Delta^2(s,t) = \begin{vmatrix} 0 & 1 & 1 & 1 & 1 & 1 \\ 1 & 0 & m^2 & t & m^2 & m^2 \\ 1 & m^2 & 0 & m^2 & s & m^2 \\ 1 & t & m^2 & 0 & m^2 & m^2 \\ 1 & m^2 & s & m^2 & 0 & m^2 \\ 1 & m^2 & m^2 & m^2 & m^2 & 0 \end{vmatrix} \tag{3}$$

and

$$\begin{pmatrix} \alpha_i & \ldots\ldots & \alpha_m \\ \beta_i & \ldots\ldots & \beta_m \end{pmatrix} \tag{4}$$

is the usual signed minor of Δ^2 obtained by the indicated row and column deletions; the quantities F_{ij} are symmetric with respect to the sufficies and F_{12}, F_{14}, F_{23}, F_{34} are constants while F_{13} and F_{24} are respectively functions of s and t only. Equations for the F_{ij} for general mass values have been written down by EVANS [5] following the method of [4]; the equation for F_{13} in our case is

$$\frac{\partial}{\partial s}\left[\left\{\sqrt{(s^2 - 4m^2 s)}\right\} F_{13}\right] \alpha \frac{\partial}{\partial s}\left[\log\left\{\frac{2m^2 - s + \sqrt{(s^2 - 4m^2 s)}}{2m^2 - s - \sqrt{(s^2 - 4m^2 s)}}\right\}\right]. \tag{5}$$

3. High energy behaviour

Asymptotically as $s \sim \infty$ it follows from Eq. (5) that

$$F_{13} \underset{s\sim\infty}{\sim} \frac{\log s}{s}\,. \tag{6}$$

It now follows from Eq. (1) that

$$\frac{\partial}{\partial t}(\Delta F) \underset{s\sim\infty}{\sim} \Delta^{-1} s \log s \tag{7}$$

all other terms in the sum diverging like s. The t-dependence of Eq. (7) is given explicitly by Eq. (3)

$$\Delta^2 \underset{s\sim\infty}{\sim} s^2 t(t - 4m^2). \tag{8}$$

Thus the asymptotic behaviour of F is given by

$$\{s\sqrt{t^2-4m^2t}\}\, F \underset{s\sim\infty}{\sim} \log s \int \frac{dt}{\sqrt{(t^2-4m^2t)}} \tag{9}$$

provided that the function $g(s)$ introduced by the partial integration of Eq. (7) is constrained by Eq. (2) to diverge no more rapidly than $\log s$ as $s \to \infty$. In Eq. (2) as $s \to \infty$ the non vanishing terms in the sum tend to a definite function $G(t)$ and

$$\frac{\partial}{\partial s}(\Delta F) \underset{s\sim\infty}{\sim} \Delta^{-1} G(t)\,, \tag{10}$$

which implies that $g'(s)$ vanishes at least as rapidly as s^{-1}. Thus the result is

$$F \underset{s\sim\infty}{\sim} \left\{\frac{1}{\sqrt{(4m^2t-t^2)}} \tan^{-1}\sqrt{\left(\frac{t}{4m^2-t}\right)}\right\} \frac{\log s}{s}\,, \tag{11}$$

which agrees with previous derivations. To find the next term in the asymptotic expansion a function of t arising from the partial integration of Eq. (5) must be retained and this leads to the addition to Eq. (11) of a term $0(s^{-1})$.

4. Conclusion

While the above example is manifestly elementary and leads only to known results its approach is quite different from those based directly on integral representations. Quite clearly whenever the differential equations of DE ALFARO et al. [3] can be written down the exhibition of asymptotic behaviour s likely to be fairly straightforward.

REFERENCES

1. R. J. EDEN, P. V. LANDSHOFF, D. I. OLIVE and J. C. POLKINGHORNE, The analytic S-matrix, Cambridge, 1966.
2. C. RISK, High energy behaviour of Feynman diagrams. Lectures at Michigan, 1969.
3. V. DE ALFARO, B. JACKSIC and T. REGGE, Differential properties of Feynman amplitudes. Lectures at Trieste, 1965.
4. M. GIFFON, Nuovo Cimento, **61A**, 663, 1969.
5. M. A. EVANS, M. Sc. Thesis, Wales, 1969.

ДИФФЕРЕНЦИАЛЬНОЕ ПРИБЛИЖЕНИЕ ПОВЕДЕНИЯ АМПЛИТУД ФЕЙНМАНА В ОБЛАСТИ ВЫСОКИХ ЭНЕРГИЙ

ДЖ. КАНИНГЭМ

Р е з ю м е

Определяется асимптотическое поведение диаграммы рассеяния типа «ящик», используя при этом вместо обычного интегрального представления амплитуды дифференциальные уравнения в частных производных.

Acta Physica Academiae Scientiarum Hungaricae, Tomus 29 (4), pp. 383—390 (1970)

ON THE APPARENT DEVIATION FROM OHM'S LAW IN GaP

By

K. SOMOGYI

RESEARCH INSTITUTE FOR TECHNICAL PHYSICS OF THE HUNGARIAN ACADEMY OF SCIENCES, BUDAPEST

(Received 14. IV. 1970)

Deviation from Ohm's Law was observed during the investigations of galvanomagnetic effects in GaP single crystals at the temperature range of 50—150 °K [9, 10]. An assumption was made that the increase of conductivity and decrease of Hall coefficient as a function of applied electric field may be caused by temperature rise and carrier increase due to impact ionization [9]. On the basis of pulse measurements (and other experimental data) a different assumption is given: the sample is overheated above the ambient temperature by Joule heat arising even with a relatively low sample current. It has been shown that the sample holder must have a significant role in the origin of the apparent deviation from Ohm's law.

GaP is one of the most frequently investigated compounds among the $A^{III}B^{V}$ semiconductors. Several papers have dealt with the electrical properties of the doped *n*- and *p*-type ([1—5] [6—8]) and undoped [9] GaP recently. Their results were in agreement with one another.

For the first time MIYAUCHI, SONOMURA and YAMAMOTO observed the deviation from Ohm's law [9]. It was observed that at low temperature when increasing the voltage applied on the sample, above a critical field strength, the Hall-coefficient began to decrease, whereas the specific conductivity increased. They interpreted this phenomenon as a result of the increase in charge carrier concentration owing to the impact ionization [9, 10]. They, however, did not go into the detailed analysis of this phenomenon in their work. In the present work we intend to give another explanation of this phenomenon. Preliminary results of these investigations have been published in [11].

Experimental

The GaP single crystals used in our experiments were grown by the solid-solution method in a closed system at 1040 °C [12]. The Ga and P used to grow the crystals were of 5N purity. Crystals of different types were obtained by Zn (*p*-type) and Te (*n*-type) doping. Rectangular samples with average dimensions of $4 \times 1.5 \times 0.1$ mm^3 were cut out from the polished crystals. Six ohmic contacts were alloyed to the sides of the samples for classical resistivity and Hall measurements. The current and potential leads were made of 60 μm gold wire. Contact dimensions were of 0.2×0.1 mm^2. According to our con-

ductivity and Hall measurements the concentration of the impurities in the investigated samples was between 5×10^{17} and 3×10^{18} cm^{-3}, whereas the compensation degree was 5—20%.

The measurements were carried out with the conventional d.c. compensation method. Some measurements were performed with the pulse method, and the voltages were measured with an oscilloscope. A sample holder similar to that described by URE [13, 14] was used during the measurements between 85 and 400 °K temperatures. To perform the measurements at 77 °K the samples were directly submerged in liquid nitrogen. The construction of the sample holder plays a considerable role in the interpretation of the deviation from Ohm's law. In the holder described above the sample was in the interior of a copper block surrounded by nitrogen vapour. Thus, the sample placed in the ambient gas is not in direct contact with the good heat-conducting copper holder and heat exchange cannot take place except through the nitrogen vapour (but for the electrical leads). The temperature in the sample holder was measured with a chromel-alumel thermocouple, whose sensing junction lies in the same ambient gas, and is electrically insulated from the sample.

Results and discussion

Figs. 1 and 2 show the change of the conductivity as a function of the electric field strength and current, respectively, at several temperatures, from d.c. measurements.

The critical field strength generally lies about 10 Vcm^{-1} (it is even below 100 Vcm^{-1} in paper [9]) which is supposedly not enough for the occurrence of impact ionization. The supposition of the presence of impact ionization is not in contradiction with the experimental fact that with increasing temperature the critical field strength decreases. However, it does not explain why this phenomenon disappears approaching room temperature, where not all the impurities are yet ionized.

It also remains unexplained why the sample submerged in liquid nitrogen behaves differently. In this case the avalanche-like increase of the conductivity does not occur in spite of the fact that the field strength achieved is higher by an order of magnitude (see Fig. 1, curve 5 and Fig. 2, curve 5). The supposition of impact ionization is in contradiction with the results of the pulse measurements, too, as will be shown later (Fig. 5).

Here we propose an alternative explanation for the non-linearity of the curves $\sigma(E)$, $\sigma(I)$ and $I(U)$ (deviation from Ohm's law) measured on GaP at low temperatures taking into account the overheating of the sample compared with the ambient temperature. Thin samples of small volume might change their temperature in ambient gas by dissipating relatively little Joule heat.

Owing to the small cross-section and the comparatively low conductivity (the concentration and mobility of the charge carriers are low [1—9]) relatively low currents are sufficient for a considerable temperature increase (Fig. 2). At the same time, however, the thermocouple of great volume, in poor thermal contact with the sample, does not show the overheating of the sample at all

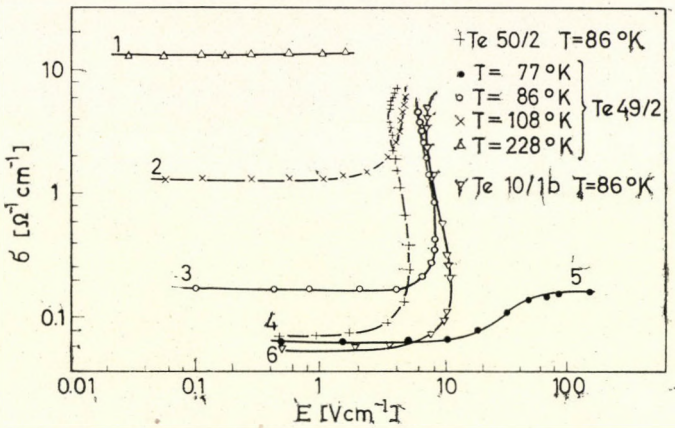


Fig. 1. Conductivity vs electric field on several samples at several ranges of temperature

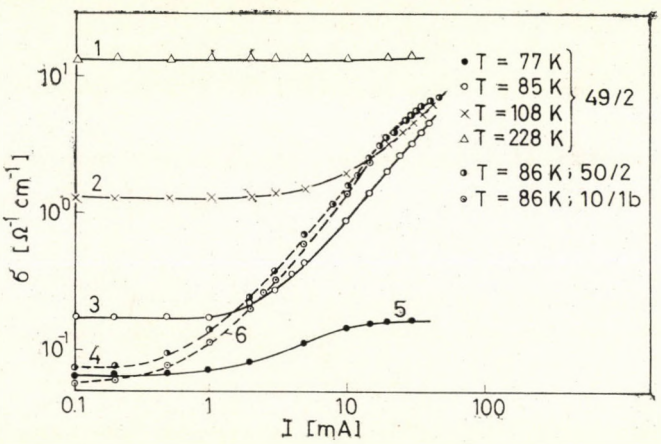


Fig. 2. Conductivity vs sample current

or only slightly. Owing to the great heat capacity of the copper block the change of the ambient temperature is insignificant. Thus, the data measured on the sample belong to some higher temperature than the temperature registered by the thermocouple due to the overheating of the sample.

In the temperature range of 50—150 °K the concentration of the charge carriers and conductivity strongly depend upon the temperature [1], [3—9]. Consequently, the overheating of the sample considerably changes the measured

data. If we chose a high current during the galvanomagnetic measurements, in such a current range where this apparent deviation from Ohm's law exists, the slope of the curves $\sigma(T^{-1})$ and $R(T^{-1})$ would be different, and the ionization energy of the impurities calculated from these curves might be smaller than it really is.

The supposition of local overheating is in good agreement with the experimental results:

1. If the sample is submerged in liquid nitrogen, the heat transfer is far better, and consequently the overheating of the sample is considerably

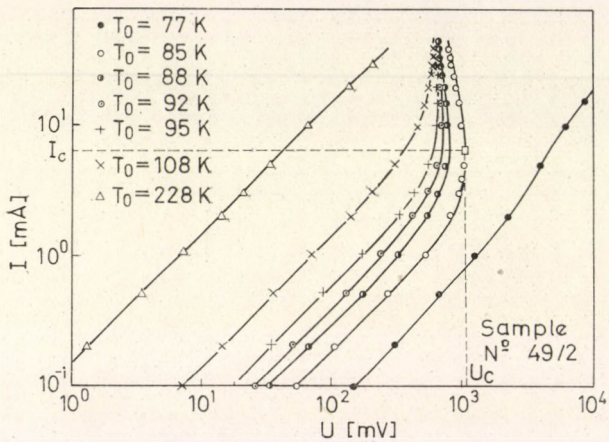


Fig. 3. I—V characteristics for the sample N° 49|2 at several temperatures

lower. In this case the avalanche-like increase of conductivity does not take place (Fig. 1, curve 5, Fig. 2, curve 5).

2. On the curves measured in samples submerged in liquid nitrogen only a small increase followed by saturation could be observed. This is due to the following: increasing the heat dissipation the liquid nitrogen begins to boil vigorously at the surface of the sample. The bubbles, however, decrease the heat transfer and only slight overheating can occur. However, the decrease of the heat transfer is limited. Thus the $\sigma(E)$ and $\sigma(I)$ curves become saturated and do not change any more. (In the case of sample 49|2 the overheating going with the saturation is about 5 K).

3. Fig. 3 shows voltage-current characteristics related to a typical sample at different temperatures. The negative characteristics figuring on one part of the curves $\sigma(E)$ in Fig. 1 and $I(U)$ in Fig. 3 can also be explained by the overheating of the sample. It is a well-known phenomenon in thermistors [15].

In [16] the stationary thermal break-down in semiconductors was investigated based on the calculations of O'DWYER [17] with the assumption of

the validity of Newton's cooling law [18]. From the formulae obtained we make use of the following [16]:

$$\frac{\sigma}{\left(\frac{d\sigma}{dT}\right)_c} = T_c - T_0 , \tag{1}$$

$$I_c = (T_c - T_0)\sqrt{\beta F \frac{q}{l}\left(\frac{d\sigma}{dT}\right)_c} , \tag{2}$$

$$U_c = \sqrt{\beta F \frac{l}{q} \frac{1}{\left(\frac{d\sigma}{dT}\right)_c}} , \tag{3}$$

where index c stands for the reversion point of the $I(U)$ characteristics (Fig. 3), T_0 is the ambient temperature, β is the heat dissipation factor, F is the surface on which the heat dissipation takes place, q is the thickness of the sample, l is the length of the sample.

The temperature dependence of σ is known from our measurements, so we obtain the differential quotient $d\sigma/dT$ graphically. On this basis we plot the curve: $\sigma(d\sigma/dT)^{-1} = \varphi(T)$ and cut it by straights $T_c - T_0 = f(T)$ going with the different T_0 values. The cross-point values according to the relation (1) give the curve $T_c = \psi(T_0)$. Applying now Eqs. (2) and (3) we obtain the temperature dependence of I_c and U_c. This calculation was made for the sample N° 49/2 so that from (2) and (3) we obtained the factors $\beta Fq/l$ and $\beta Fl/q$ by fitting them in one point. We displayed in Fig. 4 the calculated values by a continuous line beside the experimental points which might be read off Fig.3. The good agreement between the calculated values and the experimental results proves the origin of the deviations from Ohm's law to be of thermal origin.

4. Pulse-operated measurements were carried out, too, for the investigation of this phenomenon. Fig. 5 shows the comparison of the d.c. and pulse-operated I—V characteristics at several temperatures. It can be seen that the deviation from Ohm's law does not occur in the investigated current and voltage range if we use pulses of $\tau = 10\ \mu\text{sec}$ at $\omega = 200\ \text{sec}^{-1}$ frequency. If the duty ratio of the pulses is $k = \tau\omega$ then the power fed into the sample is $P = I^2Rk$ (where R means the resistivity of the sample). Consequently, by increasing k that current range might be reached again, where the deviation from Ohm's law has to appear. This can be seen in Fig. 6a where the change of σ is displayed as a function of ω at different τ. As can be seen in Fig. 2 the 40 mA current applied is far above the current needed at the given temperature to originate non-linearity. For choosing k-values suitable for the measurements (i.e. for choosing the adequate τ and ω) the change of σ is shown in Fig. 6b as a

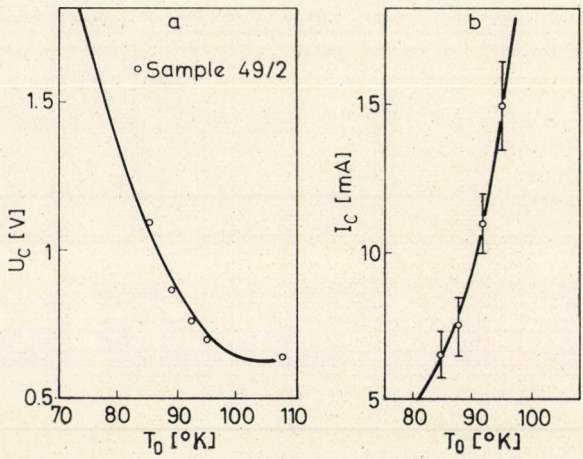


Fig. 4a) U_c as a function of T_0; *b)* I_c as a function of T_0. (The calculated values are shown by full lines)

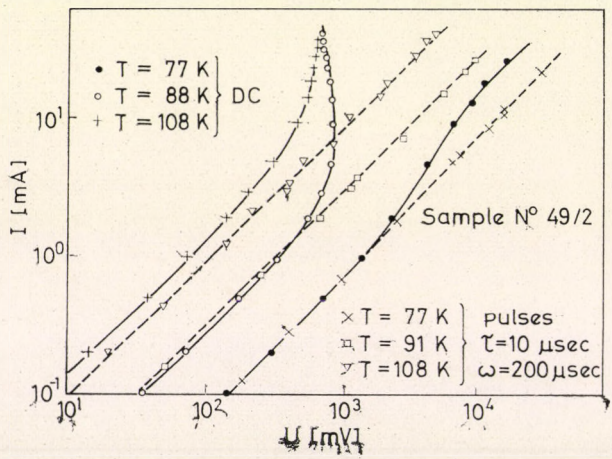


Fig. 5. I—V characteristics measured by d.c. and pulses on the sample N° 49|2

function of k at $I = 40$ mA. The values obtained by d.c. measurements ($k = 1$) are also shown.

5. In the interval of 200—400 °K the conductivity of GaP crystals is relatively high and depends on the temperature only to a small extent (the function of $\sigma(T^{-1})$ reaches its maximum and then decreases). Thus

(i) the curves $\sigma(I)$ and $\sigma(E)$ taken on the same sample at different T_0
a) have to approach each other (Fig. 1, curves 2,3 and Fig. 2, curves 2,3)
b) have to become saturated.

(ii) On approaching room temperature the deviation from Ohm's law should occur hardly or not at all. (Curves going with 228 °K in Figs. 1 and 2).

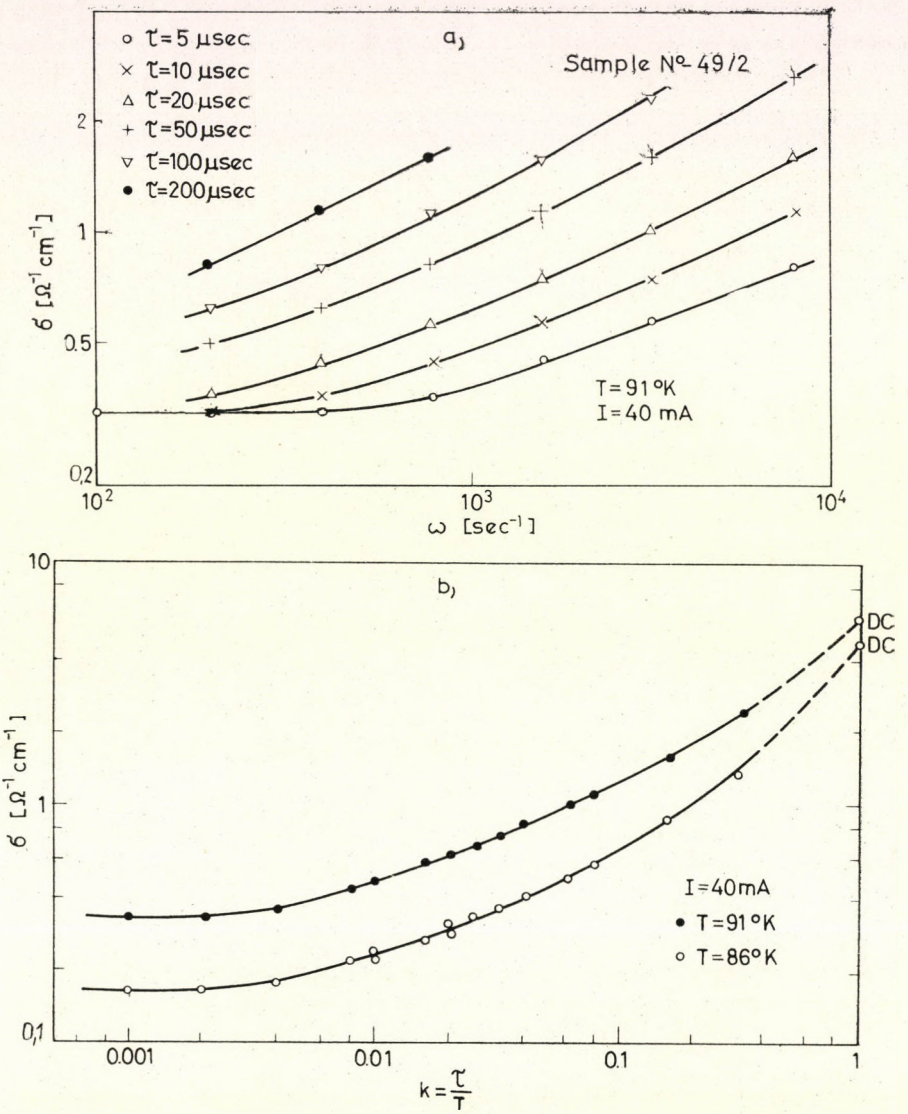


Fig. 6. a) Conductivity vs frequency at a critically high current value and several τ-s; *b)* Conductivity vs duty ratio. (At the d.c. $k = 1$)

Conclusions

Our experimental results can obviously be explained by supposing the overheating of the sample. No contradictions were found between this supposition and the experimental results. The supposition of overheating proved to be right based on the pulse-operated measurements and thermal breakdown at d.c. measurements. A considerable influence of the impact ionization and

other current conduction mechanisms causing the deviation from Ohm's law is out of the question in our and other similar cases, according to our opinion.

The authors of [9] do not describe the sample holder used during their measurements. However, by comparing their data and ours it seems to be plausible that the phenomenon observed by them might be explained similarly.

Acknowledgements are due to Dr. G. GERGELY for having supported the work. I wish to thank I. BERTÓTI for having provided me with the crystals, J. HAGYÓ for having prepared the samples as well as Dr. G. PATAKI, B. PŐDÖR, J. BALÁZS and B. RÖSNER for valuable discussions.

REFERENCES

1. T. HARA and I. AKASAKI J. Appl. Phys., **39**, 285, 1958.
2. А. Д. Ременюк, Л. Г. Забелина, Ю. И. Уханов, Ю. В. Шмарцев, ФТП, **2**, 666, 1968.
3. Д. Н. Наследов, В. В. Негрескул, С. В. Слободчиков, ФТТ, **7**, 1912, 1965.
4. D. N. NASLEDOV, V. V. NEGRESKUL, S. I. RADAUTSAN and S. V. SLOBODCHIKOV, phys. stat. sol., **10**, 37, 1965.
5. H. C. MONTGOMERY, J. Appl. Phys., **39**, 2002, 1968.
6. M. M. COHEN and F. D. BEDARD, J. Appl. Phys., **39**, 75, 1968.
7. С. Л. Пышкин, С. Н. Радауцан, С. В. Слободчиков, ФТП, **1**, 1013, 1967.
8. I. BERTÓTI and K. SOMOGYI, Híradástechnika, **21**, 133, 1970.
9. T. MIYAUCHI, H. SONOMURA and N. YAMAMOTO: Jap. J. Appl. Phys., **6**, 1409, 1967.
10. T. MIYAUCHI, H. SONOMURA and N. YAMAMOTO, Jap. J. Appl. Phys., **8**, 711, 1969.
11. K. SOMOGYI, Jap. J. Appl. Phys., **9**, 232, 1970.
12. I. BERTÓTI et al, to be published.
13. R. W. URE, Rev. Sci. Inst., **28**, 836, 1957.
14. K. SOMOGYI and V. G. SZIDJAKIN, Híradástechnika, **20**, 262, 1969.
15. В. В. Пасынков, Л. К. Чиркин, А. Д. Шинков, Полупроводниковые приборы, Москва, 1966.
16. G. PATAKI and S. DEMETER: to be published.
17. J. J. O'DWYER, The Theory of Dielectric Breakdown of Solids, Oxford, 1964.
18. K. N. WAGNER, Trans. A. I. M. E., **41**, 283, 1922.

О ПОЯВЛЕНИИ КАЖУЩЕГОСЯ ОТКЛОНЕНИЯ ОТ ЗАКОНА ОМА В GaP

К. ШОМОДИ

Резюме

При исследовании гальваномагнитных эффектов на фосфиде галлия наблюдалось отклонение от закона Ома при низких температурах (50—150 °K) [9, 10]. О природе такого отклонения предполагалось, что рост электропроводности и уменьшение постоянной Холла вызывается ростом концентрации носителей тока и температуры в последствии ударной ионизации [9]. В настоящей работе излагается другое объяснение этого эффекта. На основании экспериментальных данных (в первую очередь на основании измерений в импульсном режиме) показано, что отклонение от закона Ома является следствием перегрева образца по сравнению с окружающей средой, под действием выделяющегося Джоулевого тепла. Показано так же, что устройство держателя образца имеет существенное значение для появления кажущегося отклонения от закона Ома.

Acta Physica Academiae Scientiarum Hungaricae, Tomus 29 (4), pp. 391—398 (1970)

POTENTIAL ENERGY CURVES FOR DIATOMIC MOLECULES

By

T. TIETZ*

DEPARTMENT OF PHYSICS, WEST VIRGINIA UNIVERSITY, MORGANTOWN, WEST VIRGINIA 26506, U. S. A.

(Received 14. IV. 1970)

The purpose of this paper is to give a simple expression for the potential-energy function for diatomic molecules for which one can solve exactly the Schrödinger equation for both discrete and continuous energy parameters, E. The analytical expression for this potential curve is illustrated numerically. The possible appearance of the hump and the double-minimum in the potential curve has also been investigated.

I. Introduction

Curves of the potential energy versus internuclear distance form a convenient way of displaying the energy levels of diatomic molecules. In addition, they permit the ready application of the Franck-Condon principle to radiative transitions, electron-molecule collisions, predissociations, etc. Such curves for atmospheric molecules and molecular ions are helpful in determining the thermodynamic properties and radiation and reaction rates of heated or excited air. It is known that the Schrödinger equation is solvable only for the potential-energy function given by MORSE [1], MANNING [2], EISENHART [3] and the author of this paper [4] and then only if the quantum number $L = 0$. The purpose of this paper is to give a simple potential function for which one can solve exactly the Schrödinger equation for arbitrary L and for both discrete and continuous energy parameters E. Recently, VANDERSLICE, MASON and MAISCH [5] have modified a method due to RYDBERG [6], KLEIN [7] and RESS [8] to permit numerical calculation of accurate potential curves over the range for which spectroscopic data are available but this method is connected with burdensome numerical calculations.

II. Potential function

We write our potential function $U(r)$ in the form

$$U(r) = \frac{D_e H^2}{A}(r-r_e)^2\left[\frac{B+Gr+Ar^2}{r^2(F+Hr)^2}\right] + \frac{C(r-r_e)^2}{r(F+Hr)^2}, \tag{1}$$

* On leave of absence from the Department of Physics of Łódź University, Łódź, Poland.

where D_e is the dissociation energy, r_e is the equilibrium internuclear distance and A, B, C, F, G and H are constants. The six constants can be determined from the criteria that (1) the Schrödinger equation is exactly solvable and (2) $U(r)$ fulfills all necessary physical conditions [9]. Our potential curve given by Eq. (1) is infinite at $r = 0$ and $U(r_e) = U'(r_e) = 0$. For infinite values of r this potential curve is $U(\infty) = D_e$. Since $U(r)$ should have a minimum at $r = r_e$, we obtain the first relation for the constants

$$U''(r_e) = \frac{2D_e H^2}{A}\left[\frac{B+Gr_e+Ar_e^2}{r_e(F+Hr_e)^2}\right] + \frac{2C}{r_e(F+Hr_e)^2} = K_e, \tag{2}$$

where K_e is the force constant. In order to solve the Schrödinger equation exactly we next seek the condition which must be fulfilled for these constants.

III. The Schrödinger equation

The Schrödinger equation for our potential function is

$$Y_L'' + \left\{\frac{2m_0}{\hbar^2}\left[E - D_e\left(\frac{H^2}{A}\right)(r-r_e)^2\left(\frac{B+Gr+Ar^2}{r^2(F+Hr)^2}\right) - \frac{C(r-r_e)^2}{r(F+Hr)^2}\right] - \frac{L(L+1)}{r^2}\right\} Y_L = 0, \tag{3}$$

where m_0 is the reduced mass of the molecule. Substituting

$$Y_L(r) = r^p \exp\left[-\sqrt{D_1-\alpha^2}\right]r \cdot f(r) \tag{4}$$

and setting

$$(2m_0/E\hbar^2) = \alpha^2,\ (2m_0 D_e/\hbar^2) = D_1,\ (2m_0 C/\hbar^2) = C_1 \tag{5}$$

we obtain for $f(r)$ the equation,

$$f'' + 2\left[\frac{p}{r} - \sqrt{D_1-\alpha^2}\right]f' + \left[-\frac{2p}{r}\sqrt{D_1-\alpha^2} + \frac{\varepsilon_1+\gamma_1 r+\delta_1 r^2}{r(F+Hr)^2} - \frac{C_1(r-r_e)^2}{r(F+Hr)^2}\right]f = 0, \tag{6}$$

where p, ε_1, γ_1 and δ_1 are given by

$$[p(p-1) - L(L+1)] = \frac{D_1 B}{A}\left(\frac{Hr_e^2}{F}\right)^2, \tag{7}$$

$$-D_1\left(\frac{H^2 r_e}{A}\right)(Gr_e-2B)+2D_1\left(\frac{BH^3 r_e^2}{AF}\right)=\varepsilon_1\,, \tag{8}$$

$$-D_1\left(\frac{H^2}{A}\right)(Ar_e^2-2Gr_e+B)+D_1\left(\frac{BH^4 r_e^2}{AF^2}\right)+D_1F^2=\gamma_1\,, \tag{9}$$

$$-D_1\left(\frac{H^2}{A}\right)(G-2Ar_e)+2D_1HF=\delta\,. \tag{10}$$

In order to solve Eq. (6) exactly for $f(r)$ we must take the following substitution

$$f(r)=(F+Hr)^m\,g(r) \tag{11}$$

which gives us the equation for $g(r)$

$$g''+2\left[\frac{mH}{F+Hr}+\frac{p}{r}-\sqrt{D_1-\alpha^2}\right]g'+\left[\frac{m(m-1)H^2}{(F+Hr)^2}\right.$$
$$\left.+\frac{2mpH}{r(F+Hr)}-\frac{2mH\sqrt{D_1-\alpha^2}}{F+Hr}-\frac{2p}{r}\sqrt{D_1-\alpha^2}+\frac{\varepsilon+\gamma r+\delta r^2}{r(F+Hr)^2}\right]g=0\,, \tag{12}$$

where

$$\varepsilon=\varepsilon_1-C_1r_e^2\,,\qquad \gamma=\gamma_1+2C_1r_e\,,$$
$$\delta=\delta_1-C_1. \tag{13}$$

Putting

$$\varepsilon+[\gamma+m(m-1)H^2]r+\delta r^2$$
$$=(F+Hr)\;(N+Mr)\,, \tag{14}$$

we have

$$g''+2\left[\frac{mH}{F+Hr}+\frac{p}{r}-\sqrt{D_1-\alpha^2}\right]g'+\left[\frac{2mpH}{r(F+Hr)}-\right.$$
$$\left.-\frac{2mH\sqrt{D_1-\alpha^2}}{F+Hr}-\frac{2p}{r}\sqrt{D_1-\alpha^2}+\frac{N+Mr}{r(F+Hr)}\right]g=0\,, \tag{15}$$

where m, N and M are given by

$$AF(F+Hr_e)^2C_1=-m(m-1)AF^2H^3+D_1(F+Hr_e)^2\;H(BH^2-$$
$$-GFH+AF^2)\,, \tag{16}$$

$$\frac{AF^2N}{HD_1}=B(Hr_e+2F)\,Hr_e-AF^2\,r_e^2+\frac{m(m-1)AF^2H^2r_e^2}{D_1(F+Hr_e)^2}\,, \tag{17}$$

$$\frac{AFM}{D_1} = -BH^2 + AF(F+2Hr_e) + \frac{m(m-1)AF^2H^2}{D_1(F+Hr_e)^2}. \tag{18}$$

Our Eq. (2) takes the form

$$\frac{BH^2}{A} + \left[-\frac{m(m-1)\hbar^2 FH^3}{2m_0 D_e (F+Hr_e)^2} + \frac{H}{AF}(BH^2+AF^2) \right] r_e + H^2 r_e^2 = \Delta (F+Hr_e)^2, \tag{19}$$

where $\Delta = K_e r_e^2/2 D_e$ is the Sutherland parameter. Using Eq. (16) and Eq. (19) we rewrite Eq. (1) for $U(r)$ as follows

$$U(r) = D_e \left[\frac{1-(r_e/r)}{1+a(r/r_e)} \right]^2 \{ba^2 + [-a^2(1+b) + \Delta(1+a)^2](r/r_e) + (ar/r_e)^2\}, \tag{20}$$

where $(H/F) = (a/r_e)$ and $(B/A) = br_e^2$. In this notation using Eq. (5) we rewrite Eq. (7) for p and Eq. (16) for m as below

$$[p(p-1) - L(L+1)] = \frac{2m_0 D_e b(ar_e)^2}{\hbar^2}, \tag{21}$$

$$a^2(1+b) + a(1+ba^2) - \frac{m(m-1)\hbar^2 a^3}{2m_0 D_e r_e^2 (1+a)^2} = \Delta(1+a)^2. \tag{22}$$

In this case the solution of the Schrödinger equation $Y_L(r)$ if $U(r)$ is given by Eq. (20) has the form

$$Y_L(r) = r^p [1 + (ar/r_e)]^m \exp\left[-\frac{1}{\hbar} \sqrt{2m_0(D_e - E)}\, r \right] g(r), \tag{23}$$

where $g(r)$ fulfilles the equation

$$g'' + 2\left[\frac{ma}{r_e(1+ar/r_e)} + (p/r) - \frac{1}{\hbar}\sqrt{2m_0(D_e-E)} \right] g' + \left[\frac{2mpa}{rr_e(1+ar/r_e)} - \frac{2ma\sqrt{2m_0(D_e-E)}}{\hbar r_e(1+ar/r_e)} - \frac{2p}{\hbar r}\sqrt{2m_0(D_e-E)} + \frac{N_1 + M_1 r}{r(1+ar/r_e)} \right] g = 0. \tag{24}$$

The symbols N_1 and M_1 appearing in the last equation are

$$\frac{\hbar^2 N_1}{2m_0 D_e} = a^2 br_e(a+2) - ar_e + \frac{m(m-1)\hbar^2 a^3}{2m_0 D_e r_e (1+a)^2}, \tag{25}$$

$$\frac{\hbar^2 M_1}{2m_0 D_e} = a\,(2-ba) + 1 + \frac{m(m-1)\,a^2\hbar^2}{2m_0 D_e r_e^2 (1+a)^2}\,. \tag{26}$$

Setting $g(r)$ in the form of an infinite series

$$g(r) = \sum_s c_s r^s \tag{27}$$

we get for the coefficient c_s the recurrence formula

$$\left[M_1 - \frac{2a}{\hbar r_e}(s+m+p)\sqrt{2m_0(D_e-E)}\right]c_s + \left\{N_1 + \frac{a}{r_e}[(s+1)(s+2p+2m) + 2mp] - \frac{2}{\hbar}(p+s+1)\sqrt{2m_0(D_e-E)}\right\}c_{s+1} + (s+2)(2p+s+1)\,c_s + 2 = 0, \tag{28}$$

where $c_1 = 0$, $s = -1, 0, 1, 2, \ldots$. The requirement that $g(r)$ is a polynomial of degree $n = 1, 2, 3, \ldots$, yields the eigenvalues E_{nL} given by

$$M_1 = \frac{2a}{\hbar r_e}(n+m+p)\sqrt{2m_0(D_e-E_{nL})}\,, \tag{29}$$

where M_1 has the form of Eq. (25). The corresponding eigenfunctions to the eigenvalues E_{nL} we obtain using Eqs. (23), (24) and the last Eq. (29). In Table I we display numerical values of our potential energy function $U(r)$, as given by Eq. (20), for a range of (r/r_e) and $\Delta = 5$.

Table I shows that our potential energy curve has one maximum. The maximum lies above the dissociation energy. The change of the numerical values of the constants a and b causes this maximum to be larger, to be smaller or to disappear. This case is given in Table I. Since we have there two curves with a hump and one smooth curve. Both smooth curves as well as curves with a hump are observed experimentally [9]. The same case exists for another values of Δ then $\Delta = 5$.

In Table II we have numerical values of our potential energy function $U(r)$ for other numerical values of the constants a and b.

Table II shows that our potential energy curve $U(r)$ for the numerical values of the constants a and b given in Table II has one maximum or it has a double-minimum. The second-minimum lies above $U(r_e) = 0$. The change of the numerical values of the constants a and b causes the hump and the second-minimum to be larger, to be smaller or to disappear. It is possible to select the numerical values of the constant a and b in order that the second-minimum is below $U(r_e) = 0$. The requirement that our potential function gives correct

Table I

$U(r)/D_e$ as a function of (r/r_e) for $\Delta = 5$ for several values of the constants a and b

(r/r_e)	$U(r)/D_e$		
	$a = 40,\ b = 2.0$	$a = 20,\ b = 2.0$	$a = 20,\ b = 2.5$
0.0	$+\infty$	$+\infty$	$+\infty$
0.2	787.16	650.88	753.28
0.4	38.133	35.167	38.499
0.6	4.2233	4.0684	4.2788
0.8	0.40794	0.40225	0.41090
1.0	0.00000	0.00000	0.00000
1.2	0.11372	0.11475	0.11298
1.4	0.28600	0.29032	0.28256
1.6	0.43482	0.44318	0.42768
1.8	0.55130	0.56344	0.54036
2.0	0.64052	0.65586	0.62611
2.5	0.78389	0.80450	0.76298
3.0	0.86257	0.88566	0.83886
3.5	0.90891	0.93291	0.88230
4.0	0.93790	0.96193	0.91049
4.5	0.95691	0.98053	0.92940
5.0	0.96987	0.99284	0.94265
10.0	1.00368	1.01949	0.98340
15.0	1.00634	1.01797	0.99105
20.0	1.00617	1.01531	0.99398
25.0	1.00559	1.01311	0.99549
30.0	1.00502	1.01141	0.99701
35.0	1.00453	1.01007	0.99701
∞	1.00000	1.00000	1.00000

experimental value for the vibration-rotation coupling constant α_e is fulfilled by [10]

$$-\left(\frac{Xr_e}{3}+1\right)=F_e=\frac{\alpha_e\,\omega_e}{6B_e^2}\,, \tag{30}$$

where $X = U'''(r_e)/U''(r_e)$, ω_e is the vibrational frequency, and B_e is the rotational constant. This equation gives us a helpful condition in order to determine the constants a and b of our potential curve given by Eq. (20). In our case we have

$$b=(F_e-1)\,\Delta\left(\frac{1}{a}+1\right)^2+1+\Delta\left(\frac{1}{a^2}-1\right). \tag{31}$$

Table II

$U(r)/D_e$ as a function of (r/r_e) for $\Lambda = 5$ for several values of the constants a and b

(r/r_e)	$U(r)/D_e$		
	$a = 1.4,\ b = 1.0$	$a = 1.4,\ b = 15$	$a = 1.4,\ b = 20$
0.0	$+\infty$	$+\infty$	$+\infty$
0.2	206.31	282.87	359.44
0.4	21.089	26.525	31.961
0.6	3.2359	3.7505	4.2651
0.8	0.37054	0.39780	0.42506
1.0	0.00000	0.00000	0.00000
1.2	0.12032	0.11274	0.10516
1.4	0.31284	0.27632	0.23980
1.6	0.48495	0.40618	0.32742
1.8	0.62146	0.49648	0.37149
2.0	0.72576	0.55609	0.38643
2.5	0.88800	0.62667	0.36534
3.0	0.96910	0.64694	0.32479
3.5	1.01059	0.65150	0.29241
4.0	1.04289	0.65353	0.26416
5.0	1.04800	0.65600	0.26400
10.0	1.03680	0.71928	0.40176
15.0	1.02446	0.77520	0.53058
20.0	1.01775	0.81794	0.61812
25.0	1.01376	0.84651	0.67929
30.0	1.01116	0.86753	0.72390
40.0	1.00935	0.89520	0.78437
50.0	1.0624	0.91475	0.82326

Acknowledgement

The author thanks Professor Dr. ROBERT G. BREENE, Jr. for helpful discussions connected with this paper as well as for the possibility to visit the Department of Physics of the West Virginia University.

REFERENCES

1. P. MORSE, Phys. Rev., **34,** 57, 1929.
2. M. F. MANNING, Phys. Rev., **48,** 161, 1935.
3. L. P. EISENHART, Phys. Rev., **74,** 87, 1948.
4. T. TIETZ, J. Chem. Phys., **38,** 3036, 1963.
5. J. T. VANDERSLICE, E. A. MASON and W. G. MAISCH, J. Mol. Spectrosc., **3,** 17, 1957; errata **5,** 83, 1960.
6. R. RYDBERG, Z. Phys., **73,** 376, 1931.

7. O. KLIEN, Z. Phys., **76**, 226, 1932.
8. A. L. G. RESS, Proc. Phys. Soc. (London) **59**, 998, 1947.
9. F. R. GILMORE, J. Quant. Spectrosc. Radiat. Transfer., **5**, 369, 1963.
10. Y. P. VARSHNI, Rev. Mod. Phys., **29**, 664, 1957.

КРИВЫЕ ПОТЕНЦИАЛЬНОЙ ЭНЕРГИИ ДЛЯ ДВУХАТОМНЫХ МОЛЕКУЛ

Т. ТИТЦ

Резюме

Цель настоящей работы — дать простое выражение для функции потенциальной энергии двухатомных молекул, для которых уравнение Шредингера решается точно, как с дискретными, так и с непрерывными значениями параметра энергии E. Аналитическое выражение кривой потенциала иллюстрируется численным примером. Исследуется возможность появления горба и двойного минимума на кривой потенциала.

Acta Physica Academiae Scientiarum Hungaricae, Tomus 29 (4), pp. 399–406 (1970)

RE-INVESTIGATION OF THE COUPLING CONSTANTS OF THE REVISED MOLECULAR STATES OF TiO

By

I. KOVÁCS and V. M. KORWAR*

DEPARTMENT OF ATOMIC PHYSICS, POLYTECHNICAL UNIVERSITY, BUDAPEST

(Received 14. IV. 1970)

The problem of anomalous triplet splitting in the α and γ band systems of the TiO molecule has been re-investigated, as it is now known that the transitions responsible for these systems are $C^3\Delta - X^3\Delta$ and $A^3\Phi - X^3\Delta$, respectively, and not $C^3\Pi - X^3\Pi$ and $A^3\Delta - X^3\Pi$ as has been formerly assumed. As has been done by KOVÁCS previously the observed splitting can be explained on the basis of anomalous triplet splittings found in $X^3\Delta$, $C^3\Delta$ and $A^3\Phi$ terms by taking into account simultaneously the spin-orbit and spin-spin interactions. Also, the exact values of the coupling constants A are given for all the three states on the levels $v = 0$.

I. Introduction

Rotational analysis of some of the bands of the α and γ systems of the TiO molecule have been carried out by CHRISTY [1] and by PHILLIPS [2]. The anomalous splittings observed in the two transitions have been investigated by KOVÁCS [3] and by TŐRÖS [4]. It was assumed that these two systems were produced by $C^3\Pi - X^3\Pi$ and $A^3\Delta - X^3\Pi$ transitions, respectively, but it is now established [5] that the transitions responsible for these systems are $C^3\Delta - X^3\Delta$ and $A^3\Phi - X^3\Delta$. Thus, all the molecular states involved have been re-designated. It therefore calls for fresh investigation. The present work is a re-investigation of the multiplet splitting in the (0,0) bands of the α and γ systems of TiO.

II. $A^3\Phi - X^3\Delta$ transition

Of the two methods of determining the multiplet splitting constant, namely, (i) the method of combination differences $\Delta_2F_3(J) - \Delta_2F_1(J)$ and (ii) the method of term differences $F_3(J) - F_1(J)$, the latter method yields more exact results than the former. In this method, in the absence of experimental data on satellite branches, the term differences cannot be obtained directly, but are given by

$$\Delta F'_{31}(J) = Q_3(J) - Q_1(J) + \Delta F''_{31}(J),$$

* On leave from Karnatak University, Dharwar, India.

$$\Delta F'_{31}(J) = R_3(J-1) - R_1(J-1) + \Delta F''_{31}(J-1) \qquad (1)$$
$$= P_3(J+1) - P_1(J+1) + \Delta F''_{31}(J+1),$$

where $\Delta F''_{31}(J)$ ($\Delta F_{ik}(J) = F_i(J) - F_k(J)$) can be calculated theoretically by means of the triplet formulae of the lower state. The earlier data for the lower state for the level $v'' = 0$, $B'' = 0.534\ \mathrm{cm}^{-1}$, $D'' = -6.1\times10^{-7}\ \mathrm{cm}^{-1}$ hold, but Y'' and A'' have to be recalculated as the lower state is now known to be a Δ state. However, the method of term differences cannot be used to determine the constant A'' for this state. By the method of combination differ-

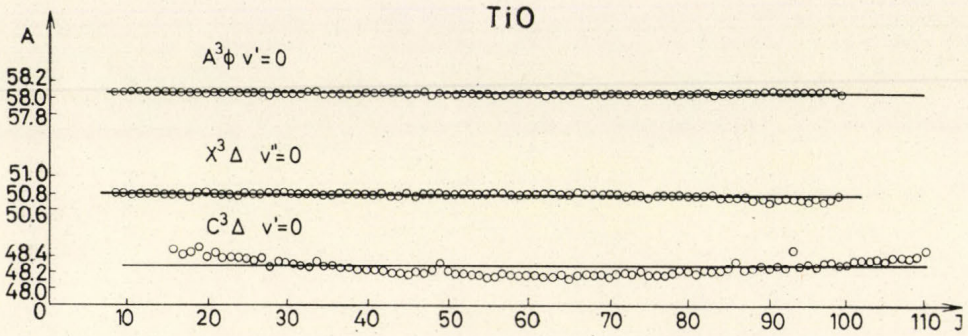


Fig. 1

ences the mean value of A'' works out to $50.795\ \mathrm{cm}^{-1}$. With these data on the lower state the term differences $\Delta F'_{31}(J)$ have been computed according to Eq. (1) for all the branches P, Q, R and then the mean calculated.

For the determination of the coupling constant A' by method (ii) above the following relation, obtained from the well known triplet formulae [6] is made use of:

$$\frac{1}{4B'^2}\left\{(F'_3 - F'_1) + \gamma'(2J+1) - 4D'[(J^2+J-8)\ (2J+1)]\right\}^2 + \qquad (2)$$
$$= 9(Y'-2)^2 - \frac{104}{3} + 4J(J+1),$$

where B', D' are the rotational constants (for the level $v' = 0$, $B' = 0.5058\ \mathrm{cm}^{-1}$, $D' = -6.99\times10^{-7}\ \mathrm{cm}^{-1}$), γ' the constant of the interaction between rotation and spin, whereas $Y' = A'/B'$. By making use of this relation, we have at the level $v' = 0$, $Y' = 114.770\ \mathrm{cm}^{-1}$, and $A' = 58.05\ \mathrm{cm}^{-1}$ and $\gamma' = +0.00126\ \mathrm{cm}^{-1}$. In Fig. 1 A' has been plotted against the rotational quantum number J and it appears to be fairly constant, as was also found by KOVÁCS previousiy.

When once one is in possession of A values for the upper state the $\Delta F''_{31}(J)$ values can be obtained from formulae similar to Eq. (1) above, and these could then be used to determine a more accurate value of A by the method of term differences. This has been done for the $X^3\Delta$ state at the level $v'' = 0$. The relation used is the same as Eq. (2) in KOVÁCS's paper [3]. It now turns out that A'' is fairly constant as can be seen from Fig. 1. However, the mean value found earlier, viz., 50.795 cm^{-1} by the method of combination differences, coincides almost exactly with the constant value (= 50.800 cm^{-1}) found by the method of term differences.

Using these data, discrepancy is found between the observed and calculated multiplet splittings if the spin–spin interaction and the perturbations of $^1\Phi$ terms arising from the spin–orbit interaction are neglected. If one is not in possession of experimental data on satellite branches, the triplet splitting cannot be produced separately for the terms involved in the transition; only the difference between the triplet splittings of the terms can be obtained. Again, as it is not certain whether the anomalous splitting is at the upper or the lower state, one has to consider that there is anomalous splitting on both the states. Then one has (for detailed explanation, see KOVÁCS [3])

$$Q_i(J) - Q_k(J) + \Delta F''^{\,\mathrm{Calc}}_{ik}(J) - \Delta F'_{ik}(J) = \\ = [\Delta F'^{\,\mathrm{Obs}}_{ik}(J) - \Delta F'^{\,\mathrm{Calc}}_{ik}(J)] - [\Delta F''^{\,\mathrm{Obs}}_{ik}(J) - \Delta F''^{\,\mathrm{Calc}}_{ik}(J)], \tag{3a}$$

$$R_i(J-1) - R_k(J-1) + \Delta F''^{\,\mathrm{Calc}}_{ik}(J-1) - \Delta F'^{\,\mathrm{Calc}}_{ik}(J) = \\ = [\Delta F'^{\,\mathrm{Obs}}_{ik}(J) - \Delta F'^{\,\mathrm{Calc}}_{ik}(J)] - [\Delta F''^{\,\mathrm{Obs}}_{ik}(J-1) - \Delta F''^{\,\mathrm{Calc}}_{ik}(J-1)], \tag{3b}$$

$$P_i(J+1) - P_k(J+1) + \Delta F''^{\,\mathrm{Calc}}_{ik}(J+1) - \Delta F'^{\,\mathrm{Calc}}_{ik}(J) = \\ = [\Delta F'^{\,\mathrm{Obs}}_{ik}(J) - \Delta F'^{\,\mathrm{Calc}}_{ik}(J)] - [\Delta F''^{\,\mathrm{Obs}}_{ik}(J+1) - \Delta F''^{\,\mathrm{Calc}}_{ik}(J+1)]. \tag{3c}$$

If one takes the mean values of (3b) and (3c) one has, to a good approximation,

$$\frac{1}{2}[\Delta F''^{\,\mathrm{Obs}}_{ik}(J-1) - \Delta F''^{\,\mathrm{Calc}}_{ik}(J-1) + \Delta F''^{\,\mathrm{Obs}}_{ik}(J+1) - \\ - \Delta F''^{\,\mathrm{Calc}}_{ik}(J+1)] \approx \Delta F''^{\,\mathrm{Obs}}_{ik}(J) - \Delta F''^{\,\mathrm{Calc}}_{ik}(J).$$

Hence one has

$$[\Delta F'^{\,\mathrm{Obs}}_{12}(J) - \Delta F'^{\,\mathrm{Calc}}_{12}(J)] - [\Delta F''^{\,\mathrm{Obs}}_{12}(J) - \Delta F''^{\,\mathrm{Calc}}_{12}(J)] = \\ = \beta'_{\Phi}(S'^{\,2}_{3,J-1} - S'^{\,2}_{3,J}) - \beta''_{\Delta}(S''^{\,2}_{2,J-1} - S''^{\,2}_{2,J}), \\ [\Delta F'^{\,\mathrm{Obs}}_{23}(J) - \Delta F'^{\,\mathrm{Calc}}_{23}(J)] - [\Delta F''^{\,\mathrm{Obs}}_{23}(J) - \Delta F''^{\,\mathrm{Calc}}_{23}(J)] = \\ = \beta'_{\Phi}(S'^{\,2}_{3,J} - S'^{\,2}_{3,J+1}) - \beta''_{\Delta}(S''^{\,2}_{2,J} - S''^{\,2}_{2,J+1}), \tag{4}$$

where the first terms on the right-hand side of (4) take into account simultaneously the spin–spin interaction and the perturbation by the $^1\Phi$ term and the

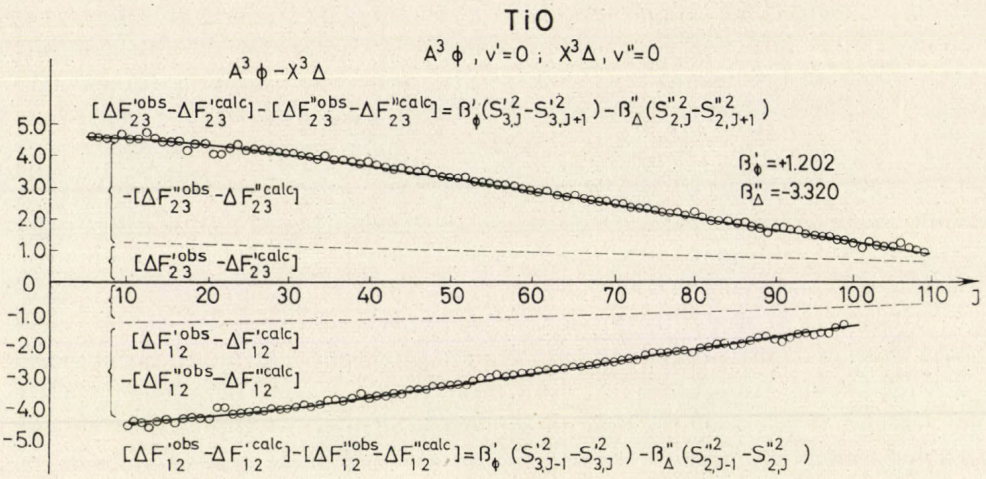


Fig. 2

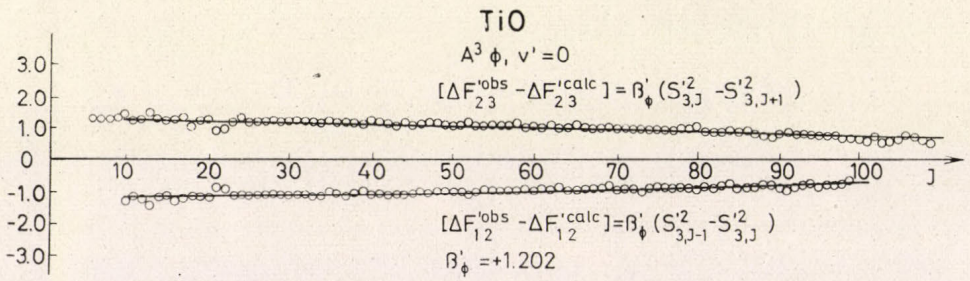


Fig. 3

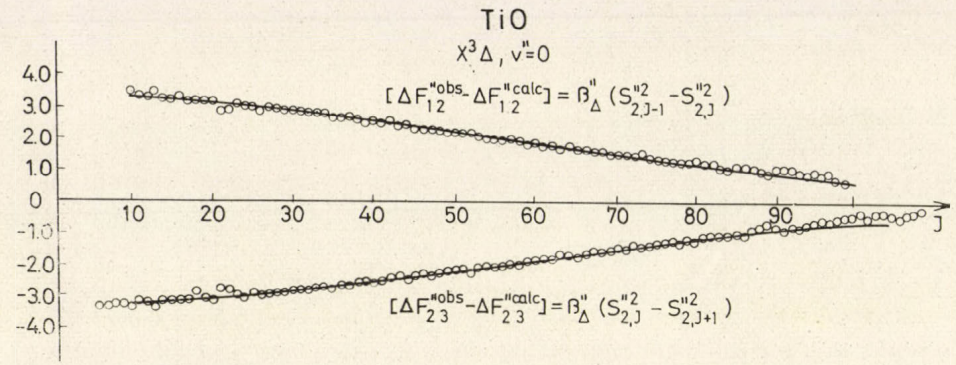


Fig. 4

second terms on the right-hand side account for spin—spin interaction and perturbation by the $^1\Delta$ term. The transformation matrix elements S are given by [7]

$$S'_{3,J-1} = \left[\frac{2(J^2-9)}{C'_1(J)}\right]^{1/2}, \quad C'_1(J) = 9Y'(Y'-4)(J-2)(J+3) + \\ + 2(2J+1)(J-3)J(J+3),$$

$$S'_{3,J} = \frac{3(Y'-2)}{[C'_2(J)]^{1/2}}, \quad C'_2(J) = 9Y'(Y'-4) + 4J(J+1),$$

$$S'_{3,J+1} = \left[\frac{2(J-2)^2(J+4)^2}{C'_3(J)}\right]^{1/2} C'_3(J) = 9Y'(Y'-4)(J-3)(J+4) + \\ + 2(2J+1)(J-2)(J+1)(J+4),$$

and

$$S''_{2,J-1} = \frac{(J-2)(J+2)}{[C''_1(J)]^{1/2}}, \quad S''_{2,J} = \frac{Y''-2}{[C''_2(J)]^{1/2}}, \quad S''_{2,J+1} = \frac{(J-1)(J+3)}{[C''_3(J)]^{1/2}},$$

where

$$C''_1(J) = 2Y''(Y''-4)(J-1)(J+2) + (2J+1)(J-2)J(J+2),$$
$$C''_2(J) = Y''(Y''-4) + J(J+1),$$
$$C''_3(J) = 2Y''(Y''-4)(J-2)(J+3) + (2J+1)(J-1)(J+1)(J+3).$$

For computing the left-hand sides of (4) the means of the values obtained from the P, Q, R branches have been taken. The results are plotted in Fig. 2, where the circles denote the values of the left-hand side of (4) determined from (3) and the lines drawn in full represent the values of the right-hand side of (4), calculated theoretically with the values $\beta'_\Phi = 1.202\ \mathrm{cm}^{-1}$ and $\beta'_\Delta = -3.320\ \mathrm{cm}^{-1}$. The dotted lines indicate how the anomalous triplet splittings are distributed between the two states involved in the transition; this is again shown separately in Figs. 3 and 4.

It can be seen from Figs. 3 and 4 that a greater deviation from the usual triplet splitting is shown on the lower state $X^3\Delta$ than on the upper state $A^3\Phi$.

III. $C^3\Delta - X^3\Delta$ transition

It is clear from the foregoing conclusions that anomalous triplet splitting is also to be expected for the $C^3\Delta - X^3\Delta$ transition. Here also it is impossible to separate the triplet splitting of the two states involved in the transition as no satellite branches are observed.

For determination of the coupling constant the relation (2) used by Kovács [3] has been used. The value A' has been plotted in Fig. 1. It can be seen from the Figure that the coupling constant does not come out to be constant, the trend of the curve being exactly the same as when the upper state was treated as a $^3\Pi$ state. (see Fig. 1 of Kovács [3]). With a view to finding if the neglect of spin—spin and spin—orbit interaction (perturbation by the $^1\Delta$

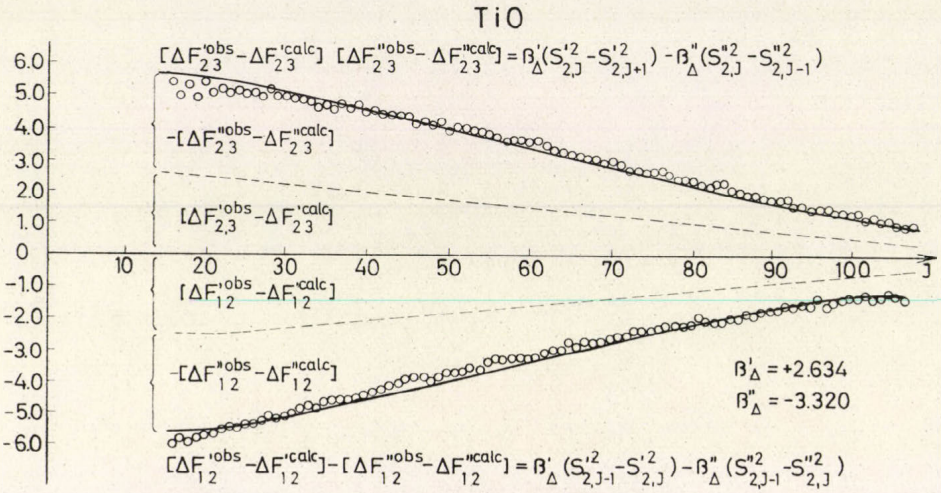


Fig. 5

term) is responsible for the non-constancy of A for the $C^3\Delta$ state, these interactions were included and the new relation for finding A' was

$$\frac{1}{16B'^2}\{\Delta F'_{31}(J)+\gamma'(2J+1)+\beta(S'^2_{1,J+1}-S'^2_{1,J-1})-4D'[J^2+(J+1)^3]\}^2=$$
$$=(Y'-2)^2-\frac{11}{3}+J(J+1)\,,$$

where S's are transformation matrix elements similar to those in Eq. (4).This however, did not yield better results, the trend of the variation of A with J remaining exactly the same as before. The mean value of $Y' = 98.869\ \mathrm{cm}^{-1}$ and mean $A' = 48.284\ \mathrm{cm}^{-1}$, $\gamma' = -0.045\ \mathrm{cm}^{-1}$. With these values of constants and with those for the lower state $X^3\Delta$, anomalous triplet splittings can be explained. This is shown in Fig. 5, where the left-hand sides of (3) have been marked by circles. The relevant theoretical formulae are

$$[\Delta F_{12}^{'Obs}(J)-\Delta F_{12}^{'Calc}(J)]-[\Delta F_{12}^{''Obs}(J)-\Delta F_{12}^{''Calc}(J)]=$$
$$=\beta'_\Delta(S'^2_{2,J-1}-S'^2_{2,J})-\beta''_\Delta(S''^2_{2,J-1}-S''^2_{2,J})\,,$$

$$[\Delta F'^{\mathrm{Obs}}_{23}(J) - \Delta F'^{\mathrm{Calc}}_{23}(J)] - [\Delta F''^{\mathrm{Obs}}_{23}(J) - \Delta F''^{\mathrm{Calc}}_{23}(J)] =$$
$$= \beta'_{\Delta}(S'^{2}_{2,J} - S'^{2}_{2,J+1}) - \beta''_{\Delta}(S''^{2}_{2,J} - S''^{2}_{2,J+1}).$$

With the value of $\beta'_{\Delta} = +2.634$ cm^{-1} and $\beta''_{\Delta} = -3.32$ cm^{-1}, the theoretical curves (drawn in full line) have been drawn. The dotted lines again indicate the separations of the anomalous triplet splittings of the upper and lower states, among which those of the upper state may be seen separately in Fig. 6.

The values of the new, modified constants used for the $C^3\Delta$, $A^3\Phi$ and $X^3\Delta$ states are presented in Table I.

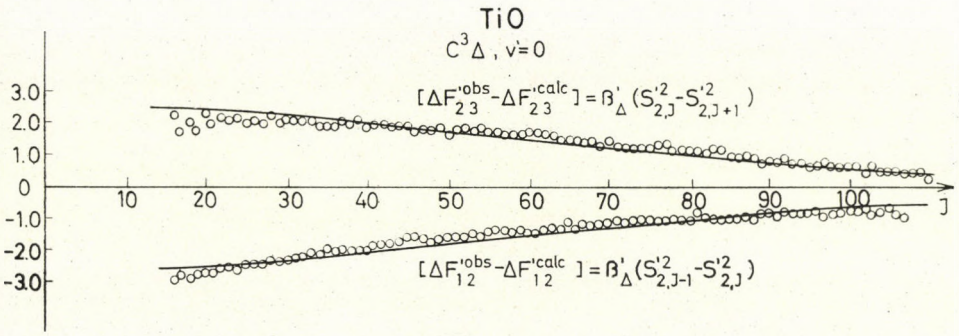


Fig. 6

Table I

	v	A	Y	γ	β
$C^3\Delta$	0	48.284	98.869	−0.045	+2.634
$A^3\Phi$	0	58.051	114.771	+0.00126	+1.202
$X^3\Delta$	0	50.800	95.122	−0.00004	−3.320

In conclusion, it may be stated that the anomalous triplet splittings observed on the $C^3\Delta$, $A^3\Phi$ and $X^3\Delta$ terms of the TiO molecule can again be interpreted as before (by Kovács and Tőrös) after the determination of the correct values of the coupling constants by taking into account simultaneously the spin–orbit and the spin–spin interactions.

REFERENCES

1. A. Christy, Phys. Rev., **33**, 701, 1929.
2. J. G. Phillips, Astrophys. J., **114**, 152, 1951.
3. I. Kovács, J. Mol. Spectr., **18**, 229, 1965.
4. R. Tőrös, Acta Phys. Hung., **20**, 91, 1966.

5. U. Uhler, Dissertation, Stockholm, 1954.
K. D. Carlson and C. Moser, J. Phys. Chem., **67**, 2644, 1963.
K. D. Carlson and R. K. Nesbet, J. Chem. Phys., **41**, 1051, 1964.
J. G. Phillips, Astrophys. J., **157**, 449, 1969.
6. A. Budó, Zs. f. Phys., **98**, 437, 1936.
7. I. Kovács, Rotational Structure in the Spectra of Diatomic Molecules, Akadémiai Kiadó, Budapest and Adam Hilger Ltd., London, pp. 69., 1969.

ПОВТОРНОЕ ИССЛЕДОВАНИЕ КОНСТАНТ СВЯЗИ ИСПРАВЛЕННЫХ МОЛЕКУЛЯРНЫХ СОСТОЯНИЙ

И. КОВАЧ и В. М. КОРВАР

Р е з ю м е

Пересматривается проблема аномального триплетного расщепления в α и γ системах полос TiO, так как в последнее время стало известным, что переходами, ответственными за эти системы, являются переходы $C^3\Delta - X^3\Delta$ и $A^3\Phi - X^3\Delta$ соответственно, а не $C^3\Pi - X^3\Pi$ и $A^3\Delta - X^3\Pi$, как это предполагалось раньше. Как уже Ковач показал, наблюдаемое расчепление объясняется с помощью аномальных триплетных расщеплений, основанных на термах $X^3\Delta$, $C^3\Delta$ и $A^3\Phi$, с учетом спин-орбитального и спин-спинового взаимодействий. Определяются точные значения констант связи A для всех трех состояний уровня $v = 0$.

Acta Physica Academiae Scientiarum Hungaricae, Tomus 29 (4), pp. 407—413 (1970)

FISSION PRODUCTS IN THE ATMOSPHERIC PRECIPITATION IN DEBRECEN, HUNGARY, DURING 1968 AND 1969

By

A. SZALAY and E. CSONGOR

INSTITUTE OF NUCLEAR RESEARCH OF THE HUNGARIAN ACADEMY OF SCIENCES (ATOMKI), DEBRECEN

(Received 22. IV. 1970)

Observations concerning the beta activity of fission products in the atmospheric precipitation were continued during 1968 and 1969. The annual sum of beta activity in these two years was double and triple that in 1967, respectively. Some samples demonstrated exceedingly high specific activity in the summer of 1969. In these samples it was possible to localize alpha-active hot particles by means of cellulose nitrate detector foil.

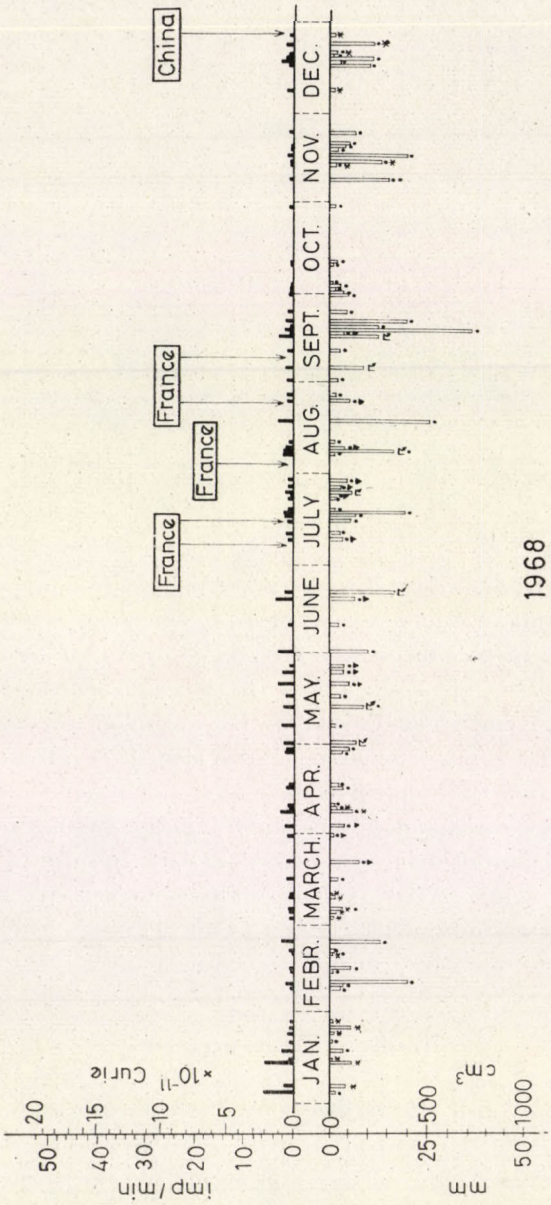
Introduction

Measurements relating to the beta activity of fission products in atmospheric precipitation were continued during 1968 and 1969. Such measurements have been carried out systematically, without interruption in our Institute since 1952 [1—9] essentially with the same method.

The precipitation is collected daily by means of an ombrometer with a 40 cm diameter PVC funnel, located on the roof of the Institute. In the absence of precipitation the deposited dust and soot is washed from the funnel into the collecting vessel and is measured together with the next precipitation. Then the precipitation is evaporated and the residue is concentrated in standardized glass cups. After two days the beta activity of the sample is measured by an end-window GM counter. The details of the measuring techniques applied have appeared in our preceding papers [4].

Results of measurements

Fig. 1 demonstrates the results of the measurements for the years 1968 and 1969. The mode of representation is the same as previously. The measured beta activity is referred to a surface of 1/50 m^2, i.e. the surface of a standard meteorological ombrometer. The beta activity of the samples is plotted on the ordinate upwards in cpm and 10^{-11} Curie units as a function of calendar time. The quantity of daily precipitation is shown on the ordinate downwards in mm and cm^3 units. Published data of atmospheric nuclear tests are denoted in Fig. 1 as well.


China
France
France
France
JAN.
FEBR.
MARCH
APR.
MAY.
JUNE
JULY
AUG.
SEPT.
OCT.
NOV.
DEC.
1968
imp/min
×10⁻¹¹ Curie
MeV

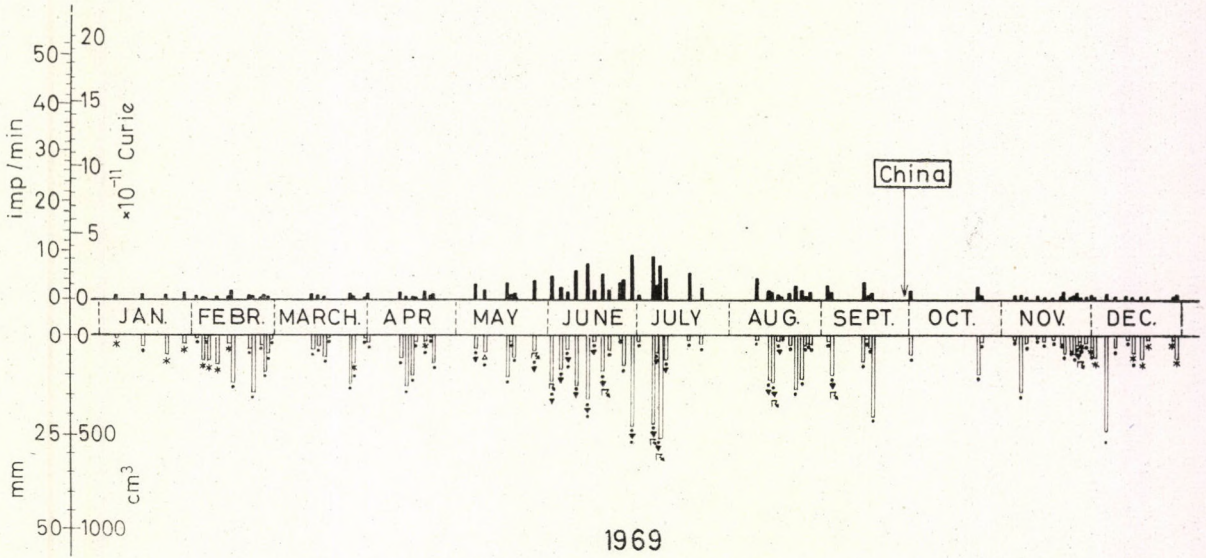


Fig. 1. Beta activity of fission products in the atmospheric precipitation in Debrecen, Hungary, during 1968 and 1969. Ordinate upwards, right: activity in 10^{-11} Curie units, corrected for the geometry of the counting equipment. Ordinate upwards, left: activity observed in cpm, both reduced to 1/50 m² ombrometer surface. Ordinate downwards, right: one day's rainfall in ml water volume collected by an exposed area of 1/50 m². Ordinate downwards, left: one day's rainfall in mm. Abscissa: calendar time

The monthly and annual sums of the beta activity of the samples are shown in Table I in mCi/km² · month, and in mCi/km² · year units.

The fission products of an atomic-bomb explosion are usually dispersed in the troposphere, from where they are washed out with the precipitation within some weeks. The maximum of tropospheric fallout is generally detectable in a zone which is within 10°—20° latitude of the place of the explosion.

Table I

Monthly and annual sum of beta activity measured in the precipitation in Debrecen

Month	1968 mCi/km² · month	1969 mCi/km² · month
January	3.327	0.6
February	1.074	1.149
March	1.101	0.729
April	1.875	1.158
May	2.610	2.682
June	1.695	9.01
July	2.256	5.757
August	2.091	3.03
September	2.112	1.95
October	0.477	1.005
November	0.672	1.281
December	1.494	1.041
Annual sum	20.784 mCi/km² · year	29.392 mCi/km² · year

In the case of a thermonuclear test, most of the fission products are injected into the stratosphere, from where the fallout is mixed in the troposphere, with a decontamination half-life of 0.7 year. A strong vertical mixing occurs between the stratospheric and tropospheric air masses in spring and early summer, in the middle latitudes, so the well known spring maxima usually appear in the activity. In the years 1966 and 1967 this maximum was not detectable at all, because the presence of the fresh fission products originating from the sporadic atmospheric nuclear tests obscured this periodicity and resulted in a practically constant activity level.

In the year 1968 and especially in 1969 the activity level in the early summer was considerably high (see Table I) and the annual sums of the activities were, respectively, more than double, and treble those of 1967, which amounted to 8.8 mCi/km² · year.

The annual sum of beta activity between 1952 and 1969 is displayed in Fig. 2 for comparison.

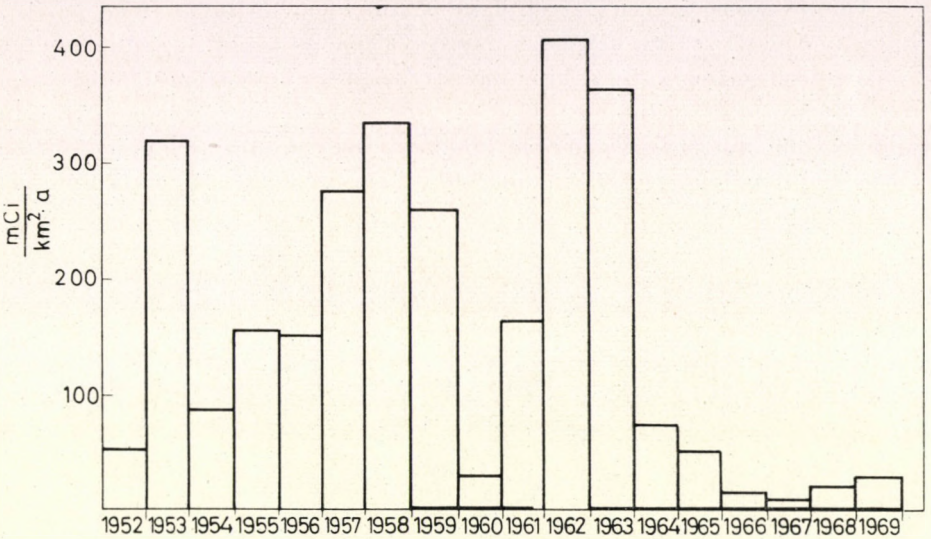


Fig. 2. Annual sum of beta activity measured in the precipitation in Debrecen, Hungary, between 1952 and 1969

Table II

Monthly and annual average specific beta activity of precipitation in Debrecen during 1968 and 1969

Month	1968 pCi/ml	1969 pCi/ml
January	0.1399	0.055
February	0.0240	0.0163
March	0.0647	0.022
April	0.0751	0.029
May	0.0864	0.095
June	0.0485	0.0923
July	0.0443	0.0919
August	0.0391	0.050
September	0.0202	0.046
October	0.0454	0.063
November	0.0104	0.033
December	0.0384	0.019
Annual average	0.0416	0.0537

The increased activity level in 1968 and 1969 can be ascribed partly to Chinese and partly to French nuclear tests. These were not directly detectable in this laboratory, only later, after the stratospheric and tropospheric mixing. To decide the origin of fallout, the decay of the most active samples, from the spring of 1968 and early summer of 1969 were measured over a period of some months but no short period component of the activity was detectable. The

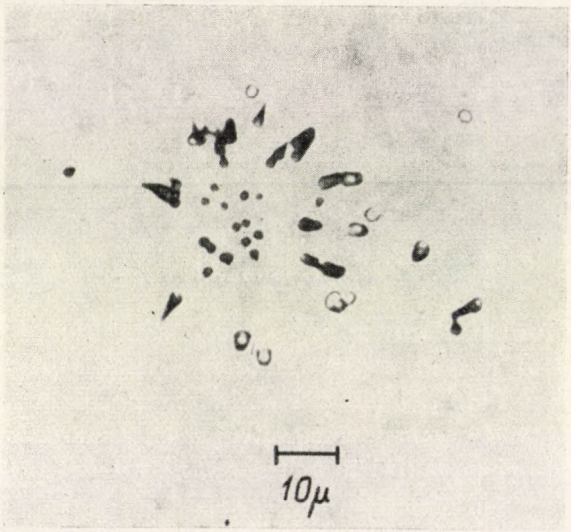


Fig. 3. Microphotograph of alpha particle tracks in a cellulose nitrate detector foil. The tracks originate from a single centre where an alpha active hot particle is localized

activities of the samples from the summer of 1969 were evaluated by the Way-Wigner formula and the fission products could be related to the Chinese H-bomb nuclear test of the previous year. Though after such a long time the fractionating effects cannot be neglected and the fission products of the French nuclear tests of the year 1968 possibly contribute to the activity.

Fresh fission products were detectable only in the precipitation collected in January 1968. The activity of the two highly active samples in January (see Fig. 1) was measured during some months and it decreased in the beginning phase rapidly. The date of the origin of the fresh fission products was definitely determinable by the Way—Wigner formula, and it was identical with the date of the Chinese atomic bomb test of 24. December 1967.

In Table II the monthly averages of the specific beta activity are shown. The annual averages of the specific beta activity increased considerably in comparison with the value of 0.0175 pCi/ml in the year 1966, and 0.0171 pCi/ml in the year 1967.

In the summer of 1969 some rainfall samples had especially high specific beta activity e.g. 2.1 pCi/ml (25. June), 0.85 pCi/ml (18. July) and 0.6 pCi/ml (10. August). It was presumable that a hot particle ought to be present in the residue after evaporation. To decide this question, the alpha activity of the sample was measured with a Si(Li) semiconductor detector and the presence of alpha activity was detected during one hour of measurement. For the localization of the alpha active particles, cellulose nitrate detector foils were placed on the samples. The foils were etched after three weeks of irradiation. The detailed description of the applied method has been published previously [10]—[11].

The detector foils were scanned by microscope. The microphotograph of the detected tracks originating from the sample of highest specific activity (2.1 pCi/ml) is shown in Fig. 3. It can be observed that the alpha particles hit the detector foil starting from a single centre and so the localization of the alpha active hot particle was possible in the sample. The microphotographs were similar in the case of the two other highly active samples, but there were fewer tracks.

The authors are grateful to Dr. G. SOMOGYI for the etching of the detector foils and for the preparation of the microphotograph; and to Mrs. ANGELI for collecting and measuring the precipitations.

REFERENCES

1. A. SZALAY and D. BERÉNYI sen., Acta Phys. Hung., **5**, 1, 1955.
2. A. SZALAY and D. BERÉNYI sen., MTA III. Oszt. Közl., **5**, 89, 1955.
3. A. SZALAY and D. BERÉNYI, sen., MTA III. Oszt. Közl., **9**, 175, 1959.
4. A. SZALAY and D. BERÉNYI sen., Proc. 2nd Geneva Conf., **18**, 570, 1958.
5. A. KOVÁCH and A. SZALAY, ATOMKI Közl., **2**, 229, 1960.
6. A. SZALAY and A. KOVÁCH, Acta Phys. Hung., **13**, 281, 1961.
7. A. SZALAY and A. KOVÁCH, Acta Phys. Hung., **16**, 321, 1964.
8. A. SZALAY and A. KOVÁCH, Acta Phys. Hung., **23**, 137, 1967.
9. A. SZALAY and E. CSONGOR, Acta Phys. Hung., **25**, 279, 1968.
10. G. SOMOGYI, ATOMKI Közl., **8**, 218, 1966.
11. G. SOMOGYI, M. VÁRNAGY and G. PETŐ, Nucl. Instr. Meth., **59**, 299, 1968.

ПРОДУКТЫ ДЕЛЕНИЯ В АТМОСФЕРНЫХ ОСАДКАХ В Г. ДЕБРЕЦЕН (ВЕНГРИЯ) В 1968 И 1969 ГГ.

А. САЛАИ и Е. ЧОНГОР

Резюме

Наблюдение бета-активности продуктов деления в атмосферных осадках было продолжано в 1968 и 1969 гг. Суммарная бета-активность за двух последних лет было соответственно два и три раза выше чем в 1967 г. Некоторые образцы показали особенно высокую удельную активность летом 1969 г. В этих образцах удалось установить присутствие альфа-активных осколков при помощи диэлектрического детектора, состоящего из нитроцеллюлозы.

Acta Physica Academiae Scientiarum Hungaricae, Tomus 29 (4), pp. 415—417 (1970)

HIGHER ORDER COHERENCE EFFECTS OF LASER LIGHT ON THE PHOTOELECTRON DISTRIBUTION DETECTED BY THIRD ORDER PHOTOEFFECT

By

GY. FARKAS

CENTRAL RESEARCH INSTITUTE OF PHYSICS, BUDAPEST

(Received 7. V. 1970)

On decreasing the coherence volume of the giant pulse laser beam the statistical distribution of the photoelectron signal peaks due to third order photoeffect (TPE) was observed to undergo a marked change, while that for the linear photoeffect (LPE) remained unchanged.

The effect of the coherence of light on statistics, expected to be much stronger for higher order process [1, 2, 3, 4, 6], was investigated by observing the statistical fluctuations of the TPE in gold by varying the coherence volume [5] of the incident laser beam.

In the experimental setup described in [7], the coherence properties were varied using different coherence volumes of the beam, determined at a given wavelength and optical bandwidth by the diameters d and D of the diaphragms, one of which was mounted at the laser output and the other at a distance L in the optical axis. After crossing the two diaphragms, the multimode giant pulse laser beam was split into two parts, which were detected simultaneously, one on the linear, the other on the third order detector. The signal peaks J_L and J_T from the linear and from the third order detector, respectively, were analysed on a two-dimensional amplitude analyser. The comparison of the average number of photoelectrons for the coherent and the less coherent cases [6] proved to be difficult with our apparatus. Therefore, we investigated the distributions of J_L and J_T. Considering that $J_T \sim J_L^3$ [7], we evaluated the distributions of the percentage deviations from the averages, i.e.,

$$\xi = [(J_L - \bar{J}_L)/\bar{J}_L] \cdot 100 \quad \text{and} \quad \eta \equiv [(J_T/J_L^3 - \overline{J_T/J_L^3})/\overline{J_T/J_L^3}] \cdot 100.$$

The distributions A, B, C of ξ and η, each averaged over 100 shots, plotted for three different values of d, D and L are shown in Fig. 1. It is apparent that there is a marked change in the TPE distributions, while the LPE distributions are left unchanged. The distribution is the strongest when C has the smallest d, i.e., the smallest aperture at the ruby output surface.

The considerable change in TPE statistics for the given decrease in coherence volume can be interpreted by the observations of the random appear-

ance of the picosecond substructure from pulse to pulse among the "hot spots" of the giant pulse beams [8, 9, 10]. This occasional partial picosecond modulation content of a single light pulse can be amplified by the strong non-linear response of TPE, while it is simply averaged out by the linear response of LPE.

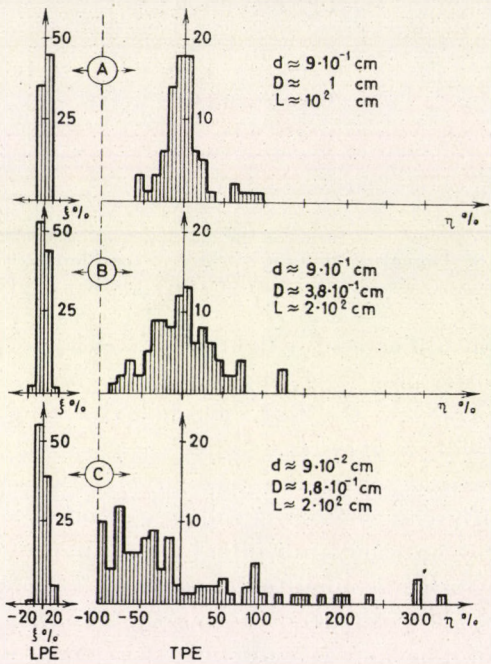


Fig. 1. Horizontal: values of ξ or η. Vertical: frequency of events, for which ξ or η have the specified values

In the currently continued experiments no considerable fluctuations have been observed in the successive TPE signal peaks during a single mode-locked giant pulse.

Thanks are due to Zs. NÁRAY, P. VARGA, I. KERTÉSZ, K. TITSCHKA, Z. HORVÁTH and Miss Zs. SÖRLEY.

REFERENCES

1. Y. R. SHEN, Phys. Rev., **155,** 921, 1967.
2. J. DUCUING and N. BLOEMBERGEN, Phys. Rev., **133,** 1493, 1964.
3. S. CARUSOTTO, C. FORNACA and E. POLACCO, Phys. Rev., **165,** 1391, 1968.
4. M. C. TEICH and P. DIAMENT, J. Appl. Phys., **40,** 625, 1969.
5. L. MANDEL, Proc. Int. School of Phys. "Enrico Fermi" Course XLII., "Quantum Optics", Academic Press, 1968.
6. F. SHIGA and S. IMAMURA, Phys. Lett., **25A,** 706, 1967.
7. GY. FARKAS, ZS. NÁRAY and P. VARGA, Phys. Lett., **24A,** 134, 1967, **25A,** 572, 1967, **28A,** 190, 1968.

8. S. L. Shapiro, M. A. Duguay, L. B. Kreuzer, J. W. Hansen and K. W. Wecht, IEEE J. Quantum El. QE4, 343, 1968.
9. H. Statz and M. Bass, J. Appl. Phys., **40**, 377, 1969.
10. R. J. Harrach, Appl. Phys. Lett. **14**, 148, 1969.

КОГЕРЕНТНЫЕ ЭФФЕКТЫ ВЫСШЕГО ПОРЯДКА РАСПРЕДЕЛЕНИЯ ФОТО-ЭЛЕКТРОНОВ ОТ ЛАЗЕРНОГО ИЗЛУЧЕНИЯ, ИЗМЕРЕННЫЕ ФОТОЭФФЕКТОМ ТРЕТЬЕГО ПОРЯДКА

Д. ФАРКАШ

Р е з ю м е

Уменьшением когерентного объема гигантского импульсного лазерного луча наблюдалось статическое распределение фотоэлектронных сигнальных пиков, обусловленных фотоэффектом третьего порядка, в то время как оно оставалось неизменным в случае линейного фотоэффекта.

Acta Physica Academiae Scientiarum Hungaricae, Tomus 29 (4), pp. 419—425 (1970)

ON THE PHYSICAL SIGNIFICANCE OF THE VECTOR POTENTIAL

By

L. JÁNOSSY

CENTRAL RESEARCH INSTITUTE FOR PHYSICS, BUDAPEST

(Received 7. VII. 1970)

AHARONOV and BOHM claimed that the vector potential of an electromagnetic field plays a specified role which is a characteristic quantum mechanical effect. In the analysis below it is shown that this is not so but that the role of the vector potential can be understood without supposing a specific quantum mechanical action.

§ 1. In classical electrodynamics the force acting upon charges is expressed by the Lorentz force density $\mathbf{F} = \varrho \left(\mathbf{E} + \frac{1}{c} \mathbf{v} \times \mathbf{B} \right)$, i.e. in terms of the field strengths only. Thus the motion of a charge distribution can be calculated with help of the field strength and there is no need to use the distribution of the vector potential **A**.

In quantum mechanics the equation of motion, i.e. the Schrödinger equation contains explicitly the vector potential; we have

$$\frac{1}{2m} \left(i\hbar \nabla + \frac{e}{c} \mathbf{A} \right)^2 \psi + (V + e\Phi) \psi = i\hbar \dot{\psi} \,. \tag{1}$$

One might respect that the quantum mechanical motion obtained from (1) has features depending on the vector potential **A**. This appears the more so as the expression for the quantum mechanical current density

$$\mathbf{i} = - \frac{i\hbar e}{2m} (\psi^* \operatorname{grad} \psi - \psi \operatorname{grad} \psi^*) - \frac{e^2}{mc} \mathbf{A} \psi \psi^* \tag{2}$$

constains also explicitly the vector potential. So as to illustrate such a supposed effect BOHM and AHARONOV [1] considered an ideal experiment of the type shown in Fig. 1.

A beam of electron falls on the screen S_1 with two holes A, B. An interference pattern is observed on the opposite screen S_2. A small magnetized rod may be placed between the screens in a position between the beams. If the rod is very thin and stands perpendicular to the paths of the interfering beams, one can produce a situation such that the main beams producing the interference pattern pass through a region where the magnetic field strength **B** is negligible. Although there seems thus to be no direct magnetic force to act upon the beams — it must be expected, that the magnet **M** modifies the inter-

ference pattern observed on the opposite screen S_2. The vector potential **A** is not negligible along the path of the interfering beams — the change of pattern appears to be caused directly by the vector potential — the effect, being according to BOHM, a specific quantum effect.*

An experiment by CHAMBERS [3] reproduces the ideal experiment thus discussed. A very thin magnetic rod is placed behind a screen in an electron

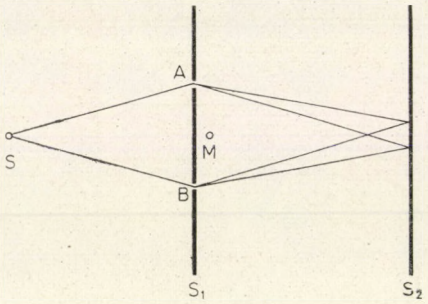


Fig. 1

microscope and a typical change of pattern is observed which is caused by the magnet. It is suggested that the effect observed is that considered theoretically by BOHM.

§ 2. We are of the opinion that the effect discussed by BOHM occurs indeed but we do not think that it proves the existence of a quantum mechanical effect connected with the vector potential.

So as to make our point of view clear we note that as we have shown elsewhere the wave equation (1) can be brought into a form which contains the Lorentz force only and does not contain the vector potential [4]. Indeed, we introduce as new variables the quantities

$$\varrho = \psi^* \psi \tag{3}$$

$$\mathbf{v} = \frac{\hbar}{m} \operatorname{grad} S - \frac{e}{mc} \mathbf{A} , \tag{4}$$

where S is the phase of the wave function, i.e.

$$\psi = Re^{iS} . \tag{5}$$

Both R and S are real functions of the variables, i.e.

$$R = R(\mathbf{r}, t) \qquad S = S(\mathbf{r},t).$$

In terms of the hydrodynamical variables $\varrho = \varrho(\mathbf{r}, t)$ and $\mathbf{v} = \mathbf{v}(\mathbf{r}, t)$ we obtain in place of (1)

$$\operatorname{div} \varrho \mathbf{v} + \frac{\partial \varrho}{\partial t} = 0 \tag{6}$$

* The view of BOHM is also accepted by FEYNMAN [2].

$$m\frac{d\mathbf{v}}{dt} = -\operatorname{grad}(Q+V) + e\left[\mathbf{E} + \frac{1}{c}(\mathbf{v}\times\mathbf{B})\right], \tag{7}$$

where

$$Q = -\frac{\hbar}{2m}\frac{\nabla^2\varrho^{\frac{1}{2}}}{\varrho^{\frac{1}{2}}}.$$

Relations (6) and (7) can be called hydrodynamical equations of motion. They are exactly equivalent to the Schrödinger equation (1) provided initial condition for ϱ and $\mathbf{v}$ are fulfilled, namely

$$\left.\begin{aligned} \int \varrho d\tau &= 1 \qquad (a)\\ \oint \mathbf{v}d\mathbf{s} &= 2\pi\frac{\hbar k}{m} - \frac{e}{mc}\int \mathbf{B}dS. \qquad (b)\end{aligned}\right\} \tag{8}$$

$$k = 0, \pm 1, \pm 2, \ldots$$

The integration $d\tau$ is to be taken over the whole of space; the integration $\oint$ in (8b) is to be taken over an arbitrary closed line L avoiding points where $\varrho = 0$. The integral on the right side of (8b) gives the magnetic flux across L. The conditions (8a, b) if fulfilled for any time $t = 0$ they will be fulfilled automatically at any time $t \neq 0$ — this can be shown with the help of the equations of motion (6) and (7). Thus relations (8) are fulfilled at any time t nevertheless they play the role of initial conditions.

The hydrodynamical equations of motion (6), (7) are exactly equivalent with the wave equation (1) this can be illustrated by the following scheme:

Scheme 1

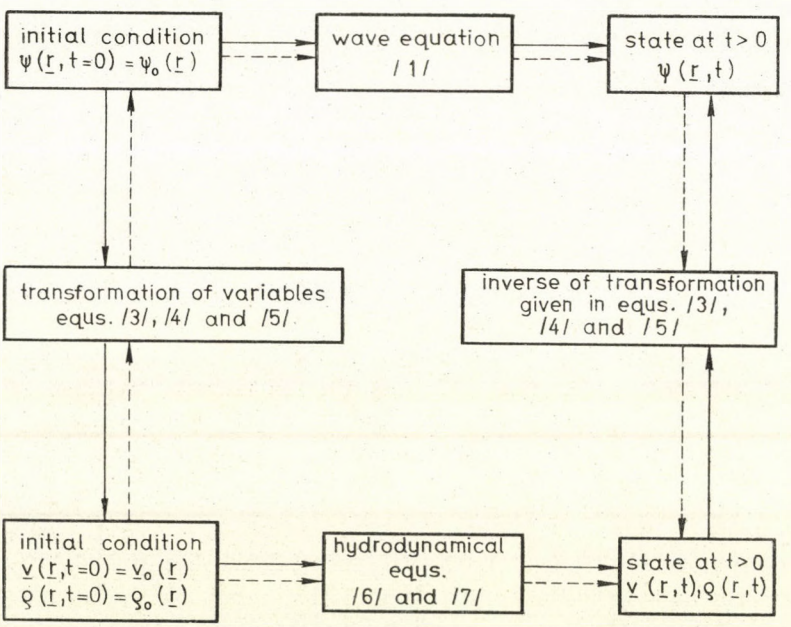


Fig. 2

The scheme shows the following. The physical state of a system at $t = 0$ can be expressed either by an initial condition

$$\psi(\mathbf{r}, 0) = \psi_0(\mathbf{r}) \tag{9}$$

or alternatively by a condition

$$\varrho(\mathbf{r}, 0) = \varrho_0(\mathbf{r}), \quad \mathbf{v}(\mathbf{r}, 0) = \mathbf{v}_0(r). \tag{10}$$

ϱ_0, $\mathbf{v}_0$ has to be chosen in accord with (8).

Considering an initial condition ψ_0 we can calculate $\psi(\mathbf{r}, t)$ for $t \neq 0$ with the help of the wave equation (1). Alternatively having an initial condition ϱ_0, $\mathbf{v}_0$ we can calculate $\mathbf{v}(\mathbf{r},t)$, $\varrho(\mathbf{r},t)$ for $t \neq 0$ from the initial condition with the help of (6) and (7). It can be shown that provided ψ_0 and ϱ_0, $\mathbf{v}_0$ are connected by the transformations (3), (4) then the $\psi(\mathbf{r}, t)$ and $\varrho(\mathbf{r}, t)$, $\mathbf{v}(\mathbf{r}, t)$ will be connected by the same relations (3), (4). Thus the changes of the system, obeying given initial conditions, can be described either by the Schrödinger equation (1) or by the hydrodynamical equations (6), (7) and both equations of motion lead to the same change in time of the system.

§ 3. From the above result we see that the changes of a physical system in the course of time can be described equally well by the Schrödinger equation containing the vector potential explicitly or by the mathematically equivalent hydrodynamical equations which contain only the Lorentz force density but which equations do not contain the vector potential.

The situation is thus somewhat similar in quantum theory, as it is in classical theory. The motion of the system can thus be described by relations containing the vector potential, but it can also be described making use of the Lorentz force only.

The quantum mechanical problem is somewhat complicated by the question whether the physical state of a system is "better" described by the wave function ψ or by the hydrodynamical variables ϱ, $\mathbf{v}$?

If we start from an initial condition of the form (10) for $\mathbf{v}$ and ϱ then the initial condition ψ_0 for ψ contains the vector potential $\mathbf{A}$ at $t = 0$. If on the other hand we start from an initial condition (9) for ψ then the initial value $\mathbf{v}_0$ of $\mathbf{v}$ contains $\mathbf{A}$ and the change of ϱ, in the course of time, also contains $\mathbf{A}$.

Without going into details of this question which is bordering on philosophy, we can make the following statement if considering interference patterns of a beam of electrons.

Observable interference patterns are obtained in a stationary state (or in states which sufficiently approximate a stationary state). The interference pattern is characterized by the distribution $\varrho(\mathbf{r})$. The fact that a state is statio-

nary can be expressed by the condition

$$\frac{\partial \varrho(\mathbf{r}, t)}{\partial t} = 0\,, \qquad \frac{\partial \mathbf{v}(\mathbf{r}, t)}{\partial t} = 0\,. \tag{11}$$

Thus the distribution of interference pattern can be obtained as a solution of the equations (6), (7) together with the initial conditions (8) and with the conditions (11) assuming the state to be stationary. The above relations are differential relations connecting ϱ, v with the field strengths **E**, **B**, thus the interference pattern can be worked out without reference to the vector potential **A** and without explicit use of the wave function ψ.

Thus using for the vector potential **A** various gauges **A**, **A**′, ... we have to use different initial conditions ψ_0, ψ_0', ... if we want to express the same physical configuration, e.g. the same stationary configuration.

§ 4. From the mathematical point of view it is thus clear that the effect of electromagnetic fields on the stationary distribution of electron streams — but also upon the motion of non-stationary streams — can be expressed with the help of the Lorentz force and there is no need to suppose that the vector potential has a particular role in the interaction. It is nevertheless interesting to discuss qualitatively how the effects of an electromagnetic field come about and in particular, how the mechanism of the effect discussed by BOHM and shown schematically in Fig. 1 can be understood.

To see this question more clearly we note that switching on an electromagnetic field we cause a perturbation which is represented by a term

$$P = \frac{i\hbar}{mc}\,\mathbf{A}\ \mathrm{grad}\ \psi + e\,\Phi + \frac{e^2}{c^2}\,\mathbf{A}^2\,, \tag{12}$$

in the Schrödinger equation.

For the sake of illustration suppose the switching on of a magnetic field. We can take $\Phi = 0$ and if the field is such that

$$\mathbf{A}\ \mathrm{grad}\ \psi = 0,$$

where ψ is the wave function of the unperturbed state, then we obtain only a small perturbation of the order of $e^2/c^2\ \mathbf{A}^2$. The switching on of the perturbation causes therefore only a very small immediate change of ψ. However, the main effect of the perturbation is this. If the original state ψ was a stationary one, the perturbed state will not be anymore stationary and a slow change is initiated by the perturbation — which change eventually may lead to a large change of the configuration.

The position is similar to that if a small perturbation is applied to a degenerate stationary state. If the state is not of the form of the *proper linear*

combination of the degenerate wave functions then a beat starts between the perturbed components of the state and in time the small perturbation causes a large change of the configuration.

We may consider as an example a homogeneous magnetic field with a vector potential

$$\mathbf{A}(\mathbf{r}) = -\frac{1}{2}(\mathbf{r}\times\mathbf{B})\,\beta(t),$$

where $\beta(t)$ is a monotonously increasing function such that

$$\beta(t) = \begin{cases} 0 & t < 0, \\ 1 & t > T. \end{cases}$$

The perturbation P changes ψ only very little at first. However, since

$$\mathbf{v} = \mathbf{v}_0 - \frac{e}{mc}\mathbf{A},$$

where

$$\mathbf{v}_0 = \frac{\hbar}{m}\,\mathrm{grad}\ S, \quad (\psi = Re^{iS})$$

thus the perturbation produces a rotation with an angular velocity

$$\boldsymbol{\omega} = -\frac{e\mathbf{B}}{2mc}\,\beta(t)\,.$$

The latter effect is the well-known Larmour precession. Unless the rotating charge has cylindrical symmetry around the axis of rotation — the rotating charge is not anymore stationary. Indeed we find

$$\frac{\partial \varrho}{\partial t} \neq 0\,.$$

The rotating charge emits thus radiation until the configuration changes into a stationary one. The latter may differ considerably from the former one.

§ 5. Applying the above considerations to the effect considered by BOHM, we come to the following picture. If an interference pattern is obtained with the help of an arrangement as shown in Fig. 1 without the magnet M, then some stationary state is obtained and the distribution of ϱ on the screen characterizes the interference pattern. If M is brought in between the main interfering beams, then the immediate effect of the magnet is small. However, the magnet upsets the stationarity of the configuration and a new state starts to

build up. For the stationary configuration the *boundary conditions* are of great importance. In the case considered the main beam travels through a region where there is only small magnetic force. However, the flux passing through the magnet **M** must return somewhere and therefore the beam is *surrounded* by magnetic lines of force. The latter enclosing the configuration of the stream effects strongly the form of the stationary state which builds up eventually and thus the effect of the magnet is felt by its effect through the boundary condition.

If we considered the case where the magnet is in its final position before the electron beam was switched on, then the position is very similar. The beam after having been switched on changes its configuration until it reaches a stationary configuration. The latter is affected by the magnetic lines of force surrounding the stream and thus the distribution of ϱ is strongly affected by the field although the main part of the beam may pass through a region where practically $\mathbf{B} = 0$.

I am greatly indebted to L. PÁL and his colleagues for interesting discussions in which the problem was raised and which discussions helped to clear the problem.

REFERENCES

1. Y. AHARONOV and D. BOHM, Phys. Rev., **115**, 485, 1959.
2. I. I. FEYNMAN et al., The Feynman Lectures on Physics. II.
3. R. G. CHAMBERS, Phys. Rev. Letters, **5**, 3, 1960.
4. L. JÁNOSSY and M. ZIEGLER-NÁRAY, Acta Phys. Hung., **16**, 345, 1964.

РОЛЬ ВЕКТОРНОГО ПОТЕНЦИАЛА

Л. ЯНОШИ

Р е з ю м е

Ахаронов и Бом утверждали, что векторный потенциал электромагнитного поля играет особую роль, которую следует рассматривать, как эффект квантовой механики. В нашей статье доказывается, что это не соответствует действительности. Роль векторного потенциала можно толковать и в том случае, если не предполагается существование такого особого явления квантовой механики.

Note added in proof. D. BOHM and C. PHILIPPIDIS reflected upon the ideas developed in this article. Their comment will appear in a subsequent article.

RECENSIONES

E. FENYVES and O. HAIMAN: The Physical Principles of Nuclear Radiation Measurements

Joint edition published by Akadémiai Kiadó, Budapest and Academic Press, New York and London, 1969, pp. 590

The present book is a revised translation of the German version (Akadémiai Kiadó, Budapest, 1965). According to the original intention of the authors it contains not only a description of the various types of counters but also track detectors, and not only the practical aspects of detectors (counters and track detectors) but also their basic physical interactions and phenomena. This large scope of the book is one of its chief values and this differentiates it from other excellent books on a similar subject.

The first three of the eight chapters deal with the interaction of nuclear radiation with matter, its penetration through various materials and the basic phenomena in different detectors. It is followed by a treatment of the operation and the construction of counters and by their application for the determination of the physical properties of particles and dosimetric problems (Chapters 4, 5 and 6). Finally, in Chapters 7 and 8 particle track detectors and their application in the determinations of the physical properties of particles are summarized. The book is completed with two Appendices, one on the methods of the discovery of elementary particles and the other dealing with electronic instruments for the acquisition and the processing of data from detectors.

Every chapter and the Appendices are followed by a very detailed list of references, which contributes to the usefulness of the present book to a high degree and makes it possible to use it as a reference book and a manual in nuclear and elementary-particle physics research in the measurements of radiations.

The value of this work is evidenced by the fact that the English version with very few modifications was published jointly by Akadémiai Kiadó, Budapest, and Academic Press, New York, four years after the issue of the German edition. Considering, however, that the development of science generally and in the field of radiation detectors in particular is very rapid nowadays it seems to us that a more thorough revision of the first (German) version would have made the book more up-to-date. With such a thorough revision, semiconductor detectors should be allotted more space as compared with the scintillation techniques, according to their present significance in nuclear research. Similarly, the inclusion of solid-state track detectors would be advisable. (Note: in the present edition no mention is made of them.)

Finally, it should be noticed that the omission of the historical section on the development of measuring methods in nuclear and elementary particle physics seems to be regrettable. This useful and interesting Section should have been included, at least in the Appendices.

D. BERÉNYI

J. L. DELCROIX: Plasma Physics

John Wiley and Sons Limited, London, New York, Sydney, 1965

Plasma physics is in a state of rapid development and it is difficult to formulate a methodical presentation which is both complete and well balanced. The author makes a very wide survey of the subject and gives a clear presentation of all the main problems and results of plasma physics. This monograph is based on physical principles; the mathematical treatment is given in the Appendices. It deals mainly with the relations between microscopic and macroscopic descriptions of plasma, but a wide range of plasma properties are also described.

Chapter 1 is introductory. It gives the general concepts on ionized gases and plasmas, a short resumé of the history of plasma physics and its main goal, the harnessing of nuclear fusion energy, which has turned out to be a more difficult problem than physicists thought in the early 1950s. In any case, the numerous studies carried out on plasmas have given us many by-products, some of which are described briefly in this Chapter.

The systematic treatment of the subject begins with the second Chapter. This, and the third Chapter give the trajectories of independent charged particles in a uniform and in a nonuniform magnetic field. The next two chapters deal with elastic collisions and give some basic cross-section formulae. Then follows a short summary of the kinetic theory of fluids, studying the state of a system at a given instant of time. The next problem is how this state has developed from the previous states and how it will evolve in the future. These topics are treated by microscopic evolution equations. The final chapters deal with the properties of plasmas in thermodynamic equilibrium, with the macroscopic equations for one component of a many-component fluid, and with lumped macroscopic properties of plasmas.

The book is recommended for research students and others entering the plasma research field. For a rapid introduction to the subject the reader may omit the material printed in smaller type which contains the more difficult or less important parts of the text.

D. KISDI

Battelle Rencontres, 1967. Lectures in Mathematics and Physics

Edited by Cecile M. DeWitt, John A. Wheeler. W. A. Benjamin, Inc. New York, Amsterdam, 1968, pp. 560

Many mathematicians and physicists feel that they are missing important developments, even ideas significant for their own work, and they would be happy to have better contact with one another's work, but nobody is able to read all the literature, or even the abstracts of it. Even electronic information retrieval could hardly help. The best information system is the mind of a colleague. That was the reason why the Battelle Memorial Institute arranged this meeting between a small number of mathematicians and physicists working in an area where fruitful interactions could be expected. The main problem of such meetings is usually the lack of time and the too many lectures which give the whole enterprise a fragmentary character. These problems were avoided by ensuring a longer time: from 16 July to 31 August, 7 weeks were available for the meeting. The topic was differential geometry and global topology on the mathematical side and Einstein's geometrical theory of gravitation and the Feynman amplitudes or integrals on the physical side. To provide a framework for discussion, four speakers were invited to give a series of lectures: S. HELGASON lectured on Lie groups and symmetric spaces, R. PENSORE on differential geometry, spinors and space-time singularities, R. BOTT on Morse theory and its applications to homotopy theory and J. LASCOUX on the topological analysis of Feynman amplitudes. These lectures and the informal accounts contributed by the participants are presented in this book. The latter were of two types: expository lectures outlining the background, significance and goals of the research field discussed and lectures on technical details. During the meeting it turned out that mathematicians are rarely interested in having the results of physics translated into mathematical terms. They wanted to get the key idea without the details. Physicists on the other hand had to realise that mathematicians will never solve their problem and that mathematics can give them general principles but solving their problems is their own business. The meeting had a great success among the participants and it is also hoped among the readers of this book, among scientists who work in these fields of mathematics and physics.

D. KISDI

AAGE BOHR and BEN R. MOTTELSON:

Nuclear Structure Vol. I. Single-Particle Motion

W. A. Benjamin, Inc. New York, Amsterdam, 1969, pp. 471

The whole three-volume work gives a systematic and up-to-date discussion of the theoretical concepts used in investigations of nuclear structure. In Volume I, single particle motion is the main topic. Before starting this subject, Chapter 1 is devoted to a summary of the important symmetry features of a nuclear system (nuclear symmetry properties associated with space-time invariance and isobaric symmetry).

The discussion of single-particle motion in nuclei is divided into two chapters dealing with independent particle motion and single-particle configurations, respectively. The first of these chapters contains the systematic discussion of the Fermi gas approximation, the nuclear shell structure, the average nuclear potential and its relation to nucleonic interactions and the optical potential. The other chapter deals with particle-hole symmetry, with the study of electric and magnetic moments and transition probabilities as a tool for testing nuclear wave functions, with beta-decay and nuclear reactions.

This systematically developed text in which each section builds only on the concepts explained in previous sections, is only approximately one third of the whole book. After almost every section there are "Illustrative Examples" which contain discussions of empirical data. As any real experiment involves a whole nucleus and the analysis may often require much more information than the systematic text could give as far as that point in these examples the authors have felt themselves free to employ results from other sections of the book, too.

After each chapter, in several Appendices, those topics are treated which are quite general, applicable within wide ranges of quantal physics, such as angular momentum algebra, creation operator formalism, statistical calculation of nuclear level densities, fluctuations in terms of random matrices, one-particle wave functions and matrix elements, the description of Fermion systems in terms of particles and holes, and the analysis of electromagnetic, beta-decay and nuclear reaction processes in terms of appropriate matrix elements. These Appendices make the book as self-contained as possible and useful for a reader who is not specialist in this field. The usefulness of the book is increased by the detailed subject index and by the wide bibliography of 15 pages.

The book can be highly recommended for any graduate physicist who is interested in nuclear physics.

D. KISDI

Men of Physics: L. D. Landau II

Pergamon Press, Oxford, 1969

The book is the second volume of a set of two paperbacks containing reprints of papers by L. D. LANDAU selected from the embarrassing riches of his contributions to various branches of physics. While the first volume was devoted to LANDAU's most important works on low temperature physics and solid state physics, the present volume includes papers on thermodynamics, plasma physics and quantum theory. The reprints are preceded by a concise but thorough introduction consisting of five chapters by D. TER HAAR intended to familiarize the reader with LANDAU's work in each field covered by the selected papers. The book is of great value for all those interested in the development of new ideas in physics. Finally, we give the list of LANDAU's papers contained in this volume:

1. On the Theory of Phase Transitions
2. The Transport Equation in the Case of Coulomb Interactions
3. On the Vibrations of the Electronic Plasma
4. On the Statistical Theory of Nuclei
5. On the Origin of Stellar Energy
6. On the Multiple Production of Particles during Collisions of Fast Particles
7. Extension of the Uncertainty Principle to Relativistic Quantum Theory (with R. PEIERLS)
8. A Theory of Energy Transfer in Collisions
9. Fundamental Problems
10. On the Conservation Laws for Weak Interactions

P. SZÉPFALUSY

Proceedings of the 1968 Heat Transfer and Fluid Mechanics Institute

Stanford University Press, 1968

This is a collection of 16 interesting papers presented at the above meeting and the abstract of 3 invited lectures on recent advances in fluid mechanics, heat transfer and related subjects. The published papers deal with current researches in the field and the invited lectures were given by L. KOVÁSZNAY on turbulence, by G. CARRIER on Tsunami propagation and by R. GENTRY on numerical computations of flow fields. The full text of these lectures is not published in this volume. The editors of the book are the General Chairmen of the meeting, A. F. EMERY and C. A. DEPEW.

J. ANTAL

N. BLOEMBERGEN: **Nonlinear Optics**

W. A. Benjamin Inc. 1965

This monograph was published in the series "Frontiers in Physics" edited by D. PINES. The book reviews the field of nonlinear optics based on lectures given by the author on quantum electronics at Harvard University.

The nonlinear response of circuit elements at various frequencies (audio, radio and microwave) is generally known to electrical engineers. This lecture note discusses the analogous phenomena at optical frequencies. The material presented is arranged in seven parts. These are: Classical Introductions, Quantum Theory of Nonlinear Susceptibilities, Maxwell's Equations in Nonlinear Media, Wave Propagation in Nonlinear Media, Experimental Results, Conclusion and the Appendices, in which three articles published originally in The Physical Review (1962, 1964) by J. A. ARMSTRONG, N. BLOEMBERGEN, J. DUCNING, P. S. PERSHAN and Y. R. SHEN, are reprinted. This excellent book is very highly recommended to all who require a relatively short but quite advanced guide to Nonlinear Optics.

J. ANTAL

G. E. R. SCHULZE: **Metallphysik**

Akademie-Verlag, Berlin 1967

Das vorliegende Buch ist ein Lehrbuch, das sich auf dem Gebiete der Festkörperphysik hauptsächlich mit den wichtigsten Eigenschaften der Metallen beschäftigt. Wie es vom Verfasser schon im Vorwort betont wird, ist die Grundeinstellung des Buches experimentell im Sinne der gewohnten Behandlungsweise der traditionellen Lehrbücher der Experimentalphysik. Diese heutzutage etwas vernachlässigte Darstellungsmethode kann jedenfalls als ein Vorteil des Buches betrachtet werden wodurch eine ganz beträchtliche Menge von Erkentnissen dem breiteren Leserkreis näher gebracht wird. Nach einer kurzgefassten Einleitung gliedert sich das Buch in vier Hauptteile: Aufbau und Zustand der Metalle, mechanische und thermische Eigenschaften des idealen Gitters, Eigenschaften des realen Gitters und Platzwechselvorgänge, — und schliesslich — elektrische und magnetische Eigenschaften. Entsprechend dem Lehrbuchcharakter des Bandes befinden sich an den letzten hundert Seiten recht nützliche Ergänzungen, wie ein ganz ausführliches Symbolverzeichnis, eine Zusammenstellung wichtiger Lehrbücher für weiterführende Studien, ein Quellenverzeichnis der von anderen Stellen übernommenen Abbildungen, ein Sachverzeichnis in drei Sprachen (deutsch, russisch und englisch), das zugleich als ein kleines Fachwörterbuch benutzt werden kann, und endlich ein aus mehreren Tabellen bestehender Anhang. Das Buch wurde in sehr klarem und leicht verfolgbarem Stil geschrieben. Die Auswahl des Materials kann, dem klar abgegrenzten Ziel des Buches entsprechend, günstig beurteilt werden. Die Verarbeitung des Stoffes erstreckt sich auf die Besprechung moderner Resultate und die theoretischen Ausführungen bieten eine nützliche Einführung zu eingehenden Studien der Festkörperphysik dar. Das Buch kann daher den Physikstundenten, Physiklehrern und sich nach der Metallphysik interessierenden Nichtphysikern gleicherweise empfohlen werden. Der Band wurde in recht formschöner Ausführung und in klarem Druck vom Akademie-Verlag hergestellt.

J. ANTAL

Printed in Hungary

A kiadásért felel az Akadémiai Kiadó igazgatója

Műszaki szerkesztő: Farkas Sándor

A kézirat nyomdába érkezett: 1970. VIII. 12. — Terjedelem: 11.25 (A/5) ív, 39 ábra

71.70215 Akadémiai Nyomda, Budapest — Felelős vezető: Bernát György

The *Acta Physica* publish papers on physics, in English, German, French and Russian.
The *Acta Physica* appear in parts of varying size, making up volumes.
Manuscripts should be addressed to:

Acta Physica, Budapest 502, P. O. B. 24.

Correspondence with the editors and publishers should be sent to the same address
The rate of subscription is $ 16.00 a volume.
Orders may be placed with "Kultúra" Foreign Trade Company for Books and News. papers (Budapest I., Fő u. 32. Account No. 43-790-057-181) or with representatives abroad.

Les *Acta Physica* paraissent en français, allemand, anglais et russe et publient des travaux du domaine de la physique.
Les *Acta Physica* sont publiés sous forme de fascicules qui seront réunis en volumes.
On est prié d'envoyer les manuscrits destinés à la rédaction à l'adresse suivante:

Acta Physica, Budapest 502, P. O. B. 24.

Toute correspondance doit être envoyée à cette même adresse.
Le prix de l'abonnement est de $ 16.00 par volume.
On peut s'abonner à l'Entreprise du Commerce Extérieur de Livres et Journaux «Kultúra» (Budapest I., Fő u. 32. — Compte-courant No. 43-790-057-181) ou à l'étranger chez tous les représentants ou dépositaires.

«*Acta Physica*» публикуют трактаты из области физических наук на русском, немецком, английском и французском языках.
«*Acta Physica*» выходят отдельными выпусками разного объема. Несколько выпусков составляют один том.
Предназначенные для публикации рукописи следует направлять по адресу:

Acta Physica, Budapest 502, P. O. B. 24.

По этому же адресу направлять всякую корреспонденцию для редакции и администрации. Подписная цена — $ 16.00 за том.
Заказы принимает предприятие по внешней торговле книг и газет «*Kultúra*» (Budapest I., Fő u. 32. Текущий счет: № 43-790-057-181) или его заграничные представительства и уполномоченные.

INDEX

N. D. Sen Gupta: On the Symmetry Properties of the Equation of Motion. — *Н. Д. Сен Гупта:* О свойствах симметрии уравнения движения 305

A. M. Molla: Punch Problem of Transversely Isotropic Material for a Half-Space with Mixed Thermal Conditions. — *А. М. Молла:* Проблема ударной волны в поперечно изотропном материале, заполняющем полупространство со смешанными термическими условиями 309

И. Киршнер: Аналогические черты матрицы энтропии и матрицы проводимости — *I. Kirschner:* Analogous Features of the Entropy and Conductivity Matrices ... 319

I. Ketskeméty and *L. Kozma:* A Method for the Spectrophotometric Investigation of Absorption and Fluorescence Emission in Media of Extremely Weak Absorption. — *И. Кечкемети* и *Л. Козма:* Метод для спектрофотометрического изучения поглощения и флуоресцентного излучения слабо поглощающих сред 331

Х. Д. Андросенко, С. Б. Ермагамбетов, Г. Н. Смиренкин, Д. Л. Шпак и *И. Ковач:* Угловая анизотропия деления ядер нейтронами и структура барьера. — *H. D. Androsenko, S. B. Ermagambetov, G. N. Smirenkin, D. L. Shpak* and *I. Kovács:* Angular Anisotropy of Nuclear Fission by Neutrons and the Barrier Structure 341

A. Dobay-Szegleth: Calculation of Electron Scattering on the Basis of the Statistical Atom Model in which the Electrons are Grouped according to the Principal Quantum Number. — *А. Добаи-Сеглет:* Расчет рассеяния электронов по статистической модели атома, в которой электроны сгруппированы по главному квантовому числу 359

L. Meskó, V. Schlenk and *A. Valek:* Experimental Study of the $^{24}Mg(d,p)^{25}Mg$ Reaction in the Energy Range 650—500 keV. — *Л. Мешко, Б. Шленк* и *А. Валек:* Исследование ядерной реакции $^{24}Mg(d, p)^{25}Mg$ в области энергии 650—500 кэв 365

J. Cunningham: A Ghostless Lee Model. — *Дж. Канингэм:* Модель Ли без призрачных состояний 373

J. Cunningham: A Differential Approach to High Energy Behaviour of Feynman Amplitudes. — *Дж. Канингэм:* Дифференциальное приближение поведения амплитуд Фейнмана в области высоких энергий 379

K. Somogyi: On the Apparent Deviation from Ohm's Law in GaP. — *К. Шомоди:* О появлении кажущегося отклонения от закона Ома в GaP 383

T. Tietz: Potential Energy Curves for Diatomic Molecules. — *Т. Титц:* Кривые потенциальной энергии для двухатомных молекул 391

I. Kovács and *V. M. Korwar:* Re-investigation of the Coupling Constants of the Revised Molecular States of TiO. — *И. Ковач* и *В. М. Корвар:* Повторное исследование констант связи исправленных молекулярных состояний 399

A. Szalay and *E. Csongor:* Fission Products in the Atmospheric Precipitation in Debrecen, Hungary, during 1968 and 1969. — *А. Салаи* и *Е. Чонгор:* Продукты деления в атмосферных осадках в г. Дебрецен (Венгрия) в 1968 и 1969 гг. 407

Gy. Farkas: Higher Order Coherence Effects of Laser Light on the Photoelectron Distribution Detected by Third Order Photoeffect. — *Д. Фаркаш:* Когерентные эффекты высшего порядка распределения фото электронов от лазерного излучения, измеренные фотоэффектом третьего порядка 415

L. Jánossy: On the Physical Significance of the Vector Potential. — *Л. Яноши:* Роль векторного потенциала 419

RECENSIONES 427